



Institut für Anorganische Chemie

# Synthesis and Characterization of Oligonuclear Naphthalene and Diphosphacyclobutadiene Transition Metal Complexes

Dissertation

Zur Erlangung des Doktorgrades der Naturwissenschaften

Dr. rer. nat.

an der Fakultät Chemie und Pharmazie der Universität Regensburg

vorgelegt von:

Jennifer Malberg

aus Essen

Regensburg 2013



Der experimentelle Teil der vorliegenden Arbeit wurde in der Zeit zwischen März 2010 und September 2013 unter Anleitung von Prof. Dr. Robert Wolf am Institut für Anorganische und Analytische Chemie der Westfälischen Wilhelms-Universität Münster und am Institut für Anorganische Chemie der Universität Regensburg angefertigt. Meinem Betreuer danke ich herzlich für die Überlassung dieses spannenden Projektes sowie für die hervorragende Betreuung und Unterstützung.

Die Arbeit wurde angeleitet von: Prof. Dr. Robert Wolf

Promotionsgesuch eingereicht am: 21.10.2013

Tag der mündlichen Prüfung: 10.12.2013

Promotionsausschuss:	Vorsitz	Prof. Dr. Henri Brunner
	Erstgutachter	Prof. Dr. Robert Wolf
	Zweitgutachter	Prof. Dr. Manfred Scheer
	Dritter Prüfer	Prof. Dr. Axel Jacobi von Wangelin



## Table of Contents

<b>1</b>	<b>Introduction</b>	
1.1	Low-Oxidation State Naphthalene and Anthracene Metal Complexes	1
1.1.1	Mononuclear Complexes	1
1.1.2	Dinuclear Complexes	4
1.2	Metal Complexes with Diphosphacyclobutadiene Ligands	6
<b>2</b>	<b>Synthesis and Electronic Structure of Dissymmetrical, Naphthalene-Bridged Sandwich Complexes <math>[\text{Cp}'\text{Fe}(\mu\text{-C}_{10}\text{H}_8)\text{MCp}^*]^x</math> (<math>x = 0, +1</math>; <math>\text{M} = \text{Fe}, \text{Ru}</math>; <math>\text{Cp}' = \eta^5\text{-C}_5\text{H}_2\text{-1,2,4-}t\text{Bu}_3</math>; <math>\text{Cp}^* = \eta^5\text{-C}_5\text{Me}_5</math>)</b>	<b>15</b>
2.1	Introduction	17
2.2	Results	19
2.2.1	Synthesis and Characterization of the Neutral Complexes $[\text{Cp}'\text{Fe}(\mu\text{-C}_{10}\text{H}_8)\text{FeCp}^*]$ ( <b>3</b> ), $[\text{Cp}'\text{Fe}(\mu\text{-C}_{10}\text{H}_8)\text{RuCp}^*]$ ( <b>4</b> ), and $[\text{Cp}^*\text{Fe}(\mu\text{-C}_{10}\text{H}_8)\text{RuCp}^*]$ ( <b>5</b> )	19
2.2.2	Cyclic Voltammetry	24
2.2.3	Synthesis and Characterization of the Mixed-Valence Compounds $[\text{Cp}'\text{Fe}(\mu\text{-C}_{10}\text{H}_8)\text{FeCp}^*][\text{PF}_6]$ ( <b>[3]PF<sub>6</sub></b> ) and $[\text{Cp}'\text{Fe}(\mu\text{-C}_{10}\text{H}_8)\text{RuCp}^*][\text{PF}_6]$ ( <b>[4]PF<sub>6</sub></b> )	26
2.2.4	Computational Results, Spectroelectrochemistry and TDDFT Calculations	30
2.2.4.1	MO and Population Analysis	30
2.2.4.2	Anodic UV/vis Spectroelectrochemistry	33
2.2.4.3	TDDFT Calculations	36
2.2.4.4	$^{57}\text{Fe}$ Mössbauer Spectra	37
2.3	Conclusion	39
2.4	Experimental Section	40
2.4.1	General Procedures	40
2.4.2	$[\text{Cp}'\text{Fe}(\mu\text{-C}_{10}\text{H}_8)\text{FeCp}^*]$ ( <b>3</b> )	40
2.4.3	$[\text{Cp}'\text{Fe}(\mu\text{-C}_{10}\text{H}_8)\text{RuCp}^*]$ ( <b>4</b> )	40
2.4.4	$[\text{Cp}'\text{Fe}(\mu\text{-C}_{10}\text{H}_8)\text{FeCp}^*][\text{PF}_6]$ ( <b>[3]PF<sub>6</sub></b> )	41
2.4.5	$[\text{Cp}'\text{Fe}(\mu\text{-C}_{10}\text{H}_8)\text{RuCp}^*][\text{PF}_6]$ ( <b>[4]PF<sub>6</sub></b> )	41
2.4.6	$[\text{Cp}^*\text{Fe}(\mu\text{-C}_{10}\text{H}_8)\text{RuCp}^*]$ ( <b>5</b> )	41
2.4.7	Spectroelectrochemistry	42
2.4.8	EPR Spectroscopy and EPR Parameter Calculations	42
2.4.9	$^{57}\text{Fe}$ Mössbauer Spectroscopy	43
2.4.10	X-Ray Crystallography	43
2.5	Supporting Information	44
2.5.1	Single-Crystal X-Ray Structure of $[\text{Cp}^*\text{Fe}(\mu\text{-}\eta^4\text{:}\eta^4\text{-C}_{10}\text{H}_8)\text{RuCp}^*]$ ( <b>5</b> )	44
2.5.2	Graphical Representations of the UV/vis Spectra of <b>3</b> , <b>4</b> , <b>[3]PF<sub>6</sub></b> , and <b>[4]PF<sub>6</sub></b>	45

2.5.3	Cyclic Voltammograms of <b>3</b> and <b>4</b>	46
2.5.4	UV/vis Spectroelectrochemistry of <b>5</b>	47
2.5.5	Calculated Frontier Orbitals of <b>3</b> <sup>+</sup> and <b>4</b> <sup>+</sup>	48
2.5.6	TDDFT Electronic Transition Calculated for the Optimized Geometries of <b>3</b> , <b>3</b> <sup>+</sup> , <b>4</b> , <b>4</b> <sup>+</sup> , <b>5</b> and <b>5</b> <sup>+</sup>	49
2.5.7	Cartesian Coordinates of the Optimized Structures of <b>3</b> , <b>3</b> <sup>+</sup> , <b>4</b> , <b>4</b> <sup>+</sup> , <b>5</b> and <b>5</b> <sup>+</sup>	50
2.5.8	Crystallographic Data of <b>3</b> , <b>4</b> , [ <b>4</b> ]PF <sub>6</sub> , and <b>5</b>	56
<b>3</b>	<b>Towards Trimethylsilylated Phospha-Organometallic Compounds: Reactions of [Co(P<sub>2</sub>C<sub>2</sub>R<sub>2</sub>)<sub>2</sub>]<sup>−</sup> Anions with Me<sub>3</sub>SiCl</b>	61
3.1	Introduction	63
3.2	Results	64
3.3	Conclusion	74
3.4	Experimental Section	75
3.4.1	General Procedures	75
3.4.2	[Co(η <sup>4</sup> -P <sub>2</sub> C <sub>2</sub> <i>t</i> Pent <sub>2</sub> SiMe <sub>3</sub> )(η <sup>4</sup> -P <sub>2</sub> C <sub>2</sub> <i>t</i> Pent <sub>2</sub> )] ( <b>1</b> )	75
3.4.3	[Co(η <sup>4</sup> -P <sub>2</sub> C <sub>2</sub> Ad <sub>2</sub> (CH <sub>2</sub> ) <sub>4</sub> OSiMe <sub>3</sub> )(η <sup>4</sup> -P <sub>2</sub> C <sub>2</sub> Ad <sub>2</sub> )] ( <b>2</b> )	76
3.4.4	[Co(η <sup>4</sup> -P <sub>2</sub> C <sub>2</sub> <i>t</i> Bu <sub>2</sub> (CH <sub>2</sub> ) <sub>4</sub> OSiMe <sub>3</sub> )(η <sup>4</sup> -P <sub>2</sub> C <sub>2</sub> <i>t</i> Bu <sub>2</sub> )] ( <b>3</b> )	77
3.4.5	[Co(η <sup>4</sup> -P <sub>2</sub> C <sub>2</sub> <i>t</i> Pent <sub>2</sub> (CH <sub>2</sub> ) <sub>4</sub> OSiMe <sub>3</sub> )(η <sup>4</sup> -P <sub>2</sub> C <sub>2</sub> <i>t</i> Pent <sub>2</sub> )] ( <b>4</b> )	77
3.4.6	[K(tol) <sub>2</sub> Co(P <sub>2</sub> C <sub>2</sub> <i>t</i> Pent <sub>2</sub> ) <sub>2</sub> ] ( <b>5</b> )	78
3.4.7	X-Ray Crystallography	78
3.5	Supporting Information	80
3.5.1	UV/vis Spectrum of [Co(η <sup>4</sup> -P <sub>2</sub> C <sub>2</sub> <i>t</i> Pent <sub>2</sub> SiMe <sub>3</sub> )(η <sup>4</sup> -P <sub>2</sub> C <sub>2</sub> <i>t</i> Pent <sub>2</sub> )] ( <b>1</b> )	80
<b>4</b>	<b>Gold(I) and Silver(I) Complexes of Diphosphacyclobutadiene Cobaltate Anions</b>	83
4.1	Introduction	85
4.2	Results	87
4.2.1	Synthesis and Structures of Potassium Salts <b>1</b> and <b>2</b>	87
4.2.2	Synthesis and Characterization of Novel Gold(I) and Silver(I) Complexes	89
4.2.2.1	Single-Crystal X-Ray Structures of <b>3</b> and <b>6–9</b>	91
4.2.2.2	Solid-State NMR Spectra of <b>3–9</b>	97
4.2.2.3	Solution NMR Spectra of Complexes <b>3</b> , <b>6</b> , and <b>7</b>	103
4.3	Conclusion	106
4.4	Experimental Section	108
4.4.1	General Procedures	108
4.4.2	[K(thf) <sub>3</sub> {Co(P <sub>2</sub> C <sub>2</sub> <i>t</i> Pent <sub>2</sub> ) <sub>2</sub> }] ( <b>1</b> )	108
4.4.3	[K(thf) <sub>4</sub> {Co(P <sub>2</sub> C <sub>2</sub> Ad <sub>2</sub> ) <sub>2</sub> }] ( <b>2</b> )	108
4.4.4	[Au{Co(η <sup>4</sup> -P <sub>2</sub> C <sub>2</sub> <i>t</i> Pent <sub>2</sub> ) <sub>2</sub> (PMe <sub>3</sub> ) <sub>2</sub> }] ( <b>3</b> )	109

4.4.5	[Au{Co( $\eta^4$ -P <sub>2</sub> C <sub>2</sub> Ad <sub>2</sub> ) <sub>2</sub> }] <sub>x</sub> ( <b>4</b> )	109
4.4.6	[Ag{Co( $\eta^4$ -P <sub>2</sub> C <sub>2</sub> Ad <sub>2</sub> ) <sub>2</sub> }] <sub>x</sub> ( <b>5</b> )	110
4.4.7	[Au(PMe <sub>3</sub> ) <sub>4</sub> ][Au{Co( $\eta^4$ -P <sub>2</sub> C <sub>2</sub> Ad <sub>2</sub> ) <sub>2</sub> }] <sub>2</sub> ( <b>6</b> )	110
4.4.8	[K(thf) <sub>6</sub> ][Au{Co( $\eta^4$ -P <sub>2</sub> C <sub>2</sub> Ad <sub>2</sub> ) <sub>2</sub> }] <sub>2</sub> ( <b>7</b> )	111
4.4.9	[K([18]crown-6)(thf) <sub>2</sub> ][Au{Co( $\eta^4$ -P <sub>2</sub> C <sub>2</sub> Ad <sub>2</sub> ) <sub>2</sub> }] <sub>2</sub> ( <b>8</b> )	111
4.4.10	[K([18]crown-6)(thf) <sub>2</sub> ][Ag{Co( $\eta^4$ -P <sub>2</sub> C <sub>2</sub> Ad <sub>2</sub> ) <sub>2</sub> }] <sub>2</sub> ( <b>9</b> )	111
4.4.11	X-Ray Crystallography	112
4.4.12	Solid-State NMR Spectroscopy	112
4.4.13	DFT Calculations on NMR Parameters	113
4.5	Supporting Information	117
4.5.1	Graphical Representations of the Single-Crystal X-ray Structures of [K(thf) <sub>6</sub> ]-[Au{Co( $\eta^4$ -P <sub>2</sub> C <sub>2</sub> Ad <sub>2</sub> ) <sub>2</sub> }] <sub>2</sub> ( <b>7</b> ), [K([18]crown-6)(thf) <sub>2</sub> ][Au{Co( $\eta^4$ -P <sub>2</sub> C <sub>2</sub> Ad <sub>2</sub> ) <sub>2</sub> }] <sub>2</sub> ( <b>8</b> ), and [K([18]crown-6)(thf) <sub>2</sub> ][Ag{Co( $\eta^4$ -P <sub>2</sub> C <sub>2</sub> Ad <sub>2</sub> ) <sub>2</sub> }] <sub>2</sub> ( <b>9</b> )	117
4.5.2	<sup>31</sup> P{ <sup>1</sup> H} and <sup>13</sup> C{ <sup>1</sup> H} CPMAS NMR Spectra of [Au{Co( $\eta^4$ -P <sub>2</sub> C <sub>2</sub> Ad <sub>2</sub> ) <sub>2</sub> }] <sub>x</sub> ( <b>4</b> ), [Ag{Co( $\eta^4$ -P <sub>2</sub> C <sub>2</sub> Ad <sub>2</sub> ) <sub>2</sub> }] <sub>x</sub> ( <b>5</b> ), [Au(PMe <sub>3</sub> ) <sub>4</sub> ][Au{Co( $\eta^4$ -P <sub>2</sub> C <sub>2</sub> Ad <sub>2</sub> ) <sub>2</sub> }] <sub>2</sub> ( <b>6</b> ), and [K([18]crown-6)(thf) <sub>2</sub> ][Ag{Co( $\eta^4$ -P <sub>2</sub> C <sub>2</sub> Ad <sub>2</sub> ) <sub>2</sub> }] <sub>2</sub> ( <b>9</b> )	119
4.5.3	Variable-Temperature <sup>1</sup> H and <sup>13</sup> C{ <sup>1</sup> H} NMR Spectra of [Au{Co( $\eta^4$ -P <sub>2</sub> C <sub>2</sub> <i>t</i> Pent <sub>2</sub> ) <sub>2</sub> (PMe <sub>3</sub> ) <sub>2</sub> }] ( <b>3</b> )	121
<b>5</b>	<b>Preparation of an Organometallic Molecular Square by Self-Assembly of Phosphorus-Containing Building Blocks</b>	127
5.1	Introduction	129
5.2	Results	130
5.3	Conclusion	134
5.4	Experimental Section	135
5.4.1	General Procedures	135
5.4.2	[Au{Co(P <sub>2</sub> C <sub>2</sub> <i>t</i> Bu <sub>2</sub> ) <sub>2</sub> }] <sub>4</sub> ( <b>1</b> )	135
5.4.3	[K(thf) <sub>2</sub> {Co(P <sub>2</sub> C <sub>2</sub> <i>t</i> Bu <sub>2</sub> ) <sub>2</sub> }] ( <b>2</b> )	135
5.4.4	[Au(PPh <sub>3</sub> ) <sub>4</sub> ][Au{Co(P <sub>2</sub> C <sub>2</sub> <i>t</i> Bu <sub>2</sub> ) <sub>2</sub> }] <sub>2</sub> ( <b>3</b> )	136
5.4.5	[Tl(thf) <sub>2</sub> {Co(P <sub>2</sub> C <sub>2</sub> <i>t</i> Bu <sub>2</sub> ) <sub>2</sub> }] ( <b>4</b> )	136
5.4.6	X-Ray Crystallography	137
5.5	Supporting Information	139
5.5.1	<sup>1</sup> H and <sup>31</sup> P{ <sup>1</sup> H} NMR Spectra of [Au{Co(P <sub>2</sub> C <sub>2</sub> <i>t</i> Bu <sub>2</sub> ) <sub>2</sub> }] <sub>4</sub> ( <b>1</b> )	139
5.5.2	Variable-Temperature <sup>1</sup> H and <sup>31</sup> P{ <sup>1</sup> H} NMR Spectra of [Au(PPh <sub>3</sub> ) <sub>4</sub> ][Au{Co(P <sub>2</sub> C <sub>2</sub> <i>t</i> Bu <sub>2</sub> ) <sub>2</sub> }] <sub>2</sub> ( <b>3</b> )	140
5.5.3	<sup>1</sup> H and <sup>31</sup> P{ <sup>1</sup> H} NMR Spectra of [Tl(thf) <sub>2</sub> {Co(P <sub>2</sub> C <sub>2</sub> <i>t</i> Bu <sub>2</sub> ) <sub>2</sub> }] ( <b>4</b> )	142
5.5.4	UV/vis Spectrum of [Tl(thf) <sub>2</sub> {Co(P <sub>2</sub> C <sub>2</sub> <i>t</i> Bu <sub>2</sub> ) <sub>2</sub> }] ( <b>4</b> )	143

<b>6</b>	<b>Copper(I) and Silver(I) Complexes of Diphosphacyclobutadiene Sandwich Anions: Synthesis, Crystal Structures, Solution and Solid-State NMR Characterization</b>	<b>147</b>
6.1	Introduction	149
6.2	Results	151
6.2.1	Synthesis and Structural Characterization of Novel Copper(I) Complexes [Cu{Co(P <sub>2</sub> C <sub>2</sub> <i>t</i> Pent <sub>2</sub> ) <sub>2</sub> }(PPh <sub>3</sub> ) <sub>2</sub> ] ( <b>1</b> ), [Cu{Co(P <sub>2</sub> C <sub>2</sub> <i>t</i> Bu <sub>2</sub> ) <sub>2</sub> }(PPh <sub>3</sub> ) <sub>2</sub> ] ( <b>2</b> ), and [Cu(PMe <sub>3</sub> ) <sub>4</sub> ][Co(P <sub>2</sub> C <sub>2</sub> <i>t</i> Pent <sub>2</sub> ) <sub>2</sub> ] ( <b>3</b> )	151
6.2.2	Synthesis and Structural Characterization of the Silver(I) Complexes [Ag{Co(P <sub>2</sub> C <sub>2</sub> <i>t</i> Pent <sub>2</sub> ) <sub>2</sub> }(PMe <sub>3</sub> ) <sub>3</sub> ] ( <b>4</b> ), [Ag{Co(P <sub>2</sub> C <sub>2</sub> <i>t</i> Pent <sub>2</sub> ) <sub>2</sub> }(PMe <sub>3</sub> ) <sub>2</sub> ] ( <b>5</b> ), and [Ag <sub>2</sub> {Co(P <sub>2</sub> C <sub>2</sub> <i>t</i> Pent <sub>2</sub> ) <sub>2</sub> }(PMe <sub>3</sub> ) <sub>5</sub> ]SbF <sub>6</sub> ( <b>6</b> )	160
6.3	Conclusion	169
6.4	Experimental Section	170
6.4.1	General Procedures	170
6.4.2	Synthesis of [K(thf) <sub>3</sub> {Co(P <sub>2</sub> C <sub>2</sub> <i>t</i> Pent <sub>2</sub> ) <sub>2</sub> }]	170
6.4.3	Synthesis of [K(thf) <sub>2</sub> {Co(P <sub>2</sub> C <sub>2</sub> <i>t</i> Bu <sub>2</sub> ) <sub>2</sub> }]	170
6.4.4	Synthesis of [Cu{Co(P <sub>2</sub> C <sub>2</sub> <i>t</i> Pent <sub>2</sub> ) <sub>2</sub> }(PPh <sub>3</sub> ) <sub>2</sub> ] ( <b>1</b> )	171
6.4.5	Synthesis of [Cu{Co(P <sub>2</sub> C <sub>2</sub> <i>t</i> Bu <sub>2</sub> ) <sub>2</sub> }(PPh <sub>3</sub> ) <sub>2</sub> ] ( <b>2</b> )	171
6.4.6	Synthesis of [Cu(PMe <sub>3</sub> ) <sub>4</sub> ][Co(P <sub>2</sub> C <sub>2</sub> <i>t</i> Pent <sub>2</sub> ) <sub>2</sub> ] ( <b>3</b> )	172
6.4.7	Synthesis of [Ag{Co(P <sub>2</sub> C <sub>2</sub> <i>t</i> Pent <sub>2</sub> ) <sub>2</sub> }(PMe <sub>3</sub> ) <sub>3</sub> ] ( <b>4</b> )	173
6.4.8	Synthesis of [Ag{Co(P <sub>2</sub> C <sub>2</sub> <i>t</i> Pent <sub>2</sub> ) <sub>2</sub> }(PMe <sub>3</sub> ) <sub>2</sub> ] ( <b>5</b> )	173
6.4.9	Synthesis of [Ag <sub>2</sub> {Co(P <sub>2</sub> C <sub>2</sub> <i>t</i> Pent <sub>2</sub> ) <sub>2</sub> }(PMe <sub>3</sub> ) <sub>5</sub> ]SbF <sub>6</sub> ( <b>6</b> )	174
6.4.10	X-Ray Crystallography	175
6.4.11	Solid-State NMR Spectroscopy	179
6.5	Supporting Information	180
6.5.1	Graphical Representation of the Single-Crystal X-Ray Structure of [Cu{Co(P <sub>2</sub> C <sub>2</sub> <i>t</i> Pent <sub>2</sub> ) <sub>2</sub> }(PPh <sub>3</sub> ) <sub>2</sub> ] ( <b>1</b> )	180
6.5.2	Variable-Temperature <sup>31</sup> P{ <sup>1</sup> H} NMR Spectra of [Cu{Co(P <sub>2</sub> C <sub>2</sub> <i>t</i> Pent <sub>2</sub> ) <sub>2</sub> }(PPh <sub>3</sub> ) <sub>2</sub> ] ( <b>1</b> ) and [Cu{Co(P <sub>2</sub> C <sub>2</sub> <i>t</i> Bu <sub>2</sub> ) <sub>2</sub> }(PPh <sub>3</sub> ) <sub>2</sub> ] ( <b>2</b> )	181
6.5.3	<sup>1</sup> H NMR Spectrum of [Cu(PMe <sub>3</sub> ) <sub>4</sub> ][Co(P <sub>2</sub> C <sub>2</sub> <i>t</i> Pent <sub>2</sub> ) <sub>2</sub> ] ( <b>3</b> )	183
6.5.4	<sup>31</sup> P{ <sup>1</sup> H} NMR Spectra of [Ag{Co(P <sub>2</sub> C <sub>2</sub> <i>t</i> Pent <sub>2</sub> ) <sub>2</sub> }(PMe <sub>3</sub> ) <sub>3</sub> ] ( <b>4</b> ), [Ag{Co(P <sub>2</sub> C <sub>2</sub> <i>t</i> Pent <sub>2</sub> ) <sub>2</sub> }(PMe <sub>3</sub> ) <sub>2</sub> ] ( <b>5</b> ), and [Ag <sub>2</sub> {Co(P <sub>2</sub> C <sub>2</sub> <i>t</i> Pent <sub>2</sub> ) <sub>2</sub> }(PMe <sub>3</sub> ) <sub>5</sub> ]SbF <sub>6</sub> ( <b>6</b> )	184
6.5.5	<sup>13</sup> C{ <sup>1</sup> H} CPMAS NMR Spectra of Complexes <b>1–6</b>	186
6.5.6	<sup>31</sup> P{ <sup>1</sup> H} CPMAS NMR Spectra of [Ag{Co(P <sub>2</sub> C <sub>2</sub> <i>t</i> Pent <sub>2</sub> ) <sub>2</sub> }(PMe <sub>3</sub> ) <sub>3</sub> ] ( <b>4</b> ), [Ag{Co(P <sub>2</sub> C <sub>2</sub> <i>t</i> Pent <sub>2</sub> ) <sub>2</sub> }(PMe <sub>3</sub> ) <sub>2</sub> ] ( <b>5</b> ), and [Ag <sub>2</sub> {Co(P <sub>2</sub> C <sub>2</sub> <i>t</i> Pent <sub>2</sub> ) <sub>2</sub> }(PMe <sub>3</sub> ) <sub>5</sub> ]SbF <sub>6</sub> ( <b>6</b> )	188
6.5.7	<sup>31</sup> P RFDR and R-TOBSY Spectra of [Ag{Co(P <sub>2</sub> C <sub>2</sub> <i>t</i> Pent <sub>2</sub> ) <sub>2</sub> }(PMe <sub>3</sub> ) <sub>3</sub> ] ( <b>4</b> ) and [Ag{Co(P <sub>2</sub> C <sub>2</sub> <i>t</i> Pent <sub>2</sub> ) <sub>2</sub> }(PMe <sub>3</sub> ) <sub>2</sub> ] ( <b>5</b> ), and [Ag <sub>2</sub> {Co(P <sub>2</sub> C <sub>2</sub> <i>t</i> Pent <sub>2</sub> ) <sub>2</sub> }(PMe <sub>3</sub> ) <sub>5</sub> ]SbF <sub>6</sub> ( <b>6</b> )	189

6.5.8	<sup>31</sup> P Chemical Shielding Anisotropy Parameters (Full Tensor Values) for Compounds <b>1–6</b>	191
<b>7</b>	<b>Summary</b>	195
<b>8</b>	<b>Zusammenfassung</b>	205
<b>9</b>	<b>Acknowledgement</b>	215
<b>10</b>	<b>Curriculum Vitae</b>	217



# 1 Introduction

## 1.1 Low-Oxidation State Naphthalene and Anthracene Metal Complexes

### 1.1.1 Mononuclear Complexes

Low-valent naphthalene and anthracene transition metal complexes are attractive sources of highly unsaturated metal units in chemical synthesis.<sup>1</sup> In many cases, they are readily accessible by the reduction of metal halides with alkali metal naphthalene and anthracene at low temperatures.<sup>1</sup> Due to the labile character of the coordinated ligands these metalates easily undergo ligand substitution reactions. The driving force for the replacement of the arene ligand is the recovery of aromaticity of the conjugated  $\pi$  system.<sup>2</sup> Homoleptic naphthalene and anthracene complexes may thus function as synthetic equivalents of “naked” metal atoms and anions, which are of high general interest for the exploration of low-valent transition metal chemistry.<sup>3–8</sup>

Although reactions of transition metal halides with alkali metal naphthalene solutions were described in a U.S Patent in 1939, over 25 years passed before *Chatt* and *Davidson* illustrated the potential of this route by the preparation of the first naphthalene transition metal complex  $[\text{Ru}(\eta^2\text{-C}_{10}\text{H}_8)(\text{dmpe})_2]$  (**1**, Figure 1, dmpe = tetramethyldiphosphanylene). They suggested that this highly reactive complex forms an equilibrium with its hydride tautomer  $\text{cis-}[\text{RuH}(\eta^1\text{-C}_{10}\text{H}_7)(\text{dmpe})]$  (**1'**).<sup>9</sup> In 1967, the group of *E. O. Fischer* reported the first homoleptic polyarene ruthenium(II) complex  $[\text{Ru}(\eta^6\text{-C}_{10}\text{H}_8)_2](\text{PF}_6)_2$  (**2**, Figure 1), in which the ruthenium atom is exclusively coordinated by two naphthalene molecules. The complex was isolated in 3% yield by a Fischer-Hafner type procedure from the reaction system  $\text{RuCl}_3/\text{AlCl}_3/\text{Al}/\text{naphthalene}/\text{hexamethylbenzene}$ .<sup>10</sup>

Polyarene transition metal chemistry caught little attention over the next decades until a seminal contribution by *Ellis et al.* reported the isolation and characterization of the anionic  $\text{tris}(\eta^4\text{-naphthalene})\text{zirconate}(2-)$  (**3**, Figure 1).<sup>1,11</sup> Following this discovery, various homoleptic naphthalene and anthracene complexes were isolated with a range of transition metals. Polyarene complexes of several early transition metals have been described.<sup>6,8,12</sup> Complexes containing electron-rich transition metals are still comparatively rare. Anions **4** and **5** (Figure 1) represent two of the few well-characterized examples with the late transition metals cobalt and iron.<sup>5,7</sup>

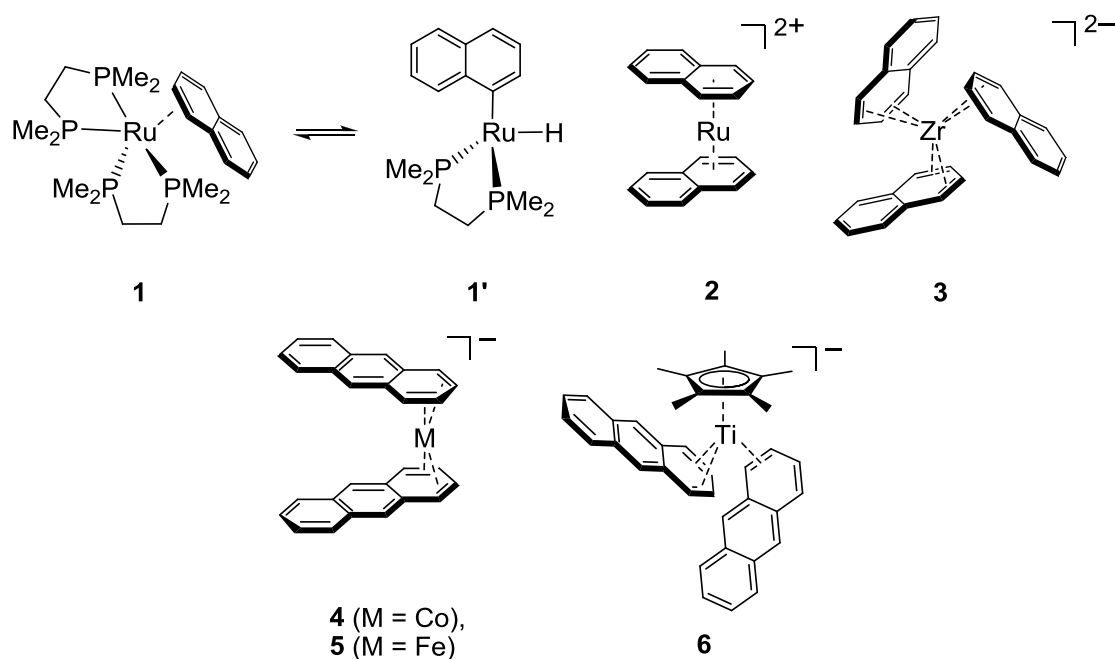
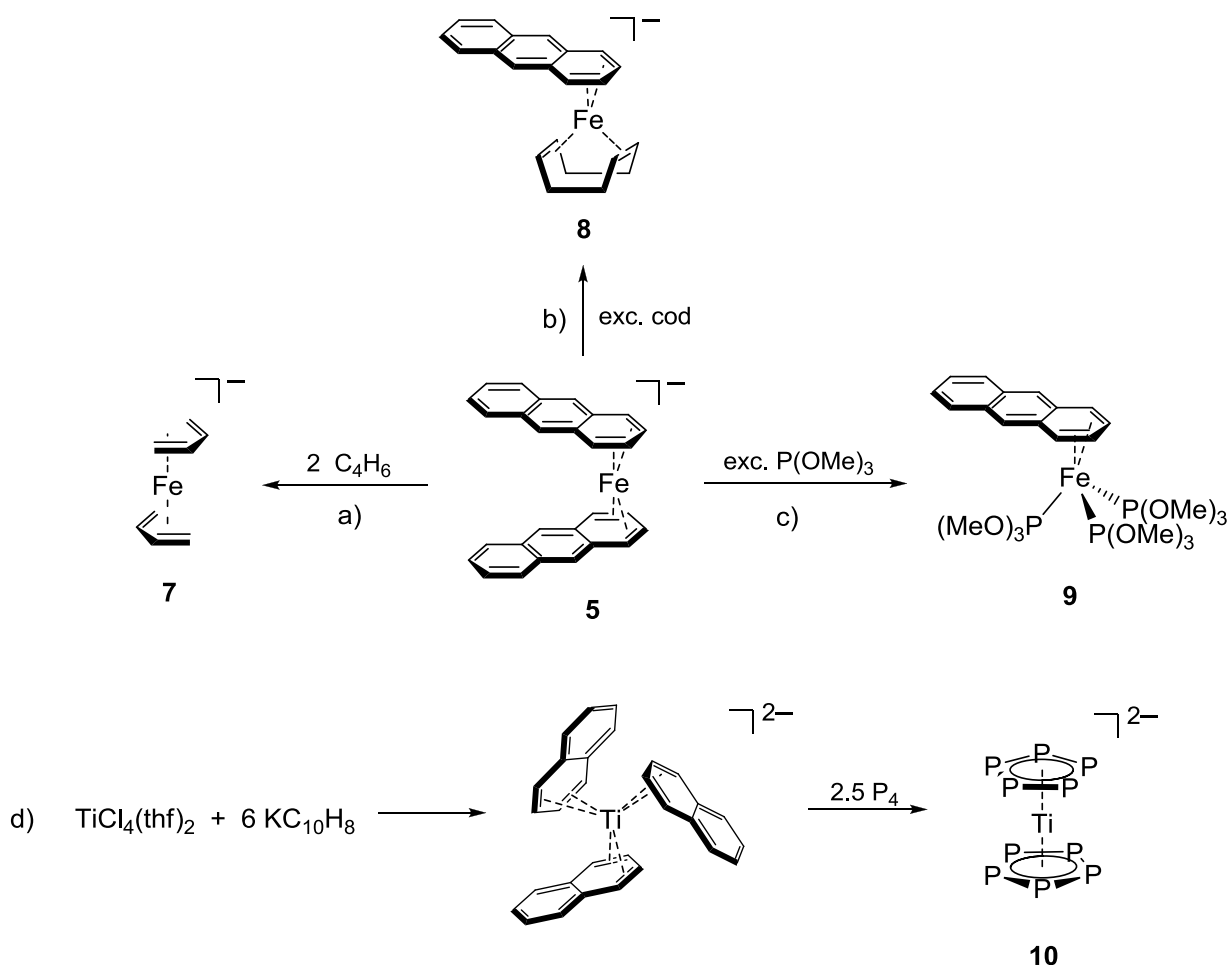


**Figure 1.** Selected examples of polyarene metalates.



**Scheme 1.** Selected examples of ligand-substitution reactions of the polyarene metalate **5**, including the synthesis of the first carbon-free metallocene  $[Ti(\eta^5-P_5)_2]^{2-}$  (**10**).

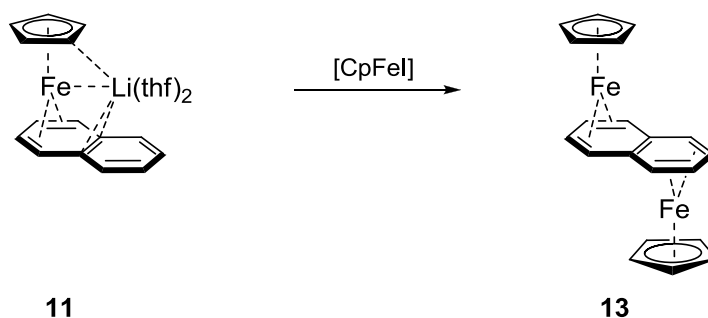
Heteroleptic polyarene metalates of type **6** (Figure 1) are still quite uncommon. Interestingly, the solid-state molecular structure of complex **6** features two anthracene molecules that bind to the metal center with different hapticities.<sup>4</sup> Based on the 18-electron formalism, the presence of the  $\eta^2$ -coordinated ligand is unexpected and is presumably a consequence of the steric demand of the  $Cp^*$  ligand.

In 1990, Jonas *et al.* reported the synthesis of the heteroleptic naphthalene iron complex  $[Li(thf)_2\{Cp^*Fe(\eta^4-C_{10}H_8)\}]$  (**11**, Scheme 2) by the reduction of ferrocene with lithium naphthalene.<sup>15</sup> Using a similar approach, our group recently prepared the low-valent naphthalene complex  $[K([18]crown-6)\{Cp^*Fe(\eta^4-C_{10}H_8)\}]$  (**12**, Figure 2) via a one-pot procedure from  $Cp^*Li$ ,  $FeCl_2(thf)_{1.5}$  (one equiv. each) and two equiv. potassium naphthalene.<sup>16</sup> Compound **12** forms the cyclobutadiene complexes  $[K([18]crown-6)\{Cp^*Fe(\eta^4-C_4Ph_4)\}]$  and  $[K([18]crown-6)\{Cp^*Fe(\eta^4-P_2C_2tBu_2)\}]$  upon reaction with diphenylacetylene and *tert*-butyl phosphalkyne, respectively. Furthermore, **12** reacts with white phosphorus to produce unusual anionic polyphosphido iron complexes.<sup>17</sup> Compound **12** therefore represents a promising source of the “ $Cp^*Fe^-$ ” synthon, and it remains exciting to see how it can be further exploited in synthetic chemistry. The anthracene analogue of **12**,  $[K([18]crown-6)\{Cp^*Fe(\eta^4-C_{14}H_{10})\}]$ , was also prepared recently along with the neutral complexes  $[Cp^*Fe(\eta^4-C_{10}H_8)]$

and  $[\text{Cp}^*\text{Fe}(\eta^4\text{-C}_{14}\text{H}_{10})]$ . The redox properties and the bonding situation of these complexes were explored in some detail.<sup>18</sup>

### 1.1.2 Dinuclear Complexes

The synthetic utility of naphthalene and anthracene metalates for the preparation of bimetallic complexes was first demonstrated by *Jonas* and coworkers. They showed that treatment of the iron(0) complex **11** with one equivalent of  $[\text{CpFeI}]$  yields the dinuclear naphthalene-bridged compound  $[\text{CpFe}(\mu\text{-C}_{10}\text{H}_8)\text{FeCp}]$  (**13**, Scheme 2).<sup>15a</sup> The related  $\text{Cp}^*$  substituted compound  $[\text{Cp}^*\text{Fe}(\mu\text{-C}_{10}\text{H}_8)\text{FeCp}^*]$  (**14**, Figure 2) has been mentioned in a dissertation and was synthesized by a similar procedure.<sup>19</sup>



**Scheme 2.** Synthesis of the homodinuclear diiron complex **13**.

The investigation of the electronic interactions between the incorporated metal centers in bimetallic compounds such as **13** and **14** is of considerable interest.<sup>20</sup> The nature of the bridging ligand is an important factor. Although homobimetallic diiron complexes are known with numerous hydrocarbon bridges, naphthalene and anthracene have rarely been used.<sup>21</sup> The dicationic complex  $[\text{CpFe}(\mu\text{-C}_{14}\text{H}_{10})\text{FeCp}][\text{PF}_6]_2$  is a rare example in which anthracene has been used as a bridging ligand.<sup>22</sup> Besides the diiron complexes **13** and **14**, the homonuclear vanadium and chromium compounds  $[\text{CpV}(\mu\text{-C}_{10}\text{H}_8)\text{VCp}]$  (**16**, Figure 2) and  $[(\text{C}_6\text{H}_6)\text{Cr}(\mu\text{-C}_{10}\text{H}_8)\text{Cr}(\text{C}_6\text{H}_6)]$  (**17**) are two examples for naphthalene-bridged complexes.<sup>15a, 23</sup> Heterobimetallic compounds in which the polyarene is coordinated by different metals are even less common. In 2005, *Sweigart et al.* reported the heterobimetallic iron-manganese complex  $[\text{CpFe}(\mu\text{-C}_{10}\text{H}_8)\text{Mn}(\text{CO})_3]$  (**18**). Spectroscopic investigations suggest a zwitterionic electronic structure for this compound in which a cationic  $\text{CpFe}^+$  fragment and an anionic  $\text{Mn}(\text{CO})_3^-$  unit bind to opposite sides of the arene ligand.<sup>24</sup> Our group recently reported that the naphthalene complex  $[\text{K}([18]\text{crown-6})\{\text{Cp}^*\text{Fe}(\eta^4\text{-C}_{10}\text{H}_8)\}]$  (**12**, Figure 2) readily reacts with  $[\text{Cp}^*\text{FeCl}(\text{tmeda})]$  ( $\text{tmeda} = N,N,N',N'$ -tetramethylethylenediamine) to yield the homobimetallic diiron compound  $[\text{Cp}^*\text{Fe}(\mu\text{-C}_{10}\text{H}_8)\text{FeCp}^*]$  (**14**, Figure 2). The related anthracene-bridged complex  $[\text{Cp}^*\text{Fe}(\mu\text{-C}_{14}\text{H}_{10})\text{FeCp}^*]$  (**15**, Figure 2) was prepared by a related one-pot procedure from “ $\text{Cp}^*\text{FeCl}$ ”, and  $\text{KC}_{14}\text{H}_{10}$ . Both complexes are diamagnetic. Cyclic voltammetry and UV/vis spectroelectrochemical studies revealed that complexes **14** and **15** can reversibly oxidized to the monocations **14**<sup>+</sup> and **15**<sup>+</sup>.<sup>18</sup> *Tatsumi* and coworkers independently reported the preparation and characterization of **14** and **15** and of the mixed-valent  $\text{Fe}^{\text{I}}\text{-Fe}^{\text{II}}$  complexes  $[\text{Cp}^*\text{Fe}(\mu\text{-C}_{10}\text{H}_8)\text{FeCp}^*]\text{BAr}^{\text{F}}_4$  (**14**) $\text{BAr}^{\text{F}}_4$ ) and  $[\text{Cp}^*\text{Fe}(\mu\text{-C}_{14}\text{H}_{10})\text{-}$

FeCp\*]BAR<sup>F</sup><sub>4</sub> ([**15**]BAR<sup>F</sup><sub>4</sub>). In contrast to the  $\eta^4$  coordination mode of the neutral complexes, the cationic species **14**<sup>+</sup> and **15**<sup>+</sup> contain  $\eta^6$ -coordinated Cp\*Fe fragments.<sup>25</sup> Thorough spectroscopic and electrochemical studies were performed, including <sup>57</sup>Fe Mössbauer investigations and spectroelectrochemistry experiments.<sup>18, 25</sup> In conjunction with DFT calculations, these investigations revealed the strong electronic coupling between the two formally 17e iron(+I) centers in these compounds.

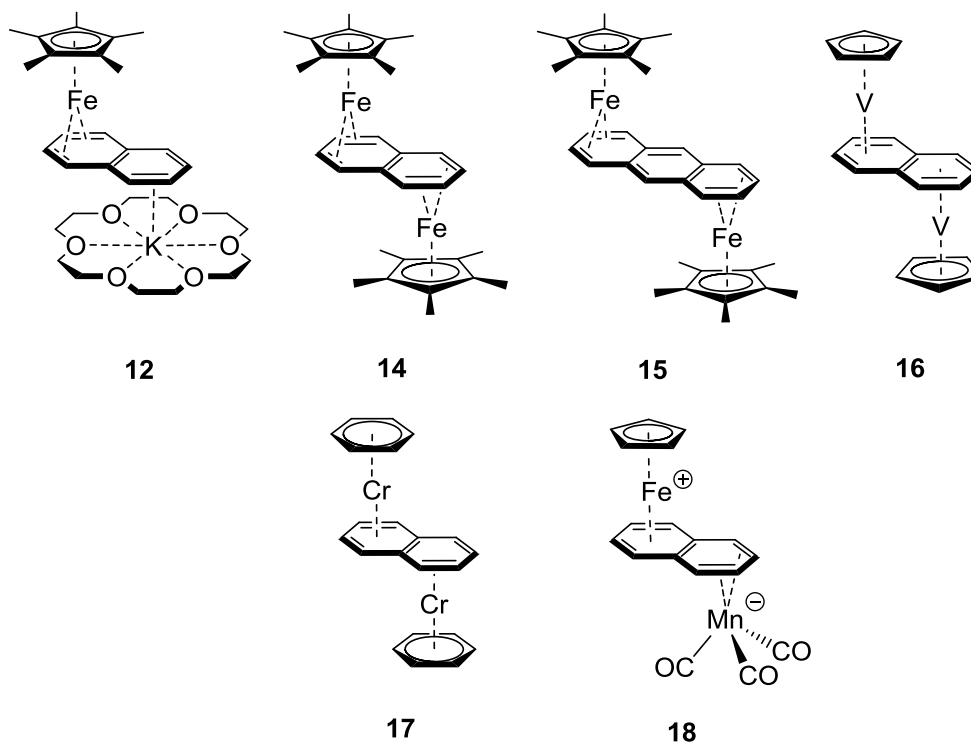


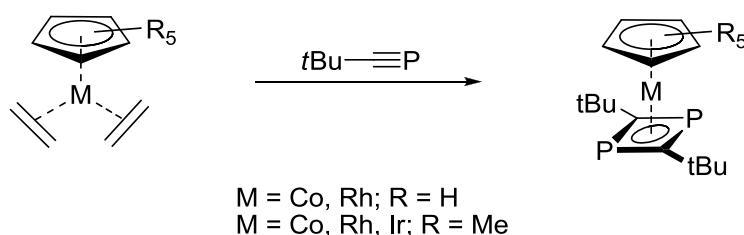
**Figure 2.** Schematic representation of mono- and bimetallic transition metal complexes **12** and **14–18**.

Subsequent to the prior investigations described above, it was an aim of this thesis to gain a deeper understanding of the influence of the Cp<sup>R</sup> ligand on structure and electronic behavior. Therefore, the effect of replacing the Cp\* ligand by the more bulky derivative Cp' (Cp' = 1,2,4-tri-*tert*-butylcyclopentadienyl) was investigated. Furthermore, we sought to investigate the effect of different metal atoms on the electronic structure by replacing one of the iron atoms by its heavier congener ruthenium. The results of these investigations are presented in Chapter 2.

## 1.2 Metal Complexes with Diphosphacyclobutadiene Ligands

Compounds containing multiple bonds were restricted to elements of the second row of the periodic table for a long time, and the ability of phosphorus to form stable  $p_{\pi}-p_{\pi}$  bonds was not recognized.<sup>26</sup> As a consequence of this so called “double bond rule”, the development of the chemistry of trivalent phosphorus derivatives bearing  $p_{\pi}-p_{\pi}$  bonds developed slowly.<sup>27</sup> In 1961, *Gier* reported the synthesis of methylidynephosphine (or phosphacetylene)  $\text{HC}\equiv\text{P}$  by the pyrolysis of  $\text{PH}_3$  using an electric arc between graphite electrodes.<sup>28</sup> Methylidynephosphine, the parent compound of phosphalkynes  $\text{RC}\equiv\text{P}$ , was reported to be highly pyrophoric and decomposed even at very low temperatures ( $-120\text{ }^{\circ}\text{C}$ ), so that this fundamentally important result remained a chemical curiosity for many years.<sup>27b, 28</sup> Almost 20 years elapsed until *Becker* and coworkers described the preparation of the first kinetically stabilized phosphalkyne  $t\text{BuC}\equiv\text{P}$ .<sup>29</sup> In the following years, the synthesis of  $t\text{BuC}\equiv\text{P}$  was further optimized so that useful amounts of this compound became readily accessible.<sup>29b</sup> Since then, both the organic chemistry of phosphalkynes as well as their coordination chemistry have been intensively explored. Many similarities between alkynes and phosphalkynes have been highlighted, while their chemical behavior is quite distinct from that of nitriles.<sup>30,31</sup>

In 1986, the groups of *Nixon* and *Binger* independently reported the first example of phosphalkyne cyclodimerization in the coordination sphere of a transition metal atom. Treatment of bis(ethene) complexes of cobalt, rhodium, and iridium with *tert*-butyl phosphalkyne led to a metal-mediated, orbital symmetry-forbidden  $[2+2]$  cycloaddition which yielded the first complex of a 1,3-diphosphacyclobutadiene ligand (Scheme 3).<sup>32</sup> The molecular structures feature essentially planar  $\eta^4$ -coordinated  $\text{P}_2\text{C}_2$  rings. The endocyclic  $\text{P}-\text{C}$  bonds are equidistant with bond lengths of  $1.80\text{ \AA}$  in accord with partial double bond character.<sup>32a,c</sup>



**Scheme 3.** Cyclodimerization of *tert*-butyl phosphalkyne at Co, Rh, and Ir centers.

1,3-Diphosphacyclobutadiene complexes containing zerovalent iron (**19**, Figure 3) and a homoleptic, zerovalent nickel sandwich compound (**20**) were reported soon afterwards.<sup>33</sup> Interestingly, the choice of the metal is an important factor. Thus, the formation of bicyclic dimers of type **23** (Figure 3) was observed in reactions of  $t\text{BuC}\equiv\text{P}$  with zirconium and hafnium complexes.<sup>32b,34</sup> In contrast, a  $[2+2]$  cycloaddition occurs in the coordination sphere of titanium, yielding  $\eta^4$ -bound diphosphacyclobutadiene rings, but less regioselectively than with appropriate late transition metals. Thus, treatment of the bis(cyclooctatetraene) titanium complex  $[\text{Ti}(\eta^4\text{-cot})(\eta^8\text{-cot})]$  with *tert*-butyl phosphalkyne or adamantyl phosphalkyne

afforded two different types of complexes which contained the 1,3- and 1,2-diphosphacyclobutadiene ligand, respectively (type **21** and **22**, Figure 3). Type **22** results from the head-to-head cyclodimerization of the phosphalkyne, which is not commonly observed in reactions with other metal fragments.<sup>35</sup> Nonetheless, computational studies suggest that the 1,2-isomer tends to be more stable than the 1,3-derivative with small substituents such as R = H or Me.<sup>35, 36</sup> The fact that 1,3-diphosphacyclobutadiene complexes are the most typical products obtained in stoichiometric [2+2] cycloadditions is explained by the use of large substituents such as R = *t*Bu, which render the formation of 1,2- isomers less energetically favorable.

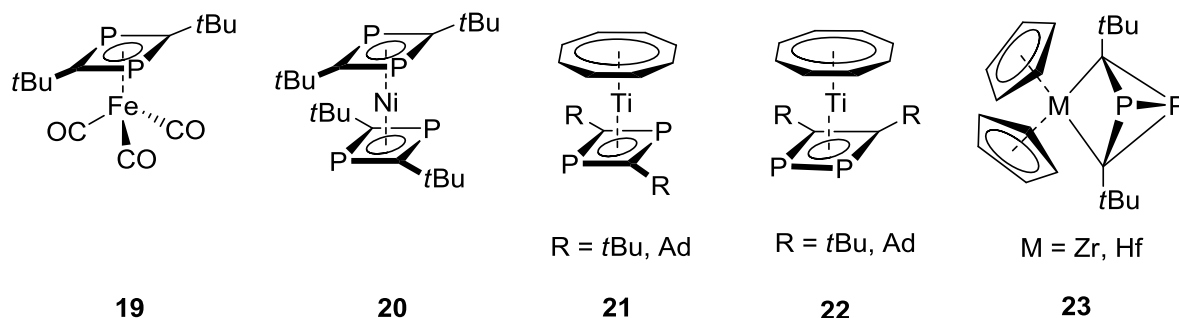
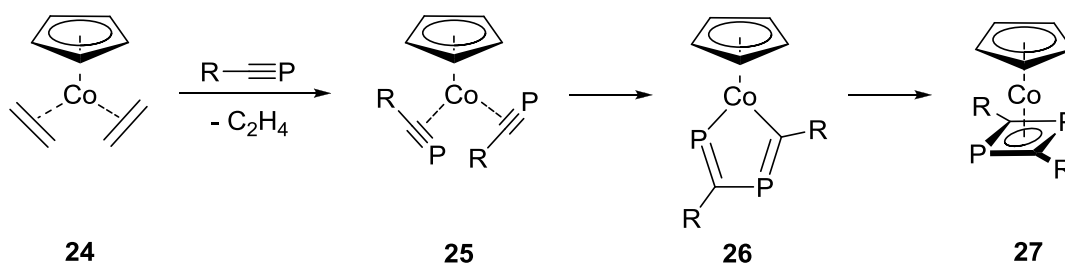


**Figure 3.** Important examples of transition metal complexes of 1,3- and 1,2-diphosphacyclobutadienes (**19-22**) and the 1,3-diphosphabicyclo[1.1.0]butanediyl ligand (**23**).

Concerning the mechanism of formation of the 1,3-diphosphacyclobutadiene fragment in metal-mediated reactions, *Binger et al.* proposed that first a di( $\pi$ -phosphalkyne)metal complex (**25**, Scheme 4) is formed, followed by a subsequent coupling process yielding a 1,4-diphospha-2-metallacyclopentadiene **26**. The diphosphacyclobutadiene-1,4-diyl ligand in **26** immediately forms the 1,3-diphosphacyclobutadiene complex (**27**).<sup>32c</sup> An analogous mechanism was proposed for the cyclodimerization of alkynes at transition metal centers.<sup>37</sup> *Binger et al.* succeeded in the isolation and characterization of a 1,4-diphospha-2-rhodacyclopentadiene species that resembles intermediate **26** soon afterwards.<sup>38</sup> NMR spectroscopic investigations revealed that this species slowly rearranges in solution to form the corresponding 1,3-diphosphacyclobutadiene derivative. The formation of the bicyclic dimers of type **23** (Figure 3) and of the 1,2-isomer **22** (Figure 3) is assumed to proceed via metallacyclopentadiene intermediates as well.<sup>38, 39</sup>



**Scheme 4.** Proposed mechanism of the formation of the 1,3-diphosphacyclobutadiene ligand.

In the course of the discovery of the first 1,3-diphosphacyclobutadiene metal complex  $[\text{Co}(\eta^5\text{-Cp})(\eta^4\text{-P}_2\text{C}_2t\text{Bu}_2)]$  (**27**, Scheme 4), *Binger et al.* already found that the diphosphacyclobutadiene moiety can act as a ligand itself to form larger, oligonuclear complexes. Each phosphorus atom possesses a lone pair that is able to form a coordinative bond to a second transition metal atom. Thus, complex **27** reacts with the bis(ethene)cobalt complex **24** to form the new di- and trimetallic complexes **28** and **29** (Figure 4).<sup>32b,c</sup> *Nixon et al.* reported that hexametallic complexes **30** are accessible from the reaction of  $[\text{M}(\eta^5\text{-Cp})(\eta^4\text{-C}_2\text{P}_2t\text{Bu}_2)_2]$  ( $\text{M} = \text{Co}, \text{Rh}, \text{Ir}$ ) with  $[\text{RhCl}(\text{C}_2\text{H}_4)_2]_2$ .<sup>40</sup> Further investigations concerning the utility of 1,3-diphosphacyclobutadiene metal complexes in the synthesis of new multimetallic aggregates revealed that the cobalt complex **27** readily forms platinum complexes. Thus, the cobalt platinum complex  $[\text{Pt}(\text{PPh}_3)_2\{\text{Co}(\eta^5\text{-Cp})(\eta^4\text{-P}_2\text{C}_2t\text{Bu}_2)_2\}]$  (**31**, Figure 4) was obtained by reacting **27** with the zero-valent platinum compound  $[\text{Pt}(\text{PPh}_3)_2(\eta^2\text{-C}_2\text{H}_4)]$ . The complexes  $[\text{trans-PtCl}_2(\text{PEt}_3)_2\{\text{Co}(\eta^5\text{-Cp})(\eta^4\text{-P}_2\text{C}_2t\text{Bu}_2)_2\}]$  (**32**) and  $[\text{trans-}\{\text{PtCl}_2(\text{PEt}_3)_2\}_2\{\text{Co}(\eta^5\text{-Cp})(\eta^4\text{-P}_2\text{C}_2t\text{Bu}_2)_2\}]$  (**33**) were isolated from the reaction of **27** with the chloro-bridged dimer  $[\{\text{Pt}(\mu\text{-Cl})\text{Cl}(\text{PEt}_3)_2\}_2]$ .<sup>40b</sup>

Besides these early examples, only few metal complexes with diphosphacyclobutadiene metalloligands have been reported.<sup>41–43</sup> In 1999, *Zenneck* and coworkers described the preparation of bimetallic 1,3- and 1,2-diphosphacyclobutadiene complexes  $[\{\text{Cr}(\text{CO})_5\}_2\{\text{Fe}(\text{CO})_3(\eta^4\text{-1,2-P}_2\text{C}_2t\text{Bu}_2)\}]$  (**34**) and  $[\{\text{Cr}(\text{CO})_5\}_2\{\text{Fe}(\text{CO})_3(\eta^4\text{-1,3-P}_2\text{C}_2t\text{Bu}_2)\}]$  (**35**) by a stepwise addition of  $\text{Cr}(\text{CO})_5$  to the  $\text{P}_2\text{C}_2$  ligand.<sup>42</sup> The structures of the above-mentioned platinum-cobalt and iron-chromium complexes are closely related to the structures of **28** and **29**. *Kramkowski* and *Scheer* isolated the tungsten complexes **36** and **37** that are shown in Figure 4.<sup>43</sup> The compounds were obtained from the reaction of  $t\text{BuC}\equiv\text{P}$  and  $\text{MesC}\equiv\text{P}$  with  $[\text{W}(\text{CO})_5(\text{thf})]$ . Besides the  $\eta^4$ -bound 1,3-diphosphacyclobutadiene ligands, both complexes contain side-on coordinated  $\text{RC}\equiv\text{P}$  units. Additionally, the P atoms of the  $\text{P}_2\text{C}_2$  ring and of the coordinated  $\text{MesC}\equiv\text{P}$  are bridged by a  $\text{W}(\text{CO})_4$  moiety in complex **36**. *Szameitat* and coworkers reported the bimetallic rhodium-gold compound  $[\text{Au}(\text{PPh}_3)\{\text{Rh}(\eta^4\text{-P}_2\text{C}_2t\text{Bu}_2)_2(\eta^4\text{-C}_2\text{B}_9\text{H}_{11})\}]$  (**38**) which represents a combination of phosphalkyne and metallacarborane chemistry.<sup>41</sup>

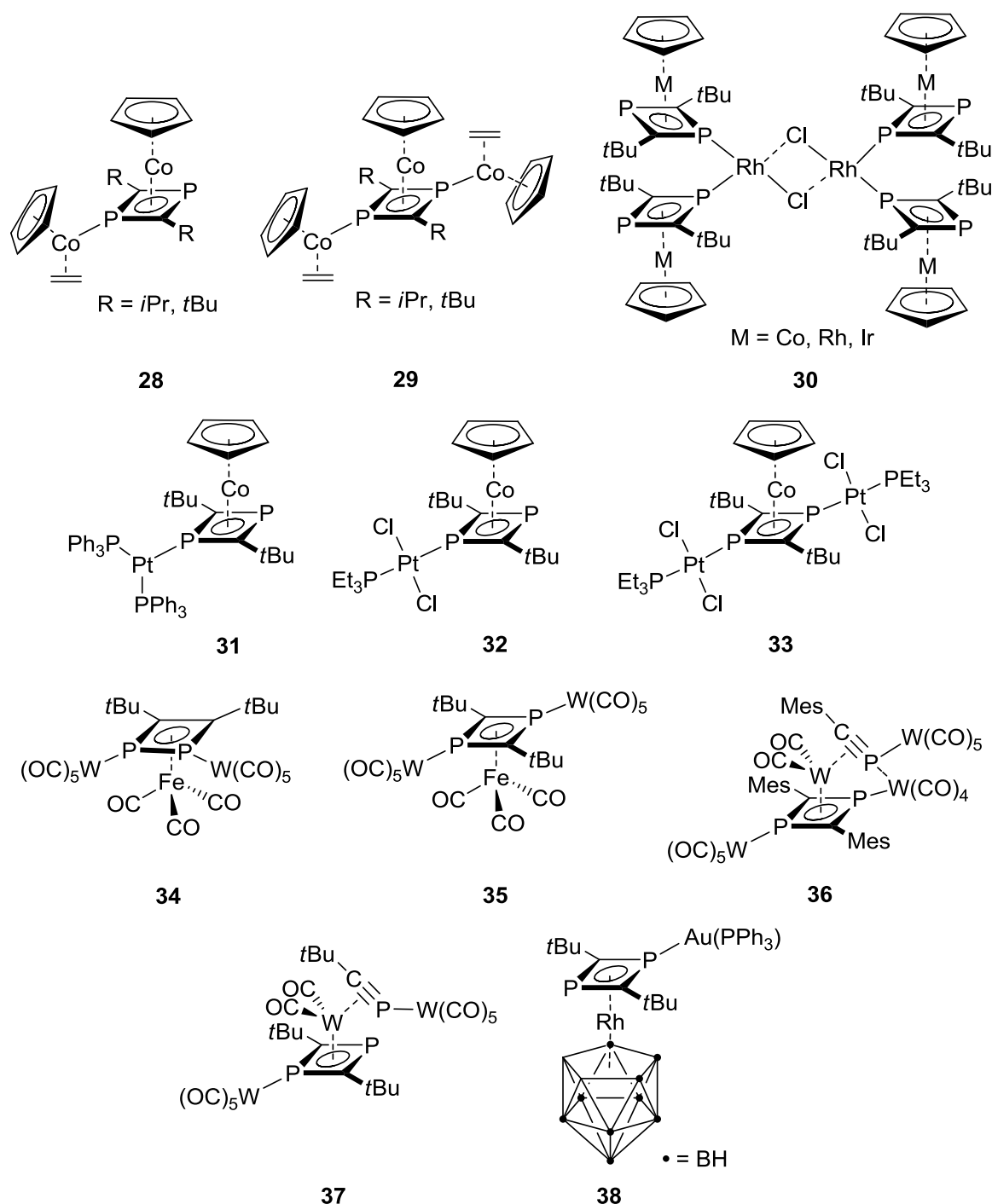
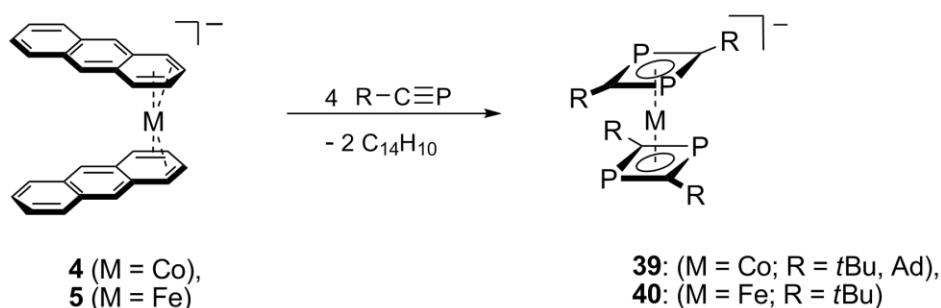


**Figure 4.** Selected examples of oligonuclear diphosphacyclobutadiene sandwich compounds.

Our group recently reported the synthesis and comprehensive characterization of anionic bis(1,3-diphosphacyclobutadiene) complexes  $[M(\eta^4-P_2C_2R_2)]^-$  (**39**:  $M = Co$ ,  $R = tBu$ ,  $Ad$ ; **40**:  $M = Fe$ ;  $R = tBu$ ). The complexes were obtained by reacting phosphalkynes with the low-valent metalates  $[M(C_{14}H_{10})_2]^-$  (**4** and **5**,  $M = Fe, Co$ ) according to Scheme 5. As described in chapter 1.1.1, these low-valent metalates serve as synthetic equivalents of “naked” “Fe<sup>-</sup>” and “Co<sup>-</sup>” anions.<sup>3–8</sup> Complexes **39** and **40** are formed by the substitution of both arene ligands and a head-to-tail cyclodimerization of the phosphalkyne at the metal center.<sup>5–6,44–45</sup> They were characterized by X-ray crystallography, NMR and EPR spectroscopy and

elemental analysis and their spectroelectrochemistry and bonding situation was thoroughly analyzed.<sup>44c</sup> Both complexes show identical 1,3-diphosphacyclobutadiene ligands and differ only in the metal center.<sup>44b</sup> In contrast to the diamagnetic cobalt compound **39**, the iron complex **40** is a paramagnetic 17 electron species. Determination of the magnetic moment and EPR spectroscopic investigations revealed the presence of one unpaired electron per iron center. Density functional studies (DFT) on **39** and **40** showed that the metal-ligand bonding is highly covalent. The calculations revealed that the electronic structure ought to be considered an intermediate between two extreme cases: the presence of a low-valent metal ion ( $M^{-I}$ ) that is stabilized by two neutral and  $\pi$ -accepting ligands ( $L^0$ ,  $L = C_2P_2R_2$ ) or a high-valent metal ion ( $M^{III}$ ) that interacts with two  $\pi$ -donating dianions ( $L^{2-}$ ).



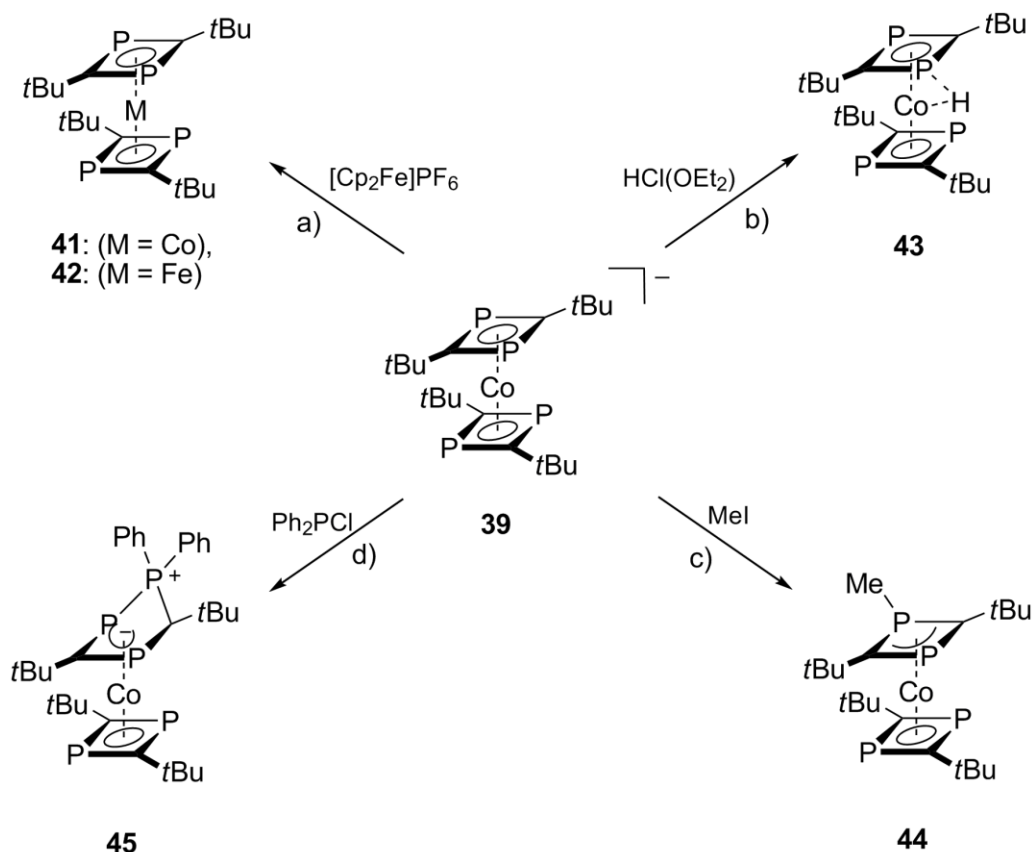
**Scheme 5.** Synthesis of the homoleptic bis(1,3-diphosphacyclobutadiene)metalates **39** and **40**.

Electrochemical investigations revealed that the anions **39** and **40** can be reversibly oxidized to the neutral sandwiches  $[M(\eta^4\text{-P}_2\text{C}_2\text{R}_2)_2]$  ( $M = \text{Co, Fe}$ ) by a one-electron-transfer reaction. Subsequently, the neutral complexes  $[M(\eta^4\text{-P}_2\text{C}_2\text{R}_2)]_2$  (**41**:  $M = \text{Co}$ , **42**:  $M = \text{Fe}$ ) were isolated by reacting **39** and **40** with  $[\text{Cp}_2\text{Fe}]\text{PF}_6$  (Scheme 6a).<sup>44c</sup>

Apart from their redox chemistry, anions **39** and **40** show a rich chemistry towards electrophilic compounds. Treatment of the cobalt complex **39** with the simplest electrophile, a proton, afforded the neutral compound  $[\text{CoH}(\eta^4\text{-P}_2\text{C}_2t\text{Bu}_2)_2]$  (**43**, Scheme 6b). Interestingly, the proton of **43** occupies a bridging position between the cobalt center and one phosphorus atom of the  $\text{P}_2\text{C}_2$  ligands. NMR spectroscopic investigations revealed that the proton is not statically bound to cobalt or one of the phosphorus atoms of the  $\text{P}_2\text{C}_2$  rings. Instead, the hydrogen atom adopts a bridging position between cobalt and one of the phosphorus and carbon atoms of the  $\text{P}_2\text{C}_2$  rings. It appears to exchange between the different  $\text{Co-H-P}$  and  $\text{Co-H-C}$  bridged structures at room temperature. Complex **43** therefore shows a dynamic behavior both in solution and in the solid state, that was proven by  $^{31}\text{P}$  NMR spectroscopy. Contrary to this, bulkier electrophiles show no interaction with the cobalt center, but attack the diphosphacyclobutadiene ligand instead. Treatment of **39** with methyl iodide gave  $[\text{Co}(\eta^4\text{-P}_2\text{C}_2t\text{Bu}_2\text{Me})(\eta^4\text{-P}_2\text{C}_2t\text{Bu}_2)]$  (**44**, Scheme 6c), in which the methyl group is bound to one phosphorus atom of the  $\text{P}_2\text{C}_2$  ring. Complex **44** is the first example of a transition metal complex of a 1,3-diphosphacyclobuten-4-yl ( $\text{P}_2\text{C}_2t\text{Bu}_2\text{Me}$ ) ligand. A product similar to **44** was expected in the reaction of **39** with  $\text{Ph}_2\text{PCl}$ , but an insertion of the  $\text{PPh}_2^+$  fragment into a  $\text{P-C}$  bond of the diphosphacyclobutadiene ring

occurred, and the complex  $[\text{Co}(\eta^4\text{-P}_3\text{C}_2t\text{Bu}_2\text{Ph}_2)(\eta^4\text{-P}_2\text{C}_2t\text{Bu}_2)]$  (**45**) was obtained (Scheme 6d).<sup>44a</sup> The structure of **45** features an unusual triphosphacyclopentadienylium ( $\text{P}_3\text{C}_2t\text{Bu}_2\text{Ph}_2$ )<sup>+</sup> ligand.<sup>46</sup>

Complexes of type **39** and **40** promise an intriguing coordination chemistry due to the presence of the lone pairs on the four phosphorus atoms. However, their coordination chemistry was not explored prior to this thesis. Therefore, a major aim of this thesis was to investigate the coordination behavior of these novel organometallic building blocks. For our initial investigations, we decided to concentrate on complexes with the coinage metals. In Chapters 4–6, we present the synthesis and comprehensive characterization of copper(I), silver(I) and gold(I) complexes of diphosphacyclobutadiene sandwich anions.



**Scheme 6.** Reactions of the homoleptic sandwich anion **39** with electrophiles.

## References

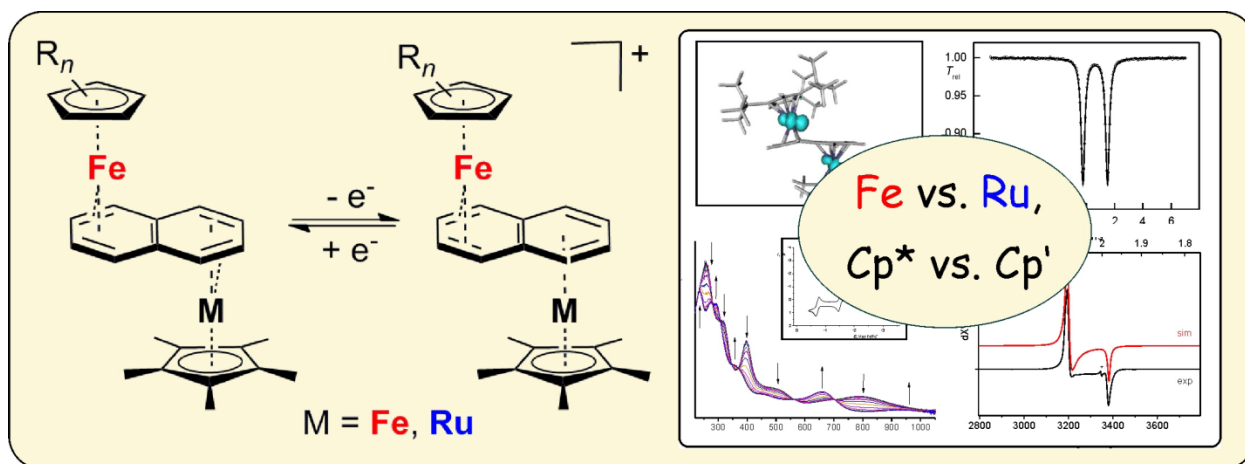
- 1 J. E. Ellis, *Inorg. Chem.* **2006**, *45*, 3167.
- 2 a) E. P Kündig, C. Perret, S. Spichiger, *J. Organomet. Chem.* **1985**, 286, 183; b) G. Zhu, K. E. Janak, J. S. Figueroa, G. Parkin, *J. Am. Chem. Soc.* **2006**, *128*, 5452.
- 3 a) G. Wilke, *Angew. Chem. Int. Ed.* **1963**, *2*, 105; b) G. Wilke, B. Bogdanović, P. Hardt, P. Heimbach, W. Keim, M. Kröner, W. Oberkirch, K. Tanaka, E. Steinrücke, D. Walter, H. Zimmermann, *Angew. Chem. Int. Ed.* **1966**, *5*, 151.
- 4 J. K. Seaburg, P. J. Fischer, V. G. Young, Jr., J. E. Ellis, *Angew. Chem. Int. Ed.* **1998**, *37*, 155.
- 5 W. W. Brennessel, V. G. Young, Jr., J. E. Ellis, *Angew. Chem. Int. Ed.* **2002**, *41*, 1211.
- 6 W. W. Brennessel, V. G. Young, Jr., J. E. Ellis, *Angew. Chem. Int. Ed.* **2006**, *45*, 7268.
- 7 W. W. Brennessel, R. E. Jilek, J. E. Ellis, *Angew. Chem. Int. Ed.* **2007**, *46*, 6132.
- 8 R. E. Jilek, M. Jang, E. D. Schmolensky, J. D. Britton, J. E. Ellis, *Angew. Chem. Int. Ed.* **2008**, *47*, 1.
- 9 a) N. D. Scott, J. F Walker, U.S Patent 2,177,412, Oct. 24, 1939; b) J. Chatt, J.M. Davidson, *J. Chem. Soc.* **1965**, 843.
- 10 E. O. Fischer, C. Elschenbroich, C. G. Kreiter, *J. Organomet. Chem.* **1967**, *7*, 481.
- 11 M. Jang, J. E. Ellis, *Angew. Chem. Int. Ed.* **1994**, *33*, 1973.
- 12 a) W. W. Brennessel, S. N. Roush, B. R. Strandberg, O. E. Woisetschläger, V. G. Young, Jr., J. E. Ellis, *Chem. Commun.* **2002**, 2356; b) W. W. Brennessel, M. K. Pomije, V. J. Sussmann, E. Urnezis, V. G. Young, Jr., J. E. Ellis, *J. Am. Chem. Soc.* **2002**, *124*, 10258.
- 13 a) K. M. Chi, S. R. Frerichs, S. B. Philson, J. E. Ellis, *Angew. Chem. Int. Ed.* **1987**, *26*, 1190; b) J. E. Ellis, *Organometallics* **2003**, *22*, 3322.
- 14 E. U. Urnezis, W. W. Brennessel, C. J. Cramer, P. von Rague-Schleyer, J. E. Ellis, *Science* **2002**, *295*, 832.
- 15 a) K. Jonas, *Pure Appl. Chem.* **1990**, *62*, 1169; b) A. Frings, *Dissertation*, Ruhr-Universität Bochum **1988**.
- 16 E. M. Schnöckelborg, R. Wolf, *Chem. Commun.* **2010**, *46*, 2832.
- 17 E. M. Schnöckelborg, J. J. Weigand, R. Wolf, *Angew. Chem.* **2011**, *50*, 6657.
- 18 a) E. M. Schnöckelborg, M. M. Khusniyarov, B. de Bruin, F. Hartl, T. Langer, M. Eul, S. Schulz, R. Pöttgen, R. Wolf, *Inorg. Chem.* **2012**, *51*, 6719; b) E. M. Schnöckelborg, F. Hartl, T. Langer, R. Pöttgen, R. Wolf, *Eur. J. Inorg. Chem.* **2012**, 1632.
- 19 P. Klusmann, *Dissertation*, Ruhr-Universität Bochum **1993**.
- 20 a) D. O. Cowan, C. LeVanda, J. Park, F. Kaufman, *Acc. Chem. Res.* **1973**, *6*, 1; b) D. Astruc, *Acc. Chem. Res.* **1997**, *30*, 383; c) S. Barlow, D. O'Hare, *Chem. Rev.* **1997**, *97*, 637; d) A. Ceccon, S. Santi, L. Orian, A. Bisello, *Coord. Chem. Rev.* **2004**, *248*, 683; e) P. Aguirre-Etcheverry, D. O'Hare, *Chem. Rev.* **2010**, *110*, 4839.
- 21 a) U. T. Mueller-Westerhoff, P. J. Eilbracht, *J. Am. Chem. Soc.* **1972**, *94*, 9272; b) D. O. Cowan, C. LeVanda, R. L. Collins, G. A. Candela, U. T. Mueller-Westerhoff, P. J. Eilbracht, *J. Chem. Soc., Chem. Commun.* **1973**, *0*, 329; c) C. LeVanda, K. Bechgaard, D. O. Cowan, U. T. Mueller-Westerhoff, P. Eilbracht, G. A. Candela, R. L. Collins, *J. Am. Chem. Soc.* **1976**, *98*, 3181; d) M. H. Desbois, D. Astruc, J. Guillin, J. P. Mariot, F. Varret, *J. Am. Chem. Soc.* **1985**, *107*, 5280; d) R. J. Webb, S.J. Geib, D. L. Staley, A. L. Rheingold, D. N. Hendrickson, *J. Am. Chem. Soc.* **1990**, *112*, 5031; f) J. M. Manriquez, M. D. Ward, W. M. Reiff, J. C. Calabrese, N. L. Jones, P. J. Carroll, E. E. Bunel, J. S. Miller, *J. Am. Chem. Soc.* **1995**, *117*, 6182; g) M. Lacoste, M.-H. Delville-Desbois, N. Ardoin, D. Astruc, *Organometallics* **1997**, *16*, 2343.
- 22 W. H. Morrison, Jr., E. Y. Ho, D. N. Hendrickson, *J. Am. Chem. Soc.* **1974**, *96*, 3603.

- 23 a) M. N. Bochkarev, I. L. Fedushkin, H. Schumann, J. Loeb, *J. Organomet. Chem.* **1991**, 410, 321; b) B. F. Bush, V. M. Lynch, J. J. Lagowski, *Organometallics* **1987**, 6, 1267; c) B. F. Bush, J. J. Lagowski, *Organometallics* **1988**, 7, 1945; d) B. F. Bush, J. J. Lagowski, *J. Organomet. Chem.* **1990**, 386, 37.
- 24 J. A. Reingold, K. L. Virkaitis, G. B. Carpenter, S. Sun, D. A. Sweigart, P. T. Czech, K. R. Overly, *J. Am. Chem. Soc.* **2005**, 127, 11146.
- 25 T. Hatanaka, Y. Ohki, T. Kamachi, T. Nakayama, K. Yoshizawa, M. Katada, K. Tatsumi, *Chem. Asian. J.* **2012**, 7, 1231.
- 26 a) K. S. Pitzer, *J. Am. Chem. Soc.* **1948**, 70, 2140; b) R. S. Mulliken, *J. Am. Chem. Soc.* **1950**, 72, 4493.
- 27 a) M. Regitz, *Chem. Rev.* **1990**, 90, 191; b) A. C. Gaumont, J. M. Denis, *Chem. Rev.* **1994**, 94, 1413.
- 28 T. E. Gier, *J. Am. Chem. Soc.* **1961**, 83, 1764.
- 29 a) G. Becker, G. Gresser, W. Uhl, *Z. Naturforsch. B*, **1981**, 36,16; b) T. Allspach, M. Regitz, G. Becker, W. Becker, *Synthesis* **1986**, 31.
- 30 a) M. Regitz, O. J. Scherer, *Multiple Bonds and Low Coordination in Phosphorus Chemistry*, Thieme, Stuttgart **1990**; b) K. B. Dillon, F. Mathey, J. F. Nixon, *Phosphorus: The Carbon Copy*, Wiley Chichester **1998**; c) F. Mathey, *Angew. Chem. Int. Ed.* **2003**, 42, 1578.
- 31 a) J. F. Nixon, *Chem. Rev.* **1995**, 145, 201; b) C. A. Russel, N. S. Townsend, in *Phosphorus(III) Ligands in Homogeneous Catalysis: Design and Synthesis*, P. C. J. Kamer, W.N.M. van Leeuwen (eds.), John Wiley & Sons Ltd **2012**, p. 343.
- 32 a) P. B. Hitchcock, M. J. Maah, J. F. Nixon, *J. Chem. Soc., Chem. Commun.* **1986**, 737; b) P. Binger, R. Milczarek, R. Mynott, M. Regitz, W. Rösch, *Angew. Chem., Int. Ed. Engl.* **1988**, 7, 644; c) P. Binger, R. Milczarek, R. Mynott, C. Krüger, Y. H. Tsay, E. Raabe, M. Regitz, *Chem. Ber.* **1988**, 121, 637.
- 33 M. Driess, D. Hu, H. Pritzkow, H. Schäufele, U. Zenneck, M. Regitz, W. Rösch, *J. Organomet. Chem.* **1987**, 334, C35; b) P. Binger, B. Biedenbach, R. Schneider, M. Regitz, *Synthesis* **1989**, 960; c) T. Wettling, G. Wolmershäuser, P. Binger, M. Regitz, *J. Chem. Soc., Chem. Commun.* **1990**, 1541; d) G. Brauers, M. Green, C. Jones, J. F. Nixon, *J. Chem. Soc., Chem. Commun.* **1995**, 1125.
- 34 T. Wettling, B. Geissler, R. Schneider, S. Barth, P. Binger, M. Regitz, *Angew. Chem. Int. Ed.* **1992**, 31, 758.
- 35 P. Binger, G. Glaser, S. Albus, C. Krüger, *Chem. Ber.* **1995**, 128, 1262.
- 36 S. Creve, M. T. Nguyen, L. G. Vanquickenborne, *Eur. J. Inorg. Chem.* **1999**, 1281.
- 37 a) K. P. C. Vollhardt, *Angew. Chem. Int. Ed. Engl.* **1984**, 23, 539; b) K. Jonas, *Angew. Chem. Int. Ed. Engl.* **1985**, 24, 295.
- 38 P. Binger, B. Biedenbach, R. Mynott, C. Krüger, P. Betz, M. Regitz, *Angew. Chem. Int. Ed.* **1988**, 27, 1157.
- 39 see ref. 30b, p. 284.
- 40 a) P. B. Hitchcock, M. J. Maah, J. F. Nixon, *J. Chem. Soc., Chem. Commun.* **1987**, 844; b) P. B. Hitchcock, M. J. Maah, J. F. Nixon, *Heteroatom. Chem.* **1991**, 2, 253.
- 41 a) H. F. Dare, J. A. K. Howard, M. U. Pilotti, F. G. A. Stone, J. Szameitat, *J. Chem. Soc., Chem. Commun.* **1989**, 1409; b) H. F. Dare, J. A. K. Howard, M. U. Pilotti, F. G. A. Stone, J. Szameitat, *J. Chem. Soc. Dalton Trans.* **1990**, 2263.
- 42 F. W. Heinemann, S. Kummer, U. Seiss-Brandl, U. Zenneck, *Organometallics* **1999**, 18, 2021.
- 43 P. Kramkowski, M. Scheer, *Eur. J. Inorg. Chem.* **2000**, 1869.

- 44 a) R. Wolf, A. W. Ehlers, J. C. Slootweg, M. Lutz, D. Gudat, M. Hunger, A. L. Spek, K. Lammertsma, *Angew. Chem. Int. Ed.* **2008**, *47*, 4584; b) R. Wolf, J. C. Slootweg, A. W. Ehlers, F. Hartl, B. de Bruin, M. Lutz, A. L. Spek, K. Lammertsma, *Angew. Chem. Int. Ed.* **2009**, *48*, 3104; c) R. Wolf, A. W. Ehlers, M. M. Khusniyarov, F. Hartl, B. de Bruin, G. J. Long, F. Grandjean, F. M. Schappacher, R. Pöttgen, J. C. Slootweg, M. Lutz, A. L. Spek, K. Lammertsma, *Chem. Eur. J.* **2010**, *16*, 14322.
- 45 S. Güлак, O. Stepanek, J. Malberg, B. Rezaei Rad, M. Kotora, R. Wolf, A. Jacobi von Wangelin, *Chem. Sci.* **2013**, *4*, 776.
- 46 a) V. Caliman, P. B. Hitchcock, J. F. Nixon, *J. Chem. Soc. Chem. Commun.* **1995**, 1661; b) P. B. Hitchcock, J. F. Nixon, N. Sakarya, *Chem. Commun.* **1996**, 2751; c) V. Caliman, P. B. Hitchcock, J. F. Nixon, L. Nyulaszi, N. Sakarya, *Chem. Commun.* **1997**, 1305; d) V. Caliman, P. B. Hitchcock, J. F. Nixon, *Heteroatom. Chem.* **1998**, *9*, 1.

## 2 Synthesis and Electronic Structure of Dissymmetrical, Naphthalene-Bridged Sandwich Complexes $[\text{Cp}'\text{Fe}(\mu\text{-C}_{10}\text{H}_8)\text{MCp}^*]^x$ ( $x = 0, +1$ ; $\text{M} = \text{Fe}, \text{Ru}$ ; $\text{Cp}' = \eta^5\text{-C}_5\text{H}_2\text{-1,2,4-}t\text{Bu}_3$ ; $\text{Cp}^* = \eta^5\text{-C}_5\text{Me}_5$ )<sup>[a],[b]</sup>

Jennifer Malberg, Elizabeth Lupton, Eva-Maria Schnöckelborg, Bas de Bruin, Jörg Sutter, Karsten Meyer, Frantisek Hartl and Robert Wolf



[a] Reprinted (adapted) with permission from: J. Malberg, E. Lupton, E.-M. Schnöckelborg, B. de Bruin, J. Sutter, K. Meyer, F. Hartl, R. Wolf, *Organometallics* **2013**, published online on 10/09/2013. DOI: 10.1021/om4005862. Copyright 2013 American Chemical Society.

[b] Elizabeth Lupton performed the computational studies (Figures 4–6 and S6–S7, Table 3 and S1). Complex **5** (Scheme 2, Figure S1, Table 2) was synthesized and characterized by Eva-Maria Schnöckelborg and Robert Wolf. Bas de Bruin carried out the EPR measurements (Figure 3, Table 4) and analyzed these with the aid of DFT calculations. Mössbauer measurements (Figure 11, Table 6) were performed by Jörg Sutter and Karsten Meyer. František Hartl performed the spectroelectrochemistry (Schemes S3–S4, Figures 7–10 and S7–S8, Table 3). Robert Wolf carried out the X-ray crystal structure analyses.



## 2.1 Introduction

Ferrocene is the prototype of an organometallic sandwich complex with widespread applications that range from materials science to its use as a ligand scaffold in catalysis.<sup>1</sup> Since the initial discovery and structural elucidation of ferrocene<sup>2,3</sup>, the chemistry of cyclopentadienyl iron complexes has been of unabated interest. In extension to the well-investigated mononuclear sandwich compounds, bimetallic species, where two cyclopentadienyl iron units or related metal fragments are connected by a bridging hydrocarbon ligand, have been attracting considerable attention.<sup>4</sup> The electron communication between the metal atoms in such species is potentially relevant to applications in molecular electronics. This aspect has therefore been the subject of numerous studies.<sup>5</sup> Although naphthalene represents the simplest polyaromatic hydrocarbon, it has scarcely been considered as a bridging ligand in bimetallic complexes.<sup>6–10</sup> The few structurally characterized naphthalene-bridged bimetallic compounds include the homobimetallic diiron complex  $[\text{CpFe}(\mu\text{-C}_{10}\text{H}_8)\text{FeCp}^*]$  (**A**), and the MnFe complex  $[\text{CpFe}(\mu\text{-}\eta^6\text{:}\eta^4\text{-C}_{10}\text{H}_8)\text{Mn}(\text{CO})_3]$  (**B**). The latter complex, reported by *Sweigart et al.*, is a rare example of a heterobimetallic, naphthalene-bridged complex.<sup>8</sup> Its spectroscopic and structural data indicate a zwitterionic electronic structure with an  $\eta^6$ -coordinated  $\text{CpFe}^+$  fragment, and an  $\eta^4$ -coordinated  $\text{Mn}(\text{CO})_3^-$  moiety.

In the course of our ongoing investigations into the chemistry of polyarene iron complexes with iron in a low formal oxidation state,<sup>11,12</sup> we became interested in bimetallic iron complexes with naphthalene and anthracene as bridging ligands. Our group, and an independent report by *Tatsumi* and coworkers, recently described the synthesis of the compounds  $[\text{Cp}^*\text{Fe}(\mu\text{-C}_{10}\text{H}_8)\text{FeCp}^*]$  (**1**,  $\text{Cp}^* = \text{C}_5\text{Me}_5$ , chart 1) and  $[\text{Cp}^*\text{Fe}(\mu\text{-C}_{14}\text{H}_{10})\text{FeCp}^*]$  (**2**) by the reduction of  $[\text{Cp}^*\text{FeCl}(\text{tmeda})]$  with potassium naphthalenide and potassium anthracenide or, in the case of **1**, by salt metathesis from  $[\text{Cp}^*\text{FeCl}(\text{tmeda})]$  and the anionic complex  $[\text{K}([18]\text{crown-6})\{\text{Cp}^*\text{Fe}(\eta^4\text{-C}_{10}\text{H}_8)\}]$ .<sup>13,14</sup> The iron atoms in complexes **1** and **2** display the formal oxidation state +I. Electrochemical, spectroscopic, and DFT investigations revealed that in **1** and **2** the naphthalene and anthracene bridging ligands efficiently mediate the electronic coupling between the iron centers, resulting in diamagnetic ground states for these compounds. The reversible oxidation of **1** and **2** resulted in the mixed-valent  $\text{Fe}^{\text{I}}\text{-Fe}^{\text{II}}$  monocations  $[\text{Cp}^*\text{Fe}(\mu\text{-C}_{10}\text{H}_8)\text{FeCp}^*]^+(\mathbf{1}^+)$  and  $[\text{Cp}^*\text{Fe}(\mu\text{-C}_{14}\text{H}_{10})\text{FeCp}^*]^+(\mathbf{2}^+)$ , which were isolated and fully characterized as  $[\text{BAr}^{\text{F}}_4]^-$  salts by *Tatsumi et al.*<sup>14</sup>

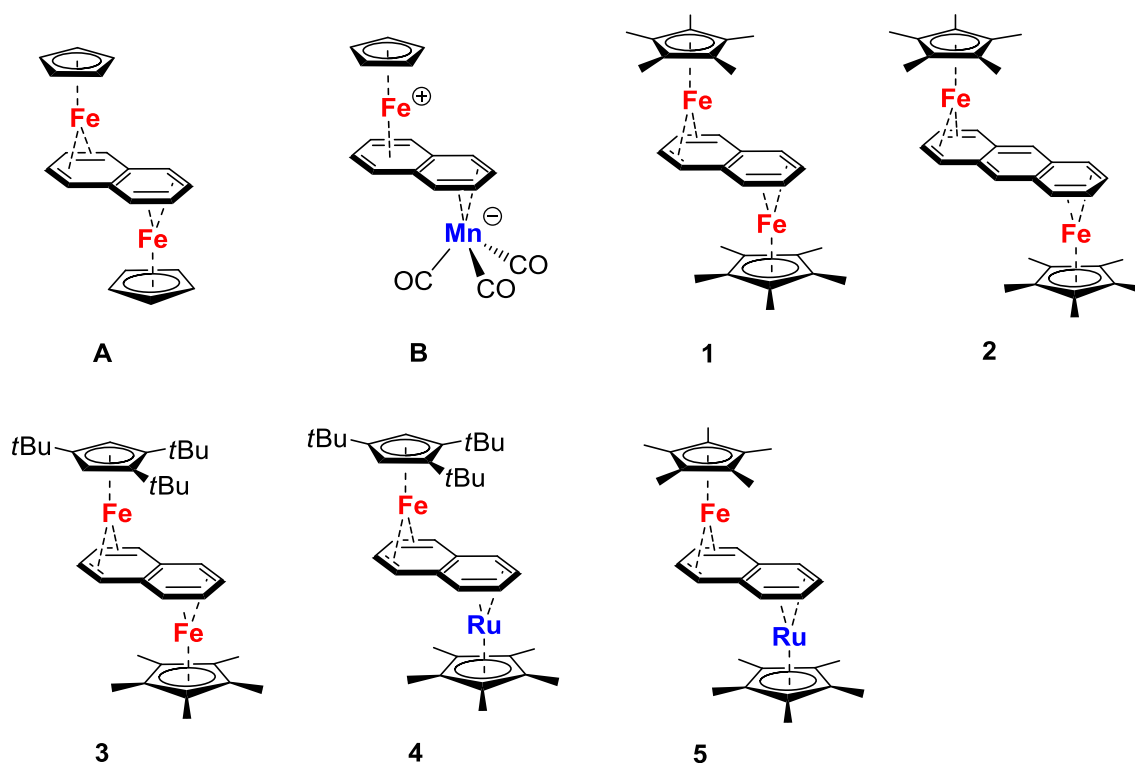


**Chart 1**

In this chapter, we wish to address the following questions:

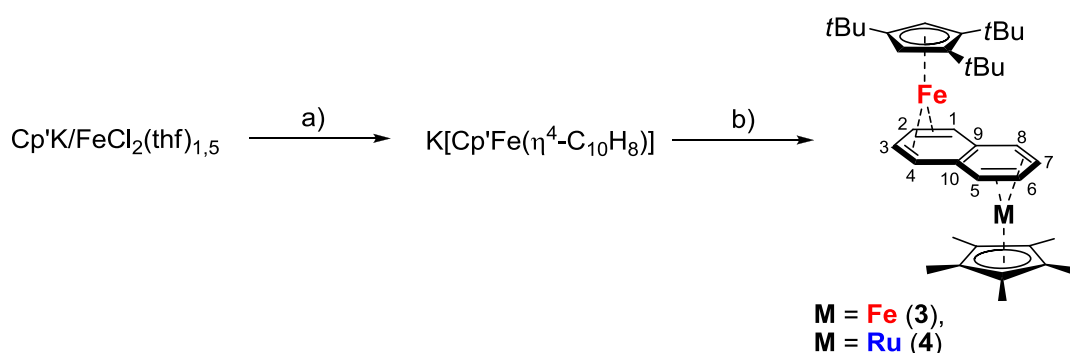
- How does replacing the Cp\* ligand by a related cyclopentadienyl derivative affect the properties of this type of bimetallic complex?
- What is the effect of substituting one of the iron centers by a heavier group 8 congener?

In order to answer these questions, we have synthesized and fully characterized the new dinuclear naphthalene complexes  $[\text{Cp}'\text{Fe}(\mu\text{-C}_{10}\text{H}_8)\text{FeCp}^*]$  (**3**,  $\text{Cp}' = \text{C}_5\text{H}_2\text{-1,2,4-}t\text{Bu}_3$ ) and  $[\text{Cp}'\text{Fe}(\mu\text{-C}_{10}\text{H}_8)\text{RuCp}^*]$  (**4**, Chart 1), and their one-electron oxidation products  $[\text{Cp}'\text{Fe}(\mu\text{-C}_{10}\text{H}_8)\text{RuCp}^*]\text{PF}_6$  (**[4]PF<sub>6</sub>**).  $[\text{Cp}'\text{Fe}(\mu\text{-C}_{10}\text{H}_8)\text{FeCp}^*]\text{PF}_6$  (**[3]PF<sub>6</sub>**). Different from **1** and **2**, these new complexes display a heteroleptic structure with one tri-*tert*-butyl-substituted Cp' ligand instead of Cp\* on iron. The Cp\*Fe moiety in the diiron complexes **3** and **[3]PF<sub>6</sub>** has been replaced by the Cp\*Ru group in **4** and **[4]PF<sub>6</sub>**. For comparison, we furthermore report the synthesis and electrochemical data of the homoleptic FeRu complex  $[\text{Cp}^*\text{Fe}(\mu\text{-C}_{10}\text{H}_8)\text{RuCp}^*]$  (**5**). The new complexes have been characterized by cyclic voltammetry, spectroscopic techniques such as NMR, EPR, UV/vis and  $^{57}\text{Fe}$  Mössbauer spectroscopy and X-ray crystallography. DFT calculations support the analysis of the experimental data and give valuable insight into the effects of the heterometallic and Cp\* ligand substitution.

## 2.2 Results

### 2.2.1 Synthesis and Characterization of the Neutral Complexes [Cp'Fe( $\mu$ -C<sub>10</sub>H<sub>8</sub>)FeCp\*] (**3**), [Cp'Fe( $\mu$ -C<sub>10</sub>H<sub>8</sub>)RuCp\*] (**4**), and [Cp\*Fe( $\mu$ -C<sub>10</sub>H<sub>8</sub>)RuCp\*] (**5**)

The naphthalene-bridged complexes [Cp'Fe( $\mu$ -C<sub>10</sub>H<sub>8</sub>)FeCp\*] (**3**) and [Cp'Fe( $\mu$ -C<sub>10</sub>H<sub>8</sub>)RuCp\*] (**4**) were synthesized by a one-pot protocol according to Scheme 1. In the first step, Cp'FeCl was prepared *in situ* from Cp'K and FeCl<sub>2</sub>(thf)<sub>1.5</sub> in DME. Subsequently, this “Cp'FeCl” solution was reacted with two equiv. of potassium naphthalenide in THF to form the iron(0) complex K[Cp'Fe( $\eta^4$ -C<sub>10</sub>H<sub>8</sub>)]. Subsequent addition of one equiv. of [Cp\*FeCl(tmeda)] to this deep red-brown reaction solution afforded the homodinuclear FeFe complex **3** in 42% yield. The heterodinuclear FeRu complex **4** was isolated in 23% yield after addition of 0.25 equiv. [Cp\*RuCl]<sub>4</sub> to the K[Cp'Fe( $\eta^4$ -C<sub>10</sub>H<sub>8</sub>)] solution.



**Scheme 1.** Synthesis of **3** and **4**. Reagents: a) +2 K<sub>2</sub>C<sub>10</sub>H<sub>8</sub>/–KCl, b) [Cp\*FeCl(tmeda)] or 0.25 [Cp\*RuCl]<sub>4</sub>/–KCl.

The molecular structures of **3** and **4** were established by single crystal X-ray crystallography and are displayed in Figure 1. Table 1 summarizes important bond lengths and angles. The two metal fragments Cp'Fe and Cp\*M (M = Fe and Ru) bind to opposite faces of the naphthalene bridge. Both metal centers are clearly  $\eta^4$ -coordinated. For **3**, Fe1 and Fe2 display similar Fe–C distances (Fe1–C1,C2,C3,C4 2.008(4)–2.136(4) Å; Fe2–C5,C6,C7,C8 2.034(5)–2.094(5) Å). The ruthenium atom in **4** shows somewhat larger metal carbon distances (Ru1–C5,C6,C7,C8 2.174(5)–2.220(4) Å) in agreement with the larger atomic radius of ruthenium. For the C–C distances of the naphthalene molecule, the typical long-short-long pattern is observed that is characteristic of naphthalene coordinated to electron-rich metal centers.<sup>11,12</sup>

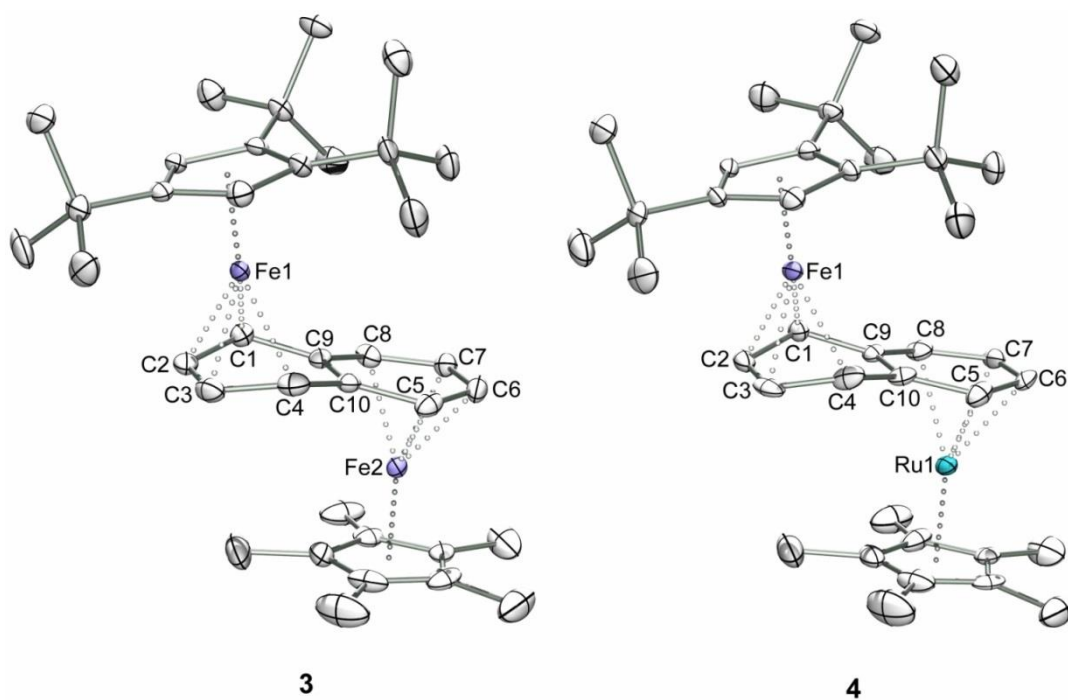


**Figure 1.** Single crystal X-ray structures of  $[\text{Cp}'\text{Fe}(\mu\text{-C}_{10}\text{H}_8)\text{FeCp}^*]$  (**3**) and  $[\text{Cp}'\text{Fe}(\mu\text{-C}_{10}\text{H}_8)\text{RuCp}^*]$  (**4**). Displacement ellipsoids are drawn at the 50% level, hydrogen atoms are not shown for clarity.

**Table 1.** Selected bond lengths (Å) and angles [ $^\circ$ ] of **3**, **3**<sup>+</sup>, **4**, **4**<sup>+</sup>, **5**, and **5**<sup>+</sup> determined by X-ray crystallography and DFT calculations. Values given in *italics* are from DFT calculations.

	<b>3</b>	<b>3</b> <sup>+</sup>	<b>4</b>	<b>4</b> <sup>+</sup>	<b>5</b>	<b>5</b> <sup>+</sup>
	(M = Fe2)	(M = Fe2)	(M = Ru1)	(M = Ru1)	(M = Ru1)	(M = Ru1)
Fe1–C1	2.136(4)	/	2.134(4)	2.082(3)	/	/
	<i>2.14</i>	<i>2.12</i>	<i>2.14</i>	<i>2.12</i>	<i>2.12</i>	<i>2.11</i>
Fe1–C2	2.013(4)	/	2.003(5)	2.030(3)	/	/
	<i>2.02</i>	<i>2.04</i>	<i>2.02</i>	<i>2.04</i>	<i>2.03</i>	<i>2.00</i>
Fe1–C3	2.008(4)	/	2.012(5)	2.027(3)	/	/
	<i>2.01</i>	<i>2.04</i>	<i>2.02</i>	<i>2.04</i>	<i>2.03</i>	<i>2.00</i>
Fe1–C4	2.109(4)	/	2.105(4)	2.100(3)	/	/
	<i>2.12</i>	<i>2.12</i>	<i>2.12</i>	<i>2.12</i>	<i>2.11</i>	<i>2.11</i>
Fe1–C9	2.678(2)	/	2.718(2)	2.677(3)	/	/
	<i>2.67</i>	<i>2.56</i>	<i>2.65</i>	<i>2.63</i>	<i>2.47</i>	<i>2.46</i>
Fe1–C10	2.654(2)	/	2.696(2)	2.690(3)	/	/
	<i>2.66</i>	<i>2.55</i>	<i>2.65</i>	<i>2.63</i>	<i>2.47</i>	<i>2.46</i>
av. Fe1–C(Cp')	2.085(4)	/	2.080(4)	2.119(3)	/	/
	<i>2.10</i>	<i>2.11</i>	<i>2.09</i>	<i>2.12</i>	<i>2.07</i>	<i>2.10</i>
M–C5	2.083(4)	/	2.220(4)	2.222(3)	/	/
	<i>2.12</i>	<i>2.12</i>	<i>2.25</i>	<i>2.24</i>	<i>2.25</i>	<i>2.27</i>
M–C6	2.034(5)	/	2.191(4)	2.211(3)	/	/
	<i>2.04</i>	<i>2.07</i>	<i>2.17</i>	<i>2.21</i>	<i>2.16</i>	<i>2.23</i>

M–C7	2.044(4)	/	2.174(5)	2.210(3)	/	/
	2.04	2.07	2.17	2.21	2.16	2.23
M–C8	2.094(3)	/	2.220(4)	2.227(3)	/	/
	2.11	2.12	2.24	2.24	2.25	2.27
M–C9	2.330(3)	/	2.436(4)	2.269(3)	/	/
	2.43	2.26	2.64	2.38	2.74	2.44
M–C10	2.336(3)	/	2.434(4)	2.277(3)	/	/
	2.43	2.44	2.64	2.38	2.74	2.44
av. M–C(Cp*)	2.062(4)	/	2.179(5)	2.178(3)	/	/
	2.08	2.09	2.20	2.20	2.20	2.22
C1–C2	1.421(6)	/	1.440(6)	1.416(5)	/	/
	1.43	1.42	1.43	1.43	1.43	1.43
C2–C3	1.405(5)	/	1.395(6)	1.396(5)	/	/
	1.42	1.42	1.42	1.42	1.42	1.42
C3–C4	1.433(6)	/	1.427(7)	1.415(5)	/	/
	1.44	1.43	1.44	1.43	1.43	1.43
C4–C10	1.437(5)	/	1.457(6)	1.469(5)	/	/
	1.44	1.45	1.44	1.46	1.43	1.45
C5–C10	1.427(5)	/	1.417(6)	1.418(4)	/	/
	1.43	1.43	1.44	1.43	1.44	1.43
C5–C6	1.411(6)	/	1.418(7)	1.415(5)	/	/
	1.43	1.42	1.44	1.42	1.44	1.42
C6–C7	1.396(5)	/	1.398(6)	1.414(5)	/	/
	1.42	1.42	1.42	1.42	1.43	1.42
C7–C8	1.419(5)	/	1.418(6)	1.412(5)	/	/
	1.43	1.42	1.44	1.42	1.44	1.42
C8–C9	1.411(5)	/	1.427(6)	1.422(5)	/	/
	1.43	1.43	1.44	1.43	1.44	1.43
C9–C1	1.448(5)	/	1.440(6)	1.470(4)	/	/
	1.44	1.45	1.44	1.46	1.43	1.45
C9–C10	1.416(5)	/	1.413(4)	1.420(4)	/	/
	1.43	1.44	1.43	1.44	1.43	1.45
fold angles	22.7 <sup>[a]</sup> , 11.7 <sup>[a]</sup>	/, 10.4 <sup>[a]</sup>	25.2 <sup>[a]</sup> , 11.2 <sup>[a]</sup>	28.7 <sup>[a]</sup> , 12.4 <sup>[a]</sup>	/, 13.9 <sup>[a]</sup>	/, 15.5 <sup>[a]</sup>
	9.5 <sup>[b]</sup> , 5.9 <sup>[b]</sup>	/, 2.7 <sup>[b]</sup>	8.6 <sup>[b]</sup> , 7.8 <sup>[b]</sup>	1.7 <sup>[b]</sup> , 2.4 <sup>[b]</sup>	/, 21.1 <sup>[b]</sup>	/, 6.2 <sup>[b]</sup>

<sup>[a]</sup> Dihedral angle between planes C1,C2,C3,C4/C1,C9,C10,C4; <sup>[b]</sup> Dihedral angle between planes C5,C6,C7,C8/C5,C10,C9,C8.

The  $\eta^4$ -coordination of naphthalene to Fe1, Fe2, and Ru1 results in a significant folding of the coordinated arene rings. This folding is more pronounced for the ring coordinated to the Cp'Fe moiety (Fe1) than for the second arene ring, which binds to the Cp\*Fe or Cp\*Ru fragment (Fe2 or Ru1), respectively. For **3**, a fold angle C1,C2,C3,C4/C1,C9,C10,C4 of 22.7° is observed for the ring coordinated to Fe1, which displays the sterically encumbered Cp' ligand. The folding is significantly less pronounced for the ring coordinated to Fe2 with a fold angle C5,C6,C7,C8/C5,C9,C10,C8 of only 9.5°. Similar fold angles (25.2° vs. 8.6°) are observed in the structure of **4**. The differences in ring folding at the different metal atoms are also apparent from the Fe–C distances to the bridgehead carbon atoms. The Fe1–C9 and Fe1–C10 distances in **3** and **4** are larger than 2.6 Å whereas the distances of Fe2 and Ru1 to the bridgehead carbons C9 and C10 are much shorter (Fe2–C9 2.330(3) Å, Fe2–C10 2.336(3) Å, Ru1–C9 2.434(4) Å, and Ru1–C10 2.436(4) Å).

We also calculated the structures of **3** and **4** using DFT methods at the BP86<sup>15,16,17</sup> / def2-TZVP<sup>18,19</sup> level of theory as implemented in the ORCA<sup>20</sup> package. The calculated structures support the discussion above of the X-ray crystallographic structures, with the metal centers being  $\eta^4$ -coordinated to the rings of the naphthalene bridge.

The structures of the previously characterized homobimetallic complexes [Cp\*Fe( $\mu$ -C<sub>10</sub>H<sub>8</sub>)FeCp\*] (**1**) and [Cp\*Fe( $\mu$ -C<sub>14</sub>H<sub>10</sub>)FeCp\*] (**2**) are similar to those of **3** and **4**.<sup>13,14</sup> However, from inspection of the Fe–C distances of the bridgehead carbons (**1**: Fe1–C9 2.441(1) Å, Fe1–C10 2.435(2) Å, **2**: Fe1–C15,C15' 2.359(2) Å) it becomes apparent that the coordinated arene rings are significantly less folded in **1** and **2**. The fold angles of 12.4° for **1** and 9.1° for **2** are more than 10° smaller than those of **3** and **4**.

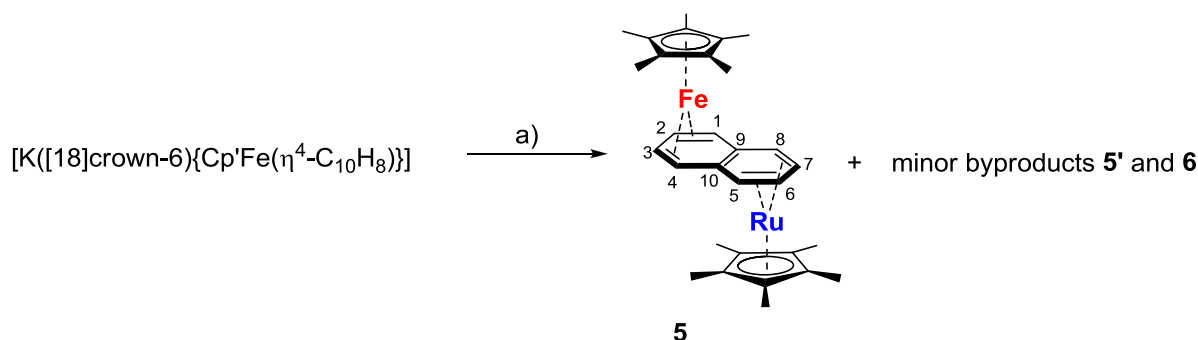
Complexes **3** and **4** are diamagnetic in contrast to related polyarene-bridged complexes [Cp\*Fe( $\mu$ -L)FeCp\*] (L = fluorene, diphenylmethane, phenanthrene, triphenylmethane, pyrene), which are paramagnetic, with weakly coupled iron centers.<sup>6g</sup> Well-resolved <sup>1</sup>H and <sup>13</sup>C{<sup>1</sup>H} NMR spectra were recorded for **3** and **4** in C<sub>6</sub>D<sub>6</sub> at room temperature. The NMR signatures fully support the molecular structures formulated by X-ray crystallography. The assignment of the NMR data is summarized in Table 2. The <sup>1</sup>H NMR spectra of both complexes feature four broad peaks that can be assigned to the naphthalene ligand. Low-frequency resonances observed at 1.30 ppm for **3** and 1.00 ppm for **4** are assigned to the 1,4-protons of the naphthalene ligand and are indicative of an  $\eta^4$ -coordination of the corresponding arene ring.<sup>11h,12</sup> The resonances of the hydrogen atoms in the 2,3-position are significantly more deshielded and are observed at 6.94 ppm (**3**) and 6.85 ppm (**4**), respectively. Similar resonances were observed for the symmetrical complex **1**.<sup>13</sup> Signals at 2.01 and 4.86 ppm for **3**, and 2.87 and 4.27 ppm for **4** are assigned to the arene ring coordinated to the Cp\*Fe and Cp\*Ru moieties, respectively. Interestingly, the difference between the chemical shifts of these resonances is significantly smaller than the chemical shift difference of the resonances assigned to the arene ring bound to the Cp'Fe unit. This observation correlates with the smaller fold angle of these arene rings in the X-ray structures (*vide supra*). The Cp\* ligands give rise to singlets in the expected range at 1.38 ppm for **3** and 1.53 ppm for **4**. A set of three signals observed in the aliphatic range with a 9:18:2 ratio arises from the Cp' ligand.

**Table 2.** The assignment of the  $^1\text{H}$  NMR and  $^{13}\text{C}\{^1\text{H}\}$  NMR resonances of **1**, **3**, **4**, and **5**. The  $^{13}\text{C}\{^1\text{H}\}$  NMR resonances are given in parentheses; the labeling scheme for **3** and **4** is given in Scheme 1; the labeling scheme for **1** and **5** is given in Scheme 2.

	<b>1</b>	<b>3</b>	<b>4</b>	<b>5</b>
$\text{H}_{1,4}(\text{C}_{1,4})$	1.11 (58.0)	1.30 (48.0)	1.00 (42.7)	1.31 (58.8)
$\text{H}_{2,3}(\text{C}_{2,3})$	5.72 (77.5)	6.94 (74.8)	6.85 (73.9)	5.10 (72.0)
$\text{H}_{5,8}(\text{C}_{5,8})$	1.11	2.01 (68.8)	2.87 (73.1)	1.80 (59.5)
$\text{H}_{6,7}(\text{C}_{6,7})$	5.72	4.86 (77.7)	4.27 (74.9)	5.37 (76.4)
$\text{C}_{9,10}$	110.1	(108.1)	(117.1)	(110.8)
CH of $\text{Cp}'$	/	3.35 (66.1)	3.43 (65.9)	/
$\text{CH}_3$ of $\text{Cp}'$	/	1.27, 1.49 (31.6, 34.4)	1.44, 1.59 (32.0, 34.6)	/
$\text{C}(\text{CH}_3)_3$ of $\text{Cp}'$	/	/ (31.2, 33.2)	/ (31.6, 33.3)	/
quart. C of $\text{Cp}'$	/	/ (95.1, 96.7)	/ (95.1, 95.7))	/
$\text{CH}_3$ of $\text{Cp}^*$	1.49 (10.1)	1.38 (9.9)	1.53 (10.8)	1.64, 1.77 (10.3, 11.5)
quart. C. of $\text{Cp}^*$	(83.8)	(83.4)	(88.3)	(82.6), (85.1)

The  $^{13}\text{C}\{^1\text{H}\}$  NMR data show a similar trend as the  $^1\text{H}$  NMR resonances (Table 2). Compared to the free ligand, the resonances are shifted to lower frequencies. The carbon atoms in the 1,4-position, which are connected to the  $\text{Cp}'\text{Fe}$  moiety, are significantly more deshielded than the resonances of the carbons connected to the  $\text{Cp}^*\text{Fe}$  and  $\text{Cp}^*\text{Ru}$  fragments.

In addition to the dissymmetrical complexes **3** and **4** we also synthesized the symmetrical FeRu complex  $[\text{Cp}^*\text{Fe}(\mu\text{-C}_{10}\text{H}_8)\text{RuCp}^*]$  (**5**) which bears two  $\text{Cp}^*$  ligands. Complex **5** is accessible by reacting the mononuclear compound  $[\text{K}([18]\text{crown-6})\{\text{Cp}^*\text{Fe}(\eta^4\text{-C}_{10}\text{H}_8)\}]$  with one equiv.  $[\text{Cp}^*\text{RuCl}]_4$  in THF at  $-78^\circ\text{C}$  (Scheme 2). It was isolated in 43% yield by crystallization from *n*-hexane.



**Scheme 2.** Synthesis of **5**. Reagents: a) 0.25  $[\text{Cp}^*\text{RuCl}]_4$ .

A single-crystal X-ray structure analysis (Figure S1) confirmed that the molecular structure of **5** is analogous to those of **1–4**. A detailed interpretation of the structural parameters is not meaningful due the disorder of iron and ruthenium over both metal sites in this structure. However, the calculated structure

(DFT BP86/def2-TZVP, Table 1) is similar overall to the calculated molecular structure for the analogous Cp-substituted derivative **4**. An interesting effect of replacing Cp' by Cp\* is observed for the fold angles of the arene rings coordinated to Fe1 and Ru1, respectively. For **5**, the calculated fold angle at Ru1 is significantly larger (21.1°) than the fold angle at Fe1 (13.9°), whereas the opposite trend is observed for the calculated structure of **4** (7.8° at Ru1 vs. 11.7° at Fe1, Table 1). A larger fold angle is usually identified with increased back-bonding from the metal into the ligand  $\pi^*$  orbitals.<sup>11h</sup> However, the calculated structure of cation **5**<sup>+</sup> (BP86/def2-TZVP) shows a significantly smaller fold angle of 6.2° at Ru1. The Ru1–C9,C10 distances to the bridgehead carbons are also shorter by 0.30 Å than in **5**. The ring folding at Fe1 does not change very much on oxidation. A very similar trend is observed for **4** vs. **4**<sup>+</sup> (*vide supra*). Most of the structural parameters are practically unaffected by the oxidation **5** to **5**<sup>+</sup>.

The NMR data of **5** are given in Table 2. The <sup>1</sup>H-NMR spectrum in C<sub>6</sub>D<sub>6</sub> features four multiplets at 1.31, 1.80, 5.10 and 5.37 ppm for the naphthalene ligand, a singlet at 1.64 for the Cp\*Fe moiety and a singlet at 1.77 ppm for the Cp\*Ru unit. In addition to these signals, we observed two sets of minor signals that presumably arise from additional components present in low concentrations (<5% each). We tentatively assign these resonances to the homoleptic RuRu complex [Cp\*Ru( $\mu$ -C<sub>10</sub>H<sub>8</sub>)RuCp\*] (**6**) and an isomer **5'** that presumably corresponds to the *cis*-isomer of **5**, where iron and ruthenium coordinate to the same side of the plane of the bridging naphthalene ligand.<sup>21</sup> Attempts to completely remove these minor impurities in compound **5** by recrystallization were unsuccessful. Nevertheless, the purity of **5** was sufficient to carry out cyclic voltammetry and UV/vis spectroelectrochemistry experiments (see below).

### 2.2.2 Cyclic Voltammetry

In order to gain insight into the redox properties, we carried out cyclic voltammetry on the dinuclear complexes **3–5**. The results of UV/vis spectroelectrochemistry measurements are presented further below. The redox properties of **3** and **4** determined by cyclic (and in some cases also square wave) voltammetry are summarized in Table 3. The cyclic voltammograms are depicted in the Supporting Information (Figures S3 and S4, respectively). For better understanding of the influence of the metal center (Fe, Ru) and cyclopentadienyl ligand (Cp', Cp\*) variations, two reference compounds have been included in the spectroelectrochemical study, *viz.* the fully symmetric complex **1** (Chart 1) and its FeRu derivative [Cp\*Fe( $\mu$ -C<sub>10</sub>H<sub>8</sub>)RuCp\*] (**5**).<sup>13,22</sup>

**Table 3.** Electrochemical data<sup>a</sup> for dissymmetrical **Cp'MMCp\*** complexes **3** and **4** and for the homoleptic **Cp\*MMCp\*** reference compounds **1** and **5**.<sup>22</sup>

	<b>3</b>	<b>4</b>	<b>1</b>	<b>5</b>
$E_{1/2}$ (Ox2)	−0.73	−0.70	−0.95	−1.05
$E_{1/2}$ (Ox1)	−1.51	−1.54	−1.61	−1.64
$E_{1/2}$ (Red)	−3.02	−3.06 <sup>b</sup>	−3.10	−3.09 <sup>b</sup>

<sup>a</sup> Anodic (Ox) and cathodic (Red) electrode potentials in Volt vs  $E_{1/2}$ (ferrocene/ferrocenium); Pt microdisc electrode, THF/TBAH, 293 K,  $\nu = 100 \text{ mV s}^{-1}$ . <sup>b</sup> Electrochemically quasi reversible:  $\Delta E_p$  exceeds the value recorded for the ferrocene/ferrocenium (Fc/Fc<sup>+</sup>) internal standard.

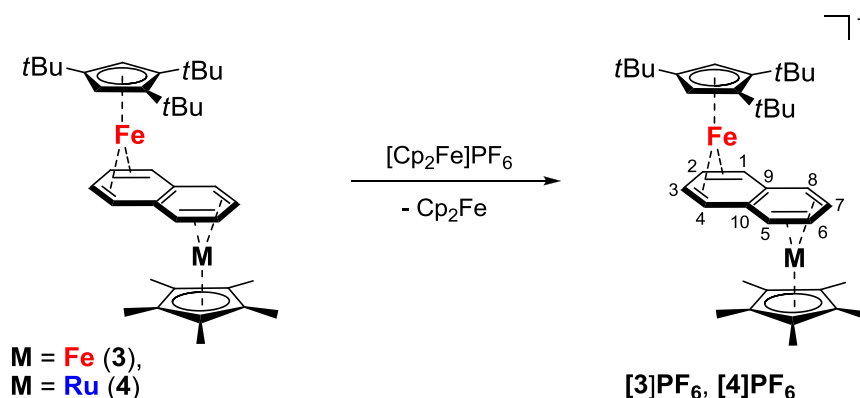
The cyclic voltammograms of all four complexes show two well-separated anodic waves ( $\Delta E_{1/2} = 660 \text{ mV}$  for **1**,  $780 \text{ mV}$  for **3**,  $840 \text{ mV}$  for **4**, and  $590 \text{ mV}$  for **5**) at rather negative potentials, belonging to fully reversible  $1e^-$  oxidations of the parent compounds to the corresponding cations and dications. While for symmetric **1** the large  $\Delta E_{1/2}$  value points to a strong electronic communication between the formally Fe(I) centers through the naphthalene bridge,<sup>13,14</sup> in the case of the asymmetric heterometallic complexes this argument needs to be considered with caution. The reduction of complexes **3** and **4** to the corresponding anions was observed close to the cathodic potential limit of the electrolyte as a reversible wave, in the case of **4** affected by slow electron transfer kinetics. A very similar situation was encountered for the reduction of the other FeRu complex **5**.

Remarkably, the cathodic waves of all four complexes in Table 3 lie in a very narrow potential region and remain largely unaffected by the variation of the substituents on the Cp rings as well as by the replacement of the Cp\*Fe moiety with Cp\*Ru. The same conclusion can also be drawn for the first  $1e^-$  oxidation of the complexes. Their LUMOs and HOMOs can therefore be considered as receiving a significant contribution from delocalized  $\pi^*$  and  $\pi$  Cp-metal-naphthalene systems, respectively, in line with the results of theoretical calculations (see below). The oxidations can be seen as residing more at the cyclopentadienyl iron termini while the reductions shift more to the naphthalene bridge. Due to the delocalized nature of the frontier orbitals (see below, Figures 5 and 6) the Cp\*Ru moiety is also involved in the redox processes, although somewhat less than the Cp\*Fe or Cp'Fe terminus.

The slightly less negative potentials for the oxidation and reduction of **3** and **4** compared to **1** and **5** reflect the overall electronic effect of the less donating Cp' group in the former two complexes.<sup>23</sup> The potential difference increases for the oxidation of the corresponding cationic complexes (Table 3). This observation agrees with the theoretically supported very similar contribution of the Cp'Fe and Cp\*Fe moieties<sup>14</sup> to the characters of the highest occupied MOs (see below).

### 2.2.3 Synthesis and Characterization of the Mixed-Valence Compounds [Cp'Fe( $\mu$ -C<sub>10</sub>H<sub>8</sub>)FeCp\*]PF<sub>6</sub> ([3]PF<sub>6</sub>) and [Cp'Fe( $\mu$ -C<sub>10</sub>H<sub>8</sub>)RuCp\*]PF<sub>6</sub> ([4]PF<sub>6</sub>)

Encouraged by the cyclic voltammetry results, we subsequently prepared the cations **3**<sup>+</sup> and **4**<sup>+</sup> on a preparative scale. The preparative oxidations of **3** and **4** with an equimolar amount of ferrocenium hexafluorophosphate in THF proceeded according to Scheme 3 and afforded crystalline salts of green [Cp'Fe( $\mu$ -C<sub>10</sub>H<sub>8</sub>)FeCp\*][PF<sub>6</sub>] (**[3]PF<sub>6</sub>**) and violet [Cp'Fe( $\mu$ -C<sub>10</sub>H<sub>8</sub>)RuCp\*][PF<sub>6</sub>] (**[4]PF<sub>6</sub>**) in 56% yield each.



**Scheme 3.** Synthesis of the cationic complexes **[3]PF<sub>6</sub>** and **[4]PF<sub>6</sub>**.

X-ray quality crystals of **[4]PF<sub>6</sub>** were grown from THF/toluene. The molecular structure of **[4]PF<sub>6</sub>** (Figure 2) shows a contraction of the Ru1–C9 and Ru1–C10 distances by approximately 0.16 Å compared to neutral **4** (see Table 1). This contraction corresponds to a significant flattening of the arene ring coordinated to Ru1, which displays a fold angle C5,C6,C7,C8/C5,C10,C9,C8 of merely 1.7°. The bonding pattern of Ru1 in **4**<sup>+</sup> thus resembles an  $\eta^6$ -coordination, while Fe1 is still  $\eta^4$ -coordinated (fold angle 28.7°). The C–C distances within the  $\eta^6$ -coordinated arene ring (1.412(5)–1.422(5) Å) are equal within experimental error. The remaining metal carbon distances are largely similar to **4**.

Unfortunately, we could not characterize the FeFe compound **[3]PF<sub>6</sub>** by X-ray crystallography so far. Repeated attempts to grow suitable single crystals from various solvents remained unsuccessful. However, inspection of the DFT-calculated structure (Table 1) shows that the oxidation of neutral **3** by one electron to give **3**<sup>+</sup> only has a modest effect on the molecular structure. The general structural arrangement is not changed by the oxidation. The largest structural change is observed for the Fe1–C9 and Fe1–C10 distances, which decrease by 0.08 and 0.11 Å upon oxidation. The calculated fold angles at Fe1 and Fe2 (Fe1: 10.4°, Fe2: 2.7°) are slightly smaller than in neutral **3** (11.7 and 5.9°). Most other structural parameters remain practically the same.

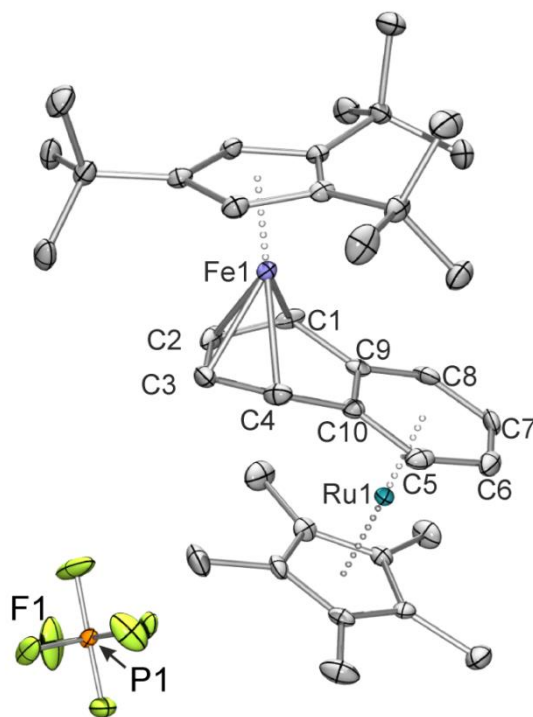


**Figure 2.** Single crystal X-ray structures of  $[\text{Cp}'\text{Fe}(\mu\text{-C}_{10}\text{H}_8)\text{RuCp}^*]\text{PF}_6$  (**[4]PF<sub>6</sub>**). Displacement ellipsoids are drawn at the 40% level, hydrogen atoms are omitted for clarity.

The cationic complexes **[3]PF<sub>6</sub>** and **[4]PF<sub>6</sub>** show uninformative, very poorly resolved  $^1\text{H}$  NMR spectra due to their paramagnetism. The determination of their solution magnetic moments by Evans's method gave a value of  $\mu_{\text{eff}} = 1.7(1) \mu_{\text{B}}$  for both **3<sup>+</sup>** and **4<sup>+</sup>**. These experimental values are in excellent agreement with the calculated spin-only value of  $1.73 \mu_{\text{B}}$  for a complex featuring one unpaired electron. The UV/Vis spectra recorded in THF agree well with those obtained by the spectroelectrochemistry experiments and the *TDDFT* calculations (see below).

The EPR spectra of **[3]PF<sub>6</sub>** and **[4]PF<sub>6</sub>** were recorded at 20 K in a THF matrix. The spectra reveal a slightly rhombic, nearly axial *g*-tensor characteristic for  $S = 1/2$  systems, without any resolved hyperfine couplings (Figure 3). Satisfactory spectral simulations were obtained with the parameters shown in Table 4.

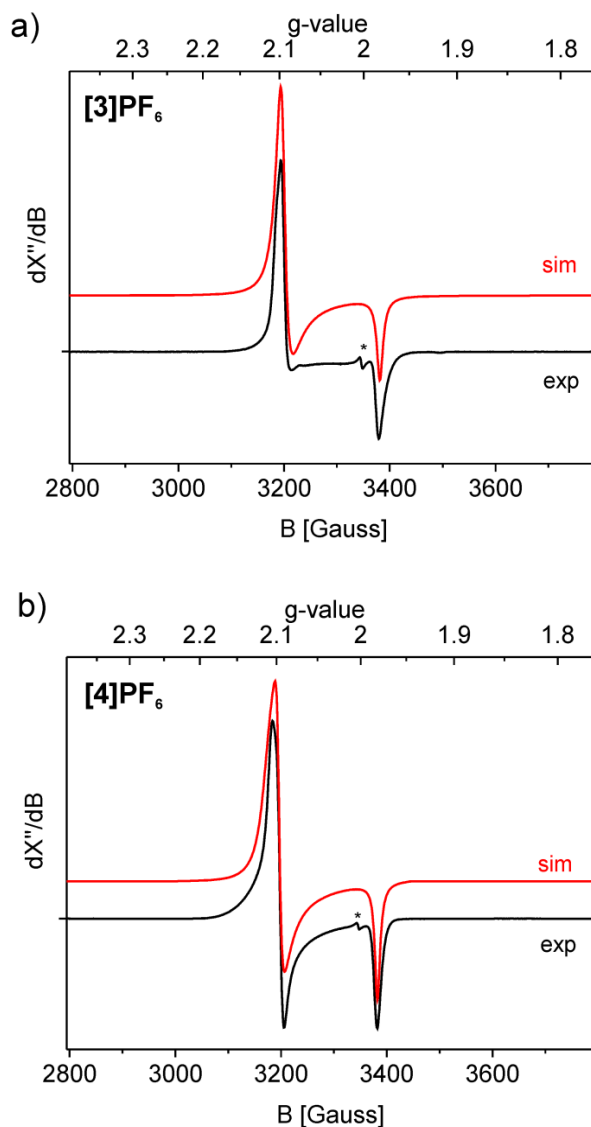


**Figure 3.** Experimental and simulated X-band EPR spectra of **[3]PF<sub>6</sub>** (a) and **[4]PF<sub>6</sub>** (b). Experimental conditions:  $T = 20$  K, microwave power of 0.2 mW, field modulation amplitude of 4 G, microwave frequency of 9.379557 GHz. The simulated spectrum was obtained with the parameters shown in Table 4. The small signal marked with an asterisk is an impurity in the glass wall of the EPR cryostat.

The results of DFT EPR property calculations performed with ORCA are shown in Table 4. The calculated EPR parameters are in qualitative agreement with the experimental values, but the DFT calculated  $g$ -tensor is somewhat more rhombic compared to the near axial  $g$ -tensor obtained from the experimental spectra. Both in the experimental spectra and in the calculations, the rhombicity of the RuFe compound **[4]PF<sub>6</sub>** is slightly larger than in the FeFe compound **[3]PF<sub>6</sub>**.

**Table 4.** Experimental and DFT calculated EPR parameters of **[3]PF<sub>6</sub>** and **[4]PF<sub>6</sub>**.

	<b>[3]PF<sub>6</sub></b> <sup>[a]</sup>	<b>3<sup>+</sup></b> <sup>[b]</sup>	<b>[4]PF<sub>6</sub></b> <sup>[a]</sup>	<b>4<sup>+</sup></b> <sup>[b]</sup>
<i>g</i> <sub>11</sub>	2.099	2.074	2.108	2.091
<i>g</i> <sub>22</sub>	2.093	2.050	2.097	2.069
<i>g</i> <sub>33</sub>	1.982	1.991	1.981	1.992
<i>W</i> <sub>11</sub>	19	-	20	-
<i>W</i> <sub>22</sub>	10	-	8	-
<i>W</i> <sub>33</sub>	7	-	6	-

<sup>[a]</sup> Parameters from spectral simulations (least square “best fit”). Hyperfine couplings in MHz.

<sup>[b]</sup> DFT calculated parameters (ORCA, B3LYP, def2-TZVP).

DFT-calculated spin density plots of cations **3<sup>+</sup>** and **4<sup>+</sup>** (Figure 4) are consistent with these EPR results. The spin density plots reveal that both complexes are essentially iron-centered radicals, which may explain the similar EPR parameters. For **3<sup>+</sup>**, large contributions to the unpaired electron density are observed at Fe1 and Fe2. For **4<sup>+</sup>**, the spin density is mainly localized on Fe1 with a smaller contribution on Ru1. The latter contribution may account for the slightly larger rhombicity of the EPR spectrum of **4** due to the larger spin-orbit couplings of the heavier Ru atom.

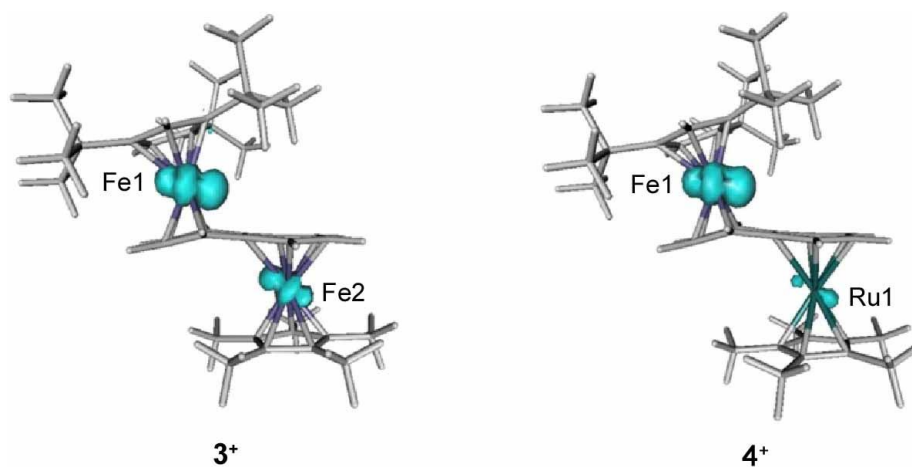


**Figure 4.** Spin densities of **3<sup>+</sup>** and **4<sup>+</sup>** calculated at the BP86/def2-TZVP level of theory. (Spin densities generated using Gabedit<sup>24</sup>).

## 2.2.4 Computational Results, Spectroelectrochemistry, and TDDFT Calculations

We reproduced the structures of **3–5** and **3<sup>+</sup>–5<sup>+</sup>** using DFT calculations at the BP8615<sup>15–17</sup> / def2-TZVP<sup>15,16</sup> level of theory as implemented in the ORCA<sup>15</sup> package. As shown in Table 1, there is very good agreement between the calculated structures and experiment, with the difference in bond lengths remaining within 0.05 Å. There is a greater discrepancy between the fold angles, where, although the calculated angles are significantly smaller, the trend of decreasing fold angle with increasing charge of the complex is reproduced. The calculated structures therefore support the discussion above of the X-ray crystallographic structures.

### 2.2.4.1 MO and Population Analysis

We analyzed the electronic structures from the DFT calculations by examining the frontier orbitals of the neutral species and comparing the populations of the localized metal d atomic orbitals in **3**, **3<sup>+</sup>**, **4**, and **4<sup>+</sup>**. The frontier molecular orbitals shown in Figures 5 and 6 indicate the degree of interaction between the metal atom and the naphthalene bridging ligand. Firstly we note the similarities between **3** and **4** in that the HOMOs and LUMOs extend over the metal atoms and the naphthalene bridge. Lower lying orbitals have then more d-orbital character associated with the metal atoms. In both cases the HOMO-1 and HOMO-2 are localized on the Fe1 atom bound to the Cp' ligand, and the HOMO-4 and HOMO-5 on the metal atom associated with the Cp\* ligand (Fe2 or Ru1, respectively). Given the fact that Cp' should be less electron donating than Cp\*,<sup>23</sup> this is somewhat unexpected and may be explained by the steric influence of the sterically crowded Cp' ligand, which results in a more acute fold angle of naphthalene for Fe1 (11.7° compared to 5.9° for **3**, and 11.2° compared to 7.8° for **4**, Table 1) and increases the metal-to-ligand back-bonding. Covalent interactions between metal d-orbitals and the arene rings in the naphthalene bridge can be identified in the HOMO, HOMO-2, HOMO-3, HOMO-5 and HOMO-6 for both **3** and **4**. The LUMO orbitals display larger contributions from naphthalene and the Cp\* and Cp' ligands. The HOMO-LUMO gap is 0.15 eV smaller for **3** (1.27 eV) than for **4** (1.42 eV).

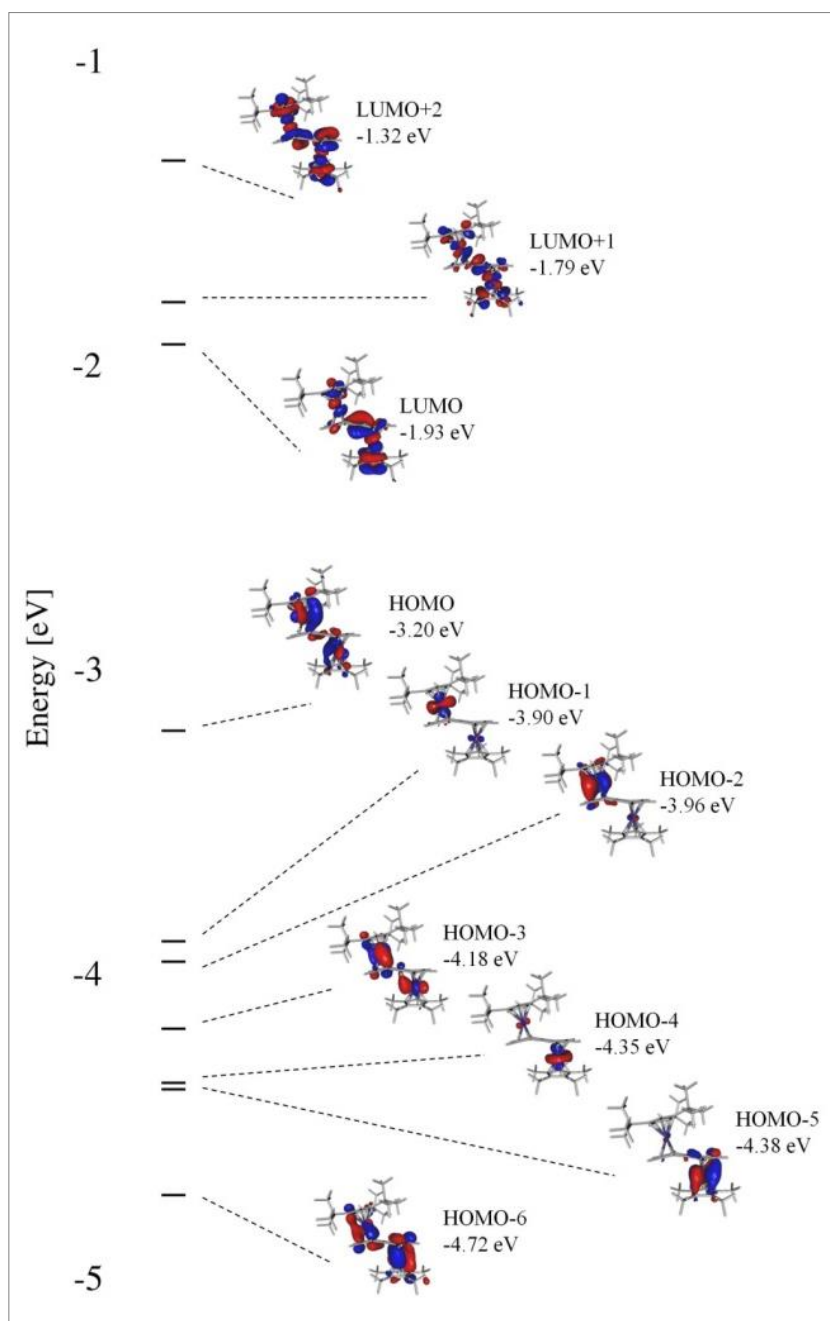


**Figure 5.** The frontier molecular orbitals of **3** calculated with DFT at the BP86 / def2-TZVP level of theory. (Molecular orbitals generated using Gabedit.<sup>15</sup>).

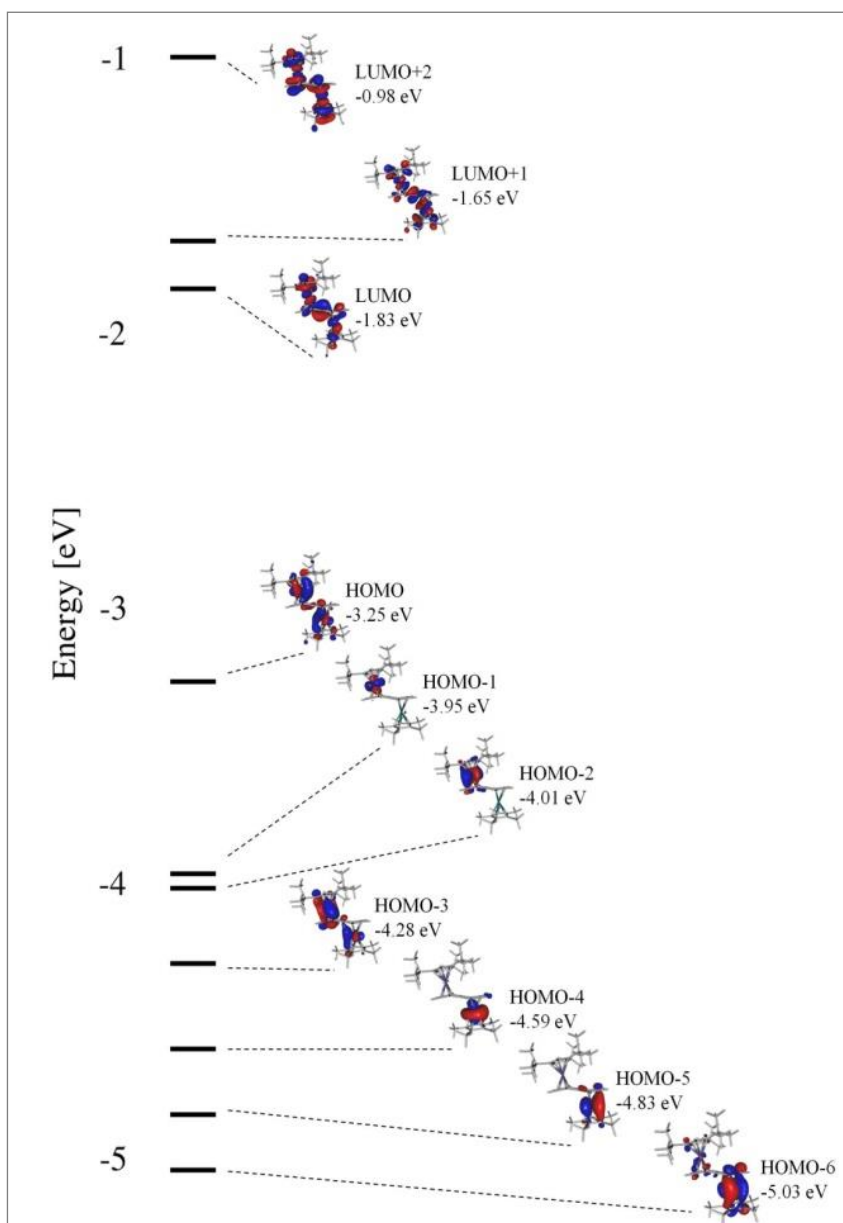


**Figure 6.** The frontier molecular orbitals of **4** calculated with DFT at the BP86 / def2-TZVP level of theory. (Molecular orbitals generated using Gabedit.<sup>15</sup>).

We analyzed the spin densities presented in Table 5 (determined according to the population analysis scheme of Löwdin) in order to determine where electron density is removed on oxidation. Here we note that the greatest change in spin for **3**<sup>+</sup> is associated with Fe2 attached to the Cp\* ligand, whereas in **4**<sup>+</sup> and **5**<sup>+</sup> the greatest change in spin is associated with the Fe atom attached to Cp'. Therefore an electron is preferentially removed from the metal atom associated with the Cp\* ligand in the homometallic compound **3** on oxidation, but this can be switched on substitution of iron by ruthenium in compounds **4** and **5**.

**Table 5.** The spin densities from a Löwdin population analysis on the DFT calculations at the BP86/def2-TZVP level of theory associated with the metal atomic d-orbitals.

	<b>3<sup>+</sup></b>		<b>4<sup>+</sup></b>	
	Fe1	Fe2	Fe1	Ru1
d <sub>z<sup>2</sup></sub>	0.06	0.23	0.25	0.02
d <sub>xy</sub>	0.01	0.05	0.07	0.00
d <sub>yz</sub>	0.01	0.04	0.06	0.00
d <sub>x<sup>2</sup>-y<sup>2</sup></sub>	0.12	0.18	0.16	0.04
d <sub>xy</sub>	0.00	0.17	0.22	0.00
Σd <sub>i</sub>	0.21	0.66	0.77	0.06

#### 2.2.4.2 Anodic UV/Vis Spectroelectrochemistry

The investigated complexes are highly air and moisture sensitive. Therefore, care must be taken when preparing solutions in the THF/TBAH electrolyte (see experimental) in order to avoid irreversible decomposition of the parent compounds, which is indicated by gradual appearance of new redox waves in the cyclic voltammograms.

The stepwise 2e<sup>-</sup> electrochemical oxidation of the dinuclear complexes **3–5** was monitored by UV/vis spectroscopy, using an OTTLE cell.<sup>25</sup> The spectroelectrochemical study of reference compound **1** has already been published elsewhere.<sup>13</sup> Thin-layer cyclic voltammograms were recorded to probe the reversibility of the forward anodic steps (Table 3) by recording the reverse cathodic responses. The results show that all cationic products **3<sup>+</sup>–5<sup>+</sup>** are completely stable on the spectroelectrochemistry time scale, *viz.* 10–20 min. Further oxidation to the corresponding dications **3<sup>2+</sup>–5<sup>2+</sup>** proved to be reversible only for **4<sup>+</sup>** and **5<sup>+</sup>**. Unlike the stable symmetric derivative **1<sup>2+</sup>**,<sup>13</sup> dication **3<sup>2+</sup>** was slowly decomposing at room temperature and the recovery of **3<sup>+</sup>** and parent **3** was limited. In this case, **3<sup>2+</sup>** was generated in situ by rapid potential step oxidation on the time scale of seconds synchronized with the collection of UV/vis spectra on a diode-array spectrophotometer.

The 1e<sup>-</sup> oxidation of diiron complex **3** is depicted in Figure 7. The broad visible absorption band of **3** at 791 nm lies at a lower energy compared to reference **1** (675 and 760sh nm). This red shift is not consistent with the slightly less negative oxidation potential of **3** (Table 3) caused by the substitution of one of the Cp\* ligands in **1** with Cp', reflecting a lower HOMO energy, and with a larger HOMO-LUMO gap for **3** compared to **5**. This implies that the frontier redox orbitals are not exclusively involved in these visible electronic transitions. Indeed, although the calculated contribution of the HOMO to LUMO transition to this electronic absorption is the dominant factor, it constitutes 39% in **3** and merely 16% in **5** (see Table S1) of the transition. The other visible absorption at 397 nm with a broad shoulder at ca. 500 nm is similar for both neutral diiron complexes. The combined nature of the corresponding electronic transitions involving several vertical 1e<sup>-</sup> excitations is revealed by the calculated data in Table S1.

The UV/vis spectrum of oxidized  $\mathbf{3}^+$  shows a prominent absorption band at 659 nm, resembling closely that of  $\mathbf{1}^+$  (633 nm). This also applies to the broad and relatively weak NIR absorption of  $\mathbf{3}^+$  at 945 nm (or at 937 and 1151 nm in neat THF). For  $\mathbf{1}^+$  these two NIR bands (820 and 1145 nm) were tentatively assigned to intervalence charge transfer (IVCT) electronic transitions, although careful TDDFT analysis proved their more complex nature, revealing mixed vertical  $1e^-$  excitations between delocalized orbitals.<sup>14</sup> Three less resolved absorption bands of  $\mathbf{3}^+$  are located between 350-600 nm, followed by composed intense UV absorptions with maxima at 277 and 293 nm that replaced the strong absorption band of parent  $\mathbf{3}$  at 258 nm (with a shoulder at 318 nm).

Further oxidation of  $\mathbf{3}^+$  to  $\mathbf{3}^{2+}$  results in the disappearance of the NIR bands whilst the visible absorption is reduced to two fairly weak bands at 498 and 624 nm (Figure 8) accompanied by a more intense band at 376 nm with a shoulder at ca 410 nm. At the same time,  $\mathbf{3}^{2+}$  exhibits strong UV absorptions at 223, 259 and 291 nm. A very similar UV/vis spectrum was also recorded for stable reference  $\mathbf{1}^{2+}$ ,<sup>10b,13</sup> reflecting almost identical bonding properties in both redox series.

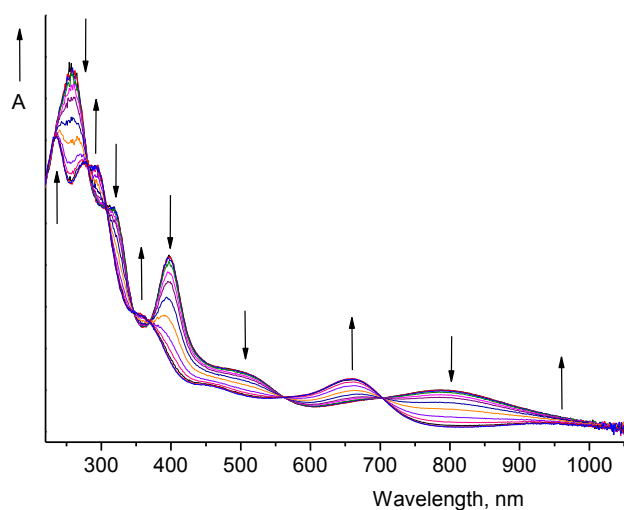


**Figure 7.** The anodic step  $\mathbf{3} \rightarrow \mathbf{3}^+$  monitored in the UV/Vis region. Conditions: OTTLE cell equipped with a Pt minigrid working electrode, THF/TBAH under Ar, 293 K.

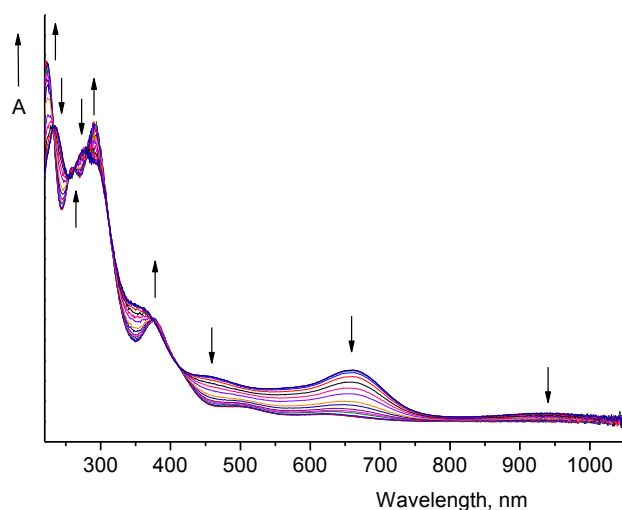


**Figure 8.** The anodic step  $3^+ \rightarrow 3^{2+}$  monitored in the UV/Vis region. Conditions: cf. Figure 7. Rapid potential step electrolysis was completed within less than 1 min.

The replacement of the FeCp\* moiety in complex **3** with RuCp\* to obtain complex **4** results in the shift of the visible absorption to a higher energy (bands at 621 and 440 nm) while the UV absorption remains almost unchanged (bands at 394, 319 and 260 nm), keeping a similar intensity pattern as well. The oxidation of **4** to  $4^+$  leads to the appearance of new bands in the NIR and visible region at 800, 544, and 403 nm (Figure 9), lying again at a higher energy compared to the corresponding visible electronic absorption of  $3^+$ . The UV spectral region of both cations is not significantly different,  $4^+$  absorbing at 294 and 316 nm similar to  $3^+$ .

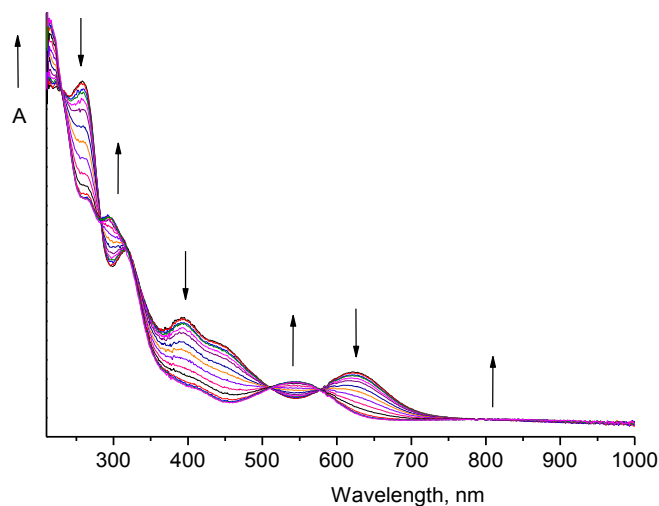


**Figure 9.** The anodic step  $4 \rightarrow 4^+$  monitored in the UV/Vis region. Conditions: cf. Figure 7.

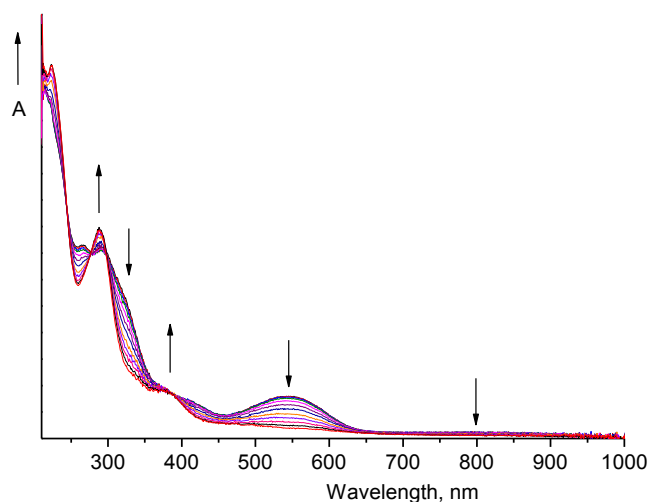


**Figure 10.** The anodic step  $4^+ \rightarrow 4^{2+}$  monitored in the UV/Vis region. Conditions: cf. Figure 7.

Further oxidation of  $4^+$  to  $4^{2+}$  reduces the visible absorption to two poorly resolved weak bands between 450-650 nm (Figure 10). The additional bands of  $4^{2+}$  at 223, 289, and 377 nm have almost identical positions as the UV absorption maxima of  $3^{2+}$  (see above).

The UV/vis absorption spectrum of reference heterometallic complex **5** reveals slight blue shifts of the absorption bands in the visible and UV region (599, 388sh, 344, and 280 nm) as a consequence of the replacement of the Cp' ligand in **4** with the stronger donor Cp\* to obtain the symmetric complex (Figure S5).

Similar to  $4^+$ , also the UV/vis spectrum of  $5^+$  shows a dominant absorption band at 591 nm accompanied by a weak NIR absorption at 796 and 920 nm. In the UV region  $5^+$  absorbs at 380 and 296 nm (Figure S5). The second anodic step producing  $5^{2+}$  leads typically to strongly diminished visible absorption represented by weak bands at 567 and 450 nm (Figure S6). In addition, a strong UV absorption band of  $5^{2+}$  arose at 280 nm together with shoulders at 340 and 360 nm.

#### 2.2.4.3 TDDFT Calculations

To gain more insight into the nature of the electronic transitions, the UV/vis spectra were calculated using the TDDFT method at the B3LYP<sup>26,27</sup>/def2-SVP<sup>16,17</sup> level of theory. The experimental spectra (see above and Figure S2) are well-reproduced. The calculated electronic transitions are summarized in Table S1 of the supporting information, and the relevant molecular orbitals are depicted in Figures 5, 6, S7, and S8. The NIR absorptions of the cations  $3^+$ ,  $4^+$ , and  $5^+$  are reproduced by the calculations. They display large contributions from the HOMO-2( $\beta$ ) $\rightarrow$ SOMO( $\beta$ )  $1e^-$  vertical transition. This transition corresponds to an excitation from an iron-centered orbital (HOMO-2) to a delocalized orbital with bonding contributions of naphthalene and metal orbitals (Figures S7 and S8). The electronic transitions in the visible and UV regions have contributions from a number of different frontier orbitals, the most significant of which are listed in Table S1. The lowest energy absorptions of neutral **3–5** (**3**: 780 and 630sh nm, **4**: 627 and

**5:** 594 sh nm) have significant contributions from HOMO→LUMO transitions, although other orbitals such as the HOMO–2 and the LUMO+1 also participate.

#### 2.2.4.4 <sup>57</sup>Fe Mössbauer Spectra

The <sup>57</sup>Fe Mössbauer spectra of **3**, **4**, [**3**]PF<sub>6</sub>, and [**4**]PF<sub>6</sub> are displayed in Figure 11, and the <sup>57</sup>Fe Mössbauer parameters obtained by simulation of these spectra are summarized in Table 6. One quadrupole doublet is observed in each of the spectra, which show very narrow line widths for neutral **3** ( $\Gamma_{FWHM} = 0.32(1) \text{ mms}^{-1}$ ) and **4** ( $\Gamma_{FWHM} = 0.28(1) \text{ mms}^{-1}$ ). These line widths are only slightly higher than the natural line width of  $0.19 \text{ mm s}^{-1}$ . This value of  $0.19 \text{ mms}^{-1}$  is equal to the minimum experimental line width of the used <sup>57</sup>Fe Mössbauer spectrometer. The spectra of [**3**]PF<sub>6</sub> and [**4**]PF<sub>6</sub> show somewhat larger line widths of  $0.49(1) \text{ mms}^{-1}$ , which we attribute to the paramagnetism of the latter two complexes. Most notably, the distinct environments of the two iron centers in **3** and [**3**]PF<sub>6</sub> are not resolved in the spectra, despite the narrow experimental line width. This observation appears to indicate that both iron nuclei have a very similar electronic environment although they carry different cyclopentadienyl substituents Cp' vs. Cp\*. The observation of only one fully averaged quadrupole doublet for [**3**]PF<sub>6</sub> furthermore indicates complete charge delocalization on the Mössbauer timescale ( $>10^{-8} \text{ s}$ ) at 77 K in this mixed-valent complex.

**Table 6.** Experimental <sup>57</sup>Fe Mössbauer spectroscopic parameters of **3**, **4**, [**3**]PF<sub>6</sub>, and [**4**]PF<sub>6</sub>, recorded at 77 K.

	<b>3</b>	[ <b>3</b> ]PF <sub>6</sub>	<b>4</b>	[ <b>4</b> ]PF <sub>6</sub>
$\delta (\text{mms}^{-1})$	0.63(1)	0.58(1)	0.61(1)	0.59(1)
$\Delta E_Q (\text{mms}^{-1})$	1.74(1)	1.42(1)	1.92(1)	1.17(1)
$\Gamma_{FWHM}$	0.32(1)	0.49(1)	0.28(1)	0.49(1)

Substituting Cp\* by Cp', or replacing Fe by Ru, has a very small effect on the <sup>57</sup>Fe Mössbauer isomer shifts of **3**, **4**, [**3**]PF<sub>6</sub>, and [**4**]PF<sub>6</sub>. The isomers shifts recorded at 77 K are in a remarkably narrow range of  $0.58(1)$  to  $0.62(1) \text{ mms}^{-1}$ . Recent theoretical studies show that the assignment of metal oxidation states on the basis of <sup>57</sup>Fe Mössbauer isomer shifts is not straightforward, since there is no obvious correlation between the 4s orbital contribution and the valence contribution to the isomer shift.<sup>28</sup> Instead, the metal-ligand bond length appears to be the most important factor that determines the variation of the isomer shift in a series of complexes.<sup>29</sup> Accordingly, the observed similarity of the isomer shift values might be attributed to the Fe–C bond lengths, which are in a similar range in the neutral and oxidized complexes due to the effect of metal to ligand backbonding (see Table 1). The previously characterized complexes [Cp\*Fe( $\mu$ -C<sub>10</sub>H<sub>8</sub>)FeCp\*] (**1**), [Cp\*Fe( $\mu$ -C<sub>14</sub>H<sub>10</sub>)FeCp\*] (**2**), [Cp\*Fe( $\mu$ -C<sub>10</sub>H<sub>8</sub>)FeCp\*][BAr<sup>F</sup><sub>4</sub>] ([**1**]BAr<sup>F</sup><sub>4</sub>), and [Cp\*Fe( $\mu$ -C<sub>10</sub>H<sub>8</sub>)FeCp\*][BAr<sup>F</sup><sub>4</sub>] ([**2**]BAr<sup>F</sup><sub>4</sub>) also show very similar isomer shifts of  $0.58$  and  $0.60 \text{ mms}^{-1}$  at 78 K,<sup>13,14</sup> which are comparable to mononuclear [Cp\*Fe( $\eta^4$ -C<sub>10</sub>H<sub>8</sub>)] ( $0.65(1) \text{ mms}^{-1}$ ) and other dinuclear complexes [Cp\*Fe( $\mu$ -L)FeCp\*] with dihydrophenanthrene, phenanthrene, triphenylene, and pyrene bridging ligands ( $0.59(1)$ – $0.66(1) \text{ mms}^{-1}$ ).<sup>6g,11h</sup>

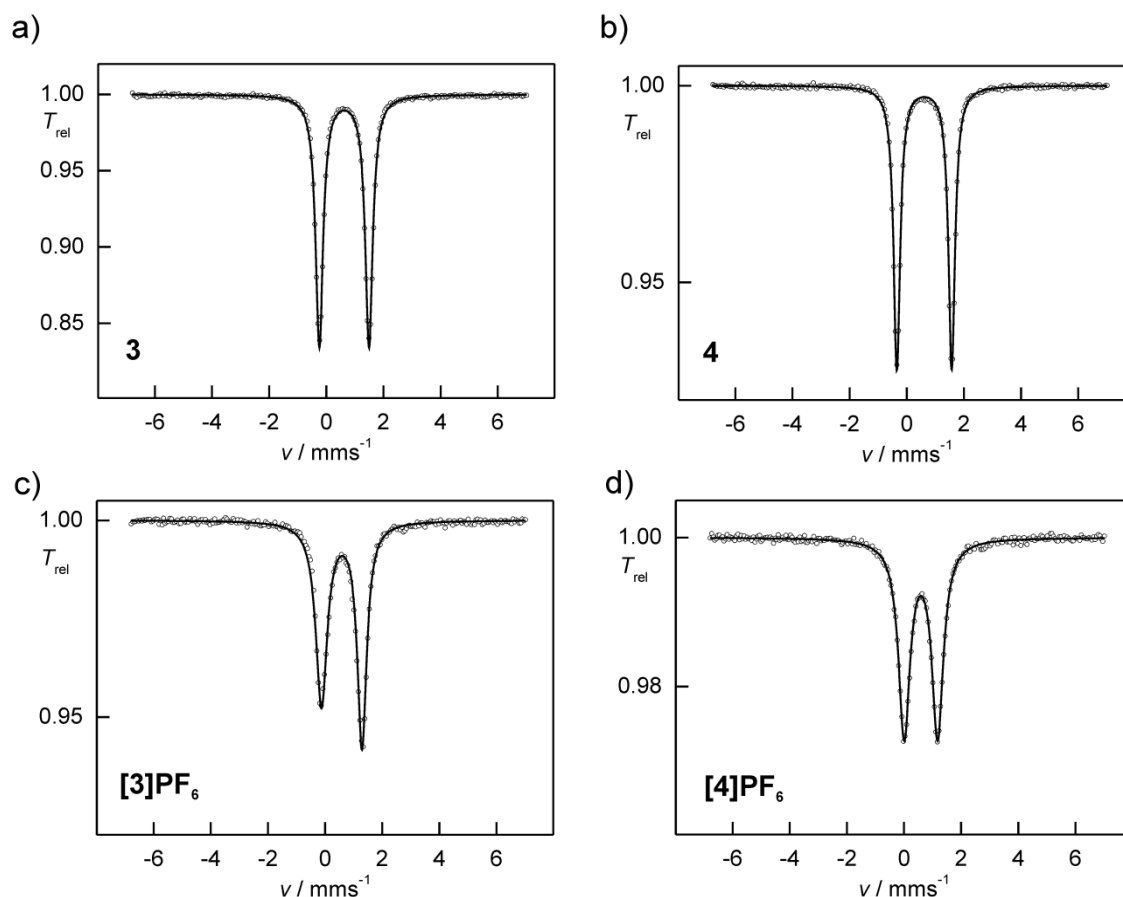


**Figure 11.** Experimental (data points) and simulated (continuous lines)  $^{57}\text{Fe}$  Mössbauer spectra of complexes **3** (a), **4** (b), **[3]PF<sub>6</sub>** (c), and **[4]PF<sub>6</sub>** (d), recorded at 77 K.

Neutral **3** and **4** display similar quadrupole splittings of  $1.74(1) \text{ mms}^{-1}$  (**3**) and  $1.92(1) \text{ mms}^{-1}$  (**4**). The quadrupole splittings are smaller for the oxidation products **[3]PF<sub>6</sub>** ( $1.42(1) \text{ mms}^{-1}$ ) and **[4]PF<sub>6</sub>** ( $1.17(1) \text{ mms}^{-1}$ ). The quadrupole splittings of the related Cp\*-substituted complexes **1** ( $1.57(1) \text{ mms}^{-1}$ ), and **2** ( $1.57(1) \text{ mms}^{-1}$ ) vs. **[1]BAR<sup>F</sup><sub>4</sub>** ( $1.17 \text{ mms}^{-1}$ ), and **[2]BAR<sup>F</sup><sub>4</sub>** ( $1.44 \text{ mms}^{-1}$ ) show the same trend. A reduction in the quadrupole splittings has also been observed for mononuclear  $[\text{Cp}^*\text{Fe}(\eta^4\text{-C}_{10}\text{H}_8)]$  ( $\Delta E_Q = 1.04(1) \text{ mms}^{-1}$ ) vs. the anionic complex  $[\text{K}([18]\text{crown-6})\{\text{Cp}^*\text{Fe}(\eta^4\text{-C}_{10}\text{H}_8)\}]$  ( $\Delta E_Q = 1.68(1) \text{ mms}^{-1}$ ).<sup>11h</sup> We suggest that the observation of smaller quadrupole splitting parameters for the cations might be attributed to the mixed-valent nature of these cations, where the iron atoms are partially oxidized to the iron(II) oxidation state, with its low-spin  $d^6$  electron configuration.

Finally, we note that our  $^{57}\text{Fe}$  Mössbauer results are in line with observations for related ferrocene derivatives and mixed-valent biferrocenium complexes.<sup>30,31</sup> The isomer shifts in these species are almost insensitive to iron oxidation whereas the quadrupole splitting strongly decrease on oxidation of iron(II) to iron(III) in these species. Interestingly, decrease of the quadrupole splittings upon oxidizing **4** to **[4]PF<sub>6</sub>** ( $\Delta\Delta E_Q = 0.75(1) \text{ mms}^{-1}$ ) is substantially larger than the difference in quadrupole splitting between **3** and **[3]PF<sub>6</sub>** ( $\Delta\Delta E_Q = 0.32(1) \text{ mms}^{-1}$ ). This in the magnitude of the quadrupole coupling constant of **[4]PF<sub>6</sub>**

might indicate that a larger proportion of charge density is removed from the Cp'-substituted iron atom (Fe1) in this complex, which is in agreement with our EPR and DFT results (see above).

## 2.3 Conclusion

The aim of this study was to investigate the effect of Cp\* ligand and metal substitution in naphthalene-bridged bimetallic sandwich complexes. To this end, we have successfully prepared and fully characterized the new dissymmetrical sandwich complexes [Cp'Fe( $\mu$ -C<sub>10</sub>H<sub>8</sub>)FeCp\*] (**3**) and [Cp'Fe( $\mu$ -C<sub>10</sub>H<sub>8</sub>)RuCp\*] (**4**) bearing Cp\* and Cp' ligands. Compounds **3** and **4** are accessible by straightforward one-pot procedures. The corresponding PF<sub>6</sub><sup>-</sup> salts of the monocations **3**<sup>+</sup> and **4**<sup>+</sup> have been isolated by oxidation of **3** and **4** with ferrocenium hexafluorophosphate. The electrochemical, structural and spectroscopic characteristics of these complexes have been analyzed and compared with those of the symmetrically-substituted complexes [Cp\*Fe( $\mu$ -C<sub>10</sub>H<sub>8</sub>)RuCp\*] (**1**) and [Cp\*Fe( $\mu$ -C<sub>10</sub>H<sub>8</sub>)RuCp\*] (**5**) bearing two Cp\* units.

Our results show that the substitution of Cp\* by Cp' and Fe by Ru in the investigated complexes only leads to relatively modest perturbations of the electronic structures. These substitutions apparently do not significantly affect the compositions and shapes of the frontier orbitals. The redox-active frontier orbitals of **3** and **4** involve major contributions from the Cp'Fe moieties and the naphthalene bridging ligand as is evident from DFT calculations. Accordingly, a moderate shift of the anodic redox potentials of **3** and **4** to more positive values was observed in comparison with **1** and **5**, while the substitution of a Cp\*Fe unit in complex **3** by a Cp\*Ru fragment (complex **4**) only has a small effect. The redox potentials thus appear to be more strongly affected by the substitution of Cp\* by Cp' than by substitution of Fe by Ru. Complexes **1** and **3–5** show qualitatively similar electronic absorption spectra. This apparent resemblance of the electronic absorption spectra persists even for the 1e<sup>-</sup> and 2e<sup>-</sup> oxidized complexes. The <sup>57</sup>Fe Mössbauer spectra revealed very similar isomer shifts, but substantially smaller quadrupole splittings for the cationic complexes [**3**]PF<sub>6</sub> and [**4**]PF<sub>6</sub> in comparison with neutral **3** and **4**. Related polyarene complexes and ferrocene derivatives show similar trends of the parameters. The Mössbauer data of [**3**]PF<sub>6</sub> provide additional evidence for the charge delocalized nature of the mixed-valent cation **3**<sup>+</sup>, which thus shows two strongly electronically coupled iron centers.

## 2.4 Experimental Section

### 2.4.1 General Procedures

All reactions were carried out under an inert atmosphere of purified argon using rigorous Schlenk and glovebox techniques. Solvents were purified, dried, and degassed by standard techniques.  $\text{FeCl}_2(\text{thf})_{1.5}$  was prepared by Soxhlet extraction of commercially available, anhydrous  $\text{FeCl}_2$ .  $\text{Cp}^*\text{H}$  was prepared by a slightly modified literature procedure.<sup>32</sup>  $\text{Cp}^*\text{K}$  was prepared by metalation of  $\text{Cp}^*\text{H}$  with *n*BuLi and exchange of the cation with KO*t*Bu in toluene.  $[\text{Cp}^*\text{RuCl}]_4$ ,  $[\text{Cp}^*\text{FeCl}(\text{tmeda})]$  and  $[\text{K}([18]\text{crown-6})\{\text{Cp}^*\text{Fe}(\eta^4\text{-C}_{10}\text{H}_8)\}]$  were prepared according to the literature procedure.<sup>11h,33,34</sup>  $[\text{Cp}_2\text{Fe}]\text{PF}_6$  was purchased from Aldrich and used as received. NMR spectra were recorded on Bruker Advance 300 ( $^3\text{P}$ ; 85%  $\text{H}_3\text{PO}_4$ ,  $^{19}\text{F}$ ;  $\text{CF}_3\text{CO}_2\text{H}$ ) and Bruker MSL 400 spectrometers ( $^1\text{H}$ ,  $^{13}\text{C}$ ;  $\text{SiMe}_4$ ), internally referenced to residual solvent resonances. The spectra were recorded at 293 K. The  $^1\text{H}$  and  $^{13}\text{C}\{^1\text{H}\}$  NMR resonances were assigned using HSQC and HMBC spectra. Melting points were measured on samples in sealed capillaries and are uncorrected. Elemental analyses were determined at Vario ELIII CHNS and Elementar Micro Vario Cube instruments. EI MS spectra were recorded on a Varian MAT 212 spectrometer.

#### 2.4.2 $[\text{Cp}^*\text{Fe}(\mu\text{-C}_{10}\text{H}_8)\text{FeCp}^*]$ (**3**)

$\text{Cp}^*\text{K}$  (1.09 g, 4.00 mmol) was added slowly to a suspension of  $\text{FeCl}_2(\text{thf})_{1.5}$  (0.94 g, 4.00 mmol) in DME (40 mL) at  $-30\text{ }^\circ\text{C}$ , and the reaction mixture was stirred at this temperature for 2 h. The resulting green-brown solution was then added by cannula to a deep green solution of potassium naphthalenide (8.00 mmol) in 120 mL THF at  $-78\text{ }^\circ\text{C}$ , whereupon a dark orange-red solution was formed. After stirring for 2 h at  $-78\text{ }^\circ\text{C}$ , a solution of  $[\text{Cp}^*\text{FeCl}(\text{tmeda})]$  (1.37 g, 4.00 mmol) in THF (25 mL) was added, and the reaction mixture was allowed to warm to room temperature overnight. The solvent was then removed in *vacuo* and the residue was extracted with *n*-hexane ( $3\times 25\text{ mL}$ ). The *n*-hexane extract was reduced to ca. 30 mL. Dark brown crystals of **3** were isolated in 42% (1.03 g, 1.69 mmol) yield from the concentrated *n*-hexane extract after storage at  $-18\text{ }^\circ\text{C}$  for two days. M.p.  $265\text{ }^\circ\text{C}$  (decomp.).  $^1\text{H}$  NMR (400.13 MHz,  $\text{C}_6\text{D}_6$ ):  $\delta = 1.27$  (s, 9H, *t*Bu of  $\text{Cp}^*$ ), 1.30 (bs, 2H,  $\text{H}_{1,4}$ ), 1.38 (s, 15 H,  $\text{Cp}^*$ ), 1.49 (s, 18H, *t*Bu of  $\text{Cp}^*$ ), 2.01 (bs, 2H,  $\text{H}_{5,8}$ ), 3.35 (s, 2H, CH of  $\text{Cp}^*$ ), 4.86 (bs, 2H,  $\text{H}_{6,7}$ ), 6.94 (bs, 2H,  $\text{H}_{2,3}$ ).  $^{13}\text{C}\{^1\text{H}\}$  NMR (100.59 MHz,  $\text{C}_6\text{D}_6$ ):  $\delta = 9.9$  (s,  $\text{CH}_3$  of  $\text{Cp}^*$ ), 31.2 (s,  $\text{C}(\text{CH}_3)_3$  of  $\text{Cp}^*$ ), 31.6 (s,  $\text{CH}_3$  of  $\text{Cp}^*$ ), 33.2 (s,  $\text{C}(\text{CH}_3)_3$  of  $\text{Cp}^*$ ), 34.4 (s,  $\text{CH}_3$  of  $\text{Cp}^*$ ), 48.0 (s,  $\text{C}_{1,4}$ ), 66.1 (s, CH of  $\text{Cp}^*$ ), 68.8 (s,  $\text{C}_{5,8}$ ), 74.8 (s,  $\text{C}_{2,3}$ ), 77.7 (s,  $\text{C}_{6,7}$ ), 83.4 (s,  $\text{C}(\text{CH}_3)_3$  of  $\text{Cp}^*$ ), 95.1 (s,  $\text{Cp}^*$ ), 96.7 (s,  $\text{Cp}^*$ ), 108.1 (s,  $\text{C}_{9,10}$ ). Elemental analysis for  $\text{C}_{37}\text{H}_{52}\text{Fe}_2$  (608.5 g/mol): calcd. C 73.03, H 8.61; found C 73.08, H 8.5. UV/vis (*n*-hexane,  $\lambda_{\text{max}}/\text{nm}$  ( $\epsilon_{\text{max}}/\text{dm}^3\text{mol}^{-1}\text{cm}^{-1}$ )): 318 (35000); 397 (30000); 498 (shoulder); 630 (shoulder); 780 (6500).

#### 2.4.3 $[\text{Cp}^*\text{Fe}(\mu\text{-C}_{10}\text{H}_8)\text{RuCp}^*]$ (**4**)

Compound **4** was prepared by an analogous procedure to **3**.  $\text{Cp}^*\text{K}$  (1.09 g, 4.00 mmol) was added slowly to a suspension of  $\text{FeCl}_2(\text{thf})_{1.5}$  (0.94 g, 4.00 mmol) in DME (40 mL) at  $-30\text{ }^\circ\text{C}$ , and the reaction mixture was stirred for 2 h at  $-30\text{ }^\circ\text{C}$ . The resulting green-brown solution was then added by cannula to a deep green

solution of potassium naphthalenide (8.00 mmol) in THF (120 mL) at  $-78\text{ }^{\circ}\text{C}$ , whereupon a dark orange-red solution was formed. After stirring for 2 h at  $-78\text{ }^{\circ}\text{C}$ , a suspension of  $[\text{Cp}^*\text{RuCl}]_4$  (1.09 g, 4.00 mmol) in THF (25 mL) was added, and the reaction mixture was allowed to warm up to room temperature overnight. The solvent was then removed in *vacuo*, and the residue was extracted with *n*-hexane (3×25 mL). The *n*-hexane extract was reduced to ca. 30 mL. Dark green crystals of **4** were isolated in 23 % (0.60 g, 0.91 mmol) yield from the concentrated *n*-hexane extract after storage at  $-18\text{ }^{\circ}\text{C}$  for two days. M.p.  $265\text{ }^{\circ}\text{C}$  (decomp.).  $^1\text{H}$  NMR (400.13 MHz,  $\text{C}_6\text{D}_6$ ):  $\delta$  = 1.00 (bs, 2H,  $\text{H}_{1,4}$ ), 1.44 (s, 9H, *t*Bu of Cp'), 1.53 (s, 15 H, Cp\*), 1.59 (s, 18H, *t*Bu of Cp'), 2.87 (bs, 2H,  $\text{H}_{5,8}$ ), 3.43 (s, 2H, CH of Cp'), 4.27 (bs, 2H,  $\text{H}_{6,7}$ ), 6.85 (bs, 2H,  $\text{H}_{2,3}$ ).  $^{13}\text{C}\{^1\text{H}\}$  NMR (100.59 MHz,  $\text{C}_6\text{D}_6$ ):  $\delta$  = 10.8 (s,  $\text{CH}_3$  of Cp\*), 31.6 (s,  $\text{C}(\text{CH}_3)_3$  of Cp'), 32.0 (s,  $\text{CH}_3$  of Cp'), 33.3 (s,  $\text{C}(\text{CH}_3)_3$  of Cp'), 34.6 (s,  $\text{CH}_3$  of Cp'), 42.7 (s,  $\text{C}_{1,4}$ ), 65.9 (s, CH of Cp'), 73.1 (s,  $\text{C}_{5,8}$ ), 73.9 (s,  $\text{C}_{2,3}$ ), 74.9 (s,  $\text{C}_{7,6}$ ), 88.3 (s,  $\text{C}(\text{CH}_3)_3$  of Cp\*), 95.1 (s, Cp'), 95.7 (s, Cp'), 117.1 (s,  $\text{C}_{9,10}$ ). Elemental analysis for  $\text{C}_{37}\text{H}_{52}\text{FeRu}$  (653.7 g/mol): calcd. C 67.98, H 8.02; found C 67.59, H 7.97. UV/Vis (*n*-hexane,  $\lambda_{\text{max}}/\text{nm}$  ( $\epsilon_{\text{max}}/\text{dm}^3\text{mol}^{-1}\text{cm}^{-1}$ ): 321 (25000); 402 (20000); 441 (shoulder); 627 (10000).

#### 2.4.4 $[\text{Cp}'\text{Fe}(\mu\text{-C}_{10}\text{H}_8)\text{FeCp}^*]\text{PF}_6$ (**[3]PF<sub>6</sub>**)

$[\text{Cp}_2\text{Fe}]\text{PF}_6$  (0.15 g, 0.45 mmol) was added slowly to a dark brown solution of **3** (0.27 g, 0.45 mmol) in THF (60 mL) at room temperature. A green reaction mixture formed. After stirring at room temperature overnight, the solvent was removed in *vacuo*. The dark green residue was washed with *n*-hexane (4×25 mL) and then dissolved in THF (ca. 50 mL). The green solution was filtered and the volume reduced to ca. 20 mL. After addition of toluene (20 mL) and storage at  $-18\text{ }^{\circ}\text{C}$  for three days, compound **[3]PF<sub>6</sub>** precipitated as a dark green solid in 56% (0.19 g, 0.25 mmol) yield. M.p.  $285\text{ }^{\circ}\text{C}$  (decomp.). Magnetic susceptibility (Evans NMR Method,  $[\text{D}_8]\text{-THF}$ ):  $\mu_{\text{eff}} = 1.7(1)\ \mu_{\text{B}}$ . Elemental analysis for  $\text{C}_{37}\text{H}_{52}\text{Fe}_2\text{PF}_6$  (753.4 g/mol): calcd. C 58.98, H 6.96; found C 58.51, H 6.65. UV/Vis/near-IR (THF,  $\lambda_{\text{max}}/\text{nm}$  ( $\epsilon_{\text{max}}/\text{dm}^3\text{mol}^{-1}\text{cm}^{-1}$ ): 357 (shoulder); 469 (shoulder); 658 (5000); 937 (700); 1151 (400).

#### 2.4.5 $[\text{Cp}'\text{Fe}(\mu\text{-C}_{10}\text{H}_8)\text{RuCp}^*]\text{PF}_6$ (**[4]PF<sub>6</sub>**)

Compound **[4]PF<sub>6</sub>** was prepared by a procedure analogous to the synthesis of **[3]PF<sub>6</sub>** by adding  $[\text{Cp}_2\text{Fe}]\text{PF}_6$  (0.15 g, 0.45 mmol) to a deep green THF solution of **4**. **[4]PF<sub>6</sub>** was isolated in 0.20 g (0.25 mmol, 56%) yield as a violet solid. M.p.  $290\text{ }^{\circ}\text{C}$  (decomp.). Magnetic susceptibility (Evans NMR Method,  $[\text{D}_8]\text{THF}$ ):  $\mu_{\text{eff}} = 1.7(1)\ \mu_{\text{B}}$ . Elemental analysis calcd. for  $\text{C}_{37}\text{H}_{52}\text{FeRuPF}_6$  (798.7 g/mol): C 55.64, H 6.56; found C 55.15, H 6.30. UV/Vis/near-IR (THF,  $\lambda_{\text{max}}/\text{nm}$  ( $\epsilon_{\text{max}}/\text{dm}^3\text{mol}^{-1}\text{cm}^{-1}$ ): 409 (shoulder); 450 (shoulder); 544 (7500); 795 (400); 1336 (100).

#### 2.4.6 $[\text{Cp}^*\text{Fe}(\mu\text{-C}_{10}\text{H}_8)\text{RuCp}^*]$ (**5**)

$[\text{Cp}^*\text{RuCl}]_4$  (0.407 g, 1.50 mmol) was dissolved in THF (30 mL) and added dropwise to a THF solution (30 mL) of  $[\text{K}([18]\text{crown-6})\{\text{Cp}^*\text{Fe}(\eta^4\text{-C}_{10}\text{H}_8)\}]$  (0.933 g, 1.50 mmol) at  $-78\text{ }^{\circ}\text{C}$ . The reaction mixture was stirred for four days at room temperature. The color of the solution gradually turned dark green. The mixture was filtered with a cannula, the solvent was evaporated to dryness and the dark residue was

extracted with *n*-hexane (5×20 mL). Concentration of the *n*-hexane solution to 40 mL and storage at +8 °C yielded dark green crystals of **5** in 43% (0.360 g, 0.65 mmol) yield. The <sup>1</sup>H-NMR spectrum of the isolated crystalline compound shows the presence of minor amounts (<5%) of two byproducts that we assign to the *cis* isomer *cis*-[Cp\*Fe(η<sup>4</sup>-C<sub>10</sub>H<sub>8</sub>)RuCp\*] (**5'**) and the RuRu complex [Cp\*Ru(μ-C<sub>10</sub>H<sub>8</sub>)RuCp\*] (**6**). M.p. 214–219 °C (decomp.). <sup>1</sup>H-NMR (400.03 MHz, C<sub>6</sub>D<sub>6</sub>, 300 K): δ = 1.31 (m, 2H, H<sub>1,4</sub> of **5**), 1.64 (s, 15H, Cp\*Fe of **5**), 1.70 (s, 0.8H, Cp\*Fe of **5'**), 1.77 (s, 15H, Cp\*Ru of **5**), 1.80 (m, 2H, H<sub>5,8</sub> of **5**), 1.85 (s, 0.8H, Cp\*Ru of **5'**), 2.03 (m, 0.1H, C<sub>10</sub>H<sub>8</sub> of **5'**), 2.13 (s, 0.8H, Cp\* of **6**), 2.17 (m, 0.1H, C<sub>10</sub>H<sub>8</sub> of **5'**), 3.84 (m, 0.1H, C<sub>10</sub>H<sub>8</sub> of **6**), 4.00 (m, 0.1H, C<sub>10</sub>H<sub>8</sub> of **6**), 4.69 (m, 0.1H, C<sub>10</sub>H<sub>8</sub> of **5'**), 4.89 (m, 0.1H, C<sub>10</sub>H<sub>8</sub> of **5'**), 5.10 (m, 2H, H<sub>2,3</sub> of **5**), 5.37 (m, 2H, H<sub>6,7</sub> of **5**). <sup>13</sup>C{<sup>1</sup>H} NMR (100.59 MHz, C<sub>6</sub>D<sub>6</sub>, 300 K, only the signals of the major product **5** were detected): δ = 10.3 (C<sub>5</sub>(CH<sub>3</sub>)<sub>5</sub> of Cp\*Fe), 11.5 (C<sub>5</sub>(CH<sub>3</sub>)<sub>5</sub> of Cp\*Ru), 58.8 (C<sub>1,4</sub>), 59.5 (C<sub>5,8</sub>), 72.0 (C<sub>2,3</sub>), 76.4 (C<sub>6,7</sub>), 82.6 (C<sub>5</sub>(CH<sub>3</sub>)<sub>5</sub> of Cp\*Fe), 85.1 (C<sub>5</sub>(CH<sub>3</sub>)<sub>5</sub> of Cp\*Ru), 110.8 (C<sub>9,10</sub>). UV/vis (*n*-hexane, λ<sub>max</sub>/nm, ε<sub>max</sub>/dm<sup>3</sup>mol<sup>-1</sup>cm<sup>-1</sup>): 279 (20500), 344 (11500), 400 (shoulder), 594 (6500). EI MS (*m/z* (%)): 601 (9.20, [Cp\*Ru(μ-C<sub>10</sub>H<sub>8</sub>)RuCp\*]<sup>+</sup> (**6**<sup>+</sup>)), 556 (100, **5**<sup>+</sup>), 372 (5.7, [Cp\*<sub>2</sub>Ru]<sup>+</sup>), 365 (93.2, [**5**-Cp\*Fe]<sup>+</sup>), 326 (6.8, [Cp\*<sub>2</sub>Fe]<sup>+</sup>), 319 (14.9, [**5**-Cp\*Ru]<sup>+</sup>), 235 (21.2, [Cp\*Ru-2H]), 135 (31.2, [Cp\*]<sup>+</sup>), 128 (86.3, [C<sub>10</sub>H<sub>8</sub>]<sup>+</sup>), 121 (19.1), 119 (18.5). Elemental analysis calcd. for C<sub>30</sub>H<sub>38</sub>FeRu (M = 555.5 g/mol): C 64.86, H 6.89; found C 64.71, H 6.94.

#### 2.4.7 Spectroelectrochemistry

Conventional cyclic voltammetry (CV) was performed in a rigorously pre-dried air-tight single-compartment cell connected to a MetrohmAutolab PGSTAT302N potentiostat. The cell was equipped with a Pt microdisc (0.14 mm<sup>2</sup>) working electrode carefully polished with a 25-μm diamond paste, a Pt coil auxiliary electrode and an Ag coil pseudoreference electrode. The solutions of the studied dinuclear complexes (10<sup>-3</sup> mol dm<sup>-3</sup>) were carefully prepared under an atmosphere of dry argon in THF freshly distilled from Na/benzophenone. The supporting electrolyte, tetrabutylammonium hexafluorophosphate (TBAH, 10<sup>-1</sup> mol dm<sup>-3</sup>) was recrystallized twice from absolute ethanol and dried overnight in *vacuo* at 80°C. All redox potentials are reported against the ferrocene/ferrocenium (Fc/Fc<sup>+</sup>) redox couple used as an internal standard.

Controlled-potential electrolyses within the OTTLE cell<sup>25</sup> were carried out using a PA4 potentiostat (Laboratory Devices, Polná, Czech Republic). The concentrations of the dinuclear complexes and TBAH used in these measurements were ca. 5×10<sup>-4</sup> and 3×10<sup>-1</sup> mol dm<sup>-3</sup>, respectively. The UV/Vis spectra were obtained using the Scinco S3100 diode array spectrophotometer. The different redox steps were localized with the aid of the contemporarily recorded thin-layer cyclic voltammograms.

#### 2.4.8 EPR Spectroscopy and EPR Parameter Calculations

Experimental X-band EPR spectra were recorded on a Bruker EMX spectrometer equipped with a He temperature control cryostat system (Oxford Instruments). The spectra were simulated by iteration of the anisotropic *g*-values, (super) hyperfine coupling constants and line widths using the W95EPR program.<sup>35</sup> The geometries of the full atom model of **3**<sup>+</sup> and **4**<sup>+</sup> were fully optimized with the Turbomole program<sup>36a</sup> coupled to the PQS Baker optimizer<sup>37</sup> at the BP86 level<sup>38</sup> using the def2-TZVP basis.<sup>36c,f</sup> EPR parameters<sup>39</sup>

were subsequently calculated with the ORCA<sup>20</sup> program systems, using the coordinates from the structure optimized in Turbomole as input. In the ORCA calculations we used the Ahlrich's def2-TZVP basis set and the B3LYP functional.<sup>40</sup>

#### 2.4.9 <sup>57</sup>Fe Mössbauer Spectroscopy

<sup>57</sup>Fe Mössbauer spectra were recorded on a WissElMössbauer spectrometer (MRG-500) at 77 K in constant acceleration mode. <sup>57</sup>Co/Rh was used as the radiation source. WinNormos for Igor Pro software has been used for the quantitative evaluation of the spectral parameters (least-squares fitting to Lorentzian peaks). The minimum experimental line widths were 0.19 mm·s<sup>-1</sup>. The temperature of the samples was controlled by an MBBC-HE0106 Mössbauer He/N<sub>2</sub> cryostat within an accuracy of ±0.3 K. Isomer shifts were determined relative to  $\alpha$ -iron at 298 K.

#### 2.4.10 X-Ray Crystallography

The crystals were processed with an Agilent Technologies SuperNova (**3**, **4**, and [**4**]PF<sub>6</sub>) or a Bruker APEXII diffractometer (**5**). Either semi-empirical multi-scan absorption corrections<sup>41</sup> or analytical ones<sup>42</sup> were applied to the data. The crystal data are given in Table S2 of the supporting information. The structures were solved with SHELXS<sup>43</sup> or SIR<sup>44</sup> and least-square refinements on  $F^2$  were carried out with SHELXL<sup>43</sup>. Details are given in the corresponding CIF files. Structure and refinement data are given in Table S2 of the supporting information.

The crystal of **3** was non-merohedrally twinned. Two twin components to the data were identified with the Agilent Technologies CrySalisPro software (version 1.171.35.19), and the structure was refined with the HKLF5 instruction to a final BASF of 0.52. The crystal of **4** was pseudo-merohedrally twinned about a crystallographic  $C_2$  axis. The twinning was refined with the TWIN 1 0 0 0 -1 0 0 0 -1 instruction with a final BASF of 0.49. The structure of **5** showed a disorder of the two metal atoms, which were each refined over the two metal sites using a split model with an occupancy ratio of 0.34:0.66 using the EADP constraint. The disorder resulted in large displacement parameters for the carbon atoms in the Cp\* ligands. Due to the disorder, a detailed discussion of bond lengths and angles for this structure would not be meaningful.

## 2.5 Supporting Information

### 2.5.1 Single-Crystal X-Ray Structure of $[\text{Cp}^*\text{Fe}(\mu\text{-}\eta^4\text{:}\eta^4\text{-C}_{10}\text{H}_8)\text{RuCp}^*]$ (**5**)

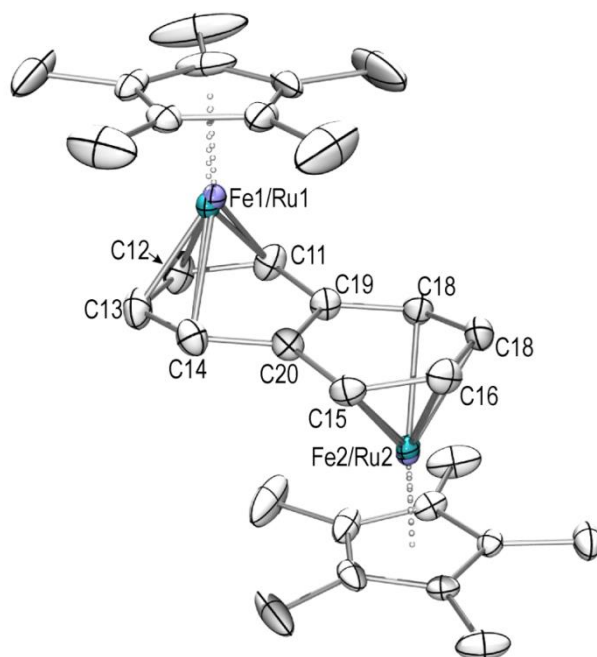


**Figure S1.** The single-crystal X-ray structure of **5** with the metal atoms disordered over two sites in a 0.66:0.34 ratio (Fe1/Fe2 and Ru1/Ru2). Thermal ellipsoids are drawn at the 30% level; H atoms have been omitted for clarity.

## 2.5.2 Graphical Representations of the UV/vis Spectra of **3**, **4**, [3]PF<sub>6</sub>, and [4]PF<sub>6</sub>

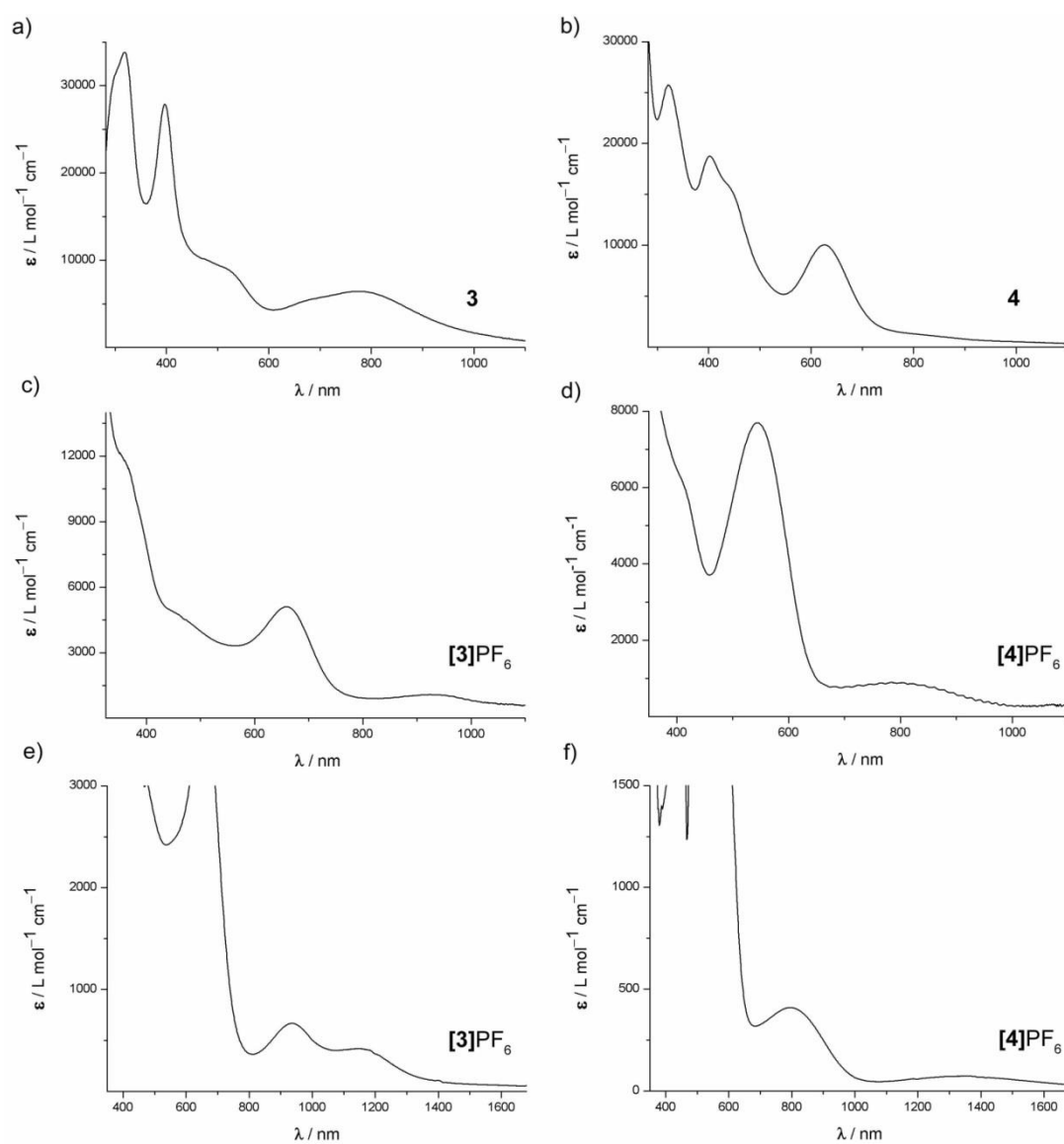


**Figure S2.** The UV/vis spectra of **3**, **4**, [3]PF<sub>6</sub>, and [4]PF<sub>6</sub>. The spectra of **3** and **4** were recorded in *n*-hexane, those of [3]PF<sub>6</sub>, and [4]PF<sub>6</sub> in THF.

### 2.5.3 Cyclic Voltammograms of 3 and 4

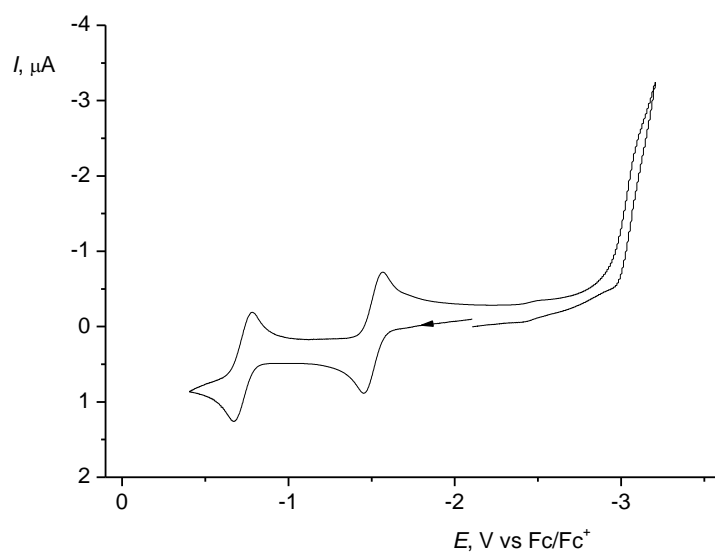


**Figure S3.** The cyclic voltammogram of complex **3**. Conditions: a Pt microdisc working electrode, THF/ $10^{-1}$  M TBAH,  $T = 293$  K,  $\nu = 100$  mV s<sup>-1</sup>.

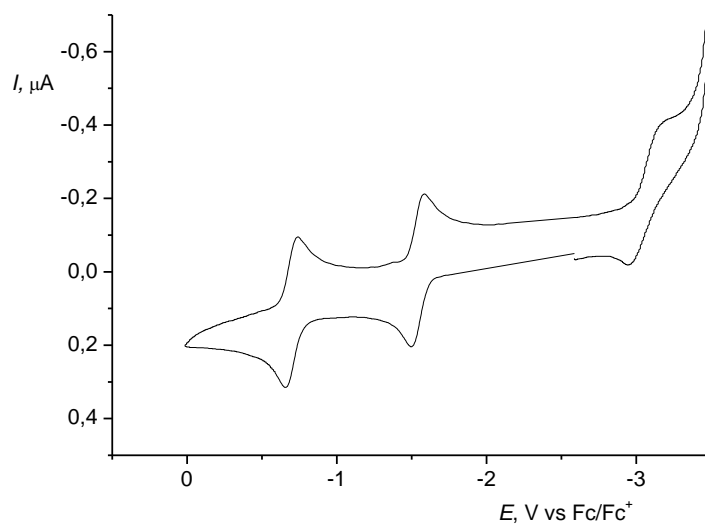


**Figure S4.** The cyclic voltammogram of complex **4**. Conditions: a Pt microdisc working electrode, THF/ $10^{-1}$  M TBAH,  $T = 293$  K,  $\nu = 100$  mV s<sup>-1</sup>.

#### 2.5.4 UV/vis Spectroelectrochemistry of **5**

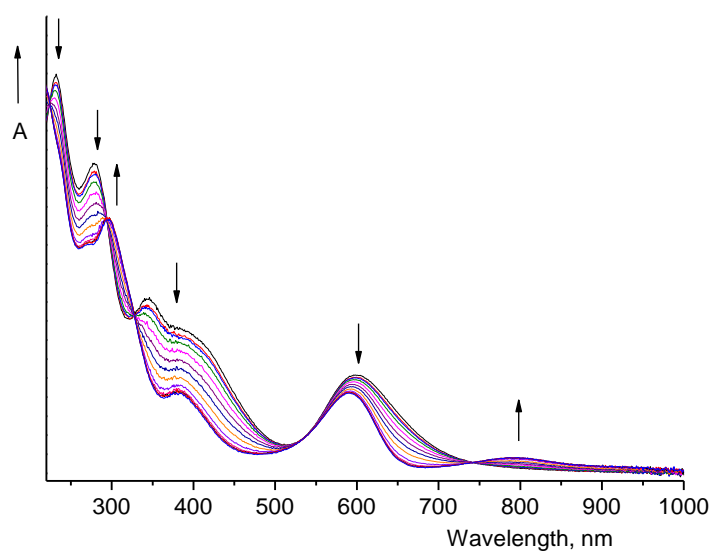


**Figure S5.** The anodic step  $5 \rightarrow 5^+$  monitored in the UV/Vis region. Conditions: OTTLE cell equipped with a Pt minigrid working electrode, THF/TBAH under Ar, 293 K.

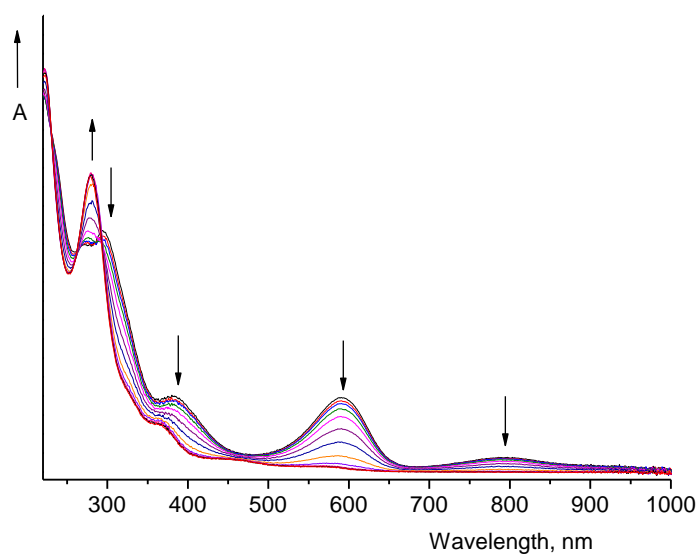


**Figure S6.** The anodic step  $5^+ \rightarrow 5^{2+}$  monitored in the UV/Vis region. Conditions: cf. Figure S5.

### 2.5.5 Calculated Frontier Molecular Orbitals of $3^+$ and $4^+$

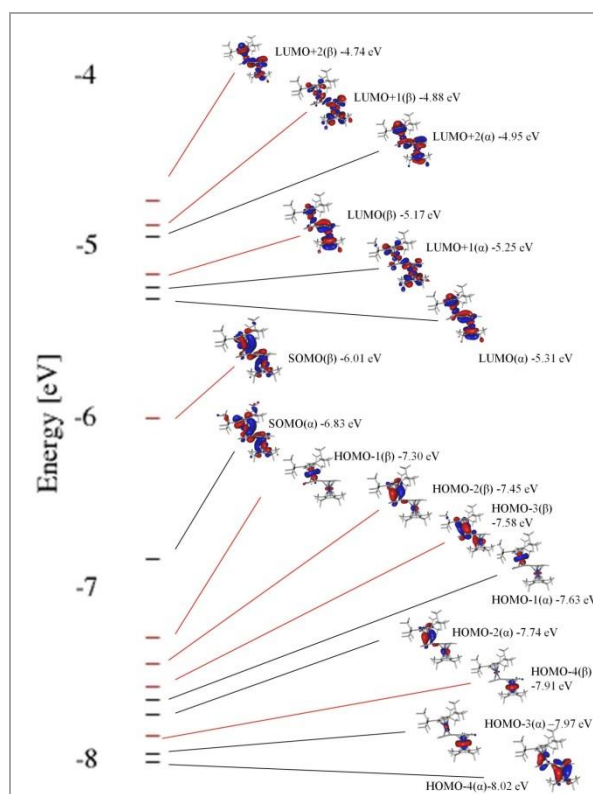


**Figure S7.** The frontier molecular orbitals of  $3^+$  calculated with DFT at the BP86 / def2-TZVP level of theory.

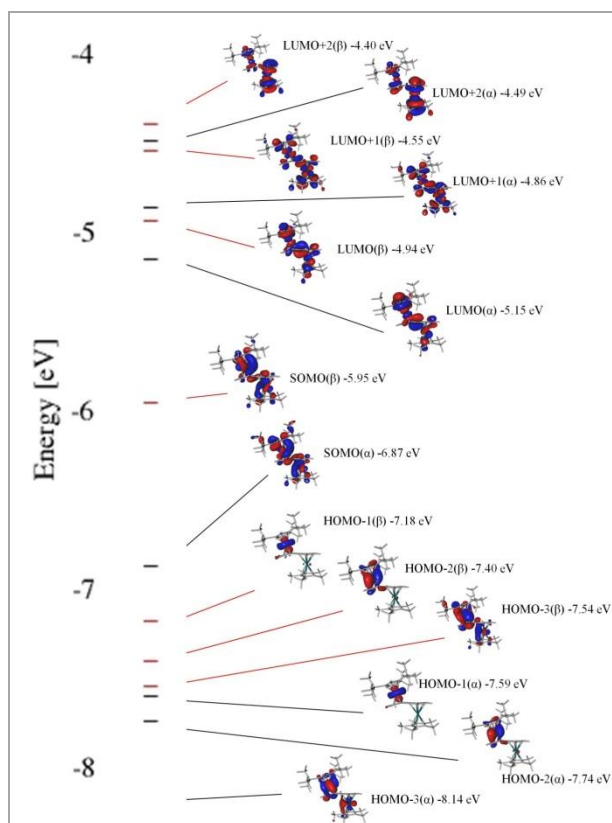


**Figure S8.** The frontier molecular orbitals of  $4^+$  calculated with DFT at the BP86 / def2-TZVP level of theory.

## 2.5.6 TDDFT Electronic Transition Calculated for the Optimized Geometries of **3**, **3<sup>+</sup>**, **4**, **4<sup>+</sup>**, **5**, and **5<sup>+</sup>**

**Table S1.** TDDFT electronic transitions calculated for the optimized geometries at the B3LYP/def2-SVP level. The relevant molecular orbitals are depicted in Figures 5 and 6 (for **3** and **4**), and Figures S7 and S8 in the supporting information (for **3<sup>+</sup>** and **4<sup>+</sup>**).

	$\nu$ [nm]	$f$	%	Character	Exptl. $\nu$ [nm]
<b>3</b>	813	0.00001	79	HOMO-1→LUMO+1	
	658	0.061	39	HOMO→LUMO	780, 630sh
	374	0.176	17	HOMO-2→LUMO	498sh, 397
			10	HOMO→LUMO	
			18	HOMO→LUMO+3	
	299	0.152	15	HOMO-3→LUMO+2	318
			22	HOMO-3→LUMO+3	
<b>3<sup>+</sup></b>	974	0.00048	69	HOMO-2( $\beta$ )→SOMO( $\beta$ )	1151sh
	781	0.002	14	SOMO( $\alpha$ )→LUMO( $\alpha$ )	937
			23	HOMO-5( $\beta$ )→SOMO( $\beta$ )	
			13	HOMO-1( $\beta$ )→SOMO( $\beta$ )	
	644	0.036	15	HOMO-1( $\beta$ )→SOMO( $\beta$ )	658
	597	0.042	21	SOMO( $\alpha$ )→LUMO( $\alpha$ )	469sh
			11	HOMO-9( $\beta$ )→SOMO( $\beta$ )	
			14	HOMO-9( $\beta$ )→LUMO+1( $\beta$ )	
	514	0.016	12	HOMO-1( $\alpha$ )→LUMO( $\alpha$ )	
			23	SOMO( $\alpha$ )→LUMO+3( $\alpha$ )	
			10	HOMO-1( $\beta$ )→LUMO+3( $\beta$ )	
<b>4</b>	779	0.0001	65	HOMO→LUMO+1	
	640	0.049	24	HOMO-2→LUMO+1	627
			26	HOMO→LUMO	
	421	0.313	37	HOMO→LUMO	402, 441sh
	316	0.235	15	HOMO-1→LUMO+1	321
			18	HOMO-1→LUMO+2	
			11	HOMO→LUMO+5	
			13	HOMO→LUMO+6	
<b>4<sup>+</sup></b>	1058	0.0004	72	HOMO-2( $\beta$ )→SOMO( $\beta$ )	1336
	926	0.0011	53	HOMO-3( $\beta$ )→SOMO( $\beta$ )	
	736	0.0068	59	HOMO-1( $\beta$ )→SOMO( $\beta$ )	795
	546	0.115	15	HOMO-3( $\alpha$ )→LUMO( $\alpha$ )	544

			23	HOMO-2( $\beta$ ) $\rightarrow$ LUMO( $\beta$ )	
			19	HOMO-2( $\beta$ ) $\rightarrow$ LUMO+4( $\beta$ )	
	401	0.066	12	SOMO( $\alpha$ ) $\rightarrow$ LUMO+3( $\alpha$ )	409sh, 450sh
			19	HOMO-1( $\beta$ ) $\rightarrow$ LUMO+3( $\beta$ )	
<b>5</b>	751	0.0001	46	HOMO $\rightarrow$ LUMO+1	
	602	0.067	11	HOMO-2 $\rightarrow$ LUMO+1	594
			16	HOMO $\rightarrow$ LUMO	
			11	HOMO $\rightarrow$ LUMO+1	
	426	0.263	22	HOMO $\rightarrow$ LUMO	400sh
			15	HOMO $\rightarrow$ LUMO+1	
	343	0.209	12	HOMO-4 $\rightarrow$ LUMO+2	344
			10	HOMO-1 $\rightarrow$ LUMO+3	
<b>5<sup>+</sup></b>	915	0.0006	69	HOMO-2( $\beta$ ) $\rightarrow$ SOMO( $\beta$ )	920, 796
	590	0.151	46	HOMO( $\alpha$ ) $\rightarrow$ LUMO( $\alpha$ )	591
	455	0.017	26	HOMO( $\alpha$ ) $\rightarrow$ LUMO+3( $\alpha$ )	
	435	0.012	11	HOMO-2( $\beta$ ) $\rightarrow$ LUMO( $\beta$ )	
			12	HOMO-2( $\beta$ ) $\rightarrow$ LUMO+4( $\beta$ )	
	418	0.046	15	HOMO-6( $\beta$ ) $\rightarrow$ HOMO( $\beta$ )	380
			13	HOMO-5( $\beta$ ) $\rightarrow$ HOMO( $\beta$ )	

## 2.5.7 Cartesian Coordinates of the Optimized Structures of 3, 3<sup>+</sup>, 4, 4<sup>+</sup>, 5, and 5<sup>+</sup>

### [Cp'Fe( $\mu$ -C<sub>10</sub>H<sub>8</sub>)FeCp\*] (3)

C	-0.507648	3.516304	1.500698	H	-1.260106	-1.484562	2.780536
C	0.898899	3.659060	1.260492	C	0.724046	-1.081929	1.928435
C	1.076030	4.443353	0.056790	H	1.299750	-1.482452	2.763058
C	-0.227358	4.786721	-0.445093	C	1.379039	-0.551774	0.758982
C	-1.206936	4.203629	0.435366	C	-0.714457	0.364441	-0.123184
C	1.995696	3.140923	2.140166	C	0.711084	0.362080	-0.134778
H	2.228449	3.860008	2.944051	C	0.711244	-4.340293	0.389940
H	2.922256	2.971287	1.575539	C	1.162347	-3.734964	-0.843526
H	1.718751	2.190678	2.616211	C	0.002411	-3.371938	-1.630405
C	2.387863	4.889625	-0.513483	C	-1.166745	-3.720822	-0.852163
H	2.323703	5.057989	-1.597246	C	-0.731869	-4.331481	0.384803
H	3.180990	4.149677	-0.338315	Fe	-0.006802	2.723581	-0.355610
H	2.719696	5.836686	-0.054527	Ru	0.003059	-2.256567	0.267636
C	-0.514193	5.655752	-1.632158	H	2.467359	-0.612063	0.701776
H	-1.479844	5.407501	-2.093247	H	-2.457049	-0.616082	0.735710
H	0.259125	5.555921	-2.406321	C	1.583389	-4.975237	1.430864
H	-0.553536	6.720489	-1.345271	H	1.757215	-6.042319	1.207359
C	-2.692835	4.364693	0.327360	H	2.566273	-4.488387	1.486522

H	-3.032006	5.269211	0.860700
H	-3.225828	3.509944	0.765001
H	-3.018148	4.461791	-0.717606
C	-1.143022	2.839858	2.676398
H	-1.332354	3.558226	3.492898
H	-0.504706	2.041919	3.077794
H	-2.106919	2.384221	2.411208
C	1.377225	1.265386	-1.022831
H	2.464878	1.338110	-0.967351
C	0.693294	1.927983	-2.090589
H	1.251509	2.460794	-2.860775
C	-0.725151	1.927292	-2.081624
H	-1.293499	2.458339	-2.845617
C	-1.393899	1.265852	-1.002778
H	-2.480695	1.337508	-0.932365
C	-1.368057	-0.553234	0.778284
C	-0.696712	-1.083018	1.938089

**[Cp'Fe( $\mu$ -C<sub>10</sub>H<sub>8</sub>)FeCp\*]<sup>+</sup> (3<sup>+</sup>)**

C	-0.507648	3.516304	1.500698
C	0.898899	3.659060	1.260492
C	1.076030	4.443353	0.056790
C	-0.227358	4.786721	-0.445093
C	-1.206936	4.203629	0.435366
C	1.995696	3.140923	2.140166
H	2.228449	3.860008	2.944051
H	2.922256	2.971287	1.575539
H	1.718751	2.190678	2.616211
C	2.387863	4.889625	-0.513483
H	2.323703	5.057989	-1.597246
H	3.180990	4.149677	-0.338315
H	2.719696	5.836686	-0.054527
C	-0.514193	5.655752	-1.632158
H	-1.479844	5.407501	-2.093247
H	0.259125	5.555921	-2.406321
H	-0.553536	6.720489	-1.345271
C	-2.692835	4.364693	0.327360
H	-3.032006	5.269211	0.860700
H	-3.225828	3.509944	0.765001
H	-3.018148	4.461791	-0.717606
C	-1.143022	2.839858	2.676398
H	-1.332354	3.558226	3.492898
H	-0.504706	2.041919	3.077794
H	-2.106919	2.384221	2.411208
C	1.377225	1.265386	-1.022831
H	2.464878	1.338110	-0.967351
C	0.693294	1.927983	-2.090589

H	1.128218	-4.919619	2.429271
C	2.588064	-3.627633	-1.295785
H	3.275588	-3.522948	-0.445777
H	2.892736	-4.526828	-1.858562
H	2.736793	-2.760668	-1.953094
C	0.010655	-2.858085	-3.037974
H	0.898874	-2.243819	-3.237570
H	0.009781	-3.686405	-3.769374
H	-0.870111	-2.235541	-3.244829
C	-2.588004	-3.595417	-1.313491
H	-2.721371	-2.726881	-1.972066
H	-2.900430	-4.491070	-1.877698
H	-3.279654	-3.481603	-0.467968
C	-1.619579	-4.955415	1.419255
H	-2.595371	-4.454081	1.470322
H	-1.808080	-6.019247	1.192457
H	-1.169557	-4.908798	2.420397

C	0.724046	-1.081929	1.928435
H	1.299750	-1.482452	2.763058
C	1.379039	-0.551774	0.758982
C	-0.714457	0.364441	-0.123184
C	0.711084	0.362080	-0.134778
C	0.711244	-4.340293	0.389940
C	1.162347	-3.734964	-0.843526
C	0.002411	-3.371938	-1.630405
C	-1.166745	-3.720822	-0.852163
C	-0.731869	-4.331481	0.384803
Fe	-0.006802	2.723581	-0.355610
Ru	0.003059	-2.256567	0.267636
H	2.467359	-0.612063	0.701776
H	-2.457049	-0.616082	0.735710
C	1.583389	-4.975237	1.430864
H	1.757215	-6.042319	1.207359
H	2.566273	-4.488387	1.486522
H	1.128218	-4.919619	2.429271
C	2.588064	-3.627633	-1.295785
H	3.275588	-3.522948	-0.445777
H	2.892736	-4.526828	-1.858562
H	2.736793	-2.760668	-1.953094
C	0.010655	-2.858085	-3.037974
H	0.898874	-2.243819	-3.237570
H	0.009781	-3.686405	-3.769374
H	-0.870111	-2.235541	-3.244829
H	2.566273	-4.488387	1.486522
C	-2.588004	-3.595417	-1.313491

H	1.251509	2.460794	-2.860775
C	-0.725151	1.927292	-2.081624
H	-1.293499	2.458339	-2.845617
C	-1.393899	1.265852	-1.002778
H	-2.480695	1.337508	-0.932365
C	-1.368057	-0.553234	0.778284
C	-0.696712	-1.083018	1.938089

H	-2.721371	-2.726881	-1.972066
H	-2.900430	-4.491070	-1.877698
H	-3.279654	-3.481603	-0.467968
C	-1.619579	-4.955415	1.419255
H	-2.595371	-4.454081	1.470322
H	-1.808080	-6.019247	1.192457
H	-1.169557	-4.908798	2.420397

**[Cp'Fe( $\mu$ -C<sub>10</sub>H<sub>8</sub>)RuCp\*] (4)**

Fe	2.199194	8.016406	10.614390
Fe	1.414802	3.202080	10.414435
C	-0.340635	2.350394	9.627481
C	0.785382	1.451068	9.494461
C	1.335884	1.136521	10.770977
C	0.559471	1.876661	11.714245
C	-0.496690	2.623796	11.058852
C	2.025056	4.710247	9.019981
C	3.075604	3.835243	9.455685
C	3.305390	3.743282	10.852417
C	2.453520	4.518680	11.711880
C	1.317087	6.766567	12.077668
C	0.430526	7.781079	11.600220
C	0.207516	7.880365	10.202014
C	0.883413	6.963866	9.337887
C	1.555301	5.802172	9.835096
C	1.777843	5.702025	11.239851
C	4.065846	8.252991	9.719996
C	4.192806	8.274311	11.148174
C	3.383724	9.362306	11.655929
C	2.762419	10.016290	10.534885
C	3.169838	9.324598	9.339207
C	4.781626	7.329703	8.782676
H	4.988241	6.358204	9.250463
H	5.746854	7.761049	8.465375
H	4.194412	7.136992	7.874382
C	5.061717	7.368357	11.966275
H	6.087963	7.767669	12.037803
H	5.125878	6.363544	11.527656
H	4.681566	7.258412	12.990946
C	3.285808	9.786604	13.089851
H	3.379800	8.932459	13.774502
H	2.328314	10.281525	13.303464
H	4.087431	10.500048	13.347238
C	1.900114	11.240988	10.595175
H	1.326155	11.289313	11.531001
H	1.183682	11.275176	9.762951
H	2.510455	12.158570	10.538654

H	0.398515	2.404836	6.918964
H	-1.246005	2.314230	6.256637
C	-2.615960	2.052517	8.583294
H	-3.185157	2.530148	9.389472
H	-2.533871	0.980522	8.815812
H	-3.200916	2.156565	7.656113
C	-1.353381	4.188788	8.085514
H	-2.093336	4.332927	7.281896
H	-0.395166	4.594459	7.738241
H	-1.668065	4.781600	8.947023
C	2.384357	0.074024	11.073673
C	3.495198	0.053938	10.006571
H	3.086172	-0.117342	9.000514
H	4.209369	-0.757098	10.216687
H	4.048559	1.002661	9.990135
C	3.019196	0.283794	12.460729
H	3.511888	1.263211	12.534302
H	3.774083	-0.493891	12.651953
H	2.268746	0.219480	13.261882
C	1.667006	-1.299651	11.066591
H	0.862848	-1.326503	11.816263
H	2.378597	-2.108570	11.295829
H	1.218819	-1.504541	10.083598
C	-1.593933	3.268852	11.931202
C	-2.637255	2.174977	12.276760
H	-2.155865	1.325410	12.782743
H	-3.138441	1.789204	11.379339
H	-3.408611	2.581754	12.949976
C	-2.318086	4.476758	11.313308
H	-3.020229	4.893608	12.051911
H	-2.905520	4.212140	10.426987
H	-1.606869	5.269556	11.042089
C	-0.993130	3.769990	13.266781
H	-0.189719	4.497041	13.088661
H	-0.593755	2.952067	13.881087
H	-1.780240	4.262646	13.857210
H	2.543892	4.383867	12.791579
H	0.740203	1.881354	12.784554

C	2.810459	9.707356	7.935524	H	1.568377	6.739619	13.139481
H	3.533517	10.434618	7.528083	H	1.163982	1.075247	8.549738
H	1.815775	10.171076	7.880654	H	4.069633	3.083721	11.264114
H	2.811414	8.837577	7.264635	H	1.782128	4.731260	7.956199
C	-1.214882	2.683569	8.395593	H	3.646975	3.243936	8.739561
C	-0.619969	2.042651	7.119678	H	-0.020675	8.492191	12.292563
H	-0.594895	0.945290	7.180790	H	-0.419663	8.670765	9.788865
Fe	2.199194	8.016406	10.614390	H	0.791855	7.090750	8.257971

**[Cp'Fe( $\mu$ -C<sub>10</sub>H<sub>8</sub>)RuCp\*]<sup>+</sup> (4<sup>+</sup>)**

Fe	2.199465	7.864278	10.604884	H	-1.253415	2.354493	6.269764
Fe	1.390362	3.357420	10.423265	C	-2.606984	2.068931	8.597243
C	-0.339046	2.432009	9.634011	H	-3.193110	2.534626	9.397580
C	0.829742	1.580849	9.495267	H	-2.498113	1.000248	8.831558
C	1.363362	1.229202	10.765446	H	-3.190314	2.152703	7.668569
C	0.561515	1.932851	11.712566	C	-1.403233	4.240840	8.097636
C	-0.514705	2.646365	11.072431	H	-2.143016	4.365535	7.292751
C	2.052582	4.784862	8.997163	H	-0.456737	4.673057	7.746690
C	3.094872	3.925590	9.449442	H	-1.741923	4.822897	8.958331
C	3.331288	3.830825	10.844250	C	2.423497	0.176980	11.059021
C	2.501575	4.587730	11.724222	C	3.530859	0.161621	9.988902
C	1.234367	6.753172	12.114689	H	3.123860	0.001606	8.980445
C	0.392969	7.782883	11.615691	H	4.234981	-0.658225	10.190593
C	0.164197	7.884942	10.219625	H	4.103343	1.099716	9.982786
C	0.781726	6.957548	9.338874	C	3.053938	0.371952	12.450183
C	1.530661	5.847276	9.834587	H	3.557323	1.345027	12.541045
C	1.762013	5.742619	11.254471	H	3.803656	-0.410830	12.632974
C	4.078899	8.125903	9.722182	H	2.305090	0.298594	13.251614
C	4.188821	8.160202	11.156072	C	1.696922	-1.193935	11.037580
C	3.368402	9.245812	11.639912	H	0.893050	-1.229947	11.786549
C	2.754393	9.881485	10.504117	H	2.409447	-2.001305	11.262325
C	3.184551	9.184029	9.320070	H	1.253489	-1.393913	10.051907
C	4.829785	7.214532	8.804043	C	-1.619420	3.264655	11.954050
H	5.045154	6.246795	9.274279	C	-2.636352	2.137613	12.274866
H	5.795274	7.668300	8.525620	H	-2.143024	1.294751	12.779488
H	4.279655	7.023761	7.873405	H	-3.122730	1.750943	11.370819
C	5.072532	7.286823	11.989905	H	-3.419957	2.522732	12.944355
H	6.084211	7.719944	12.054404	C	-2.366974	4.463391	11.346924
H	5.173657	6.280667	11.562885	H	-3.082347	4.851344	12.086652
H	4.697030	7.184340	13.016275	H	-2.943301	4.198253	10.454438
C	3.256020	9.694176	13.063461	H	-1.677232	5.280566	11.091216
H	3.379425	8.862089	13.768680	C	-1.033668	3.752398	13.301144
H	2.291348	10.176080	13.269084	H	-0.244605	4.501894	13.148397
H	4.042597	10.432120	13.291455	H	-0.625430	2.934385	13.908756
C	1.889672	11.102734	10.541038	H	-1.833992	4.218818	13.892642
H	1.305593	11.167151	11.468406	H	2.604007	4.449514	12.800930
H	1.191606	11.139239	9.694765	H	0.731143	1.919044	12.784360

H	2.512970	12.010344	10.486836	H	1.473082	6.718968	13.178129
C	2.844128	9.557768	7.911229	H	1.226704	1.239359	8.545274
H	3.563412	10.302804	7.533305	H	4.067291	3.132558	11.239932
H	1.844557	10.004903	7.832779	H	1.806318	4.802603	7.935571
H	2.886871	8.694399	7.234957	H	3.637288	3.295318	8.745470
C	-1.224928	2.739136	8.403382	H	-0.014654	8.530540	12.295311
C	-0.612679	2.111988	7.129115	H	-0.420933	8.711793	9.818400
H	-0.550146	1.016657	7.193607	H	0.667617	7.079272	8.261635
H	0.390076	2.508530	6.912514	H	-1.253415	2.354493	6.269764

**[Cp\*Fe( $\mu$ -C<sub>10</sub>H<sub>8</sub>)RuCp\*] (5)**

Ru	2.280664	8.069160	10.712597	H	-1.576368	2.461759	6.318232
Fe	1.369442	3.092985	10.324810	C	-2.797848	2.108008	8.715251
C	-0.454882	2.315963	9.620552	H	-3.303419	2.554077	9.579942
C	0.638451	1.400968	9.371313	H	-2.722455	1.024485	8.889137
C	1.263696	1.013765	10.592294	H	-3.440511	2.268091	7.835488
C	0.569631	1.725012	11.618222	C	-1.528179	4.244864	8.239783
C	-0.509481	2.524090	11.070382	H	-2.310919	4.441338	7.489650
C	1.931146	4.643057	8.955532	H	-0.584764	4.653428	7.857279
C	2.983306	3.723983	9.280744	H	-1.781574	4.797857	9.146794
C	3.305473	3.560645	10.651461	C	2.302046	-0.085562	10.775198
C	2.540437	4.314020	11.605674	C	3.339103	-0.081939	9.636160
C	1.455391	6.552772	12.151464	H	2.860569	-0.195556	8.652871
C	0.476376	7.543571	11.800573	H	4.043215	-0.918995	9.760455
C	0.158248	7.712685	10.426039	H	3.916443	0.852409	9.625465
C	0.838746	6.886770	9.467623	C	3.031985	0.043658	12.124675
C	1.534760	5.691405	9.854918	H	3.553982	1.006755	12.210220
C	1.851666	5.520550	11.234932	H	3.777267	-0.759228	12.229652
C	4.368467	8.416779	10.089747	H	2.334572	-0.041099	12.970592
C	4.213557	8.759798	11.483944	C	1.549170	-1.439840	10.753670
C	3.255911	9.839751	11.588347	H	0.795509	-1.483166	11.553315
C	2.798693	10.155595	10.255067	H	2.252174	-2.275404	10.897761
C	3.473920	9.269269	9.332615	H	1.032008	-1.587721	9.794622
C	5.351108	7.439654	9.520507	C	-1.532390	3.145270	12.044947
H	5.561695	6.623570	10.224164	C	-2.569180	2.051678	12.409771
H	6.311416	7.931444	9.283630	H	-2.070473	1.171719	12.841585
H	4.976832	6.983825	8.594064	H	-3.136670	1.716589	11.531570
C	5.004010	8.178065	12.617517	H	-3.286155	2.436971	13.152108
H	5.951798	8.725944	12.756439	C	-2.276520	4.391005	11.535519
H	5.254268	7.124624	12.435159	H	-2.919173	4.781451	12.339725
H	4.451704	8.230824	13.565204	H	-2.928401	4.177115	10.681032
C	2.899255	10.581984	12.840950	H	-1.573048	5.186627	11.252940
H	2.949439	9.932226	13.725054	C	-0.832350	3.573645	13.357119
H	1.883338	10.997003	12.790477	H	-0.029834	4.296108	13.157804
H	3.591049	11.424849	13.012844	H	-0.407032	2.722052	13.904584
C	1.884980	11.284510	9.883591	H	-1.567667	4.049855	14.022976
H	1.145943	11.483726	10.671663	H	2.702722	4.125941	12.668745

H	1.334641	11.071491	8.957396
H	2.453513	12.216686	9.721913
C	3.375493	9.318017	7.837211
H	4.126401	10.008225	7.415716
H	2.387425	9.665792	7.506909
H	3.548390	8.330134	7.389918
C	-1.399936	2.724232	8.465995
C	-0.901305	2.137970	7.124393
H	-0.893428	1.038664	7.129914
H	0.108740	2.493244	6.874727

H	0.820668	1.674841	12.673007
H	1.761069	6.462784	13.195159
H	0.945000	1.062470	8.387256
H	4.077639	2.863588	10.976942
H	1.617499	4.719954	7.913152
H	3.487418	3.151905	8.501534
H	0.009373	8.161491	12.567459
H	-0.560431	8.465612	10.102532
H	0.656828	7.058327	8.405587
H	-1.576368	2.461759	6.318232

**[Cp\*Fe( $\mu$ -C<sub>10</sub>H<sub>8</sub>)RuCp\*]<sup>+</sup> (5<sup>+</sup>)**

Ru	2.244023	7.963031	10.680462
Fe	1.280538	3.308883	10.373479
C	-0.470489	2.384345	9.647622
C	0.703691	1.574871	9.363312
C	1.333787	1.143758	10.561471
C	0.591643	1.756472	11.612224
C	-0.542842	2.489635	11.107165
C	1.825927	4.834371	9.006139
C	2.919801	3.992973	9.370924
C	3.209847	3.844657	10.749822
C	2.379661	4.537364	11.685187
C	1.181551	6.722111	12.215195
C	0.339934	7.787999	11.784981
C	0.053652	7.941812	10.401036
C	0.613887	7.029627	9.461292
C	1.370639	5.897215	9.891208
C	1.659016	5.739739	11.294586
C	4.378064	8.131721	10.104883
C	4.213997	8.535840	11.481639
C	3.330133	9.680488	11.511627
C	2.940419	9.977323	10.150361
C	3.584255	9.015957	9.283255
C	5.289302	7.054123	9.608342
H	5.409764	6.251111	10.346224
H	6.290559	7.467673	9.402366
H	4.921024	6.605868	8.676809
C	4.936510	7.952567	12.656634
H	5.914776	8.444557	12.783391
H	5.123496	6.878822	12.528057
H	4.376939	8.092059	13.590212
C	2.990428	10.496215	12.720789
H	2.965959	9.886080	13.632710
H	2.018142	10.994676	12.618236
H	3.747712	11.282777	12.872773
C	2.126182	11.153296	9.706909

H	-1.630828	2.518752	6.361792
C	-2.803211	2.040672	8.753687
H	-3.336616	2.433457	9.626869
H	-2.657812	0.960775	8.900407
H	-3.455923	2.177356	7.878971
C	-1.678975	4.269905	8.326947
H	-2.470714	4.434662	7.580741
H	-0.764735	4.749398	7.952638
H	-1.974675	4.778969	9.247795
C	2.443277	0.110267	10.698758
C	3.487407	0.235525	9.573442
H	3.028311	0.157681	8.577740
H	4.227058	-0.573706	9.656613
H	4.028837	1.190386	9.628244
C	3.147100	0.208020	12.064649
H	3.616139	1.190977	12.215175
H	3.936546	-0.553810	12.133302
H	2.450384	0.030785	12.896323
C	1.765930	-1.281422	10.593212
H	1.007215	-1.414648	11.377472
H	2.517648	-2.076560	10.706526
H	1.274702	-1.411684	9.618577
C	-1.589221	3.017805	12.110975
C	-2.559400	1.848803	12.425108
H	-2.014688	0.984521	12.831020
H	-3.104351	1.514778	11.533447
H	-3.298067	2.167943	13.175519
C	-2.401147	4.239252	11.648535
H	-3.063940	4.559213	12.465749
H	-3.039608	4.025211	10.785073
H	-1.746108	5.087088	11.400416
C	-0.912411	3.425607	13.441875
H	-0.152911	4.204033	13.283188
H	-0.440793	2.578731	13.956976
H	-1.674469	3.828211	14.123928

H	1.391114	11.451825	10.465163	H	2.519056	4.354598	12.751255
H	1.588460	10.949652	8.772248	H	0.842738	1.672287	12.664688
H	2.781419	12.021164	9.526098	H	1.439310	6.630096	13.270582
C	3.544513	9.019390	7.786091	H	1.037480	1.314730	8.364420
H	4.360138	9.644355	7.386897	H	3.981285	3.155285	11.090463
H	2.601450	9.429154	7.402818	H	1.531397	4.887817	7.957848
H	3.672011	8.011106	7.372136	H	3.453833	3.413970	8.618156
C	-1.451566	2.754845	8.509867	H	-0.046947	8.503908	12.509159
C	-0.923071	2.233922	7.152918	H	-0.554284	8.777032	10.055353
H	-0.833104	1.138733	7.134956	H	0.431752	7.173300	8.396216
H	0.052429	2.670380	6.893124				

### 2.5.8 Crystallographic Data of 3, 4, 4[PF<sub>6</sub>], and 5

**Table S2.** Crystallographic data and structure refinement of 3, 4, 4[PF<sub>6</sub>], and 5.

	3	4	4[PF <sub>6</sub> ]	5
Empirical formula	C <sub>37</sub> H <sub>52</sub> Fe <sub>2</sub>	C <sub>37</sub> H <sub>52</sub> FeRu	C <sub>37</sub> H <sub>52</sub> F <sub>6</sub> PFeRu	C <sub>30</sub> H <sub>38</sub> FeRu
Crystal size [mm <sup>3</sup> ]	0.30×0.14×0.03	0.09×0.0×0.02	0.00×0.18×0.21	0.10×0.05×0.02
Color and shape	red rods	red plates	red plates	dark green plates
Formula weight [g mol <sup>-1</sup> ]	608.49	653.71	798.68	555.52
Crystal system	monoclinic	monoclinic	orthorhombic	orthorhombic
Space group	<i>P</i> 2/ <i>c</i>	<i>P</i> 2 <sub>1</sub> / <i>c</i>	<i>Pbca</i>	<i>P</i> 2 <sub>1</sub> 2 <sub>1</sub> 2 <sub>1</sub>
Absorption correction	analytical	multi-scan	multi-scan	multi-scan
Transmission min/max	0.926/0.615	0.9811/0.9188	0.41251/1.0000	0.9769/0.8917
<i>a</i> [Å]	14.1265(3)	9.2059(11)	16.2256(2)	8.0972(5)
<i>b</i> [Å]	9.1841(2)	24.692(3)	17.4125(2)	15.1917(9)
<i>c</i> [Å]	24.2253(5)	13.9429(16)	25.6091(2)	20.7875(12)
α[°]	90	90	90	90
β[°]	91.143(2)	89.984(2)	90	90
γ[°]	90	90	90	90
<i>V</i> [Å <sup>3</sup> ]	3142.35(12)	3169.4(6)	7235.29(13)	2557.1(3)
<i>Z</i>	4	4	8	4
<i>T</i> [K]	123(2)	153(2)	123(2)	123(2)
λ[Å]	1.54178	0.71073	1.54184	0.71073
ρ <sub>calc</sub> [g/cm <sup>3</sup> ]	1.286	1.370	1.466	1.443
μ (mm <sup>-1</sup> )	7.556	0.958	7.489	1.173
Theta range [°]	3.13–73.67	0.82–28.76	3.5–73.5	1.66–28.73
Reflections collected to θ <sub>max</sub> [°]	9466	34235	32092	27449
Unique reflections ( <i>R</i> <sub>int</sub> )	9466 (0.0000)	8234 (0.0583)	7165 (0.042)	6619 (0.0334)
Refl. obs. [ <i>I</i> > 2σ( <i>I</i> )]	8881	7000	6217	
Parameters	367	367	469	307
Completeness to θ	0.998	0.998	0.999	0.100

<i>R</i> -values [ $I > 2\sigma(I)$ ]	0.0553/0.1663	0.0916/0.0404	0.0884/0.0463	0.0302/0.0727
<i>R</i> -values (all data)	0.1739/0.0605	0.0967/0.0518	0.0827/0.0370	0.0335/0.0741
GOF on $F^2$	1.126	1.024	1.062	1.053
Residual density [ $\text{e}\text{\AA}^{-3}$ ]	-0.609/0.605	-0.813/0.773	-0.53/0.87	-0.349/0.549
Flack parameter	/	/	/	0.69(3)
CCDC-	942393	942394	942395	942396

## References

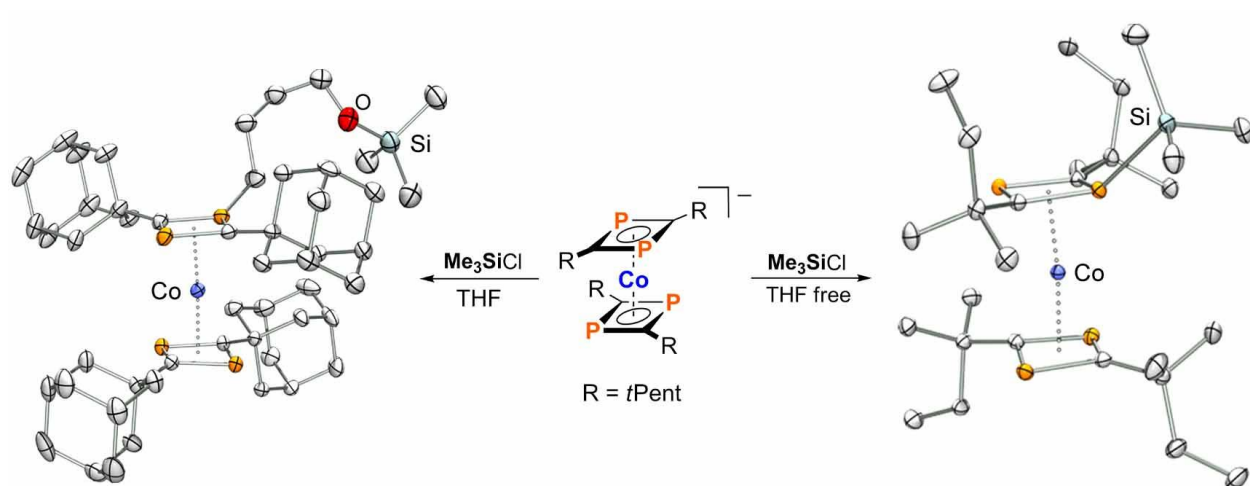
- 1 (a) A. Togni, R. L. Halterman, *Metallocenes*, Wiley-VCH, Weinheim, **2008**; (b) P. Štěpnička, *Ferrocenes: Ligands, Materials and Biomolecules*, J. Wiley, Hoboken, **2008**.
- 2 (a) T. J. Kealy, P. L. Pauson, *Nature* **1951**, *168*, 1039; (b) G. Wilkinson, M. Rosenblum, M. C. Whiting, R. B. Woodward, *J. Am. Chem. Soc.* **1952**, *74*, 2125; (c) E. O. Fischer, W. Z. Pfab, *Z. Naturforsch. B.* **1952**, *7*, 377.
- 3 Reviews on the history of ferrocene's discovery: (a) P. Laszlo, R. Hoffmann, *Angew. Chem. Int. Ed.* **2000**, *39*, 123; (b) P. L. Pauson, *J. Organomet. Chem.* **2001**, *3*, 637; (c) H. Werner, *Angew. Chem. Int. Ed.* **2012**, *51*, 6052.
- 4 (a) D. Astruc, *Electron Transfer and Radical Processes in Transition Metal Chemistry*, VCH Publishers: New York, **1995**, chapter 4; (b) D. O. Cowan, C. LeVanda, J. Park, F. Kaufman, *Acc. Chem. Res.* **1973**, *6*, 1; (c) D. Astruc, *Acc. Chem. Res.* **1997**, *30*, 383; (d) A. Ceccon, S. Santi, L. Orian, A. Bisello, *Coord. Chem. Rev.* **2004**, *248*, 683; (e) P. Aguirre-Etcheverry, D. O'Hare, *Chem. Rev.* **2010**, *110*, 4839.
- 5 (a) F. Paul, C. Lapinte, *Coord. Chem. Rev.* **1998**, *178-180*, 431; (b) S. Barlow, D. O'Hare, *Chem. Rev.* **1997**, *97*, 637; (c) W. Kaim, A. Klein, M. Glöckle, *Acc. Chem. Res.* **2000**, *33*, 755; (d) K. D. Demadis, C. M. Hartshorn, T. J. Meyer, *Chem. Rev.* **2001**, *101*, 2655; (e) M. D. Ward, J. A. McCleverty, *J. Chem. Soc., Dalton Trans.* **2002**, 275; (f) J.-P. Launay, *Chem. Soc. Rev.* **2001**, *30*, 386; (g) S. Szafert, J. A. Gladysz, *Chem. Rev.* **2003**, *103*, 4175; (h) T. Ren, *Organometallics* **2005**, *24*, 4854.
- 6 Selected examples of homobimetallic diiron complexes with hydrocarbon bridges other than naphthalene or anthracene, including, for example, biphenyl, triphenylene, pyrene, phenanthrene, the fulvalene dianion, the pentalene dianion, and the s-indacene dianion: (a) U. T. Mueller-Westerhoff, P. Eilbracht, *J. Am. Chem. Soc.* **1972**, *94*, 9272; (b) D. O. Cowan, C. LeVanda, R. L. Collins, G. A. Candela, U. T. Mueller-Westerhoff, P. Eilbracht, *Chem. Soc. Chem. Commun.* **1973**, *0*, 329; (c) C. LeVanda, K. Bechgaard, D. O. Cowan, U. T. Mueller-Westerhoff, P. Eilbracht, G. A. Candela, R. L. Collins, *J. Am. Chem. Soc.* **1976**, *98*, 3181; (d) M. H. Desbois, D. Astruc, J. Guillin, J. P. Mariot, F. Varret, *J. Am. Chem. Soc.* **1985**, *107*, 5280; (e) R. J. Webb, S. J. Geib, D. L. Staley, A. L. Rheingold, N. D. Hendrickson, *J. Am. Chem. Soc.* **1990**, *112*, 5031; (f) J. M. Manriquez, M. D. Ward, W. M. Reiff, J. C. Calabrese, N. L. Jones, P. J. Carroll, E. E. Bunel, J. S. Miller, *J. Am. Chem. Soc.* **1995**, *117*, 6182; (g) H. Rabaa, M. Lacoste, M.-H. Delville-Desbois, J. Ruiz, B. Gloaguen, N. Ardoin, D. Astruc, A. L. Beuze, J.-Y. Saillard, *Organometallics* **1995**, *14*, 5078; (h) M. Lacoste, M.-H. Delville-Desbois, N. Ardoin, D. Astruc, *Organometallics* **1997**, *16*, 2343; (i) J. Moss, J. Thomas, A. Ashley, A. R. Cowley, D. O'Hare, *Organometallics* **2006**, *25*, 4279.
- 7 A. Frings, *Dissertation*, Ruhr-Universität Bochum **1988**.
- 8 J. A. Rheingold, K. L. Virkaitis, G. B. Carpenter, S. Sun, D. A. Sweigart, P. T. Czech, K. R. Overly, *J. Am. Chem. Soc.* **2005**, *127*, 11146.
- 9 P. Klusmann, *Dissertation*, Ruhr-Universität-Bochum **1993**.
- 10 An anthracene-bridged dication  $[\text{CpFe}(\mu\text{-C}_{14}\text{H}_{10})\text{FeCp}]^{2+}$  related to type **A** was characterized by polarographic measurements, NMR and UV/vis spectroscopy: (a) W. H. Morrison Jr., E. Y. Ho, D. N. Hendrickson, *J. Am. Chem. Soc.* **1974**, *96*, 3603; (b) W. H. Morrison Jr., E. Y. Ho, D. N. Hendrickson, *Inorg. Chem.* **1975**, *14*, 500.

- 11 (a) R. Wolf, A. W. Ehlers, J. C. Slootweg, M. Lutz, D. Gudat, M. Hunger, A. L. Spek, K. Lammertsma, *Angew. Chem. Int. Ed.* **2008**, *47*, 4584; (b) R. Wolf, J. C. Slootweg, A. W. Ehlers, F. Hartl, B. de Bruin, M. Lutz, A. L. Spek, K. Lammertsma, *Angew. Chem. Int. Ed.* **2009**, *48*, 3104; (c) R. Wolf, A. W. Ehlers, M. M. Khusniyarov, F. Hartl, B. de Bruin, G. J. Long, F. Grandjean, M. Schappacher, R. Pöttgen, J. C. Slootweg, M. Lutz, A. L. Spek, K. Lammertsma, *Chem. Eur. J.* **2010**, *16*, 14322; (d) R. Wolf, N. Ghavtadze, K. Weber, E.-M. Schnöckelborg, B. de Bruin, A. W. Ehlers, K. Lammertsma, *Dalton Trans.* **2010**, *39*, 1453; (e) K. Weber, E.-M. Schnöckelborg, R. Wolf, *Chem. Cat. Chem.* **2011**, *3*, 1572; (f) R. Wolf, E.-M. Schnöckelborg, *Chem. Commun.* **2010**, 2832; (g) E.-M. Schnöckelborg, J. J. Weigand, R. Wolf, *Angew. Chem. Int. Ed.* **2011**, *50*, 6657; (h) E.-M. Schnöckelborg, M. Khusniyarov, B. de Bruin, F. Hartl, T. Langer, M. Eul, S. Schulz, R. Pöttgen, R. Wolf, *Inorg. Chem.* **2012**, *51*, 6719.
- 12 Lead references to related pioneering work in the area: (a) K. Jonas, *Pure Appl. Chem.* **1990**, *62*, 1169; (b) C. Brodt, S. Niu, H. Pritzkow, M. Stephan, U. Zenneck, *J. Organomet. Chem.* **1993**, *459*, 283; (c) C. Brodt, S. Niu, H. Pritzkow, M. Stephan, U. Zenneck, *J. Organomet. Chem.* **1993**, *459*, 283. (d) H. Kubo, M. Hirano, S. Komiya, *J. Organomet. Chem.* **1998**, *556*, 89; (e) J. E. Ellis, *Inorg. Chem.* **2006**, *45*, 3167; (f) W. W. Brennessel, R. E. Jilek, J. E. Ellis, *Angew. Chem. Int. Ed.* **2007**, *46*, 6132; (g) W. W. Brennessel, J. E. Ellis, *Inorg. Chem.* **2012**, *51*, 9076.
- 13 E.-M. Schnöckelborg, F. Hartl, T. Langer, R. Pöttgen, R. Wolf, *Eur. J. Inorg. Chem.* **2012**, 1632.
- 14 T. Hatanaka, Y. Ohki, T. Kamachi, T. Nakayama, K. Yoshizawa, M. Katada, K. Tatsumi, *Chem. Asian J.* **2012**, *7*, 1231.
- 15 A. D. Becke, *Phys. Rev. A* **1988**, *38*, 3098.
- 16 J. P. Perdew, *Phys. Rev. B* **1986**, *33*, 8822.
- 17 J. P. Perdew, *Phys. Rev. B* **1986**, *34*, 7406.
- 18 A. Schäfer, H. Horn, R. J. Ahlrichs, *J. Chem. Phys.* **1992**, *97*, 2571.
- 19 F. Weigend, R. Ahlrichs, *J. Chem. Phys.* **2005**, *7*, 3297.
- 20 F. Neese, The Orca program system *Wiley Interdiscip. Rev.-Comput. Mol. Sci.* **2012**, *2*, 73.
- 21 The isomer **5'** features very similar <sup>1</sup>H NMR resonances as **5**. Two resonances at 1.70 ppm und 1.85 ppm presumably correspond to the Cp\* ligands on iron and ruthenium, while resonances at 2.03, 2.17, 4.69 and 4.89 ppm are assigned to the naphthalene ligand. A singlet at +2.13 ppm may be assigned to homobimetallic [Cp\*Ru(μ-C<sub>10</sub>H<sub>8</sub>)RuCp\*] (**6**), which gives rise to one singlet at 2.13 ppm for Cp\* and only two resonances for the naphthalene ligand at 3.84 und 4.00 ppm.  
Support for the presence of **6** stems from the EI mass spectrum of the isolated compound where the molecular ion **6**<sup>+</sup> (m/z = 601) was detected with an intensity of 9.2%. The molecular ion **5**<sup>+</sup> (m/z = 556, 100.0%) is the base peak. Further peaks may be assigned to the fragments [Cp\*Ru(η<sup>4</sup>-C<sub>10</sub>H<sub>8</sub>)]<sup>+</sup> (m/z = 365, 93.2%), [Cp\*Fe(η<sup>4</sup>-C<sub>10</sub>H<sub>8</sub>)]<sup>+</sup> (m/z = 319, 14.9%), [Cp\*<sub>2</sub>Ru]<sup>+</sup> (m/z = 372, 5.7%), [Cp\*<sub>2</sub>Fe]<sup>+</sup> (m/z = 326, 6.8%), and [C<sub>10</sub>H<sub>8</sub>]<sup>+</sup> (m/z = 128, 86.3%).
- 22 E.-M. Schnöckelborg, *Dissertation*, University of Münster, **2011**.
- 23 M. Maekawa, C. G. Daniliuc, M. Freytag, P. J. Jones, M. D. Walter, *Dalton Trans.* **2012**, *41*, 10317.
- 24 A. R. Allouche, *J. Comput. Chem.* **2011**, *32*, 174.
- 25 M. Krejčík, M. Daněk, F. Hartl, *J. Electroanal. Chem.* **1991**, *317*, 179.
- 26 A. D. Becke, *J. Chem. Phys.* **1993**, *98*, 5648.
- 27 C. T. Lee, W. T. Yang, R. G. Parr, *Phys. Rev. B* **1988**, *37*, 785.
- 28 F. Neese, *Inorg. Chim. Acta* **2002**, *337*, 181.
- 29 F. Neese, T. Petrenko, P. in Gülich, E. Bill, A. X. Trautwein, (eds.), *Mössbauer Spectroscopy and Transition Metal Chemistry*, Springer, Heidelberg, **2011**, p.163.
- 30 C. K. Wertheim, R. H. Herber, *J. Chem. Phys.* **1963**, *38*, 2106.

- 31 (a) T. Y. Dong, D. N. Hendrickson, C. G. Pierpont, M. F. Moore, *J. Am. Chem. Soc.* **1986**, *108*, 963;  
 (b) T. Y. Dong, T. Kambara, D. N. Hendrickson, *J. Am. Chem. Soc.* **1986**, *108*, 4423; (c) T. Y. Dong,  
 T. Kambara, D. N. Hendrickson, *J. Am. Chem. Soc.* **1986**, *108*, 5857; (d) T. Y. Dong, X. H. Huang, C.  
 K. Chang, Y. S. Wen, S. L. Lee, J. A. Chen, W. Y. Yeh, A. Yeh, *J. Am. Chem. Soc.* **1993**, *115*, 6357.
- 32 E. V. Dehmlow, C. Bollmann, *Z. Naturforsch. B*, **1993**, *48*, 457.
- 33 (a) N. Oshima, H. Suzuki, Y. Moro-Oka, *Chem. Lett.*, **1984**, 1161; (b) P. J. Fagan, M. D. Ward, J. C.  
 Calabrese, *J. Am. Chem. Soc.*, **1989**, *111*, 1698.
- 34 K. Jonas, P. Klusmann, R. Goddard, *Z. Naturforsch. B*, **1995**, *50*, 394.
- 35 Prof. Frank Neese, Max Planck Institute for Chemical Energy Conversion, Mülheim/Ruhr, Germany
- 36 (a) R. Ahlrichs, M. Bär, H.-P. Baron, R. Bauernschmitt, S. Böcker, M. Ehrig, K. Eichkorn, S. Elliott, F.  
 Furche, F. Haase, M. Häser, C. Hättig, H. Horn, C. Huber, U. Huniar, M. Kattannek, A. Köhn, C.  
 Kölmel, M. Kollwitz, K. May, C. Ochsenfeld, H. Öhm, A. Schäfer, U. Schneider, O. Treutler, K.  
 Tsereteli, B. Unterreiner, M. von Arnim, F. Weigend, P. Weis, H. Weiss, Turbomole Version 5,  
 January **2002**. Theoretical Chemistry Group, University of Karlsruhe; (b) O. Treutler, R. Ahlrichs,  
*J. Chem. Phys.* **1995**, *102*, 346; (c) Turbomole basis set library, Turbomole Version 6.4, see (a);  
 (d) A. Schäfer, H. Horn, R. Ahlrichs, *J. Chem. Phys.* **1992**, *97*, 2571; (e) D. Andrae, U.  
 Haeussermann, M. Dolg, H. Stoll, H. Preuss, *Theor. Chim. Acta* **1990**, *77*, 123; (f) A. Schäfer, C.  
 Huber, R. Ahlrichs, *J. Chem. Phys.* **1994**, *100*, 5829.
- 37 (a) PQS version 2.4, **2001**, Parallel Quantum Solutions, Fayetteville, Arkansas, USA (the Baker  
 optimizer is available separately from PQS upon request). (b) J. Baker, *J. Comput. Chem.* **1986**, *7*,  
 385.
- 38 (a) C. Lee, W. Yang, R. G. Parr, *Phys. Rev. B* **1988**, *37*, 785; (b) A. D. Becke, *J. Chem. Phys.* **1993**, *98*,  
 1372; (c) A. D. Becke, *J. Chem. Phys.* **1993**, *98*, 5648.
- 39 Some references and reviews on DFT approaches to EPR parameters: (a) E. van Lenthe, A. van der  
 Avoird, P. E. S. Wormer, *J. Chem. Phys.* **1997**, *107*, 2488. (b) E. van Lenthe, A. van der Avoird, P. E.  
 S. Wormer, *J. Chem. Phys.* **1998**, *108*, 4783; (c) F. Neese, *Curr. Opin. Chem. Biol.* **2003**, *7*, 125;  
 (d) F. Neese, E. Solomon, in *Magnetoscience - From Molecules to Materials*; J. S. Miller, M. Drillon,  
 Eds.; Wiley: New York, **2003**; pp 345; (e) G. Peng, J. Nichols, E. A. McCullough, J. Spence, *J. Inorg.*  
*Chem.*, **1994**, *33*, 2857.
- 40 (a) C. Lee, W. Yang, R. G. Parr, *Phys. Rev. B* **1988**, *37*, 785; (b) A. D. Becke, *J. Chem. Phys.* **1993**, *98*,  
 1372; (c) A. D. Becke, *J. Chem. Phys.* **1993**, *98*, 5648.
- 41 a) *SCALE3ABS*, *CrysAlisPro*, Aglient Technologies Inc., Oxford, GB, **2012**; b) G. M. Sheldrick,  
*SADABS*, Bruker AXS, Madison, USA, **2007**.
- 42 R. C. Clark, J. S. Reid, *Acta Cryst.* **1995**, *A51*, 887.
- 43 G. M. Sheldrick, *Acta Cryst.* **2008**, *A64*, 112.
- 44 A. Altomare, M. C. Burla, M. Camalli, G. L. Cascarno, C. Giacovazzo, A. G. G. Moliterni, G. Polidori,  
 R. Spagna, *J. Appl. Cryst.* **1999**, *32*, 115.

### 3 Towards Trimethylsilylated Phospha-Organometallic Compounds: Reactions of $[\text{Co}(\text{P}_2\text{C}_2\text{R}_2)_2]^-$ Anions with $\text{Me}_3\text{SiCl}$ <sup>[a]</sup>

Jennifer Malberg, and Robert Wolf



[a] Unpublished results



### 3.1 Introduction

The cyclodimerization of phosphalkynes  $R-C\equiv P$  in the coordination sphere of a transition metal atom is an elegant method for the preparation of metal-coordinated diphosphacyclobutadienes.<sup>1–3</sup> Typically, 1,3-diphosphacyclobutadienes are formed by a head-to-tail dimerization of phosphalkynes with bulky substituents such as  $tBu-C\equiv P$ . The less sterically demanding phosphalkyne  $Me-C\equiv P$  or specific transition metal fragments favor the formation of 1,2-diphosphacyclobutadienes through a head-to-head dimerization, however.<sup>4–6</sup> Recently, we have found that anionic bis(diphosphacyclobutadiene) complexes of type  $[M(\eta^4-P_2C_2R_2)_2]^-$  (**A–D**, Chart 1,  $M = Co$ ,  $R = tBu$ ,  $tPent$ ,  $Ad$ ;  $M = Fe$ ,  $R = tBu$ ) are readily accessible by reacting the low-valent metalates  $[M(C_{14}H_{10})_2]^-$  with phosphalkynes.<sup>7–11</sup> Complexes **A–D** were thoroughly characterized by spectroscopic techniques, electrochemical methods and DFT calculations.<sup>9</sup> The molecular structures feature  $\eta^4$ -coordinated diphosphacyclobutadiene ligands in a staggered orientation due to steric repulsion of the substituents. A reactivity study of the diamagnetic cobalt complex **B** with different electrophiles revealed its versatile reactivity.<sup>7</sup> The neutral compound  $[CoH(\eta^4-P_2C_2tBu_2)_2]$  (**E**) was obtained from the reaction of the cobalt complex with  $HCl(OEt_2)$ . In the  $^1H$  NMR spectrum, the proton gives rise to a remarkably shifted quintet at  $-4.5$  ppm. The solution and solid-state  $^{31}P$  NMR spectra show only one broad resonance at room temperature, indicating a dynamic structure. Upon lowering the temperature, the slow limit exchange is approached, and the broad resonances split into three distinct signals. These observations reveal the dynamic behavior of complex **E**, in which the hydrogen introduced by the protonation of **B** is not statically bound to cobalt or one of the phosphorus atoms of the  $P_2C_2$  rings. The hydrogen atom instead appears to interact with cobalt and phosphorus at the same time. The temperature dependent NMR spectra are explained by a fluxional process, where the hydrogen adopts a bridging position as shown in Chart 1. At higher temperature, the hydrogen interconverts rapidly between all eight  $Co-H-P$  and  $Co-H-C$ -bridged minima of lower-energy transition states calculated by DFT methods at 8.0 and 4.5 kcal mol<sup>-1</sup>. At very low temperatures, the slow exchange limit is approached, which results in the observed asymmetric  $^{31}P\{^1H\}$  NMR spectrum with three peaks in a 1:2:1 ratio.

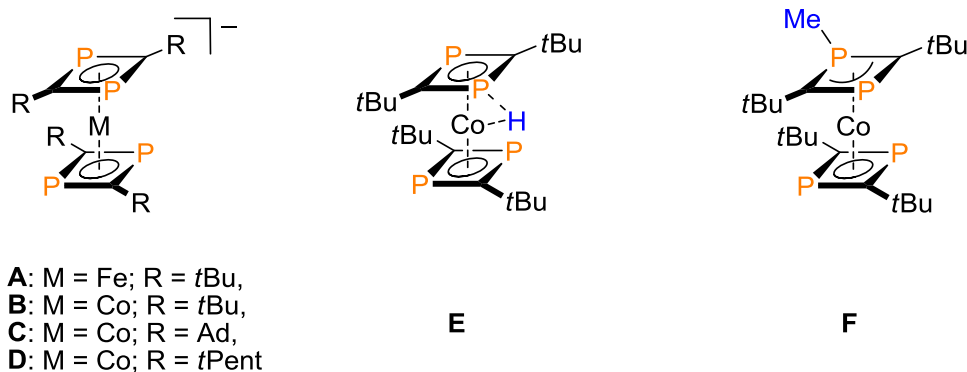


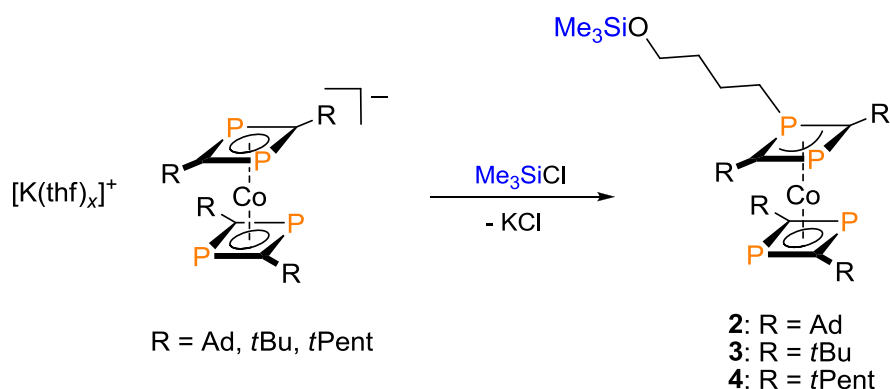
Chart 1

The reaction of **B** with methyl iodide led to an entirely different result. The methyl group shows no interaction with the cobalt center, but binds exclusively to one phosphorus atom of the diphosphacyclobutadiene ligand in complex  $[\text{Co}(\eta^4\text{-P}_2\text{C}_2t\text{Bu}_2\text{Me})(\eta^4\text{-P}_2\text{C}_2t\text{Bu}_2)]$  (**F**).<sup>7</sup>

Encouraged by these results, we became interested to extend the reactivity profile of our homoleptic sandwich anions further. We wondered if silylated compounds of type  $[\text{Co}(\eta^4\text{-P}_2\text{C}_2\text{R}_2\text{SiR}'_3)(\eta^4\text{-P}_2\text{C}_2\text{R}_2)]$ , which should contain a phosphorus-silicon bond, are also accessible by reacting complexes of type **B–D** with silicon electrophiles. For our initial studies, we decide to focus on reactions with the “bulky proton”  $\text{Me}_3\text{Si}^+$ . Here, we present the synthesis, characterization and first insights into the reactivity of the silylated phospho-organometallic compound  $[\text{Co}(\eta^4\text{-P}_2\text{C}_2t\text{Pent}_2\text{SiMe}_3)(\eta^4\text{-P}_2\text{C}_2t\text{Pent}_2)]$  (**1**).

## 3.2 Results

Initial attempts to synthesize the targeted trimethylsilylated sandwich complexes via straightforward salt metathesis of the potassium salts  $[\text{K}(\text{thf})_2\{\text{Co}(\text{P}_2\text{C}_2t\text{Bu}_2)_2\}]$  (**K-B**),  $[\text{K}(\text{thf})_4\{\text{Co}(\text{P}_2\text{C}_2\text{Ad}_2)_2\}]$  (**K-C**), and  $[\text{K}(\text{thf})_3\{\text{Co}(\text{P}_2\text{C}_2t\text{Pent}_2)_2\}]$  (**K-D**) with  $\text{Me}_3\text{SiCl}$  in THF led to an unexpected result. NMR spectroscopic monitoring revealed that  $[\text{Co}(\eta^4\text{-P}_2\text{C}_2\text{R}_2(\text{CH}_2)_4\text{OSiMe}_3)(\eta^4\text{-P}_2\text{C}_2\text{Ad}_2)]$  (**2**:  $\text{R} = \text{Ad}$ , **3**:  $\text{R} = t\text{Bu}$ , **4**:  $\text{R} = t\text{Pent}$ ) are formed in these reactions in high yield (Scheme 1). Complexes **2–4** result from the cleavage of a C–O bond of THF and the insertion of the cleaved THF molecule between phosphorus and silicon. The formation of complex **2–4** might be explained by the *in situ* generation of the  $\text{Me}_3\text{Si}^+$  cation, which is highly oxophilic and attacks a THF molecule instead of the  $[\text{Co}(\text{P}_2\text{C}_2\text{R}_2)_2]^-$  anion. Attempts to avoid the C–O bond cleavage by changing the solvent to toluene also led to the same products **2–4**. This observation indicates that even small amounts of THF, which remain coordinated to potassium in the dried compound, are entirely sufficient to cause a cleavage reaction. The cleavage and insertion is observed with similar efficiency irrespective of whether the bulky adamantyl substituent or the less strongly shielding *t*Bu and *t*Pent substituents are used.



**Scheme 1.** Synthesis of the insertion products **2–4**.

Compounds **2–4** were isolated in moderate yields of 37–56% from *n*-hexane or *n*-pentane. They were initially characterized by multinuclear NMR spectroscopy in C<sub>6</sub>D<sub>6</sub> solution. Each <sup>1</sup>H and <sup>13</sup>C{<sup>1</sup>H} NMR spectrum features one signal for the SiMe<sub>3</sub> group in the usual range (0.06–0.09 ppm) with clearly resolved <sup>29</sup>Si-<sup>1</sup>H couplings in the <sup>1</sup>H NMR spectra. In addition, four resonances for the CH<sub>2</sub> groups of the (CH<sub>2</sub>)<sub>4</sub>OSiMe<sub>3</sub> fragment and three sets of signals for the different adamantyl, *tert*-butyl or *tert*-pentyl substituents are detected. The <sup>13</sup>C{<sup>1</sup>H} NMR spectra of **3** and **4** show three signals for the chemically different carbon atoms of the diphosphacyclobutadiene ligands. The NMR data are comparable to those found for the methylated complex **F** (Chart 1). The <sup>31</sup>P{<sup>1</sup>H} NMR spectra of complexes **2–4** feature three resonances in the expected ratio of 1:2:1. The assignment of the <sup>31</sup>P{<sup>1</sup>H} NMR resonances of **2**, **3**, and **4** is summarized in Table 1. Based on their intensity, the singlets at 19.1 (**2**), 25.8 (**3**), and 29.4 ppm (**4**), respectively, may be assigned to the phosphorus atoms of the “free” ligand (P3 and P4, see Figure 1 for the labeling scheme). The phosphorus atoms of the substituted ring (P1 and P2) give rise to doublets due to coupling of both phosphorus nuclei. In agreement with the NMR data of complex **F**, we assign the resonances shifted to higher field at –57.3 (**2**; <sup>2</sup>*J*(P,P) = 16.38 Hz), –50.0 (**3**; <sup>2</sup>*J*(P,P) = 14.71 Hz), and –45.5 ppm (**4**, <sup>2</sup>*J*(P,P) = 15.04 Hz) to the alkylated phosphorus atom P1. The remaining doublets at 55.5 ppm for both **2** (<sup>2</sup>*J*(P,P) = 15.85 Hz) and **3** (<sup>2</sup>*J*(P,P) = 14.57 Hz), and 55.4 ppm for **4** (<sup>2</sup>*J*(P,P) = 14.41 Hz) arise from the “free” phosphorus atom P2.

**Table 1.** The assignment of the <sup>31</sup>P{<sup>1</sup>H} NMR resonances of **2**, **3**, and **4**. The <sup>31</sup>P{<sup>1</sup>H} NMR shifts of [Co(η<sup>4</sup>-P<sub>2</sub>C<sub>2</sub>*t*Bu<sub>2</sub>Me)(η<sup>4</sup>-P<sub>2</sub>C<sub>2</sub>*t*Bu<sub>2</sub>)] (**F**) are given for comparison; chemical shifts are given in ppm, the multiplicity and the <sup>2</sup>*J*(P,P) couplings are given in parenthesis; the labeling scheme for complexes **2–4**, and **F** is given in Figure 1.

	<b>2</b>	<b>3</b>	<b>4</b>	<b>F</b>
P1	–57.3 (d, 16 Hz)	–50.0 (d, 15 Hz)	–45.5 (d, 15 Hz)	–50.5 (br d, ~10 Hz)
P2	55.5 (d, 16 Hz)	55.5 (d, 15 Hz)	55.4 (d, 15 Hz)	41.7 (s)
P3 and P4	19.1 (s)	25.8 (s)	29.4 (s)	25.5 (s)

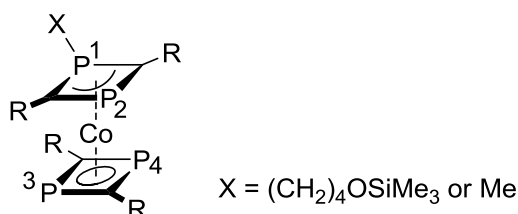


**Figure 1.** Labelling scheme for the insertion complexes **2–4** (X = (CH<sub>2</sub>)<sub>4</sub>OSiMe<sub>3</sub>) and for the methylated complex **F** (X = Me).

Unfortunately, the NMR spectroscopic characterization revealed that the isolated compounds **2** and **4** are contaminated with small amounts of the protonated complexes  $[\text{CoH}(\text{P}_2\text{C}_2\text{R}_2)_2]$  (**2'**: R = Ad, **4'**: R = *t*Pent). The formation of these byproducts is presumably caused by traces of HCl in the  $\text{Me}_3\text{SiCl}$  solution. According to the  $^1\text{H}$  NMR spectra, compound **2** contains 12% of **2'**, compound **4** 16% of **4'**.

While complexes **3** and **4** were isolated as orange oils that could not be recrystallized, compound **2** was obtained as an orange, crystalline solid. Repeated attempts to grow crystals suitable for X-ray crystallography of **3** and **4** were frustrated by their eminently high solubility also in apolar solvents such as *n*-pentane even at very low temperatures ( $-80\text{ }^\circ\text{C}$ ). X-ray quality crystals of **2** were obtained from a concentrated toluene solution at  $-18\text{ }^\circ\text{C}$ . The molecular structure of **2** (see Figure 2) shows that the  $(\text{CH}_2)_4\text{OSiMe}_3$  group is directly bound to one phosphorus atom (P1) of one diphosphacyclobutadiene ligand, resulting in a slightly pyramidalized geometry of the coordinated phosphorus atom P1 (sum of angles around P1:  $349.80^\circ$ ).

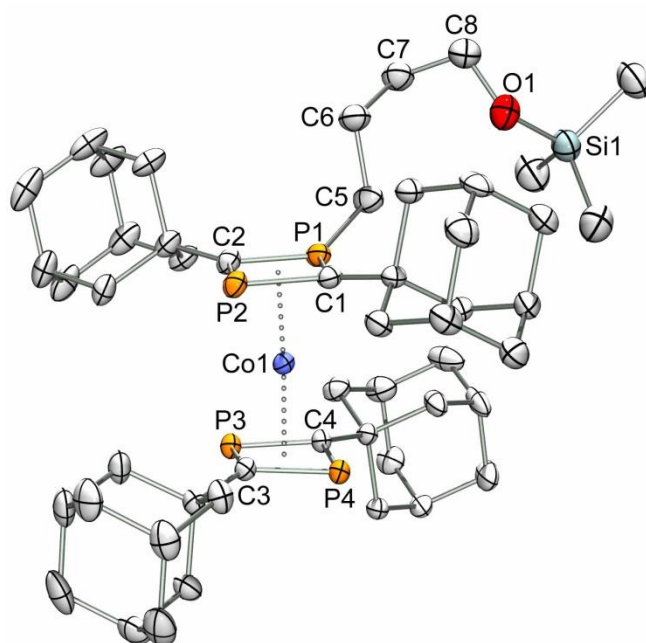


**Figure 2.** Solid-state molecular structure of  $[\text{Co}(\eta^4\text{-P}_2\text{C}_2\text{Ad}_2(\text{CH}_2)_4\text{OSiMe}_3)(\eta^4\text{-P}_2\text{C}_2\text{Ad}_2)]$  (**2**). Displacement ellipsoids are drawn at the 40% probability level. H-atoms and the toluene solvate molecule are omitted for clarity. Selected bond lengths (Å) and angles ( $^\circ$ ): C1–P1 1.759(3), C1–P2 1.806(3), C2–P1 1.763(3), C2–P2 1.803(4), C3–P3 1.803(3), C3–P4 1.797(3), C4–P3 1.803(3), C4–P4 1.799(3), C5–P1 1.813(4), Co1–P1 2.1324(10), Co1–P2 2.2731(10), Co1–P3 2.2621(10), Co1–P4 2.2612(10), Co1–C1 2.142(3), Co1–C2 2.138(3), Co1–C3 2.085(3), Co1–C4 2.070(3), C1–P1–C2 86.56(16), C1–P1–C5 130.37(18), C2–P1–C2 132.87(17), C1–P2–C2 83.59(15), P1–C1–P2 94.77(16), P1–C2–P2 94.72(17), C3–P3–C4 80.57(14), C3–P4–C4 80.50(14), P3–C3–P4 99.46(15), P3–C4–P4 99.03(15).

The Co–P distance (Co–P1 2.1324(10) Å) and the intra-ring P–C bond lengths of P1 (P1–C1,C2 1.759(3) and 1.763(3) Å) are slightly shorter than those of the remaining P atoms (Co–P2,P3,P4 2.2612(9)–2.2731(10) Å; P2–C1,C2 1.806(3) and 1.803(3) Å) and of the starting material K-C (Co–P1 2.2532(5); P1–C1,C2 1.8066(17) and 1.8118(16) Å). In accord with the comparative short P1–C bond lengths, the P<sub>2</sub>C<sub>2</sub> ligand of **2**, which is bound to the (CH<sub>2</sub>)<sub>4</sub>OSiMe<sub>3</sub> moiety, shows slightly wider C–P–C bond angles (C1–P1–C2 86.56(16), C1–P2–C2 83.95(15), C3–P3–C4 80.50(14), C3–P4–C4 80.57(15)°) and slightly smaller P–C–P bond angles (P1–C1–P2 94.77(16), P1–C2–P2 94.72(17), P3–C3–P4 99.03(15), P3–C4–P4 99.46(15)°). Analogous structural parameters were found for the methylated complex **F** (Co–P1 2.1089(8); P1–C1,C2 1.747(3) and 1.746(3) Å).<sup>7</sup>

Reasoning that the direct silylation of our sandwich anions [Co(P<sub>2</sub>C<sub>2</sub>R<sub>2</sub>)<sub>2</sub>]<sup>−</sup> is prevented even if traces of THF are present, we synthesized the new potassium salt [K(tol)<sub>2</sub>{Co(P<sub>2</sub>C<sub>2</sub>*t*Pent<sub>2</sub>)<sub>2</sub>}] (**5**) by recrystallization of [K(thf)<sub>3</sub>{Co(P<sub>2</sub>C<sub>2</sub>*t*Pent<sub>2</sub>)<sub>2</sub>}] (K-D) in hot toluene and storage at −18 °C overnight. The single crystal X-ray structure of **5** is shown in Figure 3. The molecular structure is closely related to that previously found for the potassium salt [K(thf)<sub>4</sub>{Co(P<sub>2</sub>C<sub>2</sub>Ad<sub>2</sub>)<sub>2</sub>}] (K-C).<sup>10a</sup>

The potassium cation interacts with one 1,3-diphosphacyclobutadiene ring of the cobaltate anion in an η<sup>4</sup>-fashion. Additionally, contacts between K1 and a CH<sub>3</sub>-group and a disordered CH<sub>2</sub> group from the *tert*-pentyl substituents (K1–C11 3.258(4) Å and K1–C23a,C23b 3.363(11), 3.280(11) Å) are observed. The coordination sphere of the potassium is completed by two toluene molecules that coordinate to K1 in an η<sup>6</sup>-fashion (K–C<sub>tol</sub> 3.148(4)–3.270(4) Å). The K–C (K1–C1,C2 3.246(3) and 3.302(3) Å) and K–P bond lengths (K1–P1,P2 3.2720(11) and 3.3129(11) Å) between potassium and the coordinated P<sub>2</sub>C<sub>2</sub> ring of **5** are shorter than those found in K-C (K1–C1,C2 3.475(2) and 3.421(2) Å; K1–P1,P2 3.465(9) and 3.429(9) Å).

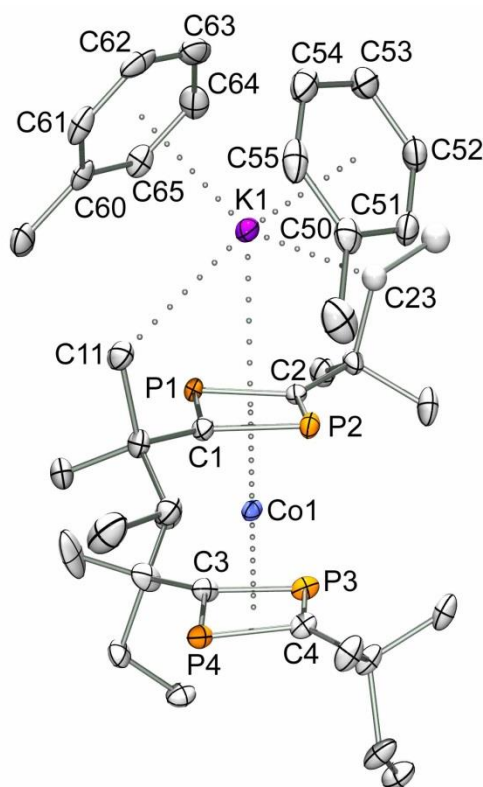
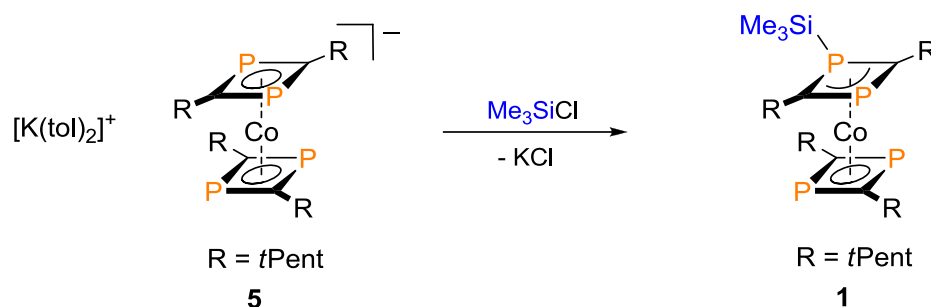


**Figure 3.** Solid-state molecular structure of  $[K(tol)_2\{Co(P_2C_2tPent_2)_2\}]$  (**5**). Displacement ellipsoids are drawn at the 40% probability level. Hydrogen atoms and disorder in the *tert*-pentyl substituents are omitted for clarity. Selected bond lengths (Å) and angles (°): C1–P1 1.812(3), C1–P2 1.800(4), C2–P1 1.807(4), C2–P2 1.800(3), C3–P3 1.790(3), C3–P4 1.804(3), C4–P3 1.796(4), C4–P4 1.799(4), Co1–P1 2.2450(10), Co1–P2 2.2467(10), Co1–P3 2.2512(10), Co1–P4 2.2564(10), Co1–C1 2.072(3), Co1–C2 2.068(3), Co1–C3 2.077(4), Co1–C4 2.079(3), K1–P1 3.2720(11), K1–P2 3.3129(11), K1–C1 3.246(3), K1–C2 3.302(3), K1–C11 3.258(4), K1–C23 K1–C23a 3.363(11), K1–C23b 3.280(11), K1–C50 3.270(4), K1–C51 3.198(4), K1–C52 3.148(4), K1–C53 3.156(4), K1–C54 3.210(4), K1–C55 3.263(4), K1–C60 3.238(4), K1–C61 3.256(4), K1–C62 3.259(6), K1–C63 3.232(4), K1–C64 3.192(4), K1–C65 3.192(4), C1–P1–C2 80.35(16), C1–P1–C2 80.86(16), P1–C1–P2 99.14(17), P1–C2–P2 99.33(17), C3–P3–C4 81.52(17), C3–P4–C4 81.07(17), P3–C3–P4 98.50(18), P3–C4–P4 98.46(19).

The new toluene complex **5** was investigated by multinuclear NMR spectroscopy in solution. Complex **5** and the THF complex **K-D** show identical  $^{31}P\{^1H\}$  NMR spectra in  $[D_8]THF$  solution displaying a single resonance at 9.6 ppm, which shows that the  $[Co(P_2C_2tPent_2)_2]^-$  anions are chemically identical in both salts. The  $^1H$  and  $^{13}C\{^1H\}$  NMR spectra show one set of signals for the *tert*-pentyl substituent and for the coordinated toluene molecules. Additionally, the  $^{13}C\{^1H\}$  NMR spectrum features a triplet at 101.2 ppm ( $^1J(C,P) = 51.93$  Hz) which is characteristic for the carbon atoms of the  $P_2C_2tPent_2$  ligands.  $^1H$  and  $^{13}C\{^1H\}$  NMR spectroscopy also convincingly supported the identity of **5**. No resonances for coordinated THF were observed in the spectra of the toluene-containing compound **5**.

The new toluene complex **5** was successfully employed to synthesize the silylated compound **1** according to Scheme 2. The reaction of **5** with Me<sub>3</sub>SiCl in the absence of THF afforded complex **1** as deep red-brown crystalline solid in 72% yield.



**Scheme 2.** Synthesis of the silylated complex **1**.

X-ray quality crystals of **1** (see Figure 4) were obtained from a concentrated *n*-pentane solution at  $-80\text{ }^\circ\text{C}$ . The structural parameters of **1** are similar to those found for the complexes  $[Co(\eta^4-P_2C_2Ad_2(CH_2)_4OSiMe_3)(\eta^4-P_2C_2Ad_2)]$  (**2**) and  $[Co(\eta^4-P_2C_2tBu_2Me)(\eta^4-P_2C_2tBu_2)]$  (**F**). The SiMe<sub>3</sub> group in **1** is directly bound to one of the phosphorus atoms (P1) of the P<sub>2</sub>C<sub>2</sub>tPent<sub>2</sub> ligand (sum of angles around P1: 338.8°). The P–Si bond lengths of 2.2893(8) Å is in the normal range reported for phosphorus–silicon single bonds (additive single-bond covalent radii: 2.27 Å).<sup>12</sup> The Co–P and C–P bond lengths (Co–P 2.1866(6)–2.2651(6) Å; P–C 1.7840(16)–1.7940(16) Å) and C–P–C and P–C–P bond angles (C–P–C 80.71(8)–84.42(7)°, P–C–P 95.81(7)–99.25(11)°) are similar to those of **2** and of the methylated derivative  $[Co(\eta^4-P_2C_2tBu_2Me)(\eta^4-P_2C_2tBu_2)]$  (**F**).

The identity of complex **1** was supported by multinuclear NMR spectroscopy in C<sub>6</sub>D<sub>6</sub> solution. The <sup>1</sup>H and <sup>13</sup>C{<sup>1</sup>H} NMR spectra feature one doublet for the SiMe<sub>3</sub> group (<sup>3</sup>*J*(H,P) = 7.88 Hz and <sup>2</sup>*J*(C,P) = 8.27 Hz) and three separate sets of signals for the chemically different *tert*-pentyl substituents. In agreement with its crystal structure, the <sup>31</sup>P{<sup>1</sup>H} NMR spectrum features three singlets at 25.6, 23.1, and  $-2.6$  ppm in a ratio of 2:1:1. Based on its intensity, the resonance at 25.6 ppm can be assigned to the chemically identical phosphorus atoms of the free P<sub>2</sub>C<sub>2</sub>tPent<sub>2</sub> ligand (P3 and P3a, labeling scheme according to Figure 4). The <sup>31</sup>P NMR singlet shifted to higher field at  $-2.6$  ppm may be assigned to the silylated phosphorus atom P1. This signal is significantly broadened in the coupled <sup>31</sup>P NMR spectrum (*v*<sub>FWHM</sub> = 41 Hz) compared to the proton-decoupled <sup>31</sup>P{<sup>1</sup>H} NMR spectrum due to the unresolved P–H coupling to the SiMe<sub>3</sub> group. The remaining signal at 23.1 ppm arises from the non-silylated phosphorus atom P2 of the P<sub>2</sub>C<sub>2</sub>tPent<sub>2</sub>SiMe<sub>3</sub> ligand.

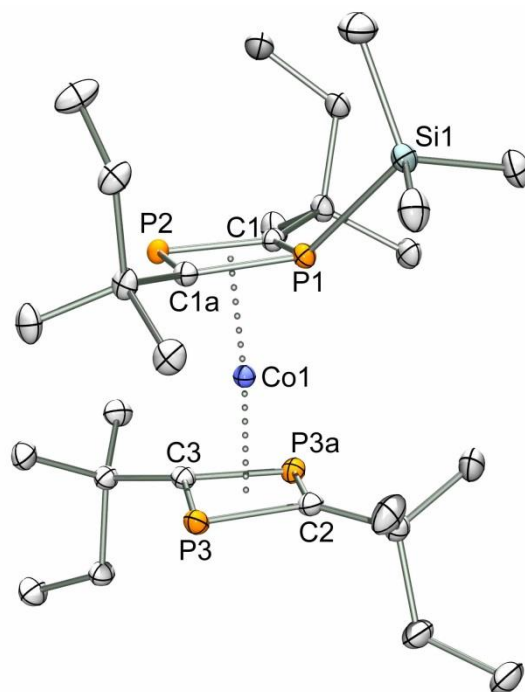


**Figure 4.** Solid-state molecular structure of  $[\text{Co}(\eta^4\text{-P}_2\text{C}_2t\text{Pent}_2\text{SiMe}_3)(\eta^4\text{-P}_2\text{C}_2t\text{Pent}_2)]$  (**1**). Displacement ellipsoids are drawn at the 40% probability level. Hydrogen atoms are omitted for clarity. Selected bond lengths (Å) and angles (°): C1–P1 1.7840(16), C1–P2 1.7940(16), C1a–P1 1.7840(16), C1a–P2 1.7940(16), C2–P3 1.7962(15), C3–P3 1.8006(15), Co1–P1 2.1866(6), Co1–P2 2.2651(6), Co1–P3 2.2570(6), Co1–P3a 2.2570(6); Co1–C1 2.1176(15), Co1–C1a 2.1176(15), Co1–C2 2.080(2), Co1–C3 2.073(2), Co1–C4 2.070(3), P1–Si1 2.2893(8), C1–P1–C1a 84.42(7), C1–P2–C1a 83.84(7), Si1–P1–C1 127.20(5), Si1–P1–C1a 127.20(5), P1–C1–P2 95.81(7), P1–C1a–P2 95.81(7), C2–P3–C3 80.71(8), C2–P3a–C3 80.71(8), P3–C2–P3a 99.25(11), P3–C3–P3a 98.92(11).

Unfortunately, the isolated compound **1** contains ca. 7% of the protonated complex  $[\text{CoH}(\text{P}_2\text{C}_2t\text{Pent}_2)_2]$  (**4'**) according to  $^1\text{H}$  NMR spectroscopy and elemental analysis. The UV/vis spectrum of **1** in *n*-hexane (see the Supporting Information, Figure S1) shows two intense absorptions in the UV region at  $\lambda = 251$  and 326 nm, which may arise as a result of metal-to-ligand charge transfer. Compared to the potassium salts  $[\text{K}([\text{18}]\text{crown-6})(\text{thf})_2][\text{Co}(\text{P}_2\text{C}_2\text{Ad}_2)_2]$  and  $[\text{K}([\text{18}]\text{crown-6})(\text{thf})_2][\text{Co}(\text{P}_2\text{C}_2t\text{Bu}_2)_2]$ , these charge transfer absorptions are shifted to higher energy.<sup>13</sup>

Since the phosphorus-silicon bond is known to be remarkably reactive and readily reacts with small inorganic and organic electrophiles, e.g. water, oxygen, carbon dioxide, halogens and organyl halides, we wondered if the reaction of THF with **1** would afford the previously observed insertion product **4**.<sup>14</sup> The reaction was monitored by  $^1\text{H}$  and  $^{31}\text{P}\{^1\text{H}\}$  NMR spectroscopy. The NMR data clearly reveal the formation of compound **4** (see Figure 5 for  $^{31}\text{P}\{^1\text{H}\}$  NMR data). Similar C–O bond cleavage reactions were also observed in NMR experiments with 2-methyltetrahydrofuran (2-Me-THF) and 1,4-dioxane (Figures 6 and 7). In contrast to the reaction with THF, the NMR spectra of these reactions indicate the presence of a second species. The  $^{31}\text{P}\{^1\text{H}\}$  NMR spectrum of the reaction with 2-Me-THF (see Figure 6)

features two sets of three signals each in a ratio of 1:2:1. We presume that this indicates the formation of two different products by the cleavage of the C–O bond at the 2- or 5-position, respectively. Besides the typical three resonances in a ratio of 1:2:1, the  $^3\text{P}\{^1\text{H}\}$  NMR spectrum of the reaction with 1,4-dioxane (Figure 7) shows two minor doublets ( $J(\text{P},\text{P}) = 14.9$  and  $14.8$  Hz) in ratio of approx. 1:1, which arises from a second, unidentified species.

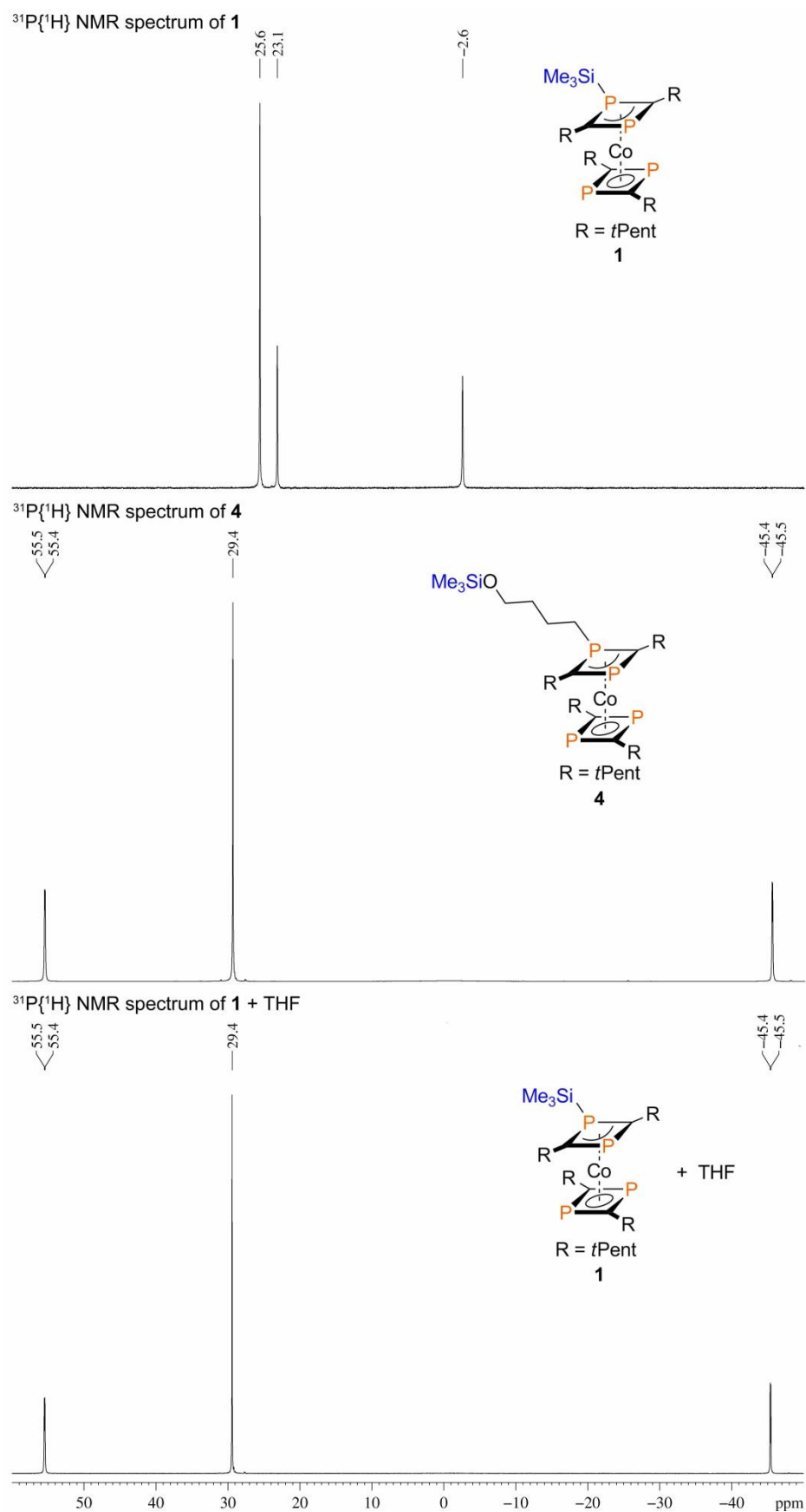


**Figure 5.**  $^{31}\text{P}\{^1\text{H}\}$  NMR spectra (161.16 MHz, 300 K,  $\text{C}_6\text{D}_6$ ) of complexes **1** (top), **4** (middle), and of the reaction mixture of **1** with THF (bottom). The signal of the impurity **4'** is not observed due to the fluxional behavior of this compound.



### 3.3 Conclusion

In summary, reactions of sandwich complexes of type  $[\text{Co}(\text{P}_2\text{C}_2\text{R}_2)_2]^-$  with the silicon electrophile  $\text{Me}_3\text{Si}^+$  gave two different types of products: In the presence of THF, the complexes  $[\text{Co}(\eta^4\text{-P}_2\text{C}_2\text{R}_2(\text{CH}_2)_4\text{OSiMe}_3)(\eta^4\text{-P}_2\text{C}_2\text{R}_2)_2]$  (**2–4**,  $\text{R} = \text{Ad}, t\text{Bu}, t\text{Pent}$ ) were formed through the C–O bond cleavage of a THF molecule. In contrast, the silylated complex  $[\text{Co}(\eta^4\text{-P}_2\text{C}_2t\text{Pent}_2\text{SiMe}_3)(\eta^4\text{-P}_2\text{C}_2t\text{Pent}_2)_2]$  (**1**), in which the  $\text{SiMe}_3$  group is directly bound to one phosphorus atom of a diphosphacyclobutadiene ligand, was isolated in the absence of THF. As expected, the P–Si bond of **1** is remarkably reactive. Thus, complex **1** readily reacts with THF, 2-methyltetrahydrofuran and 1,4-dioxane to yield complexes of type **4**. This initial study paves the way for further investigations concerning the reactivity profile of **1**. Due to the presence of a reactive phosphorus-silicon bond, compound **1** should be a versatile precursor for the preparation of new phospho-organometallic complexes. The formation of phosphorus-element bonds should be feasible by reacting **1** with main-group- and transition metal halides, which might enable the synthesis of a plethora of new compounds.

## 3.4 Experimental Section

### 3.4.1 General Procedures

All experiments were performed under an atmosphere of dry argon, by using standard Schlenk and glovebox techniques. Solvents were purified, dried, and degassed by standard techniques. NMR spectra were recorded (298K) on Bruker Avance 300 ( $^{31}\text{P}$ ; 85%  $\text{H}_3\text{PO}_4$ ) and Avance 400 spectrometers ( $^1\text{H}$ ,  $^{13}\text{C}$ ,  $^{29}\text{Si}$ ;  $\text{SiMe}_4$ ), internally referenced to residual solvent resonances. The spectra were recorded at 293 K unless noted otherwise. Melting points were measured on samples in sealed capillaries and are uncorrected. Compounds  $[\text{K}(\text{thf})_2\{\text{Co}(\text{P}_2\text{C}_2\text{tBu}_2)_2\}]$  (**K-B**),  $[\text{K}(\text{thf})_4\{\text{Co}(\text{P}_2\text{C}_2\text{Ad}_2)_2\}]$  (**K-C**), and  $[\text{K}(\text{thf})_3\{\text{Co}(\text{P}_2\text{C}_2\text{tPent}_2)_2\}]$  (**K-D**) were prepared according to literature procedures.<sup>10</sup> The dried solids contain a variable amount of THF molecules. The number of THF molecules present per formula unit was determined by  $^1\text{H}$  NMR spectroscopy on each sample.  $\text{Me}_3\text{SiCl}$  was purchased from ABCR and distilled prior to use. Elemental Analyses were determined on Vario ELIII CHNS and Elementar Micro Vario Cube instruments and are uncorrected.

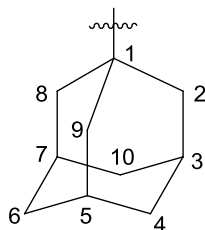
### 3.4.2 $[\text{Co}(\eta^4\text{-P}_2\text{C}_2\text{tPent}_2\text{SiMe}_3)(\eta^4\text{-P}_2\text{C}_2\text{tPent}_2)]$ (**1**)

A solution of  $\text{Me}_3\text{SiCl}$  in toluene (0.39 M, 1.45 mmol, ca. 3.7 mL) was added to a suspension of  $[\text{K}(\text{tol})_{1.5}\{\text{Co}(\text{P}_2\text{C}_2\text{tPent}_2)_2\}]$  (**5**, 0.91 g, 1.32 mmol) in toluene (60 mL) at room temperature. The reaction mixture was stirred overnight whereupon a dark red solution was formed. The solvent was then removed *in vacuo* and the deep red residue was dissolved in ca. 50 mL *n*-pentane. The dark red solution was filtered and concentrated to ca. 10 mL. Dark reddish brown crystals of complex **1** were isolated after storage at  $-78^\circ\text{C}$  for three days. Yield 0.56 g (72%). Compound **1** is contaminated with ca. 7%  $[\text{CoH}(\text{P}_2\text{C}_2\text{tPent}_2)_2]$  (**4'**) according to the  $^1\text{H}$  NMR spectrum and elemental analysis and with small amounts of an unidentified silicon containing species ( $\delta(^{29}\text{Si}) = 7.5$  and  $-21.4$  ppm) according to the  $^{29}\text{Si}$  NMR spectrum. The isolated compound still contains traces (0.13 molecules per formula unit) of *n*-pentane after drying *in vacuo* for 45 min according to the  $^1\text{H}$ -NMR spectrum. X-ray quality crystals of **1** were obtained by storing a concentrated *n*-pentane solution at  $-78^\circ\text{C}$  for three days. M.p.  $170^\circ\text{C}$  (decomp.). Elemental analysis calcd. for  $0.93(\text{C}_{27}\text{H}_{53}\text{CoP}_4\text{Si}) \cdot 0.07(\text{C}_{24}\text{H}_{45}\text{CoP}_4) \cdot 0.13\text{C}_5\text{H}_{12}$  ( $M = 592.96$ ): C 55.58, H 9.18; found: C 55.41, H 8.70. UV/vis (*n*-hexane,  $\lambda_{\text{max}}/\text{nm}$  ( $\epsilon_{\text{max}}/\text{dm}^3\text{mol}^{-1}\text{cm}^{-1}$ )): 251 (26500); 281 (shoulder); 326 (13500).  $^1\text{H}$  NMR (400.13 MHz, 300 K,  $\text{C}_6\text{D}_6$ ):  $\delta = 0.28$  (d,  $^3J(\text{P},\text{H}) = 7.9$  Hz, 9H;  $\text{SiMe}_3$ ), 0.86 (t, 0.8 H;  $\text{CH}_3$  of *n*-pentane), 1.00–1.34 (overlapping s, t and q, 42 H;  $\text{C}(\text{CH}_3)_3\text{CH}_2\text{CH}_3$  and  $\text{C}(\text{CH}_3)_3\text{CH}_2\text{CH}_3$  and  $\text{C}(\text{CH}_3)_3\text{CH}_2\text{CH}_3$  of **1** and **4'**,  $\text{CH}_2$  of *n*-pentane), 1.46–1.73 (overlapping q, 7H;  $\text{C}(\text{CH}_3)_3\text{CH}_2\text{CH}_3$  of **1** and **4'**).  $^{13}\text{C}\{^1\text{H}\}$  NMR (100.61 MHz, 300 K,  $\text{C}_6\text{D}_6$ ):  $\delta = -1.0$  (d,  $^2J(\text{C},\text{P}) = 8.3$  Hz;  $\text{SiMe}_3$ ), 10.0–10.4 (br. overlapping s;  $\text{C}(\text{CH}_3)_3\text{CH}_2\text{CH}_3$ ), 14.2 (s;  $\text{CH}_3$  of *n*-pentane), 22.7 (s; 2,4- $\text{CH}_2$  of *n*-pentane), 27.4 (s;  $\text{C}(\text{CH}_3)_2\text{CH}_2\text{CH}_3$ ), 29.1 (s;  $\text{C}(\text{CH}_3)_2\text{CH}_2\text{CH}_3$ ), 29.9 (s;  $\text{C}(\text{CH}_3)_2\text{CH}_2\text{CH}_3$ ), 32.2 (s;  $\text{C}(\text{CH}_3)_2\text{CH}_2\text{CH}_3$ ), 34.4 (s; 3- $\text{CH}_2$  of *n*-pentane), 37.2 (s;  $\text{C}(\text{CH}_3)_2\text{CH}_2\text{CH}_3$ ), 38.3 (s;  $\text{C}(\text{CH}_3)_2\text{CH}_2\text{CH}_3$ ), 38.9–39.3 (overlapping s;  $\text{C}(\text{CH}_3)_2\text{CH}_2\text{CH}_3$ ). The signals for the  $\text{C}_2\text{P}_2$  rings were not observed.  $^{31}\text{P}$  NMR (161.98 MHz, 300 K,  $\text{C}_6\text{D}_6$ , see Figure 4 for labeling scheme):  $\delta = 25.5$  (s,  $\nu_{\text{FWHM}} = 12.9$  Hz, 2P; P3 and P4), 23.1 (s,  $\nu_{\text{FWHM}} = 17.2$  Hz,

1P; P2),  $-2.6$  (br s,  $\nu_{\text{FWHM}} = 40.9$  Hz, 1P; P1).  $^{31}\text{P}\{^1\text{H}\}$  NMR (161.98 MHz, 300 K,  $\text{C}_6\text{D}_6$ ):  $\delta = 25.6$  (s, 2P; P3 and P4),  $23.1$  (s, 1P; P2),  $-2.6$  (s, 1P; P1).  $^{29}\text{Si}$  DEPT NMR (79.49 MHz, 300 K,  $\text{C}_6\text{D}_6$ ):  $\delta = 11.8$  (dd,  $^1J(\text{Si},\text{P}) = 28.6$  Hz,  $^3J(\text{Si},\text{P}) = 23.8$  Hz),  $7.5$  (impurity),  $-21.4$  (impurity).

### 3.4.3 $[\text{Co}(\eta^4\text{-P}_2\text{C}_2\text{Ad}_2(\text{CH}_2)_4\text{OSiMe}_3)(\eta^4\text{-P}_2\text{C}_2\text{Ad}_2)]$ (**2**)

$\text{Me}_3\text{SiCl}$  (0.13 mL, 1.00 mmol) was added to a light red solution of  $[\text{K}(\text{thf})_4\{\text{Co}(\text{P}_2\text{C}_2\text{Ad}_2)_2\}]$  (1.10 g, 1.00 mmol) in THF (ca. 45 mL) at room temperature, and the reaction mixture was stirred overnight. The solvent was then removed in *vacuo*, and the deep red residue was dissolved in ca 30 mL *n*-hexane, filtered, and concentrated to ca. 15 mL. Complex **2** precipitates a red solid after storage at  $-18$  °C for two days. Yield: 0.35 g (38 %). Crystals suitable for X-ray crystallography were obtained from a concentrated toluene solution at  $-18$  °C. The isolated compound still contains one *n*-hexane molecule per formula unit after drying in *vacuo* for 30 min according to the  $^1\text{H}$ -NMR spectrum. Complex **2** is contaminated with the protonated compound  $[\text{CoH}(\text{C}_2\text{P}_2\text{Ad}_2)_2]$  (**2'**) (ca. 12% according to  $^1\text{H}$  NMR spectroscopy). Attempts to remove the impurity by recrystallization failed due to the similar solubility of both compounds. M.p.  $235$  °C (decomp.).  $^1\text{H}$  NMR (400.13 MHz, 300 K,  $\text{C}_6\text{D}_6$ ):  $\delta = 0.09$  (s with  $^{29}\text{Si}$  satellites,  $^2J(\text{Si},\text{H}) = 58.5$  Hz, 9H;  $\text{SiMe}_3$ ),  $0.89$  (t, 6 H;  $\text{CH}_3$  of *n*-hexane),  $1.24$  (br m, 8H;  $\text{CH}_2$  of *n*-hexane),  $1.49\text{--}2.24$  (overlapping m, 69 H; Ad-H of **2**, Ad-H of **2'**,  $\text{PCH}_2\text{CH}_2\text{CH}_2\text{CH}_2\text{O}$ ),  $2.21$  (m, 2H;  $\text{PCH}_2\text{CH}_2\text{CH}_2\text{CH}_2\text{O}$ ),  $2.59$  (m, 2H;  $\text{PCH}_2\text{CH}_2\text{CH}_2\text{CH}_2\text{O}$ ),  $3.44$  (t,  $^3J(\text{H},\text{H}) = 5.64$  Hz, 2H;  $\text{PCH}_2\text{CH}_2\text{CH}_2\text{CH}_2\text{O}$ ).  $^{13}\text{C}\{^1\text{H}\}$  NMR (100.61 MHz, 300 K,  $\text{C}_6\text{D}_6$ ):  $\delta = -0.6$  (s;  $\text{SiMe}_3$ ),  $14.3$  (s;  $\text{CH}_3$  of *n*-hexane),  $23.1$  (s; 2- $\text{CH}_2$  and of *n*-hexane),  $26.2$  (d,  $^2J(\text{C},\text{P}) = 7.7$  Hz;  $\text{PCH}_2\text{CH}_2\text{CH}_2\text{CH}_2\text{O}$ ),  $29.3$  (br s; C-3, C-5 and C-7 of Ad),  $29.5$  (br s; C-3, C-5 and C-7 of Ad),  $29.6$  (br s; C-3, C-5 and C-7 of Ad),  $31.9$  (s; 3- $\text{CH}_2$  of *n*-hexane),  $33.7$  (d,  $^1J(\text{C},\text{P}) = 12.4$  Hz;  $\text{PCH}_2\text{CH}_2\text{CH}_2\text{CH}_2\text{O}$ ),  $35.3$  (d,  $^3J(\text{C},\text{P}) = 6.9$  Hz;  $\text{PCH}_2\text{CH}_2\text{CH}_2\text{CH}_2\text{O}$ ),  $36.7$  (br s; C-1 of Ad),  $36.9$  (br s; C-4, C-6 and C-10 of Ad),  $37.1$  (br s; C-4, C-6 and C-10 of Ad),  $37.1$  (br s; C-4, C-6 and C-10 of Ad),  $46.0$  (br s; C-2, C-3 and C-9 of Ad),  $46.4$  (br s; C-2, C-3 and C-9 of Ad),  $47.1$  (br s; C-2, C-3 and C-9 of Ad),  $61.6$  (s;  $\text{PCH}_2\text{CH}_2\text{CH}_2\text{CH}_2\text{O}$ ). The signals for the  $\text{P}_2\text{C}_2$  rings were not observed.  $^{31}\text{P}\{^1\text{H}\}$  NMR (161.98 MHz, 300 K,  $\text{C}_6\text{D}_6$ , see Figure 1 for the labeling scheme):  $\delta = 55.5$  (d,  $^2J(\text{P},\text{P}) = 16$  Hz, 1P; P1),  $19.1$  (s, 2P; P3 and P4),  $-57.3$  (d,  $^2J(\text{P},\text{P}) = 16$  Hz, 1P; P2).  $^{29}\text{Si}\{^1\text{H}\}$ DEPT (79.49 MHz, 300 K,  $\text{C}_6\text{D}_6$ ):  $\delta = 16.8$ .



### 3.4.4 [Co( $\eta^4$ -P<sub>2</sub>C<sub>2</sub>tBu<sub>2</sub>(CH<sub>2</sub>)<sub>4</sub>OSiMe<sub>3</sub>)( $\eta^4$ -P<sub>2</sub>C<sub>2</sub>tBu<sub>2</sub>)] (3)

Compound **3** was prepared by an analogous procedure to **2** by adding a solution of Me<sub>3</sub>SiCl in toluene (0.39 M, 0.39 mmol, ca 1.0 mL) to a suspension of [K(thf)<sub>1.75</sub>{Co(P<sub>2</sub>C<sub>2</sub>tBu<sub>2</sub>)<sub>2</sub>}] (0.20 g, 0.35 mmol) in toluene (ca. 35 mL) at room temperature. The reaction mixture was stirred overnight at room temperature whereupon a light red solution was formed. The solvent was then removed in *vacuo*, and the dark red residue was dissolved in ca. 25 mL *n*-hexane. After filtration the solution was concentrated to ca. 10 mL. Complex **3** precipitated as a red oily solid after storage at -18 °C for ten days. Yield: 78.6 mg (37%). An elemental analysis could not be performed due to the oily consistence of the isolated compound. <sup>1</sup>H NMR (400.13 MHz, 300 K, C<sub>6</sub>D<sub>6</sub>):  $\delta$  = 0.06 (s with <sup>29</sup>Si satellites, <sup>2</sup>J(Si,H) = 58.4 Hz, 9H; SiMe<sub>3</sub>), 1.23 (s, 18 H; *t*Bu), 1.28 (s, 9H; *t*Bu), 1.32 (s, 9 H; *t*Bu), 1.42 (m, 2H; PCH<sub>2</sub>CH<sub>2</sub>CH<sub>2</sub>CH<sub>2</sub>O), 2.04 (m, 2H; PCH<sub>2</sub>CH<sub>2</sub>CH<sub>2</sub>CH<sub>2</sub>O), 2.33 (m, 2H; PCH<sub>2</sub>CH<sub>2</sub>CH<sub>2</sub>CH<sub>2</sub>O), 3.37 (t, <sup>3</sup>J(H,H) = 5.64 Hz, 2H; PCH<sub>2</sub>CH<sub>2</sub>CH<sub>2</sub>CH<sub>2</sub>O). <sup>13</sup>C{<sup>1</sup>H} NMR (100.61 MHz, 300 K, C<sub>6</sub>D<sub>6</sub>):  $\delta$  = -0.6 (s; SiMe<sub>3</sub>), 25.2 (d, <sup>2</sup>J(C,P) = 7.7 Hz; PCH<sub>2</sub>CH<sub>2</sub>CH<sub>2</sub>CH<sub>2</sub>O), 27.8 (dd, <sup>1</sup>J(C,P) = 19.6 Hz, <sup>3</sup>J(C,P) = 6.8 Hz; PCH<sub>2</sub>CH<sub>2</sub>CH<sub>2</sub>CH<sub>2</sub>O), 32.3 (very br s; PCH<sub>2</sub>CH<sub>2</sub>CH<sub>2</sub>CH<sub>2</sub>O), 33.0–33.9 (br overlapping s; C(CH<sub>3</sub>)<sub>3</sub> of *t*Bu), 35.8–36.2 (very br overlapping s; C(CH<sub>3</sub>)<sub>3</sub> of *t*Bu), 61.3 (s; PCH<sub>2</sub>CH<sub>2</sub>CH<sub>2</sub>CH<sub>2</sub>O), 77.8 (dd, <sup>1</sup>J(C,P) = 66.5 Hz, <sup>3</sup>J(C,P) = 3.3 Hz, 2C; substituted P<sub>2</sub>C<sub>2</sub> ring), 114.4 (t, <sup>1</sup>J(C,P) = 51.4 Hz, 1C; free P<sub>2</sub>C<sub>2</sub> ring), 122.2 (d, <sup>1</sup>J(C,P) = 54.6 Hz, 1C; free P<sub>2</sub>C<sub>2</sub> ring). <sup>31</sup>P{<sup>1</sup>H} NMR (161.98 MHz, 300 K, C<sub>6</sub>D<sub>6</sub>, labeling scheme analogous to **2**):  $\delta$  = 55.5 (d, <sup>2</sup>J(P,P) = 15 Hz, 1P; P1), 25.8 (s, 2P; P3 and P4), -50.0 (d, <sup>2</sup>J(P,P) = 15 Hz, 1P; P2). <sup>29</sup>Si NMR (79.49 MHz, 300 K, C<sub>6</sub>D<sub>6</sub>):  $\delta$  = 17.2.

### 3.4.5 [Co( $\eta^4$ -P<sub>2</sub>C<sub>2</sub>tPent<sub>2</sub>(CH<sub>2</sub>)<sub>4</sub>OSiMe<sub>3</sub>)( $\eta^4$ -P<sub>2</sub>C<sub>2</sub>tPent<sub>2</sub>)] (4)

Compound **4** was prepared by two synthetic routes.

Method A: A solution of Me<sub>3</sub>SiCl in toluene (0.39 M, 0.35 mmol, ca 0.9 mL) was added to a light red solution of [K(thf)<sub>1.25</sub>{Co(P<sub>2</sub>C<sub>2</sub>tPent<sub>2</sub>)<sub>2</sub>}] (0.21 g; 0.31 mmol) in THF (ca. 40 mL) at room temperature. After the reaction mixture had been stirred overnight the solvent was removed in *vacuo*, and the red residue was dissolved in ca. 30 mL *n*-pentane. The mixture was filtered, and the solvent was evaporated to dryness. Complex **4** was obtained as a dark red oil. Yield: 0.12 g (56%). Complex **4** is contaminated with the protonated compound [CoH(C<sub>2</sub>P<sub>2</sub>tPent<sub>2</sub>)<sub>2</sub>] (**4'**) (ca. 16% according to <sup>1</sup>H NMR spectroscopy). Attempts to remove the impurity by recrystallization failed due to the similar solubility of both compounds. <sup>1</sup>H NMR (400.13 MHz, 300 K, C<sub>6</sub>D<sub>6</sub>):  $\delta$  = 0.06 (s with <sup>29</sup>Si satellites, <sup>2</sup>J(Si,H) = 58.5 Hz, 9H; SiMe<sub>3</sub>), 0.96–1.18 (overlapping s, and t, 40 H; C(CH<sub>3</sub>)<sub>2</sub>CH<sub>2</sub>CH<sub>3</sub> and C(CH<sub>3</sub>)<sub>2</sub>CH<sub>2</sub>CH<sub>3</sub> of **4** and **4'**), 1.35–1.50 (overlapping q and m, 5H; C(CH<sub>3</sub>)<sub>2</sub>CH<sub>2</sub>CH<sub>3</sub> of **4** and **4'** and PCH<sub>2</sub>CH<sub>2</sub>CH<sub>2</sub>CH<sub>2</sub>O), 1.62–1.69 (overlapping q, 6 H; C(CH<sub>3</sub>)<sub>2</sub>CH<sub>2</sub>CH<sub>3</sub> of **4** and **4'**), 2.01 (m, 2H; PCH<sub>2</sub>CH<sub>2</sub>CH<sub>2</sub>CH<sub>2</sub>O), 2.38 (m, 2H; PCH<sub>2</sub>CH<sub>2</sub>CH<sub>2</sub>CH<sub>2</sub>O), 3.36 (t, <sup>3</sup>J(H,H) = 5.77 Hz, 2H; PCH<sub>2</sub>CH<sub>2</sub>CH<sub>2</sub>CH<sub>2</sub>O). <sup>13</sup>C{<sup>1</sup>H} NMR (100.61 MHz, 300 K, C<sub>6</sub>D<sub>6</sub>):  $\delta$  = -0.6 (s; SiMe<sub>3</sub>), 10.0 (s; C(CH<sub>3</sub>)<sub>3</sub>CH<sub>2</sub>CH<sub>3</sub>), 10.3 (s; C(CH<sub>3</sub>)<sub>3</sub>CH<sub>2</sub>CH<sub>3</sub>), 10.4 (s; C(CH<sub>3</sub>)<sub>3</sub>CH<sub>2</sub>CH<sub>3</sub>), 25.2 (d, <sup>1</sup>J(C,H) = 7.1 Hz; PCH<sub>2</sub>CH<sub>2</sub>CH<sub>2</sub>CH<sub>2</sub>O), 27.8–29.7 (overlapping s; C(CH<sub>3</sub>)<sub>2</sub>CH<sub>2</sub>CH<sub>3</sub>), 33.5 (d, <sup>1</sup>J(C,P) = 12.9 Hz; PCH<sub>2</sub>CH<sub>2</sub>CH<sub>2</sub>CH<sub>2</sub>O), 36.7 (d, <sup>1</sup>J(C,H) = 5.6 Hz;

PCH<sub>2</sub>CH<sub>2</sub>CH<sub>2</sub>CH<sub>2</sub>O), 38.4–38.7 (br overlapping s; C(CH<sub>3</sub>)<sub>3</sub>CH<sub>2</sub>CH<sub>3</sub>), 38.9 (br s; C(CH<sub>3</sub>)<sub>3</sub>CH<sub>2</sub>CH<sub>3</sub>), 39.2 (br s; C(CH<sub>3</sub>)<sub>3</sub>CH<sub>2</sub>CH<sub>3</sub>), 39.6 (br s; C(CH<sub>3</sub>)<sub>3</sub>CH<sub>2</sub>CH<sub>3</sub>), 61.3 (s; PCH<sub>2</sub>CH<sub>2</sub>CH<sub>2</sub>CH<sub>2</sub>O), 77.0 (d, <sup>1</sup>J(C,P) = 66.1 Hz, 2C; substituted P<sub>2</sub>C<sub>2</sub> ring), 113.2 (t, <sup>1</sup>J(C,P) = 54.3 Hz, 1C; free P<sub>2</sub>C<sub>2</sub> ring), 120.4 (t, <sup>1</sup>J(C,P) = 54.8 Hz, 1C; free P<sub>2</sub>C<sub>2</sub> ring). <sup>31</sup>P{<sup>1</sup>H} NMR (161.98 MHz, 300 K, C<sub>6</sub>D<sub>6</sub>, labeling scheme analogous to **2** and **3**): δ = 55.4 (d, <sup>2</sup>J(P,P) = 15 Hz, 1P; P1), 29.4 (s, 2P; P3 and P4), –45.5 (d, <sup>2</sup>J(P,P) = 15 Hz, 1P; P2). <sup>29</sup>Si NMR (79.49 MHz, 300 K, C<sub>6</sub>D<sub>6</sub>): δ = 17.2.

Method B: Complex **1** (69.2 mg; 0.12 mmol) was dissolved in ca. 1 mL THF at room temperature and stirred overnight. The deep red solution was then filtered and evaporated to dryness giving complex **4** as red oil in 59% yield (45.7 mg). The isolated compound was contaminated with ca. 7% [CoH(P<sub>2</sub>C<sub>2</sub>tPent)<sub>2</sub>] (**4'**) (according to the <sup>1</sup>H-NMR spectrum) due to presence of **4'** in the starting material **1**. The spectroscopic properties for this sample are identical within experimental error to that of the sample prepared by method A.

### 3.4.6 [K(tol)<sub>2</sub>{Co(P<sub>2</sub>C<sub>2</sub>tPent)<sub>2</sub>}] (**5**)

Complex **5** was obtained as a light red crystalline solid by recrystallization of [K(thf)<sub>2.5</sub>{Co(P<sub>2</sub>C<sub>2</sub>tPent)<sub>2</sub>}] (K-**D**, 0.86 g, 1.17 mmol) in hot toluene (ca. 180 mL) and storage at –18 °C overnight. The dried solid contains a variable amount of toluene molecules. The number of toluene molecules present per formula unit was determined by <sup>1</sup>H NMR spectroscopy individually on each sample. Yield 0.69 g (88%, *x* = 1.25). X-ray quality crystals were obtained from a concentrated toluene solution at –18 °C. M.p.: 180 °C. Elemental analysis calcd. for C<sub>24</sub>H<sub>44</sub>CoKP<sub>4</sub>·1.5C<sub>7</sub>H<sub>8</sub> (*M* = 692.76, calculated for a sample which contains 1.5 molecules toluene): C 59.82, H 8.12; found: C 59.97, H 8.12. <sup>1</sup>H NMR (400.13 MHz, 300 K, [D<sub>8</sub>]THF): δ = 0.90–0.94 (overlapping s and t, 36 H; C(CH<sub>3</sub>)<sub>2</sub>CH<sub>2</sub>CH<sub>3</sub> and C(CH<sub>3</sub>)<sub>2</sub>CH<sub>2</sub>CH<sub>3</sub>), 1.45 (q, 8 H; C(CH<sub>3</sub>)<sub>2</sub>CH<sub>2</sub>CH<sub>3</sub>), 2.30 (s, 3.75 H; CH<sub>3</sub> of toluene); 7.06–7.17 (m, 6.25 H; CH of toluene). <sup>13</sup>C{<sup>1</sup>H} NMR (100.61 MHz, 300 K, [D<sub>8</sub>]THF/C<sub>7</sub>D<sub>8</sub> ca. 1:1): δ = 10.6 (s; C(CH<sub>3</sub>)<sub>2</sub>CH<sub>2</sub>CH<sub>3</sub>), 21.2 (s; CH<sub>3</sub> of toluene), 29.3 (s; C(CH<sub>3</sub>)<sub>2</sub>CH<sub>2</sub>CH<sub>3</sub>), 38.4 (s; C(CH<sub>3</sub>)<sub>2</sub>CH<sub>2</sub>CH<sub>3</sub>), 40.1 (s; C(CH<sub>3</sub>)<sub>2</sub>CH<sub>2</sub>CH<sub>3</sub>), 101.2 (t, <sup>1</sup>J(C,P) = 51.93 Hz; P<sub>2</sub>C<sub>2</sub> ring), 125.8 (s; 4-CH of toluene), 129.5 (s; 3,5-CH of toluene), 138.2 (s; 2,6-CH of toluene). <sup>31</sup>P{<sup>1</sup>H} NMR (161.98 MHz, 300 K, [D<sub>8</sub>]THF): δ = 9.6.

### 3.4.7 X-Ray Crystallography

The crystals were processed with Agilent Technologies SuperNova (**1** and **5**) and Bruker AXS APEX II (**2**) devices, respectively. Either semi-empirical multi-scan absorption corrections<sup>15</sup> or analytical ones<sup>16</sup> were applied to the data. The structures were solved by SHELXS<sup>17</sup> or SIR<sup>18</sup> and least-square refinements on *F*<sup>2</sup> were carried out with SHELXL<sup>17</sup>. Crystallographic data are given in Table 2.

**Table 2.** Crystallographic data and structure refinement of **1**, **2**, and **5**.

	<b>1</b>	<b>2</b>	<b>5</b>
Empirical formula	C <sub>27</sub> H <sub>53</sub> CoP <sub>4</sub> Si	C <sub>51</sub> H <sub>77</sub> CoOP <sub>4</sub> Si·C <sub>7</sub> H <sub>8</sub>	C <sub>38</sub> H <sub>60</sub> CoKP <sub>4</sub>
Crystal size [mm <sup>3</sup> ]	0.10 x 0.16 x 0.21	0.24 x 0.18 x 0.10	0.30 x 0.30 x 0.20
Color and shape	yellow blocks	orange blocks	orange blocks
Formula weight [g mol <sup>-1</sup> ]	588.59	1009.16	738.77
Crystal system	orthorhombic	monoclinic	monoclinic
Space group	<i>Pnma</i>	<i>P2<sub>1</sub>/n</i>	<i>P2<sub>1</sub>/n</i>
Absorption correction	multi-scan	semi-empirical	semi-empirical
Transmission min/max	1.00000/0.35868	0.6811/0.4351	0.65045/1.00000
<i>a</i> [Å]	16.9382(3)	13.4814(2)	11.3548(2)
<i>b</i> [Å]	11.0030(2)	20.6464(3)	20.4325(3)
<i>c</i> [Å]	17.2884(2)	19.7044(2)	17.0180(3)
$\alpha$ [°]	90	90	90
$\beta$ [°]	90	103.5210(10)	90.789(2)
$\gamma$ [°]	90	90	90
<i>V</i> [Å <sup>3</sup> ]	3222.06(9)	5332.56(12)	3947.92(11)
<i>Z</i>	4	4	4
<i>T</i> [K]	123(9)	153(1)	123(2)
$\lambda$ [Å]	1.54180	1.54178	1.54178
$\rho_{\text{calc}}$ [g/cm <sup>3</sup> ]	1.213	1.257	1.243
$\mu$ (mm <sup>-1</sup> )	6.499	4.160	6.056
Theta range [°]	3.7–73.6	3.15–71.75	3.38–59.99
Reflections collected to $\theta_{\text{max}}$ [°]	17036	31033	10610
Unique reflections ( <i>R</i> <sub>int</sub> )	3321 (0.033)	10038 (0.0503)	5250 (0.0304)
Refl. obs. [ <i>I</i> > 2 $\sigma$ ( <i>I</i> )]	3051	7361	5250
Parameters	176	585	417
Completeness to $\theta$	0.992	0.961	0.895
<i>R</i> -values [ <i>I</i> > 2 $\sigma$ ( <i>I</i> )]	0.0641/0.0272	0.0556/0.1590	0.0464/0.1193
<i>R</i> -values (all data)	0.0660/0.0311	0.0762/0.1687	0.0500/0.1218
GOF on <i>F</i> <sup>2</sup>	1.037	1.067	1.073
Residual density [eÅ <sup>-3</sup> ]	–0.25/0.28	–0.637/1.093	–0.474/0.732

### 3.5 Supporting Information

#### 3.5.1 UV/vis Spectrum of $[\text{Co}(\eta^4\text{-P}_2\text{C}_2t\text{Pent}_2\text{SiMe}_3)(\eta^4\text{-P}_2\text{C}_2t\text{Pent}_2)]$ (**1**)

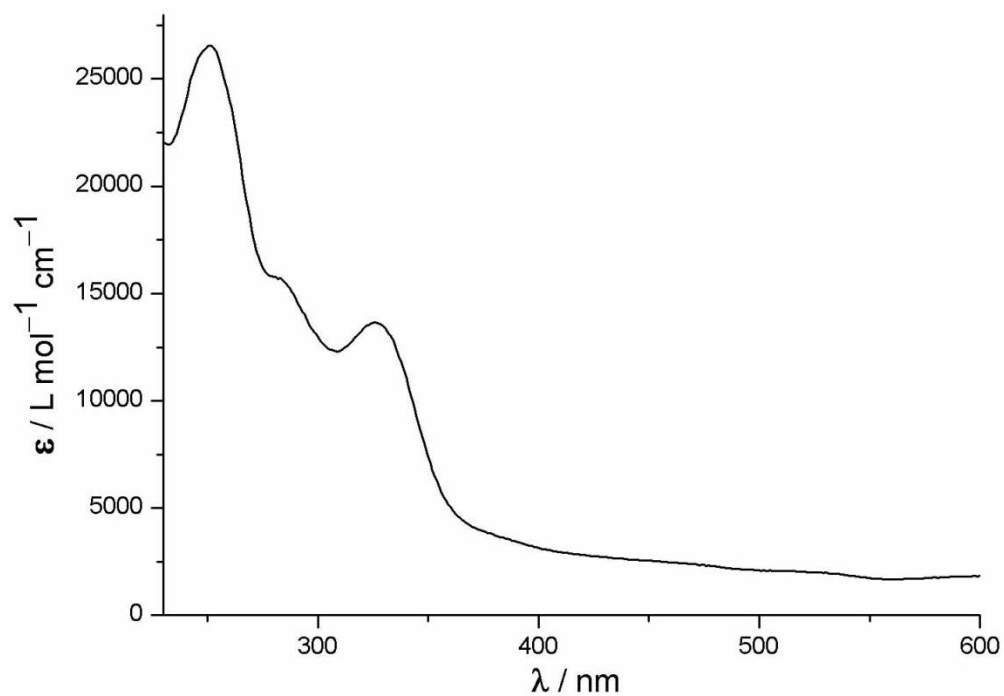


**Figure S1.** UV/vis spectrum of  $[\text{Co}(\eta^4\text{-P}_2\text{C}_2t\text{Pent}_2\text{SiMe}_3)(\eta^4\text{-P}_2\text{C}_2t\text{Pent}_2)]$  (**1**) in *n*-hexane.

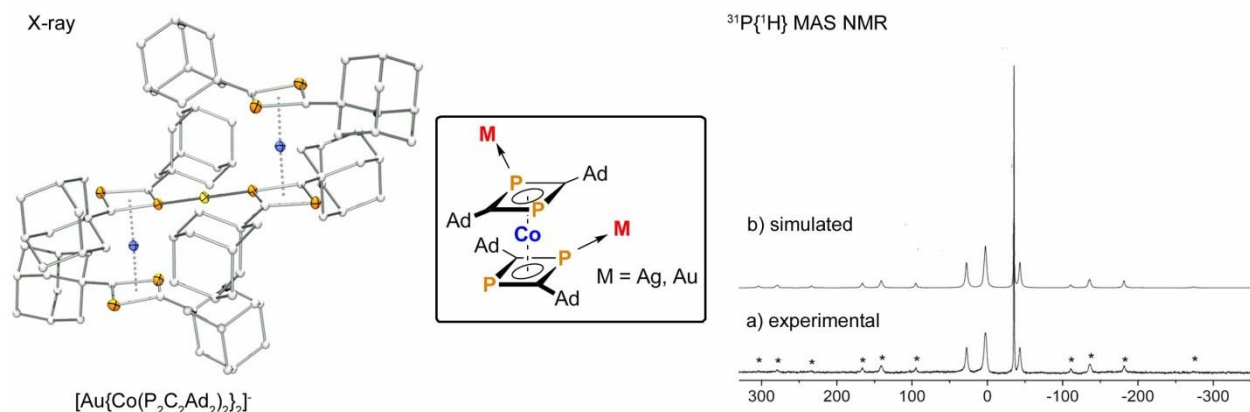
## References

- 1 P. Binger, R. Milczarek, R. Mynott, M. Regitz, W. Rösch, *Angew. Chem. Int. Ed. Engl.* **1986**, 25, 644;  
b) P. B. Hitchcock, M. J. Maah, J. F. Nixon, *J. Chem. Soc., Chem. Commun.* **1986**, 737; c) P. Binger,  
R. Milczarek, R. Mynott, C. Krüger, Y. H. Tsay, E. Raabe, M. Regitz, *Chem. Ber.* **1988**, 121, 637; d) P.  
Binger, B. Biedenbach, R. Schneider, M. Regitz, *Synthesis* **1989**, 960
- 2 M. Regitz, *Chem. Rev.* **1990**, 90, 191; b) A. C. Gaumont, J. Denis, *Chem. Rev.* **1994**, 94, 1413; d) J. F.  
Nixon, *Coord. Chem. Rev.* **1995**, 145, 201; c) M. Regitz, O. J. Scherer, *Multiple Bonds and Low  
Coordination Phosphorus Chemistry*, Thieme, Stuttgart, **1990**; d) K. B. Dillon, F. Mathey, J. F. Nixon,  
*Phosphorus: The Carbon Copy*, Wiley, Chichester, **1998**; e) F. Mathey, *Angew. Chem. Int. Ed.* **2003**,  
42, 1578.
- 3 A. Efraty, *Chem. Rev.* **1977**, 77, 692; b) L. Veiros, G. Dazinger, K. Kirchner, M. C. Calhorda, R.  
Schmid, *Chem. Eur. J.* **2005**, 10, 5860, and ref. therein; c) D. Seyferth, *Organometallics* **2003**, 22, 2; d)  
U. H. F. Bunz, *Top. Curr. Chem.* **1999**, 201, 131
- 4 P. Binger, G. Glaser, S. Albus, C. Krüger, *Chem. Ber.* **1995**, 128, 1261.
- 5 P. Kramkowski, M. Scheer, *Eur. J. Inorg. Chem.* **2000**, 1869.
- 6 C. Jones, C. Schulten, A. Stasch, *Dalton. Trans.* **2006**, 3733.
- 7 R. Wolf, A. W. Ehlers, J. C. Slootweg, M. Lutz, D. Gudat, M. Hunger, A. L. Spek, K. Lammertsma,  
*Angew. Chem. Int. Ed.* **2008**, 47, 4584.
- 8 R. Wolf, J. C. Slootweg, A. W. Ehlers, F. Hartl, B. de Bruin, M. Lutz, A. L. Spek, K. Lammertsma,  
*Angew. Chem. Int. Ed.* **2009**, 48, 3104.
- 9 R. Wolf, A. W. Ehlers, M. M. Khusniyarov, F. Hartl, B. de Bruin, G. J. Long, F. Grandjean, F. M.  
Schappacher, R. Pöttgen, J. C. Slootweg, M. Lutz, A. L. Spek, K. Lammertsma, *Chem. Eur. J.* **2010**,  
16, 14322.
- 10 a) J. Malberg, T. Wiegand, H. Eckert, M. Bodensteiner, R. Wolf, *Chem. Eur. J.* **2013**, 19, 2356;  
b) J. Malberg, T. Wiegand, H. Eckert, M. Bodensteiner, R. Wolf, *Eur. J. Inorg. Chem.* **2013**,  
DOI: 10.1002/ejic.201301173 .
- 11 S. Güllak, O. Stepanek, J. Malberg, B. Rezaei Rad, M. Kotora, R. Wolf, A. Jacobi von Wangelin,  
*Chem. Sci.* **2013**, 4, 776.
- 12 P. Pykkö, M. Atsumi, *Chem. Eur. J.* **2009**, 15, 186.
- 13 R. Wolf, A. W. Ehlers, M. M. Khusniyarov, F. Hartl, B. de Bruin, G. J. Long, F. Grandjean, F. M.  
Schappacher, R. Pöttgen, J. C. Slootweg, M. Lutz, A. L. Spek, K. Lammertsma, *Chem. Eur. J.* **2010**,  
16, 14322.
- 14 D. A. Armittage in *The Silicon-Heteroatom Bond* (Eds. S. Patai, Z. Rappoport), Wiley, **1991**, p. 183.
- 15 a) *SCALE3ABS*, *CrysAlis<sup>Pro</sup>*, Agilent Technologies Inc. , Oxford, GB, **2012**, b) G. M. Sheldrick,  
*SADABS*, Bruker AXS, Madison, USA, **2007**.
- 16 R. C. Clark, J. S. Reid, *Acta Cryst. Sect. A* **1995**, 51, 887.
- 17 G. M. Sheldrick, *Acta Cryst. Sect. A* **2008**, 64, 112.
- 18 A. Altomare, M. C. Burla, M. Camalli, G. L. Cascarno, C. Giacovazzo, A. G. G. Moliterni, G. Polidori,  
R. Spagna, *J. Appl. Cryst.* **1999**, 32, 115.



## 4 Gold(I) and Silver(I) Complexes of Diphosphacyclobutadiene Cobaltate Anions<sup>[a],[b],[c]</sup>

Jennifer Malberg, Thomas Wiegand, Hellmut Eckert, Michael Bodensteiner, and Robert Wolf



[a] Reproduced with permission from: J. Malberg, T. Wiegand, H. Eckert, M. Bodensteiner, R. Wolf, *Chem. Eur. J.* **2013**, *19*, 2356-2369. Copyright 2013 WILEY-VCH.

[b] Figure 4 is reproduced with permission from: T. Wiegand, H. Eckert, S. Grimme, J. Malberg, R. Wolf, *Solid State Nucl. Magn. Res.* **2013**, *53*, 13-19. Copyright 2013 WILEY-VCH.

[c] Thomas Wiegand and Hellmut Eckert recorded and analyzed the solid-state NMR spectra (Figures 5–9 and S4–S6, Tables 2–4). Michael Bodensteiner refined the single crystal X-ray structures.



## 4.1 Introduction

Phospha-organometallic chemistry has attracted much interest over the years due to the analogies between hydrocarbon-based organometallic species and their phospha-organometallic counterparts, in which one or several carbon atoms in the ligand framework have been replaced by phosphorus.<sup>1</sup> The structural and electronic similarities between organometallic and phospha-organometallic complexes have frequently been highlighted, but the incorporation of phosphorus nonetheless has a profound influence on the electronic structure and reactivity.<sup>1,2</sup> One intriguing aspect of phospha-organometallic complexes is the possibility to coordinate metal ions through the lone pairs of phosphorus.<sup>3</sup>

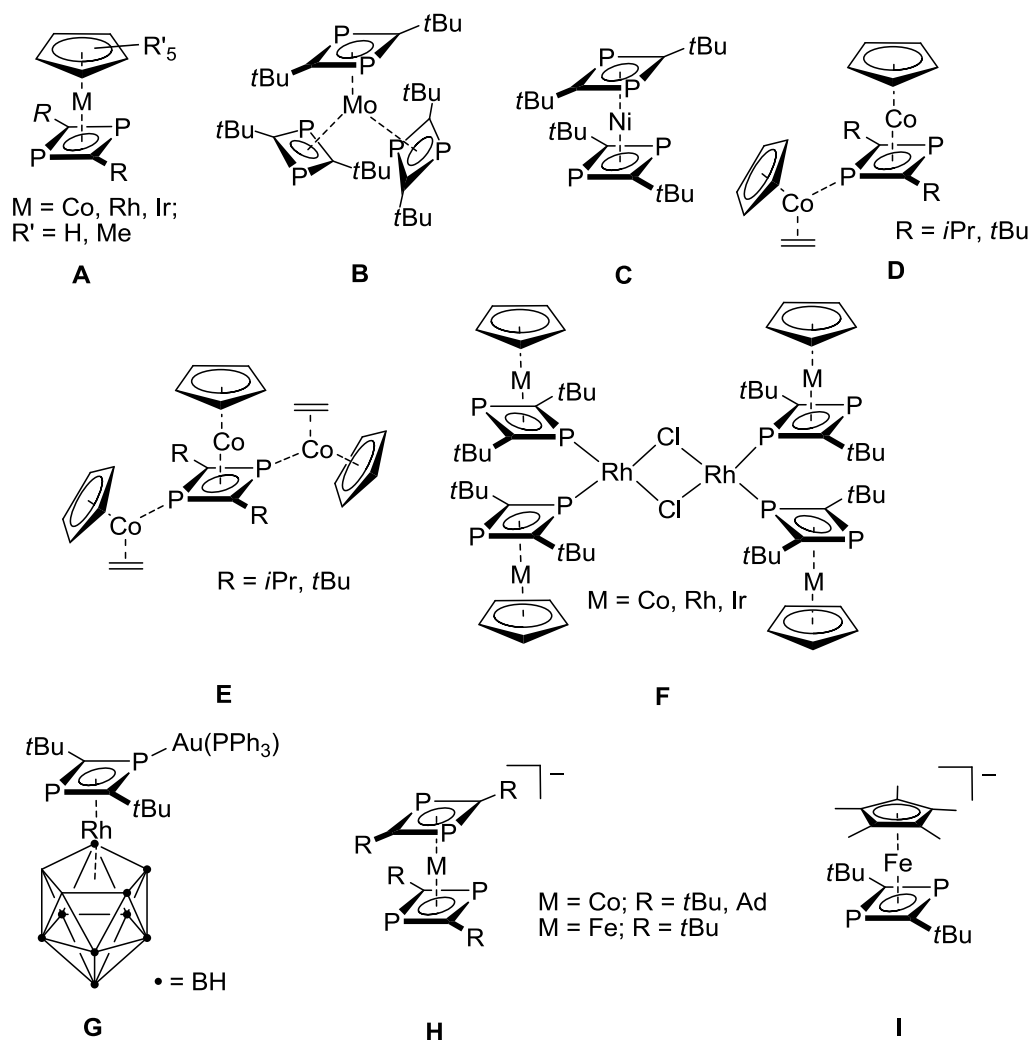
The cyclodimerization of phosphaalkynes  $R-C\equiv P$  in the coordination sphere of a transition metal atom is an elegant method for the preparation of metal-coordinated diphosphacyclobutadienes.<sup>1,4</sup> The formation of the 1,2-diphosphacyclobutadienes via head-to-head dimerization is observed with small substituents on the phosphaalkyne, e.g.  $R = Me$ , while bulkier substituents favor the formation of 1,3-diphosphacyclobutadienes via head-to-tail dimerization.<sup>5</sup> 1,3-diphosphacyclobutadiene complexes of type **A** were first prepared independently by the groups of Regitz, Binger and Nixon in 1986 via the reaction of ethene complexes  $[(C_5R'_5)M(\eta^2-C_2H_2)_2]$  ( $M = Co, Rh, Ir, R' = H, Me$ ) with *tert*-butylphosphaalkyne  $tBu-C\equiv P$ .<sup>6</sup> Since then, various heteroleptic diphosphacyclobutadiene complexes have been synthesized with a range of different early and late transition metals.<sup>7</sup> Homoleptic complexes, which exclusively contain two or three diphosphacyclobutadiene ligands (type **B** and **C**) are still rather scarce.<sup>8,9</sup>

Only few metal complexes with diphosphacyclobutadiene metalloligands have been reported so far.<sup>6c,10-13</sup> Examples are the oligonuclear compounds **D–E**, which were obtained by reacting type **A** complexes  $[CpM(\eta^4-P_2C_2R_2)_2]$  ( $R = tBu, iPr$ ) with  $[CpCo(\eta^2-C_2H_4)_2]$  and  $[RhCl(\eta^2-C_2H_4)_2]_2$ , respectively.<sup>6c,10</sup> The (1,2-dicarbaborane)rhodium complex **G** is the only complex in which a 1,3-diphosphacyclobutadiene ligand is coordinated to a coinage metal atom, more specifically gold(I).<sup>13</sup>

We recently found that anionic bis(1,3-diphosphacyclobutadiene) complexes of type **H** are readily prepared by reacting  $tBuC\equiv P$  and  $AdC\equiv P$  with the low valent metalates  $[K([18]crown\ 6)(thf)_2][M(\eta^4-C_{10}H_{14})_2]$  ( $M = Fe, Co$ ).<sup>14-16</sup> We reported the synthesis and structural characterization of the potassium salts  $[K([18]crown-6)(thf)_2][Co(P_2C_2R_2)_2]$  ( $R = tBu, Ad$ ) and  $[K([18]crown-6)(thf)_2][Fe(C_2P_2tBu_2)_2]$ , which feature similar homoleptic sandwich anions composed of two  $\eta^4$ -coordinated 1,3-diphosphacyclobutadiene ligands. The cobalt complexes are diamagnetic 18e species, whereas the iron compound has 17 valence electrons and is paramagnetic. The heteroleptic 18 electron iron complex **I** can be prepared in an analogous fashion to **H** from  $[K([18]crown-6)(thf)_2][Cp^*Fe(\eta^4-C_{10}H_8)]$  ( $Cp^* = C_5Me_5$ ) and  $tBu-C\equiv P$ .<sup>17</sup> An analysis of the spectroscopic properties and the electronic structures of the  $[M(P_2C_2tBu_2)_2]^-$  ( $M = Fe, Co$ ) anions highlighted the strongly covalent nature of the bonding in these complexes, which makes it difficult to assign the oxidation state of the metal atom unambiguously based on spectroscopic results.<sup>16</sup> By using preparative

and electrochemical methods, we showed that the oxidation of the  $[\text{M}(\text{P}_2\text{C}_2\text{tBu}_2)_2]^-$  affords the neutral sandwich complexes  $[\text{M}(\text{P}_2\text{C}_2\text{tBu}_2)_2]$ .<sup>14,16</sup>

Reactions of  $[\text{Co}(\text{P}_2\text{C}_2\text{tBu}_2)_2]^-$  with a range of different electrophiles ( $\text{H}^+$ ,  $\text{Me}^+$  and  $\text{Ph}_2\text{P}^+$ ) furthermore demonstrate that such sandwich anions may serve as versatile synthetic building blocks for a diverse family of phospho-organometallic complexes.<sup>13</sup>



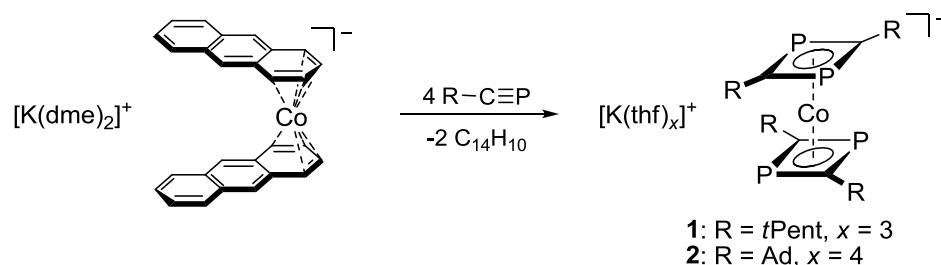
Although bis(diphosphacyclobutadiene) complexes of type **H** promise an intriguing coordination chemistry with transition metal cations due to the presence of four phosphorus atoms carrying lone pairs in their ligand shell, their coordination behavior has not been explored to date. Here, we present first results of coordination studies of the  $[\text{Co}(\text{P}_2\text{C}_2\text{R}_2)_2]^-$  anion with gold(I) and silver(I) cations. We describe the synthesis and characterization of the novel complexes  $[\text{Au}\{\text{Co}(\text{P}_2\text{C}_2\text{tPent}_2)_2\}(\text{PMe}_3)_2]$  (**3**),  $[\text{Au}\{\text{Co}(\text{P}_2\text{C}_2\text{Ad}_2)_2\}]_x$  (**4**),  $[\text{Ag}\{\text{Co}(\text{P}_2\text{C}_2\text{Ad}_2)_2\}]_x$  (**5**),  $[\text{Au}(\text{PMe}_3)_4][\text{Au}\{\text{Co}(\text{P}_2\text{C}_2\text{Ad}_2)_2\}_2]$  (**6**),  $[\text{K}(\text{thf})_6][\text{Au}\{\text{Co}(\text{P}_2\text{C}_2\text{Ad}_2)_2\}_2]$  (**7**),  $[\text{K}([18]\text{crown-6})(\text{thf})_2][\text{Au}\{\text{Co}(\text{P}_2\text{C}_2\text{Ad}_2)_2\}_2]$  (**8**) and  $[\text{K}([18]\text{crown-6})(\text{thf})_2][\text{Ag}\{\text{Co}(\text{P}_2\text{C}_2\text{Ad}_2)_2\}_2]$  (**9**). These complexes were prepared by salt metathesis using the new potassium salts  $[\text{K}(\text{thf})_3\{\text{Co}(\text{P}_2\text{C}_2\text{tPent}_2)_2\}]$  (**1**) and  $[\text{K}(\text{thf})_4\{\text{Co}(\text{P}_2\text{C}_2\text{Ad}_2)_2\}]$  (**2**). The molecular structures of the complexes **2**, **3**, and **6–9** are analyzed by X-ray crystallography. The formation of

dynamic equilibria in THF solution by **3** and **6** is elucidated by variable-temperature NMR spectroscopy. Moreover, we show that multinuclear solid-state NMR is a highly useful complementary tool to analyze the molecular structures of phospho-organometallic coordination compounds such as **3–9**.

## 4.2 Results

### 4.2.1 Syntheses and Structures of the Potassium Salts **1** and **2**

For this initial study, we decided to focus on reactions of the diamagnetic cobalt complexes  $[\text{Co}(\text{P}_2\text{C}_2\text{R}_2)_2]^-$  ( $\text{R} = t\text{Pent}, \text{Ad}$ ) with silver(I) and gold(I) salts. The resulting gold(I) and silver(I) complexes can be easily examined by NMR spectroscopy. As precursors for the preparation of the targeted metal complexes, we decided to prepare the potassium salts  $[\text{K}(\text{thf})_3\{\text{Co}(\text{P}_2\text{C}_2t\text{Pent}_2)_2\}]$  (**1**) and  $[\text{K}(\text{thf})_4\{\text{Co}(\text{P}_2\text{C}_2\text{Ad}_2)_2\}]$  (**2**). Unlike the previously described complexes  $[\text{K}([18]\text{crown-6})(\text{thf})_2][\text{Co}(\text{P}_2\text{C}_2\text{R}_2)_2]$  ( $\text{R} = t\text{Bu}, \text{Ad}$ ), **1** and **2** do not contain crown ether. The presence of *tert*-pentyl and adamantyl substituents ensures good solubility and is less likely to give disorder problems that are sometimes encountered with *tert*-butyl substituted complexes.<sup>14</sup> Compounds **1** and **2** are accessible by reacting the bis(anthracene)cobaltate  $[\text{K}(\text{dme})_2\{\text{Co}(\eta^4\text{-C}_{14}\text{H}_{10})_2\}]$ <sup>18,19</sup> with four equivalents of the corresponding phosphalkyne (*t*Pent–C≡P or Ad–C≡P, respectively) in THF according to Scheme 1. They were isolated as light-red plates (**1**) and light-red blocks (**2**) in good yields (75%) by crystallization from THF/*n*-hexane. Both compounds are very sensitive towards air and moisture. The adamantyl-substituted complex **2** is thermally very stable and decomposes only above 300 °C. The *tert*-pentyl substituted analogue **1** melts at 175 °C.



**Scheme 1.** Synthesis of complexes **1** and **2**.

Compounds **1** and **2** were initially characterized by multinuclear NMR spectroscopy in  $[\text{D}_8]\text{THF}$  and microanalysis. The analytical data indicate the presence of three THF molecules per formula unit for **1** and two THF molecules per formula unit for **2**. Four THF molecules are observed in the X-ray structure of **2** (*vide infra*), but the THF is partly removed by drying the samples in high vacuum.

The  $^1\text{H}$  and  $^{13}\text{C}\{^1\text{H}\}$  NMR spectra confirm the identities of **1** and **2**. Each spectrum shows one set of signals for the *tert*-pentyl and adamantyl substituents, respectively. The formation of the desired bis(diphosphacyclobutadiene) complex is also verified by a triplet in the  $^{13}\text{C}\{^1\text{H}\}$  NMR spectrum at 101.1 ppm for **1** ( $^1J_{\text{CP}} = 52.4$  Hz) and 103.6 ppm for **2** ( $^1J_{\text{CP}} = 51.5$  Hz) assigned to the carbons of the  $\text{C}_2\text{P}_2$  rings. The  $^{31}\text{P}\{^1\text{H}\}$ -NMR spectrum of **1** shows a singlet at 9.6 ppm for the chemically identical

phosphorus atoms of the anion. This resonance is shifted downfield compared to that of the *tert*-butyl-substituted compound  $[\text{K}([18]\text{crown-6})(\text{thf})_2][\text{Co}(\text{P}_2\text{C}_2t\text{Bu}_2)_2]$  (+2.4 ppm).<sup>15</sup> The  $^{31}\text{P}\{^1\text{H}\}$  NMR resonance of the adamantyl-substituted complex **2** of  $-1.1$  ppm is also shifted slightly downfield compared to the crown ether complex  $[\text{K}([18]\text{crown-6})(\text{thf})_2][\text{Co}(\text{P}_2\text{C}_2\text{Ad}_2)_2]$  ( $-2.6$  ppm).<sup>16</sup> These slight discrepancies in the observed  $^{31}\text{P}$  NMR chemical shifts between similar compounds may in part arise from the influence of the potassium cation. Coordination by an [18]crown-6 molecule to potassium should result in an ion-separated arrangement. In contrast, the potassium cations may still be able to bind to the anion in compounds **1** and **2**, as observed in the crystal structure of **2** (*vide infra*).

Whereas our attempts to grow X-ray quality crystals of complex **1** were not successful so far, we were able to determine the molecular structure of **2** in the solid state (Figure 1) by single-crystal X-ray crystallography.

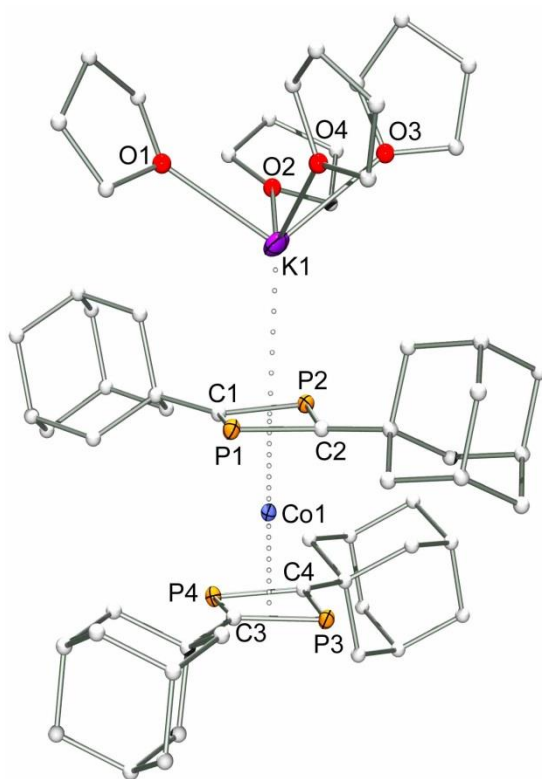


**Figure 1.** Solid-state structure of  $[\text{K}(\text{thf})_4\{\text{Co}(\text{P}_2\text{C}_2\text{Ad}_2)_2\}]$  (**2**), displacement ellipsoids are drawn at the 35% probability level, H atoms and disorder in the THF molecules are omitted for clarity. Selected bond lengths (Å) and angles (°) of **2**: C1–P1 1.8066(17), C1–P2 1.8060(17), C2–P1 1.8118(16), C2–P2 1.8079(17), C3–P3 1.8033(17), C3–P4 1.7970(17), C4–P3 1.7970(17), C4–P4 1.8008(16), K1–P1 3.4296(6), K1–P2 3.4644(7), K1–C1 3.4751(17), K1–C2 3.4217(16), K1–C6 3.468(2), K1–C16 3.3106(17), K1–O1 2.6527(15), K1–O2 2.736(5), K1–O3 2.605(4), K1–O4 3.080(7), Co1–C1 2.0704(16), Co1–P1 2.2532(5), Co1–C2 2.0584(16), Co1–P2 2.2565(5), Co1–C3 2.0732(16), Co1–P3 2.2625(5), Co1–C4 2.0662(16), Co1–P4 2.2634(5), C1–P1–C2 80.51(8), C1–P2–C2 80.63(8), P1–C1–P2 99.31(8), P1–C2–P2 99.05(8), C3–P3–C4 80.78(7), C3–P4–C4 80.85(8), P3–C3–P4 98.83(8), P3–C4–P4 98.92(8).

Unlike the previously characterized crown ether complex  $[\text{K}([18]\text{crown-6})(\text{thf})_2][\text{Co}(\text{P}_2\text{C}_2\text{Ad}_2)_2]$ , which shows an ion-separated arrangement<sup>16</sup>, complex **2** displays an ion-contact structure where the potassium cation interacts with one 1,3-diphosphacyclobutadiene ligand of the cobaltate sandwich anion in an  $\eta^4$ -fashion. The K–P distances of K1–P1 3.465(9) Å and K1–P2 3.429(9) Å are in the range observed for ionic potassium phosphanides.<sup>20</sup> The K–C distances (K1–C1 3.475(2) Å, K1–C2 3.421(2) Å) are similar to the K–C interactions observed in potassium arene compounds.<sup>21</sup> Close contacts observed between K1 and CH<sub>2</sub> groups from the adamantyl substituents (K1–C6 3.468(2) Å and K1–C16 3.3106(17) Å) indicate an interaction of the potassium cation with these substituents. The coordination sphere of potassium is completed by four THF molecules. The  $[\text{Co}(\text{P}_2\text{C}_2\text{Ad}_2)]^-$  unit features two  $\eta^4$ -coordinated diphosphacyclobutadiene rings in a staggered orientation due to the steric repulsion of the adamantyl substituents. The bond lengths and angles within the  $[\text{Co}(\text{P}_2\text{C}_2\text{Ad}_2)]^-$  anion are identical to those in the previously characterized salt  $[\text{K}([18]\text{crown-6})(\text{thf})_2][\text{Co}(\text{P}_2\text{C}_2\text{Ad}_2)_2]$ .<sup>16</sup>

#### 4.2.2 Synthesis and Characterization of Novel Gold(I) and Silver(I) Complexes

Treatment of a THF solution of  $\text{AuCl}(\text{PPh}_3)$  with one equivalent of potassium salt **1**, followed by the subsequent addition of an excess of  $\text{PMe}_3$  at low temperatures ( $-78^\circ\text{C}$ ), affords the neutral gold(I) compound  $[\text{Au}\{\text{Co}(\text{P}_2\text{C}_2\text{Ad}_2)_2\}(\text{PMe}_3)_2]$  (**3**) (Scheme 2a). Compound **3** was isolated as light-red crystals by layering a concentrated THF solution with *n*-hexane in 62% yield. So far, we could not identify the product formed by the 1:1 reaction of **1** with  $\text{AuCl}(\text{PPh}_3)$  in the *absence* of  $\text{PMe}_3$ . This reaction gave an insoluble orange precipitate at room temperature in THF which we could not characterize successfully to date.

Insoluble microcrystalline solids were also obtained when we reacted one equivalent of the adamantyl derivative  $[\text{K}(\text{thf})_4\{\text{Co}(\text{P}_2\text{C}_2\text{Ad}_2)_2\}]$  (**2**) with  $\text{AuCl}(\text{tht})$  (tht = tetrahydrothiophene) and  $\text{AgSbF}_6$  at  $-78^\circ\text{C}$  (Scheme 2b). After addition of **2** to a solution of  $\text{AuCl}(\text{tht})$  at  $-78^\circ\text{C}$ , the colour of the reaction mixtures changes rapidly from light-red to deep red. A red-brown, light-sensitive precipitate of  $[\text{Au}\{\text{Co}(\text{P}_2\text{C}_2\text{Ad}_2)_2\}]_x$  (**4**) is formed upon warming to room temperature. The reaction of **2** with  $\text{AgSbF}_6$  takes a similar course with the initial formation of a deep red-brown solution, followed by the precipitation of a brown microcrystalline powder of the silver complex  $[\text{Ag}\{\text{Co}(\text{P}_2\text{C}_2\text{Ad}_2)_2\}]_x$  (**5**). Compounds **4** and **5** precipitate together with the by-products KCl and  $\text{KSbF}_6$ . Elemental analyses indicate that the isolated solid of compound **4** contains one equiv. KCl per monomeric unit, while the silver complex **5** precipitates with ca. 0.16 equiv.  $\text{KSbF}_6$ . The lack of solubility in common organic solvents prevented their spectroscopic characterization in solution. Multinuclear NMR spectra of solid **4** and **5** suggest that the complexes are polymeric compounds that are formed by the association of  $[\text{Co}(\text{P}_2\text{C}_2\text{Ad}_2)_2]^-$  units with gold(I) or silver(I) cations (*vide infra*).



#### 4.2.2.1 Single-Crystal X-Ray Structures of **3**, and **6–9**

The molecular structure of  $[\text{Au}\{\text{Co}(\text{P}_2\text{C}_2t\text{Pent}_2)_2\}(\text{PMe}_3)_2]$  (**3**) (Figure 2) comprises an  $\text{Au}^+$  cation (Au1) that is coordinated by one phosphorus atom of a  $[\text{Co}(\text{P}_2\text{C}_2\text{Ad}_2)_2]^-$  anion and two  $\text{PMe}_3$  molecules, resulting in a trigonal planar coordination environment (sum of angles around Au1:  $360.0^\circ$ ).

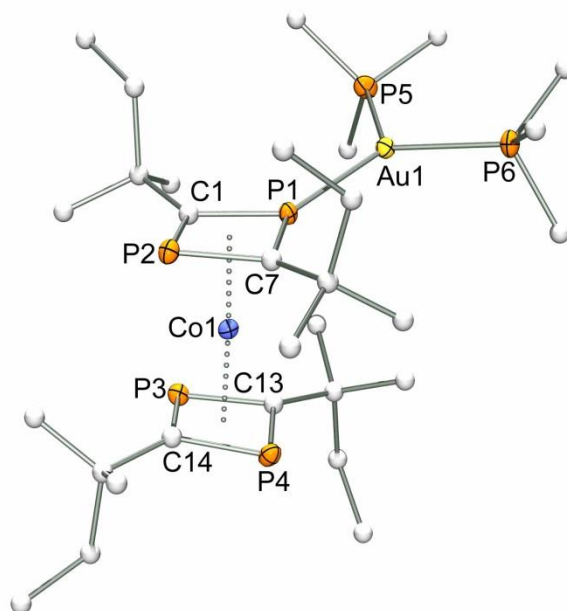


**Figure 2.** Solid-state structure of  $[\text{Au}\{\text{Co}(\text{P}_2\text{C}_2t\text{Pent}_2)_2\}(\text{PMe}_3)_2]$  (**3**). Displacement ellipsoids are at 35% probability, H atoms and solvent molecules are omitted for clarity. Selected bond lengths and angles of **3** are given in Table 1.

Although the preferred geometry for gold(I) complexes is linear, two-coordinate, trigonal planar coordination is well-known.<sup>22</sup> For example, trigonal planar  $[\text{AuL}_3]^+$  species (L = tertiary phosphane) are formed by addition of an excess of phosphane to complexes of type  $[\text{AuL}_2]^+$ .<sup>23</sup> Inspection of the structural parameters of **3** (Table 1) reveals that the angle formed by the two  $\text{PMe}_3$  molecules and the gold atom ( $\text{P5–Au1–P6}$   $114.52^\circ$ ) is narrower than the angles formed by  $\text{PMe}_3$ , Au1 and P1 of the sandwich anion ( $\text{P1–Au1–P5}$   $123.79^\circ$ ;  $\text{P1–Au1–P6}$   $121.67^\circ$ ). This is probably caused by the comparatively large steric demand of the  $[\text{Co}(\text{P}_2\text{C}_2t\text{Pent}_2)_2]^-$  anion. The Au–P bond lengths (Au1–P1 2.366(19), Au1–P5 2.371(2), Au1–P6 2.374(2) Å) are identical within experimental error. Slightly shorter Au–P distances have been observed for other tricoordinate gold(I) complexes which contain tertiary phosphane ligands, e.g.  $[\text{Au}(\text{PPh}_3)_3]^+$  [2.345–2.408 Å] and  $[\text{Au}(\text{dppf})(\text{PPh}_3)]\text{ClO}_4$  [2.343(2)–2.409(2) Å, dppf = 1,1'-bis(diphenyl)-phosphanylferrocene].<sup>24,25</sup> The structural parameters of the  $[\text{Co}(\text{P}_2\text{C}_2t\text{Pent}_2)_2]^-$  anion in the structure of **3** are essentially identical to those of complex **2**, indicating that the structure is robust and not perturbed significantly by the coordination to gold.

The solid-state molecular structure of  $[\text{Au}(\text{PMe}_3)_4][\text{Au}\{\text{Co}(\text{P}_2\text{C}_2\text{Ad}_2)_2\}_2]$  (**6**) is displayed in Figure 3. Graphical representations of the structures of **7–9** are given in the supporting information (Figures S1 to S3). Selected bond lengths and angles of **6–9** are summarized in Table 1. The structures display ion-

separated arrangements that are comprised of centrosymmetrical  $[\text{M}\{\text{Co}(\text{P}_2\text{C}_2\text{Ad}_2)_2\}_2]^-$  anions (**6–8**:  $\text{M} = \text{Au}$ , **9**:  $\text{M} = \text{Ag}$ ) and the counter cations  $[\text{Au}(\text{PMe}_3)_4]^+$  (**6**),  $[\text{K}(\text{thf})_6]^+$  (**7**), and  $[\text{K}([18]\text{crown-6})(\text{thf})_2]^+$  (**8** and **9**). The anions (Figure 3a) are centrosymmetric and consist of  $[\text{Co}(\text{P}_2\text{C}_2\text{Ad}_2)_2]^-$  sandwich units bridged by a linearly coordinated gold or silver atom ( $\text{P1–M1–P1}'$   $180^\circ$ ). The  $[\text{Au}\{\text{Co}(\text{P}_2\text{C}_2\text{Ad}_2)_2\}_2]^-$  moieties of **6–8** feature similar Au–P distances in the range of 2.267(2)–2.272(2) Å. The structure of the only previously characterized gold complex of a diphosphacyclobutadiene metalloligand,  $[\text{Au}\{\text{Rh}(\text{P}_2\text{C}_2t\text{Bu}_2)(\text{C}_2\text{B}_9\text{H}_{11})\}(\text{PPh}_3)]$  (**G**), shows a very similar Au–P bond length (2.269(3) Å).<sup>13</sup> Interestingly, the structure of the silver complex **9** shows a substantially longer Ag–P bond length of 2.3387(7) Å. This discrepancy is probably a consequence of the lanthanoid contraction and relativistic effects.

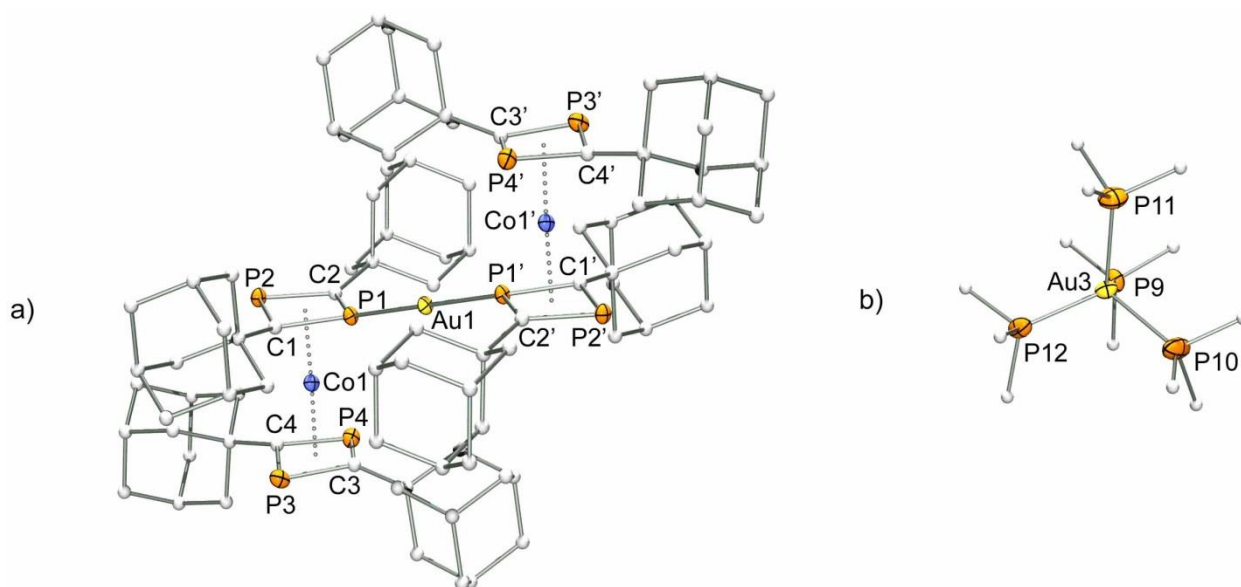


**Figure 3.** a) Solid-state molecular structure of the  $[\text{Au}\{\text{Co}(\text{P}_2\text{C}_2\text{Ad}_2)_2\}_2]^-$  anion of **6**. Thermal ellipsoids are shown at the 35% probability level; the hydrogens and a second crystallographically independent  $[\text{Au}\{\text{Co}(\text{P}_2\text{C}_2\text{Ad}_2)_2\}_2]^-$  anion have been omitted for clarity; b) solid-state molecular structure of the  $[\text{Au}(\text{PMe}_3)_4]^+$  cation of **6**. Thermal ellipsoids are drawn at the 35% probability level. The hydrogen atoms and a second crystallographically independent  $[\text{Au}(\text{PMe}_3)_4]^+$  cation have been omitted for clarity. Selected bond lengths and angles of **6** are given in Table 1.

An intriguing aspect of the structure of  $[\text{Au}(\text{PMe}_3)_4][\text{Au}\{\text{Co}(\text{P}_2\text{C}_2\text{Ad}_2)_2\}_2]$  (**6**) is the  $[\text{Au}(\text{PMe}_3)_4]^+$  cation (Figure 3b), in which the gold atom is tetrahedrally coordinated by four  $\text{PMe}_3$  ligands. Compounds of type  $[\text{Au}(\text{PMe}_3)_4]\text{X}$  ( $\text{X} = \text{BF}_4, \text{NO}_3, \text{Cl}, \text{Br}, \text{I}$ ) have been described by Schmidbaur and Franke as early as 1972.<sup>26</sup> The presence of the  $[\text{Au}(\text{PMe}_3)_4]^+$  cation in these compounds was unequivocally proven by  $^1\text{H}$  NMR, IR spectroscopy, and elemental analysis, but a crystal structure was not obtained at that time. To our knowledge, only two tetrahedral tetrakis(phosphane) gold(I) complexes have previously been crystallographically characterized. The structure of  $[\text{Au}(\text{TPA})_4]\text{X}$  [ $\text{TPA} = 1,3,5\text{-triaz-7-phosphaadamantene}$ ] shows Au–P distances of 2.371–2.395 Å ( $\text{X} = \text{PF}_6^-$ ) and 2.385(5) Å ( $\text{X} = \text{Cl}^-$ ).<sup>27</sup> The

complex  $[\text{Au}(\text{PPh}_2\text{Me})_4]\text{PF}_6$  displays a much longer Au–P bond length [2.449(1) Å] compared to **3**, probably due to the steric repulsion of the more bulky  $\text{PPh}_2\text{Me}$  ligands.<sup>28</sup> The  $[\text{Au}(\text{PMe}_3)_4]^+$  moiety in the structure of **6** features Au–P bond lengths of 2.3789(14)–2.3914(12) Å and P–Au–P angles of 107.82(4)°–112.68(5)°. The average P–Au–P angle of 109.46(5)° corresponds exactly to the ideal tetrahedral angle.



**Table 1.** Selected bond lengths (Å) and angles (°) of **2**, **3** and **6–9**.

	<b>2</b> (M = K)	<b>3</b> (M = Au)	<b>6</b> (M = Au)	<b>7</b> (M = Au)	<b>8</b> (M = Au)	<b>9</b> (M = Ag)
M1–P	3.4296(6)–3.4644(7)	2.365(1)–2.374(1)	2.2707(9)	2.272(2)	2.267(2)	2.3382(5)
P–Au–P	-	114.54(3)–123.73(3)	180.0	180.0	180.00	180.0
P5–Au2–P5'	-	-	180.0	-	-	-
Au3–P9,10,11,12	-	-	2.379(2)–2.391(2)	-	-	-
P–Au3–P	-	-	107.82(4)–112.68(5)	-	-	-
M–P1–Cr(C1,P1,C2,P2)	178.06	165.16	161.22	162.68	165.57	167.63
P–C	1.797(2)–1.812(2)	1.784(3)–1.825(5)	1.764(3)–1.807(3)	1.756(6)–1.818(8)	1.769(5)–1.806(5)	1.774(2)–1.806(2)
Co–C	2.058(2)–2.073(2)	2.082(4)–2.093(4)	2.060(4)–2.093(3)	2.060(8)–2.102(6)	2.060(6)–2.086(5)	2.060(2)–2.081(2)
Co–P	2.2533(5)–2.2635(5)	2.234(1)–2.263(2)	2.184(2)–2.273(2)	2.180(2)–2.265(3)	2.188(2)–2.262(2)	2.2016(6)–2.2639(7)
P–C–P	98.82(8)–99.31(8)	97.3(2)–98.8(2)	96.3(2)–98.7(2)	96.2(3)–99.0(4)	96.4(2)–99.3(3)	96.6(2)–98.9(2)
C–P–C	80.51(8)–80.85(8)	81.0(2)–82.8(2)	80.9(2)–84.7(2)	80.8(3)–84.1(3)	80.5(2)–84.3(2)	80.8(2)–84.0(2)



#### 4.2.2.2 Solid-State NMR Spectra of 3–9

Further insights into the molecular structures of complexes **3–9** and their covalent linking were obtained by solid-state NMR spectroscopy. We start our discussion with the  $^{31}\text{P}$  MAS NMR spectrum of  $[\text{Au}(\text{PMe}_3)_2\{\text{Co}(\text{P}_2\text{C}_2\text{tPent}_2)_2\}]$  (**3**), which is displayed in Figure 4. The six crystallographically unique phosphorus atoms of **3** (Figure 2) are clearly separated into distinct resonances. Due to strong indirect spin-spin interactions, the sharp resonances at 0.5 and 1.7 ppm can be assigned to P5 and P6 of the  $\text{PMe}_3$  ligands. The remaining rather broad signals at 26.4, 15.2, 6.4, and  $-18.2$  ppm arise from the phosphorus atoms of the bis(diphosphacyclobutadiene) sandwich unit. 2D MAS NMR experiments (RFDR **R**adio**F**requency**D**riven**R**ecoupling and R-TOBSY) revealed a correlation between the signals at 26.4 and  $-18.2$  ppm indicating that these signals belong to the constituent phosphorus atoms of one  $\text{P}_2\text{C}_2$  ring. The constituent phosphorus atoms of the other  $\text{P}_2\text{C}_2$  ring were identified by a cross-peak between the resonances at 15.2 and 6.4 ppm. Based on a single cross-peak linking the resonances of the  $\text{PMe}_3$  molecules at 0.5 and 1.7 ppm with the signal at 26.4 ppm, we assign the latter resonance to the gold-coordinated phosphorus atom (P1). Consequently the signal at  $-18.2$  ppm belongs to P2, and the resonances at 15.2 and 6.4 ppm arise from the phosphorus atoms of the non-coordinated diphosphacyclobutadiene ring (P3 and P4).<sup>29</sup> We note that the  $^{31}\text{P}$  resonances of the  $\text{C}_2\text{P}_2$ -ligands are rather broad, most probably due to unresolved indirect spin-spin couplings to the  $^{59}\text{Co}$  nucleus. Comparable results were found for the “ate complexes”  $[\text{Au}(\text{PMe}_3)_4][\text{Au}\{\text{Co}(\text{P}_2\text{C}_2\text{Ad}_2)_2\}_2]$  (**6**) (Figure 5) and  $[\text{K}([18]\text{crown-6})(\text{thf})_2][\text{Au}\{\text{Co}(\text{P}_2\text{C}_2\text{Ad}_2)_2\}_2]$  (**8**) (Figure 7).

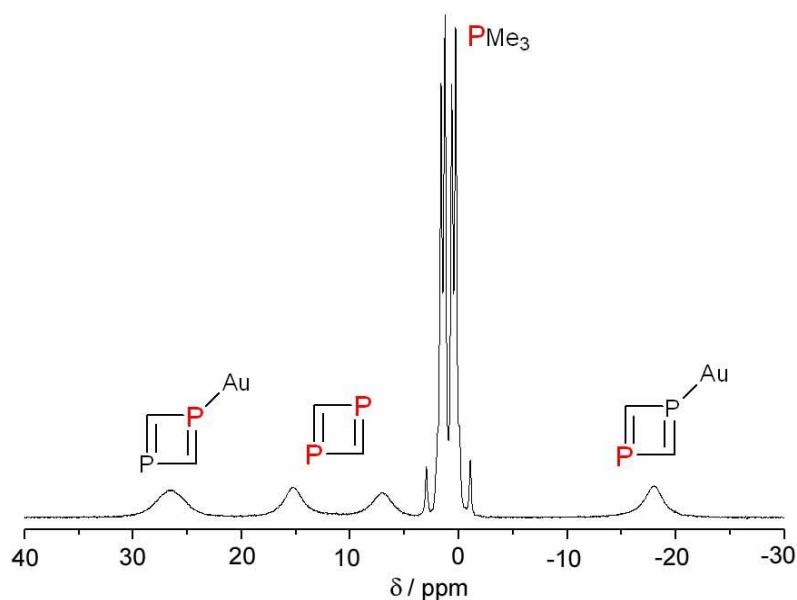


**Figure 4.**  $^{31}\text{P}$  solid-state NMR spectrum of  $[\text{Au}(\text{PMe}_3)_2\{\text{Co}(\text{P}_2\text{C}_2\text{tPent}_2)_2\}]$  (**3**). Recorded at 161.9 MHz, MAS centerband region.

The  $^{31}\text{P}\{^1\text{H}\}$  MAS NMR spectrum of  $[\text{Au}(\text{PMe}_3)_4][\text{Au}\{\text{Co}(\text{P}_2\text{C}_2\text{Ad}_2)_2\}_2]$  (**6**) is displayed in Figure 5. In agreement with the X-ray crystal structure (Figure 3), the spectrum consists of three rather broad resonances at 27.5, 2.4, and  $-43.4$  ppm in a 1:2:1 ratio, and one significantly narrower resonance at

−35.4 ppm. The latter resonance is assigned to the  $[\text{Au}(\text{PMe}_3)_4]^+$  cation. The absence of spinning sidebands clearly indicates the presence of highly symmetric or highly mobile phosphorus centers as expected for this cationic molecular unit. The strong spinning sidebands observed for the remaining  $^{31}\text{P}$  signals reveal large magnetic shielding anisotropies (Table 2) consistent with the nearly planar structure of the diphosphacyclobutadiene ligands. Based on its intensity, the signal at +2.4 ppm is assigned to the two magnetically equivalent phosphorus sites of the “free”, non-gold coordinated  $\text{P}_2\text{C}_2$  ring (P3 and P4 in Figure 3a). The resonances at +27.5 ppm and −43.4 ppm are assigned to the two crystallographically distinct  $^{31}\text{P}$  sites of the diphosphacyclobutadiene ligand which is  $\eta^1$ -coordinated to  $\text{Au}^+$  (P2, −43.4 ppm and P1, 27.5 ppm). Due to extremely short transverse relaxation times of the phosphorus nuclei (most probably due to rapid fluctuations occurring in the Zeeman states of the quadrupolar cobalt nuclei in close proximity to the  $^{31}\text{P}$  nuclei), standard 2-D MAS NMR techniques for assigning the resonances<sup>30</sup> were unsuccessful. Nevertheless,  $^{31}\text{P}$  SPARTAN (Selective Population Anti-z and Rate of Transfer to Adjacent Nuclei) experiments, using cross-relaxation effects between spatially close or bonded phosphorus nuclei,<sup>31</sup> clearly confirm the proposed peak assignments since significant spectral spin-diffusion is observed between the P atoms detected at 27.5 and −43.4 ppm (Figure 6). Based on the results obtained on complex **3**, we assign the resonance at the highest frequency (27.5 ppm) to P1.

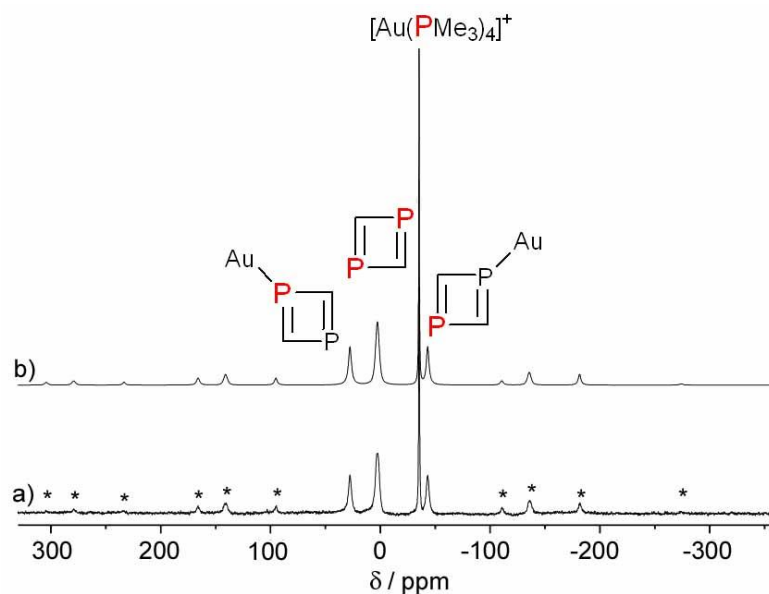


**Figure 5.**  $^{31}\text{P}\{^1\text{H}\}$  MAS NMR spectrum of the gold “ate-complex”  $[\text{Au}(\text{PMe}_3)_4][\text{Au}\{\text{Co}(\text{P}_2\text{C}_2\text{Ad}_2)_2\}_2]$  (**6**) acquired at 11.74 T under rigorously quantitative conditions with a spinning frequency of 28 kHz (a) and corresponding line shape simulation (b). The simulation reveals an intensity ratio of 1:2:2:1 for the resonances at 27.5, 2.4, −35.4 and −43.4 ppm, respectively. \* marks spinning sidebands.

**Table 2.**  $^{31}\text{P}$  chemical shielding anisotropy parameters of compounds **6** and **8**, in the first case extracted from a slow-spinning  $^{31}\text{P}\{^1\text{H}\}$  CPMAS experiment (see Figure S4 of the Supporting Information). The following convention is used:  $\Delta\sigma = \sigma_{zz} - 1/2(\sigma_{xx} + \sigma_{yy})$  and  $\eta_\sigma = (\sigma_{yy} - \sigma_{xx})/(\sigma_{zz} - \sigma_{iso})$  and  $|\sigma_{zz} - \sigma_{iso}| > |\sigma_{xx} - \sigma_{iso}| > |\sigma_{yy} - \sigma_{iso}|$ . In case of **8** all resonances split up in a 3:2 ratio, suggesting either slightly inequivalent molecules or the presence of two polymorphs.

<b>6</b>			<b>8</b>		
$\delta_{iso}/\text{ppm}$	$ \Delta\sigma /\text{ppm}$	$\eta_\sigma$	$\delta_{iso}/\text{ppm}$	$ \Delta\sigma /\text{ppm}$	$\eta_\sigma$
27.5	287.7	0.83	29.1 / 25.9	277.9 / 360.2	0.94 / 0.68
2.4	317.0	0.47	2.9 / -0.3	309.8 / 397.6	0.58 / 0.42
-35.4	-	-	-35.4	-	-
-43.4	346.4	0.39	-42.0 / -45.0	327.7 / 424.6	0.01 / 0.02

The identification of the  $^{31}\text{P}$  site coordinated to the coinage metal (P1) is simplified in case of the corresponding silver compound,  $[\text{K}([18]\text{crown-6})(\text{thf})_2][\text{Ag}\{\text{Co}(\text{P}_2\text{C}_2\text{Ad}_2)_2\}_2]$  (**9**), due to spin-spin couplings between the phosphorus site P1 and the two silver isotopes  $^{107}\text{Ag}$  and  $^{109}\text{Ag}$ . A clear doublet is observed for the resonance at -22.5 ppm with an averaged  $^1J(^{31}\text{P}^{107/109}\text{Ag})$  coupling constant of 1339 Hz (Figure 8 and Table 3). The singlet at a comparable chemical shift value (-22.6 ppm) is assigned to P2 while the phosphorus sites of the “free” ligand (P3 and P4) resonate at higher frequencies. The line shapes of the latter resonances as well as the symmetry of the doublet differ slightly with the magnetic field strength. We attribute this observation to unresolved  $^{31}\text{P}^{59}\text{Co}$   $J$  couplings and dipolar splittings that are influenced by the quadrupolar interactions of the cobalt nucleus.<sup>32</sup> Our peak assignments are supported by DFT calculations of magnetic shielding constants in the gas phase (B3-LYP/def2-TZVP,<sup>33,34</sup> for more details see the Experimental Section) for a negatively charged anionic molecular ( $[\text{Ag}\{\text{Co}(\text{P}_2\text{C}_2\text{Ad}_2)_2\}_2]^-$ ) unit of **9**, which are in good agreement with the experimentally observed values (Table 3).

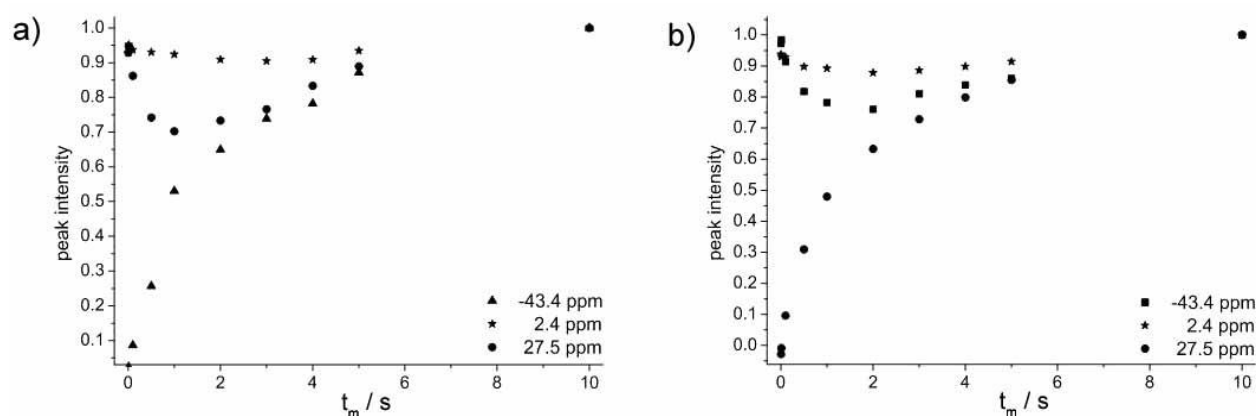


**Figure 6.**  $^{31}\text{P}$  peak intensities as a function of mixing times in SPARTAN experiments for **6** performed with selective excitation of the resonance at  $-43.4$  ppm (a) and  $27.5$  ppm (b). In both cases significant spectral spin diffusion is observed between the resonances at  $-43.4$  ppm and  $27.5$  ppm leading to the conclusion that both species belong to the same  $\text{C}_2\text{P}_2$ -ligand. The signals are normalized in both cases to the spectrum obtained with the longest mixing time applied.

**Table 3.** Experimentally and quantum-chemically (B3-LYP/def2-TZVP) determined  $^{31}\text{P}$  isotropic chemical shifts of **9**, referenced to phosphoric acid, for more details see the Experimental Section.

	$\delta_{\text{exp}}/\text{ppm}$	$\delta_{\text{calc}}/\text{ppm}$
P1	$-22.5^{[\text{a}]}$	$-30.9$
P2	$-22.6$	$-28.2$
P3/ P4	$0.^{[\text{b}]}/ 1.5^{[\text{c}]}$	$0.1$
P4/ P3	$-2.^{[\text{b}]}/ -3.3^{[\text{c}]}$	$-2.7$

[a] The simulation is based on a  $^1J(^{31}\text{P}, ^{107/109}\text{Ag})$  coupling constant of  $1339$  Hz. [b] Determined at  $11.74$  T.

[c] Determined at  $7.05$  T

The  $^{13}\text{C}\{^1\text{H}\}$  CPMAS spectra of **6** and **9** (see Figures S5a and S6a of the Supporting Information) reveal in both cases two equally intense resonances for the carbon sites C1/C2 and C3/C4, again significantly broadened by unresolved  $^{13}\text{C}^{59}\text{Co}$   $J$  couplings. DFT calculations of  $^{13}\text{C}$  magnetic shieldings for **9** reveal that the  $^{13}\text{C}$  nuclei of the diphosphacyclobutadiene ligand coordinated to the coinage metal are shifted to lower frequencies than the “free” ligands, which leads to the assignments shown in Table 4.

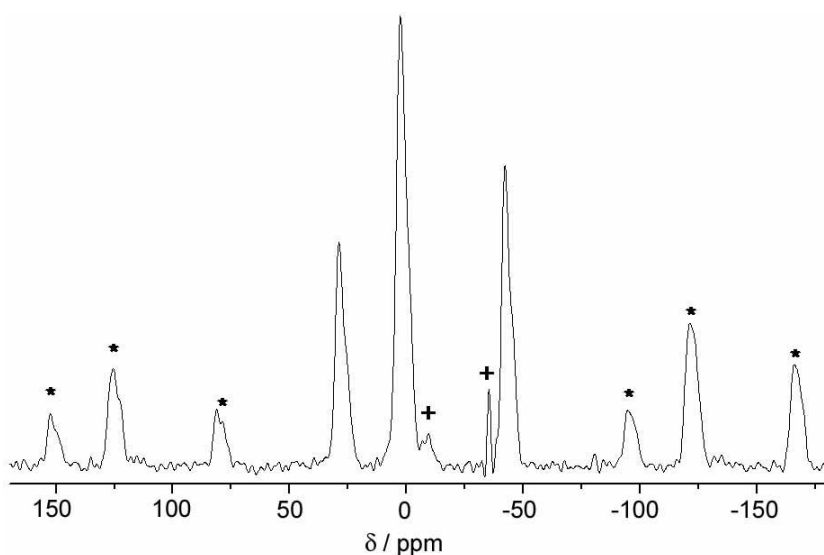


**Figure 7.**  $^{31}\text{P}\{^1\text{H}\}$  CPMAS NMR spectrum of the “ate-complex”  $[\text{K}([18]\text{crown-6})(\text{thf})_2][\text{Au}\{\text{Co}(\text{P}_2\text{C}_2\text{Ad}_2)_2\}_2]$  (**8**) acquired at 11.74 T with a spinning frequency of 25 kHz. \* marks spinning sidebands, + impurities.

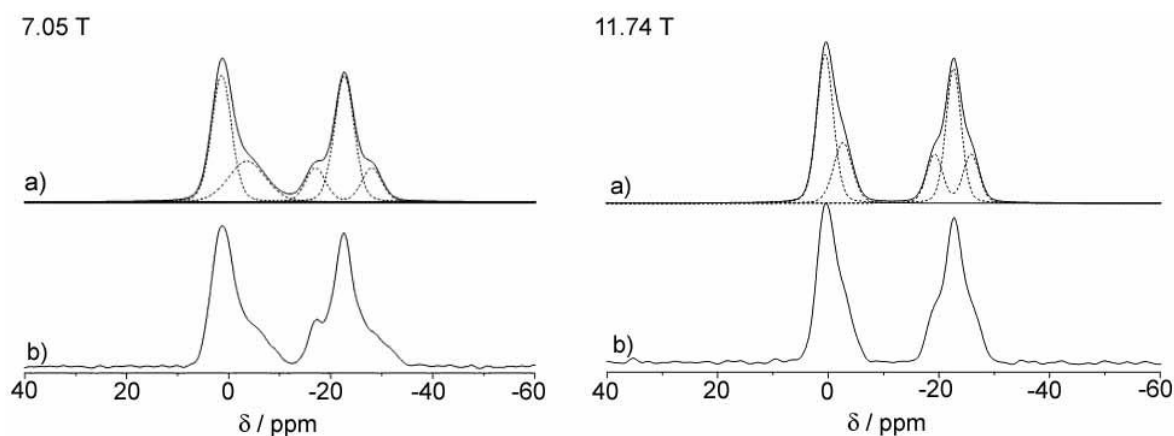


**Figure 8.**  $^{31}\text{P}\{^1\text{H}\}$  MAS NMR spectra of the “ate complex”  $[\text{K}([18]\text{crown-6})(\text{thf})_2][\text{Ag}\{\text{Co}(\text{P}_2\text{C}_2\text{Ad}_2)_2\}_2]$  (**9**) acquired at 7.05 T (a, left) and 11.74 T (a, right) and corresponding line shape simulations (b). The simulation parameters are given in Table 3.

**Table 4.** Experimentally and quantum-chemically (B3-LYP/def2-TZVP) determined  $^{13}\text{C}$  isotropic chemical shifts of **6** and **9**, referenced to TMS, for more details see the Experimental Section.

	$\delta_{\text{exp}}/\text{ppm}$ ( <b>6</b> )	$\delta_{\text{exp}}/\text{ppm}$ ( <b>9</b> )	$\delta_{\text{calc}}/\text{ppm}$ ( <b>9</b> )
C1/C2	94.3	96.7	106.6; 108.0
C3/C4	111.2	111.5	121.0; 122.3

Analyzing the results described above, we can additionally propose a structure for the polymeric compounds  $[\text{Au}\{\text{Co}(\text{P}_2\text{C}_2\text{Ad}_2)_2\}]_x$  (**4**) and  $[\text{Ag}\{\text{Co}(\text{P}_2\text{C}_2\text{Ad}_2)_2\}]_x$  (**5**). In case of **4**, two broad  $^{31}\text{P}\{^1\text{H}\}$  MAS NMR spectrum (Figure 9) in close agreement with the measured chemical shifts of the phosphorus sites P1 and P2 in the “ate-complex” **6**. Since no signal characteristic for the free ligand is detected, we propose a “zig-zag” rather than a symmetrically linked structure (Figure 10) for these polymers. These conclusions are supported by the  $^{13}\text{C}\{^1\text{H}\}$  CPMAS NMR spectrum of **4** (see Figure S5b of the Supporting Information) in which only one  $^{13}\text{C}$  resonance is apparent. This observation clearly indicates that the two diphosphacyclobutadiene ligands are both coordinated to the gold or silver cations, forming in this way the backbone of a polymeric arrangement. The same argument is valid for **5** except that, in agreement with the results obtained for the “ate-complex” **9**, the two phosphorus sites are overlapping in the  $^{31}\text{P}\{^1\text{H}\}$  CPMAS NMR spectrum (see Figure 9c).

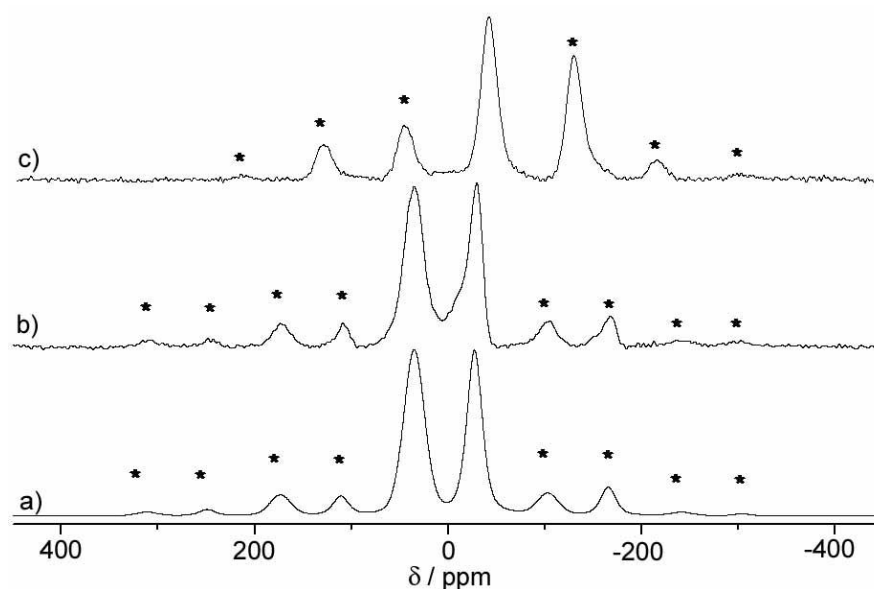


**Figure 9.**  $^{31}\text{P}\{^1\text{H}\}$  MAS-NMR spectrum of  $[\text{Au}\{\text{Co}(\text{P}_2\text{C}_2\text{Ad}_2)_2\}]_n$  (**4**) acquired at 11.74 T with a spinning frequency of 28 kHz under rigorously quantitative conditions (b) and corresponding line shape simulation (a) and rotor synchronized  $^{31}\text{P}\{^1\text{H}\}$  CPMAS NMR Hahn spin echo spectrum of  $[\text{Ag}\{\text{Co}(\text{P}_2\text{C}_2\text{Ad}_2)_2\}]_n$  (**5**) acquired at 9.4 T with a spinning frequency of 14 kHz (c). \* marks spinning sidebands. Right: Schematic representation of the proposed “zig-zag” coordination of  $\text{Au}^+$  and  $\text{Ag}^+$  cations by the  $[\text{Co}(\text{P}_2\text{C}_2\text{Ad}_2)_2]^-$  anions in complexes **4** and **5**.

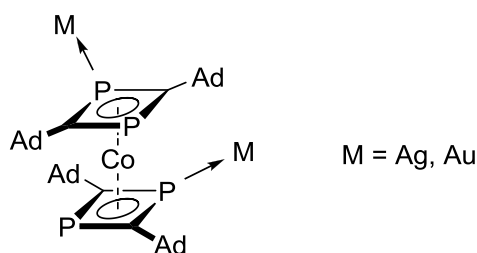


**Figure 10.** Schematic representation of the proposed “zig-zag” coordination of  $\text{Au}^+$  and  $\text{Ag}^+$  by the  $[\text{Co}(\text{P}_2\text{C}_2\text{Ad}_2)_2]^-$  anions in complexes **4** and **5**.

### 4.2.2.3 Solution NMR Spectra of Complexes 3, 6 and 7:

The complexes **3**, **6** and **7** are soluble in  $[D_8]THF$  and were therefore investigated by multinuclear NMR spectroscopy in that solvent. Interestingly, the  $^{31}P\{^1H\}$  NMR spectra of  $[Au\{Co(P_2C_2tPent)_2\}(PMe_3)_2]$  (**3**) (Figure 11) show temperature-dependent behavior, indicating a dynamic process. The temperature-dependent NMR behavior of **3** is consistent with the equilibrium proposed in Scheme 3.

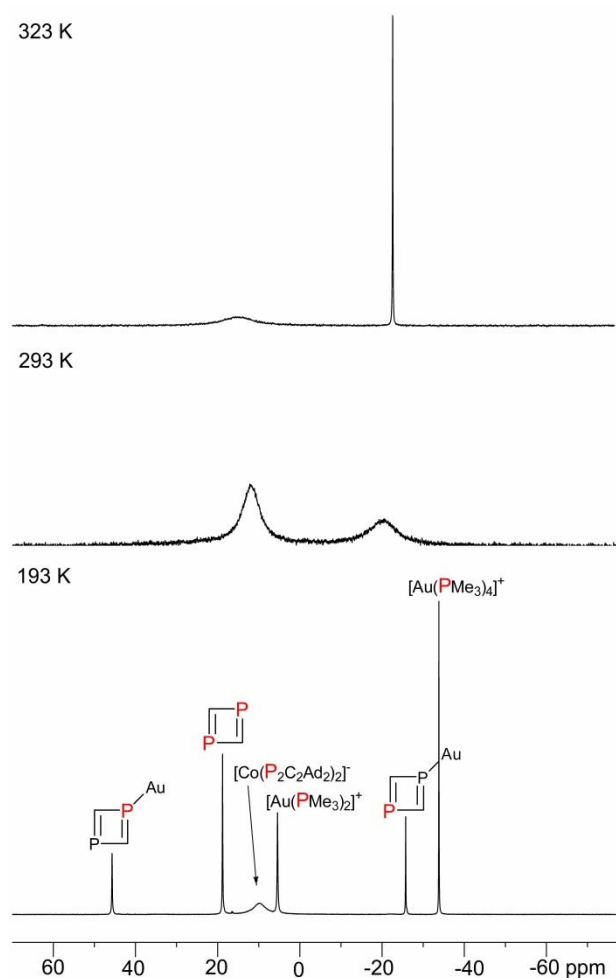
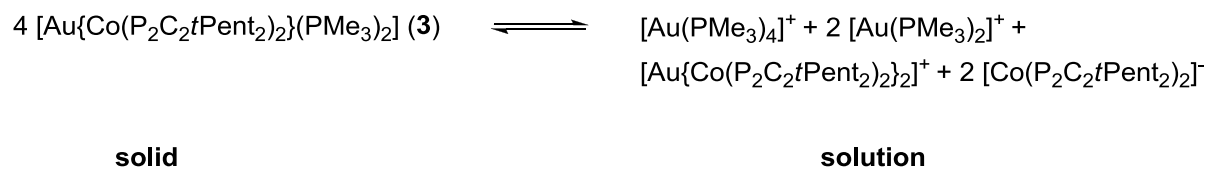


**Figure 11.** Temperature-dependent  $^{31}P\{^1H\}$  NMR spectra of  $[Au\{Co(P_2C_2tPent)_2\}(PMe_3)_2]$  (**3**) in  $[D_8]THF$ . The drawings denote the different phosphorus environments in the species observed in solution.



**Scheme 3.** Equilibrium of the ion-contact complex **3** with the ion pair **3'** in  $[D_8]THF$  solution.

The low-temperature spectrum recorded at  $-80\text{ }^{\circ}\text{C}$  displays six distinct signals whereas only four signals, that is, one signal for  $\text{PMe}_3$  and three signals for the  $[\text{Co}(\text{P}_2\text{C}_2\text{Ad}_2)_2]^-$  moiety, are expected according to the solid-state structure of **3** (see above). According to this scenario, complex **3** does not stay intact in the polar solvent  $[\text{D}_8]\text{THF}$ , but forms a mixture of the ionic species  $[\text{Au}(\text{PMe}_3)_4]^+$ ,  $[\text{Au}(\text{PMe}_3)_2]^+$ ,  $[\text{Co}(\text{P}_2\text{C}_2t\text{Pent}_2)_2]^-$ , and  $[\text{Au}\{\text{Co}(\text{P}_2\text{C}_2t\text{Pent}_2)_2\}_2]^-$ . In the low-temperature spectrum at  $-80\text{ }^{\circ}\text{C}$ , the resonance at 5.4 ppm can be assigned to the  $[\text{Au}(\text{PMe}_3)_2]^+$  cation. A similar chemical shift is reported for this cation in the literature ( $\delta = 3.4$  ppm in  $\text{CDCl}_3$ ).<sup>27,35</sup> The signal at  $-33.7$  ppm may be assigned to the tetracoordinate  $[\text{Au}(\text{PMe}_3)_4]^+$  cation. The same resonance is observed in the solution and solid-state NMR spectra of complex **6** (Figures 5 and 12). The signal at  $+9.9$  ppm (broad singlet) arises from the  $[\text{Co}(\text{P}_2\text{C}_2t\text{Pent}_2)_2]^-$  anion, which exhibits a very similar chemical shift in the potassium salt  $[\text{K}(\text{thf})_3\{\text{Co}(\text{P}_2\text{C}_2t\text{Pent}_2)_2\}]$  (**1**,  $\delta = 9.6$  ppm) (see above). In analogy to the structures of **7–9**, we assign the remaining three peaks at 45.7, 18.8, and  $-25.7$  ppm (1:2:1 ratio) to the “ate-complex”  $[\text{Au}\{\text{Co}(\text{P}_2\text{C}_2t\text{Pent}_2)_2\}_2]^-$ . At higher temperatures, the signals of the diphosphacyclobutadiene ligands coalesce into a broad peak, which is observed at 12.8 ppm at room temperature. A single broad resonance is also observed for the  $\text{PMe}_3$  ligand at  $-16.7$  ppm at room temperature, which is attributed to the formation of an equilibrium between the  $[\text{Au}(\text{PMe}_3)_2]^+$  and  $[\text{Au}(\text{PMe}_3)_4]^+$  cations in solution. The resonances at 12.8 and  $-16.7$  ppm are in an approximate intensity ratio of 4:2 at room temperature. The spectrum at  $50\text{ }^{\circ}\text{C}$  shows a broad signal at 15.0 ppm and a sharper peak at  $-20.2$  ppm. The  $^1\text{H}$  and  $^{13}\text{C}\{^1\text{H}\}$  NMR spectra of **3** in  $[\text{D}_8]\text{THF}$  (Figures S7 and S8 in the Supporting Information) are also temperature-dependent. The spectra are consistent with the proposed formation of an equilibrium between the ionic species shown in Scheme 3. A well-resolved  $^1\text{H}$  NMR spectrum recorded at  $50\text{ }^{\circ}\text{C}$  shows one *tert*-pentyl environment and one doublet for coordinated  $\text{PMe}_3$  ( $\delta = 1.47$  ppm,  $^2J(\text{P},\text{H}) = 7.0$  Hz). Similarly, the  $^{13}\text{C}\{^1\text{H}\}$  NMR spectrum shows only one set of signals for the *tert*-pentyl substituents and a doublet for the methyl groups of  $\text{PMe}_3$  ( $\delta = 18.9$  ppm,  $^1J(\text{P},\text{C}) = 17.8$  Hz) above room temperature. A single, broad peak at 102.4 ppm is observed for the carbon atoms of the  $\text{C}_2\text{P}_2$  rings at  $50\text{ }^{\circ}\text{C}$ , indicating equivalent diphosphacyclobutadiene rings. These observations indicate that the  $[\text{Au}(\text{PMe}_3)_4]^+$ ,  $[\text{Au}(\text{PMe}_3)_2]^+$ ,  $[\text{Co}(\text{P}_2\text{C}_2t\text{Pent}_2)_2]^-$ , and  $[\text{Au}\{\text{Co}(\text{P}_2\text{C}_2t\text{Pent}_2)_2\}_2]^-$  ions rapidly exchange on the NMR timescale. Upon lowering the temperature, the slow exchange limit is approached, which results in severe line broadening and the observation of distinct, overlapping  $^1\text{H}$  NMR resonances. The  $^{13}\text{C}\{^1\text{H}\}$  NMR spectra also become more complex upon decreasing the temperature. At  $-80\text{ }^{\circ}\text{C}$ , four sets of signals are observed for the *tert*-pentyl groups: one for the  $[\text{Co}(\text{P}_2\text{C}_2t\text{Pent}_2)_2]^-$  anion and three for the chemically inequivalent *t*Pent substituents of the “ate complex”  $[\text{Au}\{\text{Co}(\text{P}_2\text{C}_2t\text{Pent}_2)_2\}_2]^-$ . Four distinct resonances are also observed for the quarternary carbon atoms of the diphosphacyclobutadiene rings ( $\delta = 92.0, 100.8, 106.7$  and  $109.4$  ppm at  $-80^{\circ}\text{C}$ ). The  $^{13}\text{C}\{^1\text{H}\}$  NMR doublet observed for  $\text{PMe}_3$  at room temperature splits into two broad resonances at 17.7 and 20.7 ppm at  $-80\text{ }^{\circ}\text{C}$  that are assigned to the  $[\text{Au}(\text{PMe}_3)_4]^+$  and  $[\text{Au}(\text{PMe}_3)_2]^+$  cations, respectively.

The  $^{31}\text{P}\{^1\text{H}\}$  NMR spectrum of the “ate complex”  $[\text{K}(\text{thf})_6][\text{Au}\{\text{Co}(\text{P}_2\text{C}_2\text{Ad}_2)_2\}_2]$  (**7**) displays three resonances in a ratio of 1:2:1 at  $-36.5$ ,  $9.4$ , and  $33.9$  ppm. This pattern is in agreement with the solid-state structure of the compound (see Supporting Information, Figure S1). The resonances agree well with those observed for the same compound by solid-state NMR spectroscopy (Table 2 and Figure 7). The signal at  $9.4$  ppm can be assigned to the non-coordinated bis(diphosphacyclobutadiene) rings, whereas the resonances at  $-36.5$  and  $33.9$  ppm are assigned to the  $\text{C}_2\text{P}_2$  rings that are coordinated to gold.

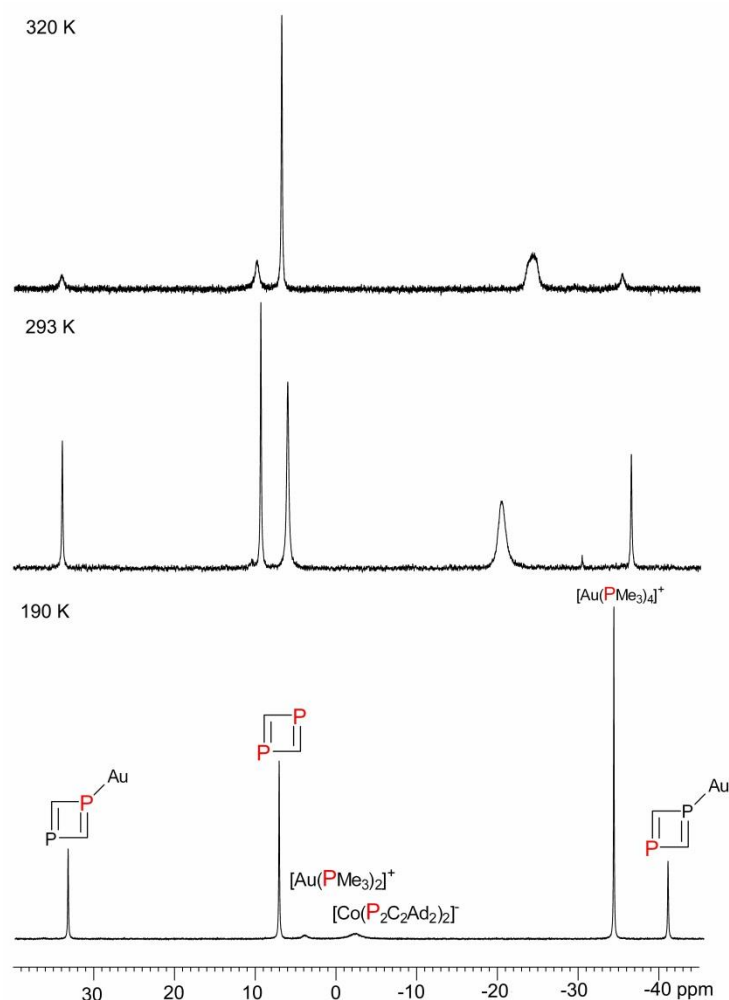
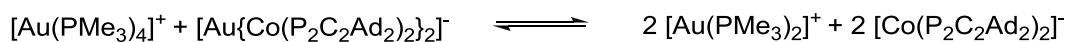


**Figure 12.** Temperature-dependent  $^{31}\text{P}\{^1\text{H}\}$  NMR spectrum of  $[\text{Au}(\text{PMe}_3)_4][\text{Au}\{\text{Co}(\text{P}_2\text{C}_2\text{Ad}_2)_2\}_2]$  (**6**) in  $[\text{D}_8]\text{THF}$ . The drawings denote the different phosphorus environments in the species observed in solution.

Similar to **7**, the low-temperature ( $-80$  °C)  $^{31}\text{P}\{^1\text{H}\}$  NMR spectrum of  $[\text{Au}(\text{PMe}_3)_4][\text{Au}\{\text{Co}(\text{P}_2\text{C}_2\text{Ad}_2)_2\}_2]$  (**6**) features three resonances for the  $[\text{Au}\{\text{Co}(\text{P}_2\text{C}_2\text{Ad}_2)_2\}_2]^-$  anion at  $33.4$ ,  $7.4$ , and  $-40.5$  ppm (Figure 12). A sharp resonance observed at  $-33.9$  ppm is assigned to the  $[\text{Au}(\text{PMe}_3)_4]^+$  cation. These signals are consistent with the solid state NMR spectrum (Table 2 and Figure 5), which shows comparable signals at  $27.5$ ,  $2.4$ ,  $-35.4$ , and  $-43.4$  ppm. Integration of the resonance of  $[\text{Au}(\text{PMe}_3)_4]^+$  at  $-33.9$  ppm indicates the presence of an excess of this cation in solution. This observation could be due to the presence of  $[\text{Au}(\text{PMe}_3)_4]\text{Cl}$ , which is soluble in THF.<sup>27</sup> From the NMR integrals and the elemental analysis we derive the presence of approximately 0.25 equiv of  $[\text{Au}(\text{PMe}_3)_4]\text{Cl}$  per formula unit of **6**.

It is important to note that the solution  $^{31}\text{P}$  NMR spectrum of **6** at  $-80\text{ }^{\circ}\text{C}$  displays two additional broad signals at 4.5 and  $-2.1$  ppm. We attribute these resonances to the partial decomposition of **6** in solution into the  $[\text{Au}(\text{PMe}_3)_2]^+$  cation and the  $[\text{Co}(\text{P}_2\text{C}_2\text{Ad}_2)_2]^-$  anion according to Scheme 4.



**Scheme 4.** Equilibrium observed for  $[\text{Au}(\text{PMe}_3)_4][\text{Au}\{\text{Co}(\text{P}_2\text{C}_2\text{Ad}_2)_2\}_2]$  (**6**) in  $[\text{D}_8]\text{THF}$ .

The  $[\text{Au}(\text{PMe}_3)_2]^+$  cation shows a broad  $^{31}\text{P}\{^1\text{H}\}$  resonance at 4.5 ppm, which is close to the chemical shift of 5.4 ppm observed for the same species in the  $^{31}\text{P}\{^1\text{H}\}$  NMR spectrum of **3**. The  $[\text{Co}(\text{P}_2\text{C}_2\text{Ad}_2)_2]^-$  anion shows a singlet at  $-2.1$  ppm (compare with  $\delta = -2.6$  ppm for  $[\text{K}([18]\text{crown-6})(\text{thf})_2][\text{Co}(\text{P}_2\text{C}_2\text{Ad}_2)_2]$ ).<sup>16</sup> The partial degradation of the  $[\text{Au}\{\text{Co}(\text{P}_2\text{C}_2\text{Ad}_2)_2\}_2]^-$  anion in THF solution is probably caused by nucleophilic attack of  $\text{PMe}_3$ , which dissociates from the  $[\text{Au}(\text{PMe}_3)_4]^+$  cation. In their pioneering report on gold(I) trimethylphosphane complexes, *Schmidbaur* and *Franke* already noted that the complexes  $[\text{Au}(\text{PMe}_3)_4]\text{X}$  ( $\text{X}=\text{BF}_4, \text{NO}_3, \text{Cl}, \text{Br}, \text{I}$ ) readily lose  $\text{PMe}_3$  on storing at room temperature under vacuum. This observation indicates that the Au–P bonds in the  $[\text{Au}(\text{PMe}_3)_4]^+$  cation are rather labile.<sup>26</sup>

According to the  $^{31}\text{P}\{^1\text{H}\}$  NMR spectra ( $[\text{D}_8]\text{THF}$ ), the  $[\text{Au}(\text{PMe}_3)_4]^+$  and the  $[\text{Au}(\text{PMe}_3)_2]^+$  cations of **6** are in rapid equilibrium at room temperature and  $50\text{ }^{\circ}\text{C}$  (Figure 12). Thus, only one broad  $\text{PMe}_3$  resonance is detected at  $\delta = -20.4$  ppm at room temperature. The characteristic resonances of the  $[\text{Co}(\text{P}_2\text{C}_2\text{Ad}_2)_2]^-$  and  $[\text{Au}\{\text{Co}(\text{P}_2\text{C}_2\text{Ad}_2)_2\}_2]^-$  anions are observed even at  $50\text{ }^{\circ}\text{C}$ , although the resonances of the latter species is much less intense and significantly broadened at this temperature compared to the low-temperature spectra. Integration of the  $^{31}\text{P}$  NMR spectra yielded a 3:1 ratio of  $[\text{Co}(\text{P}_2\text{C}_2\text{Ad}_2)_2]^-/[\text{Au}\{\text{Co}(\text{P}_2\text{C}_2\text{Ad}_2)_2\}_2]^-$  at  $50\text{ }^{\circ}\text{C}$ , whereas a ratio of 0.4:1 is observed at  $-80\text{ }^{\circ}\text{C}$ . This indicates that the equilibrium displayed in Scheme 4 is shifted to the right side upon raising the temperature.

### 4.3 Conclusion

The results of this study can be summarized as follows:

- 1) Gold(I) and silver(I) complexes of the  $[\text{Co}(\text{P}_2\text{C}_2\text{R}_2)_2]^-$  ( $\text{R}=t\text{Pent}, \text{Ad}$ ) anions are readily accessible through salt elimination reactions of the potassium salts **1** and **2** with suitable gold(I) and silver(I) halides. A range of new complexes possessing 1:1 (**3–5**) and 2:1 ratios (**6–9**) of anion/cation have been prepared by using this approach. Compounds **3–9** are the first transition-metal complexes with bis(diphosphacyclobutadiene) sandwich anions of type  $[\text{M}(\text{P}_2\text{C}_2\text{R}_2)_2]^-$ .
- 2) The  $[\text{Co}(\text{P}_2\text{C}_2\text{R}_2)_2]^-$  anions coordinate to the coinage metal ion through their phosphorus atoms. This coordination mode results in the formation of a polymeric arrangement for the 1:1 complexes  $[\text{Au}\{\text{Co}(\text{P}_2\text{C}_2\text{Ad}_2)_2\}_x]$  (**4**) and  $[\text{Ag}\{\text{Co}(\text{P}_2\text{C}_2\text{Ad}_2)_2\}_x]$  (**5**). Depending on the substituent ( $t\text{Pent}$  or  $\text{Ad}$ ), two

different types of adducts are formed upon the addition of the donor molecule  $\text{PMe}_3$  to reaction mixtures of gold(I) chloride with **1** and **2**. The complex  $[\text{Au}(\text{PMe}_3)_2\{\text{Co}(\text{P}_2\text{C}_2\text{tPent}_2)_2\}]$  (**3**) shows an ion-contact structure, whereas  $[\text{Au}(\text{PMe}_3)_4][\text{Au}\{\text{Co}(\text{P}_2\text{C}_2\text{Ad}_2)_2\}_2]$  (**6**) displays an ion-separated arrangement and contains the rare  $[\text{Au}(\text{PMe}_3)_4]^+$  cation. The structure of **6** shows the new “ate-complex” anion  $[\text{Au}\{\text{Co}(\text{P}_2\text{C}_2\text{Ad}_2)_2\}_2]^-$ . Similar anions are observed in the structures of complexes **7–9**.

- 3) Our results demonstrate the utility of solid-state NMR spectroscopy as a powerful tool to probe the structural composition of phospho-organometallic complexes and coordination polymers. The results are additionally supported by DFT calculations. The solid-state NMR data of **6–9** agree well with the single-crystal X-ray structures, demonstrating that the crystallographically-characterized species represent the bulk material. The microcrystalline complexes  $[\text{Au}\{\text{Co}(\text{P}_2\text{C}_2\text{Ad}_2)_2\}]_x$  (**4**) and  $[\text{Ag}\{\text{Co}(\text{P}_2\text{C}_2\text{Ad}_2)_2\}]_x$  (**5**) could not be structurally characterized by X-ray crystallography. However, the NMR spectroscopic results clearly show that these compounds exist as coordination polymers formed by the interaction of two phosphorus atoms from different  $\text{P}_2\text{C}_2$  rings to two  $\text{Au}^+$  and  $\text{Ag}^+$  cations. This results in a “zig-zag” structure as indicated in Figure 10.
- 4) Multinuclear solution NMR spectroscopy has been used to elucidate the solution behavior of the complexes  $[\text{Au}\{\text{Co}(\text{P}_2\text{C}_2\text{tPent}_2)_2\}(\text{PMe}_3)_2]$  (**3**),  $[\text{Au}(\text{PMe}_3)_4][\text{Au}\{\text{Co}(\text{P}_2\text{C}_2\text{Ad}_2)_2\}_2]$  (**6**) and  $[\text{K}(\text{thf})_6][\text{Au}\{\text{Co}(\text{P}_2\text{C}_2\text{Ad}_2)_2\}_2]$  (**7**) in  $[\text{D}_8]\text{THF}$ . The spectra of **7** confirm the presence of an intact  $[\text{Au}\{\text{Co}(\text{P}_2\text{C}_2\text{Ad}_2)_2\}_2]^-$  unit in solution. In contrast, the temperature-dependent NMR spectra of **3** and **6** demonstrate the formation of equilibria between the ionic species  $[\text{Au}(\text{PMe}_3)_2]^+$ ,  $[\text{Au}(\text{PMe}_3)_4]^+$ ,  $[\text{Co}(\text{P}_2\text{C}_2\text{R}_2)_2]^-$  and  $[\text{Au}\{\text{Co}(\text{P}_2\text{C}_2\text{R}_2)_2\}_2]^-$  (Scheme 3 and 4). These observations highlight the Au–P bonding in these complexes is reversible.
- 5) Although this work presents valuable first insights into the coordination properties of diphosphacyclobutadiene sandwich anions, it seems likely that a much more extensive and versatile coordination chemistry can be unraveled for these anions in the near future. An important aspect for future work will be the synthesis of complexes with a wider range of transition-metal cations. The molecular structure of the potassium salt  $[\text{K}(\text{thf})_4\{\text{Co}(\eta^4\text{-P}_2\text{C}_2\text{Ad}_2)_2\}]$  (**2**) (Figure 1) suggests that the preparation of  $\pi$ -coordination complexes should be feasible. An extension of the present work to coordination polymers that contain the paramagnetic  $[\text{Fe}(\text{P}_2\text{C}_2\text{R}_2)_2]^-$  anion could be of interest in view of the potentially cooperative magnetic interactions between the paramagnetic ( $S=1/2$ ) iron centers in these compounds.<sup>15,16</sup> The chemistry of diphosphacyclobutadiene sandwich compounds continues to be actively investigated in our laboratory.

## 4.4 Experimental Section

### 4.4.1 General Procedures

All experiments were performed under an atmosphere of dry argon, by using standard Schlenk and glovebox techniques. Solvents were purified, dried, and degassed by standard techniques. NMR spectra were recorded on Bruker Avance 300 ( $^{31}\text{P}$ ; 85%  $\text{H}_3\text{PO}_4$ ) and Avance 400 spectrometers ( $^1\text{H}$ ,  $^{13}\text{C}$ ;  $\text{SiMe}_4$ ), internally referenced to residual solvent resonances. The spectra were recorded at 293 K unless noted otherwise. Melting points were measured on samples in sealed capillaries and are uncorrected. Compounds  $t\text{Bu-C}\equiv\text{P}$ ,<sup>36</sup>  $\text{AdC}\equiv\text{P}$ ,<sup>36</sup>  $t\text{PentC}\equiv\text{P}$ ,<sup>37</sup>  $\text{AuCl}(\text{tht})$ <sup>38</sup> and  $[\text{K}(\text{dme})_2][\text{Co}(\eta^4\text{-C}_{14}\text{H}_{10})_2]$ <sup>18,19</sup> were prepared by slightly modified literature procedures.  $\text{AuCl}(\text{PPh}_3)$  and  $\text{AgSbF}_6$  were purchased from ABCR and used as received. Elemental Analyses were determined on Vario ELIII CHNS and Elementar Micro Vario Cube instruments.

### 4.4.2 $[\text{K}(\text{thf})_3\{\text{Co}(\eta^4\text{-P}_2\text{C}_2t\text{Pent}_2)_2\}]$ (**1**)

$t\text{PentC}\equiv\text{P}$  (17.57 mL, 20.00 mmol, 1.14 M solution in *n*-hexane) was added dropwise to a deep red-brown solution of  $[\text{K}(\text{dme})_2][\text{Co}(\eta^4\text{-C}_{14}\text{H}_{10})_2]$  (2.72 g, 5.00 mmol) in THF (65 mL). The mixture was allowed to warm to room temperature overnight. The dark-orange solution was filtered and concentrated to ca. 20 mL. The addition of *n*-hexane (50 mL) gave a yellow-orange crystalline solid of **1**, which was recrystallized from THF/*n*-hexane (1:2) and dried in *vacuo* for 2 h. The dried solid still contains three THF molecules per formula unit according to the elemental analysis. Yield 3.01 g (75%); m.p.: 175 °C; Elemental analysis calcd. for  $\text{C}_{36}\text{H}_{68}\text{O}_3\text{P}_4\text{CoK}$  ( $M = 770.31$ ): C 56.09, H 8.89, found: C 56.29, H 8.37;  $^1\text{H}$  NMR (400.13 MHz,  $[\text{D}_8]\text{THF}$ ):  $\delta = 0.92$  (overlapping s and t, 36H;  $\text{CH}_3$ ), 1.45 (m, 8H;  $\text{CH}_2$ ), 1.78 (m, 12H; THF), 3.62 (m, 12H; THF);  $^{13}\text{C}\{^1\text{H}\}$  NMR (100.61 MHz,  $[\text{D}_8]\text{THF}$ ):  $\delta = 10.6$  (s;  $\text{C}(\text{CH}_3)_2\text{CH}_2\text{CH}_3$ ), 29.2 (s;  $\text{C}(\text{CH}_3)_2\text{CH}_2\text{CH}_3$ ), 38.4 (s;  $\text{C}(\text{CH}_3)_2\text{CH}_2\text{CH}_3$ ), 40.1 (s;  $\text{C}(\text{CH}_3)_2\text{CH}_2\text{CH}_3$ ), 101.1 (t,  $^1J(\text{C},\text{P}) = 52.4$  Hz;  $\text{C}_2\text{P}_2t\text{Pent}_2$ ); the signals for THF were not observed due to overlap with solvent signals.  $^{31}\text{P}\{^1\text{H}\}$  NMR (161.98 MHz,  $[\text{D}_8]\text{THF}$ ):  $\delta = 9.6$ .

### 4.4.3 $[\text{K}(\text{thf})_4\{\text{Co}(\eta^4\text{-P}_2\text{C}_2\text{Ad}_2)_2\}]$ (**2**)

The compound was prepared by an analogous procedure to **1**.  $\text{AdC}\equiv\text{P}$  (2.88 g, 16.15 mmol) was added dropwise to a deep red-brown solution of  $[\text{K}(\text{dme})_2][\text{Co}(\eta^4\text{-C}_{14}\text{H}_{10})_2]$  (2.20 g, 4.08 mmol) in THF (ca. 65 mL) at -78 °C, and the mixture was allowed to warm to room temperature overnight. The dark-orange solution was filtered and concentrated to ca. 20 mL. Then, *n*-hexane (50 mL) was added. Yellow-orange crystals of **2** precipitated at room temperature, which were recrystallized from THF:*n*-hexane(1:2) and dried in *vacuo* for 2 h. Crystals of  $[\text{K}(\text{thf})_4][\text{Co}(\eta^4\text{-P}_2\text{C}_2\text{Ad}_2)_2]$  (**2**) suitable for X-ray crystallography were grown by layering a THF solution of **2** with *n*-hexane. The crystals contain four THF molecules per formula unit, two of which can be removed by drying in high vacuum according to the  $^1\text{H}$  NMR spectra and the elemental analysis. Yield 2.94 g (76%); m.p.: (slow decomp.) >300 °C; Elemental analysis calcd. for  $\text{C}_{52}\text{H}_{76}\text{O}_2\text{P}_4\text{CoK}$  (**2**·2THF;  $M = 955.09$ ): C 65.39, H 8.02, found: C 64.96, H 7.75.  $^1\text{H}$  NMR (400.13 MHz,  $[\text{D}_8]\text{THF}$ ):  $\delta = 1.40$  (m, 8H; THF), 1.65 (br m, 24 H; Ad), 1.86 (br s, 24H; Ad), 1.96 (br s, 12H; Ad), 3.49 (m, 8H; THF).  $^{13}\text{C}\{^1\text{H}\}$  NMR (100.61 MHz,  $[\text{D}_8]\text{THF}$ ):  $\delta = 30.6$  (s; C-3,

C-5, C-7 of Ad), 37.2 (s; C-1 of Ad), 38.2 (s; C-4, C-6, C-10 of Ad), 46.3 (s; C-2, C-8, C-9 of Ad), 103.6 (t,  $^1J(\text{C,P}) = 51.5$  Hz;  $\text{C}_2\text{P}_2\text{Ad}_2$ ).  $^{31}\text{P}\{^1\text{H}\}$  NMR (121.49 MHz,  $[\text{D}_8]\text{THF}$ ):  $\delta = -1.10$ .

#### 4.4.4 $[\text{Au}\{\text{Co}(\eta^4\text{-P}_2\text{C}_2\text{tPent}_2)_2(\text{PMe}_3)_2\}]$ (**3**)

A solution of **1** (0.35 g, 0.44 mmol) in THF (20 mL) was added dropwise to a solution of  $\text{AuCl}(\text{PPh}_3)$  (0.22 g, 0.44 mmol) in THF (30 mL) at  $-78$  °C. Subsequently,  $\text{PMe}_3$  (0.2 mL, 2.00 mmol) was added, and the mixture was allowed to warm to room temperature overnight. The light-red solution was filtered, concentrated to ca. 20 mL and layered with *n*-hexane. Light red crystals of **3** were isolated after storage at room temperature overnight. Crystals suitable for X-ray crystallography were grown by layering a THF solution of **3** with *n*-hexane at room temperature. Yield 0.23 g (62%); m.p.:  $210$  °C. Elemental analysis calcd. for  $\text{C}_{30}\text{H}_{62}\text{P}_6\text{AuCo}$  ( $M = 864.56$ ): C 41.68, H 7.23, found: C 41.74, H 6.93;  $^1\text{H}$  NMR (400.13 MHz, 193 K,  $[\text{D}_8]\text{THF}$ ):  $\delta = 0.86\text{--}1.04$  (overlapping t and s, 36H;  $\text{C}(\text{CH}_3)_2\text{CH}_2\text{CH}_3$ ) and  $\text{C}(\text{CH}_3)_2\text{CH}_2\text{CH}_3$ ), 1.48 (overlapping d and q, 26H;  $\text{C}(\text{CH}_3)_2\text{CH}_2\text{CH}_3$  and coordinated  $\text{PMe}_3$ );  $^1\text{H}$  NMR (400.13 MHz, 293 K,  $[\text{D}_8]\text{THF}$ ):  $\delta = 0.95$  (t, 12H;  $\text{C}(\text{CH}_3)_2\text{CH}_2\text{CH}_3$ ), 1.01 (s, 24H;  $\text{C}(\text{CH}_3)_2\text{CH}_2\text{CH}_3$ ), 1.46–1.53 (overlapping d and q, 26H;  $\text{C}(\text{CH}_3)_2\text{CH}_2\text{CH}_3$  and coordinated  $\text{PMe}_3$ );  $^1\text{H}$  NMR (400.13 MHz, 323 K,  $[\text{D}_8]\text{THF}$ ):  $\delta = 0.95$  (t, 12H;  $\text{C}(\text{CH}_3)_2\text{CH}_2\text{CH}_3$ ), 1.01 (s, 24H;  $\text{C}(\text{CH}_3)_2\text{CH}_2\text{CH}_3$ ), 1.46–1.54 (overlapping d and q, 26H;  $\text{C}(\text{CH}_3)_2\text{CH}_2\text{CH}_3$  and coordinated  $\text{PMe}_3$ );  $^{13}\text{C}\{^1\text{H}\}$  NMR (100.61 MHz, 193 K,  $[\text{D}_8]\text{THF}$ ):  $\delta = 10.7$  (s;  $\text{C}(\text{CH}_3)_2\text{CH}_2\text{CH}_3$ ), 10.9–11.0 (overlapping s;  $\text{C}(\text{CH}_3)_2\text{CH}_2\text{CH}_3$ ), 17.7 (br t  $^1J(\text{C,P}) = 12.4$  Hz; coordinated  $\text{PMe}_3$ ), 20.7 (br t,  $^1J(\text{C,P}) = 11.1$  Hz; coordinated  $\text{PMe}_3$ ), 28.4–30.4 (overlapping s;  $\text{C}(\text{CH}_3)_2\text{CH}_2\text{CH}_3$ ), 37.6–41.0 (overlapping s;  $\text{C}(\text{CH}_3)_2\text{CH}_2\text{CH}_3$  and  $\text{C}(\text{CH}_3)_2\text{CH}_2\text{CH}_3$ ), 92.0 (d,  $^1J(\text{C,P}) = 61.2$  Hz;  $\text{C}_2\text{P}_2$ ), 100.8 (br s;  $\text{C}_2\text{P}_2$ ), 106.7 (t,  $^1J(\text{C,P}) = 61.1$  Hz;  $\text{C}_2\text{P}_2$ ), 109.4 (t,  $^1J(\text{C,H}) = 54.9$  Hz;  $\text{C}_2\text{P}_2$ );  $^{13}\text{C}\{^1\text{H}\}$  NMR (100.61 MHz, 293 K,  $[\text{D}_8]\text{THF}$ ):  $\delta = 10.4$  (s;  $\text{C}(\text{CH}_3)_2\text{CH}_2\text{CH}_3$ ), 18.9 (br d  $^1J(\text{C,P}) = 17.8$  Hz; coordinated  $\text{PMe}_3$ ), 29.4 (br s;  $\text{C}(\text{CH}_3)_2\text{CH}_2\text{CH}_3$ ), 38.2 (br s;  $\text{C}(\text{CH}_3)_2\text{CH}_2\text{CH}_3$ ), 40.1 (br s;  $\text{C}(\text{CH}_3)_2\text{CH}_2\text{CH}_3$ );  $^{13}\text{C}\{^1\text{H}\}$  NMR (100.61 MHz, 323 K,  $[\text{D}_8]\text{THF}$ ):  $\delta = 10.5$  (s;  $\text{C}(\text{CH}_3)_2\text{CH}_2\text{CH}_3$ ), 18.9 (br d,  $^1J(\text{C,P}) = 17.6$  Hz; coordinated  $\text{PMe}_3$ ), 29.5 (br s;  $\text{C}(\text{CH}_3)_2\text{CH}_2\text{CH}_3$ ), 38.3 (br s;  $\text{C}(\text{CH}_3)_2\text{CH}_2\text{CH}_3$ ), 40.2 (br s;  $\text{C}(\text{CH}_3)_2\text{CH}_2\text{CH}_3$ );  $^{31}\text{P}\{^1\text{H}\}$  NMR (161.98 MHz, 193 K,  $[\text{D}_8]\text{THF}$ ):  $\delta = -33.7$  (s, 4P;  $[\text{Au}(\text{PMe}_3)_4]^+$ );  $-25.7$  (s, 2P; non-coordinated P atoms of the coordinated  $\text{C}_2\text{P}_2$  rings of  $[\text{Au}\{\text{Co}(\text{P}_2\text{C}_2\text{tPent}_2)_2\}_2]^-$ ); 5.5 (br, 4P;  $[\text{Au}(\text{PMe}_3)_2]^+$ ), 9.9 (very br. s, 8P;  $[\text{Co}(\text{P}_2\text{C}_2\text{tPent}_2)_2]^-$ ), 18.8 (s, 4P; non-coordinated  $\text{C}_2\text{P}_2$  rings of  $[\text{Au}\{\text{Co}(\text{P}_2\text{C}_2\text{tPent}_2)_2\}_2]^-$ ), 45.7 (s, 2P; Au–P of  $[\text{Au}\{\text{Co}(\text{P}_2\text{C}_2\text{tPent}_2)_2\}_2]^-$ ).  $^{31}\text{P}\{^1\text{H}\}$  NMR (161.98 MHz, 293 K,  $[\text{D}_8]\text{THF}$ ):  $\delta = -16.7$  (br s, 2P; coordinated  $\text{PMe}_3$ ); 12.8 (br s, 4P;  $[\text{Co}(\text{P}_2\text{C}_2\text{tPent}_2)_2]^-$ );  $^{31}\text{P}\{^1\text{H}\}$  NMR (161.98 MHz, 323 K,  $[\text{D}_8]\text{THF}$ ):  $\delta = -20.2$  (s, 2P; coordinated  $\text{PMe}_3$ ); 15.0 (very br s, 4P;  $[\text{Co}(\text{P}_2\text{C}_2\text{tPent}_2)_2]^-$ ).

#### 4.4.5 $[\text{Au}\{\text{Co}(\eta^4\text{-P}_2\text{C}_2\text{Ad}_2)_2\}]_x$ (**4**)

A solution of **2** (0.33 g, 0.35 mmol) in THF (20 mL) was added dropwise to a solution of  $\text{AuCl}(\text{tht})$  (0.11 g, 0.35 mmol) in THF (40 mL) at  $-78$  °C. The mixture was allowed to warm to room temperature overnight. The orange-red suspension was then centrifuged and the solid washed with THF (20 mL). This procedure was repeated twice. Compound **4** was isolated as an orange solid after drying *in vacuo* for

30 min. The solid contains one equiv. of KCl per formula unit of **4** according to the microanalysis. Yield 0.24 g (66%) of **4**; m.p.: (slow decomp.) >265 °C; Elemental analysis calcd. for C<sub>44</sub>H<sub>60</sub>P<sub>4</sub>AuCoKCl (**4**+KCl, *M* = 1043.29): C 50.65, H 5.80, found: C 49.75; H 5.69.

#### 4.4.6 [Ag{Co(η<sup>4</sup>-P<sub>2</sub>C<sub>2</sub>Ad<sub>2</sub>)<sub>2</sub>}]<sub>n</sub> (**5**)

Compound **5** was prepared by an analogous procedure to **5** by adding a light red solution of **2** (0.33 g, 0.35 mmol) in THF (20 mL) to a suspension of AgSbF<sub>6</sub> (0.12 g, 0.35 mmol) in THF (30 mL). Compound **5** was isolated as an orange solid after centrifugation and washing the precipitate (3 x 20 mL THF) and dried in *vacuo* for 30 min. The isolated solid contains about 0.16 equiv. KSbF<sub>6</sub> per formula unit according to the microanalysis. Yield 0.26 g (80%) of **5**; m.p.: >230 °C (slow decomp.); Elemental analysis calcd. for C<sub>264</sub>H<sub>360</sub>P<sub>24</sub>Ag<sub>6</sub>Co<sub>6</sub>KSbF<sub>6</sub> (**5**+1/6 KSbF<sub>6</sub>, *M* = 925.45): C 57.10, H 6.53, found: C 57.47; H 6.58.

#### 4.4.7 [Au(PMe<sub>3</sub>)<sub>4</sub>][Au{Co(η<sup>4</sup>-P<sub>2</sub>C<sub>2</sub>Ad<sub>2</sub>)<sub>2</sub>}]<sub>2</sub> (**6**)

A solution of **2** (0.53 g, 0.55 mmol) in THF (20 mL) was added dropwise to a solution of AuCl(tht) (0.18 g, 0.55 mmol) in THF (50 mL) at -78 °C. The reaction mixture was allowed to warm to room temperature overnight. The orange-red suspension was treated with an excess of PMe<sub>3</sub> (0.3 mL, 2.90 mmol) and stirred for an additional 30 min. The resulting red solution was then filtered, concentrated to ca. 15 mL and layered with *n*-hexane (50 mL). Compound **6** crystallized in form of orange blocks after storage at room temperature overnight. The crystals were isolated and dried in *vacuo*. Crystals suitable for X-ray crystallography were grown by layering a THF solution of **6** with *n*-hexane at +8 °C. The isolated compound contained 0.25 equiv. of the by-product [Au(PMe<sub>3</sub>)<sub>4</sub>]Cl per formula unit according to NMR spectroscopy and the microanalysis. Yield 0.49 g (38%); m.p.: >285 °C (slow decomp.); Elemental analysis calcd. for C<sub>512</sub>H<sub>816</sub>P<sub>64</sub>Au<sub>11</sub>Co<sub>10</sub>Cl (**6**+0.25 [Au(PMe<sub>3</sub>)<sub>4</sub>]Cl; *M* = 2349.14): C 52.36, H 7.00, found: C 53.64; H 6.85; <sup>1</sup>H NMR (400.13 MHz, 190 K, [D<sub>8</sub>]THF): δ = 1.27 (br. s; coordinated PMe<sub>3</sub>), 1.48–1.96 (br overlapping m; Ad), integration of the signals could not be performed due to overlap with solvent signals; <sup>1</sup>H NMR (400.13 MHz, 293 K, [D<sub>8</sub>]THF): δ = 1.44 (d, <sup>1</sup>J(H,P) = 5.8 Hz; coordinated PMe<sub>3</sub>), 1.55–1.96 (br overlapping m; Ad), integration of the signals could not be performed due to overlap with solvent signals; <sup>1</sup>H NMR (400.13 MHz, 320 K, [D<sub>8</sub>]THF): δ = 1.30–1.85 (br. m; coordinated PMe<sub>3</sub> and Ad), integration of the signals could not be performed due to overlap with solvent signals; <sup>13</sup>C{<sup>1</sup>H} NMR (100.61 MHz, [D<sub>8</sub>]THF): δ = 18.6 (br. d, <sup>1</sup>J(C,P) = 15.5 Hz; coordinated PMe<sub>3</sub>), 30.3 (br. s; C-3, C-5, C-7 of Ad), 37.8 (br. s; C-1 and C-4, C-6, C-10 of Ad), 46.6 (br. s; C-2, C-8, C-9 of Ad); due to the low solubility of the isolated compound, the signals for the C<sub>2</sub>P<sub>2</sub> rings were not observed; <sup>31</sup>P{<sup>1</sup>H} NMR (101.23 MHz, 190 K, [D<sub>8</sub>]THF): δ = -40.5 (s, 2P; non-coordinated P atoms of the coordinated C<sub>2</sub>P<sub>2</sub> rings of [Au{Co(P<sub>2</sub>C<sub>2</sub>Ad<sub>2</sub>)<sub>2</sub>}]<sup>-</sup>), -33.9 (s, 6P; [Au(PMe<sub>3</sub>)<sub>4</sub>]<sup>+</sup>), -2.1 (br s, 1.5P; [Co(P<sub>2</sub>C<sub>2</sub>Ad<sub>2</sub>)<sub>2</sub>]<sup>-</sup>), 4.2 (br s, 0.5P; [Au(PMe<sub>3</sub>)<sub>2</sub>]<sup>+</sup>), 7.4 (s, 4P; non-coordinated C<sub>2</sub>P<sub>2</sub> rings of [Au{Co(P<sub>2</sub>C<sub>2</sub>Ad<sub>2</sub>)<sub>2</sub>}]<sup>-</sup>), 33.4 (s, 2P; Au-P of [Au{Co(P<sub>2</sub>C<sub>2</sub>Ad<sub>2</sub>)<sub>2</sub>}]<sup>-</sup>); <sup>31</sup>P{<sup>1</sup>H} NMR (101.23 MHz, 293 K, [D<sub>8</sub>]THF): δ = -36.4 (s, 2P; non-coordinated P atoms of the coordinated C<sub>2</sub>P<sub>2</sub> rings of [Au{Co(P<sub>2</sub>C<sub>2</sub>Ad<sub>2</sub>)<sub>2</sub>}]<sup>-</sup>), -30.3 (s, 0.1P; [Au(PMe<sub>3</sub>)<sub>4</sub>]<sup>+</sup>), -20.4 (br s, 6P; coordinated PMe<sub>3</sub>), 6.1 (br s, 5.5P; [Co(P<sub>2</sub>C<sub>2</sub>Ad<sub>2</sub>)<sub>2</sub>]<sup>-</sup>), 9.4 (s; non-coordinated C<sub>2</sub>P<sub>2</sub> rings of

[Au{Co(P<sub>2</sub>C<sub>2</sub>Ad<sub>2</sub>)<sub>2</sub>}<sub>2</sub>]<sup>−</sup>), 33.9 (s, 2P; Au–P of [Au{Co(P<sub>2</sub>C<sub>2</sub>Ad<sub>2</sub>)<sub>2</sub>}<sub>2</sub>]<sup>−</sup>); <sup>31</sup>P{<sup>1</sup>H} NMR (101.23 MHz, 320 K, [D<sub>8</sub>]THF): δ = −35.4 (s, 2P; non-coordinated P atoms of the coordinated C<sub>2</sub>P<sub>2</sub> rings of [Au{Co(P<sub>2</sub>C<sub>2</sub>Ad<sub>2</sub>)<sub>2</sub>}<sub>2</sub>]<sup>−</sup>), −24.2 (br s, 10P; coordinated PMe<sub>3</sub>), 6.8 (s, 12P; [Co(P<sub>2</sub>C<sub>2</sub>Ad<sub>2</sub>)<sub>2</sub>]<sup>−</sup>), 9.9 (br s, 4P; non-coordinated C<sub>2</sub>P<sub>2</sub> rings of [Au{Co(P<sub>2</sub>C<sub>2</sub>Ad<sub>2</sub>)<sub>2</sub>}<sub>2</sub>]<sup>−</sup>), 33.1 (br s, 2P; Au–P of [Au{Co(P<sub>2</sub>C<sub>2</sub>Ad<sub>2</sub>)<sub>2</sub>}<sub>2</sub>]<sup>−</sup>).

#### 4.4.8 [K(thf)<sub>6</sub>][Au{Co(η<sup>4</sup>-P<sub>2</sub>C<sub>2</sub>Ad<sub>2</sub>)<sub>2</sub>}<sub>2</sub>] (7)

A solution of **2** (0.57 g, 0.60 mmol) in THF (30 mL) was added dropwise to a solution of AuCl(tht) (0.10 g, 0.30 mmol) in THF (40 mL). The reaction mixture was allowed to warm to room temperature overnight. The resulting red solution was then filtered and concentrated to ca. 30 mL. Crystals suitable for X-ray crystallography were obtained by storing a concentrated THF solution at −18 °C. Compound **7** was isolated as an orange-red solid which was dried in *vacuo* for 30 min. The crystals contain six THF molecules per formula unit which are partly removed on evacuation in high vacuum. The dried product still contains ca. 1.5 THF molecules per formula unit. Yield 0.28 g (50%); m.p.: (slow decomp.) > 230 °C; Elemental analysis calcd. for C<sub>94</sub>H<sub>132</sub>O<sub>1.5</sub>P<sub>8</sub>Co<sub>2</sub>AuK (*M* = 1887.78): C 59.81, H 7.05, found: C 59.61; H 6.94; <sup>1</sup>H NMR (400.13 MHz, [D<sub>8</sub>]THF): δ = 1.54–1.95 (br overlapping m; Ad and THF), 3.61 (m; THF); integration of the signals for THF and Ad was not performed due to overlap with solvent signals. <sup>13</sup>C{<sup>1</sup>H} NMR (100.61 MHz, [D<sub>8</sub>]THF): δ = 30.3 (br s; C–3, C–5, C–7 of Ad), 37.8 (br s; C–1 and C–4, C–6, C–10 of Ad), 46.5 (br s; C–2, C–8, C–9 of Ad); the signals for the C<sub>2</sub>P<sub>2</sub> rings were not observed due to the low solubility of the isolated compound, the signals for coordinated THF were not observed due to overlap with solvent signals. <sup>31</sup>P{<sup>1</sup>H} NMR (161.98 MHz, [D<sub>8</sub>]THF): δ = −36.5 (s, 2P; non-coordinated P atoms of the coordinated C<sub>2</sub>P<sub>2</sub> rings), 9.4 (s, 4P; non-coordinated C<sub>2</sub>P<sub>2</sub> rings), 33.9 (s, 2P; Au–P of [Au{Co(P<sub>2</sub>C<sub>2</sub>Ad<sub>2</sub>)<sub>2</sub>}<sub>2</sub>]<sup>−</sup>).

#### 4.4.9 [K([18]crown-6)(thf)<sub>2</sub>][Au{Co(η<sup>4</sup>-P<sub>2</sub>C<sub>2</sub>Ad<sub>2</sub>)<sub>2</sub>}<sub>2</sub>] (8)

[18]crown-6 (0.23 g, 0.88 mmol) was added to a light red solution of **2** (0.76 g, 0.80 mmol) in THF (40 mL), and the mixture was stirred for 15 min at room temperature. Afterwards, the resulting solution was added dropwise to a solution of AuCl(tht) (0.13 g, 0.40 mmol) in THF (30 mL) at −78 °C. The reaction mixture was allowed to warm to room temperature overnight. The resulting orange suspension was then treated with PMe<sub>3</sub> (ca. 3 mL) and stirred for further 30 min. After filtration, the filtrate was concentrated to 20 mL and layered with *n*-hexane (20 mL). Orange crystals suitable for X-ray crystallography formed over several days. The crystals were isolated and dried in *vacuo*. Yield 0.58 g (67%); m.p.: (slow decomp.) > 320 °C; Elemental analysis calcd. for C<sub>108</sub>H<sub>160</sub>O<sub>8</sub>P<sub>8</sub>Co<sub>2</sub>AuK (*M* = 2188.14): C 59.28, H 7.37, found: C 59.49, H 7.34. An NMR spectroscopic characterization was not performed due to the lack of solubility of **8** in common organic solvents.

#### 4.4.10 [K([18]crown-6)(thf)<sub>2</sub>][Ag{Co(η<sup>4</sup>-P<sub>2</sub>C<sub>2</sub>Ad<sub>2</sub>)<sub>2</sub>}<sub>2</sub>] (9)

Compound **9** was prepared by an analogous procedure to **8** by adding a light red THF (40 mL) solution of [18]crown-6 (0.23 g, 0.88 mmol) and **2** (0.76 g, 0.80 mmol) to a suspension of AgSbF<sub>6</sub> (0.14 g,

0.40 mmol) in THF (ca. 30 mL). Work-up was performed according to the procedure for compound **8**. Yield 0.50 g (60%); m.p.: >310 °C (slow decomp.); Elemental analysis calcd. for  $C_{108}H_{160}O_8P_8AgCo_2K$  ( $M = 2099.04$ ): C 61.80, H 7.68, found: C 61.55; H 7.39. An NMR spectroscopic characterization was not performed due to the lack of solubility of **9** in common organic solvents.

#### 4.4.11 X-Ray Crystallography

The crystals were processed at Agilent Technologies SuperNova (**3**, **7**, **8**, **9**) and Bruker AXS APEX II (**2** and **6**) devices, respectively. Either semi-empirical multi-scan absorption corrections<sup>39</sup> or analytical ones<sup>40</sup> were applied to the data. The structures were solved by SHELXS<sup>41</sup> or SIR<sup>42</sup> and least-square refinements on  $F^2$  were carried out with SHELXL<sup>41</sup>. A very minor pseudo-merohedral twin component (3.5 %) was found for **3**. Disordered solvent molecules connected to the potassium cation were refined with restraints (SAME, SIMU, DELU), free solvent molecules located at special positions were treated with SQUEEZE.<sup>43</sup> The structure of **2** contained a DME molecule coordinated to potassium as a minor component (18%) in place of THF molecules. Details are given in the corresponding CIF files. CCDC-903858–90363 (see Table 5) contain the supplementary crystallographic data for this paper. These data can be obtained free of charge from The Cambridge Crystallographic Data Center via [www.ccdc.cam.ac.uk/data\\_request/cif](http://www.ccdc.cam.ac.uk/data_request/cif).

#### 4.4.12 Solid-State NMR Spectroscopy

Solid State NMR measurements were carried out on BRUKER Avance III+ 300, BRUKER Avance DSX 400, and BRUKER Avance DSX 500 spectrometers, corresponding to magnetic flux densities of 7.05, 9.4 T, and 11.74 T, respectively. All spectrometers were equipped with 2.5 mm and 4 mm NMR double and triple resonance probes operating at MAS rotation frequencies between 10 and 28 kHz.  $^{31}P\{^1H\}$  MAS NMR spectra were measured at 7.05 and 11.74 T with a  $^{31}P$  90° excitation pulse length ranging in-between 2.0  $\mu s$  and 4.0  $\mu s$ . All spectra were acquired with TPPM-15<sup>44</sup> proton decoupling during the data acquisition applying decoupling pulses ranging in-between 4.6–8.3  $\mu s$  (~10/12  $\pi$  pulses). The relaxation delays were set to 125 s in case of **6**, 40 s for **4** and 250–500 s for **9**. Line shape analysis was done by using the DMFIT software (version 2011).<sup>45</sup> Chemical shifts are reported relative to an 85%  $H_3PO_4$  solution.

$^{31}P\{^1H\}$  cross-polarization magic-angle spinning (CPMAS) NMR spectra were measured at 9.4 T with a  $^1H$  90° pulse length of 4.9–5.5  $\mu s$ , contact times of 1.5–5 ms and relaxation delays of 2–5 s. Hartmann-Hahn matching conditions were adjusted on  $NH_4H_2PO_4$ . An efficient polarization transfer was achieved by a ramped-amplitude CP step<sup>46</sup> with the proton nutation frequency  $\nu_{RF}(^1H)$  being swept from 51 kHz to 25.5 kHz in 64 steps for a  $^1H$  90° pulse of 4.9  $\mu s$ .  $^1H$  heteronuclear decoupling was done by applying the TPPM-15 scheme with a  $^1H$  pulse length of 7.1–8.2  $\mu s$  (~10/12  $\pi$  pulses). In case of CPMAS measurements on compound **5**, the signal is detected after a rotor-synchronized Hahn echo. The spectrum of **8** was measured at 11.74 T using similar conditions described above for the  $^{31}P\{^1H\}$  MAS experiments.

$^{31}P$  SPARTAN (Selective Population Anti-z and Rate of Transfer to Adjacent Nuclei)<sup>28</sup> experiments were performed at 7.05 T with a spinning frequency of 14 kHz, beginning with a selective excitation by a soft 180° DANTE pulse<sup>47</sup> composed of 30 6° pulses (1.33  $\mu s$  in length, corresponding to a radio frequency

power of 12.5 kHz) spaced by one rotor period. After variable mixing times ranging in-between 0.01 s and 10 s, during which cross-relaxation processes, e.g. spectral spin diffusion processes, might affect the population of Zeeman spin states, the z-magnetization is detected by a non-selective 90° pulse of 4  $\mu$ s in length. All spectra were acquired using a presaturation comb consisting of 80 90° pulses and a relaxation delay of 22 s.

$^{13}\text{C}\{^1\text{H}\}$  CPMAS NMR experiments were performed at 7.05 T and 9.4 T. Hartmann-Hahn conditions were adjusted on adamantane with  $^1\text{H}$  90° pulse length ranging in-between 4.5-6.0  $\mu$ s, a contact time of 5 ms and a relaxation delay of 5 s. An efficient polarization transfer was achieved by a ramped-amplitude CP step. All the spectra were acquired with  $^1\text{H}$  SW-TPPM15 or TPPM-15<sup>48</sup> proton decoupling using  $\sim 10/12 \pi$  pulses in both cases.  $^{13}\text{C}$  chemical shifts are reported relative to TMS using adamantane ( $\delta(^{13}\text{CH}_2) = 38.56$  ppm for the methylene resonance) as a secondary standard.

#### 4.4.13 DFT Calculations of NMR Parameters

All calculations were carried out using the program package TURBOMOLE 6.3.<sup>49</sup> As a model the positions of the heavy atoms for one negatively charged molecular unit of **9** were taken from the crystal structure, whereas the positions of the hydrogen atoms have been optimized on a DFT GGA (BP86)<sup>50</sup> level of theory with Ahlrich's TZVP<sup>51</sup> basis set which was used for all atoms except Ag for which the all-electron basis TZVPPalls2<sup>52</sup> was applied. In all TURBOMOLE SCF calculations an energy convergence criterion of  $10^{-7} E_h$  and in all geometry optimizations an energy convergence criterion of  $5 \cdot 10^{-7} E_h$  was chosen. The integration grid was set to m4<sup>53</sup> and the RI approximation<sup>54</sup> was used.

The magnetic shielding calculations were performed within the GIAO (gauge independent atomic orbitals) framework.<sup>55</sup>  $^{13}\text{C}$  and  $^{31}\text{P}$  chemical shifts were calculated with the B3-LYP<sup>33</sup> functional and the def2-TZVP<sup>34</sup> basis set for all atoms, except Ag wherefore the TZVPPalls2 basis was used.  $^{31}\text{P}$  chemical shifts were referenced to phosphoric acid ( $\sigma^{\text{B3-LYP}} = 274.31$  ppm),  $^{13}\text{C}$  chemical shifts are reported relative to TMS. The shielding of TMS is determined by adding the calculated shielding of methane (same level of theory as mentioned above) to the experimental chemical shift of methane in the gas phase ( $\delta = -11.0$  ppm) that is referenced to TMS under consideration of susceptibility corrections ( $\sigma^{\text{TMS}} = 184.1$  ppm).<sup>56</sup> The calculated magnetic shielding of TMS on the level of theory discussed above is determined to 179.3 ppm.



**Table 5.** Crystal data and structure refinement of **2**, **3** and **6–9**.

	<b>2</b>	<b>3</b>	<b>6</b>	<b>7</b>	<b>8</b>	<b>9</b>
Empirical formula	C <sub>58.60</sub> H <sub>89.90</sub> CoKO <sub>4</sub> P <sub>4</sub>	C <sub>30</sub> H <sub>62</sub> AuCoP <sub>6</sub>	C <sub>108</sub> H <sub>171</sub> Au <sub>2</sub> Co <sub>2</sub> P <sub>12</sub>	C <sub>114</sub> H <sub>172</sub> AuCo <sub>2</sub> KO <sub>6.3</sub> P <sub>8</sub>	C <sub>117</sub> H <sub>180</sub> AuCo <sub>2</sub> KO <sub>9</sub> P <sub>8</sub>	C <sub>117</sub> H <sub>180</sub> AgCo <sub>2</sub> KO <sub>9</sub> P <sub>8</sub>
Crystal size [mm <sup>3</sup> ]	0.10 × 0.10 × 0.05	0.26 × 0.17 × 0.10	0.10 × 0.03 × 0.02	0.17 × 0.10 × 0.08	0.22 × 0.14 × 0.04	0.18 × 0.12 × 0.04
Colour and shape	red block	orange block	orange block	orange block	red plate	orange plate
Formula weight [g mol <sup>-1</sup> ]	1080.32	864.52	2384.88	2212.15	2188.05	2098.95
Crystal system	monoclinic	monoclinic	triclinic	orthorhombic	triclinic	Triclinic
Space group	<i>P</i> 2 <sub>1</sub> / <i>n</i>	<i>P</i> 2 <sub>1</sub> / <i>n</i>	<i>P</i> - <i>I</i>	<i>Pbcn</i>	<i>P</i> - <i>I</i>	<i>P</i> - <i>I</i>
Absorption correction	multi-scan	analytical	multi-scan	analytical	multi-scan	analytical
Transmission min/max	0.951/0.975	0.129/0.449	0.744/0.940	0.356/0.529	0.679/1.000	0.327/0.734
<i>a</i> [Å]	12.1489(4)	10.6919(2)	14.3920(5)	24.2645(4)	12.782(5)	12.794(4)
<i>b</i> [Å]	21.5192(7)	16.7835(3)	18.1462(6)	18.5964(3)	14.452(6)	14.424(5)
<i>c</i> [Å]	23.0112(8)	20.9370(4)	24.0864(8)	26.8044(8)	17.889 (7)	18.006 (6)
$\alpha$ [°]	90	90	72.336 (10)	90	110.849(4)	110.717(3)
$\beta$ [°]	98.949 (10)	90.244(2)	78.298 (10)	90	93.337(3)	93.278(3)
$\gamma$ [°]	90	90	68.7670(10)	90	113.621(2)	113.776(3)
<i>V</i> [Å <sup>3</sup> ]	5942.7(3)	3757.06(12)	5556.3(3)	12095.0(5)	2750.5(2)	2765.6(2)
<i>Z</i>	4	4	2	4	1	1
<i>T</i> [K]	153(2)	123(1)	153(2)	123(1)	123(1)	123(1)
$\lambda$ [Å]	0.71073	1.54178	0.71073	1.54178	1.54178	1.54178
$\rho_{\text{calc}}$ [g/cm <sup>3</sup> ]	1.207	1.528	1.425	1.215	1.321	1.260
$\mu$ (mm <sup>-1</sup> )	0.509	13.236	3.144	6.024	6.631	5.557
Theta range [°]	1.30–28.75	3.36–66.97	0.89–29.76	3.30–67.50	3.55–73.50	3.55–73.53

Reflections collected to $\theta_{\max}$ [°]	64045	18913	64427	57066	23540	20966
Unique reflections ( $R_{\text{in}}$ )	15416 (0.0366)	7335 (0.0275)	31392 (0.0383)	11482 (0.0546)	10638 (0.0261)	10647 (0.0333)
Refl. obs. [ $I > 2\sigma(I)$ ]	12234	6935	22559	8924	9985	9834
Parameters	728	361	1177	722	634	636
Completeness to $\theta$	0.999	1.000	0.990	0.998	0.960	0.955
$R$ -values [ $I > 2\sigma(I)$ ]	0.0408/0.1130	0.0297/0.0780	0.0390/0.0920	0.0796/0.2416	0.0481/0.1373	0.0333/0.1054
$R$ -values (all data)	0.0530/0.1187	0.0317/0.0803	0.0689/0.1089	0.0906/0.2512	0.0506/0.1391	0.0427/0.1084
GOF on $F^2$	1.072	1.084	0.817	1.025	1.061	1.036
Residual density [ $\text{e}\text{\AA}^{-3}$ ]	−0.409/1.118	−1.673/0.591	−1.092/1.441	−1.004/0.139	−1.882/0.138	−0.594/0.077
CCDC-	903858	903859	903860	903861	903862	903863

## 4.5 Supporting Information

### 4.5.1 Graphical Representations (Figures S1–S3) of the Single-Crystal Structures of $[\text{K}(\text{thf})_6][\text{Au}\{\text{Co}(\text{P}_2\text{C}_2\text{Ad}_2)_2\}_2]$ (7), $[\text{K}([18]\text{crown-6})(\text{thf})_2][\text{Au}\{\text{Co}(\text{P}_2\text{C}_2\text{Ad}_2)_2\}_2]$ (8) and $[\text{K}[18]\text{crown-6})(\text{thf})_2][\text{Ag}\{\text{Co}(\text{P}_2\text{C}_2\text{Ad}_2)_2\}_2]$ (9).

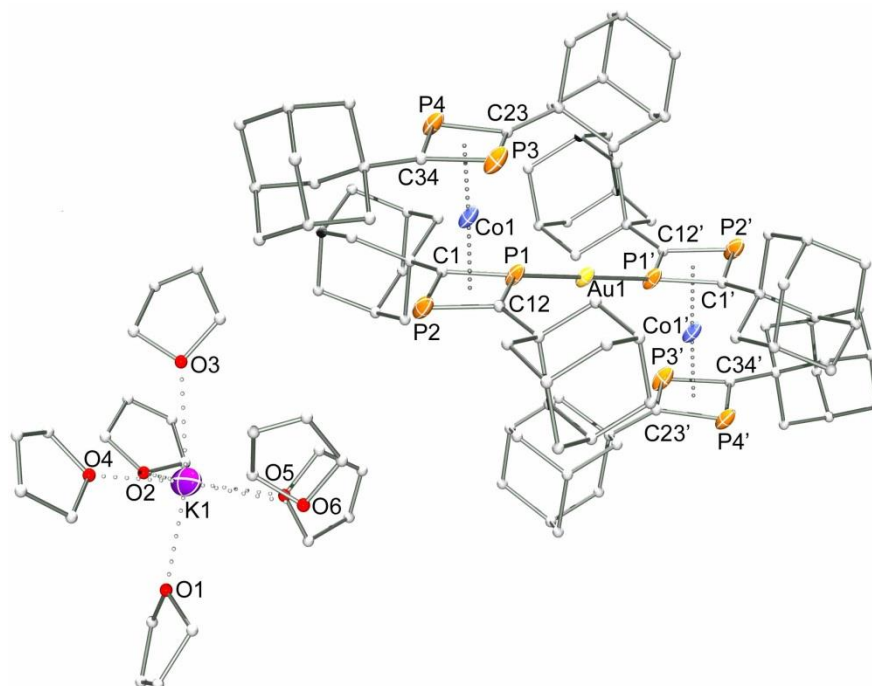


**Figure S1.** Solid-state structure of  $[\text{K}(\text{thf})_6][\text{Au}\{\text{Co}(\text{P}_2\text{C}_2\text{Ad}_2)_2\}_2]$  (7). Displacement ellipsoids are at 20% probability, H atoms and solvent molecules are omitted for clarity.

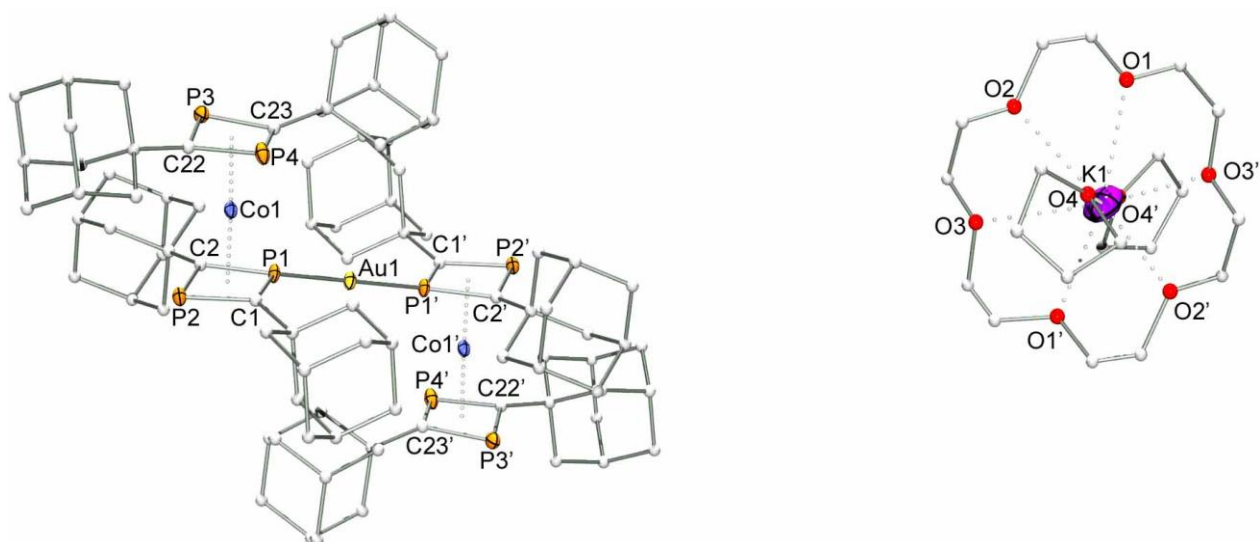


**Figure S2.** Solid-state structure of  $[\text{K}([18]\text{crown-6})(\text{thf})_2][\text{Au}\{\text{Co}(\text{P}_2\text{C}_2\text{Ad}_2)_2\}_2]$  (8). Displacement ellipsoids are at 35% probability, H atoms and solvent molecules are omitted for clarity.

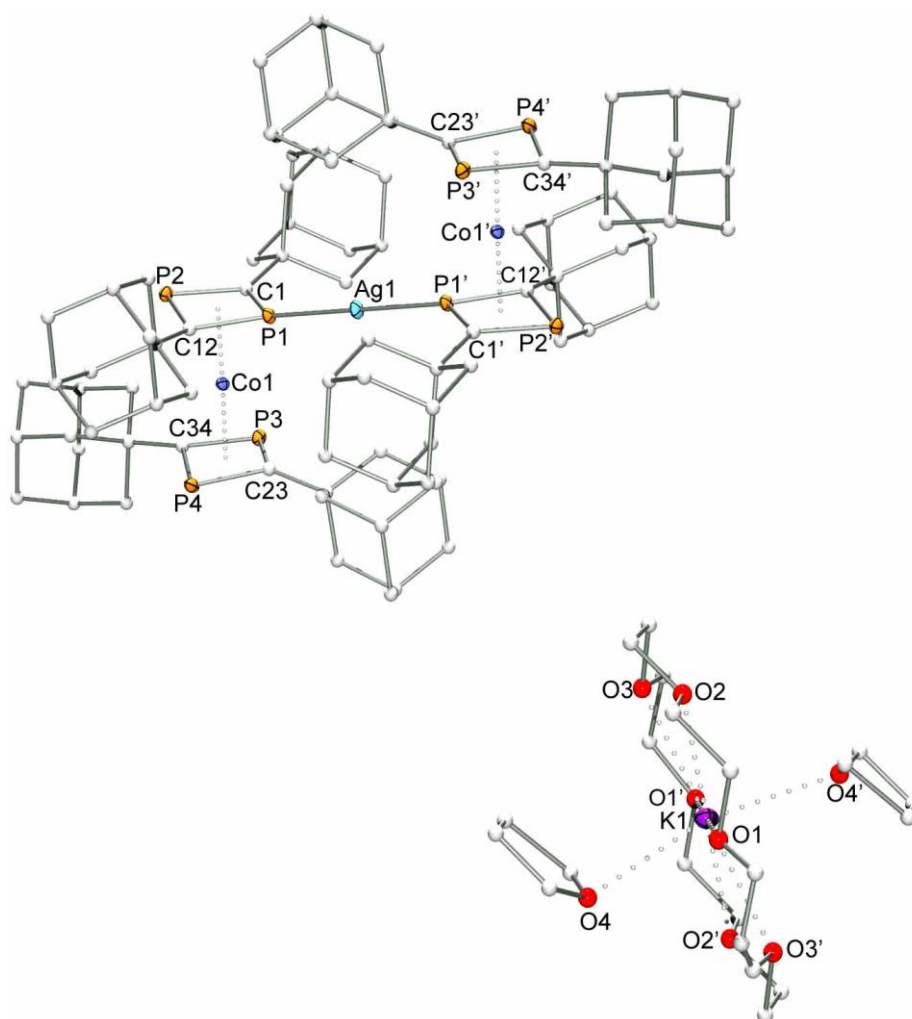


**Figure S3.** Solid-state structure of  $[K([18]\text{crown-6})(\text{thf})_2][\text{Ag}\{\text{Co}(\text{P}_2\text{C}_2\text{Ad}_2)_2\}_2]$  (**9**). Displacement ellipsoids are at 35% probability, H atoms and solvent molecules are omitted for clarity.

**4.5.2  $^{31}\text{P}\{^1\text{H}\}$  and  $^{13}\text{C}\{^1\text{H}\}$  CPMAS NMR Spectra of  $[\text{Au}\{\text{Co}(\text{P}_2\text{C}_2\text{Ad}_2)_2\}]_x$  (4),  $[\text{Ag}\{\text{Co}(\text{P}_2\text{C}_2\text{Ad}_2)_2\}]_x$  (5),  $[\text{Au}(\text{PMe}_3)_4][\text{Au}\{\text{Co}(\text{P}_2\text{C}_2\text{Ad}_2)_2\}_2]$  (6), and  $[\text{K}([18]\text{crown-6})(\text{thf})_2][\text{Ag}\{\text{Co}(\text{P}_2\text{C}_2\text{Ad}_2)_2\}_2]$  (9) (Figures S4–S6)**

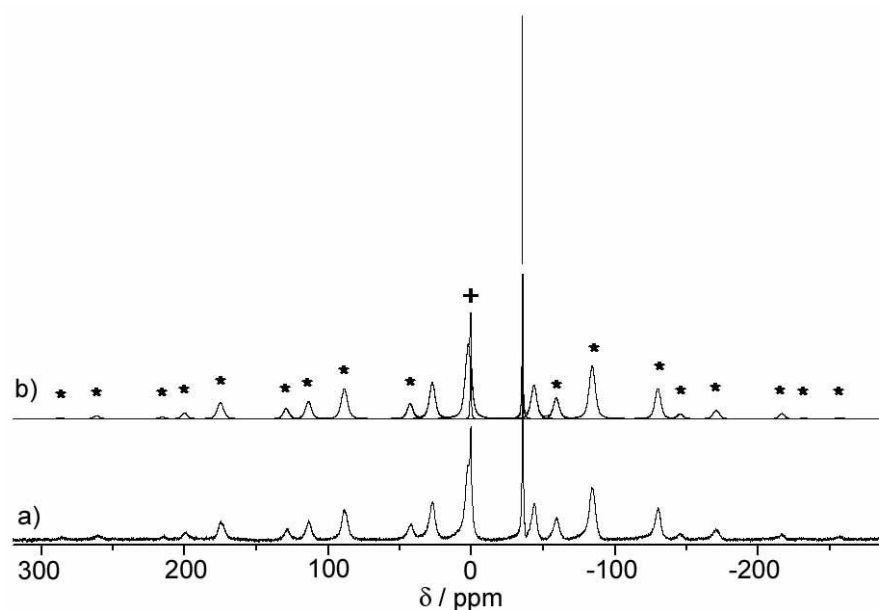


**Figure S4.**  $^{31}\text{P}\{^1\text{H}\}$  CPMAS NMR spectrum of **6** acquired at 9.4 T with a spinning frequency of 14 kHz (a) and corresponding simulation of the CSA pattern (b). + marks an impurity and \* spinning sidebands. The extracted CSA parameters are given in Table 2.

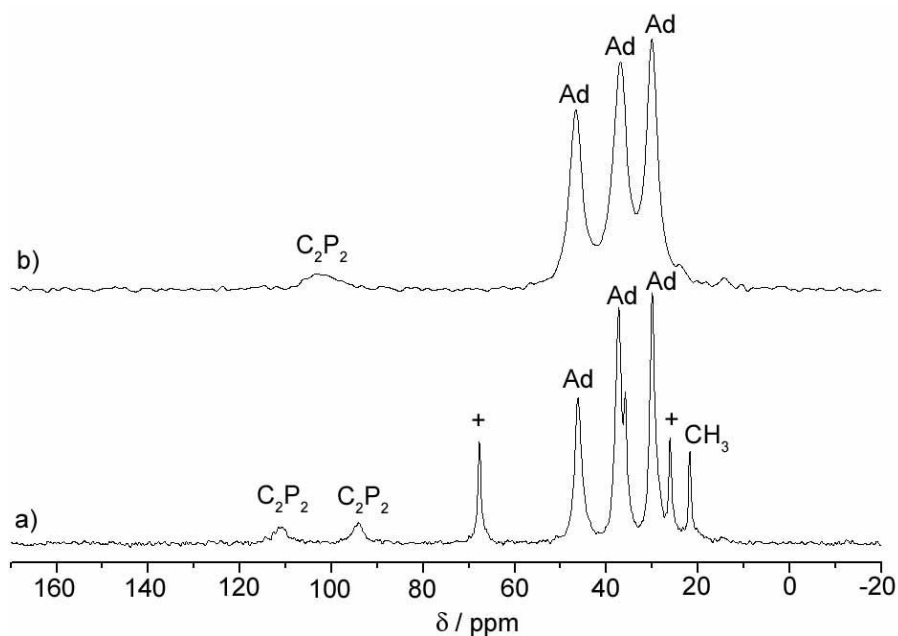


**Figure S5.**  $^{13}\text{C}\{^1\text{H}\}$  CPMAS NMR spectra of **6** (a) and **4** (b) acquired at 7.05 T with a spinning frequency of 10 kHz. + marks impurities of residual THF.

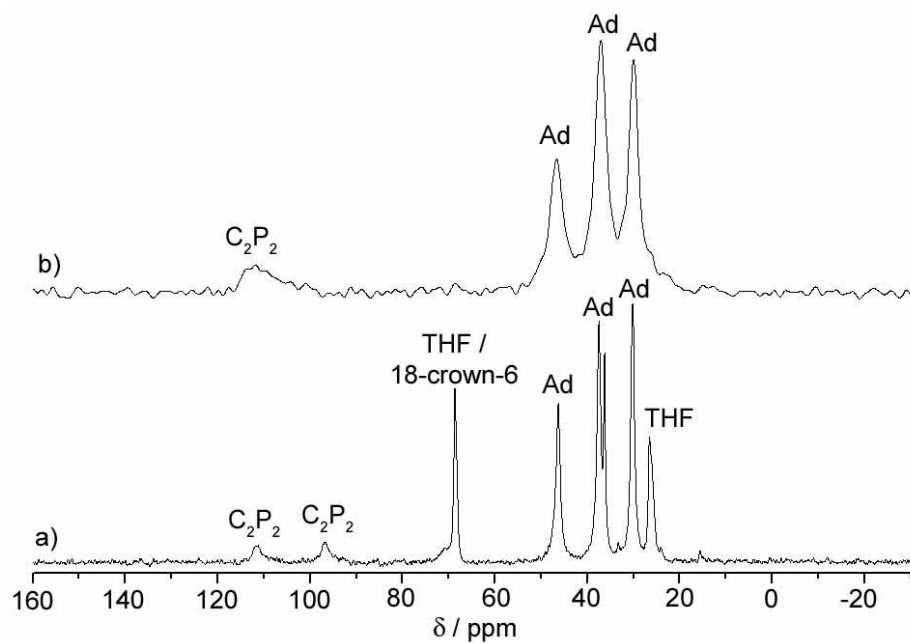


**Figure S6.**  $^{13}\text{C}\{^1\text{H}\}$  CPMAS NMR spectra of **9** acquired at 9.4 T with a rotation frequency of 10 kHz (a) and of **5** acquired at 7.05 T with a spinning frequency of 10 kHz (b).

### 4.5.3 Variable-Temperature $^1\text{H}$ and $^{13}\text{C}\{^1\text{H}\}$ NMR Spectra of $[\text{Au}\{\text{Co}(\text{P}_2\text{C}_2\text{Ad}_2)_2(\text{PMe}_3)_2\}]$ (**3**) (Figures S7 and S8).

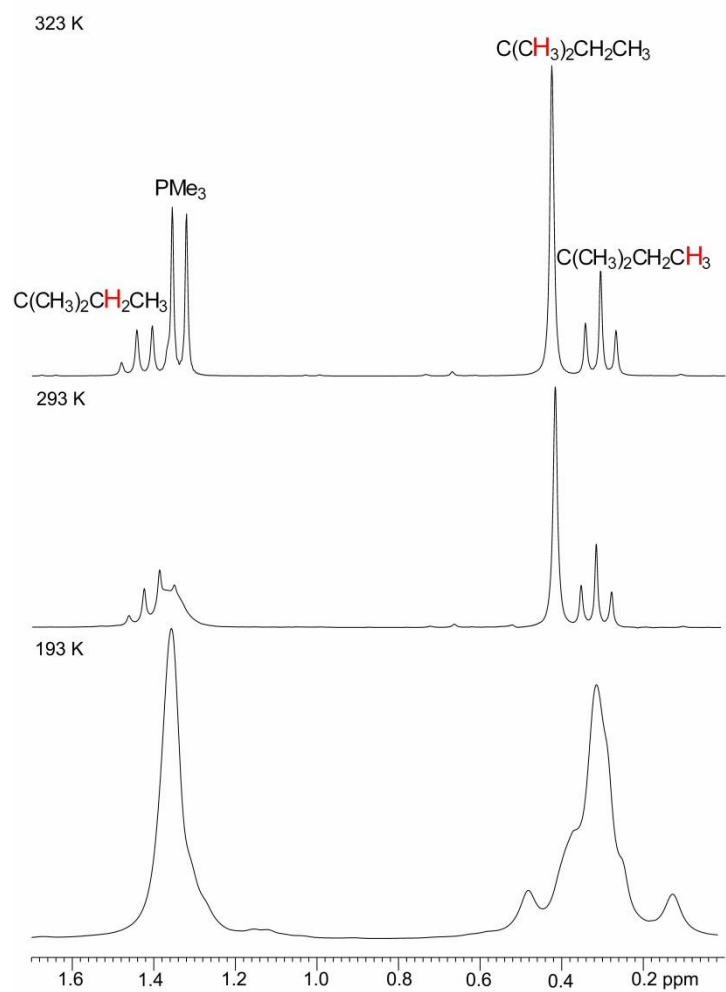


**Figure S7.** Temperature-dependent  $^1\text{H}$  NMR spectra of  $[\text{Au}\{\text{Co}(\text{P}_2\text{C}_2\text{Ad}_2)_2(\text{PMe}_3)_2\}]$  (**3**) in  $[\text{D}_8]\text{THF}$ .

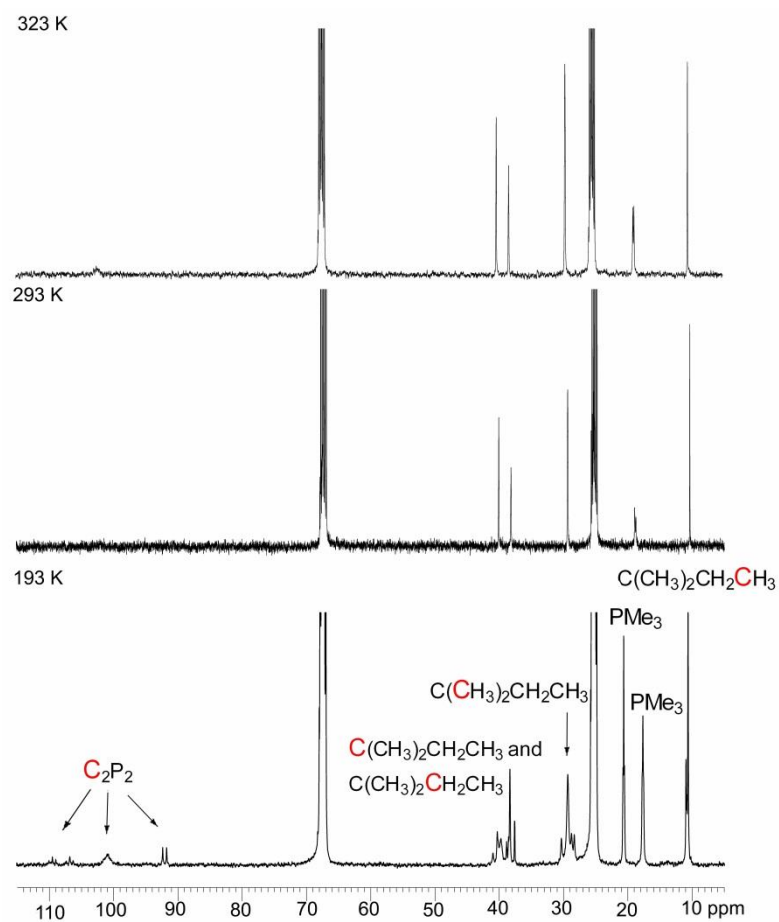


**Figure S8.** Temperature-dependent  $^{13}\text{C}\{^1\text{H}\}$  NMR spectra of  $[\text{Au}\{\text{Co}(\text{P}_2\text{C}_2\text{Ad}_2)_2\}_2(\text{PMe}_3)_2]$  (**3**) in  $[\text{D}_8]\text{THF}$ .

## References

- 1 a) M. Regitz, *Chem. Rev.* **1990**, 90, 191; b) A. C. Gaumont, J. Denis, *Chem. Rev.* **1994**, 94, 1413; c) J. F. Nixon, *Coord. Chem. Rev.* **1995**, 145, 201; d) M. Regitz, O. J. Scherer, *Multiple Bonds and Low Coordination Phosphorus Chemistry*, Thieme, Stuttgart, **1990**; e) K. B. Dillon, F. Mathey, J. F. Nixon, *Phosphorus: The Carbon Copy*, Wiley, Chichester, **1998**; f) F. Mathey, *Angew. Chem. Int. Ed.* **2003**, 42, 1578.
- 2 R. Wolf, N. Ghavtadze, K. Weber, E.-M. Schnöckelborg, B. de Bruin, A. W. Ehlers, K. Lammertsma, *Dalton Trans.* **2010**, 39, 1453.
- 3 M. Scheer, *Dalton Trans.*, **2008**, 4372.
- 4 For related metal-mediated cyclodimerizations of alkynes see: a) A. Efraty, *Chem. Rev.* **1977**, 77, 692; b) L. Veiros, G. Dazinger, K. Kirchner, M. C. Calhorda, R. Schmid, *Chem. Eur. J.* **2004**, 10, 5860, and ref. therein; c) D. Seyferth, *Organometallics* **2003**, 22, 2; d) U. H. F. Bunz, *Top. Curr. Chem.* **1999**, 201, 131.
- 5 a) C. Jones, C. Schulten, A. Stasch, *Dalton. Trans.* **2006**, 3733; b) P. Binger, G. Glaser, S. Albus, C. Krüger, *Chem. Ber.* **1995**, 128, 1261.
- 6 a) P. Binger, R. Milczarek, R. Mynott, M. Regitz, W. Rosch, *Angew. Chem. Int. Ed. Engl.* **1986**, 25, 644; b) P. B. Hitchcock, M. J. Maah, J. F. Nixon, *J. Chem. Soc., Chem. Commun.* **1986**, 737; c) P. Binger, R. Milczarek, R. Mynott, C. Krüger, Y. H. Tsay, E. Raabe, M. Regitz, *Chem. Ber.* **1988**, 121, 637.
- 7 Pertinent examples: a) P. Binger, B. Biedenbach, R. Schneider, M. Regitz, *Synthesis* **1989**, 960; b) D. Himmel, M. Seitz, M. Scheer, *Z. Anorg. Allg. Chem.* **2004**, 630, 1220; c) P. A. Arnold, F. G. N. Cloke, P. B. Hitchcock, J. F. Nixon, *J. Am. Chem. Soc.* **1996**, 118, 7630; d) A. G. Avent, F. G. N. Cloke, K. R. Flower, P. B. Hitchcock, J. F. Nixon, D. M. Vickers, *Angew. Chem. Int. Ed.* **1994**, 33, 2330; e) F. G. N. Cloke, P. B. Hitchcock, J. F. Nixon, D. M. Vickers, *J. Organomet. Chem.* **2001**, 635, 212.
- 8 F. G. N. Cloke, K. R. Flower, P. B. Hitchcock, J. F. Nixon, *J. Chem. Soc., Chem. Commun.* **1994**, 489.
- 9 T. Wettling, G. Wolmershäuser, P. Binger, M. Regitz, *J. Chem. Soc., Chem. Commun.* **1990**, 1541.
- 10 a) P. B. Hitchcock, M. J. Maah, J. F. Nixon, C. Woodward, *J. Chem. Soc., Chem. Commun.* **1987**, 844; b) P. B. Hitchcock, M. J. Maah, J. F. Nixon, *Heteroatom Chem.* **1991**, 2, 253.
- 11 F. W. Heinemann, S. Kummer, U. Seiss-Brandl, U. Zenneck, *Organometallics* **1999**, 18, 2021.
- 12 P. Kramkowski, M. Scheer, *Eur. J. Inorg. Chem.* **2000**, 1869.
- 13 H. F. Dare, J. A. K. Howard, M. U. Pilotti, F. G. A. Stone, J. Szameitat, *J. Chem. Soc., Chem. Commun.* **1989**, 1409; b) H. F. Dare, J. A. K. Howard, M. U. Pilotti, F. G. A. Stone, J. Szameitat, *J. Chem. Soc., Dalton Trans.* **1990**, 2263.
- 14 R. Wolf, A. W. Ehlers, J. C. Slootweg, M. Lutz, D. Gudat, M. Hunger, A. L. Spek, K. Lammertsma, *Angew. Chem. Int. Ed.* **2008**, 47, 4584.
- 15 R. Wolf, J. C. Slootweg, A. W. Ehlers, F. Hartl, B. de Bruin, M. Lutz, A. L. Spek, K. Lammertsma, *Angew. Chem. Int. Ed.* **2009**, 48, 3104.
- 16 R. Wolf, A. W. Ehlers, M. M. Khusniyarov, F. Hartl, B. de Bruin, G. J. Long, F. Grandjean, F. M. Schappacher, R. Pöttgen, J. C. Slootweg, M. Lutz, A. L. Spek, K. Lammertsma, *Chem. Eur. J.* **2010**, 16, 14322.
- 17 R. Wolf, E.-M. Schnöckelborg, *Chem. Commun.* **2010**, 46, 2832.
- 18 S. Gülak, O. Stepanek, J. Malberg, B. Rezaei Rad, M. Kotora, R. Wolf, A. Jacobi von Wangelin, *Chem. Sci* **2012**, 4, 776.
- 19 W. W. Brennessel, J. V. G. Young, J. E. Ellis, *Angew. Chem. Int. Ed.* **2002**, 41, 1211.
- 20 a) R. Wolf, A. Schisler, P. Lönnecke, C. Jones, E. Hey-Hawkins, *Eur. J. Inorg. Chem.* **2004**, 3277; b) R. Wolf, E. Hey-Hawkins, *Z. Anorg. Allg. Chem.* **2006**, 632, 727.

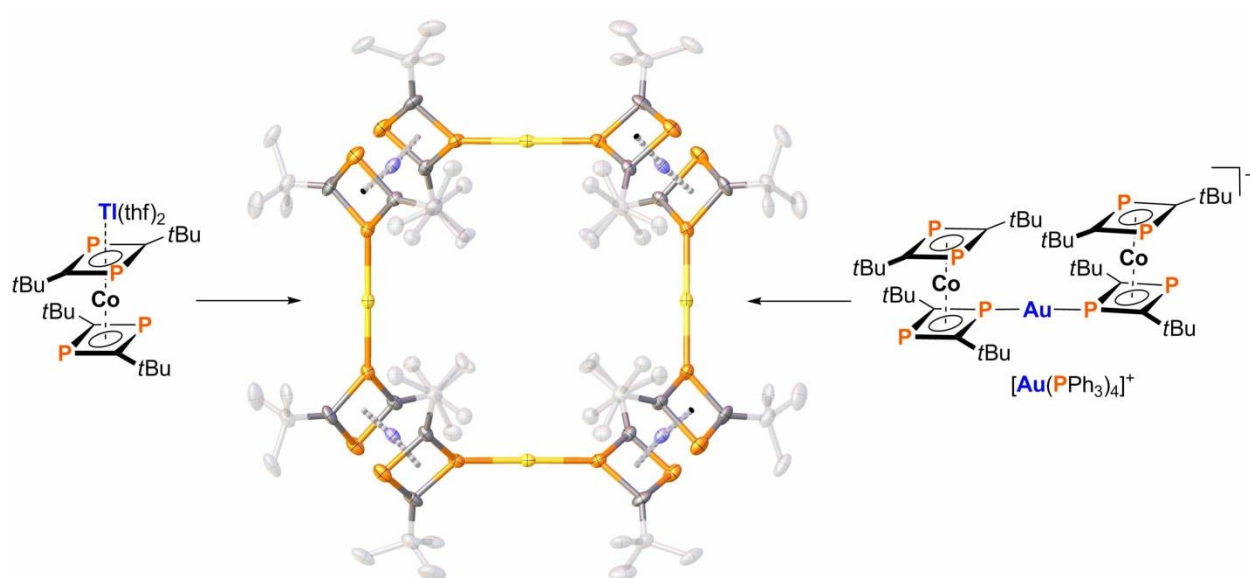
- 21 J. D. Smith, *Adv. Organomet. Chem.* **1998**, 43, 267.
- 22 G. Wilkinson, *Comprehensive Coordination Chemistry*, Pergamon Press: Oxford, **1987**, Vol 5, 869;
- 23 b) R. J. Puddephatt, *The Chemistry of Gold*, Elsevier: New York, **1978**.
- 24 a) R. V. Parish, O. Parry, C. A. McAuliffe, *J. Chem. Soc., Chem. Commun.* **1981**, 2098; b) M. J. Mays, P. A. Vergnano, *J. Chem. Soc., Dalton Trans.* **1979**, 1112.
- 25 a) P. G. Jones, *J. Chem. Soc., Chem. Commun.* **1980**, 1031; b) P. G. Jones, *Acta Crystallogr., Sect. B* **1980**, 36, 3105; c) L. J. Guggenberger, *J. Organomet. Chem.* **1984**, 81, 271.
- 26 M. C. Gimeno, P. C. Jones, A. Laguna, C. Sarroca, *Inorg. Chem.* **1993**, 32, 5927.
- 27 H. Schmidbaur, R. Franke, *Chem. Ber.* **1972**, 105, 2985.
- 28 J. M. Forward, Z. Assefa, R. J. Staples, J. P. Fackler, Jr., *Inorg. Chem.* **1996**, 35, 16.
- 29 R. C. Elder, E. H. Kelle Zeiher, M. Onady, R. R. Whittle, *J. Chem. Soc., Chem. Commun.* **1981**, 900.
- 30 T. Wiegand, H. Eckert, S. Grimme, J. Malberg, R. Wolf, *Solid State Nuclear Magnetic Resonance* **2013**, 53, 13.
- 31 T. Wiegand, H. Eckert, S. Grimme, D. Hoppe, M. Ruck, *Chem. Eur. J.* **2011**, 17, 8739.
- 32 a) L. B. Moran, J. K. Berkowitz and J. P. Yesinowski, *Phys. Rev. B* **1992**, 45, 5347; b) Z. Zhang, J. H. Kennedy and H. Eckert, *J. Am. Chem. Soc.* **1992**, 114, 5775.
- 33 a) K. L. Moran, T. E. Gier, W. T. A. Harrison, G. D. Stucky, H. Eckert, K. Eichele, R. E. Wasylshen, *J. Am. Chem. Soc.* **1993**, 115, 10553; b) A. Olivieri, *J. Am. Chem. Soc.* **1992**, 114, 5758; c) R. K. Harris, A. C. Olivieri, *Prog. Nucl. Magn. Reson. Spectrosc.* **1992**, 24, 435.
- 34 a) A. D. Becke, *J. Chem. Phys.* **1993**, 98, 5648-652; b) P. J. Stephens, F. J. Devlin, C. F. Chabalowski, M. J. Frisch, *J. Phys. Chem.* **1994**, 98, 11623.
- 35 F. Weigend, R. Ahlrichs, *Phys. Chem. Chem. Phys.* **2005**, 7, 3297.
- 36 K. Angermaier, E. Zeller, H. Schmidbaur, *J. Organomet. Chem.* **1994**, 472, 371.
- 37 H. H. Karsch in W. A. Hermann, D. J. Brauer (eds.), *Synthetic Methods of Organometallic and Inorganic Chemistry*; Vol. 3, Georg Thieme Verlag Stuttgart, **1996**.
- 38 T. Allspach, Phosphaalkine: Synthese und Charakterisierung durch ausgewählte [3+2]-Cycloadditionen, *Dissertation* **1986**, University of Kaiserslautern, Germany.
- 39 S. Ahrland, K. Dreisch, B. Noren, A. Oskarsson, *Materials Chemistry and Physics* **1993**, 35, 281.
- 40 a) SCALE3ABS, CrysAlis<sup>Pro</sup>, Aglient Technologies Inc., Oxford, GB, **2012**; b) G. M. Sheldrick, SADABS, Bruker AXS, Madison, USA, **2007**.
- 41 R.C. Clark, J. S. Reid, *Acta Cryst.* **1995**, A51, 887.
- 42 G. M. Sheldrick, *Acta Cryst.* **2008**, A64, 112.
- 43 A. Altomare, M. C. Burla, M. Camalli, G. L. Cascarno, C. Giacovazzo, A. G. G. Moliterni, G. Polidori, R. Spagna, *J. Appl. Cryst.* **1999**, 32, 115.
- 44 P. van der Sluis, A. L. Spek, *Acta Cryst Sect A* **1990**, 46, 194.
- 45 A. E. Bennett, C. M. Rienstra, M. Auger, K. V. Lakshmi, R. G. Griffin, *J. Chem. Phys.* **1995**, 103, 6951.
- 46 D. Massiot, F. Fayon, M. Capron, I. King, S. Le Calvé, B. Alonso, J.-O. Durand, B. Bujoli, Z. Gan, G. Hoatson, *Magn. Reson. Chem.* **2002**, 40, 70.
- 47 O. B. Peersen, X. L. Wu, I. Kustanovich, S. O. Smith, *J. Magn. Reson. A* **1993**, 104, 334.
- 48 a) G. Bodenhausen, R. Freeman, G. A. Morris, *J. Magn. Reson.* **1976**, 23, 171-175; b) G. A. Morris, R. Freeman, *J. Magn. Reson.* **1978**, 29, 433.
- 49 C. Vinod Chandran, P. K. Madhu, N. D. Kurur, T. Bräuniger, *Magn. Reson. Chem.* **2008**, 46, 943.
- 50 a) R. Ahlrichs, F. Furche, C. Hättig, *TURBOMOLE, version 6.3*, Universität Karlsruhe, **2009**; b) R. Ahlrichs, M. Bär, M. Häser, H. Horn, C. Kölmel, *Chem. Phys. Lett.* **1989**, 162, 165.
- 51 a) A. D. Becke, *Phys. Rev. A* **1988**, 38, 3098; b) J. P. Perdew, *Phys. Rev. B* **1986**, 34, 7406.

- 51 A. Schäfer, C. Huber, R. Ahlrichs, *J. Chem. Phys.* **1994**, 100, 5829.  
52 R. Ahlrichs, K. May, *Phys. Chem. Chem. Phys.* **2000**, 2, 943.  
53 O. Treutler, R. Ahlrichs, *J. Chem. Phys.* **1995**, 102, 346.  
54 a) K. Eichkorn, O. Treutler, H. Öhm, M. Häser, R. Ahlrichs, *Chem. Phys. Lett.* **1995**, 240, 283; b) K. Eichkorn, F. Weigend, O. Treutler, R. Ahlrichs, *Theor. Chim. Acta* **1997**, 97, 119.  
55 a) M. Kaupp, M. Bühl, V. G. Malkin, *Calculation of NMR and EPR parameters*, Wiley-VCH, **2004**;  
b) R. Ditchfield, *Mol. Phys.* **1974**, 27, 789.  
56 A. K. Jameson, C. J. Jameson, *Chem. Phys. Lett.* **1987**, 134, 461.



## 5 Preparation of an Organometallic Molecular Square by Self-Assembly of Phosphorus-Containing Building Blocks<sup>[a],[b]</sup>

Jennifer Malberg, Michael Bodensteiner, Daniel Paul, Thomas Wiegand, Hellmut Eckert, and Robert Wolf



[a] J. Malberg, M. Bodensteiner, D. Paul, T. Wiegand, H. Eckert, R. Wolf, manuscript in preparation.

[b] Daniel Paul assisted in the preparation of compound **1** and of the starting materials during his BSc project at the University of Münster. Michael Bodensteiner and Robert Wolf performed the X-ray crystal structure analyses.



## 5.1 Introduction

The preparation of metallosupramolecular compounds via the controlled self-assembly of suitable metal complexes has attracted much attention since the original report by *Lehn et al.* on the spontaneous formation of dinuclear helicates from bipyridine and copper(I).<sup>1</sup> A diverse range of structures has become accessible in the meantime which increasingly find application in diverse areas such as host-guest chemistry and catalysis.<sup>2–4</sup> The search for new functional building blocks for such supramolecular assemblies represents a timely challenge.

Molecular squares are among the most extensively investigated supramolecular architectures.<sup>2,3</sup> They may be rationally designed by the combination of linear building units and rectangular corner pieces. Impressive square-type structures have been prepared by combining octahedral or square planar metal cations, e.g.  $\text{Fe}^{2+}$ ,  $\text{Co}^{2+}$ ,  $\text{Ni}^{2+}$ ,  $\text{Pd}^{2+}$ , and  $\text{Pt}^{2+}$ , with bidentate ligands such as cyanide, nitrogen-based heterocycles, ditopic N-heterocyclic carbenes, and isonitriles.<sup>5</sup> However, the further diversification of square-type architectures requires novel synthetic strategies. Here, we describe for the first time the rational synthesis of a molecular square by using phospho-organometallic diphosphacyclobutadiene building blocks.<sup>6</sup>

As illustrated in Figure 1, our synthetic approach utilizes the recently reported anionic complex  $[\text{Co}(\eta^4\text{-P}_2\text{C}_2\text{R}_2)_2]^-$  (**A**,  $\text{R} = t\text{Bu}$ , Ad), which shows a  $D_{2d}$  symmetrical sandwich structure.<sup>7</sup> Anion **A** is readily accessible by the metal-mediated dimerization of *tert*-butyl phosphalkyne with the low-valent anthracene cobaltate complex  $[\text{Co}(\eta^4\text{-C}_{14}\text{H}_{10})_2]^-$ . The molecular structure of **A** features two coplanar 1,3-diphosphacyclobutadiene rings in a staggered orientation, i.e. the two  $\text{P}_2\text{C}_2$  rings are rotated by  $90^\circ$  with respect to one another.<sup>8a</sup> We hypothesized that this structural detail might allow the construction of a completely new type of molecular square by coordination of suitable metal cations that require a linear coordination geometry. Considering the established ability of 1,3-diphosphacyclobutadiene complexes to bind univalent coinage metal ions,<sup>8</sup> we decided to focus on gold(I) complexes. Here, we report the synthesis and structural characterization of the new octametallic  $\text{Au}_4\text{Co}_4$  compound  $[\text{Au}\{\text{Co}(\text{P}_2\text{C}_2t\text{Bu}_2)_2\}]_4$  (**1**), which is formed by the self-assembly of four  $\text{Au}^+$  cations and four  $[\text{Co}(\text{P}_2\text{C}_2t\text{Bu}_2)_2]^-$  units.

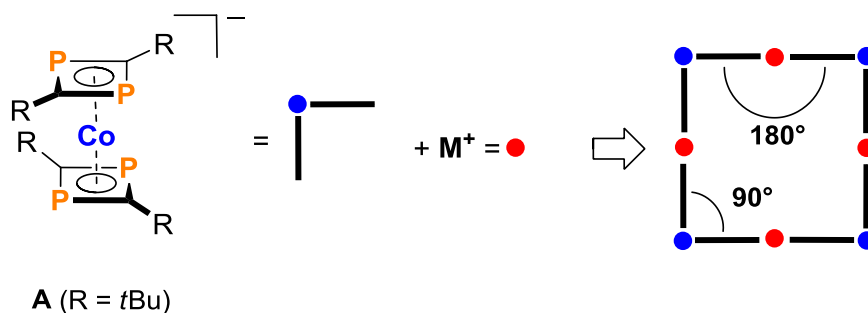
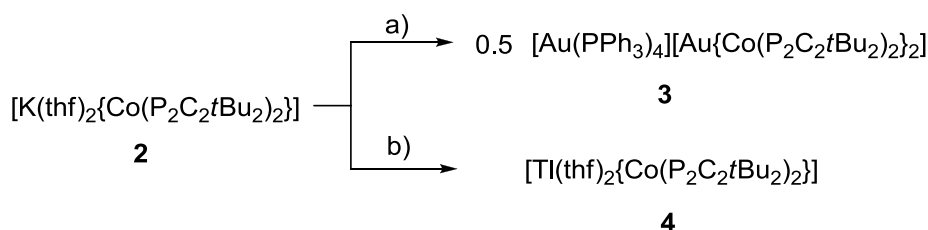


**Figure 1.** Design principle for the construction of new phospho-organometallic molecular squares.

## 5.2 Results

Initial attempts to access **1** by straightforward salt metathesis of the potassium salt  $[\text{K}(\text{thf})_2\{\text{Co}(\text{P}_2\text{C}_2\text{tBu}_2)_2\}]$  (**2**) with gold(I) halides remained unsuccessful. Instead, the reaction of **2** with  $\text{AuCl}(\text{PPh}_3)$  (Scheme 1a) afforded the ionic compound  $[\text{Au}(\text{PPh}_3)_4][\text{Au}\{\text{CoP}_2\text{C}_2\text{tBu}_2\}_2]$  (**3**) as deep red crystals in 32% yield. A single-crystal X-ray structure determination revealed an ionic structure (Figure 2a) that consists of a linear  $[\text{Au}\{\text{Co}(\text{P}_2\text{C}_2\text{tBu}_2)_2\}_2]^-$  anion (Au1–P1,P5 2.2786(11) and 2.2777(11) Å) and the  $[\text{Au}(\text{PPh}_3)_4]^+$  cation. The latter shows a distorted trigonal pyramidal structure similar to that previously reported for  $[\text{Au}(\text{PPh}_3)_4]\text{BPh}_4$ .<sup>9</sup>



**Scheme 1.** Synthesis of complexes **3** and **4**. Reagents: a) +  $\text{AuCl}(\text{PPh}_3)$ / –  $\text{KCl}$  and by-products; b) +  $\text{TlPF}_6$ / –  $\text{KPF}_6$ .

The  $^1\text{H}$  NMR and  $^{31}\text{P}\{^1\text{H}\}$  NMR spectra of **3** are temperature-dependent due to the labile coordination of the gold(I) cations.<sup>10</sup> Two very broad  $^{31}\text{P}\{^1\text{H}\}$  NMR peaks at +10.5 ppm ( $\nu_{\text{FWHM}} = 1000$  Hz) and +26.1 ppm ( $\nu_{\text{FWHM}} = 1000$  Hz) were observed in  $[\text{D}_8]\text{THF}$  at room temperature. The  $^{31}\text{P}\{^1\text{H}\}$  NMR spectrum recorded at  $-80$  °C displays three resonances for the  $[\text{Au}\{\text{Co}(\text{P}_2\text{C}_2\text{tBu}_2)_2\}_2]^-$  anion at  $-27.0$ ,  $+14.3$ , and  $+37.7$  ppm and two extremely broad peaks at  $+32.6$  ppm ( $\nu_{\text{FWHM}} = 1100$  Hz) and  $+42.2$  ppm ( $\nu_{\text{FWHM}} = 1100$  Hz) assigned to the coordinated  $\text{PPh}_3$  ligand. The large line width of the latter signal shows that the solution equilibria are not fully resolved even at this temperature. Careful integration of the  $^1\text{H}$  NMR spectra of the aromatic and *tert*-butyl signals furthermore revealed a ratio Ph:*t*Bu of 55:72, whereas a ratio of 60:72 would be expected for pure **3**. This observation is presumably explained by the presence of approximately 30% of tris(phosphane) complex  $[\text{Au}(\text{PPh}_3)_3][\text{Au}\{\text{Co}(\text{P}_2\text{C}_2\text{tBu}_2)_2\}_2]$  as a minor component in the isolated bulk solid.<sup>11</sup>

In order to facilitate the transmetalation reaction, we subsequently synthesized the thallium(I) complex  $[\text{Tl}(\text{thf})_2\{\text{Co}(\text{P}_2\text{C}_2\text{tBu}_2)_2\}]$  (**4**) in 81% yield by reacting **2** with one equivalent  $\text{TlPF}_6$  (Scheme 1b). Dark-brown **4** is the first structurally characterized example of a diphosphacylobutadiene complex of type **A** with a p-block metal. Single crystal X-ray diffraction revealed a polymeric arrangement (Figure 2b) with two similar, crystallographically independent  $[\text{Tl}(\text{thf})_2\{\text{Co}(\text{P}_2\text{C}_2\text{tBu}_2)_2\}]$  units in the asymmetric unit. The  $\text{Tl}^+$  cations are coordinated by two THF molecules and three phosphorus atoms from two different  $[\text{Co}(\text{P}_2\text{C}_2\text{tBu}_2)_2]^-$  anions with comparatively long Tl–P distances in the range of 3.252(2)–3.395(2) Å.<sup>12,13</sup>

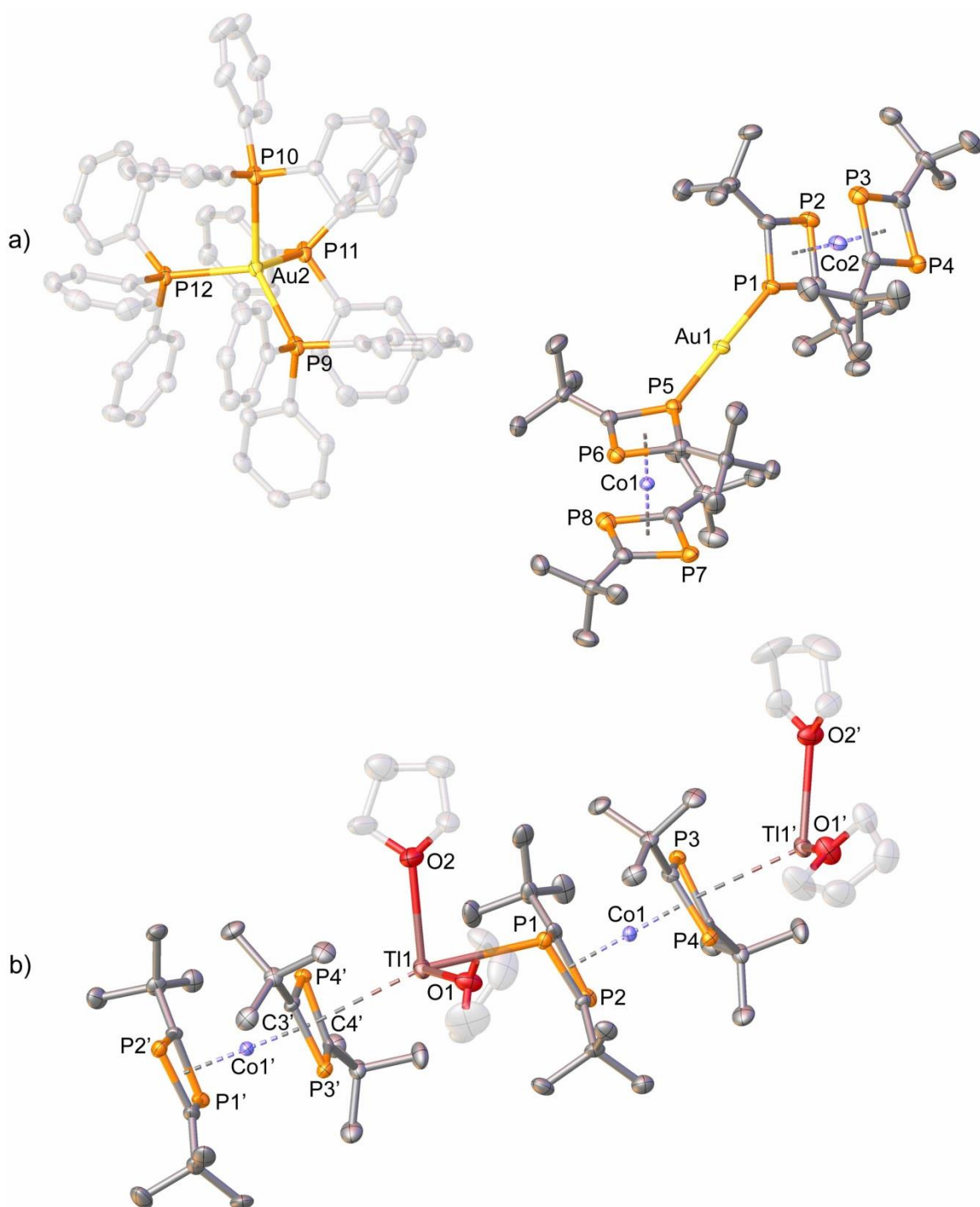
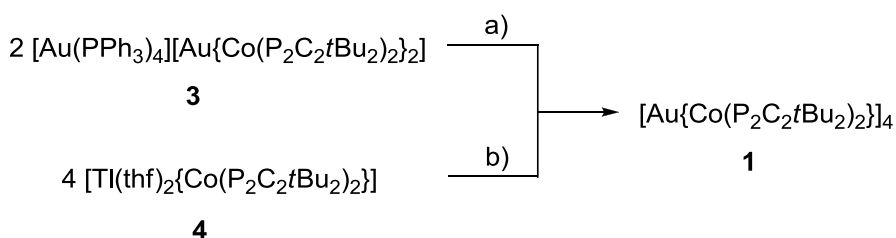


**Figure 2.** Solid-state molecular structures of a)  $[\text{Au}(\text{PPh}_3)_4][\text{Au}\{\text{Co}(\text{P}_2\text{C}_2\text{tBu}_2)_2\}_2]$  (**3**) and b)  $[\text{Tl}(\text{thf})_2\{\text{Co}(\text{P}_2\text{C}_2\text{tBu}_2)_2\}]$  (**4**). Thermal ellipsoids are drawn at the 40% probability level. Hydrogen atoms are not shown. The site disorder of Au2 and of one phenyl ring of the  $[\text{Au}(\text{PPh}_3)_4]^+$  cation of **3**, and the disorder of one THF molecule of **4** are omitted for clarity. Selected bond lengths [ $\text{\AA}$ ] and angles [ $^\circ$ ] of **3**: Au1–P1 2.2789(11), Au1–P5 2.2785(11), P1–Au1–P5 177.94(5), Au2–P9 2.4028(11), Au2–P10 2.3820(11), Au2–P11 2.3592(12), Au2–P12 3.856(17), av. P–Au2–P 107.32(5); Selected bond lengths [ $\text{\AA}$ ] of **4**: Tl1–P1 3.395(2), Tl1–P4' 3.252(2), Tl1–P3' 3.271(2), Tl1–C3' 3.271(6), Tl1–C4' 3.293(6), Tl1–O1 2.753(6), Tl1–O2 2.793(3), symmetry operation to generate the equivalent atoms of **4'**:  $+x, 0.5-y, 0.5+z$ .

The NMR spectra of **4** ( $C_7D_8/[D_8]THF$ ) display one  $^1H$  NMR resonance for the *t*Bu groups at +1.18 ppm and one  $^{31}P\{^1H\}$  NMR singlet at +30.0 ppm. The latter resonance is shifted to higher frequency by approximately 25 ppm compared to the starting compound **2** (+5.1 ppm in  $[D_8]THF$ ). No decoalescence was observed for these signals on cooling to  $-80\text{ }^\circ C$ . The symmetrical NMR spectra presumably arise either from the formation of an ionic structure  $[Ti(thf)_x]^+[Co(P_2C_2tBu_2)_2]^-$  in solution or the rapid exchange of the coordinated  $Ti^+$  cation between different  $P_2C_2$  rings via intra- or intermolecular pathways with low kinetic barriers.

Having the new complexes **3** and **4** in hand, we were gratified to discover that both compounds can be successfully employed for the preparation of our targeted  $Au_4Co_4$  square  $[Au\{Co(P_2C_2tBu_2)_2\}]_4$  (**1**): Complex **1** was obtained in 46% isolated yield by heating **3** with four equivalents of  $AuCl(PPh_3)$  in THF (Scheme 2a).<sup>14</sup> Furthermore, **1** was synthesized in 20% yield via the slow addition of **4** to a dilute THF solution of  $AuCl(tht)$  (Scheme 2b).



**Scheme 2.** Synthesis of the molecular square **1**. Reagents: a) + 8  $AuCl(PPh_3)$ / – 8  $AuCl(PPh_3)_2$ ; b) + 4  $AuCl(tht)$ / – 4  $TiCl$ , – 4  $THT$ .

Compound **1** crystallized as deep red blocks from *n*-hexane and was fully characterized by NMR spectroscopy, X-ray crystallography and elemental analysis. The solid-state molecule structure (Figure 3) shows four  $[Co(P_2C_2tBu_2)_2]^-$  units that are connected by four  $Au^+$  cations with a linear coordination environment ( $Au1-P1\ 2.276(3)\text{ \AA}$ ,  $P1-Au1-P1a\ 179.6(2)^\circ$ ). The resulting molecular square **1** has crystallographically imposed  $C_4$  symmetry (space group  $I4/mmm$  with two formula units per unit cell). The cobalt and gold atoms are located on a crystallographic mirror plane, while the phosphorus, carbon and hydrogen atoms reside above or below that plane, which results in a puckered structure (Figure 3b). The puckering of the  $[Au\{Co(P_2C_2tBu_2)_2\}]_4$  molecule is evident from the twisted  $P-Au-P$  vectors, which form a twist angle  $P1,Au1,P1a/P1d,Au1d,P1e$  of  $31.2^\circ$ .

In agreement with its solid-state structure, the  $^1H$  NMR spectrum of **1** features two sharp singlets in a 1:1 ratio that can be assigned to the two chemically different *t*Bu substituents. The  $^{31}P\{^1H\}$  NMR spectrum of **1** recorded in  $[D_8]THF$  shows two singlets at  $-19.5$  ppm and  $+38.9$  ppm. In agreement with previous solid-state NMR investigations and DFT calculations on related complexes,<sup>15</sup> we assign the high-frequency signal at  $+38.9$  ppm to the phosphorus atoms which coordinate to gold while the low-frequency resonance at  $-19.5$  ppm is assigned to the non-coordinated P atoms.

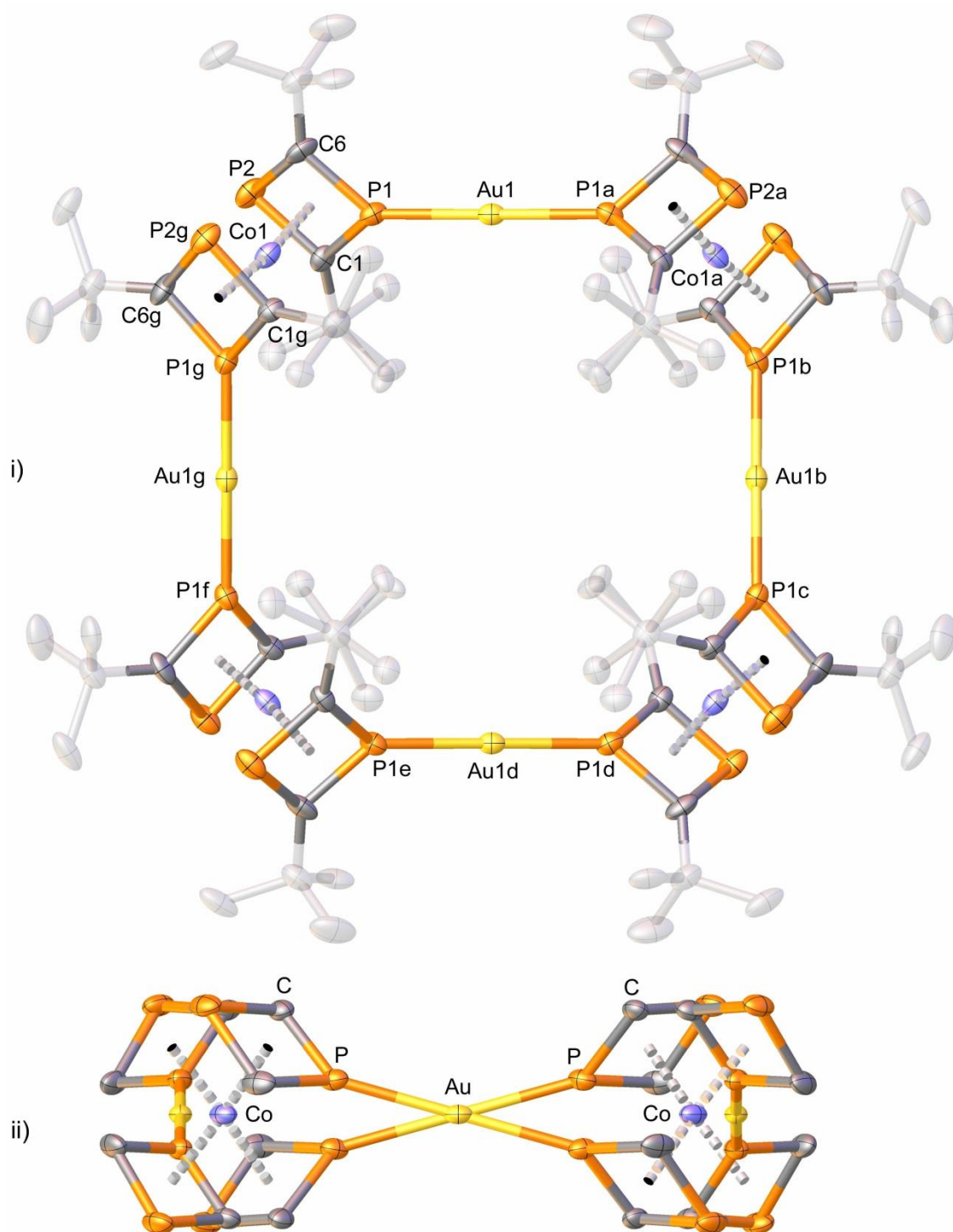


**Figure 3.** Graphical representation of the solid-state molecular structure of  $[\text{Au}\{\text{Co}(\text{P}_2\text{C}_2t\text{Bu}_2)_2\}]_4$  (**1**); i) view along the crystallographic  $c$  axis. The thermal ellipsoids are drawn at the 20% level, H atoms and the disorder of the  $[\text{Co}(\text{P}_2\text{C}_2t\text{Bu}_2)_2]^-$  anions are omitted, the  $t\text{Bu}$  groups have been made transparent for clarity; ii) view along the crystallographic  $b$  axis, H atoms and  $t\text{Bu}$  substituents are omitted for clarity. Selected bond lengths [ $\text{\AA}$ ] and angles [ $^\circ$ ]: Au1–P1 2.276(3), Co1–P1 2.193(3), Co1–C1 2.108(11), P1–C1 1.756(12), P2–C1 1.806(12), P1–Au1–P1a 179.6(2), angle between vectors P1,Au1,P1a/P1d,Au1d,P1e 31.2°, symmetry operations to generate equivalent atoms: a)  $x, 1-y, z$ ; b)  $y, 1-x, -z$ ; c)  $1-y, 1-x, z$ ; d)  $1-x, 1-y, -z$ ; e)  $1-x, y, z$ ; f)  $1-y, x, -z$ ; g)  $y, x, z$ .

### 5.3 Conclusion

In summary, we have developed a new method for the preparation of organometallic molecular squares via the self-assembly of gold(I) cations and phospho-organometallic building blocks. This new methodology was exemplified by the synthesis of the unprecedented  $\text{Au}_4\text{Co}_4$  square,  $[\text{Au}\{\text{Co}(\text{P}_2\text{C}_2t\text{Bu}_2)\}]_4$  (**1**). The two new complexes  $[\text{Au}(\text{PPh}_3)_4][\text{Au}\{\text{Co}(\text{P}_2\text{C}_2t\text{Bu}_2)_2\}_2]$  (**3**) and  $[\text{Tl}(\text{thf})_2\{\text{Co}(\text{P}_2\text{C}_2t\text{Bu}_2)_2\}]$  (**4**) are suitable starting materials for the synthesis of **1**. We are currently exploring the synthesis of a larger array of squares by using this methodology. In future work, we expect that especially the “Tl(I) route” can be easily extended to other metals beyond group 11, which should give rise to diverse oligonuclear phospho-organometallic structures with interesting electronic and magnetic properties.

## 5.4 Experimental Section

### 5.4.1 General Procedures

All experiments were performed under an atmosphere of dry argon, by using standard Schlenk and glovebox techniques. Solvents were purified, dried, and degassed by standard techniques. NMR spectra were recorded on Bruker Avance 300 ( $^{31}\text{P}$ ; 85%  $\text{H}_3\text{PO}_4$ ) and Avance 400 spectrometers ( $^1\text{H}$ ,  $^{13}\text{C}$ ;  $\text{SiMe}_4$ ), internally referenced to residual solvent resonances. The spectra were recorded at 300 K unless noted otherwise. Melting points were measured on samples in sealed capillaries and are uncorrected.  $\text{AuCl}(\text{tht})$  were prepared by a modified literature procedure.<sup>16</sup>  $\text{AuCl}(\text{PPh}_3)$  was purchased from ABCR and used as received. Elemental analyses were determined on Elementar Micro Vario Cube instruments and are uncorrected.

### 5.4.2 $[\text{Au}\{\text{Co}(\text{P}_2\text{C}_2\text{tBu}_2)_2\}]_4$ (**1**)

Method A: A colorless THF solution (20 mL) of  $\text{AuCl}(\text{PPh}_3)$  (91.7 mg, 0.19 mmol) was added to a deep red THF solution (50 mL) of  $[\text{Au}(\text{PPh}_3)_4][\text{Au}\{\text{Co}(\text{P}_2\text{C}_2\text{tBu}_2)_2\}]$  (**3**; 107.0 mg, 0.05 mmol). The reaction mixture was stirred for 12 h at room temperature and subsequently heated at 70 °C for 2 h. The solvent was removed in *vacuo* and the orange-red residue was extracted with *n*-hexane (3x10 mL). Storage of the combined *n*-hexane extracts at -30 °C for 3 days gave **1** as red crystals. Yield 27.8 mg (46%). M.p.: 235 °C (decomp.). Elemental analysis calcd. for  $\text{C}_{80}\text{H}_{144}\text{Au}_4\text{Co}_4\text{P}_{16}$  ( $M = 2625.21$ ): C 36.60, H 5.53; found: C 36.76, H 5.43.  $^1\text{H}$  NMR (400.13 MHz, 300 K,  $[\text{D}_8]\text{THF}$ ):  $\delta = 1.17$  (s, 18H; *t*Bu), 1.28 (s, 18 H; *t*Bu). A  $^{13}\text{C}\{^1\text{H}\}$  NMR spectrum was not obtained due the modest solubility of the isolated solid.  $^{31}\text{P}\{^1\text{H}\}$  NMR (161.98 MHz, 300 K,  $[\text{D}_8]\text{THF}$ ):  $\delta = -19.5$  (s; non-coordinated P atoms of  $\text{Co}(\text{P}_2\text{C}_2\text{tBu}_2)_2$ ), 38.9 (s; Au-P of  $\text{Co}(\text{P}_2\text{C}_2\text{tBu}_2)_2$ ). Method B: A THF solution (200 mL) of  $[\text{Ti}(\text{thf})\{\text{Co}(\text{P}_2\text{C}_2\text{tBu}_2)_2\}]$  (**4**; 848.8 mg, 1.15 mmol) was added slowly (45 min) to a suspension of  $\text{AuCl}(\text{tht})$  (369.8 mg, 1.15 mmol) in THF (ca. 650 mL) at -78 °C. An orange-brown suspension formed while the mixture was allowed to warm to room temperature overnight with stirring. The solvent was removed in *vacuo* and the red-brown residue was extracted with *n*-hexane (80 mL and 4x10 mL). The combined *n*-hexane solution was concentrated to 40 mL. Storage at -30 °C for three days gave red crystals of **1**. Yield 151 mg (20%). The spectroscopic properties are identical to those prepared by method A.

### 5.4.3 $[\text{K}(\text{thf})_2\{\text{Co}(\text{P}_2\text{C}_2\text{tBu}_2)_2\}]$ (**2**)

*t*BuC $\equiv$ P (24.76 mL, 33.83 mmol, 1.37 M solution in *n*-hexane) was added dropwise to a deep red-brown solution of  $[\text{K}(\text{dme})_2][\text{Co}(\text{C}_{14}\text{H}_{10})_2]$  (3.30 g, 5.21 mmol) in THF (65 mL) at -78 °C. The mixture was allowed to warm to room temperature overnight. The dark orange solution was then filtered and concentrated to ca. 30 mL. Addition of *n*-hexane (65 mL) gave a crystalline solid which was recrystallized from THF/*n*-hexane (1:2). The isolated orange, crystalline solid still contained two THF molecules per formula unit according to  $^1\text{H}$  NMR spectroscopy after drying in an oil pump vacuum for 2 h. Yield 2.92 g (87%). M.p.: 170 °C. Elemental analysis calcd. for  $\text{C}_{20}\text{H}_{36}\text{P}_4\text{CoK}\cdot 1.75(\text{C}_4\text{H}_8\text{O})$  ( $M = 605.07$ , calculated for sample which contains 1.75 THF molecules per formula unit): C 51.92, H 8.07; found: C 51.98, H 7.80.

$^1\text{H}$  NMR (400.13 MHz,  $[\text{D}_8]\text{THF}$ ):  $\delta$  = 1.07 (s, 36H; *t*Bu), 1.78 (bs, 8H; THF), 3.62 (bs, 8H; THF).  $^{13}\text{C}\{^1\text{H}\}$  NMR (100.61 MHz,  $[\text{D}_8]\text{THF}$ ):  $\delta$  = 33.6 (s;  $\text{C}(\text{CH}_3)_3$ ), 35.9 (s;  $\text{C}(\text{CH}_3)_3$ ), 102.7 (t,  $^1J(\text{C},\text{P}) = 51.7$  Hz;  $\text{C}_2\text{P}_2\text{tBu}_2$ ); the signals of coordinated THF were not observed due to overlap with solvent signals.  $^{31}\text{P}\{^1\text{H}\}$  NMR (161.98 MHz,  $[\text{D}_8]\text{THF}$ ):  $\delta$  = 5.1.

#### 5.4.4 $[\text{Au}(\text{PPh}_3)_4][\text{Au}\{\text{Co}(\text{P}_2\text{C}_2\text{tBu}_2)_2\}_2]$ (**3**)

A light red solution of  $[\text{K}(\text{thf})_2\{\text{Co}(\text{P}_2\text{C}_2\text{tBu}_2)_2\}]$  (**2**; 0.32 g, 0.50 mmol) in ca. 15 mL THF was added to a colorless solution of  $\text{AuCl}(\text{PPh}_3)$  (0.27 g, 0.50 mmol) in 50 mL THF at  $-78^\circ\text{C}$ . The reaction mixture turned deep red and was allowed to warm to room temperature overnight while stirring. Complete removal of the solvent and extraction of the dark residue with  $\text{Et}_2\text{O}$  (50 mL and 3x5 mL) gave a deep red solution, which was concentrated to ca. 15 mL and layered with *n*-hexane (ca. 10 mL). Deep red crystals of complex **3** formed after storage at  $-18^\circ\text{C}$  for three days. Compound **3** crystallized as a mixture composed of 70%  $[\text{Au}(\text{PPh}_3)_4][\text{Au}\{\text{Co}(\text{P}_2\text{C}_2\text{tBu}_2)_2\}_2]$  and 30%  $[\text{Au}(\text{PPh}_3)_3][\text{Au}\{\text{Co}(\text{P}_2\text{C}_2\text{tBu}_2)_2\}_2]$ . The isolated compound still contains one *n*-hexane molecule per formula unit after drying in an oil pump vacuum for 1 h. Yield 0.39 g (32%). M.p.:  $>320^\circ\text{C}$  (slow decomp.). Elemental analysis calcd. for  $\text{C}_{40}\text{H}_{70}\text{AuCo}_2\text{P}_8 \cdot 0.7(\text{Au}\{\text{P}(\text{C}_6\text{H}_5)_3\}_4) \cdot 0.3(\text{Au}\{\text{P}(\text{C}_6\text{H}_5)_3\}_3) \cdot \text{C}_6\text{H}_{14}$  ( $M = 2395.49$ ): C 57.08, H 6.02; found: C 56.81, H 5.81.  $^1\text{H}$  NMR (400.13 MHz, 300 K,  $[\text{D}_8]\text{THF}$ ):  $\delta$  = 0.89 (t,  $^1J(\text{H},\text{C}) = 6.89$  Hz, 6H;  $\text{CH}_3$  of *n*-hexane), 1.14 (s, 72 H; *t*Bu), 1.29 (br m, 8H;  $\text{CH}_2$  of *n*-hexane), 7.39–7.70 (overlapping m, 53H; Ph).  $^1\text{H}$  NMR (400.13 MHz, 193 K,  $[\text{D}_8]\text{THF}$ ):  $\delta$  = 0.89 (t,  $^1J(\text{H},\text{C}) = 6.84$  Hz;  $\text{CH}_3$  of *n*-hexane), 1.00–1.15 (br overlapping s; *t*Bu), 1.25 (very br. m;  $\text{CH}_2$  of *n*-hexane), 7.16–7.68 (overlapping m, 55H; Ph). Due to severe signal overlap, a reliable integration of individual signals could not be performed. Integration of the whole aliphatic (0.89–1.15 ppm) and the aromatic regions (7.16–7.68 ppm) gave a ratio (*t*Bu+*n*-hexane):Ph of 90:55.  $^{13}\text{C}\{^1\text{H}\}$  NMR (100.61 MHz, 300 K,  $[\text{D}_8]\text{THF}$ ):  $\delta$  = 14.3 (s;  $\text{CH}_3$  of *n*-hexane), 23.4 (s;  $\text{CH}_2$  of *n*-hexane), 32.4 (s;  $\text{CH}_2$  of *n*-hexane), 33.6 (s;  $\text{C}(\text{CH}_3)_3$  of *t*Bu), 35.5 (s;  $\text{C}(\text{CH}_3)_3$  of *t*Bu), 129.7 (s; C-3,5 of  $\text{PPh}_3$ ), 129.9 (s; C-4 of  $\text{PPh}_3$ ), 131.4 (br s; C-1 of  $\text{PPh}_3$ ), 134.7 (d,  $^2J(\text{C},\text{P}) = 16.38$  Hz; C-2,6 of  $\text{PPh}_3$ ). The  $^{13}\text{C}$  signals for the  $\text{P}_2\text{C}_2$  rings were not detected due to insufficient signal intensity.  $^{13}\text{C}\{^1\text{H}\}$  NMR (100.61 MHz, 193 K,  $[\text{D}_8]\text{THF}$ ):  $\delta$  = 14.8 (s;  $\text{CH}_3$  of *n*-hexane), 24.0 (s;  $\text{CH}_2$  of *n*-hexane), 33.0 (br s;  $\text{C}(\text{CH}_3)_3$  of *t*Bu), 33.6 (very br s;  $\text{C}(\text{CH}_3)_3$  of *t*Bu), 35.0 (s;  $\text{CH}_2$  of *n*-hexane), 36.0 (br s;  $\text{C}(\text{CH}_3)_3$  of *t*Bu), 36.3 (s;  $\text{C}(\text{CH}_3)_3$  of *t*Bu), 129.9 (br s; C-3,5 of  $\text{PPh}_3$ ), 131.6 (br s; C-4), 132.7 (very br m; C-2,6 of  $\text{PPh}_3$ ), 134.4 (m; C-1 of  $\text{PPh}_3$ ). The signals for the  $\text{P}_2\text{C}_2$  rings were not observed.  $^{31}\text{P}\{^1\text{H}\}$  NMR (161.98 MHz, 300 K,  $[\text{D}_8]\text{THF}$ ):  $\delta$  = 10.5 (br s;  $\text{Co}(\text{P}_2\text{C}_2\text{tBu}_2)_2$ ), 26.1 (very br s; coordinated  $\text{PPh}_3$ ).  $^{31}\text{P}\{^1\text{H}\}$  NMR (161.98 MHz, 193 K,  $[\text{D}_8]\text{THF}$ ):  $\delta$  =  $-27.0$  (s, 2P; non-coordinated P atom of  $\text{P}_2\text{C}_2\text{tBu}_2$ ), 14.3 (s, 4P;  $\text{P}_2\text{C}_2\text{tBu}_2$ ), 32.6 (very br s;  $[\text{Au}(\text{PPh}_3)_4]^+$  or  $[\text{Au}(\text{PPh}_3)_3]^+$ ), 37.7 (s, 2P; Au–P of  $\text{P}_2\text{C}_2\text{tBu}_2$ ), 42.2 (very br s;  $[\text{Au}(\text{PPh}_3)_4]^+$  or  $[\text{Au}(\text{PPh}_3)_3]^+$ ).

#### 5.4.5 $[\text{Ti}(\text{thf})_2\{\text{Co}(\text{P}_2\text{C}_2\text{tBu}_2)_2\}]$ (**4**)

$\text{TiPF}_6$  (0.47 g; 1.35 mmol) was added slowly over a period of 20 min to a light red solution of  $[\text{K}(\text{thf})_2\{\text{Co}(\text{P}_2\text{C}_2\text{tBu}_2)_2\}]$  (**2**; 0.77 g; 1.35 mmol) in 180 mL THF at room temperature. A dark red-brown reaction mixture formed immediately on addition, which was stirred for 12 h at room temperature. The

mixture was filtered, concentrated to ca. 80 mL and layered with *n*-hexane (ca. 130 mL). Deep brown crystals of **4** formed, which were recrystallized from THF/*n*-hexane (1:2). The crystals partially lose THF under vacuum. The isolated sample of **4** still contained one THF molecule per formula unit according to <sup>1</sup>H NMR spectroscopy after drying in an oil pump vacuum for 2 h. Yield 0.80 g (81%). M.p.: 185 °C (decomp.). Elemental analysis calcd. for C<sub>20</sub>H<sub>38</sub>P<sub>4</sub>CoTi·C<sub>4</sub>H<sub>8</sub>O (*M* = 735.82; *x* = 1): C 39.18, H 6.03; found: C 38.92, H 5.70. UV/vis (THF,  $\lambda_{max}/nm$  ( $\epsilon_{max}/dm^3mol^{-1}cm^{-1}$ )): 262 (shoulder); 284 (42000); 333 (17500). <sup>1</sup>H NMR (400.13 MHz, 300 K, C<sub>7</sub>D<sub>8</sub>/[D<sub>8</sub>]THF):  $\delta$  = 1.18 (s, 36H; *t*Bu), 1.51 (m, 4H; coord. THF), 3.50 (m, 4H; coord.THf). <sup>13</sup>C{<sup>1</sup>H} NMR (100.61 MHz, 300 K, C<sub>7</sub>D<sub>8</sub>/[D<sub>8</sub>]THF):  $\delta$  = 33.6 (s; C(CH<sub>3</sub>)<sub>3</sub> of *t*Bu), 35.8 (s; C(CH<sub>3</sub>)<sub>3</sub> of *t*Bu), 109.2 (t; C<sub>2</sub>P<sub>2</sub>*t*Bu<sub>2</sub>); the signals for THF were not observed due to overlap with solvent signals. <sup>31</sup>P{<sup>1</sup>H} NMR (161.98 MHz, 300 K, C<sub>7</sub>D<sub>8</sub>/[D<sub>8</sub>]THF):  $\delta$  = 30.0.

#### 5.4.6 X-Ray Crystallography

The crystals were processed with an Agilent Technologies SuperNova Atlas diffractometer. Either semi-empirical multi-scan absorption corrections,<sup>17</sup> analytical ones<sup>18</sup> or Patterson methods were applied to the data. The structures were solved by SHELXS<sup>19</sup> or SIR<sup>20</sup> and least-square refinements on *F*<sup>2</sup> were carried out with SHELXL.<sup>21,19</sup> The structure of **1** shows solvent accessible voids that contain a mixture of THF and *n*-hexane that could not be modelled due to disorder in addition to their location at a special position. The electron density associated with these voids was removed with SQUEEZE implemented in PLATON.<sup>22</sup> One of the gold atoms of **3** was disordered over two sites (Au2/Au2a 82:18 site occupancy). The structure of **4** was non-merohedrally twinned. The twinning was analyzed with CrysAlisPro software of Agilent Technologies and refined with the HKLF5 option in SHELXL.<sup>23</sup> Further details of the structure refinements are given in the corresponding .cif-files. Crystallographic data are given in Table 1.

**Table 1.** Crystallographic data and structure refinement of **1**, **3**, and **4**.

	<b>1</b>	<b>3</b>	<b>4</b>
Empirical formula	C <sub>80</sub> H <sub>144</sub> Au <sub>4</sub> Co <sub>4</sub> P <sub>16</sub>	C <sub>124</sub> H <sub>160</sub> Au <sub>2</sub> Co <sub>2</sub> P <sub>12</sub>	C <sub>28</sub> H <sub>52</sub> CoO <sub>2</sub> P <sub>4</sub> Tl
Crystal size [mm <sup>3</sup> ]	0.22 × 0.21 × 0.16	0.20 × 0.10 × 0.05	0.12 × 0.10 × 0.05
Color and shape	red block	red plate	red prism
Formula weight [g mol <sup>-1</sup> ]	2625.06	2533.95	807.88
Crystal system	tetragonal	triclinic	monoclinic
Space group	I4/ <i>mmm</i>	<i>P</i> -1	<i>P</i> 2 <sub>1</sub> / <i>c</i>
Absorption correction	numerical	numerical	multi-scan
Transmission min/max	0.619/0.284	0.752/0.430	0.68361/1.00000
<i>a</i> [Å]	24.5188(3)	14.08460(10)	19.8894(7)
<i>b</i> [Å]	24.5188(3)	17.2688(2)	17.3179(8)
<i>c</i> [Å]	11.16795(18)	26.5382(3)	19.4638(8)
$\alpha$ [°]	90	108.7950(10)	90.00
$\beta$ [°]	90	90.9390(10)	91.122(4)
$\gamma$ [°]	90	98.4060(10)	90.00
<i>V</i> [Å <sup>3</sup> ]	6713.9(2)	6030.99(11)	6702.9(5)
<i>Z</i>	2	2	8
<i>T</i> [K]	123(1)	155(2)	123(2)
$\lambda$ [Å]	1.5418	1.54184	1.54184
$\rho_{\text{calc}}$ [g/cm <sup>3</sup> ]	1.298	1.395	1.601
$\mu$ (mm <sup>-1</sup> )	13.779	8.437	14.976
Theta range [°]	4.34-76.99	3.61-77.76	3.38-74.14
Reflections collected to $\theta_{\text{max}}$ [°]	45412	98266	23542
Unique reflections ( <i>R</i> <sub>int</sub> )	2029 (0.0780)	23512 (0.0281)	23542
Refl. obs. [ <i>I</i> > 2 $\sigma$ ( <i>I</i> )]	2029	23512	23542
Parameters	111	1338	719
Completeness to $\theta$	0.952	0.992	0.983
<i>R</i> -values [ <i>I</i> > 2 $\sigma$ ( <i>I</i> )]	0.0489/0.1333	0.0428/0.1043	0.0544/0.1392
<i>R</i> -values (all data)	0.0498/0.1344	0.0507/0.1074	0.0761/0.1528
GOF on <i>F</i> <sup>2</sup>	1.073	0.916	1.045
Residual density [eÅ <sup>-3</sup> ]	-1.17/1.57	-1.22/5.49	-1.73/1.84

## 5.5 Supporting Information

### 5.5.1 $^1\text{H}$ and $^{31}\text{P}\{^1\text{H}\}$ NMR Spectra of $[\text{Au}\{\text{Co}(\text{P}_2\text{C}_2t\text{Bu}_2)_2\}]_4$ (**1**) at 300 K (Figures S1 and S2).

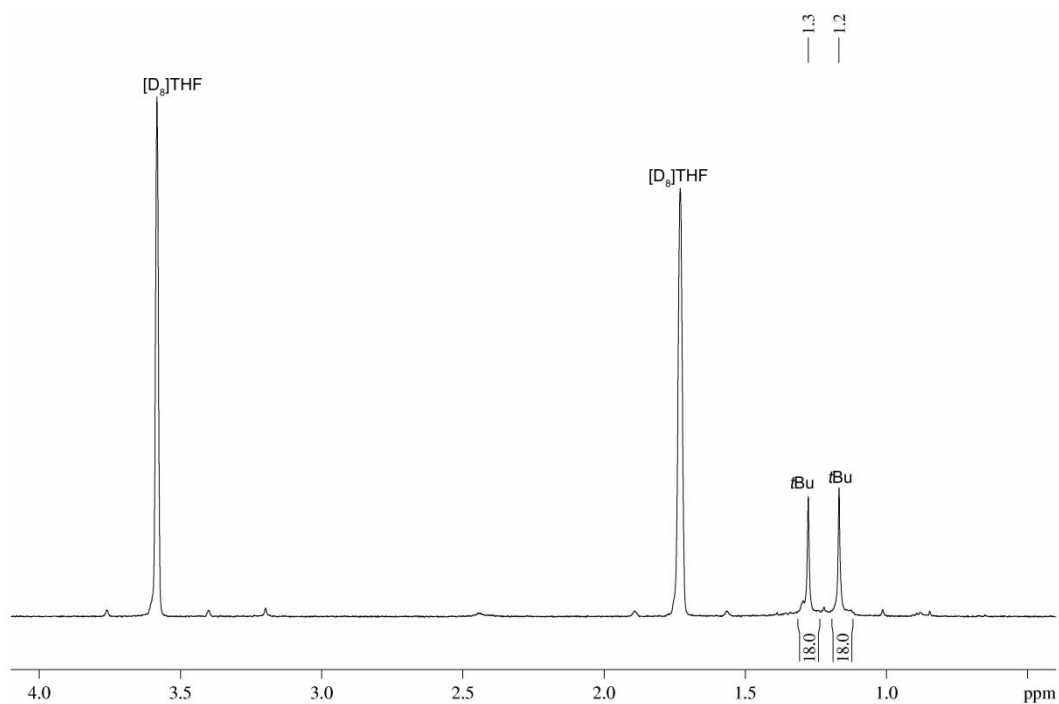


**Figure S1.**  $^1\text{H}$  NMR Spectrum of  $[\text{Au}\{\text{Co}(\text{P}_2\text{C}_2t\text{Bu}_2)_2\}]_4$  (**1**) in  $[\text{D}_8]\text{THF}$  (300 K, 400.13 MHz).

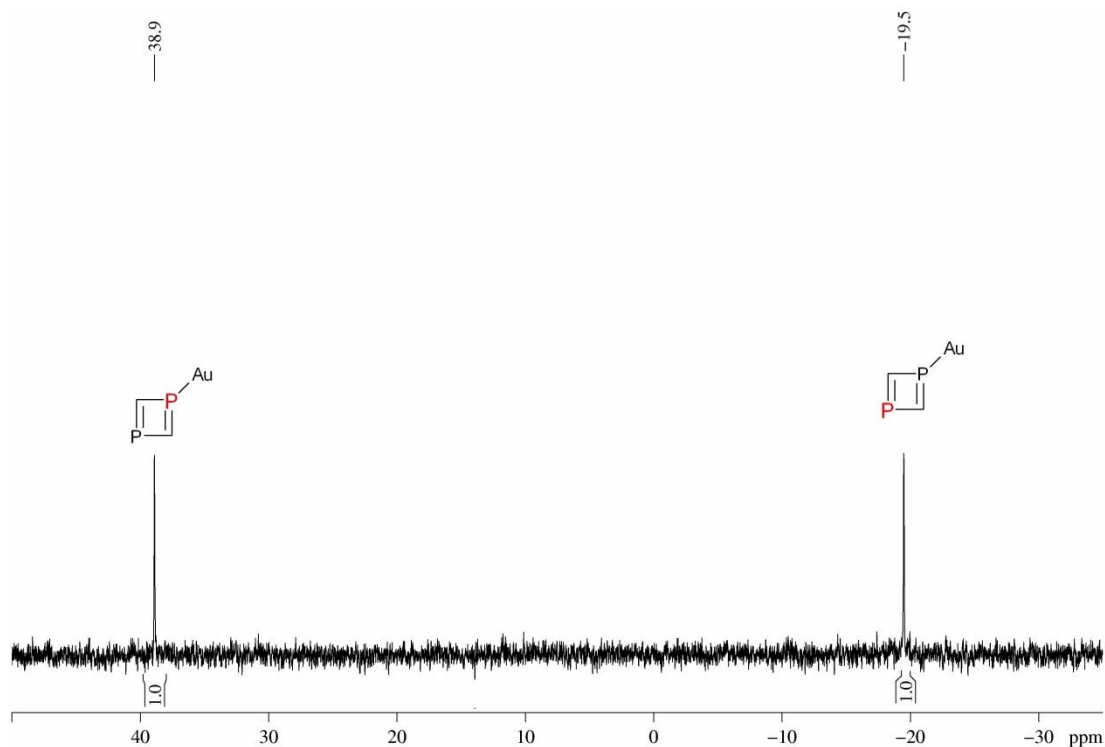


**Figure S2.**  $^{31}\text{P}\{^1\text{H}\}$  NMR Spectrum of  $[\text{Au}\{\text{Co}(\text{P}_2\text{C}_2t\text{Bu}_2)_2\}]_4$  (**1**) in  $[\text{D}_8]\text{THF}$  (300 K, 161.98 MHz).

**5.5.2 Variable-Temperature  $^1\text{H}$  and  $^{31}\text{P}\{^1\text{H}\}$  NMR Spectra of  $[\text{Au}(\text{PPh}_3)_4][\text{Au}\{\text{Co}(\text{P}_2\text{C}_2\text{tBu}_2)_2\}_2]$  (**3**) (Figures S2 and S3).**

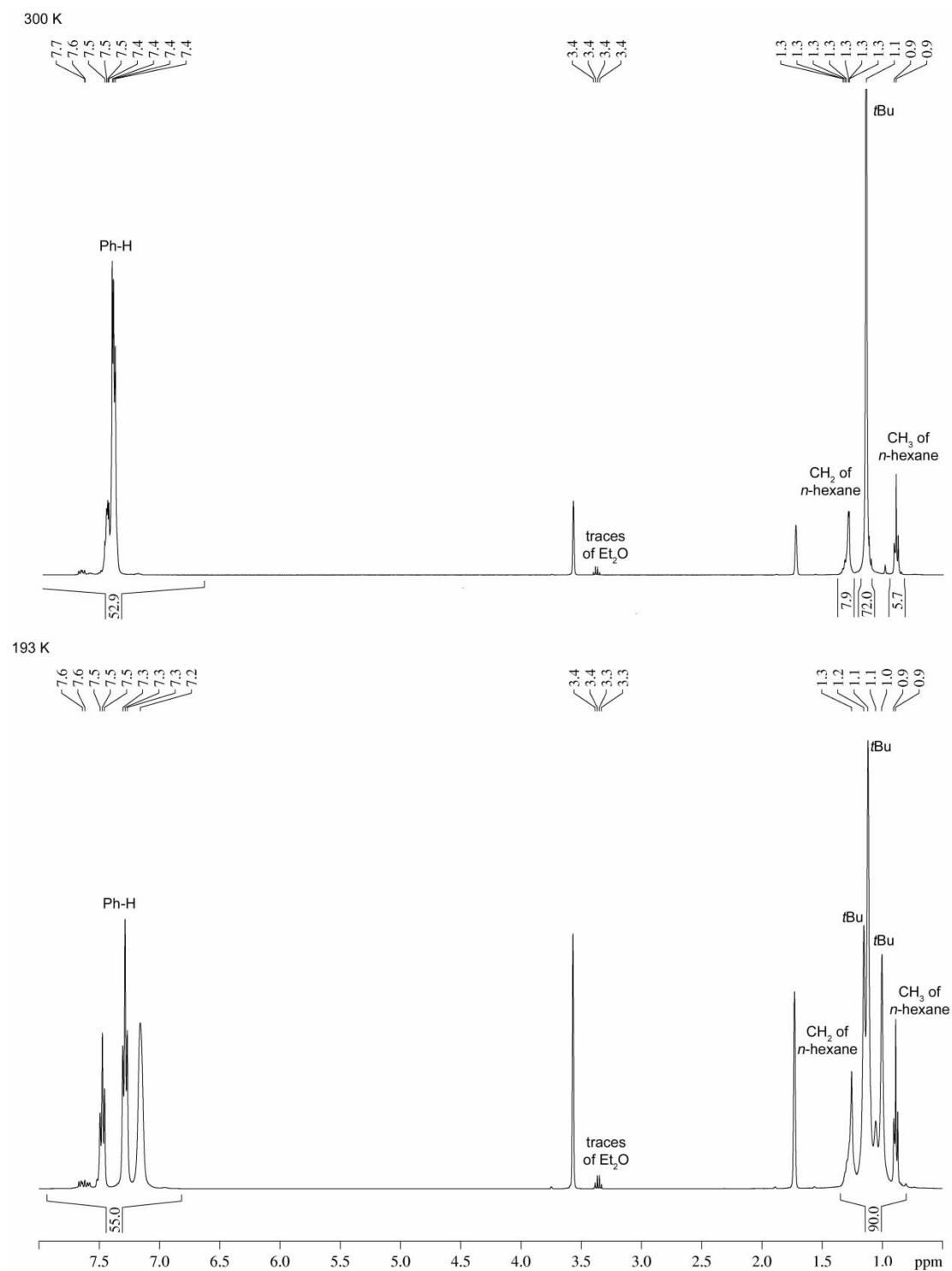


**Figure S3.** Variable-temperature  $^1\text{H}$  NMR spectra of  $[\text{Au}(\text{PPh}_3)_4][\text{Au}\{\text{Co}(\text{P}_2\text{C}_2\text{tBu}_2)_2\}_2]$  (**3**, 400.13 MHz,  $[\text{D}_8]\text{THF}$ ).

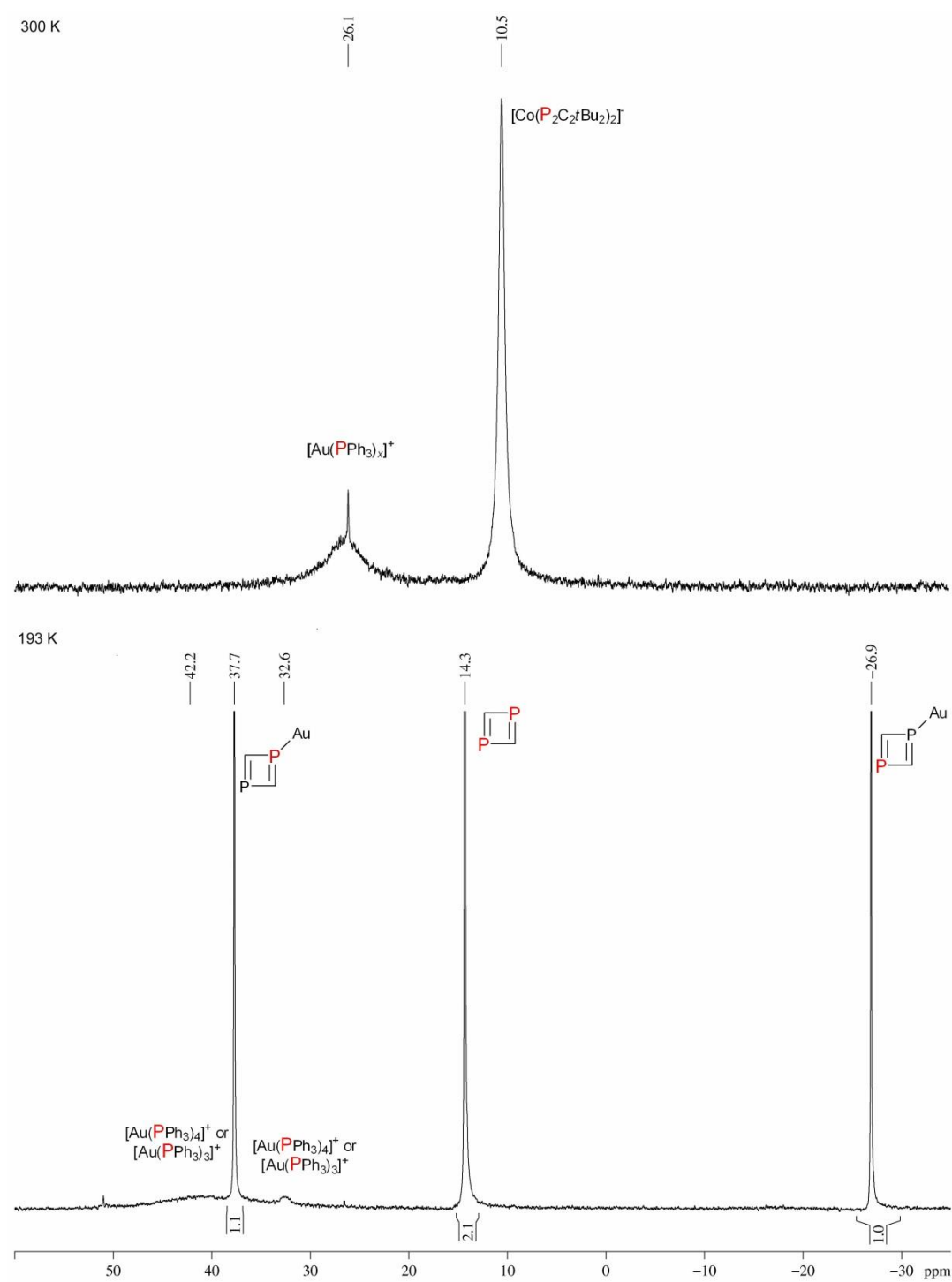


**Figure S4.** Variable-temperature  $^{31}\text{P}\{^1\text{H}\}$  NMR spectra of  $[\text{Au}(\text{PPh}_3)_4][\text{Au}\{\text{Co}(\text{P}_2\text{C}_2\text{tBu}_2)_2\}_2]$  (**3**, 161.98 MHz,  $[\text{D}_8]\text{THF}$ ).

### 5.5.3 $^1\text{H}$ and $^{31}\text{P}\{^1\text{H}\}$ NMR Spectra of $[\text{Tl}(\text{thf})_2\{\text{Co}(\text{P}_2\text{C}_2t\text{Bu}_2)_2\}]$ (**4**) at 300 K (Figures S5 and S6)

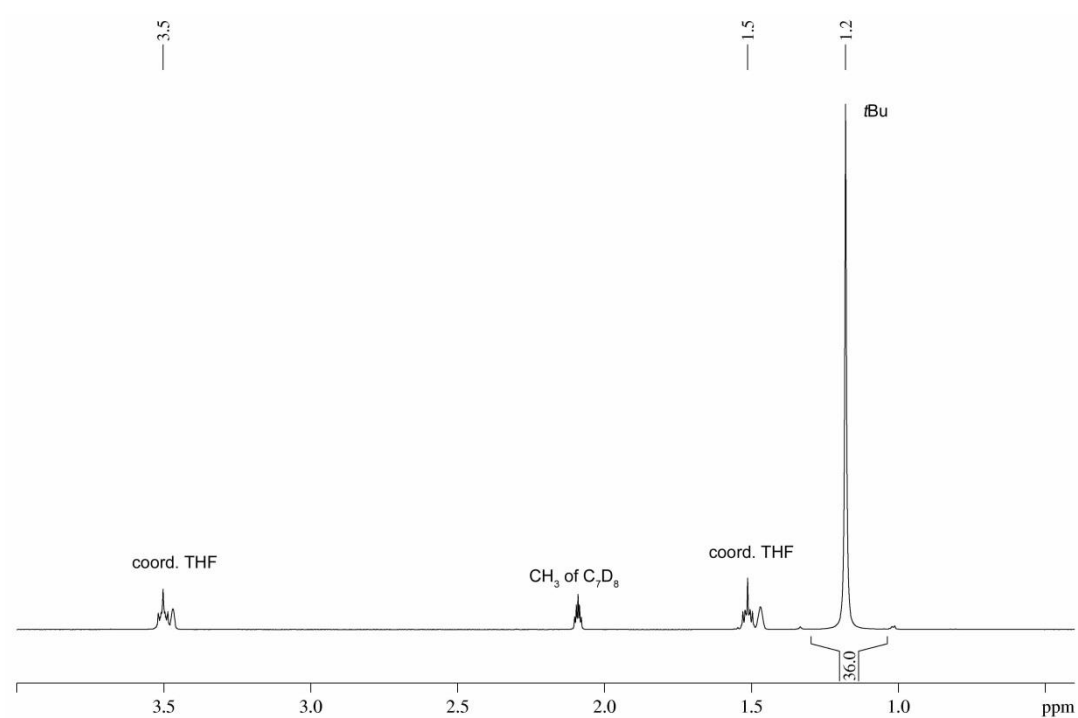


**Figure S5.**  $^1\text{H}$  NMR spectrum of  $[\text{Tl}(\text{thf})_2\{\text{Co}(\text{P}_2\text{C}_2t\text{Bu}_2)_2\}]$  (**4**) in  $[\text{D}_8]\text{THF}/\text{C}_7\text{D}_8$  (400.13 MHz,  $[\text{D}_8]\text{THF}$ ).

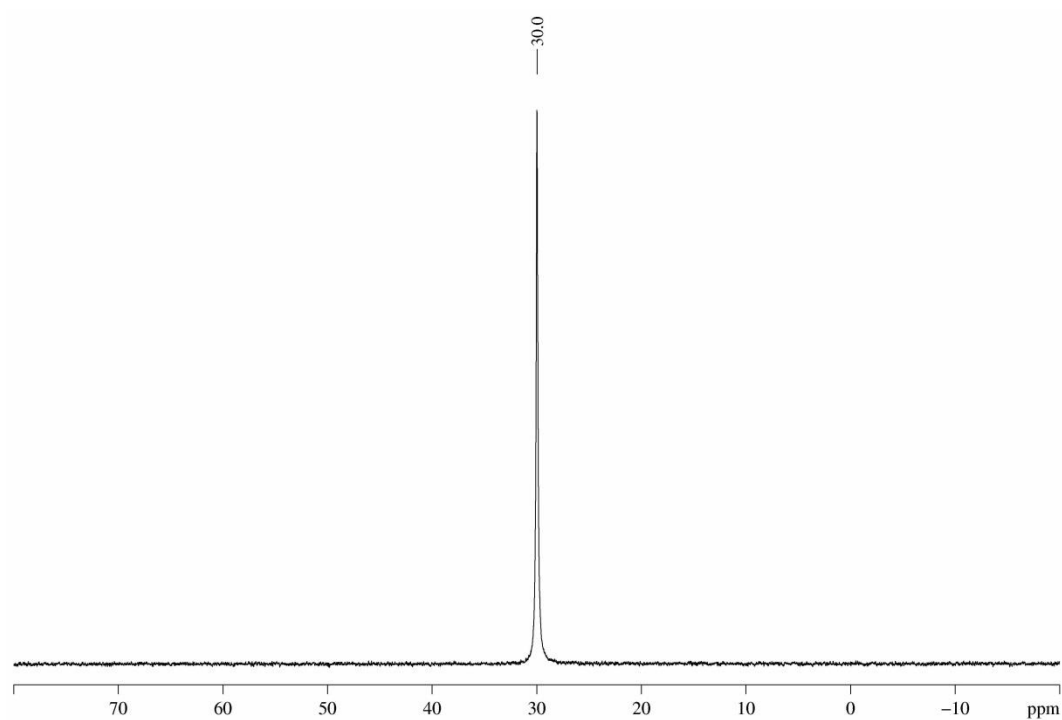


**Figure S6.**  $^{31}\text{P}\{^1\text{H}\}$  NMR spectrum of  $[\text{Tl}(\text{thf})_2\{\text{Co}(\text{P}_2\text{C}_2t\text{Bu}_2)_2\}]$  (**4**) in  $[\text{D}_8]\text{THF}/\text{C}_7\text{D}_8$  (161.98 MHz,  $[\text{D}_8]\text{THF}$ ).

#### 5.5.4 UV/vis Spectrum of $[\text{Ti}(\text{thf})_2\{\text{Co}(\text{P}_2\text{C}_2t\text{Bu}_2)_2\}]$ (**4**, Figure S7)

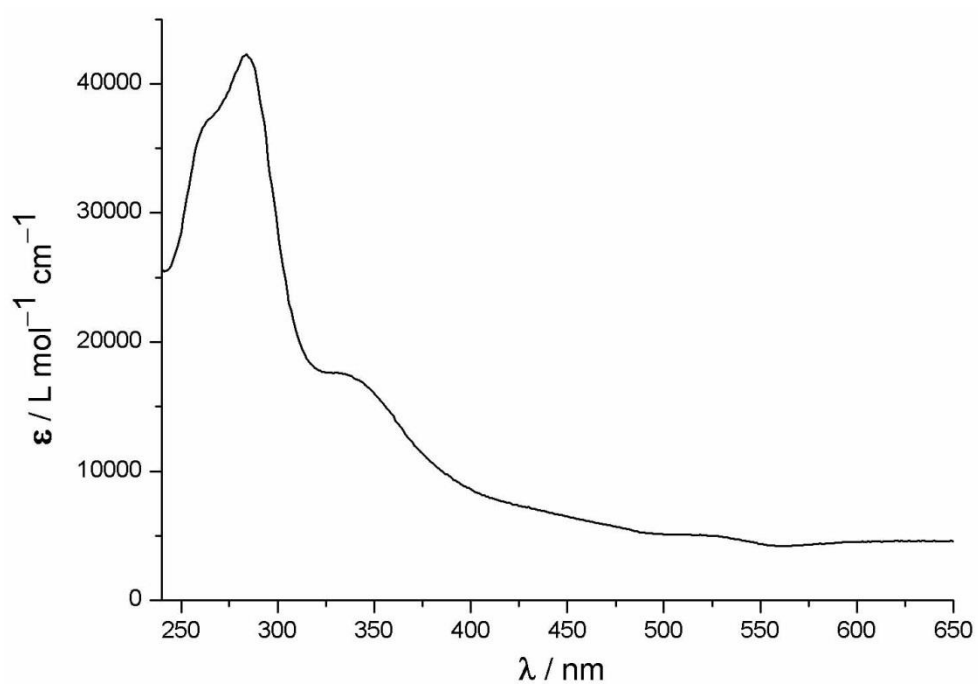


**Figure S7.** UV/vis spectrum of  $[\text{Ti}(\text{thf})_2\{\text{Co}(\text{P}_2\text{C}_2t\text{Bu}_2)_2\}]$  (**4**) in THF.

## References

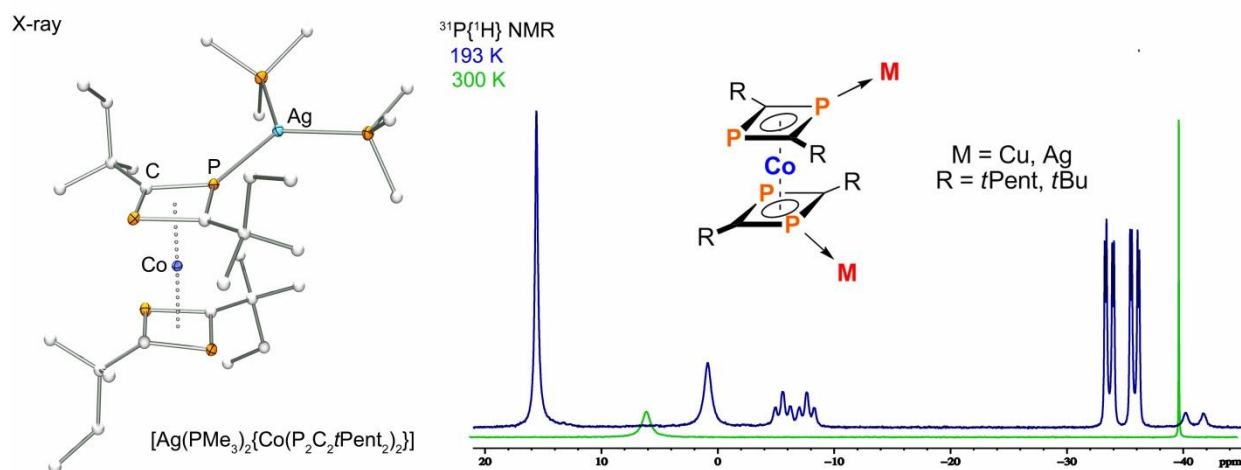
- 1 J.-M. Lehn, A. Rigault, J. Siegel, J. Harrowfield, B. Chevrier, D. Moras, *Proc. Natl. Acad. Sci. USA* **1987**, *84*, 2565.
- 2 a) J.-M. Lehn, *Supramolecular Chemistry: Concepts and Perspectives*, VCH, Weinheim, **1995**; b) L. F. Lindoy, I. M. Atkinson, *Self-Assembly in Supramolecular Systems*, RSC, Cambridge, **2000**; c) J. W. Steed, J. L. Atwood, *Supramolecular Chemistry*, 2nd ed., VCH, New York, **2009**; d) S. Sato, T. Murase, M. Fujita, in J. W. Steed, P. A. Gale (eds.), *Supramolecular Chemistry*, John Wiley & Sons, Ltd, **2012**; *Metallofoldamers: Supramolecular Architectures from Helicates to Biomimetics*, G. Maayan, M. Albrecht (eds.), Wiley-VCH, Weinheim, **2013**.
- 3 Recent reviews: a) H. Amouri, C. Desmarets, J. Moussa, *Chem. Rev.* **2012**, *112*, 2015; b) R. Chakrabarty, P. S. Mukherjee, P. J. Stang, *Chem. Rev.* **2011**, *111*, 6810; c) Y. Inokuma, M. Kawano, M. Fujita, *Nat. Chem.* **2011**, *3*, 349; d) P. Jin, S. J. Dalgarno, J. L. Atwood, *Coord. Chem. Rev.* **2010**, *254*, 1760; e) B. Therrien, *Eur. J. Inorg. Chem.* **2009**, 2445; f) B. H. Northrop, Y.-R. Zheng, K.-W. Chi, P. J. Stang, *Acc. Chem. Res.* **2009**, *42*, 1554; f) M. Yoshizawa, J. K. Klosterman, M. Fujita, *Angew. Chem. Int. Ed.* **2009**, *48*, 3418; h) P. J. Stang, B. Olenyuk, *Acc. Chem. Res.* **1997**, *30*, 502.
- 4 a) J. Bai, A. V. Virovets, M. Scheer, *Science* **2003**, *300*, 781; b) M. Yoshizawa, M. Tamura, M. Fujita, *Science* **2006**, *312*, 251; c) S. Sato, J. Iida, K. Suzuki, M. Kawano, T. Ozeki, M. Fujita, *Science* **2006**, *313*, 1273; d) M. D. Pluth, R. G. Bergman, K. N. Raymond, *Science* **2007**, *316*, 85; e) M. D. Pluth, R. G. Bergman, K. N. Raymond, *Angew. Chem. Int. Ed.* **2007**, *46*, 8587; f) C. J. Hastings, M. D. Pluth, R. G. Bergman, K. N. Raymond, *J. Am. Chem. Soc.* **2010**, *132*, 6938; g) P. Mal, B. Breiner, K. Rissanen, J. R. Nitschke, *Science* **2009**, *324*, 1697; h) Y.-F. Han, W.-G. Jia, Y.-J. Lin, G.-X. Jin, *Angew. Chem. Int. Ed.* **2009**, *48*, 6234; i) G. Steinfeld, V. Lozan, H.-J. Krüger, B. Kersting, *Angew. Chem. Int. Ed.* **2009**, *48*, 1954; j) Q.-F. Sun, J. Iwasa, D. Ogawa, Y. Ishido, S. Sato, T. Ozeki, Y. Sei, K. Yamaguchi, M. Fujita, *Science* **2010**, *328*, 1144; k) S. Bivaud, S. Goeb, V. Croué, P. I. Dron, M. Allain, M. Sallé, *J. Am. Chem. Soc.* **2013**, *135*, 10018; l) M. Han, R. Michel, B. He, Y.-S. Chen, D. Stalke, M. John, G. H. Clever, *Angew. Chem. Int. Ed.* **2013**, *52*, 1319.
- 5 Selected recent examples: a) F. Karadas, E. J. Schelter, A. V. Prosvirin, J. Bacsá, K. R. Dunbar, *Chem. Commun.* **2005**, 1414; b) S. T. Meally, K. Mason, P. McArdle, E. K. Brechin, A. G. Ryder, L. F. Jones, *Chem. Commun.* **2009**, 7024; c) C. Radloff, J. J. Weigand, F. E. Hahn, *Dalton Trans.* **2009**, 9392; d) J. Mercurol, Y. Li, E. Pardo, O. Risset, M. Seuleiman, H. Rousseliere, R. Lescouezec, M. Julve, *Chem. Commun.* **2010**, *46*, 8995; e) S. Shanmugaraju, A. K. Bar, K.-W. Chi, P. S. Mukherjee, *Organometallics* **2010**, *29*, 2971; f) F. M. Conrady, R. Fröhlich, C. Schulte-Brinke, T. Pape, F. E. Hahn, *J. Am. Chem. Soc.* **2011**, *133*, 11496; g) F. Li, J. K. Clegg, L. Goux-Capes, G. Chastanet, D. M. D'Alessandro, J.-F. Letard, C. J. Kepert, *Angew. Chem., Int. Ed.* **2011**, *50*, 2820; h) A. G. L. Olive, K. Parkan, C. Givélet, J. Michl, *J. Am. Chem. Soc.* **2011**, *133*, 20108; i) A. Rit, T. Pape, F. E. Hahn, *Organometallics* **2011**, *30*, 6393; j) A. Stephenson, M. D. Ward, *Dalton Trans.* **2011**, *40*, 10360; k) M. Schmidtendorf, T. Pape, F. E. Hahn, *Angew. Chem., Int. Ed.* **2012**, *51*, 2195; l) A. Mondal, Y. Li, M. Seuleiman, M. Julve, L. Toupet, C. M. Buron-Le, R. Lescouezec, *J. Am. Chem. Soc.* **2013**, *135*, 1653.
- 6 Reviews and books on phospho-organometallic compounds: a) J. F. Nixon, *Coord. Chem. Rev.* **1995**, *145*, 201; b) M. Regitz, O. J. Scherer, *Multiple Bonds and Low Coordination Phosphorus Chemistry*, Thieme, Stuttgart, **1990**; c) K. B. Dillon, F. Mathey, J. F. Nixon, *Phosphorus: The Carbon Copy*, Wiley, Chichester, **1998**; d) F. Mathey, *Angew. Chem. Int. Ed.* **2003**, *42*, 1578.

- 7 a) R. Wolf, A. W. Ehlers, J. C. Slootweg, M. Lutz, D. Gudat, M. Hunger, A. L. Spek, K. Lammertsma, *Angew. Chem. Int. Ed.* **2008**, *47*, 4584; b) R. Wolf, J. C. Slootweg, A. W. Ehlers, F. Hartl, B. de Bruin, M. Lutz, A. L. Spek, K. Lammertsma, *Angew. Chem. Int. Ed.* **2009**, *48*, 3104; c) R. Wolf, A. W. Ehlers, M. M. Khusniyarov, F. Hartl, B. de Bruin, G. J. Long, F. Grandjean, F. M. Schappacher, R. Pöttgen, J. C. Slootweg, M. Lutz, A. L. Spek, K. Lammertsma, *Chem. Eur. J.* **2010**, *16*, 14322.
- 8 a) H. F. Dare, J. A. K. Howard, M. U. Pilotti, F. G. A. Stone, J. Szameitat, *J. Chem. Soc., Chem. Commun.* **1989**, 1409; b) H. F. Dare, J. A. K. Howard, M. U. Pilotti, F. G. A. Stone, J. Szameitat, *J. Chem. Soc. Dalton Trans.* **1990**, 2263; c) J. Malberg, T. Wiegand, H. Eckert, M. Bodensteiner, R. Wolf, *Chem. Eur. J.* **2013**, *19*, 2356; c) J. Malberg, T. Wiegand, H. Eckert, M. Bodensteiner, R. Wolf, *Eur. J. Inorg. Chem.* **2013**, DOI:10.1002/ejic.201301173.
- 9 P. G. Jones, *J. Chem. Soc. Chem. Commun.* **1980**, 1031.
- 10 The formation of complex solution equilibria has been noted for the [AuCl(PPh<sub>3</sub>)]/PPh<sub>3</sub> system: E. C. Alyea, J. Malito, S. Attar, J. H. Nelson, *Polyhedron* **1992**, *11*, 2409.
- 11 P. G. Jones, *Acta Cryst.* **1980**, *36*, 3105; b) L. J. Guggenberger, *J. Organomet. Chem.* **1974**, *81*, 271.
- 12 A survey of thallium phosphorus compounds in the Cambridge crystal structure database, version 5.34 (Nov. 2012), gave 47 entries which show Tl–P bond lengths in the range of 2.688–3.4347 Å (median 3.044 Å).
- 13 Similar Tl–P bond lengths have been observed in Tl(I) adducts of tertiary phosphanes and transition metal polyphosphides: a) S. Welsch, L. J. Gregoriades, M. Sierka, M. Zabel, A. V. Virovets, M. Scheer, *Angew. Chem. Int. Ed.* **2007**, *46*, 9323; b) S. Kealey, N. J. Long, P. W. Miller, A. J. P. White, A. D. Gee, *Dalton Trans.* **2008**, 2677.
- 14 The colorless bis(phosphane) complex [AuCl(PPh<sub>3</sub>)<sub>2</sub>] was identified as the by-product by its <sup>31</sup>P{<sup>1</sup>H} NMR singlet at +29.7 ppm in [D<sub>8</sub>]THF and by a unit cell determination. This complex is conveniently separated during work-up due to its lack of solubility in *n*-hexane: a) G. H. Woehrle, L. O. Brown, J. E. Hutchison, *J. Am. Chem. Soc.* **2005**, *127*, 2172; b) T. J. Harrison, J. A. Kozak, M. Corbella-Pane, G. R. Dake, *J. Org. Chem.* **2006**, *71*, 4525.
- 15 T. Wiegand, H. Eckert, S. Grimme, J. Malberg, R. Wolf, *Solid State Nucl. Magn. Res.* **2013**, *53*, 13.
- 16 S. Ahrlund, K. Dreisch, B. Noren, A. Oskarsson, *Mater. Chem. Phys.* **1993**, *35*, 281.
- 17 a) SCALE3ABS, CrysAlisPro, Agilent Technologies Inc., Oxford, GB, **2012**, b) G. M. Sheldrick, SADABS, Bruker AXS, Madison, USA, **2007**.
- 18 R. C. Clark, J. S. Reid, *Acta Cryst. Sect. A* **1995**, *51*, 887.
- 19 G. M. Sheldrick, *Acta Cryst. Sect. A* **2008**, *64*, 112.
- 20 A. Altomare, M. C. Burla, M. Camalli, G. L. Cascarno, C. Giacovazzo, A. G. G. Moliterni, G. Polidori, R. Spagna, *J. Appl. Cryst.* **1999**, *32*, 115.
- 21 O. V. Dolomanov, L. J. Bourhis, R. J. Gildea, J. A. K. Howard, H. Puschmann, *J. Appl. Cryst.* **2009**, *42*, 339.
- 22 P. van der Sluis, A. L. Spek, *Acta Crystallogr. Sect. A* **1990**, *46*, 194–201.
- 23 CrysAlisPro, Agilent Technologies, Version 1.171.36.28.



## 6 Copper(I) and Silver(I) Complexes of Diphosphacyclobutadiene Sandwich Anions: Synthesis, Crystal Structures, Solution and Solid-State NMR Characterization<sup>[a],[b]</sup>

Jennifer Malberg, Thomas Wiegand, Hellmut Eckert, Michael Bodensteiner, and Robert Wolf



[a] J. Malberg, T. Wiegand, H. Eckert, M. Bodensteiner, R. Wolf, *Eur. J. Inorg. Chem.* **2013**, DOI: 10.1002/ejic.201301173, manuscript accepted on 02/10/2013.

[b] Solid-state NMR spectra (Figures 3–5, 7 and 8, 11–13, and S8–S15 and Tables 2, S1, and S2) were recorded and analyzed by Thomas Wiegand and Hellmut Eckert. The X-ray crystal structure analyses were performed by Michael Bodensteiner (Tables 1 and 3).



## 6.1 Introduction

Transition metal diphosphacyclobutadiene complexes are an important class of phospho-organometallic compounds that show many similarities to their purely hydrocarbon-based cyclobutadiene analogues.<sup>1,2</sup> Diphosphacyclobutadienes are formed in the coordination sphere of transition metals by the metal-mediated cyclodimerization of phosphalkynes.<sup>3</sup> Phosphalkynes with bulky substituents such as *t*Bu-C≡P typically form 1,3-diphosphacyclobutadienes, whereas the formation of 1,2-diphosphacyclobutadienes via head-to-head dimerization has been observed with the less sterically demanding phosphalkyne Me-C≡P and with specific transition metal fragments.<sup>4–6</sup>

One important benefit of introducing phosphorus atoms into the ligand framework of cyclobutadiene complexes is the possibility to form metal coordination complexes. A few coordination compounds have been reported so far, in which either one or both phosphorus atoms of the 1,3-diphosphacyclobutadiene ligand bind to a transition metal cation such as cobalt(I),<sup>7</sup> rhodium(I),<sup>8</sup> platinum(II) and platinum(0),<sup>8</sup> tungsten(0),<sup>8</sup> and gold(I).<sup>9</sup> We have described the synthesis of sandwich complexes of type **A** (Figure 1) by the reaction of anthracene metalates  $[M(C_{14}H_{10})_2]^-$  ( $M = Fe, Co$ ;  $C_{14}H_{10}$  = anthracene)<sup>10</sup> with the phosphalkynes *t*Bu-C≡P, *t*Pent-C≡P and Ad-C≡P.<sup>11–14</sup> The electronic structures, redox behavior and reactivity towards some electrophiles was investigated. First insights into the coordination behavior of these anions were gained from transmetalation reactions with gold(I) and silver(I) salts.<sup>15,16</sup> Three types of complexes were obtained (Figure 1):  $[Au\{Co(P_2C_2tPent_2)_2\}(PMe_3)_2]$  (**B**) was isolated from the reaction of  $[K(thf)_3\{Co(\eta^4-P_2C_2tPent_2)_2\}]$  with  $AuCl(PPh_3)$  in the presence of  $PMe_3$ . In contrast, coordination polymers of type  $[M\{Co(P_2C_2Ad_2)_2\}]_x$  (**C**,  $M = Ag, Au$ ) were obtained with the bulkier adamantyl (Ad) substituent. Reactions of two equivalents of the potassium salt  $[K(thf)_4\{Co(\eta^4-P_2C_2Ad_2)_2\}]$  with  $AuCl(tht)$  and  $AgSbF_6$  afforded “ate complexes”  $[M\{Co(P_2C_2Ad_2)_2\}_2]^-$  (**D**,  $M = Ag$  and  $Au$ ). Solid-state <sup>31</sup>P and <sup>13</sup>C NMR spectroscopy proved to be an excellent tool to study the structural composition of these complexes.

We have explored the coordination behavior of our homoleptic type **A** sandwich anions towards copper and silver cations. Here, we report the synthesis of new copper(I) and silver(I) complexes by salt metathesis of  $[K(thf)_3\{Co(\eta^4-P_2C_2tPent_2)_2\}]$  and  $[K(thf)_2\{Co(\eta^4-P_2C_2tBu_2)_2\}]$  with  $[CuCl(PPh_3)]_4$ ,  $AgCl$ , and  $AgSbF_6$  in the presence of  $PPh_3$  or  $PMe_3$ . These transmetalations afforded the novel complexes  $[Cu\{Co(P_2C_2R_2)_2\}(PPh_3)_2]$  (**1**:  $R = tPent$ , **2**:  $R = tBu$ ),  $[Cu(PMe_3)_4][Co(P_2C_2tPent_2)_2]$  (**3**),  $[Ag\{Co(P_2C_2tPent_2)_2\}(PMe_3)_3]$  (**4**),  $[Ag\{Co(P_2C_2tPent_2)_2\}(PMe_3)_2]$  (**5**), and  $[Ag_2\{Co(P_2C_2tPent_2)_2\}-(PMe_3)_5]SbF_6$  (**6**), which were characterized by variable temperature <sup>1</sup>H, <sup>13</sup>C{<sup>1</sup>H}, and <sup>31</sup>P{<sup>1</sup>H} NMR spectroscopy in solution. The molecular structures of **1–6** are discussed on the basis of <sup>31</sup>P and <sup>13</sup>C solid-state NMR and single-crystal X-ray data.

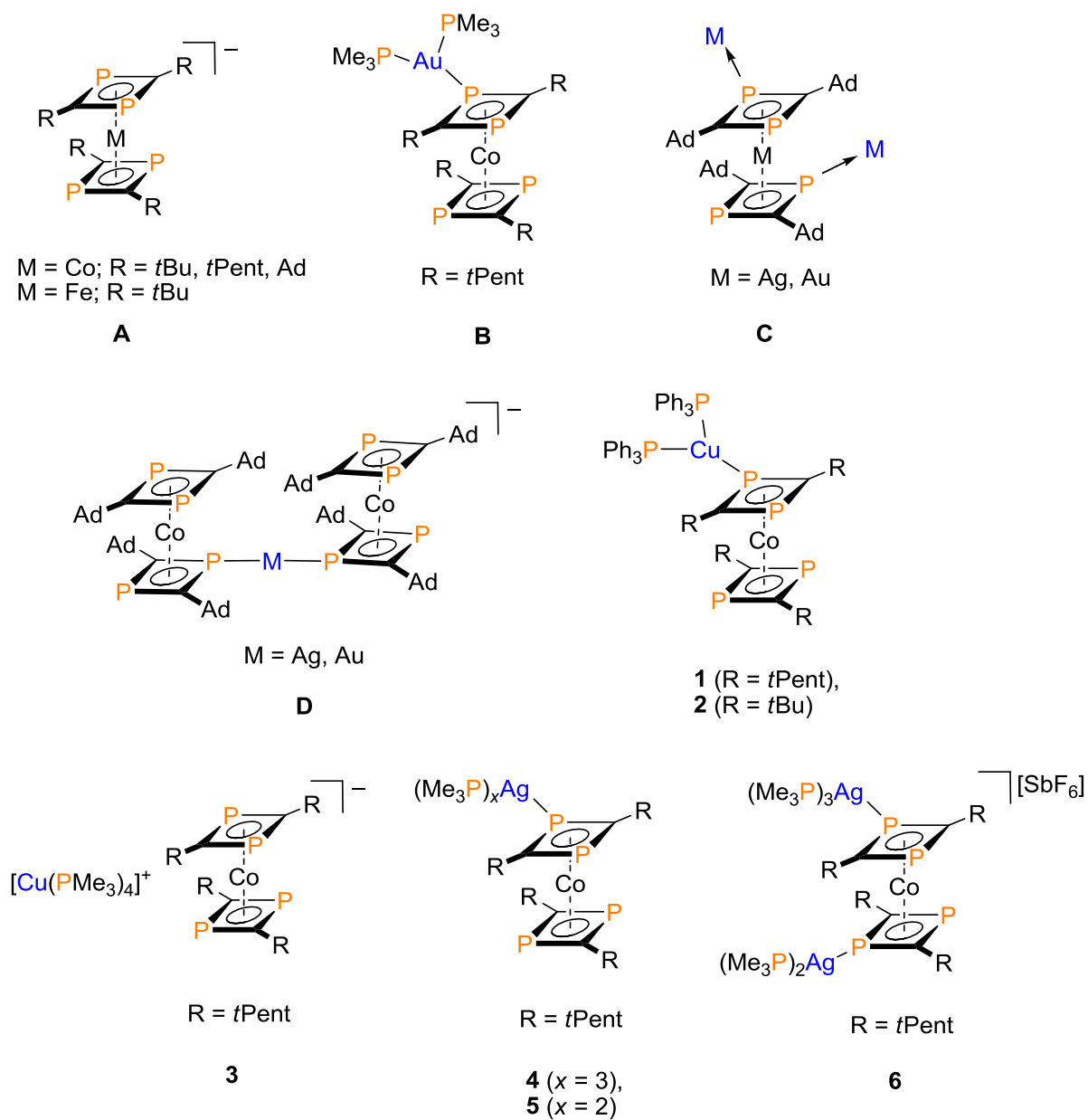
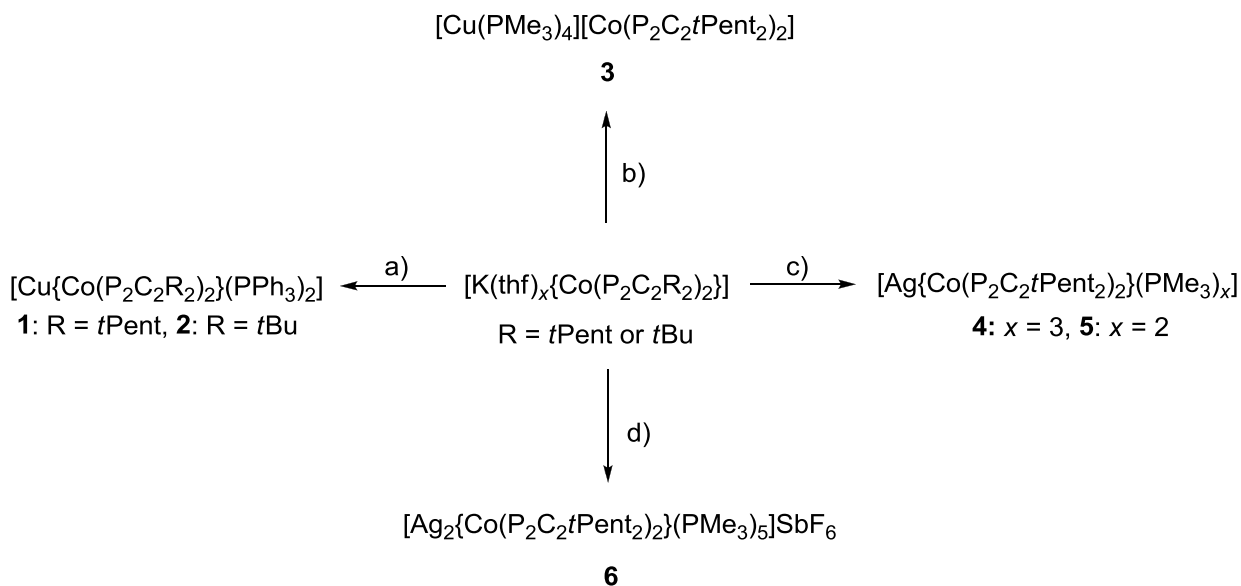


**Figure 1.** Copper(I), silver(I), and gold(I) complexes of  $[\text{Co}(\text{P}_2\text{C}_2\text{R}_2)]^-$  anions.

## 6.2 Results

### 6.2.1 Synthesis and Structural Characterization of Novel Copper(I) Complexes [Cu{Co(P<sub>2</sub>C<sub>2</sub>*t*Pent<sub>2</sub>)<sub>2</sub>}(PPh<sub>3</sub>)<sub>2</sub>] (1), [Cu{Co(P<sub>2</sub>C<sub>2</sub>*t*Bu<sub>2</sub>)<sub>2</sub>}(PPh<sub>3</sub>)<sub>2</sub>] (2), and [Cu(PMe<sub>3</sub>)<sub>4</sub>][Co(P<sub>2</sub>C<sub>2</sub>*t*Pent<sub>2</sub>)<sub>2</sub>] (3):

Treatment of a THF solution of [K(thf)<sub>3</sub>{Co(P<sub>2</sub>C<sub>2</sub>*t*Pent<sub>2</sub>)<sub>2</sub>}] or [K(thf)<sub>2</sub>{Co(P<sub>2</sub>C<sub>2</sub>*t*Bu<sub>2</sub>)<sub>2</sub>}] with 0.25 equiv. of [CuCl(PPh<sub>3</sub>)<sub>4</sub>] and one equiv. PPh<sub>3</sub> according to Scheme 1a, followed by extraction of the deep-red reaction mixtures with diethyl ether afforded the novel copper(I) complexes [Cu{Co(P<sub>2</sub>C<sub>2</sub>*t*Pent<sub>2</sub>)<sub>2</sub>}(PPh<sub>3</sub>)<sub>2</sub>] (1) and [Cu{Co(P<sub>2</sub>C<sub>2</sub>*t*Bu<sub>2</sub>)<sub>2</sub>}(PPh<sub>3</sub>)<sub>2</sub>] (2) in 52% and 75% isolated yield. The salt [Cu(PMe<sub>3</sub>)<sub>4</sub>][Co(P<sub>2</sub>C<sub>2</sub>*t*Pent<sub>2</sub>)<sub>2</sub>] (3), which contains the [Cu(PMe<sub>3</sub>)<sub>4</sub>]<sup>+</sup> cation and a non-coordinated [Co(P<sub>2</sub>C<sub>2</sub>*t*Pent<sub>2</sub>)<sub>2</sub>]<sup>−</sup> anion, was obtained by a similar procedure in 61% yield by using an excess of PMe<sub>3</sub> (Scheme 1b). Deep red, crystalline 1–3 were characterized by <sup>1</sup>H, <sup>13</sup>C{<sup>1</sup>H} and <sup>31</sup>P{<sup>1</sup>H} NMR spectroscopy in solution and by elemental analysis. According to the <sup>1</sup>H NMR spectra and the elemental analysis, the isolated solid of 2 still contains 0.5 *n*-hexane and 0.3 diethyl ether molecules per formula unit after drying in high vacuum (see the experimental section). The isolated solid of 3 still contained half a molecule of THF per formula unit.



**Scheme 1.** Synthesis of complexes 1–6. Reagents: a) 0.25 [CuCl(PPh<sub>3</sub>)<sub>4</sub>], PPh<sub>3</sub>; b) 0.25 [CuCl(PPh<sub>3</sub>)<sub>4</sub>], excess PMe<sub>3</sub>; c) AgCl, *x* PMe<sub>3</sub> (*x* = 2 or 3); d) 2 AgSbF<sub>6</sub>, excess PMe<sub>3</sub>.

Recrystallization of 1 and 2 afforded X-ray quality crystals of the *n*-hexane solvate 1·0.5*n*-hexane and the diethyl ether solvate 2·0.5Et<sub>2</sub>O, which were subjected to single crystal X-ray analysis. Compounds 1·0.5*n*-hexane and 2·0.5Et<sub>2</sub>O crystallize in the triclinic space group *P*−1 with two formula units per unit cell. Both complexes are isostructural, hence, only the structure of 2·0.5Et<sub>2</sub>O is shown in Figure 2. A graphical representation of 1·0.5*n*-hexane (R = *t*Pent) is given in Figure S1 of the Supporting Information, and important bond lengths and angles are summarized in Table 1. The structures comprise one copper(I)

cation coordinated by one phosphorus atom of a  $[\text{Co}(\text{P}_2\text{C}_2\text{R}_2)_2]^-$  anion ( $\text{R} = t\text{Pent}, t\text{Bu}$ ) and two molecules of  $\text{PPh}_3$ , resulting in a coordination number of 3 and in a distorted trigonal planar environment for copper. The sum of angles around Cu1 is approximately  $360^\circ$ . The copper–phosphorus distances are in a close range of 2.2766(9)–2.301(1) Å for **1** and 2.2630(4)–2.2864(3) Å for **2**. Similar Cu–P bond lengths have been observed for other three-coordinate copper(I) complexes that contain  $\text{PPh}_3$ -ligands such as  $[\text{Cu}(\text{PPh}_3)_3][\text{V}(\text{CO})_6]$  (Cu–P 2.293(1)–2.296(1) Å),  $[\text{Cu}(\text{PPh}_3)_3][\text{FeCl}_4]$  (2.288(2)–2.303(2) Å), and  $[\text{Cu}\{\text{cyclo}-(\text{P}_5t\text{Bu}_4)\}(\text{PPh}_3)_2]$  (2.313(3)–2.271(2) Å).<sup>17,18</sup> The structural parameters of the  $[\text{Co}(\text{P}_2\text{C}_2\text{R}_2)_2]^-$  anion are in the same range as in the related potassium salts  $[\text{K}([18]\text{crown-6})(\text{thf})_2][\text{Co}(\text{P}_2\text{C}_2t\text{Bu}_2)_2]$  and  $[\text{K}(\text{thf})_4][\text{Co}(\text{P}_2\text{C}_2\text{Ad}_2)_2]$ .<sup>8</sup>

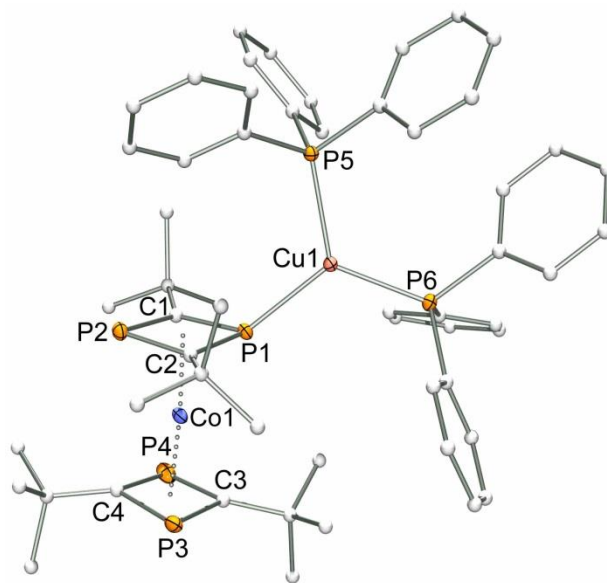


**Figure 2.** Crystallographically-determined molecular structure of  $[\text{Cu}\{(\text{P}_2\text{C}_2t\text{Bu}_2)\}(\text{PPh}_3)_2]$  (**2**·0.5 $\text{Et}_2\text{O}$ ). Thermal ellipsoids are drawn at the 35% probability level, H atoms and the  $\text{Et}_2\text{O}$  solvate molecule are omitted for clarity.

**Table 1.** Selected bond lengths (Å) and angles (°) of **1**, **2**, **5** and **6**.

	<b>1</b> (M = Cu)	<b>2</b> (M = Cu)	<b>5</b> (M = Ag)	<b>6</b> (M = Ag) <sup>a</sup>
M1-P1	2.301(1)	2.2864(3)	2.447(2)	2.4608(8), 2.482(2)
M1-P5	2.2766(9)	2.2630(4)	2.458(2)	2.4589(9), 2.588(2)
M1-P6	2.2794(9)	2.2680(4)	2.466(2)	2.4483(8), 2.5876(19)
M2-P4	-	-	-	2.5534(10), 2.451(3)
M2-P7	-	-	-	2.5306(11), 2.511(3)
M2-P8	-	-	-	2.4724(12), 2.780(3)
M2-P9	-	-	-	2.5259(13), 2.432(3)
P1-M1-P5	116.74(4)	116.830(14)	123.85(7)	120.51(3), 114.81(7)
P1-M1-P6	123.77(4)	121.926(14)	121.97(7)	121.79(3), 115.56(8)
P5-M1-P6	119.00(4)	121.097(14)	114.09(8)	117.68(3), 108.46(8)
M1-P1-P2	142.79(5)	138.724(16)	163.01(10)	165.96(4), 150.34(6)
P4-M2-P7	-	-	-	115.92(4), 120.57(12)
P4-M2-P8	-	-	-	109.19(4), 102.90(11)
P4-M2-P9	-	-	-	113.88(4), 121.33(11)
P7-M2-P8	-	-	-	103.43(4), 95.71(9)
P7-M2-P9	-	-	-	104.86(4), 108.35(11)
P8-M2-P9	-	-	-	108.89(5), 102.35(10)
M2-P3-P4	-	-	-	151.03(4), 157.66(8)
P-C	1.792(4)-1.805(6)	1.7881(13)-1.7991(14)	1.784(9)-1.808(8)	1.786(3)-1.798(3)
Co-C	2.085(4)-2.101(4)	2.0840(13)-2.0952(13)	2.080(8)-2.093(8)	2.088(3)-2.095(3)
Co-P	2.2318(10)-2.2618(13)	2.2347(4)-2.2601(4)	2.235(2)-2.263(2)	2.2394(8)-2.2535(8)
P-C-P	96.9(2)-99.2(2)	97.17(7)-98.87(7)	97.3(4)-99.0(5)	97.48(15)-97.97(14)

<sup>a</sup>The silver atoms of **6** are each disordered over two positions (Ag1/Ag11 and Ag2/Ag21). The second value relates to the minor component of the disorder, i.e. Ag11 or Ag21.



The  $^{31}\text{P}\{^1\text{H}\}$  NMR spectra of **1** and **2** (Figures S2 and S3) are complex and temperature-dependent. At room temperature, both complexes give rise to one intense, broad signal at  $-2.0$  ppm (**1**) and  $-4.4$  ppm (**2**), respectively. In addition weak, minor signals can be observed at 42.6, 21.1 and  $-5.6$  ppm for **1**. At low temperature ( $-80$  °C), several new signals appear which indicate the formation of a mixture of several unidentified species. The  $^1\text{H}$  NMR spectra of **1** and **2** in  $\text{C}_6\text{D}_6$  at room temperature show one set of well-resolved signals for the *t*Pent or *t*Bu substituents and one set of broad, overlapping phenyl resonances. The low temperature  $^1\text{H}$  NMR spectra at  $-80$  °C show the presence of several chemically different *t*Pent, *t*Bu, and phenyl substituents. These may presumably arise from the formation of equilibria between different copper phosphane species as noted for related tertiary phosphane copper(I) complexes.<sup>18–21</sup>

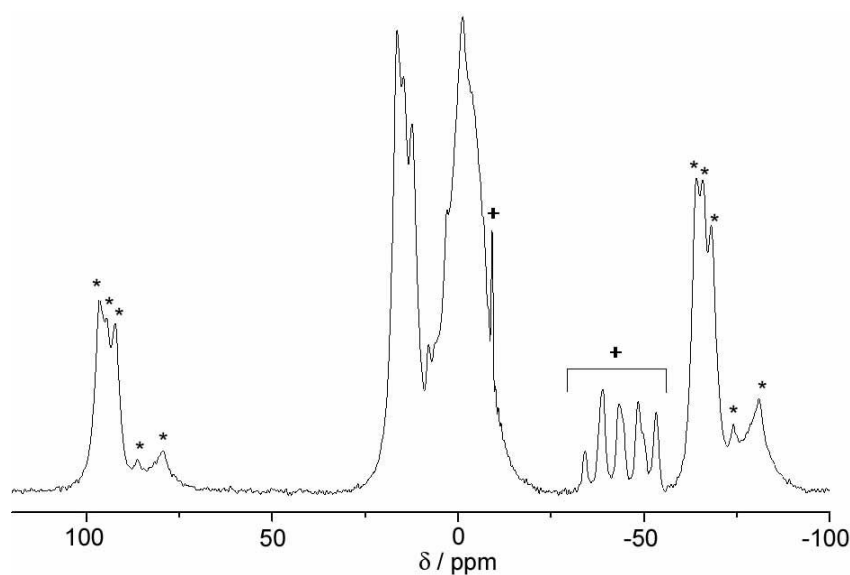


**Figure 3.**  $^{31}\text{P}\{^1\text{H}\}$  CPMAS-NMR spectrum of **1** acquired at 9.4 T and a spinning frequency of 13.0 kHz (central band region and first spinning sidebands). + denotes an impurity.

Complex  $^{31}\text{P}$  NMR spectra for **1** and **2** are also observed in the solid state. The  $^{31}\text{P}\{^1\text{H}\}$  CPMAS NMR spectrum of **1** (see Figure 3) shows two distinct groups of resonances: a group of peaks at 16.6, 14.5 and 11.7 ppm, characterized by a sizeable chemical shift anisotropy and a second group of peaks comprising a broad, poorly resolved multiplet near zero ppm. According to the spinning sideband intensity profiles observed, the P atoms giving rise to the first group of peaks have a significantly larger chemical shielding anisotropy (CSA) than the second group (see Table 2). On this basis we assign the peaks at 16.6, 14.5, and 11.7 ppm to the planar-coordinated phosphorus species P2-P4 and the broad multiplet pattern near zero ppm to the species P1 and P5/P6. These resonances are additionally affected by direct and indirect dipolar coupling to the quadrupolar  $^{63}\text{Cu}$  and  $^{65}\text{Cu}$  isotopes. Unfortunately, a line shape simulation is not possible in this case due to a strong overlap of resonances. The spinning sideband profile of this second peak group suggests that the P1 species resonating in this frequency range has a similarly sized CSA, whereas for the sites P5 and P6 the CSA is very small. This finding conforms with the expectation for tetrahedrally coordinated P atoms. The  $^{31}\text{P}\{^1\text{H}\}$  solid-state NMR spectrum of **2** is shown in Figures 4 and 5.

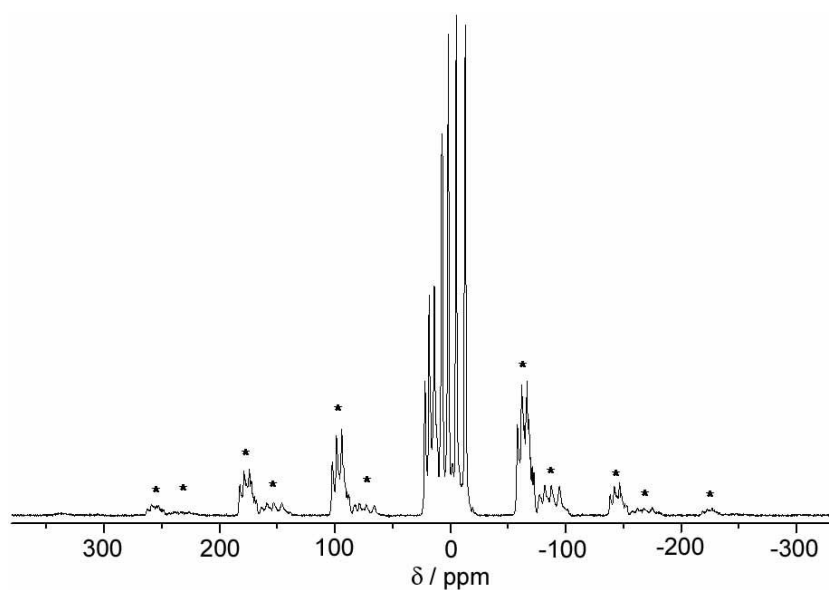


**Figure 4.**  $^{31}\text{P}\{^1\text{H}\}$  CPMAS-NMR spectrum of **2** acquired at 9.4 T and a spinning frequency of 13.0 kHz. \* marks spinning sidebands.

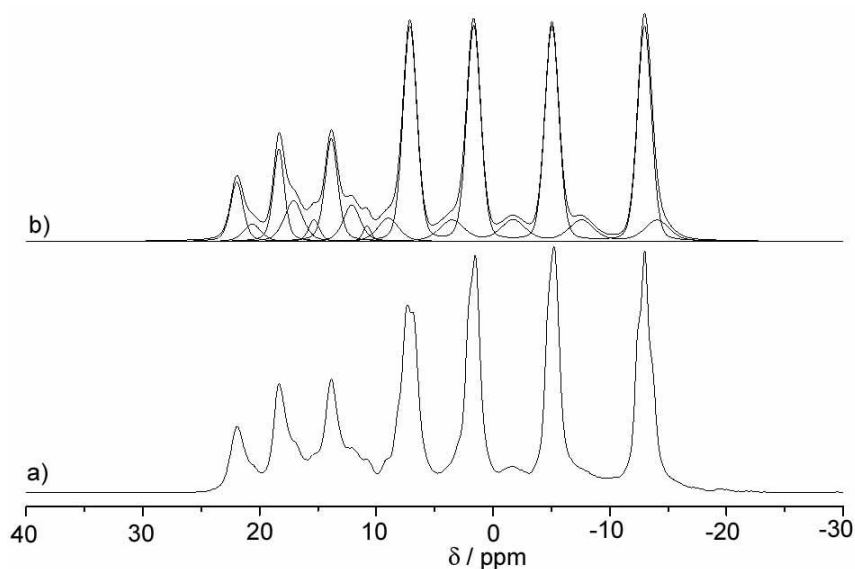


**Figure 5.**  $^{31}\text{P}\{^1\text{H}\}$  CPMAS-NMR spectrum of **2** acquired at 9.4 T and a spinning frequency of 13.0 kHz (a, central band region) and corresponding line shape simulation (b).

Again, based on the CSA argument (Table 2), the signals observed in the higher-frequency region (at 21.9, 18.3, and 13.9 ppm) can be attributed to P2, P3 and P4. The detailed simulation shows, however, additional weaker resonances, suggesting the presence of some molecular disordering effects. The spectra in the lower-frequency range are strongly influenced by heteronuclear  $^{31}\text{P}$ - $^{63/65}\text{Cu}$  spin-spin interactions,<sup>22</sup> which manifest themselves much more clearly in compound **2** than in compound **1**. Here, the four-peak pattern at  $-2.3$  ppm originates from dipolar coupling to the spin-3/2 nuclei  $^{63}\text{Cu}$  and  $^{65}\text{Cu}$  in their different Zeeman states. Note the peak spacings between these four components are different: as previously shown these differences are a consequence of the  $^{63/65}\text{Cu}$  nuclear electric quadrupolar coupling. A simulation of

this multiplet is possible, assuming  $^1J(^{31}\text{P}-^{63/65}\text{Cu}) = 1085$  Hz and a residual dipolar coupling constant  $d(^{31}\text{P}-^{63/65}\text{Cu}) = 100$  Hz determined at 9.4 T. The quantity  $d$  is given by the expression:

$$d = \frac{-3C_Q(D - \frac{\Delta J}{3})}{20\nu_s} [3\cos^2\beta^D - 1 + \eta_Q\sin^2\beta^D\cos\alpha^D]$$

with  $D$  describing the  $^{63/65}\text{Cu}$ - $^{31}\text{P}$  direct dipolar coupling constant,  $\Delta J$  the anisotropy of the indirect spin-spin coupling tensor,  $\nu_s$  the  $^{63}\text{Cu}$  or  $^{65}\text{Cu}$  Larmor frequency,  $C_Q$  the  $^{63}\text{Cu}$  or  $^{65}\text{Cu}$  quadrupolar coupling constant,  $\eta_Q$  the asymmetry parameter of the electric field gradient (EFG) at the site of the copper nuclei and  $\alpha^D$  and  $\beta^D$  the Euler angles defining the orientation of the dipolar vector in the principal axis system of the EFG.<sup>23</sup> The slightly asymmetric appearance observed for each individual spectral component can be attributed to two distinct contributions from the  $^{63}\text{Cu}$  and the  $^{65}\text{Cu}$  isotopologue, which feature different  $J$ - and dipolar coupling constants as the magnetic moments and electric quadrupole moments of these two copper nuclei are somewhat different. As the absence of spinning sideband patterns under the experimental conditions applied reveals a rather small CSA, we attribute this four-peak pattern to the magnetically equivalent nuclei P5 and P6. In addition, a second four-peak pattern is observed, which is centered at  $-5.0$  ppm and whose spinning sideband profile reveals a substantial CSA. Simulation yields a  $^1J(^{31}\text{P}-^{63/65}\text{Cu})$  coupling constant of 950 Hz and a residual dipolar coupling constant  $d(^{31}\text{P}-^{63/65}\text{Cu})$  of 50 Hz determined at 9.4 T. Thus this signal is unambiguously assigned to the copper-coordinated phosphorus site of the  $\text{C}_2\text{P}_2$  rings (P1).

Attempts to determine the molecular structure of **3** by X-ray crystallography were frustrated by severe disorder problems, which did not permit a satisfactory refinement of the structure. However, the proposed constitution as an ionic complex  $[\text{Cu}(\text{PMe}_3)_4][\text{Co}(\text{P}_2\text{C}_2t\text{Pent}_2)_2]$  is convincingly supported by the solid-state and solution NMR data.

The  $^{31}\text{P}\{^1\text{H}\}$  NMR spectrum of **3** in  $[\text{D}_8]\text{THF}$  (Figure 6) displays a singlet at  $+9.4$  ppm for the  $[\text{Co}(\text{P}_2\text{C}_2t\text{Pent}_2)_2]^-$  anion (cf. the  $^{31}\text{P}$  NMR shift of  $+9.6$  ppm for  $[\text{K}(\text{thf})_3\{\text{Co}(\text{P}_2\text{C}_2t\text{Pent}_2)_2\}]$  in the same solvent), and a symmetrical 1:1:1:1 multiplet at  $-39.1$  ppm, which we assign to the P atoms of the tetrahedral  $[\text{Cu}(\text{PMe}_3)_4]^+$  cation, coupled to  $^{63}\text{Cu}$  or  $^{65}\text{Cu}$  nuclei in their different Zeeman states. Again the contributions arising from  $^{63}\text{Cu}$  and  $^{65}\text{Cu}$ -containing isotopologue can be partially resolved. The average  $^1J(^{31}\text{P}, ^{63/65}\text{Cu})$  coupling constant of 794.6 Hz is very similar to the values observed for the closely related complexes  $[\text{Cu}(\text{PMe}_3)_4]\text{X}$  ( $\text{X} = \text{PF}_6, \text{BF}_4$ ), and  $[\text{Ni}(\text{PMe}_3)_4]$ .<sup>24,25</sup> The  $^1\text{H}$  NMR spectrum of **3** (Figure S4) features one set of well-resolved signals for the  $t\text{Pent}$  substituent. A broad singlet is observed at 1.34 ppm for the coordinated  $\text{PMe}_3$  molecules with no resolved  $^2J(^1\text{H}, ^{31}\text{P})$  spin-spin coupling. The absence of resolved P–H coupling has been noted for the related complexes  $[\text{Cu}(\text{PMe}_3)_4]\text{X}$  ( $\text{X} = \text{PF}_6, \text{BF}_4$ ) salts and  $[\text{Ni}(\text{PMe}_3)_4]$ .<sup>24,25</sup>

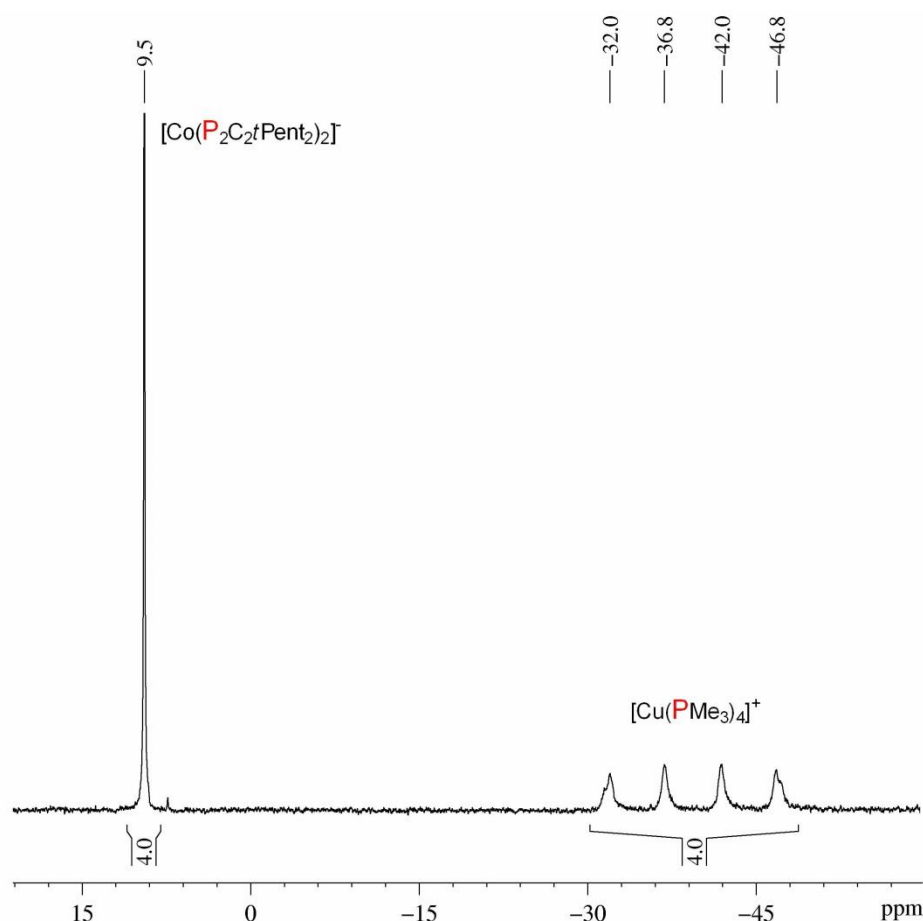


**Figure 6.**  $^{31}\text{P}\{^1\text{H}\}$  NMR spectrum of  $[\text{Cu}(\text{PMe}_3)_4][\text{Co}(\text{P}_2\text{C}_2\text{tPent})_2]$  (**3**) in  $[\text{D}_8]\text{THF}$  (161.97 MHz, 300 K).

In close correspondence with the liquid state NMR result, the  $^{31}\text{P}\{^1\text{H}\}$  CPMAS-NMR spectrum of **3** (see Figure 7) shows one single resonance for the phosphorus atoms of the  $\text{C}_2\text{P}_2$ -units at 5.3 ppm and the expected four-peak pattern ( $^1J(^{31}\text{P}-^{63/65}\text{Cu}) = 805$  Hz) for the ionic  $[\text{Cu}(\text{PMe}_3)_4]^+$  species at  $-42.4$  ppm. In this case the nearly identical peak spacings indicate  $^{63/65}\text{Cu}$  nuclear electric quadrupolar coupling constants close to zero as is expected for the highly symmetric (tetrahedral) coordination of the Cu(I) ion within the  $[\text{Cu}(\text{PMe}_3)_4]^+$  unit. It should be noted that minor signals in the region of both  $^{31}\text{P}$  resonances are also observed, possibly indicating the presence of a second polymorph within the investigated powdered sample.

Overall, the liquid and solid state NMR results clearly prove that in **3** no binding of P atoms of the  $\text{C}_2\text{P}_2$  ring to the metal atoms takes place. This conclusion is further bolstered by the  $^{13}\text{C}\{^1\text{H}\}$  CPMAS NMR spectrum, in which only a single resonance near 102 ppm is observed for the carbon atoms of the  $\text{C}_2\text{P}_2$  units (see Figure S8, Supporting Information). The  $^{65}\text{Cu}$  MAS-NMR spectrum reveals a quintet at 675.7 ppm with a  $^{65}\text{Cu}\cdots^{31}\text{P}$  spin-spin coupling constant of 851.4 Hz (see Figure 8) as expected for the  $[\text{Cu}(\text{PMe}_3)_4]^+$  unit. The line shape is not influenced by second order quadrupolar effects which is a further proof for the tetrahedral coordination of the copper atom. For compounds **1** and **2** no  $^{65}\text{Cu}$  signals were detectable, presumably because they are excessively broadened by strong quadrupolar interactions.

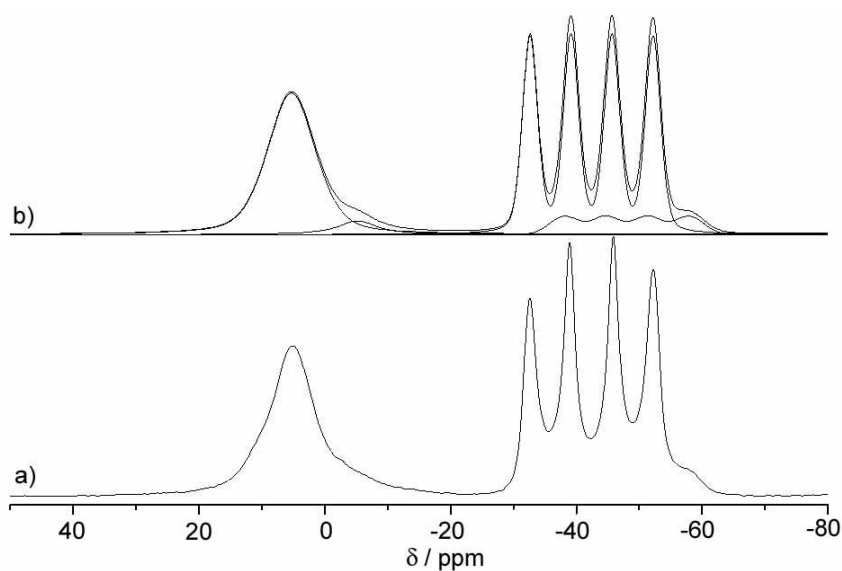


**Figure 7.**  $^{31}\text{P}\{^1\text{H}\}$  CPMAS-NMR spectrum (central band region) of **3** acquired at 7.05 T and a rotation frequency of 13.0 kHz (a) and corresponding line shape simulation (b). The minor resonances are tentatively attributed to a different polymorph.

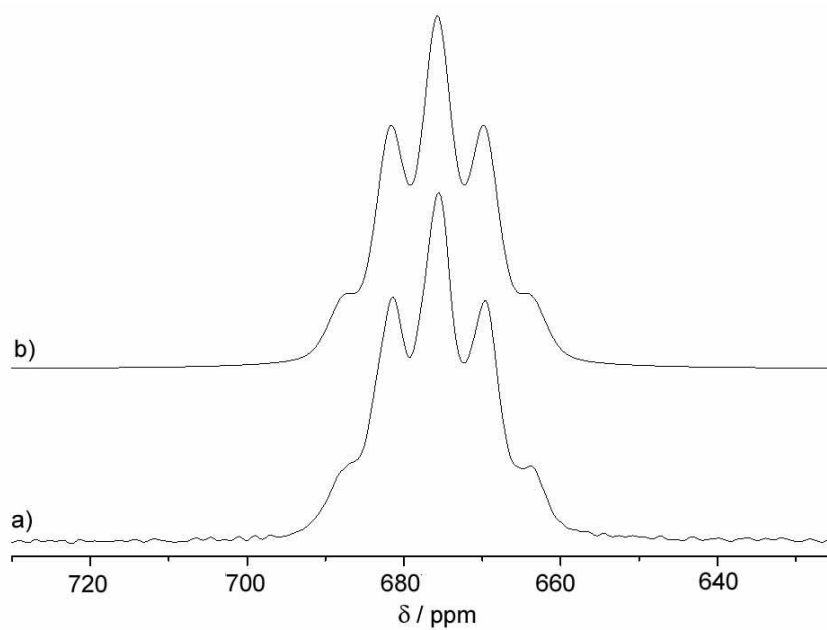


**Figure 8.**  $^{65}\text{Cu}$  MAS-NMR spectrum of **3** acquired at 11.74 T using a spinning frequency of 10.0 kHz (a) and corresponding line shape simulation (b).

## 6.2.2 Syntheses and Structural Characterization of the Silver(I) Complexes [Ag{Co(P<sub>2</sub>C<sub>2</sub>tPent<sub>2</sub>)<sub>2</sub>}(PMe<sub>3</sub>)<sub>3</sub>] (**4**), [Ag{Co(P<sub>2</sub>C<sub>2</sub>tPent<sub>2</sub>)<sub>2</sub>}(PMe<sub>3</sub>)<sub>2</sub>] (**5**) and [Ag<sub>2</sub>{Co(P<sub>2</sub>C<sub>2</sub>tPent<sub>2</sub>)<sub>2</sub>}(PMe<sub>3</sub>)<sub>5</sub>]SbF<sub>6</sub> (**6**)

Treatment of a THF suspension of anhydrous AgCl with an excess of PMe<sub>3</sub>, followed by addition of one equivalent of [K(thf)<sub>3</sub>{Co(P<sub>2</sub>C<sub>2</sub>tPent<sub>2</sub>)<sub>2</sub>}] at low temperature (−78 °C) according to Scheme 1c afforded the neutral silver(I) complex [Ag{Co(P<sub>2</sub>C<sub>2</sub>tPent<sub>2</sub>)<sub>2</sub>}(PMe<sub>3</sub>)<sub>3</sub>] (**4**) in 65% yield. Complex **4** was also prepared in lower (32%) yield using AgSbF<sub>6</sub> as the silver source. The compound was isolated from THF/*n*-hexane (1:2) and characterized by <sup>1</sup>H, <sup>13</sup>C{<sup>1</sup>H}, and <sup>31</sup>P{<sup>1</sup>H} NMR spectroscopy and microanalysis (see below). According to these data, **4** initially contains three trimethylphosphane ligands, but the compound gradually loses one of these PMe<sub>3</sub> molecules when stored as a solid at room temperature for prolonged periods (months). This process results in the formation of a mixture of **4** and the related bis(trimethylphosphane) complex [Ag{Co(P<sub>2</sub>C<sub>2</sub>tPent<sub>2</sub>)<sub>2</sub>}(PMe<sub>3</sub>)<sub>2</sub>] (**5**) as evident from the solid-state NMR investigations (Figures 11 to 13). Attempts to determine the single-crystal X-ray structure of **4** were frustrated by severe disorder problems that prevented a successful structure refinement with the acquired data sets. However, an attempt to recrystallize **4** from 1,2-difluorobenzene/*n*-hexane (ca. 1:2) gave red crystals of bis(trimethylphosphane) complex **5**, which was characterized by X-ray crystallography and multinuclear NMR spectroscopy (see below). One of the PMe<sub>3</sub> ligands of **4** is thus removed during the crystallization process. Complex **5** was prepared more conveniently in 58% yield by reacting [K(thf)<sub>3</sub>{Co(P<sub>2</sub>C<sub>2</sub>tPent<sub>2</sub>)<sub>2</sub>}] with AgCl and two equiv. PMe<sub>3</sub>.

Using a similar procedure as for **4** and **5**, we furthermore obtained the dinuclear silver(I) complex [Ag<sub>2</sub>{Co(P<sub>2</sub>C<sub>2</sub>tPent<sub>2</sub>)<sub>2</sub>}(PMe<sub>3</sub>)<sub>5</sub>]SbF<sub>6</sub> (**6**) by the reaction of [K(thf)<sub>3</sub>{Co(P<sub>2</sub>C<sub>2</sub>tPent<sub>2</sub>)<sub>2</sub>}] with two equivalents of AgSbF<sub>6</sub> and an excess of PMe<sub>3</sub> (Scheme 1d). Compound **6** was isolated in 43% yield by layering a concentrated THF solution with *n*-hexane at room temperature. Complex **6** contains 0.5 THF molecules after drying in high vacuum. In addition, the isolated solid of **6** contains 0.16 equiv. of KSbF<sub>6</sub> per formula unit, which is formed as a byproduct of the reaction and is difficult to remove by recrystallization.

The mononuclear compound **5** crystallizes in the space group *P2<sub>1</sub>/c* with four formula units per unit cell. The structure features a silver(I) atom that is surrounded by one phosphorus atom of the [Co(P<sub>2</sub>C<sub>2</sub>tPent<sub>2</sub>)<sub>2</sub>]<sup>−</sup> anion and by two molecules of PMe<sub>3</sub> (Figure 9), resulting in a trigonal planar structure similar to **1** and **2**. A similar arrangement was also observed for the gold(I) complex [Au{Co(P<sub>2</sub>C<sub>2</sub>tPent<sub>2</sub>)<sub>2</sub>}(PMe<sub>3</sub>)<sub>2</sub>] (**B**, Figure 1). In comparison with the structures of **1** and **2**, the PMe<sub>3</sub> molecules show a different orientation with respect to the C<sub>2</sub>P<sub>2</sub> plane of the 1,3-diphosphacyclobutadiene ligand (dihedral P1,P2,C1,C2/Ag1,P5,P6 14.5(1)°, cf. the angle between the planes P1,P2,C1,C2/Cu1,P5,P6 82.88(5)° in the structure of **2**). Complex **5** shows shorter Ag–P distances (2.447(2)–2.466(2) Å, see Table 1) compared to other tri-coordinate silver(I) complexes of type [Ag(PPh<sub>3</sub>)<sub>3</sub>]X (Ag–P 2.550(1)–2.556(1) Å for X = Cl; Ag–P 2.545(1)–2.630(2) Å for X = NO<sub>3</sub>), presumably due to the smaller steric demand of the methyl groups.<sup>26,27</sup> It is notable that the Ag–P bond

lengths are longer than the Au–P bonds (2.365(1)–2.474(1) Å) in the related gold(I) complex **B**. The P–Ag–P bond angles (114.09(8)–123.85(7)°) are identical to those of **B** (114.54(3)–123.73(3)°) though. The P5–Ag1–P6 angle formed by the two PMe<sub>3</sub> molecules of 114.09(8)° is smaller than the P1–Ag1–P5 and P1–Ag1–P6 angles (123.85(8)° and 121.97(7)°, respectively) between the PMe<sub>3</sub> ligands and the [Co(P<sub>2</sub>C<sub>2</sub>tPent<sub>2</sub>)<sub>2</sub>]<sup>–</sup> anion as a consequence of the comparatively large steric demand of this anion.

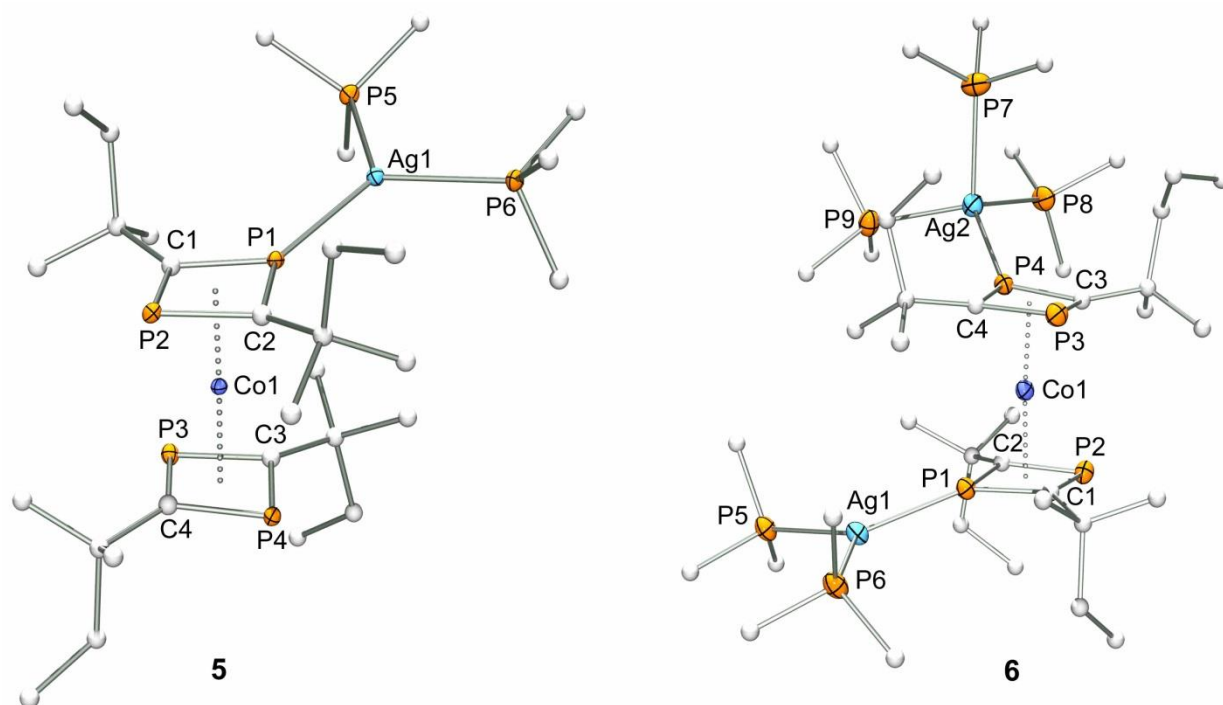


**Figure 9.** Solid-state molecular structures of [Ag{Co(P<sub>2</sub>C<sub>2</sub>tPent<sub>2</sub>)<sub>2</sub>}(PMe<sub>3</sub>)<sub>2</sub>] (**5**) and [Ag<sub>2</sub>{Co(P<sub>2</sub>C<sub>2</sub>tPent<sub>2</sub>)<sub>2</sub>}(PMe<sub>3</sub>)<sub>5</sub>]SbF<sub>6</sub> (**6**·THF). Displacement ellipsoids are drawn at the 35% probability level, and H atoms are not shown for clarity. The disorder of Ag1 and Ag2, the [SbF<sub>6</sub>]<sup>–</sup> counter anion, and a THF solvate molecule in the crystal lattice of **6**·THF are omitted.

Compound **6** crystallized as the THF solvate **6**·THF in the space group *P*-1 with two formula units per cell. The measured crystal contained one THF solvate molecule per formula unit in the crystal lattice. The structure shows an [Ag<sub>2</sub>{Co(P<sub>2</sub>C<sub>2</sub>tPent<sub>2</sub>)<sub>2</sub>}(PMe<sub>3</sub>)<sub>5</sub>]<sup>+</sup> cation and a SbF<sub>6</sub><sup>–</sup> counter ion (Figure 9). The cation comprises two distinct silver atoms which are coordinated by the [Co(P<sub>2</sub>C<sub>2</sub>tPent<sub>2</sub>)<sub>2</sub>]<sup>–</sup> sandwich unit through different C<sub>2</sub>P<sub>2</sub>-rings. Both silver atoms are disordered over two sites (Ag1/Ag11 and Ag2/Ag21) in the refined crystal. Ag1 and Ag11 are surrounded by one phosphorus atom of the sandwich anion (P1) and by two PMe<sub>3</sub> molecules (P5 and P6), resulting in a distorted trigonal planar coordination sphere with a sum of angles around Ag1 of 358.7° (338.8° for the minor disordered site Ag11). The Ag–P bond lengths (2.4522(13)–2.4609(13) Å) and bond angles (117.50(5)–121.81(4)°) are similar to those of **5** (Table 1), which features the same Ag(PMe<sub>3</sub>)<sub>2</sub><sup>+</sup> moiety. The second silver cation Ag2/Ag21 shows a distorted tetrahedral coordination environment by one phosphorus atom of the cobaltate anion (P4) and three PMe<sub>3</sub> molecules (P7–P9). The average P–Ag–P angle of 112.91° for Ag2 (108.76° for the minor disordered site

Ag21) corresponds well to the ideal tetrahedral angle. As a consequence of its higher coordination number, the Ag–P bonds (2.4724(12)–2.5534(10) Å) are longer for Ag2/Ag21 than for Ag1/Ag11. The Ag–P bonds are nevertheless shorter than in the triphenylphosphane complexes [Ag(PPh<sub>3</sub>)<sub>4</sub>]X (X = NO<sub>3</sub><sup>−</sup>, Ag–P 2.643(3)–2.671(4) Å; X = ClO<sub>4</sub><sup>−</sup>, Ag–P 2.668(5)–2.650(2) Å; X = PF<sub>6</sub><sup>−</sup>, Ag–P 2.639(2)–2.674(1) Å), which also feature four-coordinate Ag<sup>+</sup> cations.<sup>23,28,29</sup> To our knowledge, the tetrametallo-phosphido-bridged complex [Ag<sub>4</sub>(PPh<sub>2</sub>)<sub>4</sub>(PMe<sub>3</sub>)<sub>4</sub>] is the only other tetrahedral silver(I) trimethylphosphane complex. Its structure shows Ag–P(PMe<sub>3</sub>) bond lengths of 2.498(9)–2.500(1) Å and P–Ag–P angles which range from 100.9(3) to 115.4(3)°.<sup>30</sup>

The <sup>1</sup>H NMR spectra of **4–6** each feature one set of *t*Pent signals due to rapid exchange at room temperature. The coordinated PMe<sub>3</sub> molecules give rise to doublets at 1.25, 1.33 and 1.28 ppm, respectively (**4**: <sup>1</sup>J(<sup>1</sup>H, <sup>31</sup>P) = 3.30 Hz, **5**: <sup>1</sup>J(<sup>1</sup>H, <sup>31</sup>P) = 5.33 Hz, **6**: <sup>1</sup>J(<sup>1</sup>H, <sup>31</sup>P) = 3.78 Hz). Similarly, the <sup>13</sup>C{<sup>1</sup>H} NMR spectra each show only one set of *t*Pent signals and a doublet for the methyl groups of PMe<sub>3</sub> (**4**: <sup>1</sup>J(C,P) = 6.41 Hz, **5**: <sup>1</sup>J(C,P) = 12.56 Hz, **6**: <sup>1</sup>J(C,P) = 8.30 Hz). Integration of the <sup>1</sup>H and <sup>31</sup>P{<sup>1</sup>H} NMR signals observed for **4–6** at room temperature confirmed the presence of three, two and five PMe<sub>3</sub> molecules per [Co(P<sub>2</sub>C<sub>2</sub>*t*Pent<sub>2</sub>)<sub>2</sub>]<sup>−</sup> unit. At lower temperature the slow exchange limit is approached, and the <sup>1</sup>H NMR spectra become very complex.

It is interesting to compare the <sup>31</sup>P{<sup>1</sup>H} NMR spectra of **4–6**, which show similar temperature-dependent behavior in [D<sub>8</sub>]THF. At room temperature, the spectra each feature only two singlets (**4**: +6.6 and −45.2 ppm, integral ratio 4:3, **5**: +5.8 and −40.0 ppm, integral ratio 4:2, and **6**: 6.5 and −43.7 ppm, integral ratio 4:5, see Figures S5–S7 of the supporting information). The high-frequency signal is assigned to the [Co(P<sub>2</sub>C<sub>2</sub>*t*Pent<sub>2</sub>)<sub>2</sub>]<sup>−</sup> anion in each case while the low-frequency resonance arises from the PMe<sub>3</sub> ligands. No coupling to the <sup>107</sup>Ag/<sup>109</sup>Ag nuclei is observed at room temperature. The observation of just two <sup>31</sup>P NMR singlets at room temperature may be explained by rapid exchange processes in solution, which lead to equivalent <sup>31</sup>P resonances. Similar dynamic behavior was previously observed for the related gold complex [Au{Co(P<sub>2</sub>C<sub>2</sub>*t*Pent<sub>2</sub>)<sub>2</sub>}(PMe<sub>3</sub>)<sub>2</sub>] (**B**).<sup>15,16</sup>

The <sup>31</sup>P{<sup>1</sup>H} NMR spectra of **4–6** recorded at −80 °C in [D<sub>8</sub>]THF, are displayed in Figure 10. Similar resonances are observed for the [Co(P<sub>2</sub>C<sub>2</sub>*t*Pent<sub>2</sub>)<sub>2</sub>]<sup>−</sup> anion, which appear as three broad signals in an intensity ratio of 2:1:1 at +12.4, +4.2, and −6.2 ppm for **4** and +15.6, −0.8, and −6.6 ppm for **5**. The multiplet observed at −6.6 ppm in the spectrum of **5** shows resolved <sup>31</sup>P–<sup>107/109</sup>Ag and <sup>31</sup>P–<sup>31</sup>P coupling to the Ag(PMe<sub>3</sub>)<sub>2</sub> unit (<sup>1</sup>J(<sup>31</sup>P, <sup>107/109</sup>Ag) = 336 Hz and <sup>2</sup>J(<sup>31</sup>P, <sup>31</sup>P) = 104 Hz). This resonance is therefore assigned to the phosphorus atom (P1) coordinated to silver. For **6**, very broad, overlapping signals are detected at approximately at +9.9, +2.6, −0.1, −6.0, and −7.3 ppm.

The PMe<sub>3</sub> ligands of **4–6** give rise to similar, but distinct <sup>31</sup>P{<sup>1</sup>H} NMR multiplets in these low-temperature spectra. The spectrum of **4** features a major doublet at −42.8 ppm with <sup>1</sup>J(<sup>31</sup>P, <sup>107/109</sup>Ag) = 241 Hz. An additional, minor doublet is detected at −39.7 ppm (<sup>1</sup>J(<sup>31</sup>P, <sup>107/109</sup>Ag) = 256 Hz). The spectrum of the bis(trimethylphosphane) complex **5** is similar, showing

an intense, well-resolved doublet of doublets of doublets at  $-34.7$  ppm with  $^1J(^{31}\text{P}, ^{109}\text{Ag}) = 377.1$  Hz,  $^1J(^{31}\text{P}, ^{107}\text{Ag}) = 328.2$  Hz, and  $^2J(^{31}\text{P}, ^{31}\text{P}) = 104.4$  Hz. This multiplet can be assigned to the coordinated  $\text{Ag}(\text{PMe}_3)_2$  moiety. A less intense, broad doublet at  $-41.0$  ppm ( $^1J(^{31}\text{P}, ^{107/109}\text{Ag}) = 250$  Hz) indicates the presence of a second, unidentified species. Note that the latter signal is not present in the solid-state state  $^{31}\text{P}\{^1\text{H}\}$  NMR CPMAS spectrum (Figure 11, see below). The spectrum of **6** features a comparatively sharp doublet of doublets at  $-39.6$  ppm ( $^1J(^{31}\text{P}, ^{107}\text{Ag}) = 240$  Hz and  $^1J(^{31}\text{P}, ^{109}\text{Ag}) = 272$  Hz). Furthermore, two less intense broad multiplets are detected at  $-41.2$  ppm (doublet,  $^1J(^{31}\text{P}, ^{107/109}\text{Ag}) = 316$  Hz) and  $-36.3$  ppm (doublet of doublets,  $^1J(^{31}\text{P}, ^{107/109}\text{Ag}) \approx 372$  Hz and  $^2J(^{31}\text{P}, ^{31}\text{P}) \approx 70$  Hz), respectively. Based on the comparison with the spectra of **4** and **5**, it seems reasonable to suggest that the multiplets at  $-41.2$  ppm and  $-39.6$  ppm may correspond to  $\text{Ag}(\text{PMe}_3)_3$  units, whereas the broad multiplet  $-36.3$  ppm might be assigned to the  $\text{Ag}(\text{PMe}_3)_2$  moiety of **6**.

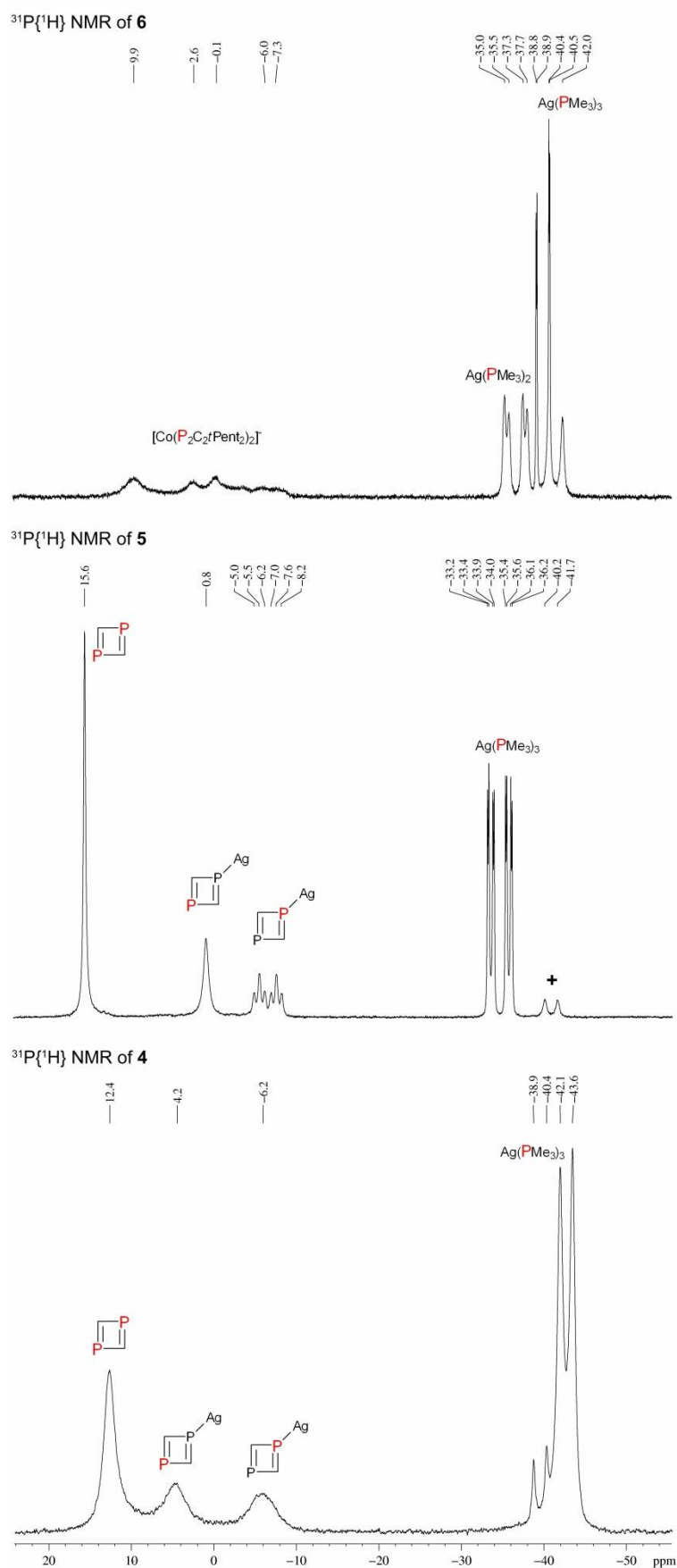


**Figure 10.**  $^{31}\text{P}\{^1\text{H}\}$  NMR spectra (161.97 MHz) of **4–6** in  $[\text{D}_8]\text{THF}$  at  $-80\text{ }^\circ\text{C}$ . + marks an impurity or an unidentified species present in solution.

Further insights can be obtained from  $^{31}\text{P}$  solid-state NMR data. The  $^{31}\text{P}\{^1\text{H}\}$  CPMAS NMR spectrum of **5** (see Figures 11 and 12) reveals four resonances for the phosphorus species of the  $\text{C}_2\text{P}_2$  ligands near 13.5, 12.1,  $-2.7$ , and  $-5.1$  ppm. As can be inferred from the liquid state NMR data, the latter signal constitutes part of a poorly resolved multiplet arising from indirect  $^{31}\text{P}$ - $^{107/109}\text{Ag}$  and  $^{31}\text{P}$ - $^{31}\text{P}$  spin-spin couplings. All these resonances show significant spinning sideband intensities under the conditions measured, reflecting sizeable chemical shielding anisotropy effects (Table 2). This is expected for the planar coordinated phosphorus atoms within the  $\text{C}_2\text{P}_2$ -rings. In agreement with previous results on  $[\text{K}([\text{18}] \text{crown-6})(\text{thf})_2][\text{Ag}\{\text{Co}(\text{P}_2\text{C}_2\text{Ad}_2)_2\}_2]^{15}$  the resonances at 13.5 and 12.1 ppm can be assigned to the  $^{31}\text{P}$  species of the non-silver coordinated  $\text{C}_2\text{P}_2$ -unit (P3 and P4). The resonances near  $-2.7$  and  $-5.1$  ppm are assigned to the silver-coordinated  $\text{C}_2\text{P}_2$ -unit (P2 and P1, respectively). The resonance of the two magnetically equivalent P atoms of the  $\text{PMe}_3$  groups (P5 and P6) is centered at  $-40.9$  ppm. The doublet of doublet pattern can be simulated with  $^1J(^{31}\text{P}-^{107}\text{Ag}) = 313$  Hz,  $^1J(^{31}\text{P}-^{109}\text{Ag}) = 360$  Hz, respectively, and  $^2J(^{31}\text{P}-^{31}\text{P}) = 91$  Hz. The proposed peak assignments are supported by a  $^{31}\text{P}$  R TOBSY experiment (see Figure 13) which uses the indirect  $^{31}\text{P}$ - $^{31}\text{P}$  spin-spin couplings for detecting interatomic connectivities.<sup>31</sup> At the chosen mixing time of 20 ms, dominant off-diagonal elements between the resonances at  $-40.9$  ppm and  $-5.1$  ppm clearly allow the assignment of the latter resonance to the silver-coordinated phosphorus species P1. For reasons unknown, the coherence transfer intensities within the coupled P1/P5,P6 spin species appear asymmetrically distributed, giving the (false) appearance of additional magnetic inequivalences in the 2-D correlation plot. The physical basis for this effect is unknown and currently under further investigation.

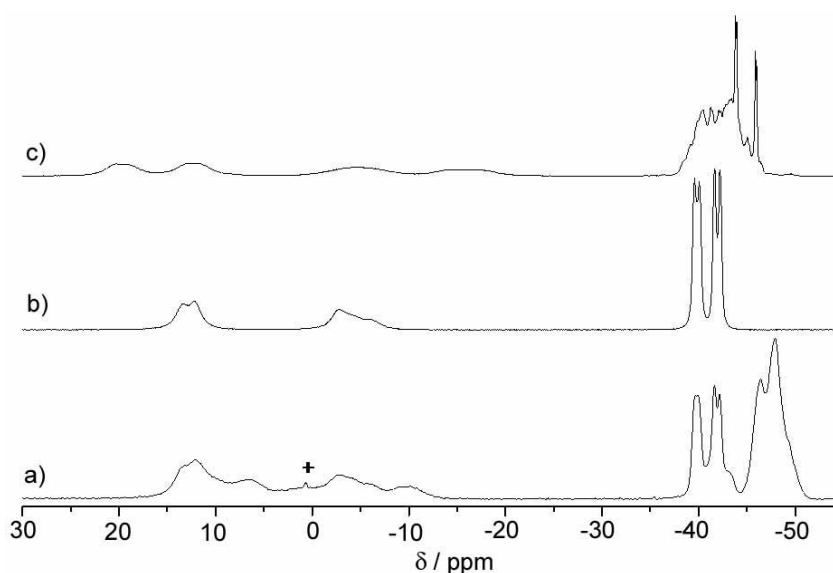


**Figure 11.**  $^{31}\text{P}\{^1\text{H}\}$  CPMAS spectra of **4** (a), **5** (b) and **6** (c) acquired at 7.05 T (c) and 9.4 T (a and b) with a spinning frequency of 13.0 kHz. + marks an impurity.

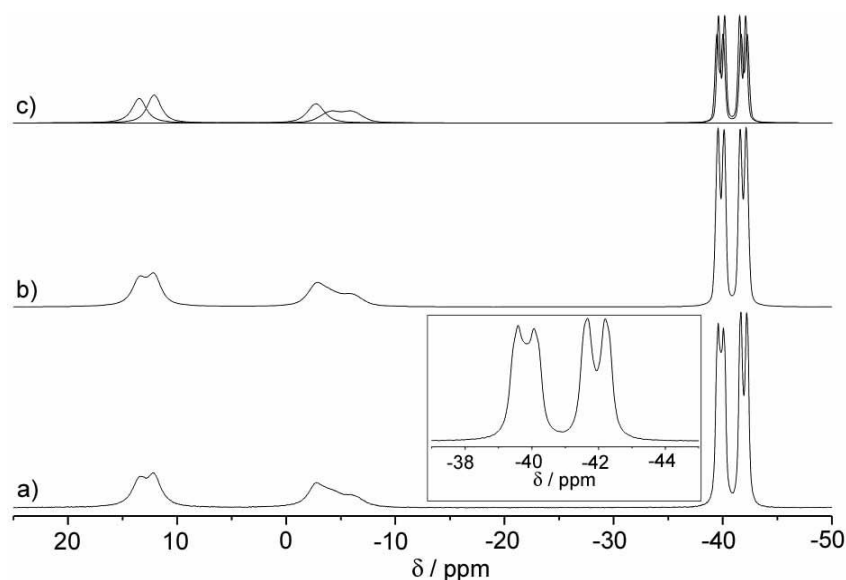


**Figure 12.**  $^{31}\text{P}\{^1\text{H}\}$  CPMAS spectrum of **5** measured at 9.4 T with a spinning frequency of 13.0 kHz (a) and corresponding line shape simulation (b), as well as the peak deconvolution (c). The inset shows the multiplet pattern at low frequencies with the characteristic splittings due to spin-spin couplings between  $^{31}\text{P}$  and the two silver isotopologue.

Since the spin-spin coupling constants  $^2J(\text{P3},\text{P4})$  and  $^2J(\text{P1},\text{P2})$ , respectively, are rather small, the expected cross-peaks between those resonances are not observed. To prove the spatial proximity of these P atoms, the through-space  $^{31}\text{P}$ - $^{31}\text{P}$  magnetic dipole-dipole interaction was re-introduced into the MAS Hamiltonian using a radio-frequency driven dipolar recoupling (RFDR) experiment.<sup>32,33</sup> At a chosen dipolar mixing time of 3.4 ms (see Figures S12 and S13), additional off-diagonal elements between the resonances at 13.5 and 12.1 ppm, and  $-2.7$  and  $-5.1$  ppm, respectively, allow the unambiguous conclusion that the resonances at highest frequencies can be assigned to P3/P4, and the resonance at  $-2.7$  ppm to the phosphorus site P2. (In this experiment, asymmetric coherence transfer effect give again a false appearance of magnetic inequivalences). At a dipolar mixing time of 8 ms additional long-range connectivities are clearly visible supporting the proposed peak assignments (see Figure S14, Supporting Information). The fact that silver coordination of the  $\text{C}_2\text{P}_2$ -rings leads to a low-frequency shift is in good agreement with previous results on comparable compounds;<sup>15</sup> the opposite effect is observed for Au coordination.<sup>16</sup>

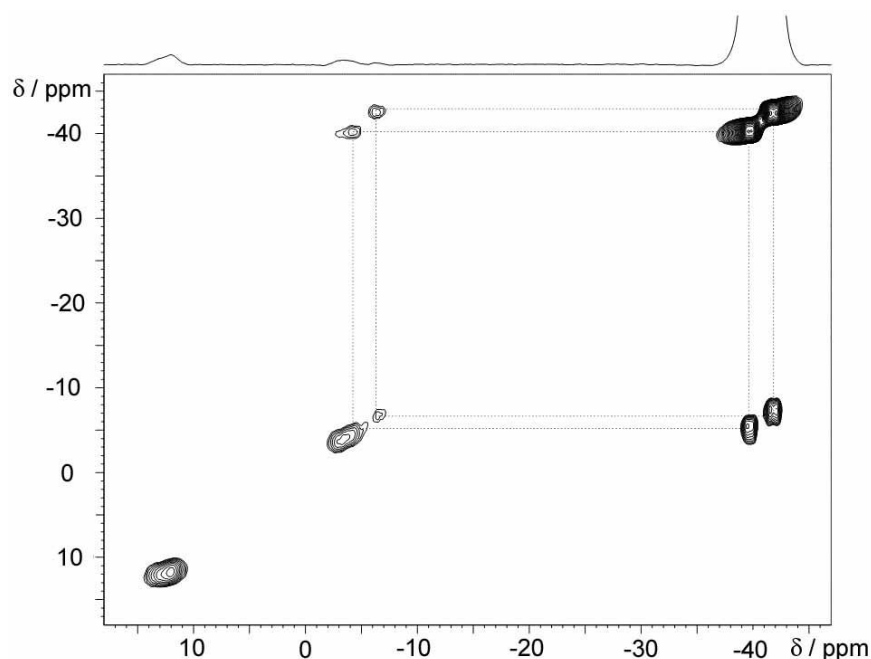


**Figure 13.**  $^{31}\text{P}\{^1\text{H}\}$  R-TOBSY spectrum of **5** acquired at 9.4 T with a rotation frequency of 12.0 kHz and an applied mixing time of ~20 ms. The off-diagonal elements arise from indirect spin-spin couplings between P1 and P5/P6.

Based on the above results on compound **5** we can further conclude from Figures 11 and 12 that the precipitated product of **4** consists of a mixture of the crystallographically described compounds **4** and **5**. Thus, compound **4** shows  $^{31}\text{P}$  resonances at 6.9, 0.8, -10.0 ppm and a complex multiplet at lower frequencies. The  $^{31}\text{P}\{^1\text{H}\}$  CP-R-TOBSY spectrum (see Supplemental Materials Section) allows the assignment of the resonance at -10.0 ppm to the phosphorus species P1 and the resonances at low frequencies to the  $\text{Ag}(\text{PMe}_3)_3$  species.

The  $^{31}\text{P}\{^1\text{H}\}$  CPMAS NMR spectrum of **6** shows four separated resonances for the phosphorus atoms of the  $\text{C}_2\text{P}_2$ -units at 19.7, 12.3, -4.6, and -15.8 ppm. Since the latter two resonances are significantly broadened and/or possess a doublet structure, it is reasonable to assign them to the silver coordinated species P1 and P4 in agreement with the experimental findings described above. Also, the sharp doublet of doublets ( $^1J(^{31}\text{P}, ^{107}\text{Ag}) = 240$  Hz and  $^1J(^{31}\text{P}, ^{109}\text{Ag}) = 272$  Hz) attributed to  $\text{Ag}(\text{PMe}_3)_3$  species is observed at -44.9 ppm. In agreement with the liquid state NMR spectrum (Figure 10) this feature is superimposed upon further multiplets, which might arise from additional  $\text{Ag}(\text{PMe}_3)_x$  species ( $x = 2$  or 3). The poorly resolved lineshape in this spectral region may result from compositional, static and dynamic disordering effects, warranting low-temperature MAS-NMR studies for further investigation.

**Table 2.** Experimental solid-state NMR values of the  $^{31}\text{P}$  isotropic chemical shifts  $\delta_{\text{iso}}$ , chemical shift anisotropies  $\Delta\sigma$  and asymmetry parameters  $\eta\sigma$  of compounds **1-6**. The following convention is used:  $\Delta\sigma = \sigma_{zz} - 1/2(\sigma_{xx} + \sigma_{yy})$  and  $\eta\sigma = (\sigma_{yy} - \sigma_{xx})/(\sigma_{zz} - \sigma_{\text{iso}})$  and  $|\sigma_{zz} - \sigma_{\text{iso}}| > |\sigma_{xx} - \sigma_{\text{iso}}| > |\sigma_{yy} - \sigma_{\text{iso}}|$ .

Compound	$\delta_{\text{iso}}$ (exp.)/ ppm	$\Delta\sigma$ (exp.)/ ppm $\pm 20$ ppm	$\eta\sigma$ (exp.) $\pm 0.1$	assignments
<b>1</b>	16.6	−284	0.51	P2/P3/P4
	14.5	−310	0.27	P2/P3/P4
	11.7	−328	0.48	P2/P3/P4
	~ 0	n.d.	n.d.	P1/P5/P6
<b>2</b>	21.9 <sup>b</sup>	−284 <sup>b</sup>	0.53 <sup>b</sup>	P2/P3/P4
	18.3 <sup>b</sup>	−273 <sup>b</sup>	0.55 <sup>b</sup>	P2/P3/P4
	13.9 <sup>b</sup>	−276 <sup>b</sup>	0.61 <sup>b</sup>	P2/P3/P4
	−5.0	n.d.	n.d.	P1
	−2.3	-	-	P5/P6
<b>3</b>	5.3 (−5.2 <sup>a</sup> )	−315 (−325 <sup>a</sup> )	0.35 (0.36 <sup>a</sup> )	C2P2
	−42.4 (−48.3 <sup>a</sup> )	-	-	[Cu(PMe <sub>3</sub> ) <sub>4</sub> ] <sup>+</sup>
<b>4</b>	6.9	n.d.	n.d.	P2/P3/P4
	0.8	n.d.	n.d.	P2/P3/P4
	−10.0	n.d.	n.d.	P1
	~ −47	-	-	P5-P7
<b>5</b>	13.5	−306	0.51	P3/P4
	12.1	−308	0.59	P3/P4
	−2.7	−307	0.45	P2
	−5.1	−335	0.45	P1
	−40.9	-	-	P5/P6
<b>6</b>	19.7	−275	0.62	P2/P3
	12.3	−308	0.52	P2/P3
	−4.6	−299	0.50	P1/P4
	−15.8	−308	0.35	P1/P4

<sup>a</sup> minor species, <sup>b</sup> main species, n.d.: not determined

### 6.3 Conclusion

Copper(I) and silver(I) complexes of the  $[\text{Co}(\text{P}_2\text{C}_2\text{R}_2)_2]^-$  anion ( $\text{R} = t\text{Pent}, t\text{Bu}$ ) were prepared by salt metathesis of  $[\text{K}(\text{thf})_3\{\text{Co}(\text{P}_2\text{C}_2t\text{Pent}_2)_2\}]$  and  $[\text{K}(\text{thf})_2\{\text{Co}(\text{P}_2\text{C}_2t\text{Bu}_2)_2\}]$  with copper(I) and silver(I) halides and the tertiary phosphanes  $\text{PMe}_3$  and  $\text{PPh}_3$ . In addition, the ionic compound  $[\text{Cu}(\text{PMe}_3)_4][\text{Co}(\text{P}_2\text{C}_2t\text{Pent}_2)_2]$  (**3**), containing the rare, four-coordinate  $[\text{Cu}(\text{PMe}_3)_4]^+$  cation, was obtained. The molecular structures of these new compounds were elucidated by X-ray crystallography and complementary liquid and solid-state NMR investigations. Complexes **1**, **2**, and **4–6** feature three-coordinate and four-coordinate coinage metal atoms that are bound to the  $[\text{Co}(\text{P}_2\text{C}_2\text{R}_2)_2]^-$  anions and coordinate with two or three phosphane ligands, depending on the reaction stoichiometry and the steric demand of the phosphane ( $\text{PPh}_3$  vs.  $\text{PMe}_3$ ). Coordination of the  $\text{C}_2\text{P}_2$  ring to copper or silver leads to a consistent low-frequency shift of the  $^{31}\text{P}$  NMR signal, opposite to the effect of Au-coordination.<sup>16</sup> In addition, the  $^{31}\text{P}$  NMR observables (chemical shifts and spin-spin coupling constants) can clearly differentiate between  $\text{Ag}(\text{PMe}_3)_2$  and  $\text{Ag}(\text{PMe}_3)_3$  groups.

The  $^1\text{H}$ ,  $^{13}\text{C}\{^1\text{H}\}$ , and  $^{31}\text{P}\{^1\text{H}\}$  NMR spectra of **1**, **2**, and **4–6** are temperature-dependent in  $[\text{D}_8]\text{THF}$  solution as revealed by variable-temperature studies. This dynamic behavior may be attributed to the partial decoordination of the copper phosphane and silver phosphane moieties in solution, which indicates that the coordinative bond between the metal atoms and the  $[\text{Co}(\text{P}_2\text{C}_2t\text{Pent}_2)_2]^-$  is labile. Similar observations have previously been made for related gold(I) complexes.<sup>15,16</sup>

## 6.4 Experimental Section

### 6.4.1 General Procedures

All experiments were performed under an atmosphere of dry argon, by using standard Schlenk and glovebox techniques. Solvents were purified, dried, and degassed by standard techniques. NMR spectra were recorded (298K) on BrukerAvance300 ( $^{31}\text{P}$ ; 85%  $\text{H}_3\text{PO}_4$ ) and Avance400 spectrometers ( $^1\text{H}$ ,  $^{13}\text{C}$ ;  $\text{SiMe}_4$ ), internally referenced to residual solvent resonances. The spectra were recorded at 300 K unless noted otherwise. Melting points were measured on samples in sealed capillaries and are uncorrected. Compounds  $t\text{PentC}\equiv\text{P}$ ,<sup>34</sup>  $t\text{Bu}-\text{C}\equiv\text{P}$ ,<sup>35</sup>  $[\text{CuCl}(\text{PPh}_3)]_4$ <sup>36</sup> and  $[\text{K}(\text{dme})_2][\text{Co}(\eta^4-\text{C}_{14}\text{H}_{10})_2]$ <sup>10</sup> were prepared by modified literature procedures. Anhydrous  $\text{AgCl}$ ,  $\text{AgSbF}_6$ ,  $\text{PPh}_3$  and  $\text{PMe}_3$  were purchased from ABCR and used as received. Elemental analyses were determined by the analytical department of Regensburg University.

### 6.4.2 Synthesis of $[\text{K}(\text{thf})_3\{\text{Co}(\text{P}_2\text{C}_2t\text{Pent}_2)_2\}]$

$t\text{PentC}\equiv\text{P}$  (17.6 mL, 20.00 mmol, 1.14 M solution in *n*-hexane) was added dropwise to a deep red-brown solution of  $[\text{K}(\text{dme})_2][\text{Co}(\eta^4-\text{C}_{14}\text{H}_{10})_2]$  (2.72 g, 5.00 mmol) in THF (65 mL). The mixture was allowed to warm to room temperature overnight. The dark-orange solution was filtered and concentrated to ca. 20 mL. The addition of *n*-hexane (50 mL) gave an orange, crystalline solid which was recrystallized from THF/*n*-hexane (1:2) and dried in *vacuo*. The dried solid contains a variable amount of THF molecules. The number of THF molecules present per formula unit was determined by  $^1\text{H}$  NMR spectroscopy individually on each sample. Yield 3.01 g (75%). M.p.: 175 °C. Elemental analysis calcd. for  $\text{C}_{24}\text{H}_{44}\text{P}_4\text{CoK}\cdot 3\text{C}_4\text{H}_8\text{O}$  ( $M = 770.31$ ): C 56.09, H 8.89; found: C 56.29, H 8.37.  $^1\text{H}$  NMR (400.13 MHz,  $[\text{D}_8]\text{THF}$ ):  $\delta = 0.92$  (overlapping s and t, 36H;  $\text{CH}_3$ ), 1.45 (m, 8H;  $\text{CH}_2$ ), 1.78 (m, 12H; THF), 3.62 (m, 12H; THF).  $^{13}\text{C}\{^1\text{H}\}$  NMR (100.61 MHz,  $[\text{D}_8]\text{THF}$ ):  $\delta = 10.6$  (s;  $\text{C}(\text{CH}_3)_2\text{CH}_2\text{CH}_3$ ), 29.2 (s;  $\text{C}(\text{CH}_3)_2\text{CH}_2\text{CH}_3$ ), 38.4 (s;  $\text{C}(\text{CH}_3)_2\text{CH}_2\text{CH}_3$ ), 40.1 (s;  $\text{C}(\text{CH}_3)_2\text{CH}_2\text{CH}_3$ ), 101.1 (t,  $^1J(\text{C},\text{P}) = 52.4$  Hz;  $\text{C}_2\text{P}_2t\text{Pent}_2$ ); the signals of coordinated THF were not observed due to overlap with solvent signals.  $^{31}\text{P}\{^1\text{H}\}$  NMR (161.98 MHz,  $[\text{D}_8]\text{THF}$ ):  $\delta = 9.6$ .

### 6.4.3 Synthesis of $[\text{K}(\text{thf})_2\{\text{Co}(\text{P}_2\text{C}_2t\text{Bu}_2)_2\}]$

This compound was prepared by an analogous procedure to  $[\text{K}(\text{thf})_3\{\text{Co}(\text{P}_2\text{C}_2t\text{Pent}_2)_2\}]$  by adding  $t\text{BuC}\equiv\text{P}$  (24.8 mL, 33.83 mmol, 1.37 M solution in *n*-hexane) to a solution of  $[\text{K}(\text{dme})_2][\text{Co}(\eta^4-\text{C}_{14}\text{H}_{10})_2]$  (3.30 g, 5.21 mmol) in THF (65 mL) at  $-78$  °C. The mixture was allowed to warm to room temperature overnight, filtered and concentrated to ca. 30 mL. Addition of *n*-hexane (65 mL) gave a crystalline solid which was recrystallized from THF/*n*-hexane (1:2). The isolated orange, crystalline solid contained a variable amount of THF molecules. The number of THF molecules present per formula unit was determined by  $^1\text{H}$  NMR spectroscopy individually on each sample. Yield 2.92 g (87%). M.p.: 170 °C. Elemental analysis calcd. for  $\text{C}_{20}\text{H}_{36}\text{P}_4\text{CoK}\cdot 1.75\text{C}_4\text{H}_8\text{O}$  ( $M = 605.07$ , calculated for a sample which contains 1.75 THF molecules per potassium atom): C 51.92, H 8.07; found: C 51.98, H 7.80.  $^1\text{H}$  NMR (400.13 MHz,  $[\text{D}_8]\text{THF}$ ):  $\delta = 1.07$  (s, 36H;  $t\text{Bu}$ ), 1.78 (bs, 8H; THF), 3.62 (bs, 8H; THF).  $^{13}\text{C}\{^1\text{H}\}$  NMR (100.61 MHz,  $[\text{D}_8]\text{THF}$ ):  $\delta = 33.6$  (s;

C(CH<sub>3</sub>)<sub>3</sub>), 35.9 (s; C(CH<sub>3</sub>)<sub>3</sub>), 102.7 (t, <sup>1</sup>J(C,P) = 51.7 Hz; C<sub>2</sub>P<sub>2</sub>tBu<sub>2</sub>); the signals of coordinated THF were not observed due to overlap with solvent signals. <sup>31</sup>P{<sup>1</sup>H} NMR (161.98 MHz, [D<sub>8</sub>]THF): δ = 5.1.

#### 6.4.4 Synthesis of [Cu{Co(P<sub>2</sub>C<sub>2</sub>tPent)<sub>2</sub>}(PPh<sub>3</sub>)<sub>2</sub>] (1)

A solution of [K(thf)<sub>1.75</sub>{Co(P<sub>2</sub>C<sub>2</sub>tPent)<sub>2</sub>}] (0.32 g, 0.50 mmol) in THF (20 mL) was added dropwise to a suspension of [CuCl(PPh<sub>3</sub>)<sub>4</sub>] (0.18 g, 0.125 mmol) in THF (35 mL) at –78 °C, and the reaction mixture was allowed to warm to room temperature overnight. Afterwards, one equivalent of PPh<sub>3</sub> (0.13 g; 0.50 mmol) was added, and the deep red solution was stirred for further 30 min at room temperature. After removal of the solvent in *vacuo*, the dark residue was extracted with 35 mL diethyl ether. The deep red solution was filtered and concentrated to ca. 20 mL. Dark red crystals of **1** were isolated after storage at –18 °C overnight. The isolated crystals contain one diethyl ether molecule per formula unit, which is completely removed on evacuation in an oil pump vacuum. Crystals of **1**·0.5*n*-hexane suitable for X-ray crystallography were grown by diffusion of *n*-hexane into a diethyl ether solution (1:1) at room temperature for two days. Yield 0.29 g (52%). M.p.: 220 °C. Elemental analysis calcd. for C<sub>60</sub>H<sub>74</sub>P<sub>6</sub>CuCo (*M* = 1103.05): C 65.30, H 6.76; found: C 65.06, H 6.62. <sup>1</sup>H NMR (400.13 MHz, C<sub>6</sub>D<sub>6</sub>): δ = 0.99 (t, 12H; C(CH<sub>3</sub>)<sub>2</sub>CH<sub>2</sub>CH<sub>3</sub>), 1.01 (s, 24H; C(CH<sub>3</sub>)<sub>2</sub>CH<sub>2</sub>CH<sub>3</sub>), 1.58 (q, 8H; C(CH<sub>3</sub>)<sub>2</sub>CH<sub>2</sub>CH<sub>3</sub>), 7.02–7.06 (m, 18 H; PPh<sub>3</sub>), 7.42–7.64 (broverlapping m, 12 H; PPh<sub>3</sub>). <sup>1</sup>H NMR (400.13 MHz, 193 K, C<sub>7</sub>D<sub>8</sub>): δ = 0.95–1.64 (overlapping m, 36H; C(CH<sub>3</sub>)<sub>2</sub>CH<sub>2</sub>CH<sub>3</sub> and C(CH<sub>3</sub>)<sub>2</sub>CH<sub>2</sub>CH<sub>3</sub>), 1.82–2.03 (overlapping m, 8H; C(CH<sub>3</sub>)<sub>2</sub>CH<sub>2</sub>CH<sub>3</sub>), 6.67–8.19 (broad overlapping m; PPh<sub>3</sub>), integration of the PPh<sub>3</sub> signals could not be performed due to overlap with solvent signals. <sup>13</sup>C{<sup>1</sup>H} NMR (100.61 MHz, [D<sub>8</sub>]THF): δ = 9.8 (s; C(CH<sub>3</sub>)<sub>2</sub>CH<sub>2</sub>CH<sub>3</sub>), 29.1 (s; C(CH<sub>3</sub>)<sub>2</sub>CH<sub>2</sub>CH<sub>3</sub>), 37.5 (s; C(CH<sub>3</sub>)<sub>2</sub>CH<sub>2</sub>CH<sub>3</sub>), 41.2 (s; C(CH<sub>3</sub>)<sub>2</sub>CH<sub>2</sub>CH<sub>3</sub>), 129.4 (s; C-4 of PPh<sub>3</sub>), 129.5 (s; C-3,5 of PPh<sub>3</sub>), 130.4 (very br s; C-1 of PPh<sub>3</sub>), 134.6 (d, <sup>2</sup>J(C,P) = 16.7 Hz; C-2,6 of PPh<sub>3</sub>). The signal for the C<sub>2</sub>P<sub>2</sub> rings was not observed. <sup>13</sup>C{<sup>1</sup>H} NMR (100.61 MHz, 193 K, [D<sub>8</sub>]THF): δ = 10.6 (s; C(CH<sub>3</sub>)<sub>2</sub>CH<sub>2</sub>CH<sub>3</sub>), 10.7 (s; C(CH<sub>3</sub>)<sub>2</sub>CH<sub>2</sub>CH<sub>3</sub>), 10.9 (s; C(CH<sub>3</sub>)<sub>2</sub>CH<sub>2</sub>CH<sub>3</sub>), 28.4 (s; C(CH<sub>3</sub>)<sub>2</sub>CH<sub>2</sub>CH<sub>3</sub>), 29.1 (s; C(CH<sub>3</sub>)<sub>2</sub>CH<sub>2</sub>CH<sub>3</sub>), 29.6 (s; C(CH<sub>3</sub>)<sub>2</sub>CH<sub>2</sub>CH<sub>3</sub>), 37.7, 38.1, 38.7, 39.2, 39.7 (overlapping s; C(CH<sub>3</sub>)<sub>2</sub>CH<sub>2</sub>CH<sub>3</sub> and C(CH<sub>3</sub>)<sub>2</sub>CH<sub>2</sub>CH<sub>3</sub>), 129.9 (broverlapping s; C-4 and C-3,5 of PPh<sub>3</sub>), 131.5 (br s; C-1 of PPh<sub>3</sub>), 134.5 (br s; C-2,6 of PPh<sub>3</sub>). Signals for the C<sub>2</sub>P<sub>2</sub> rings were not observed. <sup>31</sup>P{<sup>1</sup>H} NMR (161.98 MHz, [D<sub>8</sub>]THF): δ = –5.6 (d, *J* = 16.4 Hz); –2.0 (br s); 21.1 (br s), 42.5–42.7 (very br m). <sup>31</sup>P{<sup>1</sup>H} NMR (161.98 MHz, 193 K, [D<sub>8</sub>]THF): δ = –46.6 (br d, *J* = 71.2 Hz); –41.9 (br d, *J* = 113.9 Hz); –7.2 (t, *J* = 91.2 Hz); –4.5 (very br d, *J* = 16.2 Hz); –3.8 to 6.1 (br overlapping m); 8.5 (br s); 13.6 (br s); 14.7 to 15.1 (br. overlapping s); 18.7 (br. s); 48.3 (very br s).

#### 6.4.5 Synthesis of [Cu{Co(P<sub>2</sub>C<sub>2</sub>tBu)<sub>2</sub>}(PPh<sub>3</sub>)<sub>2</sub>] (2)

Complex **2** was prepared by an analogous procedure to **1** by adding a solution of [K(thf){Co(P<sub>2</sub>C<sub>2</sub>tBu)<sub>2</sub>}] (0.20 g, 0.35 mmol) in THF (15 mL) to a suspension of [CuCl(PPh<sub>3</sub>)<sub>4</sub>] (0.13 g, 0.087 mmol) in THF (30 mL) at –78 °C. The reaction mixture was allowed to warm to room temperature and stirred overnight. Then one equivalent of PPh<sub>3</sub> (0.09 g; 0.35 mmol) was added, and the deep red solution was stirred for further 30 min at room temperature. The solvent was removed in *vacuo*, and the dark residue was extracted with 30 mL diethyl ether. The deep red solution was filtered, concentrated to 15 mL, and layered

with 10 mL *n*-hexane. Dark red, crystalline **2** was isolated after storage at  $-32\text{ }^{\circ}\text{C}$  for two days. The isolated solid contains 0.5 *n*-hexane and ca. 0.3 diethyl ether molecules per formula unit after drying in high vacuum according to  $^1\text{H}$  NMR spectroscopy and the elemental analysis. Crystals of **2**·0.5Et<sub>2</sub>O suitable for X-ray crystallography were grown at  $-18\text{ }^{\circ}\text{C}$  by layering a diethyl ether solution with *n*-hexane (1:1). Yield 0.31 g (82%). M.p.:  $220\text{ }^{\circ}\text{C}$ . Elemental analysis calcd. for C<sub>56</sub>H<sub>66</sub>P<sub>6</sub>CoCu·0.5C<sub>6</sub>H<sub>14</sub>·0.3C<sub>4</sub>H<sub>10</sub>O ( $M = 1122.07$ ): C 64.57, H 6.64; found: C 64.69, H 6.74.  $^1\text{H}$  NMR (400.13 MHz, C<sub>6</sub>D<sub>6</sub>):  $\delta = 0.86$  (t, 3H; CH<sub>3</sub> of *n*-hexane), 1.11 (t, 6H; CH<sub>3</sub> of Et<sub>2</sub>O), 1.22 (s, 40H; *t*Bu and CH<sub>2</sub> of *n*-hexane), 3.28 (q, 1.3H; CH<sub>2</sub> of Et<sub>2</sub>O); 7.00 to 7.64 (br overlapping m; PPh<sub>3</sub>), integration of the PPh<sub>3</sub> signals could not be performed due to overlap with solvent signals.  $^1\text{H}$  NMR (400.13 MHz, 193 K, [D<sub>8</sub>]THF):  $\delta = 0.73$  (br. s; *t*Bu), 0.87 to 0.90 (overlapping t and s; CH<sub>3</sub> of *n*-hexane and *t*Bu), 1.02 (s; *t*Bu), 1.12 (t; CH<sub>3</sub> of Et<sub>2</sub>O), 1.26 (br. m; CH<sub>2</sub> of *n*-hexane), 3.36 (q; CH<sub>2</sub> of Et<sub>2</sub>O), 7.11 to 7.50 (m; PPh<sub>3</sub>). Due to the overlap of several single signals a separated integration could not be performed. Instead, integration of the whole aliphatic (0.72 to 1.32 ppm) and aromatic (7.11 to 7.48 ppm) regions was performed, which gave an intensity ratio (*t*Bu+*n*-hexane+CH<sub>3</sub> of Et<sub>2</sub>O):PPh<sub>3</sub> of 45:30.  $^{13}\text{C}\{^1\text{H}\}$  NMR (100.61 MHz, [D<sub>8</sub>]THF):  $\delta = 14.2$  (s; CH<sub>3</sub> of *n*-hexane), 15.6 (s; CH<sub>3</sub> of Et<sub>2</sub>O), 23.1 (s; CH<sub>2</sub> of *n*-hexane), 34.0 (s; C(CH<sub>3</sub>)<sub>3</sub>), 35.2 (s; C(CH<sub>3</sub>)<sub>3</sub>), 66.2 (s; CH<sub>2</sub> of Et<sub>2</sub>O), 129.5 (s; C-4 of PPh<sub>3</sub>), 129.6 (s; C-3,5 of PPh<sub>3</sub>), 130.6 (s; C-1 of PPh<sub>3</sub>), 134.6 (d,  $^2J(\text{C},\text{P}) = 16.5\text{ Hz}$ ; C-2,6 of PPh<sub>3</sub>). The signals for the C<sub>2</sub>P<sub>2</sub> ring were not observed.  $^{13}\text{C}\{^1\text{H}\}$  NMR (100.61 MHz, 193 K, [D<sub>8</sub>]THF):  $\delta = 14.8$  (s; CH<sub>3</sub> of *n*-hexane), 15.8 (s; CH<sub>3</sub> of Et<sub>2</sub>O), 23.7 (s; CH<sub>2</sub> of *n*-hexane), 32.9 (s; C(CH<sub>3</sub>)<sub>3</sub>), 33.5 (s; C(CH<sub>3</sub>)<sub>3</sub>), 33.9 (s; C(CH<sub>3</sub>)<sub>3</sub>), 35.3 (s; C(CH<sub>3</sub>)<sub>3</sub>), 35.6 (s; C(CH<sub>3</sub>)<sub>3</sub>), 36.3 (s; C(CH<sub>3</sub>)<sub>3</sub>), 66.6 (s; CH<sub>2</sub> of Et<sub>2</sub>O), 93.4 (m; C<sub>2</sub>P<sub>2</sub> ring), 106.0 (br s; C<sub>2</sub>P<sub>2</sub> ring), 113.4 (br. s; C<sub>2</sub>P<sub>2</sub> ring), 129.9 (br s; C-4 and C-3,5 of PPh<sub>3</sub>), 131.6 (br s; C-1 of PPh<sub>3</sub>), 134.4 (very br s; C-2,6 of PPh<sub>3</sub>).  $^{31}\text{P}\{^1\text{H}\}$  NMR (161.98 MHz, C<sub>6</sub>D<sub>6</sub>):  $\delta = -4.4$  (br s).  $^{31}\text{P}\{^1\text{H}\}$  NMR (161.98 MHz, 193 K, [D<sub>8</sub>]THF):  $\delta = -50.1$  (very br s);  $-43.8$  (br d,  $J = 115.4\text{ Hz}$ );  $-7.8$  (t,  $J = 91.2\text{ Hz}$ ),  $-4.9$  (br s);  $-4.4$  (br s);  $0.7$  (very br m);  $3.5$  (br. s);  $8.5$  (very br s);  $10.1$  to  $10.6$  (br overlapping s);  $19.6$  (br. s);  $43.7$  (very br s).

#### 6.4.6 Synthesis of [Cu(PMe<sub>3</sub>)<sub>4</sub>][Co(P<sub>2</sub>C<sub>2</sub>*t*Pent<sub>2</sub>)<sub>2</sub>] (**3**)

A solution of [K(thf)<sub>3.5</sub>{Co(P<sub>2</sub>C<sub>2</sub>*t*Pent<sub>2</sub>)<sub>2</sub>}] (0.40 g, 0.50 mmol) in THF was added dropwise to a suspension of [CuCl(PPh<sub>3</sub>)<sub>4</sub>] (0.18 g, 0.125 mmol) in THF at  $-78\text{ }^{\circ}\text{C}$ . Subsequently, an excess of PMe<sub>3</sub> (0.3 mL, 2.50 mmol) was added via syringe, and the reaction mixture was allowed to warm to room temperature overnight. The light-red solution was filtered, concentrated to ca. 25 mL and layered with *n*-hexane. Red crystals of **3** formed after storage at room temperature for two days. According to the  $^1\text{H}$  NMR spectra and the elemental analysis, the isolated solid of **3** still contained 0.5 THF molecules per formula unit after drying in high vacuum. Yield 0.28 g (61%). M.p.:  $240\text{ }^{\circ}\text{C}$ . Elemental analysis calcd. for C<sub>36</sub>H<sub>80</sub>P<sub>8</sub>CoCu·0.5C<sub>4</sub>H<sub>8</sub>O ( $M = 919.34$ ): C 49.64, H 9.21; found: C 49.08, H 8.89.  $^1\text{H}$  NMR (400.13 MHz, [D<sub>8</sub>]THF):  $\delta = 0.90\text{--}0.94$  (overlapping t and s, 36H; C(CH<sub>3</sub>)<sub>2</sub>CH<sub>2</sub>CH<sub>3</sub> and C(CH<sub>3</sub>)<sub>2</sub>CH<sub>2</sub>CH<sub>3</sub>), 1.34 (br. s 36 H; PMe<sub>3</sub>), 1.46 (q, 8H; C(CH<sub>3</sub>)<sub>2</sub>CH<sub>2</sub>CH<sub>3</sub>), 1.78 (m, 2H; THF), 3.62 (m, 2H; THF).  $^1\text{H}$  NMR (400.13 MHz, 193 K, [D<sub>8</sub>]THF):  $\delta = 0.89\text{--}0.95$  (br, overlapping t and s, 36H; C(CH<sub>3</sub>)<sub>2</sub>CH<sub>2</sub>CH<sub>3</sub>) and

C(CH<sub>3</sub>)<sub>2</sub>CH<sub>2</sub>CH<sub>3</sub>), 1.33–1.48 (br, overlapping s and q, 44 H; PMe<sub>3</sub> and C(CH<sub>3</sub>)<sub>2</sub>CH<sub>2</sub>CH<sub>3</sub>), 1.78 (m, 2H; coordinated THF), 3.62 (m, 2H; coordinated THF). <sup>13</sup>C{<sup>1</sup>H} NMR (100.61 MHz, [D<sub>8</sub>]THF): δ = 10.7 (s; C(CH<sub>3</sub>)<sub>2</sub>CH<sub>2</sub>CH<sub>3</sub>), 17.7 (s; PMe<sub>3</sub>), 29.3 (s; C(CH<sub>3</sub>)<sub>2</sub>CH<sub>2</sub>CH<sub>3</sub>), 38.5 (s; C(CH<sub>3</sub>)<sub>2</sub>CH<sub>2</sub>CH<sub>3</sub>), 101.2 (t, <sup>1</sup>J(C,P) = 51.8 Hz; C<sub>2</sub>P<sub>2</sub>). <sup>13</sup>C{<sup>1</sup>H} NMR (100.61 MHz, 193 K, [D<sub>8</sub>]THF): δ = 10.9 (s; C(CH<sub>3</sub>)<sub>2</sub>CH<sub>2</sub>CH<sub>3</sub>), 17.0 (s; PMe<sub>3</sub>), 29.0 (s; C(CH<sub>3</sub>)<sub>2</sub>CH<sub>2</sub>CH<sub>3</sub>), 38.4 (s; C(CH<sub>3</sub>)<sub>2</sub>CH<sub>2</sub>CH<sub>3</sub>), 100.0 (t, <sup>1</sup>J(C,P) = 55.0 Hz; C<sub>2</sub>P<sub>2</sub>). <sup>31</sup>P{<sup>1</sup>H} NMR (161.98 MHz, [D<sub>8</sub>]THF): δ = –39.1 (q, <sup>1</sup>J(<sup>31</sup>P, <sup>63/65</sup>Cu) = 794.6 Hz, 4P; [Cu(PMe<sub>3</sub>)<sub>4</sub>]<sup>+</sup>), 9.4 (s, 4P; [Co(P<sub>2</sub>C<sub>2</sub>tPent<sub>2</sub>)<sub>2</sub>]<sup>–</sup>). <sup>31</sup>P{<sup>1</sup>H} NMR (161.98 MHz, 193 K, [D<sub>8</sub>]THF): δ = –36.4 (q, <sup>1</sup>J(<sup>31</sup>P, <sup>63/65</sup>Cu) = 806.4 Hz, 4P; [Cu(PMe<sub>3</sub>)<sub>4</sub>]<sup>+</sup>), 8.5 (s, 4P; [Co(P<sub>2</sub>C<sub>2</sub>tPent<sub>2</sub>)<sub>2</sub>]<sup>–</sup>).

#### 6.4.7 Synthesis of [Ag{Co(P<sub>2</sub>C<sub>2</sub>tPent<sub>2</sub>)<sub>2</sub>}(PMe<sub>3</sub>)<sub>3</sub>] (4)

A solution of AgCl (0.07 g, 0.50 mmol) in THF was treated with an excess of PMe<sub>3</sub> (ca. 0.3 mL, 2.5 mmol) and stirred at room temperature for 5 min. Then a solution of [K(thf)<sub>1.75</sub>{Co(P<sub>2</sub>C<sub>2</sub>tPent<sub>2</sub>)<sub>2</sub>}] (0.32 g, 0.50 mmol) in THF was added at –78 °C, and the reaction mixture was allowed to warm to room temperature overnight. The deep red-brown solution was filtered, concentrated to ca. 25 mL and layered with *n*-hexane. Deep red crystals of **4** formed after storage at room temperature for two days. The isolated solid contained 0.5 THF molecules per formula unit after drying in high vacuum according to <sup>1</sup>H NMR spectroscopy. Yield 0.29 g (65%). M.p.: 230 °C. Elemental analysis calcd. for C<sub>33</sub>H<sub>71</sub>P<sub>7</sub>AgCo·0.5C<sub>4</sub>H<sub>8</sub>O (*M* = 887.60): C 47.36, H 8.52; found: C 47.86, H 8.33. <sup>1</sup>H NMR (400.13 MHz, [D<sub>8</sub>]THF): δ = 0.94 (t, 12H; C(CH<sub>3</sub>)<sub>2</sub>CH<sub>2</sub>CH<sub>3</sub>), 0.98 (s, 24H; C(CH<sub>3</sub>)<sub>2</sub>CH<sub>2</sub>CH<sub>3</sub>), 1.25 (d, <sup>1</sup>J(H,P) = 3.30 Hz, 27 H; PMe<sub>3</sub>), 1.49 (q, 8H; C(CH<sub>3</sub>)<sub>2</sub>CH<sub>2</sub>CH<sub>3</sub>), 1.78 (m, 2H; THF), 3.62 (m, 2H; THF). <sup>1</sup>H NMR (400.13 MHz, 193 K, [D<sub>8</sub>]THF): δ = 0.93 (br. s, 36H; C(CH<sub>3</sub>)<sub>2</sub>CH<sub>2</sub>CH<sub>3</sub> and C(CH<sub>3</sub>)<sub>2</sub>CH<sub>2</sub>CH<sub>3</sub>), 1.30 (br. s, 27H; PMe<sub>3</sub>), 1.42 (br. s, 8H; C(CH<sub>3</sub>)<sub>2</sub>CH<sub>2</sub>CH<sub>3</sub>), 1.78 (m, 2H; THF), 3.60 (m, 2H; THF). <sup>13</sup>C{<sup>1</sup>H} NMR (100.61 MHz, [D<sub>8</sub>]THF): δ = 10.4 (s; C(CH<sub>3</sub>)<sub>2</sub>CH<sub>2</sub>CH<sub>3</sub>), 16.7 (d, <sup>1</sup>J(C,P) = 6.41 Hz; PMe<sub>3</sub>), 29.4 (s; C(CH<sub>3</sub>)<sub>2</sub>CH<sub>2</sub>CH<sub>3</sub>), 38.4 (s; C(CH<sub>3</sub>)<sub>2</sub>CH<sub>2</sub>CH<sub>3</sub>), 39.9 (s; C(CH<sub>3</sub>)<sub>2</sub>CH<sub>2</sub>CH<sub>3</sub>), 101.3 (t, <sup>1</sup>J(C,P) = 47.95 Hz; C<sub>2</sub>P<sub>2</sub>). <sup>13</sup>C{<sup>1</sup>H} NMR (100.61 MHz, 193 K, [D<sub>8</sub>]THF): δ = 10.5 (s; C(CH<sub>3</sub>)<sub>2</sub>CH<sub>2</sub>CH<sub>3</sub>), 15.5–17.1 (br overlapping s; coordinated PMe<sub>3</sub>), 29.0 (very br s; C(CH<sub>3</sub>)<sub>2</sub>CH<sub>2</sub>CH<sub>3</sub>), 38.4 (s; C(CH<sub>3</sub>)<sub>2</sub>CH<sub>2</sub>CH<sub>3</sub>), 39.7 (very br s; C(CH<sub>3</sub>)<sub>2</sub>CH<sub>2</sub>CH<sub>3</sub>). <sup>31</sup>P{<sup>1</sup>H} NMR (161.98 MHz, [D<sub>8</sub>]THF): δ = –45.2 (s, 3P; [Ag(PMe<sub>3</sub>)<sub>3</sub>]<sup>+</sup>), 6.6 (s, 4P; [Co(P<sub>2</sub>C<sub>2</sub>tPent<sub>2</sub>)<sub>2</sub>]<sup>–</sup>). <sup>31</sup>P{<sup>1</sup>H} NMR (161.98 MHz, 193 K, [D<sub>8</sub>]THF): δ = –42.8 (br d, <sup>1</sup>J(<sup>31</sup>P, <sup>107/109</sup>Ag) = 241 Hz; coordinated PMe<sub>3</sub>), –39.7 (br d, <sup>1</sup>J(<sup>31</sup>P, <sup>107/109</sup>Ag) = 256 Hz; coordinated PMe<sub>3</sub>), –6.2 (br s; P1 of [Co(P<sub>2</sub>C<sub>2</sub>tPent<sub>2</sub>)<sub>2</sub>]<sup>–</sup>), 4.2 (br s; P2 of [Co(P<sub>2</sub>C<sub>2</sub>tPent<sub>2</sub>)<sub>2</sub>]<sup>–</sup>), 12.4 (br s; P3 and P4 of [Co(P<sub>2</sub>C<sub>2</sub>tPent<sub>2</sub>)<sub>2</sub>]<sup>–</sup>).

#### 6.4.8 Synthesis of [Ag{Co(P<sub>2</sub>C<sub>2</sub>tPent<sub>2</sub>)<sub>2</sub>}(PMe<sub>3</sub>)<sub>2</sub>] (5)

Compound **5** was prepared by a similar procedure as **4** by adding a solution of [K(thf)<sub>1.5</sub>{Co(P<sub>2</sub>C<sub>2</sub>tPent<sub>2</sub>)<sub>2</sub>}] (0.32 g; 0.46 mmol) in THF (20 mL) to a mixture of AgCl (0.07 g, 0.46 mmol) and PMe<sub>3</sub> (0.10 mL, 0.92 mmol) in THF (35 mL) at –78 °C. The light red reaction mixture was allowed to warm to room temperature overnight and the solvent was then removed in *vacuo*. The red residue was dissolved in 1,2-difluorobenzene, filtered and concentrated to ca. 30 mL. Complex **5** crystallized as an orange, crystalline solid after the addition of *n*-hexane (65 mL). Yield 0.24 g (58%).

M.p.: 230 °C. Elemental analysis calcd. for  $C_{30}H_{62}P_6AgCo$  ( $M = 775.47$ ): C 46.47, H 8.06; found: C 46.55, H 7.96.  $^1H$  NMR (400.13 MHz,  $[D_8]THF$ ):  $\delta = 0.96$  (very br s, 36H;  $C(CH_3)_2CH_2CH_3$ ) and  $C(CH_3)_2CH_2CH_3$ , 1.33 (d,  $^1J(H,P) = 5.33$  Hz, 18 H;  $PMe_3$ ), 1.49 (br q, 8H;  $C(CH_3)_2CH_2CH_3$ ).  $^{13}C\{^1H\}$  NMR (100.61 MHz,  $[D_8]THF$ ):  $\delta = 0.93$ – $0.97$  (overlapping t and s, 36H;  $C(CH_3)_2CH_2CH_3$  and  $C(CH_3)_2CH_2CH_3$ ), 1.33 (d,  $^1J(H,P) = 5.20$  Hz, 18H;  $PMe_3$ ), 1.48 (q, 8H;  $C(CH_3)_2CH_2CH_3$ ).  $^{13}C\{^1H\}$  NMR (100.61 MHz,  $[D_8]THF$ ):  $\delta = 10.3$  (s;  $C(CH_3)_2CH_2CH_3$ ), 16.1 (d,  $^1J(C,P) = 12.56$  Hz;  $PMe_3$ ), 29.4 (s;  $C(CH_3)_2CH_2CH_3$ ), 38.3 (s;  $C(CH_3)_2CH_2CH_3$ ), 40.1 (s;  $C(CH_3)_2CH_2CH_3$ ). The signal for the  $C_2P_2$  ring was not observed.  $^{13}C\{^1H\}$  NMR (100.61 MHz, 193 K,  $[D_8]THF$ ):  $\delta = 10.5$  (s;  $C(CH_3)_2CH_2CH_3$ ), 15.3 (br s;  $PMe_3$ ), 28.6 (very br s;  $C(CH_3)_2CH_2CH_3$ ), 29.1 (very br s;  $C(CH_3)_2CH_2CH_3$ ), 30.0 (very br s;  $C(CH_3)_2CH_2CH_3$ ), 38.3 (s;  $C(CH_3)_2CH_2CH_3$ ), 39.5 (very br s;  $C(CH_3)_2CH_2CH_3$ ), 40.8 (very br s;  $C(CH_3)_2CH_2CH_3$ ). The signals for the  $C_2P_2$  rings were not observed.  $^{31}P\{^1H\}$  NMR (161.98 MHz,  $[D_8]THF$ ):  $\delta = -40.0$  (s, 2P;  $[Ag(PMe_3)_2]^+$ ), 5.8 (s, 4P;  $[Co(P_2C_2tPent_2)_2]^-$ ).  $^{31}P\{^1H\}$  NMR (161.98 MHz, 193 K,  $[D_8]THF$ ):  $\delta = -41.0$  (br d,  $^1J(^{31}P, ^{107/109}Ag) = 250$  Hz; coordinated  $PMe_3$ ),  $-34.7$  (ddd,  $^1J(^{31}P, ^{109}Ag) = 377.1$  Hz,  $^1J(^{31}P, ^{107}Ag) = 328.2$  Hz,  $^2J(^{31}P, ^{31}P) = 104.4$  Hz; coordinated  $PMe_3$ ),  $-6.6$  (br dt,  $^1J(^{31}P, ^{107/109}Ag) = 336$  Hz,  $^2J(^{31}P, ^{31}P) = 104$  Hz; P1 of  $[Co(P_2C_2tPent_2)_2]^-$ ),  $-0.8$  (br s; P2 of  $[Co(P_2C_2tPent_2)_2]^-$ ), 15.6 (br s; P3 and P4 of  $[Co(P_2C_2tPent_2)_2]^-$ ).

#### 6.4.9 Synthesis of $[Ag_2\{Co(P_2C_2tPent_2)_2\}(PMe_3)_5]SbF_6$ (**6**)

A solution of  $AgSbF_6$  (0.24 g, 0.70 mmol) in THF was treated with an excess of  $PMe_3$  (ca. 0.6 mL, 6.0 mmol) and stirred at room temperature for 5 min. Then a solution of  $[K(thf)_{1.75}\{Co(P_2C_2tPent_2)_2\}]$  (0.22 g, 0.35 mmol) in THF was added at  $-78$  °C, and the reaction mixture was allowed to warm to room temperature overnight. The deep red solution was filtered, concentrated to ca. 35 mL and layered with *n*-hexane. Storage at room temperature for three days yielded a mixture of deep red crystals of **6** and pale yellow crystals of  $KSbF_6$ . The isolated compound still contains some  $KSbF_6$ , which is formed as the by-product of this reaction and is difficult to remove completely by recrystallization. According to the microanalysis we estimate that the analyzed sample contained of 0.16 equiv.  $KSbF_6$  per formula unit of **6**. In addition, the sample contained 0.5 THF solvate molecules per formula unit after drying in an oil pump vacuum. Crystals of the THF solvate **6**·THF suitable for X-ray crystallography were grown by layering a THF solution of **6** with *n*-hexane at room temperature. Yield 0.21 g (43%). M.p.: 200 °C (decomp.). Elemental analysis calcd. for  $C_{39}H_{89}Ag_2CoF_9P_9Sb \cdot 0.5C_4H_8O \cdot 0.16KSbF_6$  ( $M = 1427.34$ ): C 34.50, H 6.57; found: C 34.34, H 5.96.  $^1H$  NMR (400.13 MHz,  $[D_8]THF$ ):  $\delta = 0.94$  (t, 12H;  $C(CH_3)_2CH_2CH_3$ ), 0.98 (s, 24H;  $C(CH_3)_2CH_2CH_3$ ), 1.28 (d,  $^1J(H,P) = 3.78$  Hz, 45H;  $PMe_3$ ), 1.49 (q, 8H;  $C(CH_3)_2CH_2CH_3$ ), 1.78 (m, 2H; THF), 3.62 (m, 2H; THF).  $^1H$  NMR (400.13 MHz, 193 K,  $[D_8]THF$ ):  $\delta = 0.97$  (br overlapping t and s, 36H;  $C(CH_3)_2CH_2CH_3$  and  $C(CH_3)_2CH_2CH_3$ ), 1.31 (s, 45H;  $PMe_3$ ), 1.48 (br. s, 8H;  $C(CH_3)_2CH_2CH_3$ ), 1.78 (m, 2H; THF), 3.61 (m, 2H; THF).  $^{13}C\{^1H\}$  NMR (100.61 MHz,  $[D_8]THF$ ):  $\delta = 10.4$  (s;  $C(CH_3)_2CH_2CH_3$ ), 16.9 (d,  $^1J(C,P) = 8.3$  Hz;  $PMe_3$ ), 29.4 (s;  $C(CH_3)_2CH_2CH_3$ ), 38.4 (s;  $C(CH_3)_2CH_2CH_3$ ), 40.0 (s;  $C(CH_3)_2CH_2CH_3$ ), 101.3 (t,  $^1J(C,P) = 49.9$  Hz;  $C_2P_2$ ). The signals for coordinated THF were not observed due to overlap with solvent signals.  $^{13}C\{^1H\}$  NMR (100.61 MHz, 193 K,  $[D_8]THF$ ):  $\delta = 10.6$  (s;

C(CH<sub>3</sub>)<sub>2</sub>CH<sub>2</sub>CH<sub>3</sub>), 13.3 (s; coordinated PMe<sub>3</sub>), 16.3 (s; coordinated PMe<sub>3</sub>), 17.1 (s; coordinated PMe<sub>3</sub>), 29.8 (very br s; C(CH<sub>3</sub>)<sub>2</sub>CH<sub>2</sub>CH<sub>3</sub>), 38.4 (s; C(CH<sub>3</sub>)<sub>2</sub>CH<sub>2</sub>CH<sub>3</sub>), 40.0 (very br s; C(CH<sub>3</sub>)<sub>2</sub>CH<sub>2</sub>CH<sub>3</sub>). <sup>31</sup>P{<sup>1</sup>H} NMR (161.98 MHz, [D<sub>8</sub>]THF): δ = −43.7 (s, 5P; PMe<sub>3</sub>); 6.5 (br. s, 4P; [Co(P<sub>2</sub>C<sub>2</sub>tPent<sub>2</sub>)<sub>2</sub>]<sup>−</sup>). <sup>31</sup>P{<sup>1</sup>H} NMR (161.98 MHz, 193 K, [D<sub>8</sub>]THF): δ = −41.2 (br d, <sup>1</sup>J(<sup>31</sup>P, <sup>107/109</sup>Ag) = 316 Hz; coordinated PMe<sub>3</sub>); −39.6 (br dd, <sup>1</sup>J(<sup>31</sup>P, <sup>107</sup>Ag) = 240 Hz, <sup>1</sup>J(<sup>31</sup>P, <sup>109</sup>Ag) = 272 Hz; coordinated PMe<sub>3</sub>); −36.3 (very br dd, <sup>1</sup>J(<sup>31</sup>P, <sup>109/107</sup>Ag) ≈ 372 Hz and <sup>2</sup>J(<sup>31</sup>P, <sup>31</sup>P) ≈ 70 Hz; coordinated PMe<sub>3</sub>); −8.3 to 12.7 (very br overlapping m; [Co(P<sub>2</sub>C<sub>2</sub>tPent<sub>2</sub>)<sub>2</sub>]<sup>−</sup>). <sup>19</sup>F{<sup>1</sup>H} NMR (282.4 MHz, [D<sub>8</sub>]THF): δ = −122.6 (sept., <sup>1</sup>J(<sup>19</sup>F, <sup>123</sup>Sb) = 1940.4 Hz, the <sup>1</sup>J(<sup>19</sup>F, <sup>121</sup>Sb) coupling constant was not determined due to insufficient resolution of the signals).

#### 6.4.10 X-Ray Crystallography

The crystal data were processed with an Agilent Technologies SuperNova diffractometer. Semi-empirical multi-scan or analytical absorption corrections or were applied to the data.<sup>37</sup> The structures were solved with SHELXS<sup>38</sup> or SIR<sup>39</sup> and least-square refinements on *F*<sup>2</sup> were carried out with SHELXL.<sup>43</sup> Generally, disorder was treated with geometrical and displacement restraints where applicable. The crystal of **5** was non-merohedrally and pseudo-merohedrally twinned. Data completeness for **5** is low due to the twinning and the erroneous assumption of the mmm Laue class for the strategy computation. The non-merohedral twinning was analyzed with CrysAlisPro software of Agilent Technologies.<sup>40</sup> Two twin components were identified. The major component (>80% of the data) was used for the structure solution and refinement whereas the minor component was discarded due to the low intensity of this data. The pseudo-merohedral twin component in the space group *P*2<sub>1</sub>/*n* refined to only 0.03. This twin refinement nevertheless resulted in a significant improvement of the model.

CCDC-957390 (**1**·0.5*n*-hexane), -957391 (**2**·0.5Et<sub>2</sub>O), -957392 (**5**), and -957393 (**6**·THF) contain the supplementary crystallographic data for this paper. These data can be obtained free of charge from The Cambridge Crystallographic Data Center via [www.ccdc.cam.ac.uk/data\\_request/cif](http://www.ccdc.cam.ac.uk/data_request/cif).



**Table 3.** Crystal data and structure refinement of **1**, **2**, **5**, and **6**.

	<b>1</b> ·0.5 <i>n</i> -hexane	<b>2</b> ·0.5Et <sub>2</sub> O	<b>5</b>	<b>6</b> ·THF
Empirical formula	C <sub>60</sub> H <sub>74</sub> CoCuP <sub>6</sub> ·0.5C <sub>6</sub> H <sub>14</sub>	C <sub>56</sub> H <sub>66</sub> CoCuP <sub>6</sub> ·0.5C <sub>4</sub> H <sub>10</sub> O	C <sub>30</sub> H <sub>62</sub> P <sub>6</sub> AgCo	C <sub>39</sub> H <sub>87</sub> Ag <sub>2</sub> CoF <sub>6</sub> OP <sub>9</sub> Sb·C <sub>4</sub> H <sub>8</sub> O
Crystal size [mm <sup>3</sup> ]	0.20 × 0.20 × 0.10	0.20 × 0.10 × 0.05	0.20 × 0.20 × 0.10	0.26 × 0.16 × 0.13
Colour and shape	red block	orange block	light red block	orange plate
Formula weight [g mol <sup>-1</sup> ]	1146.56	2168.87	775.41	1419.35
Crystal system	triclinic	Triclinic	monoclinic	triclinic
Space group	<i>P</i> 1	<i>P</i> 1	<i>P</i> 2 <sub>1</sub> / <i>c</i>	<i>P</i> 1
Absorption correction	multi-scan	multi-scan	multi-scan	analytical
Transmission min/max	0.4521/1.0000	0.7610/1.0000	0.4300/1.0000	0.072/0.316
<i>a</i> [Å]	11.7040(3)	10.4101(2)	10.7545(13)	10.14800(10)
<i>b</i> [Å]	14.0289(4)	13.6771(3)	16.8715(6)	17.4725(3)
<i>c</i> [Å]	20.2509(6)	19.9098(3)	23.608(2)	19.3266(3)
α [°]	82.261(2)	90.695(2)	90	91.2190(10)
β [°]	78.686(2)	94.186(2)	117.936(16)	100.0430(10)
γ [°]	65.895(3)	100.340(2)	90	92.9220(10)
<i>V</i> [Å <sup>3</sup> ]	2970.62(14)	2780.36(9)	3784.4(8)	3368.34(9)
<i>Z</i>	2	1	4	2
<i>T</i> [K]	123(1)	123(1)	123(1)	123(1)
λ [Å]	1.5418	1.5418	1.5418	1.5418
ρ <sub>calc</sub> [g/cm <sup>3</sup> ]	1.282	1.295	1.361	1.399
μ (mm <sup>-1</sup> )	4.435	4.716	10.107	12.020
Theta range θ <sub>max</sub> [°]	3.46–76.93	3.29–73.64	8.89–67.68	3.39–73.60
Reflections collected to θ <sub>max</sub>	83787	44733	13995	26068
[°]				
Unique reflections ( <i>R</i> <sub>int</sub> )	12467(0.0690)	10914 (0.0186)	5266(0.0303)	12984(0.029)

Refl. obs. [ $I > 2\sigma(I)$ ]	11058	10611	4386	12037
Parameters	710	636	344	726
Completeness to $\theta_{\text{full}}$	1.000	0.996	0.899	0.991
$R$ -values [ $I > 2\sigma(I)$ ]	0.0683/0.1890	0.0231/0.0595	0.0575/0.1517	0.0333/0.0839
$R$ -values (all data)	0.0742/0.1953	0.0240/0.0600	0.0694/0.1587	0.0357/0.0863
GOF on $F^2$	1.062	1.028	1.100	1.033
Residual density [ $\text{e}\text{\AA}^{-3}$ ]	-0.765/1.423	-0.245/0.292	-0.687/1.931	-0.926/1.054

#### 6.4.11 Solid-State NMR Spectroscopy

$^{31}\text{P}$  solid-state NMR measurements were carried out on BRUKER Avance III+ 300 and BRUKER Avance DSX 400 spectrometers, corresponding to magnetic flux densities of 7.05 and 9.4 T, respectively. Both spectrometers were equipped with 4 mm NMR triple resonance probes operating at MAS rotation frequencies between 10.0 and 14.0 kHz. Line shape analysis was done by using the DMFIT (version 2011).<sup>41</sup> Chemical shifts are reported relative to an 85%  $\text{H}_3\text{PO}_4$  solution.  $^{31}\text{P}\{^1\text{H}\}$  cross-polarization magic-angle spinning (CPMAS) NMR spectra were measured with  $^1\text{H}$   $90^\circ$  pulse lengths of 4.5-5.0  $\mu\text{s}$ , contact times of 4-5 ms and a relaxation delay of 5 s. Hartmann-Hahn matching conditions were adjusted on  $\text{NH}_4\text{H}_2\text{PO}_4$ . An efficient polarization transfer was achieved by a ramped-amplitude CP step with the proton nutation frequency  $\nu_{\text{RF}}(^1\text{H})$  being swept from 56 kHz to 28 kHz in 64 steps for a  $^1\text{H}$   $90^\circ$  pulse of 4.5  $\mu\text{s}$  length.  $^1\text{H}$  heteronuclear decoupling was done using the TPPM-15 scheme.<sup>42</sup>

$^{31}\text{P}\{^1\text{H}\}$  CP-Radiofrequency-driven recoupling experiments<sup>32,33</sup> were done at 9.4 T using the following conditions: spinning frequency 14.0 kHz,  $^{31}\text{P}$  nutation frequency 60 kHz, dipolar mixing times of 3.4 and 8.0 ms. The chemical shift evolution time was systematically incremented in steps of 71.42  $\mu\text{s}$ . For each increment 40 scans were acquired at a relaxation delay of 5 s. TPPM decoupling was applied during the detection period. RTOBSY experiments<sup>31</sup> were done under the following conditions: rotor frequency 12.0 kHz, nutation frequency 60 kHz, fixed dipolar mixing times of 10-20 ms. The chemical shift evolution time was systematically incremented in steps of 83.33  $\mu\text{s}$ . For each increment 128 scans were acquired at a relaxation delay of 10 s. TPPM-15 decoupling was applied during the detection period.

$^{13}\text{C}\{^1\text{H}\}$  CPMAS NMR experiments were performed at 7.05 T. Hartmann-Hahn conditions were adjusted on adamantane with  $^1\text{H}$   $90^\circ$  pulse length of 4.75  $\mu\text{s}$ , a contact time of 5 ms and a relaxation delay of 5 s. An efficient polarization transfer was achieved by a ramped-amplitude CP step. All the spectra were acquired with  $^1\text{H}$  TPPM-15 proton decoupling using  $\sim 10/12 \pi$  pulses in both cases.  $^{13}\text{C}$  chemical shifts are reported relative to TMS using adamantane ( $\delta(^{13}\text{CH}_2) = 38.56$  ppm for the methylene resonance) as a secondary standard.

## 6.5 Supporting Information

### 6.5.1 Graphical Representation of the Single-Crystal Structure of $[\text{Cu}\{\text{Co}(\text{P}_2\text{C}_2t\text{Pent}_2)_2\}(\text{PPh}_3)_2]$ (**1**) (Figure S1)

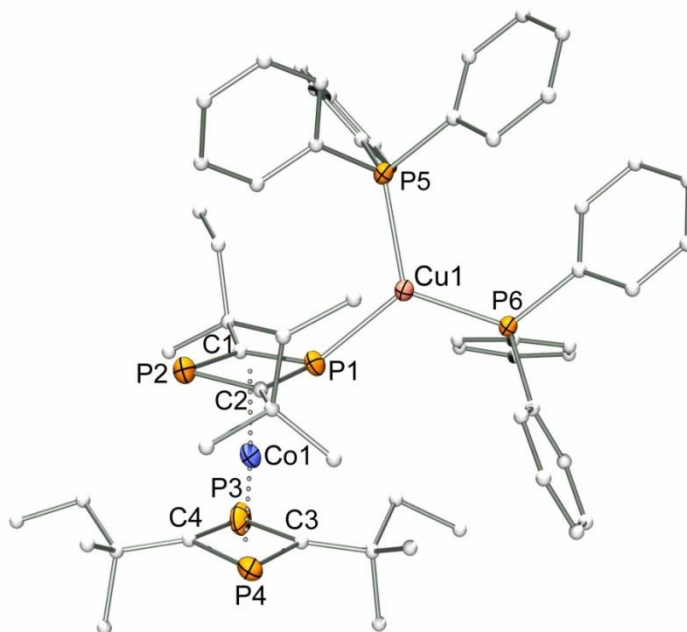


**Figure S1.** Solid-state structure of  $[\text{Cu}\{\text{Co}(\text{P}_2\text{C}_2t\text{Pent}_2)_2\}_2(\text{PPh}_3)_2]$  (**1**·0.35 *n*-hexane). Displacement ellipsoids are at 35% probability, H atoms and *n*-hexane solvate molecule in the crystal lattice are omitted for clarity.

**6.5.2 Variable-Temperature  $^{31}\text{P}\{^1\text{H}\}$  NMR Spectra of  $[\text{Cu}\{\text{Co}(\text{P}_2\text{C}_2t\text{Pent}_2)_2\}(\text{PPh}_3)_2]$  (**1**) and  $[\text{Cu}\{\text{Co}(\text{P}_2\text{C}_2t\text{Bu}_2)_2\}(\text{PPh}_3)_2]$  (**2**) (Figures S2 and S3)**

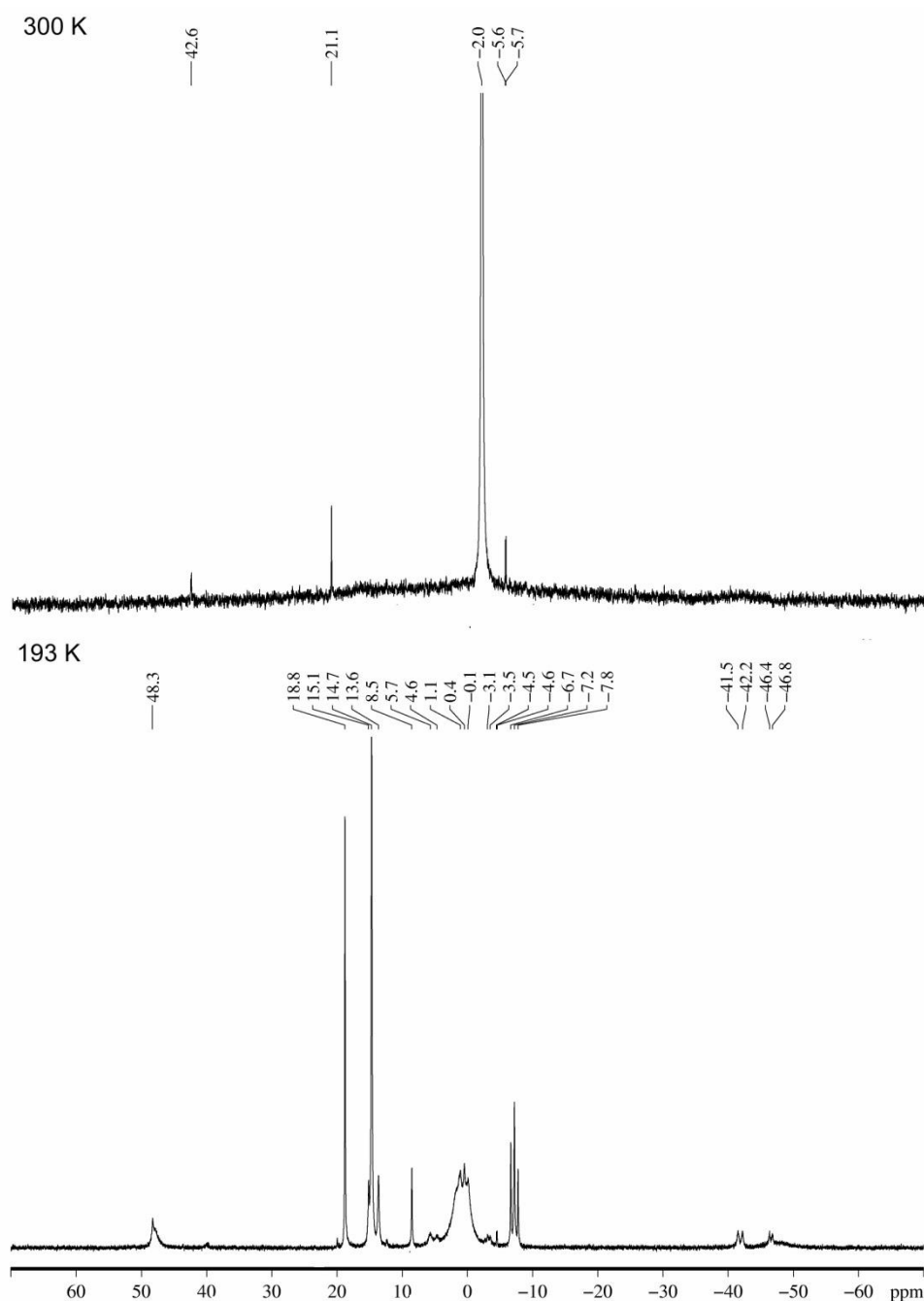


**Figure S2.** Temperature-dependent  $^{31}\text{P}\{^1\text{H}\}$  NMR spectra of  $[\text{Cu}\{\text{Co}(\text{P}_2\text{C}_2t\text{Pent}_2)_2\}(\text{PPh}_3)_2]$  (**1**) in  $[\text{D}_8]\text{THF}$  (161.97 MHz).

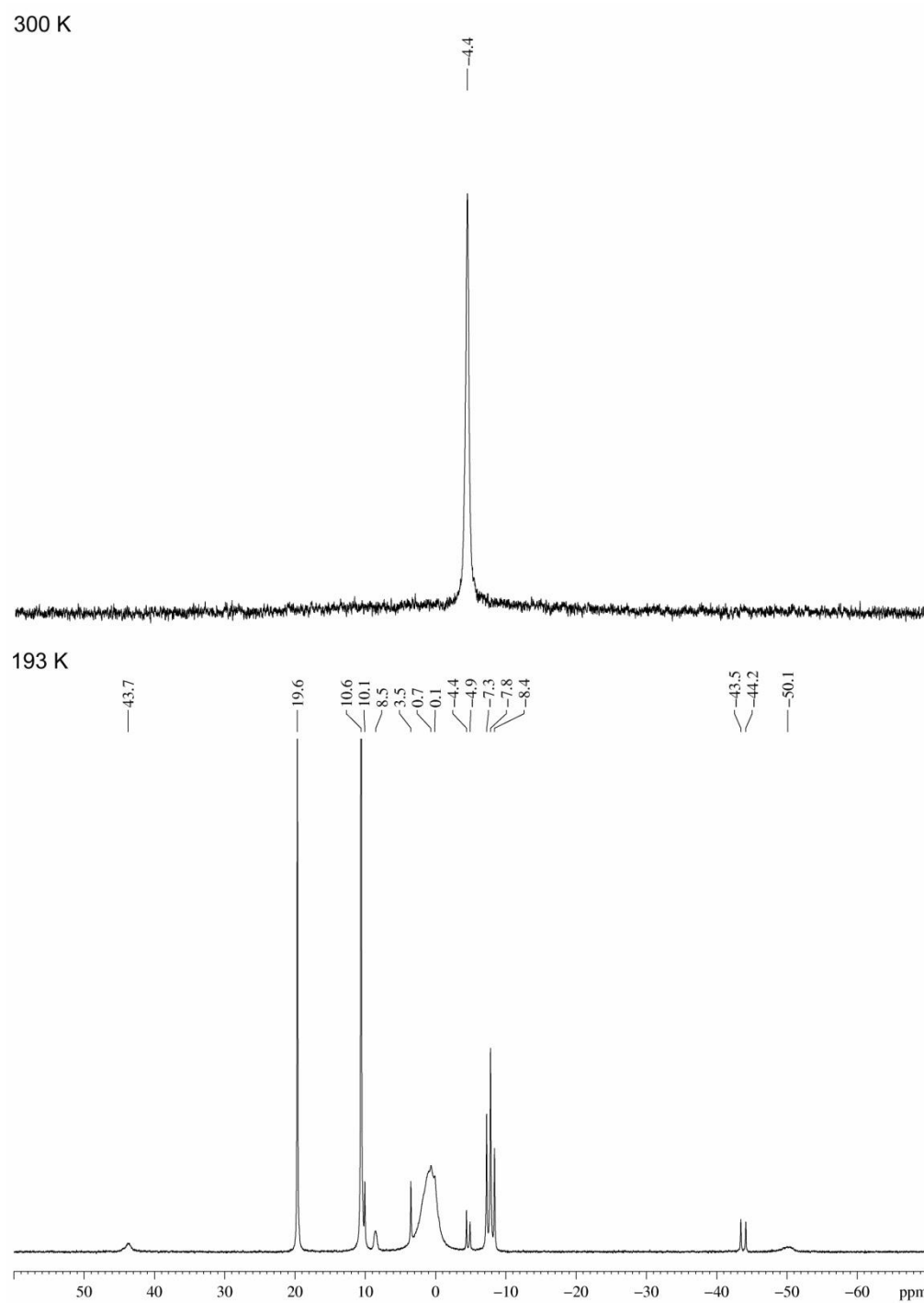


**Figure S3.** Temperature-dependent  $^{31}\text{P}\{^1\text{H}\}$  NMR spectra of  $[\text{Cu}\{\text{Co}(\text{P}_2\text{C}_2t\text{Bu}_2)_2\}(\text{PPh}_3)_2]$  (2) in  $[\text{D}_8]\text{THF}$  (161.97 MHz).

6.5.3  $^1\text{H}$  NMR Spectrum of  $[\text{Cu}(\text{PMe}_3)_4][\text{Co}(\text{P}_2\text{C}_2t\text{Pent}_2)_2]$  (**3**) at 300 K (Figure S4).

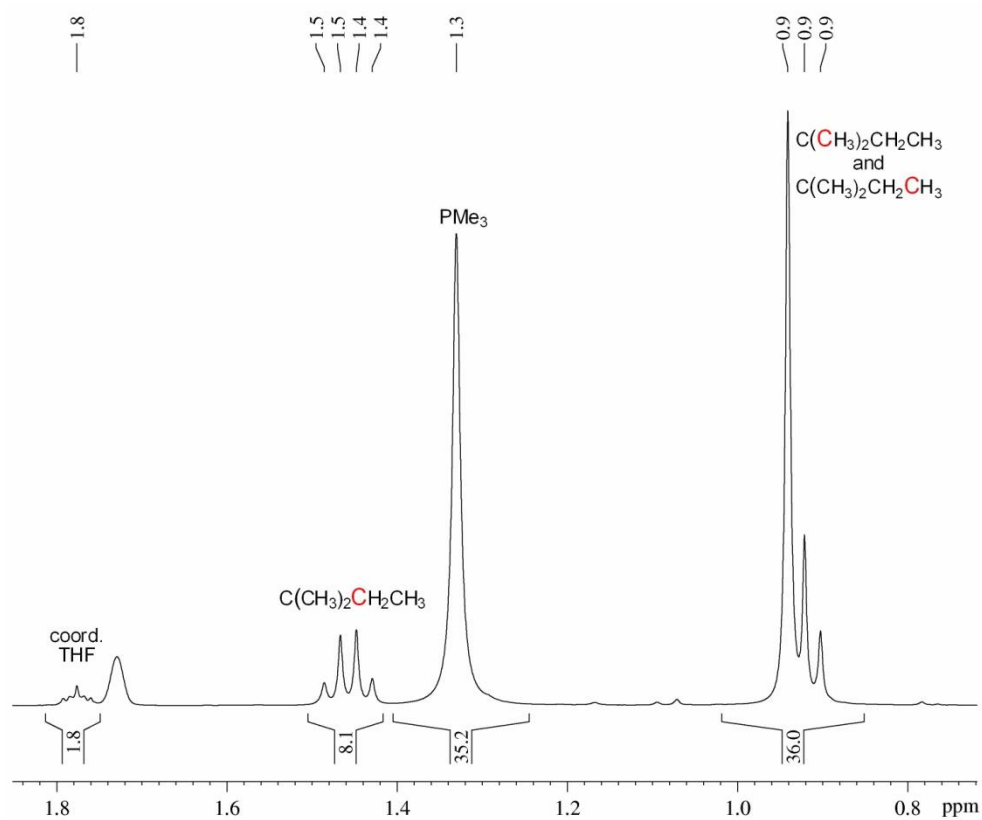
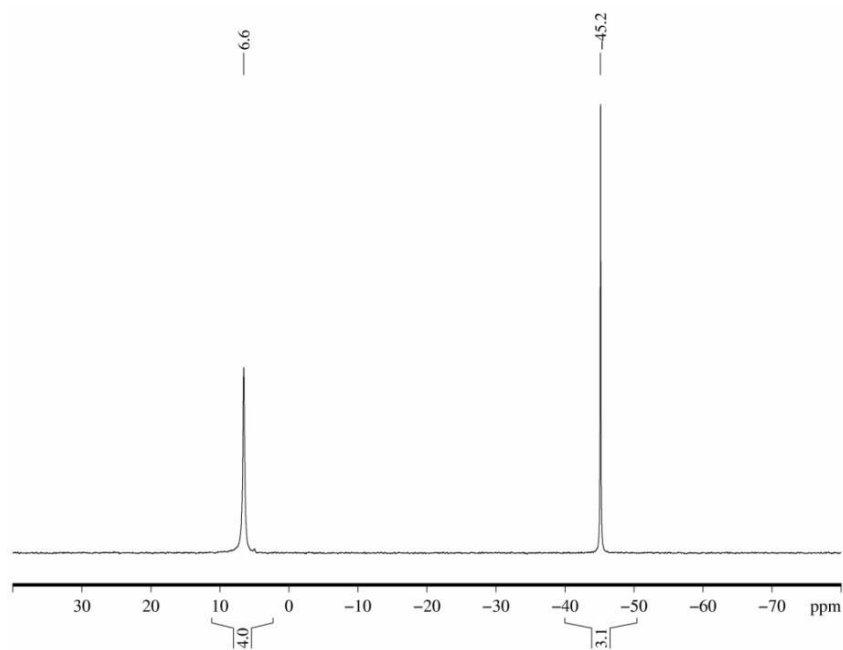
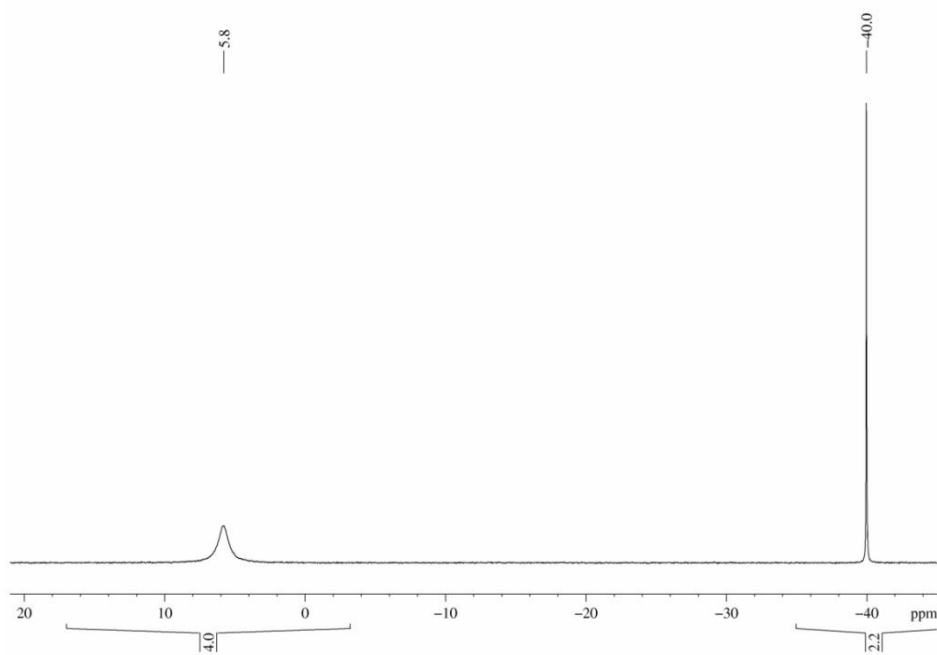


Figure S4.  $^1\text{H}$  NMR spectrum of  $[\text{Cu}(\text{PMe}_3)_4][\text{Co}(\text{P}_2\text{C}_2t\text{Pent}_2)_2]$  (**3**) in  $[\text{D}_8]\text{THF}$  (400.13 MHz, 300 K).

**6.5.4  $^{31}\text{P}\{^1\text{H}\}$  NMR Spectra of  $[\text{Ag}\{\text{Co}(\text{P}_2\text{C}_2t\text{Pent}_2)_2\}(\text{PMe}_3)_3]$  (**4**),  $[\text{Ag}\{\text{Co}(\text{P}_2\text{C}_2t\text{Pent}_2)_2\}(\text{PMe}_3)_2]$  (**5**) and  $[\text{Ag}_2\{\text{Co}(\text{P}_2\text{C}_2t\text{Pent}_2)_2\}(\text{PMe}_3)_5]\text{SbF}_6$  (**6**) at 300 K (Figures S5–S7).**



**Figure S5.**  $^{31}\text{P}\{^1\text{H}\}$  NMR spectrum of  $[\text{Ag}\{\text{Co}(\text{P}_2\text{C}_2t\text{Pent}_2)_2\}(\text{PMe}_3)_3]$  (**4**) in  $[\text{D}_8]\text{THF}$  (161.97 MHz, 300 K).



**Figure S6.**  $^{31}\text{P}\{^1\text{H}\}$  NMR spectrum of  $[\text{Ag}\{\text{Co}(\text{P}_2\text{C}_2t\text{Pent}_2)_2\}(\text{PMe}_3)_2]$  (**5**) in  $[\text{D}_8]\text{THF}$  (161.97 MHz, 300 K).

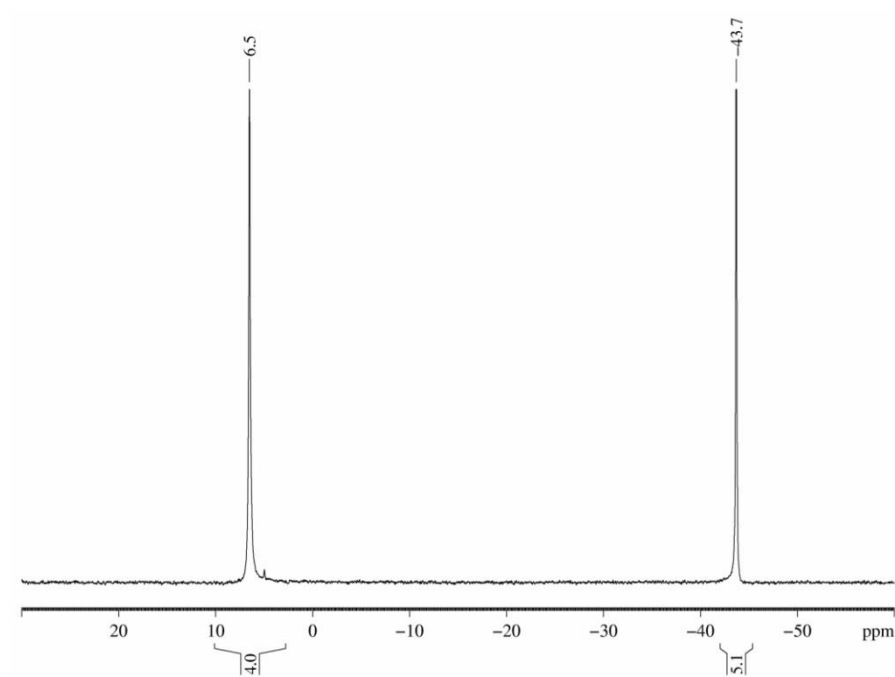


**Figure S7.**  $^{31}\text{P}\{^1\text{H}\}$  NMR spectrum of  $[\text{Ag}_2\{\text{Co}(\text{P}_2\text{C}_2t\text{Pent}_2)_2(\text{PMe}_3)_5\}\text{SbF}_6$  (**6**) in  $[\text{D}_8]\text{THF}$  (161.97 MHz, 300 K).

### 6.5.5 $^{13}\text{C}\{^1\text{H}\}$ CPMAS-NMR Spectra of Complexes 1–6 (Figures S8, S9 and Table S1)

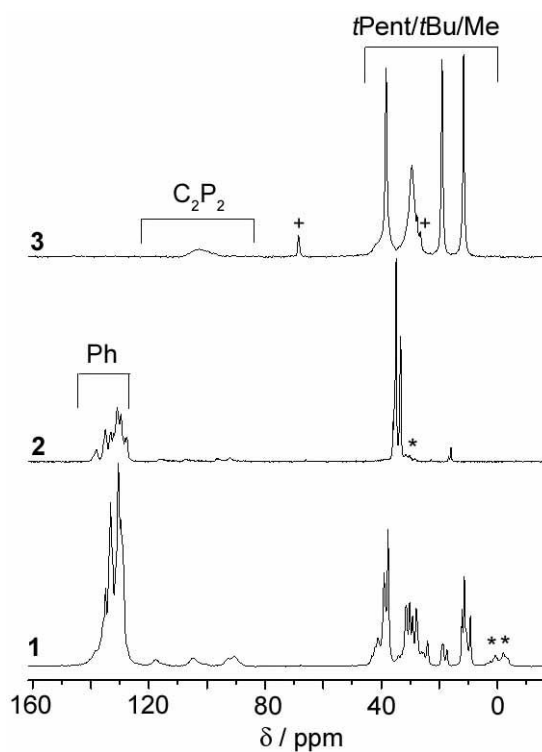


**Figure S8.**  $^{13}\text{C}\{^1\text{H}\}$  CPMAS-NMR spectra of compounds **1**, **2**, and **3**. **1** and **3** were acquired at 7.05 T with a rotation frequency of 10.0 kHz, **2** was measured at 9.4 T with a spinning frequency of 10.0 kHz. \* indicate spinning sidebands, + an impurity.

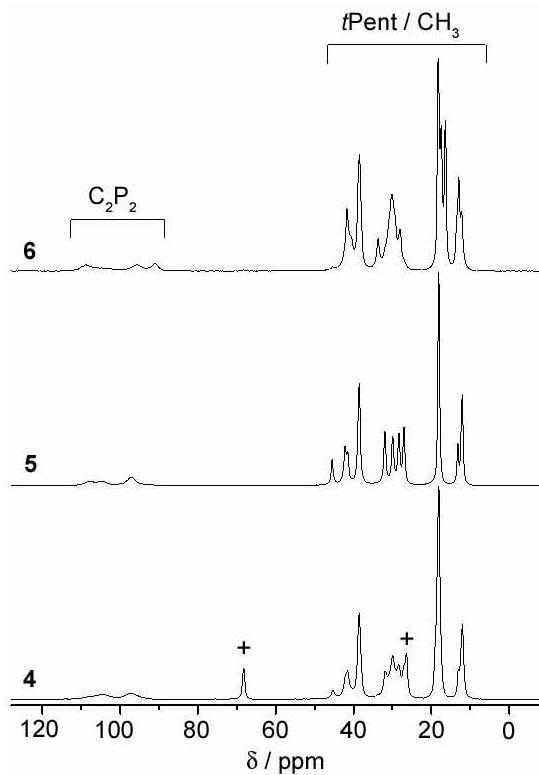


**Figure S9.**  $^{13}\text{C}\{^1\text{H}\}$  CPMAS-NMR spectra of compounds **4–6** acquired at 7.05 T with a rotation frequency of 10.0 kHz.

**Table S1.**  $^{13}\text{C}$  chemical shift values extracted from the solid-state NMR spectra.

	$\delta/\text{ppm}$
<b>1</b>	117.6; 104.7; 92.9; 90.5
<b>2</b>	-
<b>3</b>	102.2
<b>4</b>	107.9; 104.5; 97.1
<b>5</b>	107.9; 104.5; 97.1
<b>6</b>	108.9; 104.7; 95.7; 91.1

**6.5.6  $^{31}\text{P}\{^1\text{H}\}$  CPMAS-NMR Spectra of  $[\text{Ag}\{\text{Co}(\text{P}_2\text{C}_2\text{tPent}_2)_2(\text{PMe}_3)_3]$  (4),  $[\text{Ag}\{\text{Co}(\text{P}_2\text{C}_2\text{tPent}_2)_2(\text{PMe}_3)_2]$  (5) and  $[\text{Ag}_2\{\text{Co}(\text{P}_2\text{C}_2\text{tPent}_2)_2(\text{PMe}_3)_5]\text{SbF}_6$  (6) (Figure S10).**

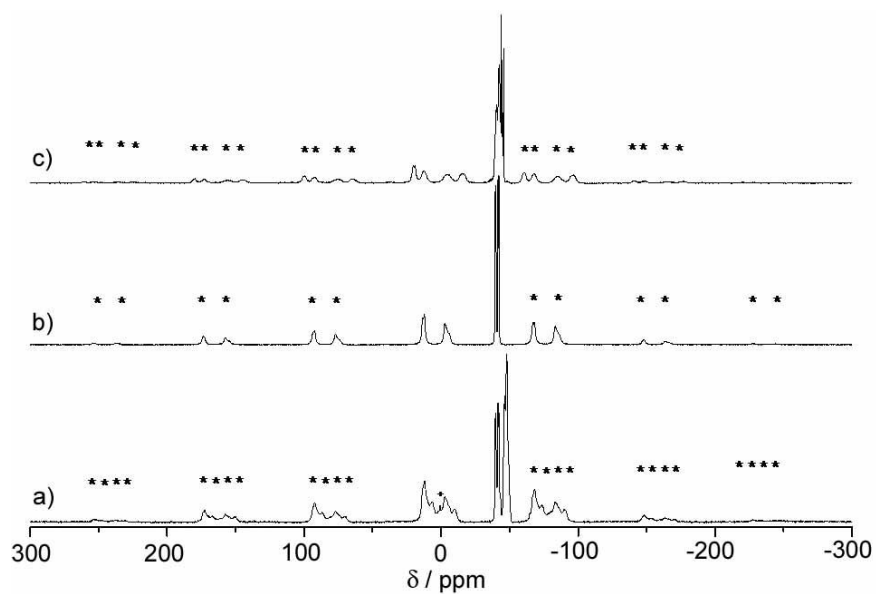


**Figure S10.**  $^{31}\text{P}\{^1\text{H}\}$  CPMAS-NMR spectra of **4** (bottom), **5** (middle) and **6** (top) acquired at 7.05 T (c) and 9.4 T (a and b) with a spinning frequency of 13.0 kHz. + marks an impurity. \* indicates spinning sidebands.

**6.5.7  $^{31}\text{P}$  RFDR and R-TOBSY Spectra of  $[\text{Ag}\{\text{Co}(\text{P}_2\text{C}_2\text{tPent}_2)_2\}(\text{PMe}_3)_3]$  (4),  $[\text{Ag}\{\text{Co}(\text{P}_2\text{C}_2\text{tPent}_2)_2\}(\text{PMe}_3)_2]$  (5), and  $[\text{Ag}_2\{\text{Co}(\text{P}_2\text{C}_2\text{tPent}_2)_2\}(\text{PMe}_3)_5]$  (6) (Figures S11–S15).**

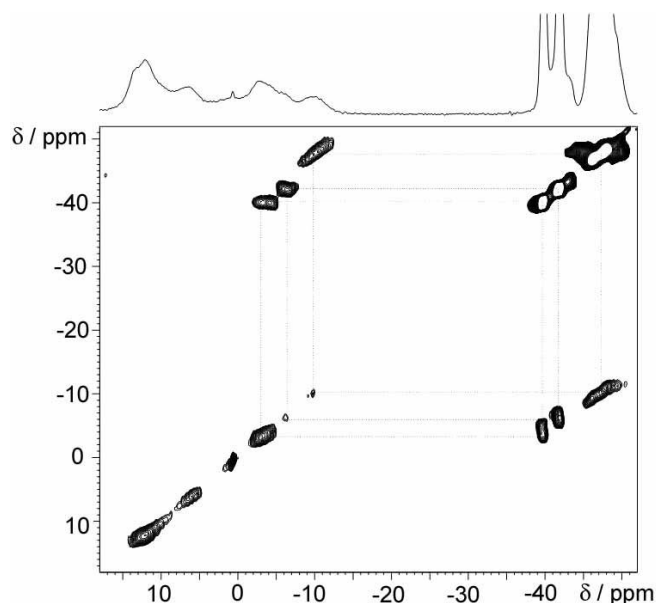


**Figure S11.**  $^{31}\text{P}\{^1\text{H}\}$  CP-R-TOBSY spectrum of **4** measured at 9.4 T with a spinning frequency of 12.0 kHz and an applied mixing time of ~10 ms. The off-diagonal elements indicate interatomic connectivities based on the scalar spin-spin coupling. The data clearly demonstrate that the studied precipitated compound represents a mixture of the compounds **4** and **5**.

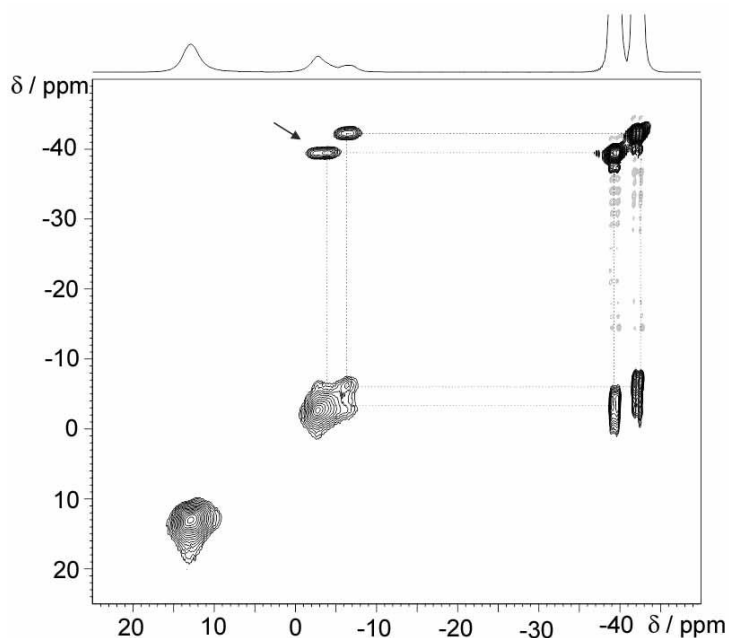


**Figure S12.**  $^{31}\text{P}\{^1\text{H}\}$  CP-RFDR spectrum of **5** measured at 7.05 T with a spinning frequency of 14.0 kHz and an applied mixing time of 3.4 ms. The off-diagonal elements indicate spatial proximities based on the direct dipolar coupling. Truncation artifacts are visible for the resonances near -40 to -42 ppm (shown in grey). The arrow indicates a long-range interaction.

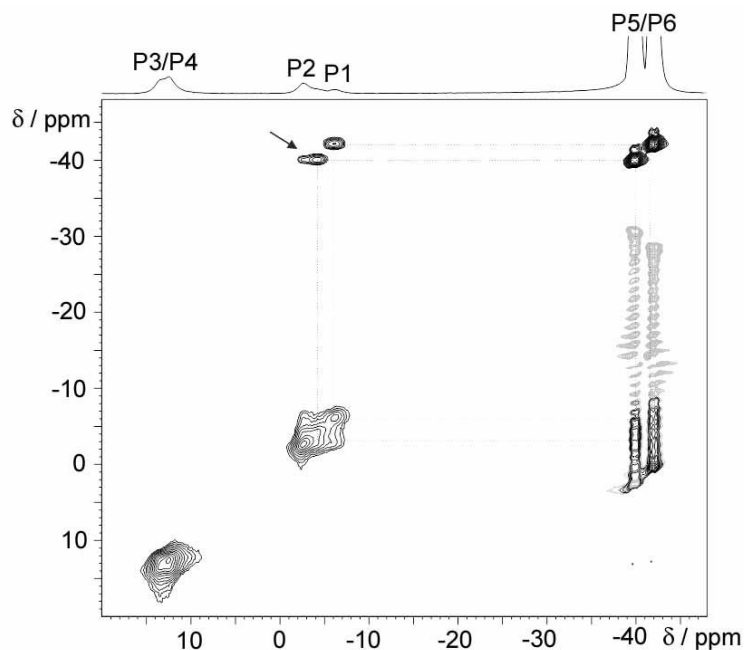


**Figure S13.**  $^{31}\text{P}\{^1\text{H}\}$  CP-RFDR spectrum of **5** measured at 9.4 T with a spinning frequency of 14.0 kHz and an applied mixing time of 3.4 ms. Truncation artifacts (shown in grey) are visible for the resonances near -40 to -42 ppm, the arrow indicates a long-range interaction.

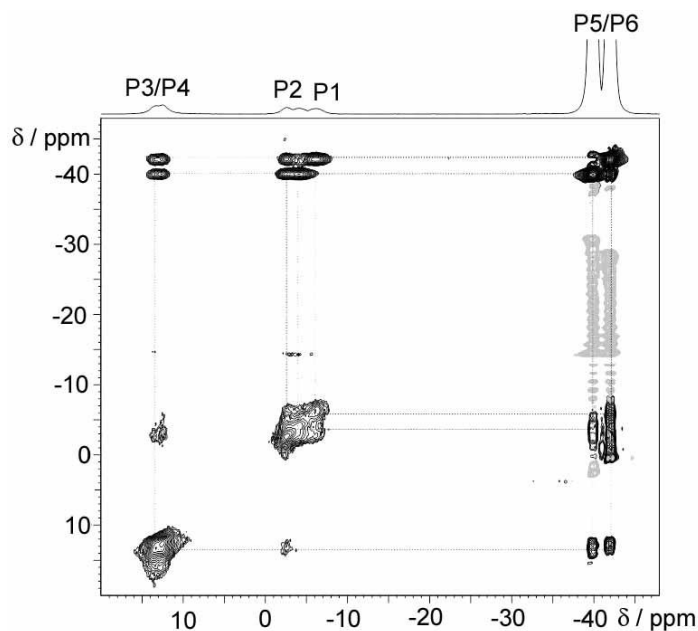


**Figure S14.**  $^{31}\text{P}\{^1\text{H}\}$  CP-RFDR spectrum of **5** measured at 9.4 T with a spinning frequency of 14.0 kHz and an applied mixing time of 8.0 ms. The off-diagonal elements indicate spatial proximities based on the direct dipolar coupling. Truncation artifacts (shown in grey) are visible for the resonances near -40 to -42 ppm.

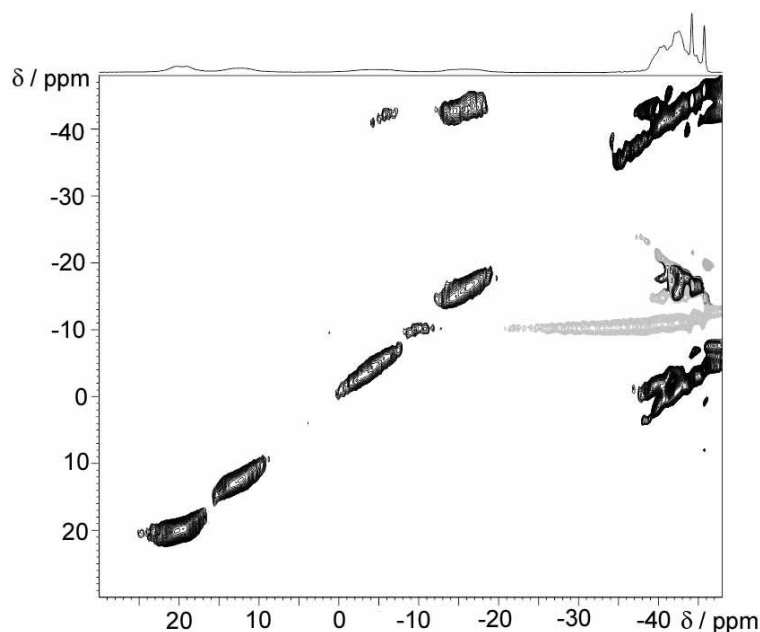


**Figure S15.**  $^{31}\text{P}\{^1\text{H}\}$  CP-RFDR spectrum of **6** measured at 9.4 T with a spinning frequency of 14.0 kHz and an applied mixing time of 3.4 ms. Truncation artifacts (shown in grey) are visible for the resonance in the low-frequency region.

### 6.5.8 $^{31}\text{P}$ Chemical Shielding Anisotropy Parameters (Full Tensor Values) for Compounds 1–6.

**Table S2.** Experimental solid-state NMR values of the  $^{31}\text{P}$  isotropic chemical shifts  $\delta_{\text{iso}}$ , chemical shift anisotropies  $\Delta\sigma$  and asymmetry parameters  $\eta_\sigma$  of compounds **1–6**. The following convention is used:  $\Delta\sigma = \sigma_{\text{zz}} - 1/2(\sigma_{\text{xx}} + \sigma_{\text{yy}})$  and  $\eta_\sigma = (\sigma_{\text{yy}} - \sigma_{\text{xx}})/(\sigma_{\text{zz}} - \sigma_{\text{iso}})$  and  $|\sigma_{\text{zz}} - \sigma_{\text{iso}}| > |\sigma_{\text{xx}} - \sigma_{\text{iso}}| > |\sigma_{\text{yy}} - \sigma_{\text{iso}}|$ . <sup>a</sup> minor species, <sup>b</sup> main species, n.d.: not determined

	$\delta_{\text{iso}}$ (exp.)/ ppm	$\Delta\sigma$ (exp.)/ $\pm 20$ ppm	$\sigma_{\text{zz}}$ (exp.)/ ppm	$\sigma_{\text{yy}}$ (exp.)/ ppm	$\sigma_{\text{xx}}$ (exp.)/ ppm	$\eta_\sigma$ (exp.) $\pm 0.1$	assignment
1	16.6	−284	−206.0	29.6	126.6	0.51	P2/P3/P4
	14.5	−310	−220.9	61.2	116.3	0.27	P2/P3/P4
	11.7	−328	−230.2	45.2	149.9	0.48	P2/P3/P4
	~ 0	n.d.	n.d.	n.d.	n.d.	n.d.	P1/P5/P6
2	21.9 <sup>b</sup>	−284 <sup>b</sup>	−211.6 <sup>b</sup>	22.1 <sup>b</sup>	123.6 <sup>b</sup>	0.53 <sup>b</sup>	P2/P3/P4
	18.3 <sup>b</sup>	−273 <sup>b</sup>	−200.3 <sup>b</sup>	22.4 <sup>b</sup>	122.9 <sup>b</sup>	0.55 <sup>b</sup>	P2/P3/P4
	13.9 <sup>b</sup>	−276 <sup>b</sup>	−197.6 <sup>b</sup>	22.0 <sup>b</sup>	134.1 <sup>b</sup>	0.61 <sup>b</sup>	P2/P3/P4
	−5.0	n.d.	n.d.	n.d.	n.d.	n.d.	P1

	-2.3	-	-	-	-	-	P5/P6
3	5.3 (-5.2 <sup>a</sup> ) -42.4 (-48.3 <sup>a</sup> )	-315 (-325 <sup>a</sup> )	-215.0 (-211.4 <sup>a</sup> )	63.0 (74.6 <sup>a</sup> )	136.2 (152.6 <sup>a</sup> )	0.35 (0.36 <sup>a</sup> )	C <sub>2</sub> P <sub>2</sub>  [Cu(PMe <sub>3</sub> ) <sub>4</sub> ] <sup>+</sup>
4	6.9	n.d.	n.d.	n.d.	n.d.	n.d.	P2/P3/P4
	0.8	n.d.	n.d.	n.d.	n.d.	n.d.	P2/P3/P4
	-10.0	n.d.	n.d.	n.d.	n.d.	n.d.	P1
	~ -47	-	-	-	-	-	P5-P7
5	13.5	-306	-217.5	36.6	140.5	0.51	P3/P4
	12.1	-308	-217.6	29.7	151.6	0.59	P3/P4
	-2.7	-307	-202.0	59.3	150.8	0.45	P2
	-5.1	-335	-218.0	66.9	166.5	0.45	P1
	-40.9	-	-	-	-	-	P5/P6
6	19.7	-275	-203.6	14.8	129.6	0.62	P2/P3
	12.3	-308	-217.6	37.2	143.1	0.52	P2/P3
	-4.6	-299	-194.5	54.8	153.7	0.50	P1/P4
	-15.8	-308	-189.3	82.2	154.5	0.35	P1/P4
	~ -42	-	-	-	-	-	P5-P9

## References

- 1 a) M. Regitz, *Chem. Rev.* **1990**, 90, 191; b) M. Regitz, O. J. Scherer, *Multiple Bonds and Low Coordination Phosphorus Chemistry*, Thieme, Stuttgart, **1990**; c) A. C. Gaumont, J. Denis, *Chem. Rev.* **1994**, 94, 1413; d) J. F. Nixon, *Coord. Chem. Rev.* **1995**, 145, 201; e) K. B. Dillon, F. Mathey, J. F. Nixon, *Phosphorus: The Carbon Copy*, Wiley, Chichester, **1998**; f) F. Mathey, *Angew. Chem. Int. Ed.* **2003**, 42, 1578.
- 2 Alkynes and phosphalkynes may also behave differently in metal-mediate oligomerization reactions: R. Wolf, N. Ghavtadze, K. Weber, E.-M. Schnöckelborg, B. de Bruin, A. W. Ehlers, K. Lammertsma, *Dalton Trans.* **2010**, 39, 1453.
- 3 Pertinent examples: a) P. Binger, R. Milczarek, R. Mynott, M. Regitz, W. Rösch, *Angew. Chem. Int. Ed. Engl.* **1986**, 25, 644; b) P. B. Hitchcock, M. J. Maah, J. F. Nixon, *J. Chem. Soc., Chem. Commun.* **1986**, 737; c) P. Binger, R. Milczarek, R. Mynott, C. Krüger, Y. H. Tsay, E. Raabe, M. Regitz, *Chem. Ber.* **1988**, 121, 637; d) P. Binger, B. Biedenbach, R. Schneider, M. Regitz, *Synthesis* **1989**, 960; e) D. Himmel, M. Seitz, M. Scheer, *Z. Anorg. Allg. Chem.* **2004**, 630, 1220; f) P. A. Arnold, F. G. N. Cloke, P. B. Hitchcock, J. F. Nixon, *J. Am. Chem. Soc.* **1996**, 118, 7630; g) A. G. Avent, F. G. N. Cloke, K. R. Flower, P. B. Hitchcock, J. F. Nixon, D. M. Vickers, *Angew. Chem. Int. Ed.* **1994**, 33, 2330; h) F. G. N. Cloke, P. B. Hitchcock, J. F. Nixon, D. M. Vickers, *J. Organomet. Chem.* **2001**, 635, 212.
- 4 a) P. Binger, G. Glaser, S. Albus, C. Krüger, *Chem. Ber.* **1995**, 128, 1261.
- 5 P. Kramkowski, M. Scheer, *Eur. J. Inorg. Chem.* **2000**, 1869.
- 6 C. Jones, C. Schulten, A. Stasch, *Dalton Trans.* **2006**, 3733.
- 7 P. Binger, R. Milczarek, R. Mynott, C. Krüger, Y. H. Tsay, E. Raabe, M. Regitz, *Chem. Ber.* **1988**, 121, 637.
- 8 a) P. B. Hitchcock, M. J. Maah, J. F. Nixon, C. Woodward, *J. Chem. Soc., Chem. Commun.* **1987**, 844; b) P. B. Hitchcock, M. J. Maah, J. F. Nixon, *Heteroatom Chem.* **1991**, 2, 253.
- 9 a) H. F. Dare, J. A. K. Howard, M. U. Pilotti, F. G. A. Stone, J. Szameitat, *J. Chem. Soc., Chem. Commun.* **1989**, 1409; b) H. F. Dare, J. A. K. Howard, M. U. Pilotti, F. G. A. Stone, J. Szameitat, *J. Chem. Soc., Dalton Trans.* **1990**, 2263.
- 10 a) W. W. Brennessel, J. V. G. Young, J. E. Ellis, *Angew. Chem. Int. Ed.* **2002**, 41, 1211; b) W. W. Brennessel, R. E. Jilek, J. E. Ellis, *Angew. Chem. Int. Ed.* **2007**, 46, 6132; c) W. W. Brennessel, J. E. Ellis, *Inorg. Chem.* **2012**, 51, 9076; d) S. Güllak, O. Stepanek, J. Malberg, B. Rezaei Rad, M. Kotora, R. Wolf, A. Jacobi von Wangelin, *Chem. Sci.* **2013**, 4, 776.
- 11 R. Wolf, A. W. Ehlers, J. C. Slootweg, M. Lutz, D. Gudat, M. Hunger, A. L. Spek, K. Lammertsma, *Angew. Chem. Int. Ed.* **2008**, 47, 4584.
- 12 R. Wolf, J. C. Slootweg, A. W. Ehlers, F. Hartl, B. de Bruin, M. Lutz, A. L. Spek, K. Lammertsma, *Angew. Chem. Int. Ed.* **2009**, 48, 3104.
- 13 R. Wolf, A. W. Ehlers, M. M. Khusniyarov, F. Hartl, B. de Bruin, G. J. Long, F. Grandjean, F. M. Schappacher, R. Pöttgen, J. C. Slootweg, M. Lutz, A. L. Spek, K. Lammertsma, *Chem. Eur. J.* **2010**, 16, 14322.
- 14 R. Wolf, E.-M. Schnöckelborg, *Chem. Commun.* **2010**, 46, 2832.
- 15 J. Malberg, T. Wiegand, H. Eckert, M. Bodensteiner, R. Wolf, *Chem. Eur. J.* **2013**, 19, 2356.
- 16 T. Wiegand, H. Eckert, S. Grimme, J. Malberg, R. Wolf, *Solid State Nucl. Magn. Res.* **2013**, 53, 13.
- 17 G. Doyle, K. A. Eriksen, *Organometallics* **1985**, 4, 2201.
- 18 S. Gómez-Ruiz, R. Wolf, S. Bauer, H. Bittig, A. Schisler, P. Lönnecke, E. Hey-Hawkins, *Chem. Eur. J.* **2008**, 14, 4511.
- 19 a) E. L. Muetterties, C. W. Alegranti, *J. Am. Chem. Soc.* **1970**, 92, 4114; b) E. L. Muetterties, C. W. Alegranti, *J. Am. Chem. Soc.* **1972**, 94, 6386.

- 20 S. Gómez-Ruiz, R. Wolf, E. Hey-Hawkins, *Dalton Trans.* **2008**, 1982.
- 21 R. Wolf, E. Hey-Hawkins, *Angew. Chem. Int. Ed.* **2005**, *44*, 6241.
- 22 a) G. Brunklaus, J. C. C.Chan, H. Eckert, S. Reiser, T. Nilges, A. Pfitzner, *Phys. Chem. Chem. Phys.* **2003**, *5*, 3768; b) M Scheer, L. Gregoriades, J. Bai, M. Sierka, G. Brunklaus, H. Eckert, *Chem. Eur. J.* **2005**, *11*, 2163.
- 23 a) A. Olivieri, *J. Am. Chem. Soc.* **1992**, *114*, 5758; b) R. K. Harris, A. C. Olivieri, *Prog. Nucl. Magn. Reson. Spectrosc.* **1992**, *24*, 435.
- 24 J. R. Black, W. Levason, M. D. Spicer, M. Webster, *J. Chem. Soc., Dalton Trans.* **1993**, *20*, 3129.
- 25 a) H. Schmidbauer, J. Adlkofer, K. Schwirten, *Chem. Ber.* **1972**, *105*, 3382; b) H. F. Klein, H. Schmidbauer, *Angew.Chem., Int. Ed. Engl.* **1970**, *9*, 903.
- 26 A. Cassel, *Acta Cryst. Sect. B.* **1981**, *37*, 229.
- 27 P. F. Barron, J. C. Dyason, P. C. Healy, L. M. Engelhardt, B. W. Skelton, A. H. White, *J. Chem. Soc., Dalton Trans.* **1986**, 1965.
- 28 L. M. Engelhardt, C. Pakawatchai, A. H. White, P. C. Healy, *J. Chem. Soc., Dalton Trans.* **1985**, 125.
- 29 F. A. Cotton, R. L. Luck, *Acta Cryst.* **1989**, *45C*, 1222.
- 30 A. Eichhöfer, J. Eisenmann, D. Fenske, F. Simon, *Z. Anorg. Allg. Chem.* **1993**, *619*, 1360.
- 31 J.C.C. Chan, G. Brunklaus, *Chem. Phys. Lett.* **2001**, *349*, 104.
- 32 A. E. Bennett, J. H. Ok, R.G. Griffin, *J. Chem. Phys.* **1992**, *96*, 8624.
- 33 A. E. Bennett, C. M. Rienstra, J.M. Griffiths, W. Zhen, P. T. Lansbury, R.G. Griffin, *J. Chem. Phys.* **1998**, *108*, 9463
- 34 T. Allspach, *Dissertation*, **1986**, University of Kaiserslautern, Germany.
- 35 Herrmann/Brauer, *Synthetic Methods of Organometallic and Inorganic Chemistry*, Vol. 3, H. H. Karsch (ed.), P, As, Sb and Bi, **1996**, Georg Thieme Verlag, Stuttgart, Germany.
- 36 a) W. T. Reichle, *Inorg. Chim. Acta* **1971**, 325; b) G. Costa, E. Reisenhofer, L. Stefani, *J. Inorg. Nucl.Chem.* **1965**, *27*, 2851.
- 37 a) *SCALE3ABS, CrysAlisPro*, Agilent Technologies Inc., Oxford, GB, **2013**; b) R. C. Clark, J. S. Reid, *Acta Cryst. Sect. A* **1995**, *51*, 887.
- 38 G. M. Sheldrick, *Acta Cryst Sect. A.* **2008**, *64*, 112-122.
- 39 A. Altomare, M. C. Burla, M. Camalli, G. L. Cascarno, C. Giacovazzo, A. G. G. Moliterni, G. Polidori, R. Spagna, *J. Appl. Cryst.* **1999**, *32*, 115.
- 40 *CrysAlisPro*, Agilent Technologies, Version 1.171.36.28.
- 41 D. Massiot, F. Fayon, M. Capron, I. King, S. Le Calvé, B. Alonso, J.O. Durand, B. Bujoli, Z. Gan, G. Hoatson, *Magn. Reson. Chem.* **2002**, *40*, 70.
- 42 A. E. Bennett, C. M. Rienstra, M. Auger, K. V. Lakshmi, R. G. Griffin, *J. Chem. Phys.* **1995**, *103*, 6951.

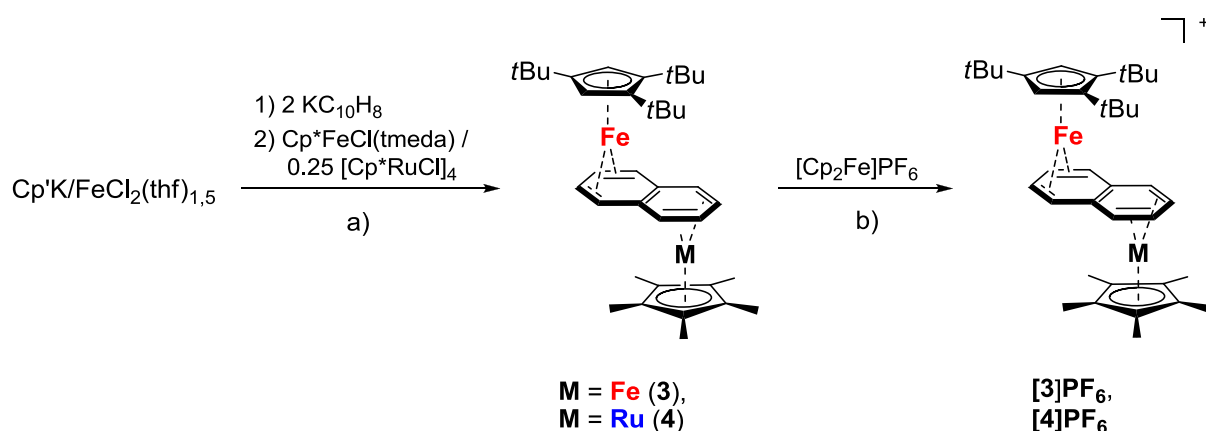
## 7 Summary

This dissertation deals with the synthesis and characterization of oligonuclear transition metal complexes, which contain two different types of bridging ligand: naphthalene ( $C_{10}H_8$ ) and 1,3-diphosphacyclobutadiene  $P_2C_2R_2$ , a phospha-organic analogue of cyclobutadiene.

Chapter 1 gives a brief introduction into the basic characteristics of polyarene and naphthalene-bridged complexes. Furthermore, the chemistry of metal complexes with diphosphacyclobutadienes is briefly introduced. In chapter 2, the synthesis and the elucidation of the electronic structure of dissymmetrical naphthalene-bridged iron-iron and iron-ruthenium complexes are discussed. Investigations concerning the reactivity of bis(diphosphacyclobutadiene) sandwich anions towards silicon electrophiles are described in chapter 3. The first results of coordination studies of these novel phospha-organometallic building blocks are presented in chapters 3–6.

*Chapter 2. Synthesis and Electronic Structure of Dissymmetrical, Naphthalene-Bridged Sandwich Complexes*  $[Cp'Fe(\mu-C_{10}H_8)MCp^*]^x$  ( $x = 0, +1$ ;  $M = Fe, Ru$ ;  $Cp' = \eta^5-C_5H_2-1,2,4-tBu_3$ ;  $Cp^* = \eta^5-C_5Me_5$ )<sup>1</sup>

An aim of the present dissertation was to gain a deeper understanding of how variations of the metal atoms and the cyclopentadienyl ligand influence the structures, spectroscopic properties, and the electronic structure of bimetallic naphthalene-bridged complexes. Therefore, the dissymmetrical sandwich complexes  $[Cp'Fe(\mu-C_{10}H_8)MCp^*]^x$  ( $M = Fe, Ru$ ;  $x = 0, 1$ ;  $Cp^* = C_5Me_5$ ,  $Cp' = 1,2,4$ -tri-*tert*-butylcyclopentdienyl) were synthesized and thoroughly characterized. The symmetrically-substituted complexes  $[Cp^*Fe(\mu-C_{10}H_8)MCp^*]$  (**1**:  $M = Fe$ ; **2**:  $M = Ru$ ) serve as reference compounds. The neutral complexes  $[Cp'Fe(\mu-C_{10}H_8)FeCp^*]$  (**3**) and  $[Cp'Fe(\mu-C_{10}H_8)RuCp^*]$  (**4**) were successfully prepared by a straightforward one-pot procedure according to Scheme 1a. The one-electron oxidation of neutral **3** and **4** with one equivalent ferrocenium hexafluorophosphate (Scheme 1b) gave the mixed-valence compounds  $[Cp'Fe(\mu-C_{10}H_8)FeCp^*]PF_6$  (**[3]PF<sub>6</sub>**) and  $[Cp'Fe(\mu-C_{10}H_8)RuCp^*]PF_6$  (**[4]PF<sub>6</sub>**).



**Scheme 1.** Synthesis of the dissymmetrical iron-iron and iron-ruthenium complexes **3**, **3<sup>+</sup>**, **4**, and **4<sup>+</sup>**.

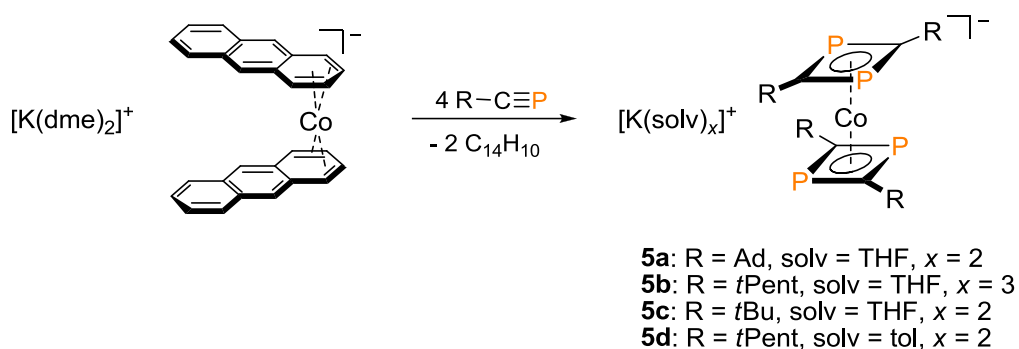
The electrochemical, structural, and spectroscopic characteristics of the dissymmetrical compounds **3**, **3**<sup>+</sup>, **4**, and **4**<sup>+</sup> bearing Cp\* and Cp' ligands were compared with those of the symmetrically-substituted derivatives **1** and **2**, which carry two Cp\* units. This analysis revealed that the substitution of Cp\* by Cp' and Fe by Ru only has a small effect on the electronic structures of the investigated complexes. The composition and shapes of the frontier molecular orbitals remain largely unaffected, and complexes **1–4** thus show qualitatively similar electronic absorption spectra. DFT calculations showed that the naphthalene bridging ligand and the Cp'Fe unit have a major contribution to the redox-active frontier orbitals. Thus, the redox potentials of dissymmetrical **3** and **4** show a moderate shift to more positive values in comparison with symmetrical **1** and **2**, whereas the substitution of Cp\*Fe in **3** by Cp\*Ru in complex **4** only has a small effect. The <sup>57</sup>Fe Mössbauer spectra show very similar isomer shifts for all investigated complexes that are in the same range as found for related polyarene complexes and ferrocene derivatives. The cations [**3**]<sup>+</sup>PF<sub>6</sub><sup>−</sup> and [**4**]<sup>+</sup>PF<sub>6</sub><sup>−</sup> show substantially smaller quadrupole splittings in comparison with neutral **3** and **4**, which might be attributed to the mixed-valent nature of these cations.

In future work, the preparation of other, related homo- and heterobimetallic naphthalene or anthracene-bridged sandwich complexes is an important aspect in order to investigate their electrochemical, spectroscopic, and structural characteristics.

### *Chapter 3. Towards Trimethylsilylated Phospha-Organometallic Compounds: Reactions of [Co(P<sub>2</sub>C<sub>2</sub>R<sub>2</sub>)<sub>2</sub>]<sup>−</sup> Anions with Me<sub>3</sub>SiCl<sup>2</sup>*

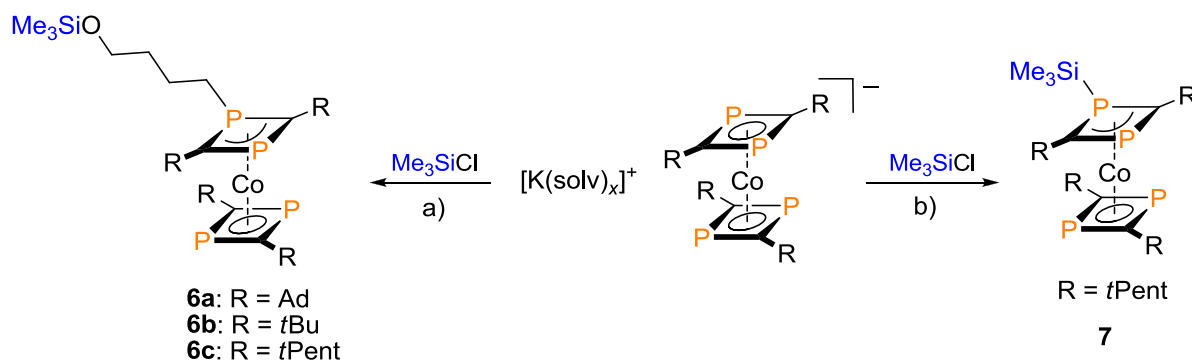
A major aim of this thesis was to investigate the coordination behaviour of anionic bis(1,3-diphosphacyclobutadiene) sandwich complexes of type [Co(P<sub>2</sub>C<sub>2</sub>R<sub>2</sub>)<sub>2</sub>]<sup>−</sup>.<sup>3–5</sup> These complexes promise an intriguing coordination chemistry due to the presence of the lone pairs on the four phosphorus atoms, which may be used for metal coordination.

The first step was the preparation of suitable precursors for our studies. Based on previous work in our group, the new potassium salts [K(thf)<sub>4</sub>{Co(P<sub>2</sub>C<sub>2</sub>Ad<sub>2</sub>)<sub>2</sub>}] (**5a**), [K(thf)<sub>3</sub>{Co(P<sub>2</sub>C<sub>2</sub>*t*Pent<sub>2</sub>)<sub>2</sub>}] (**5b**), [K(thf)<sub>2</sub>{Co(P<sub>2</sub>C<sub>2</sub>*t*Bu<sub>2</sub>)<sub>2</sub>}] (**5c**), and [K(tol)<sub>2</sub>{Co(P<sub>2</sub>C<sub>2</sub>*t*Pent<sub>2</sub>)<sub>2</sub>}] (**5d**) were synthesized by reacting the low-valent metalate [Co(C<sub>14</sub>H<sub>10</sub>)<sub>2</sub>]<sup>−</sup> with phosphalkynes according to Scheme 2. Unlike the previously described complexes [K([18]crown-6)(thf)<sub>2</sub>][Co(P<sub>2</sub>C<sub>2</sub>R<sub>2</sub>)<sub>2</sub>] (R = *t*Bu, Ad),<sup>6</sup> complexes **5a–d** do not contain crown ether molecules, which may interfere in salt metathesis reactions and may complicate the isolation of pure products.



**Scheme 2.** Synthesis of the new potassium salts **5a–d**.

The new potassium salts **5a–d** were investigated in reactions with the silicon electrophile  $\text{Me}_3\text{Si}^+$  according to Scheme 3. Unexpectedly, the complexes  $[\text{Co}(\eta^4\text{-P}_2\text{C}_2\text{R}_2(\text{CH}_2)_4\text{OSiMe}_3)(\eta^4\text{-P}_2\text{C}_2\text{R}_2)_2]$  (**6a–c**, R = Ad, *t*Bu, *t*Pent) were formed through C–O bond cleavage of a THF molecule, when the reactions were carried out in the presence of THF. The reaction also occurred in neat toluene with the THF containing starting materials **5a–c**. In order to access the targeted compound, we prepared the new, “THF-free” potassium salt  $[\text{K}(\text{tol})_2\{\text{Co}(\text{P}_2\text{C}_2\text{tPent}_2)_2\}]$  (**5d**, Scheme 2) by recrystallization of THF salt **5c** in hot toluene. The reactivity of this new toluene-containing salt **5d** with  $\text{Me}_3\text{SiCl}$  according to Scheme 3b afforded the desired complex  $[\text{Co}(\eta^4\text{-P}_2\text{C}_2\text{tPent}_2\text{SiMe}_3)(\eta^4\text{-P}_2\text{C}_2\text{tPent}_2)_2]$  (**7**), in which the  $\text{SiMe}_3$  group is bound to one phosphorus atom of one  $\text{P}_2\text{C}_2$  ring. The remarkably reactive character of the phosphorus-silicon single bond in **7** was further investigated. NMR experiments revealed that complex **7** readily reacts with THF, 2-Me-THF and 1,4-dioxane yielding complex **6c** via the ring-opening of the tetrahydrofuran or 1,4-dioxane ring. A C–O single bond has been cleaved and a P–C bond has been formed in the products.



**Scheme 3.** Synthesis of the THF-cleavage products **6a–c** and of the silylated complex **7**. a) Potassium salts **5a–c**, solv = THF, b) potassium salt **5d**, solv = toluene.

This initial study paves the way for further investigations concerning the reactivity profile of compound **7**. The remarkably reactive character of the phosphorus-silicon bond in **7** might enable the preparation of a variety of new phospho-organometallic complexes by using complex **7** as a precursor. Thus, the formation of phosphorus-element bonds should be feasible by reacting **7** with main-group and transition metal halides. In extension, investigations concerning the reactivity profile of homoleptic sandwich anions of

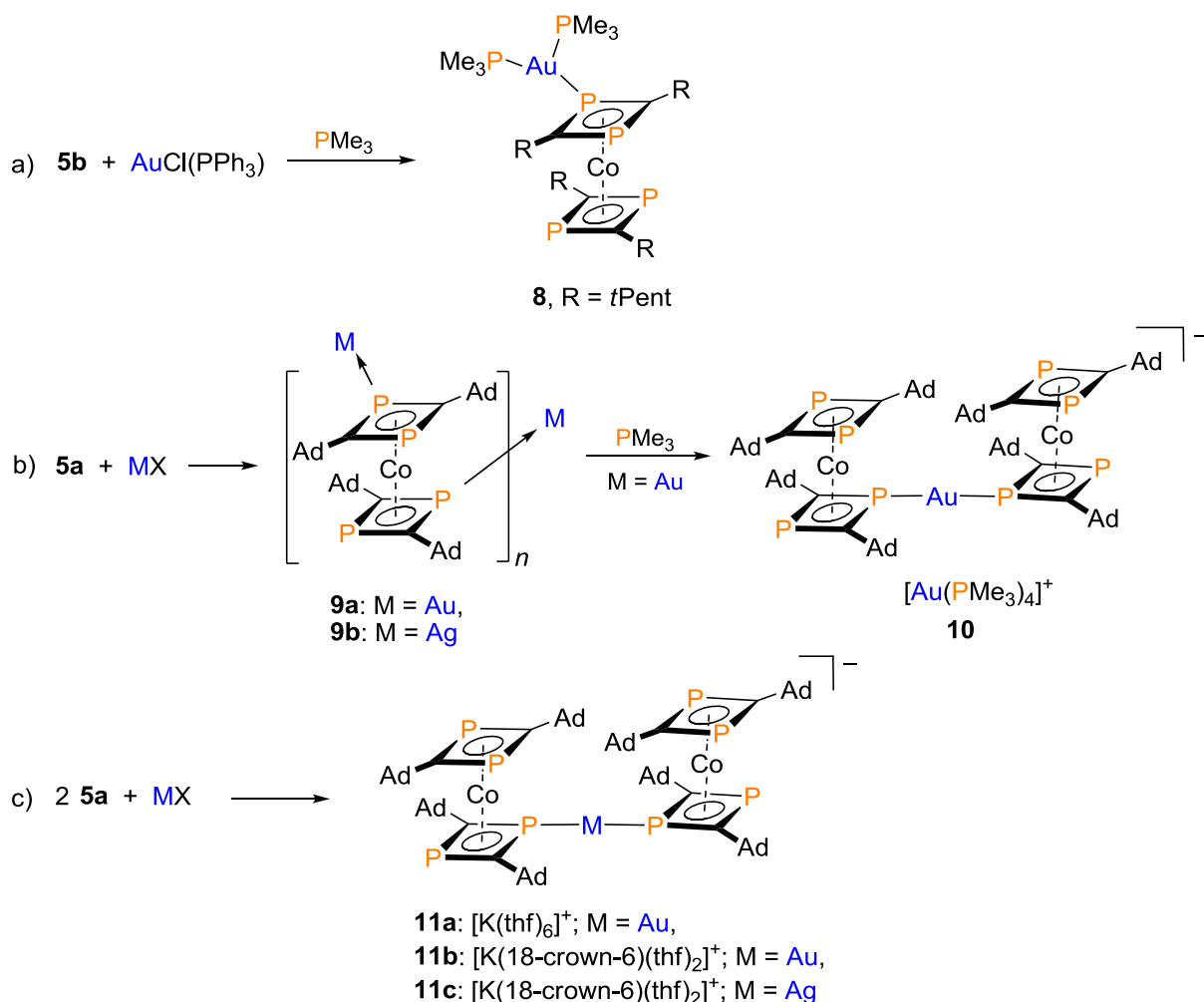
type  $[\text{Co}(\text{P}_2\text{C}_2\text{R}_2)_2]^-$  towards germanium and tin electrophiles might be of interest in order to prepare related compounds with phosphorus-germanium or phosphorus-tin bonds.

#### Chapter 4. Gold(I) and Silver(I) Complexes of Diphosphacyclobutadiene Cobaltate Anions<sup>3,4</sup>

For our initial studies of the coordination behavior of the readily accessible  $[\text{Co}(\text{P}_2\text{C}_2\text{R}_2)_2]^-$  anions, we decide to focus on reactions with coinage metal halides. A range of new copper(I), silver(I), and gold(I) complexes were obtained in these investigations. The obtained compounds represent the first transition-metal complexes of bis(diphosphacyclobutadiene) sandwich anions.

The results are summarized in Schemes 4–7. Three types of complexes (**8–11**) were obtained by reacting **5a** and **5b** with gold(I) and silver(I) salts. The adduct  $[\text{Au}(\text{PMe}_3)_2\{\text{Co}(\text{P}_2\text{C}_2t\text{Pent}_2)_2\}]$  (**8**), which features an  $[\text{Au}(\text{PMe}_3)_2]^+$  unit coordinated to the  $[\text{Co}(\text{P}_2\text{C}_2t\text{Pent}_2)_2]^-$  anion, was isolated from the reaction of  $[\text{K}(\text{thf})_3\{\text{Co}(\text{P}_2\text{C}_2t\text{Pent}_2)_2\}]$  (**5b**) with  $\text{AuCl}(\text{PPh}_3)$  in the presence of  $\text{PMe}_3$  (Scheme 4a). In contrast, coordination polymers of type  $[\text{M}\{\text{Co}(\text{P}_2\text{C}_2\text{Ad}_2)_2\}]_n$  (**9**:  $\text{M} = \text{Au}$ ,  $\text{M} = \text{Ag}$ ) were obtained reacting the more bulky complex  $[\text{K}(\text{thf})_4\{\text{Co}(\text{P}_2\text{C}_2\text{Ad}_2)_2\}]$  (**5a**) with  $\text{AuCl}(\text{tht})$  or  $\text{AgSbF}_6$ , respectively (Scheme 4b). The addition of  $\text{PMe}_3$  to the reaction mixture of **5a** with gold(I) chloride led to the formation of a different type of compound, namely  $[\text{Au}(\text{PMe}_3)_4][\text{Au}\{\text{Co}(\text{P}_2\text{C}_2\text{Ad}_2)_2\}]$  (**10**, Scheme 4b). Complex **10** displays an ion-separated structure comprising the rare  $[\text{Au}(\text{PMe}_3)_4]^+$  cation and the new “ate-complex” anion  $[\text{Au}\{\text{Co}(\text{P}_2\text{C}_2\text{Ad}_2)_2\}]^-$ .<sup>3,7</sup> Similar complexes containing the new anion  $[\text{M}\{\text{Co}(\text{P}_2\text{C}_2\text{Ad}_2)_2\}]^-$  (**11**:  $\text{M} = \text{Au}$ ,  $\text{Ag}$ ) were also obtained by reacting two equivalents of potassium salt  $[\text{K}(\text{thf})_4\{\text{Co}(\text{P}_2\text{C}_2\text{Ad}_2)_2\}]$  (**5a**) with  $\text{AuCl}(\text{tht})$  or  $\text{AgSbF}_6$  (Scheme 4c).

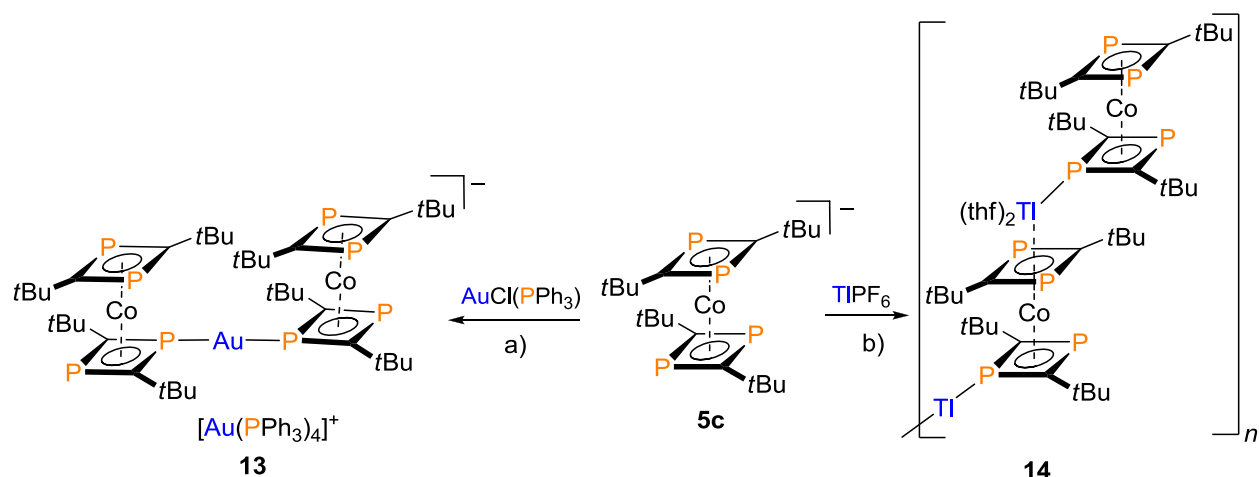
Complexes **8–11** were thoroughly characterized by X-ray crystallography and multinuclear NMR spectroscopy in solution and in the solid state. The solid-state NMR data of complexes **8**, **10**, and **11** support the single crystal X-ray structures. The microcrystalline compounds  $[\text{M}\{\text{Co}(\text{P}_2\text{C}_2\text{Ad}_2)_2\}]_n$  (**9a**:  $\text{M} = \text{Au}$ , **9b**:  $\text{M} = \text{Ag}$ ) could not be analyzed by X-ray crystallography and solution NMR spectroscopy. However, solid-state NMR experiments clearly show that these compounds exist as coordination polymers with a “zig-zag” linked structure. The solution behavior of  $[\text{Au}(\text{PMe}_3)_2\{\text{Co}(\text{P}_2\text{C}_2t\text{Pent}_2)_2\}]$  (**8**),  $[\text{Au}(\text{PMe}_3)_4][\text{Au}\{\text{Co}(\text{P}_2\text{C}_2\text{Ad}_2)_2\}]$  (**10**), and  $[\text{K}(\text{thf})_6][\text{Au}\{\text{Co}(\text{P}_2\text{C}_2\text{Ad}_2)_2\}]$  (**11a**) was additionally elucidated by multinuclear NMR spectroscopy in solution. The NMR spectra of **11a** indicate the presence of an intact  $[\text{Au}\{\text{Co}(\text{P}_2\text{C}_2\text{Ad}_2)_2\}]^-$  anion in solution as observed in the X-ray crystal structure. Contrary to that, the NMR spectra of complexes **8** and **10** are more complex and temperature-dependent, indicating the formation of equilibria between several species in solution. This observation implies that the Au–P bonds of  $[\text{Au}(\text{PMe}_3)_2\{\text{Co}(\text{P}_2\text{C}_2t\text{Pent}_2)_2\}]$  (**8**), and  $[\text{Au}(\text{PMe}_3)_4][\text{Au}\{\text{Co}(\text{P}_2\text{C}_2\text{Ad}_2)_2\}]$  (**10**) are labile.



**Scheme 4.** Synthesis of complexes **8–11**.

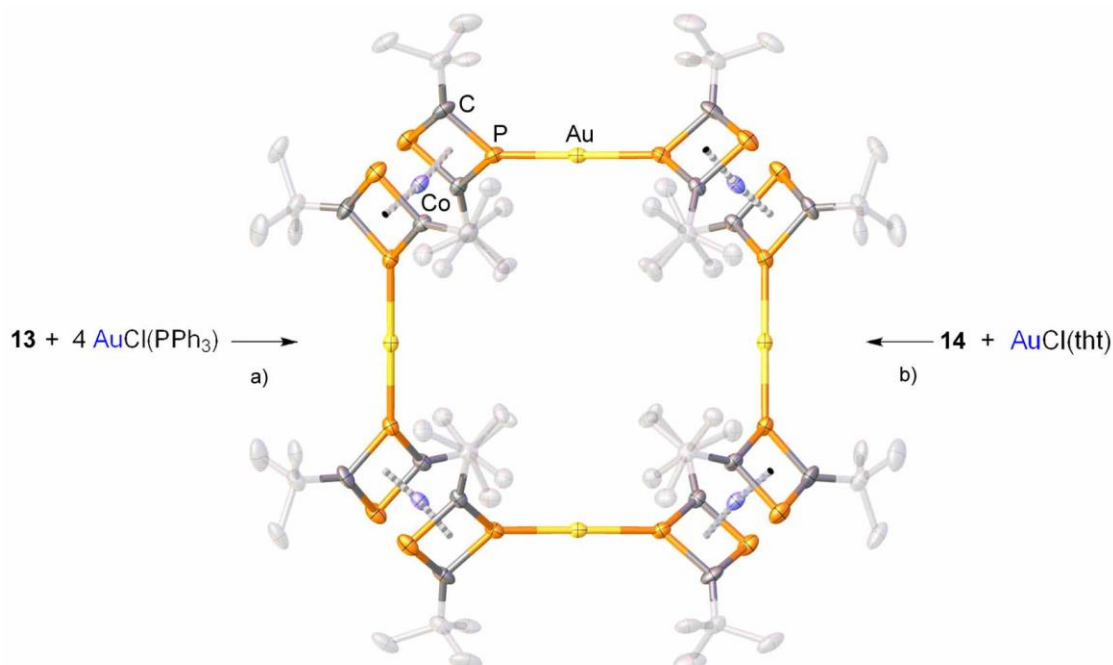
*Chapter 5. Formation of an Octanuclear Molecular Square by Self-Assembly of Phospha-Organometallic Building Block*<sup>5</sup>

This part of the thesis describes the rational synthesis of a molecular square by using bis(diphosphacyclobutadiene) sandwich anions as phospha-organometallic building blocks. Initial attempts to prepare the octanuclear gold(I) complex [Au{Co(P<sub>2</sub>C<sub>2</sub>*t*Bu<sub>2</sub>)<sub>2</sub>}]<sub>4</sub> (**12**) by a procedure analogous to the salt metathesis reactions described previously were not successful. The “ate complex” [Au(PPh<sub>3</sub>)<sub>4</sub>][Au{Co(P<sub>2</sub>C<sub>2</sub>*t*Bu<sub>2</sub>)<sub>2</sub>}]<sub>2</sub> (**13**) was isolated instead (Scheme 5a). In order to facilitate the transmetalation reaction, the novel thallium(I) compound [Tl(thf)<sub>2</sub>{Co(P<sub>2</sub>C<sub>2</sub>*t*Bu<sub>2</sub>)<sub>2</sub>}] (**14**) was prepared by reacting the potassium salt [K(thf)<sub>2</sub>{Co(P<sub>2</sub>C<sub>2</sub>*t*Bu<sub>2</sub>)<sub>2</sub>}] (**5c**) with TIPF<sub>6</sub> (Scheme 5b). Complex **14** represents the first structurally characterized complex of a [Co(P<sub>2</sub>C<sub>2</sub>R<sub>2</sub>)<sub>2</sub>]<sup>−</sup> sandwich anion with a p-block metal. Single crystal X-ray diffraction of **14** revealed a polymeric arrangement in the solid state, in which the Tl<sup>+</sup> cations are coordinated by two THF molecules and three phosphorus atoms from two different [Co(P<sub>2</sub>C<sub>2</sub>*t*Bu<sub>2</sub>)<sub>2</sub>]<sup>−</sup> sandwich units.



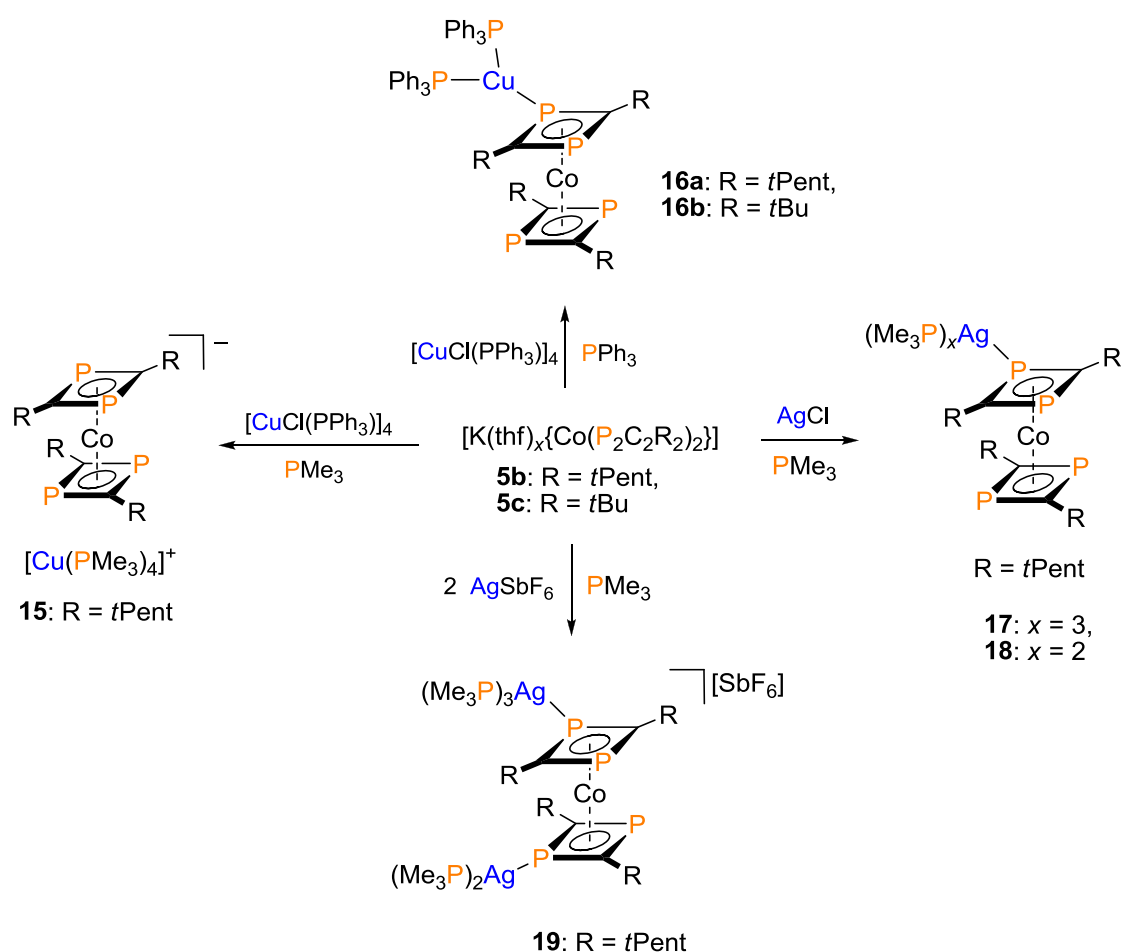
**Scheme 5.** Synthesis of the golden "ate complex" **13** and of the novel thallium salt **14**.

The synthesis of complex **12** directly through salt metathesis of the thallium complex **14** with  $\text{AuCl}(\text{tht})$  was successful and gave the target compound in 20% yield (Scheme 6a). An additional approach employed the new "ate complex"  $[\text{Au}(\text{PPh}_3)_4][\text{Au}\{\text{Co}(\text{P}_2\text{C}_2\text{tBu}_2)_2\}_2]$  (**13**) as a precursor (Scheme 6b). Compound **12** was fully characterized by X-ray crystallography, multinuclear NMR spectroscopy in solution and elemental analysis. The molecular structure of **12** shows four  $\text{Au}\{\text{Co}(\text{P}_2\text{C}_2\text{tBu}_2)_2\}$  fragments in a cyclic arrangement. Each  $\text{Au}^+$  cation is coordinated by two phosphorus atoms from different  $[\text{Co}(\text{P}_2\text{C}_2\text{tBu}_2)_2]^-$  sandwich unit in a linear fashion. The NMR spectra of **12** indicate that the complex stays intact in solution.



**Scheme 6.** Preparation of the octanuclear molecular square **12**.

In extension of the investigations on gold(I) and silver(I) complexes outlined in chapters 4 and 5, the coordination behavior of the  $[\text{Co}(\text{P}_2\text{C}_2\text{R}_2)_2]^-$  anions ( $\text{R} = t\text{Bu}, t\text{Pent}$ ) towards copper(I) and silver(I) cations was investigated. Using an analogous approach as illustrated for gold(I) compounds, complexes **15–19** were prepared by salt metathesis of  $[\text{K}(\text{thf})_3\{\text{Co}(\text{P}_2\text{C}_2t\text{Pent}_2)_2\}]$  (**5b**), and  $[\text{K}(\text{thf})_2\{\text{Co}(\text{P}_2\text{C}_2t\text{Bu}_2)_2\}]$  (**5c**) with copper(I) and silver(I) halides in the presence of the tertiary phosphanes  $\text{PMe}_3$  or  $\text{PPh}_3$ . Different types of complexes were isolated depending on the used phosphane ( $\text{PMe}_3$  or  $\text{PPh}_3$ ) and the reaction stoichiometry. The synthesis of  $[\text{Cu}(\text{PMe}_3)_4][\text{Co}(\text{P}_2\text{C}_2t\text{Pent}_2)_2]$  (**15**),  $[\text{Cu}(\text{PPh}_3)_2\{\text{Co}(\text{P}_2\text{C}_2\text{R}_2)_2\}]$  (**16a**:  $\text{R} = t\text{Pent}$ ; **16b**:  $\text{R} = t\text{Bu}$ ),  $[\text{Ag}(\text{PMe}_3)_x\{\text{Co}(\text{P}_2\text{C}_2t\text{Pent}_2)_2\}]$  (**17**:  $x = 2$ ; **18**:  $x = 3$ ), and  $[\text{Ag}_2(\text{PMe}_3)_5\{\text{Co}(\text{P}_2\text{C}_2t\text{Pent}_2)_2\}]\text{SbF}_6$  (**19**) is shown in Scheme 7.



**Scheme 7.** Synthesis of the  $[\text{Cu}(\text{PMe}_3)_4]^+$  salt **15** and the coordination complexes **16–19**.

The identity of complexes **15–19** was determined by X-ray crystallography and complementary solid-state NMR spectroscopic investigations. The structures of the coordination complexes **16–19** feature three-coordinate and four-coordinate copper(I) or silver(I) cations that are bound to one phosphorus atom of the  $[\text{Co}(\text{P}_2\text{C}_2\text{R}_2)_2]^-$  sandwich unit and to two or three phosphane ligands. Compound **15** shows an ionic structure that contains the rare, tetra-coordinate  $[\text{Cu}(\text{PMe}_3)_4]^+$  cation<sup>4,8</sup>. Analogous to the gold(I)

complexes  $[\text{Au}(\text{PMe}_3)_2\{\text{Co}(\text{P}_2\text{C}_2t\text{Pent}_2)_2\}]$  (**8**) and  $[\text{Au}(\text{PMe}_3)_4][\text{Au}\{\text{Co}(\text{P}_2\text{C}_2\text{Ad}_2)_2\}]$  (**10**) (chapter 4), the copper(I) and silver(I) complexes **16–19** show complex and temperature-dependent NMR spectra in solution which indicate a partial decoordination of the cationic copper phosphane or silver phosphane moieties from the anion.

In conclusion of chapters 4–6, we have shown that bis(diphosphacyclobutadiene) sandwich anions  $[\text{Co}(\text{P}_2\text{C}_2\text{R}_2)_2]^-$  show a versatile coordination chemistry towards coinage metals. Considering these initial investigations, it seems likely that a much more extensive coordination chemistry can be unraveled for these anions. The synthesis of complexes with a wider range of transition metals is an important aspect for future work. The solid-state molecular structure of the potassium salt  $[\text{K}(\text{thf})_4\{\text{Co}(\text{P}_2\text{C}_2\text{Ad}_2)_2\}]$  (**5a**, chapter 4) suggests, that the preparation of  $\pi$  complexes might be feasible. The preparation of coordination polymers containing the paramagnetic  $[\text{Fe}(\text{P}_2\text{C}_2\text{R}_2)_2]^-$  anions might be of interest in view of the potentially cooperative magnetic interactions between the paramagnetic iron centers. Chapter 5 highlights the ability of bis(diphosphacyclobutadiene) anions to function as phospho-organometallic building blocks. In view of the interesting electronic and magnetic properties, that can be expected for much molecular squares the synthesis of further examples will be an important aspect for future work. Especially the “Tl(I) route” appears promising for this purpose.

## References

- 1 J. Malberg, E. Lupton, E.-M. Schnöckelborg, B. de Bruin, J. Sutter, K. Meyer, F. Hartl, R. Wolf, *Organometallics* **2013**, published online on 10/09/2013. DOI: 10.1021/om4005862.
- 2 Unpublished results.
- 3 J. Malberg, T. Wiegand, H. Eckert, M. Bodensteiner, R. Wolf, *Chem. Eur. J.* **2013**, *19*, 2356.
- 4 J. Malberg, T. Wiegand, H. Eckert, M. Bodensteiner, R. Wolf, *Eur. J. Inorg. Chem.* **2013**, accepted for publication. DOI: 10.1002/ejic.201301173.
- 5 J. Malberg, M. Bodensteiner, D. Paul, T. Wiegand, H. Eckert, R. Wolf, manuscript in preparation.
- 6 R. Wolf, A. W. Ehlers, M. M. Khusniyarov, F. Hartl, B. de Bruin, G. J. Long, F. Grandjean, F. M. Schappacher, R. Pöttgen, J. C. Slootweg, M. Lutz, A. L. Spek, K. Lammertsma, *Chem. Eur. J.* **2010**, *16*, 14322.
- 7 H. Schmidbaur, R. Franke, *Chem. Ber.* **1972**, *105*, 2985.
- 8 J. R. Black, W. Levason, M. D. Spicer, M. Webster, *J. Chem. Soc., Dalton Trans.* **1993**, *20*, 3129.



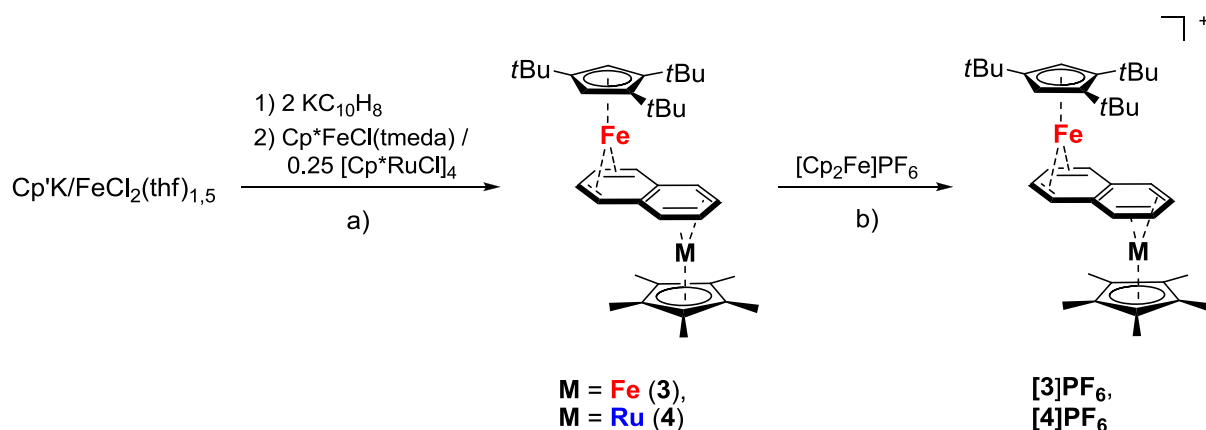
## 8 Zusammenfassung

Die vorliegende Dissertation befasst sich mit der Synthese und Charakterisierung von oligonuklearen Übergangsmetallkomplexen mit zwei verschiedenen Brückenliganden: dem Kohlenwasserstoff Naphthalin ( $C_{10}H_8$ ) und 1,3-Diphosphacyclobutadien ( $P_2C_2R_2$ ), dem Phosphor-Analogon des Cyclobutadiens.

Kapitel 1 gibt eine kurze Einleitung in die bisher bekannte Chemie von Polyaren- und Naphthalin-verbrückten Komplexen sowie von Diphosphacyclobutadien-Metallkomplexen. Kapitel 2 beschreibt ausführlich die Darstellung und Aufklärung der elektronischen Struktur neuer asymmetrischer, Naphthalin-verbrückter Eisen-Eisen und Eisen-Ruthenium-Komplexe. In Kapitel 3 werden die ersten Untersuchungen zum Reaktionsverhalten von Bis(diphosphacyclobutadien)-Sandwichanionen gegenüber Siliciumkationen als Elektrophilen vorgestellt. Die Kapitel 3–6 widmen sich den ersten Untersuchungen zum Koordinationsverhalten der genannten Anionen

*Kapitel 2. Synthese und elektronische Struktur von unsymmetrischen, Naphthalin-verbrückten Sandwichkomplexen  $[Cp'Fe(\mu-C_{10}H_8)MCp^*]^x$  ( $x = 0, +1$ ;  $M = Fe, Ru$ ;  $Cp' = \eta^5-C_5H_2-1,2,4-tBu_3$ ;  $Cp^* = \eta^5-C_5Me_5$ )<sup>1</sup>*

Ein wichtiges Ziel dieser Arbeit war es zu untersuchen, inwiefern sich unterschiedliche Metallzentren und der Cyclopentadienylligand auf die Struktur, spektroskopische Eigenschaften und elektronische Natur von bimetallic Naphthalin-verbrückten Komplexen auswirkt. Zu diesem Zweck wurden die unsymmetrischen Komplexe  $[Cp'Fe(\mu-C_{10}H_8)MCp^*]^x$  ( $M = Fe, Ru$ ;  $x = 0, 1$ ;  $Cp' = 1,2,4$ -Tri-*tert*-butylcyclopentadienyl) synthetisiert, umfassend charakterisiert und ihre Eigenschaften mit denen der symmetrisch-substituierten Komplexe  $[Cp^*Fe(\mu-C_{10}H_8)MCp^*]$  (**1**:  $M = Fe$ ; **2**:  $M = Ru$ ) verglichen. Die Darstellung der Neutralkomplexe  $[Cp'Fe(\mu-C_{10}H_8)FeCp^*]$  (**3**) und  $[Cp'Fe(\mu-C_{10}H_8)RuCp^*]$  (**4**) erfolgte durch eine einstufige Synthese entsprechend Schema 1a. Die kationischen Komplexe  $[Cp'Fe(\mu-C_{10}H_8)FeCp^*]PF_6$  (**[3]PF<sub>6</sub>**) und  $[Cp'Fe(\mu-C_{10}H_8)RuCp^*]PF_6$  (**[4]PF<sub>6</sub>**) wurden durch Oxidation von **3** und **4** mit einem Äquivalent Ferroceniumhexafluorophosphat erhalten (Schema 1b).



**Schema 1.** Synthese der unsymmetrischen Eisen-Eisen und Eisen-Ruthenium-Komplexe **3**, **3<sup>+</sup>**, **4**, and **4<sup>+</sup>**.

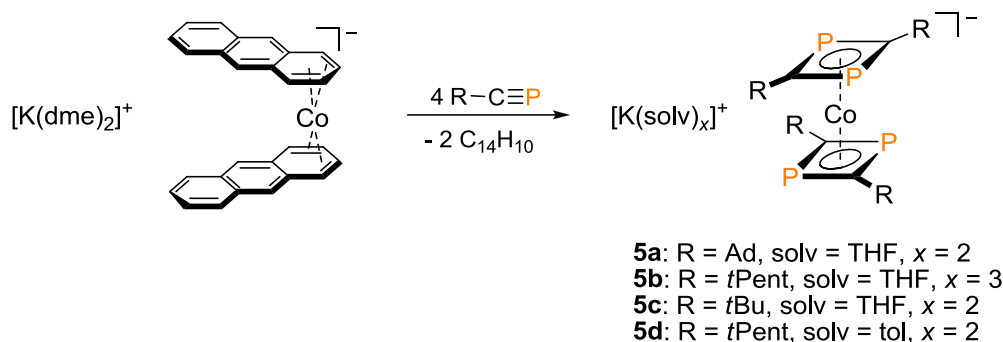
Der Vergleich der strukturellen, spektroskopischen und elektrochemischen Daten der unsymmetrischen Komplexe **3**, **3**<sup>+</sup>, **4** und **4**<sup>+</sup> mit denen der symmetrisch-substituierten Komplexe **1** und **2** ergab, dass der Austausch eines Cp\*-Liganden durch Cp' bzw. von Eisen durch Ruthenium nur einen geringen Effekt auf die elektronische Struktur der untersuchten Komplexe ausübt. So bleibt die Zusammensetzung und Form der Grenzorbitale nahezu unbeeinflusst. Daher zeigen die Komplexe **1–4** qualitativ ähnliche elektronische Absorptionsspektren. DFT Rechnungen zeigen, dass die redoxaktiven Orbitale große Beiträge vom Naphthalin-Brückenliganden und von der Cp'Fe-Einheit besitzen. Daher sind die Redoxpotentiale der unsymmetrisch substituierten Komplexe **3** und **4** im Vergleich zu denen der symmetrischen Komplexe zu geringfügig positiveren Werten verschoben, während sich der Austausch des Eisens durch Ruthenium in der Cp\*M Einheit nur wenig bemerkbar macht. Die <sup>57</sup>Fe-Mössbauer-Spektren der untersuchten Komplexe (**1–4**) zeigen sehr ähnliche Isomerieverschiebungen, die vergleichbar mit denen verwandter Polyaren- und Ferrocenkomplexe sind. Die Kationen [**3**]PF<sub>6</sub> und [**4**]PF<sub>6</sub> zeigen hingegen wesentlich geringere Quadrupolaufspaltungen als die neutralen Komplexe **3** und **4**. Dies lässt sich auf die gemischtvalente Natur der Kationen zurückführen.

Für zukünftige Arbeiten stellt die Synthese verwandter homo- und heteronuklearer Naphthalin- oder Anthracen verbrückter Komplexe ein wichtiges Ziel dar. Diese Komplexe sind aufgrund ihrer electrochemischen, strukturellen und spektroskopischen Eigenschaften interessant. Die Aufklärung dieser Eigenschaften ist daher ein weiterer wichtiger Aspekt für zukünftige Untersuchungen.

### *Kapitel 3. Reaktionen der homoleptischen Sandwichanionen [Co(P<sub>2</sub>C<sub>2</sub>R<sub>2</sub>)<sub>2</sub>]<sup>−</sup> mit Me<sub>3</sub>SiCl: Eine einfache Methode zur Herstellung silylierter Phosphaorganischer Verbindungen<sup>2</sup>*

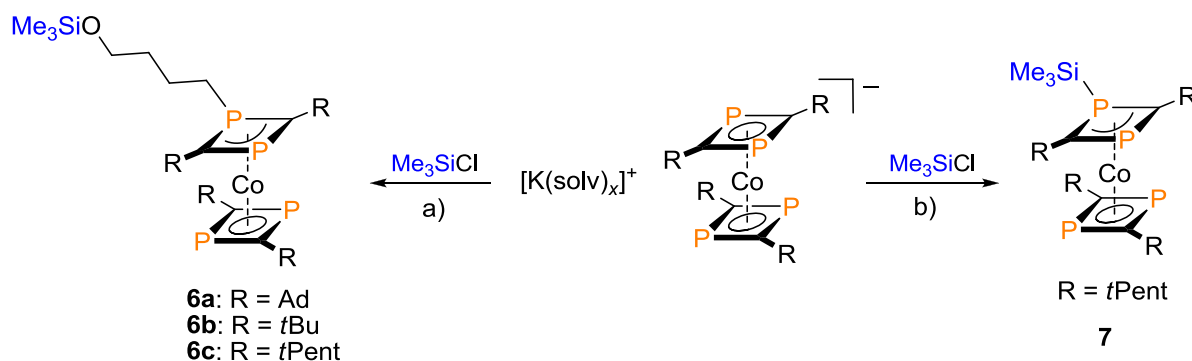
Ein wesentliches Ziel dieser Arbeit war es, das Koordinationsverhalten anionischer Bis(diphosphacyclobutadien)-Sandwichkomplexe [Co(P<sub>2</sub>C<sub>2</sub>R<sub>2</sub>)<sub>2</sub>]<sup>−</sup> zu untersuchen.<sup>3–5</sup> Die freien Elektronenpaare an den vier Phosphoratomen sollten in der Lage sein, weitere Metallatome zu koordinieren und versprechen daher eine reichhaltige Koordinationschemie dieser Komplexe.

Der erste Schritt bestand in der Synthese geeigneter Ausgangsmaterialien für diese Studien. Basierend auf Vorarbeiten in unserer Arbeitsgruppe stellten wir die neuen Kaliumsalze [K(thf)<sub>4</sub>{Co(P<sub>2</sub>C<sub>2</sub>Ad<sub>2</sub>)<sub>2</sub>}] (**5a**), [K(thf)<sub>3</sub>{Co(P<sub>2</sub>C<sub>2</sub>*t*Pent<sub>2</sub>)<sub>2</sub>}] (**5b**), [K(thf)<sub>2</sub>{Co(P<sub>2</sub>C<sub>2</sub>*t*Bu<sub>2</sub>)<sub>2</sub>}] (**5c**) und [K(tol)<sub>2</sub>{Co(P<sub>2</sub>C<sub>2</sub>*t*Pent<sub>2</sub>)<sub>2</sub>}] (**5d**) durch die Umsetzung von [Co(C<sub>14</sub>H<sub>10</sub>)<sub>2</sub>]<sup>−</sup> mit Phosphaalkinen her (Schema 2). Im Gegensatz zu den bereits beschriebenen Kaliumsalzen [K([18]Krone-6)(thf)<sub>2</sub>][Co(P<sub>2</sub>C<sub>2</sub>R<sub>2</sub>)<sub>2</sub>] (R = *t*Bu, Ad),<sup>6</sup> enthalten die neuen Salze **5a–c** keinen Kronenether, welcher sich bei der anschließenden Salzmetathese oder bei der Isolierung reiner Produkte als störend erweisen könnte.



**Schema 2.** Synthese der neuen Kaliumsalze **5a–d**.

Die neuen Kaliumsalze **5a–d** wurden hinsichtlich ihres Reaktionsverhaltens gegenüber  $\text{Me}_3\text{SiCl}$  untersucht. Die Ergebnisse dieser Untersuchungen sind in Schema 3 zusammengefasst. Unerwarteterweise bildeten sich die Komplexe  $[\text{Co}(\eta^4\text{-P}_2\text{C}_2\text{R}_2(\text{CH}_2)_4\text{OSiMe}_3)(\eta^4\text{-P}_2\text{C}_2\text{R}_2)_2]$  (**6a–c**, R = Ad, *t*Bu, *t*Pent) durch die Spaltung einer C–O Bindung eines THF-Moleküles, wenn die Reaktionen in Gegenwart von THF durchgeführt wurden. Auch bei den Umsetzungen der THF-haltigen Salze **5a–c** in Toluol wurde die Bildung von **6a–c** in hohen Ausbeuten beobachtet. Daher wurde das THF-freie Kaliumsalz  $[\text{K}(\text{tol})_2\{\text{Co}(\text{P}_2\text{C}_2\text{tPent}_2)_2\}]$  (**5d**, Schema 2) durch Umkristallisation des THF-haltigen Salzes **5c** in siedendem Toluol hergestellt. Die Umsetzung des neuen Toluol-haltigen Salzes **5d** mit  $\text{Me}_3\text{SiCl}$  lieferte, wie in Schema 3b gezeigt, den gewünschten Komplex  $[\text{Co}(\eta^4\text{-P}_2\text{C}_2\text{tPent}_2\text{SiMe}_3)(\eta^4\text{-P}_2\text{C}_2\text{tPent}_2)_2]$  (**7**), in dem die  $\text{SiMe}_3$ -Gruppe direkt an ein Phosphoratom eines  $\text{P}_2\text{C}_2\text{tPent}_2$ -Liganden gebunden ist. Der ausgesprochen reaktive Charakter der Phosphor-Silicium-Einfachbindung in **7** konnte in NMR Versuchen demonstriert werden. Komplex **7** reagiert mit THF, 2-Methyltetrahydrofuran und 1,4-Dioxan unter Spaltung einer C–O Einfachbindung und Bildung einer neuen P–C Bindung, woraus Komplexe vom Typ **6c** resultieren.



**Schema 3.** Synthese der THF-Spaltungsprodukte **6a–c** und des silylierten Komplexes **7**. a) Kaliumsalze **5a–c**, solv = THF, b) Kaliumsalz **5d**, solv = Toluol.

Zusammenfassend konnte in diesen vorläufigen Studien gezeigt werden, dass homoleptische Bis(di-phosphacyclobutadien)-Sandwichanionen  $[\text{Co}(\text{P}_2\text{C}_2\text{R}_2)_2]^-$  eine bemerkenswerte Reaktivität gegenüber Siliciumelektrophilen aufweisen. Der durch die Umsetzung des Toluol-haltigen Salzes **5d** mit  $\text{Me}_3\text{SiCl}$  erhaltene Komplex **7** enthält eine ausgesprochen reaktive Phosphor-Silicium Einfachbindung. Der

Komplex **7** stellt daher ein potenzielles Ausgangsmaterial zur Herstellung neuer phosphaoorganischer Verbindungen dar. Die Bildung neuer Phosphor-Element Bindungen sollte durch die Umsetzung von **7** mit Hauptgruppen- und Übergangsmetallhalogeniden möglich sein und zu einer Vielzahl neuartiger Verbindungen führen. Ein weiteres Ziel für zukünftige Arbeiten stellt die Untersuchung von Reaktionen der  $[\text{Co}(\text{P}_2\text{C}_2\text{R}_2)_2]^-$ -Anionen gegenüber Germanium- und Zinnelektrophilen dar. Durch ähnliche Salzmethathesen, wie in Kapitel 3 beschrieben, sollte der Zugang zu verwandten Verbindungen mit Phosphor-Germanium bzw. Phosphor-Zinn-Bindungen möglich sein.

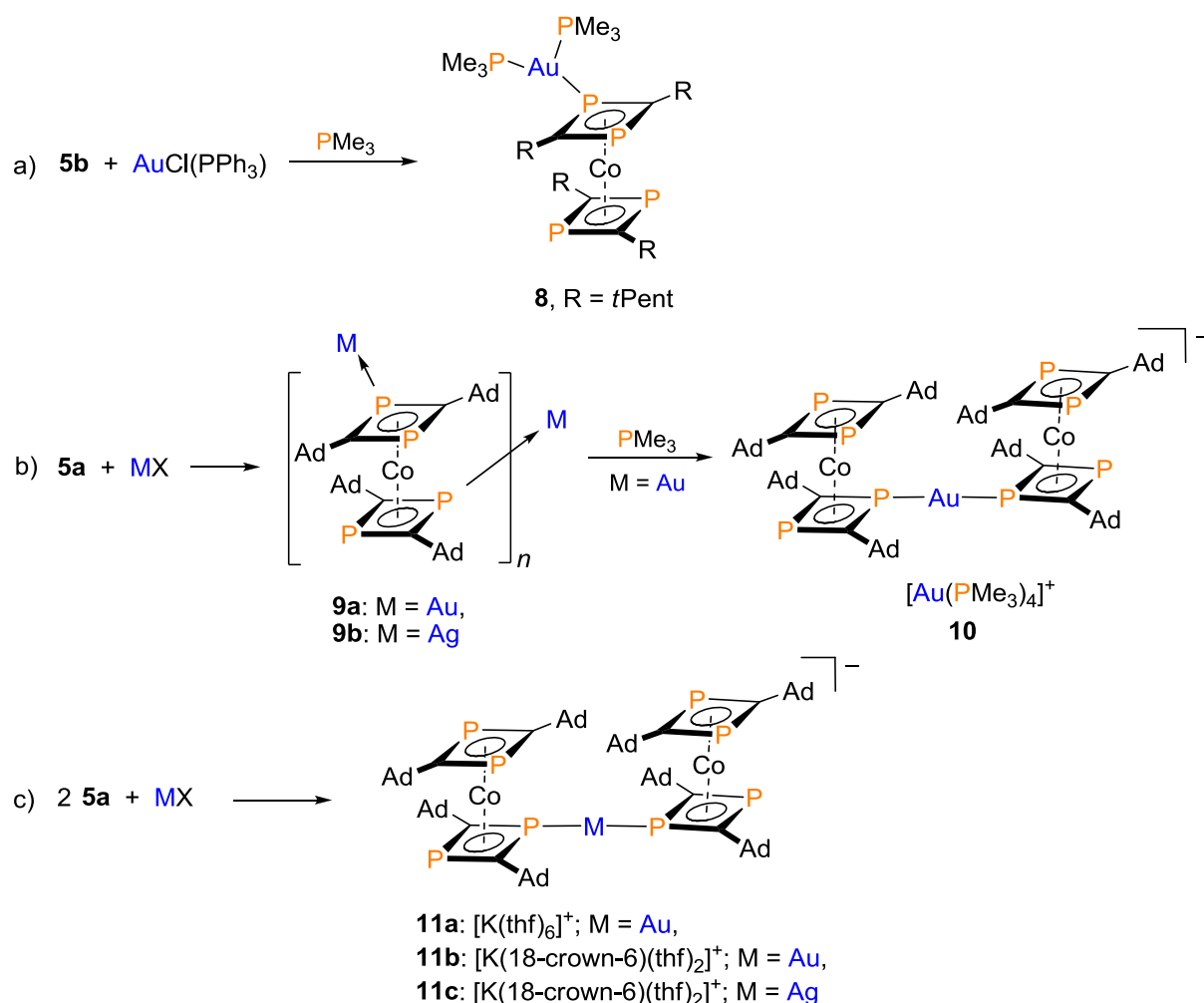
#### Kapitel 4. Gold(I)- und Silber(I)- Komplexe von Diphosphacyclobutadien Cobaltat-Anionen<sup>3,4</sup>

Dieses Kapitel beschäftigt sich mit Studien zum Reaktionsverhalten der Kaliumsalze  $[\text{K}(\text{thf})_4\{\text{Co}(\text{P}_2\text{C}_2\text{Ad}_2)_2\}]$  (**5a**),  $[\text{K}(\text{thf})_3\{\text{Co}(\text{P}_2\text{C}_2t\text{Pent}_2)_2\}]$  (**5b**) und  $[\text{K}(\text{thf})_2\{\text{Co}(\text{P}_2\text{C}_2t\text{Bu}_2)_2\}]$  (**5c**) gegenüber Münzmetallhalogeniden. Die bei diesen Untersuchungen erhaltenen Kupfer(I)-, Silber(I)- und Gold(I)-Komplexe stellen die ersten Übergangsmetallkomplexe solcher Sandwichanionen dar.

Die nachfolgenden Schemata 4–7 fassen die Ergebnisse der Untersuchungen zusammen. Drei Arten von Verbindungen wurden bei den Umsetzungen von **5a** und **5b** mit Gold(I)- und Silber(I)-Salzen erhalten: Das Addukt  $[\text{Au}(\text{PMe}_3)_2\{\text{Co}(\text{P}_2\text{C}_2t\text{Pent}_2)_2\}]$  (**8**), in welchem eine  $[\text{Au}(\text{PMe}_3)_2]^+$  Einheit an das  $[\text{Co}(\text{P}_2\text{C}_2t\text{Pent}_2)_2]^-$ -Anion koordiniert, wurde bei der Reaktion von  $[\text{K}(\text{thf})_3\{\text{Co}(\text{P}_2\text{C}_2t\text{Pent}_2)_2\}]$  (**5b**) mit  $\text{AuCl}(\text{PPh}_3)$  in Gegenwart von  $\text{PMe}_3$  erhalten (Schema 4a). Im Gegensatz dazu, lieferte die Reaktion des sterisch wesentlich anspruchsvolleren Kaliumsalzes  $[\text{K}(\text{thf})_4\{\text{Co}(\text{P}_2\text{C}_2\text{Ad}_2)_2\}]$  (**5a**) mit  $\text{AuCl}(\text{tht})$  oder  $\text{AgSbF}_6$  die Koordinationspolymere  $[\text{M}\{\text{Co}(\text{P}_2\text{C}_2\text{Ad}_2)_2\}]_n$  (**9**:  $\text{M} = \text{Au}$ ,  $\text{M} = \text{Ag}$ ; Schema 4b). Die Zugabe von  $\text{PMe}_3$  zur Reaktionslösung von **5a** und Gold(I)-chlorid führte zum Komplex  $[\text{Au}(\text{PMe}_3)_4][\text{Au}\{\text{Co}(\text{P}_2\text{C}_2\text{Ad}_2)_2\}]$  (**10**, Schema 4b). Komplex **10** zeigt eine ionenseparierte Struktur im Festkörper, bestehend aus dem bisher selten beobachteten  $[\text{Au}(\text{PMe}_3)_4]^+$ -Kation und dem neuen „At-Komplex“  $[\text{Au}\{\text{Co}(\text{P}_2\text{C}_2\text{Ad}_2)_2\}_2]^-$ .<sup>3,7</sup> Die verwandten Komplexe **11** ( $\text{M} = \text{Au}$ ,  $\text{Ag}$ ), die ebenfalls „At-Komplexe“ des Typs  $[\text{M}\{\text{Co}(\text{P}_2\text{C}_2\text{Ad}_2)_2\}_2]^-$  enthalten, wurden bei der Umsetzungen von zwei Äquivalenten Kaliumsalz **5a** mit  $\text{AuCl}(\text{tht})$  bzw.  $\text{AgSbF}_6$  isoliert (Schema 4c).

Die neuen Komplexe **8–11** wurden durch Röntgenstrukturanalysen, sowie durch NMR-Spektroskopie in Lösung und Festkörper eingehend untersucht. Die Festkörper-NMR-Daten der Verbindungen **8**, **10** und **11** bestätigen die Struktur im Einkristall. Die mikrokristallinen Verbindungen  $[\text{M}\{\text{Co}(\text{P}_2\text{C}_2\text{Ad}_2)_2\}]_n$  (**9a**:  $\text{M} = \text{Au}$ , **9b**:  $\text{M} = \text{Ag}$ ) konnten hingegen nicht durch Röntgenstrukturanalysen und NMR-Spektroskopie in Lösung charakterisiert werden. Die Festkörper-NMR-Ergebnisse zeigen, dass diese Verbindungen als Koordinationspolymere mit einer „Zick-Zack“ Struktur vorliegen. Das Verhalten von  $[\text{Au}(\text{PMe}_3)_2\{\text{Co}(\text{P}_2\text{C}_2t\text{Pent}_2)_2\}]$  (**8**) und der neuen „At-Komplexe“  $[\text{Au}(\text{PMe}_3)_4][\text{Au}\{\text{Co}(\text{P}_2\text{C}_2\text{Ad}_2)_2\}]$  (**10**) und  $[\text{K}(\text{thf})_6][\text{Au}\{\text{Co}(\text{P}_2\text{C}_2\text{Ad}_2)_2\}]$  (**11a**) in Lösung wurde durch NMR-Untersuchungen aufgeklärt. Die NMR-Spektren von **11a** stimmen gut mit der Festkörperstruktur überein, was auf ein intaktes  $[\text{Au}\{\text{Co}(\text{P}_2\text{C}_2\text{Ad}_2)_2\}_2]^-$ -Anion in Lösung hindeutet. Im Gegensatz dazu zeigen die NMR-Spektren der Komplexe **8** und **10** ein wesentlich komplexeres, temperaturabhängiges Verhalten. Dabei wird in Lösung

ein Gleichgewicht zwischen mehreren Spezies beobachtet, was darauf hin deutet, dass die Au–P Bindungen in den Komplexen  $[\text{Au}(\text{PMe}_3)_2\{\text{Co}(\text{P}_2\text{C}_2t\text{Pent}_2)_2\}]$  (**8**) und  $[\text{Au}(\text{PMe}_3)_4]\text{[Au}\{\text{Co}(\text{P}_2\text{C}_2\text{Ad}_2)_2\}]$  (**10**) labil sind.

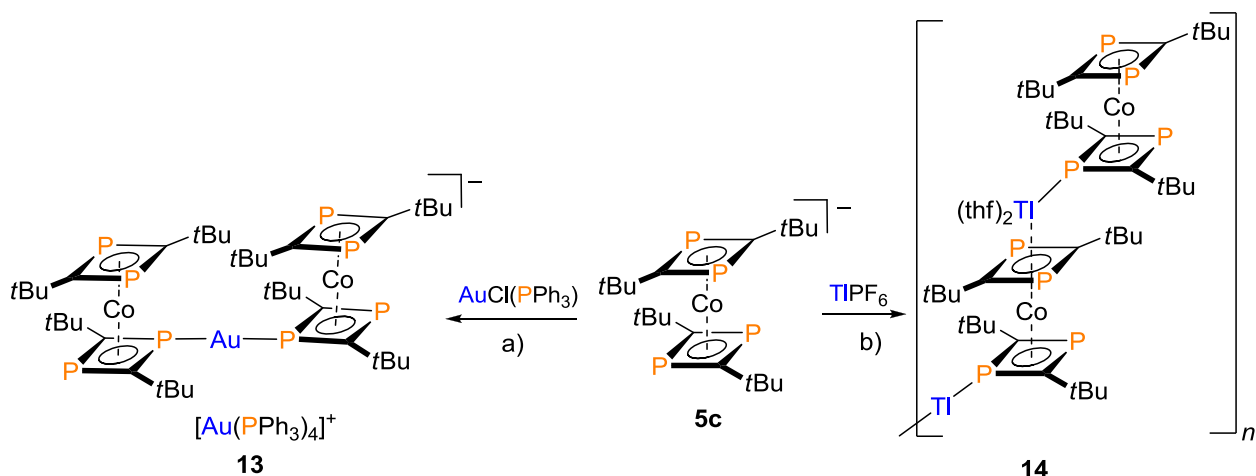


**Schema 4.** Synthese der Komplexe **8–11**.

#### Kapitel 5. Bildung eines achtkernigen, molekularen Quadrates durch Selbstorganisation von Phosphaorganometallischen Synthesebausteinen<sup>5</sup>

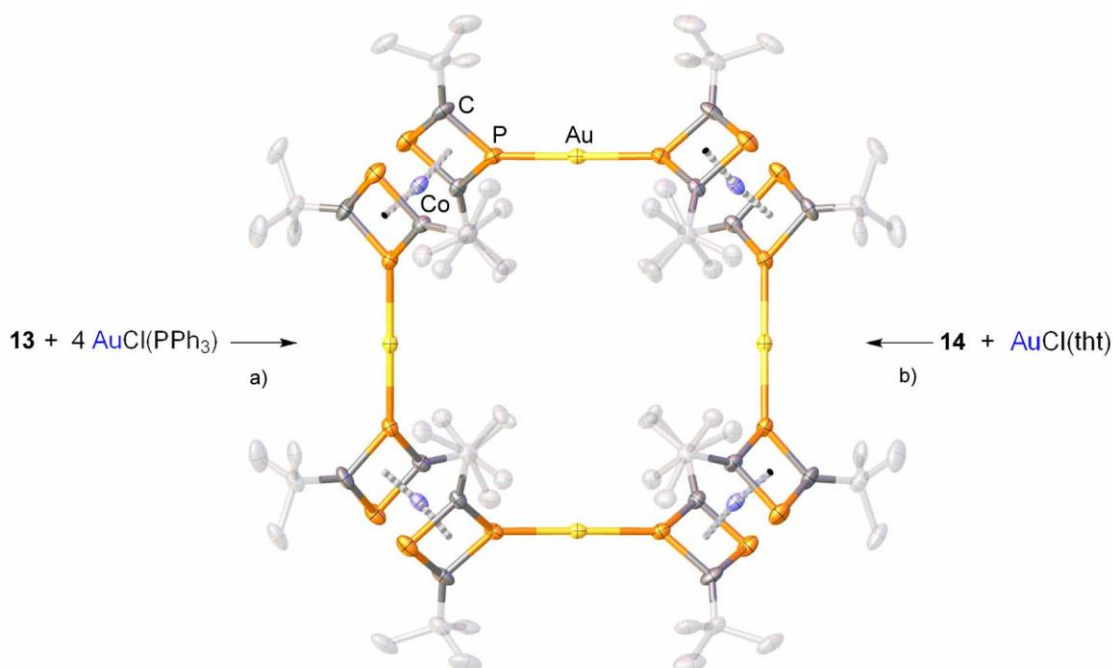
Dieser Teil der vorliegenden Arbeit beschreibt die rationale Synthese eines molekularen Quadrates unter Verwendung der  $[\text{Co}(\text{P}_2\text{C}_2\text{R}_2)_2]^-$ -Anionen als Synthesebausteine. Anfängliche Versuche, den achtkernigen Gold(I)-Komplex  $[\text{Au}\{\text{Co}(\text{P}_2\text{C}_2t\text{Bu}_2)_2\}]_4$  (**12**) durch eine gezielte Salzmethatase analog zu der bereits in Kapitel 4 beschriebenen Methode herzustellen, waren nicht erfolgreich. Stattdessen wurde der neue „At-Komplex“  $[\text{Au}(\text{PPh}_3)_4][\text{Au}\{\text{Co}(\text{P}_2\text{C}_2t\text{Bu}_2)_2\}]$  (**13**) gebildet (Schema 5a). Um die Transmetallierung zu erleichtern, synthetisierten wir daraufhin den neuartigen Thallium(I)-Komplex  $[\text{Tl}(\text{thf})_2\{\text{Co}(\text{P}_2\text{C}_2t\text{Bu}_2)_2\}]$  (**14**) durch Umsetzen des Kaliumsalzes  $[\text{K}(\text{thf})_2\{\text{Co}(\text{P}_2\text{C}_2t\text{Bu}_2)_2\}]$  (**5c**) mit  $\text{TlPF}_6$  (Schema 5b). Komplex **14** ist der erste strukturell charakterisierte Übergangsmetallkomplex eines  $[\text{Co}(\text{P}_2\text{C}_2\text{R}_2)_2]^-$ -Anions mit einem p-Block-Metall. Eine Einkristallstrukturanalyse zeigte, dass **14** eine

polymere Struktur in Festkörper aufweist, in der die  $\text{TI}^+$  Kationen von zwei THF Molekülen und durch drei Phosphoratome von zwei verschiedenen  $[\text{Co}(\text{P}_2\text{C}_2\text{tBu}_2)_2]^-$ -Sandwicheinheiten koordiniert sind.



**Schema 5.** Synthese des "Gold-At-Komplexes" **13** und des neuartigen Thalliumsalzes **14**.

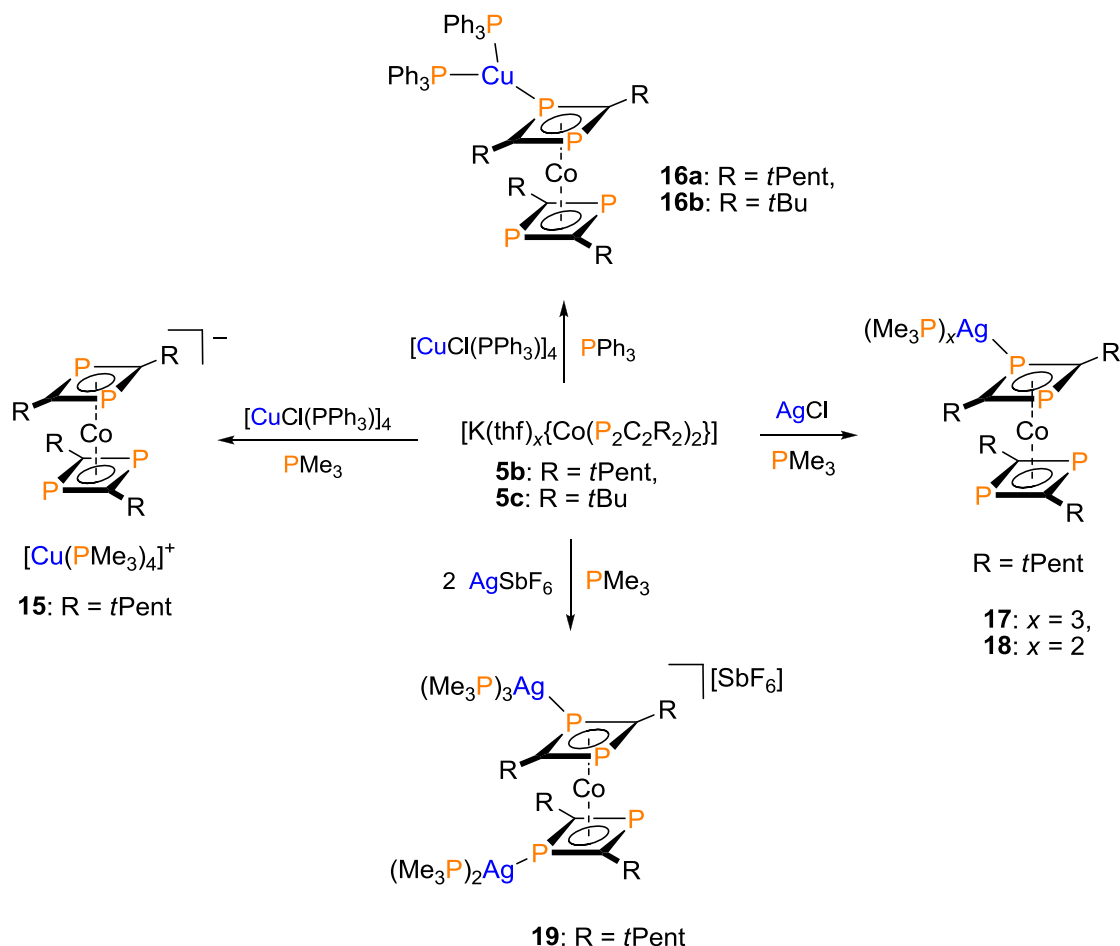
Ausgehend von dem neuen Thalliumsalz **14** ist der gewünschte Komplex gezielt durch eine Salzmetathese in 20% Ausbeute zugänglich (Schema 6a). Zusätzlich konnte der neue „At-Komplex“  $[\text{Au}(\text{PPh}_3)_4][\text{Au}\{\text{Co}(\text{P}_2\text{C}_2\text{tBu}_2)_2\}_2]$  (**13**) ebenfalls als Ausgangsmaterial für die Synthese verwendet werden (Schema 6b). Komplex **12** wurde vollständig durch Röntgenstrukturanalyse, NMR-Spektroskopie und Elementaranalyse charakterisiert. Die Festkörperstruktur von **12** besteht aus einem Makrozyklus von vier  $\text{Au}\{\text{Co}(\text{P}_2\text{C}_2\text{tBu}_2)_2\}$ -Einheiten. Jedes  $\text{Au}^+$ -Kation ist linear durch je ein Phosphoratom von zwei  $[\text{Co}(\text{P}_2\text{C}_2\text{tBu}_2)_2]^-$ -Sandwicheinheiten koordiniert. Die NMR-Spektren von **12** zeigen, dass dieser in Lösung stabil ist und intakt bleibt.



**Schema 6.** Darstellung des achtkernigen, molekularen Quadrates **12**.

Kapitel 6. Kupfer(I)- und Silber(I)-Komplexe von Diphosphacyclobutadien Sandwichanionen: Synthese, Kristallstrukturen und NMR-spektroskopische Charakterisierung in Lösung und im Festkörper.<sup>4</sup>

In Erweiterung der in den Kapiteln 4 und 5 vorgestellten Untersuchungen an Gold(I)- und Silber(I)-Komplexen wurde das Koordinationsverhalten der  $[\text{Co}(\text{P}_2\text{C}_2\text{R}_2)_2]^-$ -Anionen gegenüber Kupfer(I)- und Silber(I)-Kationen analysiert. Die neuen Komplexe **15–19** wurden, wie die zuvor beschriebenen Gold(I)-Komplexe, durch die Umsetzung der Kaliumsalze  $[\text{K}(\text{thf})_3\{\text{Co}(\text{P}_2\text{C}_2t\text{Pent}_2)_2\}]$  (**5b**) und  $[\text{K}(\text{thf})_2\{\text{Co}(\text{P}_2\text{C}_2t\text{Bu}_2)_2\}]$  (**5c**) mit Kupfer(I)- und Silber(I)-Halogeniden in Anwesenheit der tertiären Phosphane  $\text{PMe}_3$  oder  $\text{PPh}_3$  synthetisiert. In Abhängigkeit vom verwendeten Phosphan ( $\text{PMe}_3$  oder  $\text{PPh}_3$ ) und der eingesetzten Stöchiometrie wurden verschiedene Komplexe erhalten. Schema 7 fasst die Darstellung der Komplexe  $[\text{Cu}(\text{PMe}_3)_4][\text{Co}(\text{P}_2\text{C}_2t\text{Pent}_2)_2]$  (**15**),  $[\text{Cu}(\text{PPh}_3)_2\{\text{Co}(\text{P}_2\text{C}_2\text{R}_2)_2\}]$  (**16a**:  $\text{R} = t\text{Pent}$ ; **16b**:  $\text{R} = t\text{Bu}$ ),  $[\text{Ag}(\text{PMe}_3)_x\{\text{Co}(\text{P}_2\text{C}_2t\text{Pent}_2)_2\}]$  (**17**:  $x = 2$ ; **18**:  $x = 3$ ) und  $[\text{Ag}_2(\text{PMe}_3)_5\{\text{Co}(\text{P}_2\text{C}_2t\text{Pent}_2)_2\}]\text{SbF}_6$  (**19**) zusammen.



**Schema 7.** Synthese des  $[\text{Cu}(\text{PMe}_3)_4]^+$ -Salzes **15** und der Koordinationskomplexe **16–19**.

Die Komplexe **15–19** wurden durch Röntgenstrukturanalysen und ergänzend durch Festkörper-NMR-Spektroskopie untersucht. Die Festkörperstrukturen der Koordinationskomplexe **16–19** enthalten dreifach- und vierfach koordinierte Kupfer(I)- bzw. Silber(I)-Kationen. Die Metallatome sind dabei an ein

Phosphoratom einer  $[\text{Co}(\text{P}_2\text{C}_2\text{R}_2)_2]^-$ -Sandwicheinheit und an zwei bzw. drei Phosphanliganden gebunden. Das Kupfersalz **15** weist eine ionenseparierte Struktur auf, bestehend aus dem seltenen, vierfach koordinierten  $[\text{Cu}(\text{PMe}_3)_4]^+$ -Kation und einem  $[\text{Co}(\text{P}_2\text{C}_2t\text{Pent}_2)_2]^-$ -Anion.<sup>4,8</sup> Ähnlich wie die in Kapitel 4 erwähnten Gold(I)-Komplexe  $[\text{Au}(\text{PMe}_3)_2\{\text{Co}(\text{P}_2\text{C}_2t\text{Pent}_2)_2\}]$  (**8**) und  $[\text{Au}(\text{PMe}_3)_4][\text{Au}\{\text{Co}(\text{P}_2\text{C}_2\text{Ad}_2)_2\}]$  (**10**), zeigen die Kupfer(I)- und Silber(I)-Verbindungen **15–19** komplizierte und temperaturabhängige NMR-Spektren in Lösung, welche darauf hindeuten, dass die Kupfer-Phosphan- bzw. Silber-Phosphan-Einheiten in Lösung teilweise nicht an das Anion koordiniert sind.

Zusammenfassend konnte in den Kapiteln 4–6 gezeigt werden, dass die homoleptischen Sandwichanionen  $[\text{Co}(\text{P}_2\text{C}_2\text{R}_2)_2]^-$  eine reichhaltige Koordinationschemie gegenüber Münzmetallen aufweisen. Angesichts dieser Ergebnisse erscheint es sinnvoll, das Koordinationsverhalten dieser Anionen gegenüber weiteren Übergangsmetallen zu untersuchen. Durch ähnliche Salzmetathesen von  $[\text{K}(\text{thf})_x\{\text{Co}(\text{P}_2\text{C}_2\text{R}_2)_2\}]$  und insbesondere von  $[\text{Tl}(\text{thf})_2\{\text{Co}(\text{P}_2\text{C}_2\text{R}_2)_2\}]$  mit geeigneten Übergangsmetallhalogeniden sollte sich, wie in den Kapiteln 4–6 aufgezeigt, eine Vielzahl neuartiger Komplexe herstellen lassen. Die Festkörperstruktur des Kaliumsalzes  $[\text{K}(\text{thf})_4\{\text{Co}(\text{P}_2\text{C}_2\text{Ad}_2)_2\}]$  (**5a**, Kapitel 4) verdeutlicht zudem, dass die Synthese von  $\pi$ -Komplexen ebenfalls möglich sein dürfte. Ein weiteres Ziel für zukünftige Arbeiten stellt die Synthese von Koordinationspolymeren mit dem paramagnetischen Anion  $[\text{Fe}(\text{P}_2\text{C}_2\text{R}_2)_2]^-$  dar. Aufgrund potenzieller kooperativer Wechselwirkungen der paramagnetischen Eisenzentren weisen diese Verbindungen möglicherweise interessante magnetische Eigenschaften auf, deren Untersuchung ein weiteres Ziel darstellt. Das Potential von  $[\text{Co}(\text{P}_2\text{C}_2\text{R}_2)_2]^-$ -Sandwichanionen als Synthesebaustein konnte in Kapitel 5 durch die Synthese eines ungewöhnlichen, achtkernigen, molekularen Quadrates verdeutlicht werden. Derartige Verbindungen sind aufgrund ungewöhnlicher elektronischer und magnetischer Eigenschaften interessant. Die Synthese weiterer molekularen Quadrate, und evtl. auch größerer Aggregate, stellt daher eine weitere Herausforderung an zukünftigen Arbeiten dar.

## References

- 1 J. Malberg, E. Lupton, E.-M. Schnöckelborg, B. de Bruin, J. Sutter, K. Meyer, F. Hartl, R. Wolf, *Organometallics* **2013**, online veröffentlicht am 10.09.2013. DOI: 10.1021/om4005862.
- 2 Unveröffentlichte Ergebnisse.
- 3 J. Malberg, T. Wiegand, H. Eckert, M. Bodensteiner, R. Wolf, *Chem. Eur. J.* **2013**, *19*, 2356.
- 4 J. Malberg, T. Wiegand, H. Eckert, M. Bodensteiner, R. Wolf, *Eur. J. Inorg. Chem.* **2013**, am 02.10.2013 zur Veröffentlichung angenommen. DOI: 10.1002/ejic.201301173.
- 5 J. Malberg, M. Bodensteiner, D. Paul, T. Wiegand, H. Eckert, R. Wolf, Veröffentlichung in Vorbereitung.
- 6 R. Wolf, A. W. Ehlers, M. M. Khusniyarov, F. Hartl, B. de Bruin, G. J. Long, F. Grandjean, F. M. Schappacher, R. Pöttgen, J. C. Slootweg, M. Lutz, A. L. Spek, K. Lammertsma, *Chem. Eur. J.* **2010**, *16*, 14322.
- 7 H. Schmidbaur, R. Franke, *Chem. Ber.* **1972**, *105*, 2985.
- 8 J. R. Black, W. Levason, M. D. Spicer, M. Webster, *J. Chem. Soc., Dalton Trans.* **1993**, *20*, 3129.



## 9 Acknowledgement

Mein besonderer Dank gilt Herrn Prof. Dr. Robert Wolf für die interessante Aufgabenstellung, die wertvollen Anregungen, die hervorragende Betreuung während der Diplomarbeit und in der gesamten Zeit der Promotion sowie für die ausgezeichneten Arbeitsbedingungen.

Herrn Prof. Dr. Manfred Scheer (Zweitgutachter), Herrn Prof. Dr. Axel Jacobi von Wangelin (Drittprüfer) und Herrn Prof. Dr. Henri Brunner (Vorsitz) danke ich für die Bereitschaft, die Plätze des Prüfungskomitees zu besetzen.

Meinen Kooperationspartnern Frau Dr. Elizabeth Lupton (Universität Regensburg), Herrn Dr. Bas de Bruin (Universität Amsterdam), Herrn Dr. Jörg Sutter und Herrn Prof. Dr. Kasten Meyer von der Universität Erlangen-Nürnberg, Herrn Prof. Dr. Frantisek Hartl (Universität Reading) und insbesondere Herrn Dr. Thomas Wiegand und Herrn Prof. Dr. Hellmut Eckert von der Universität Münster danke ich herzlich für ihre wertvolle Unterstützung und hilfreichen Diskussionen.

Ein großer Dank gilt weiterhin den Mitarbeitern der Zentralen Analytik und Werkstätten an den Universitäten zu Münster und Regensburg. Frau Anette Schramm, Frau Georgine Stühler und Herrn Fritz Kastner von der NMR Abteilung der Universität Regensburg danke ich herzlichst für die vielen, oftmals auch komplizierteren und „außer-Routine-mäßigen“ NMR Messungen.

Allen jetzigen und früheren Mitarbeitern unseren Arbeitskreises, sowie den Mitarbeitern des AK Uhl und des AK Scheer danke ich für die ausgesprochen angenehme Laboratmosphäre und die vielen schönen Momente, auch über den Laboralltag hinaus. Mein besonderer Dank gilt dabei meinen Arbeitskollegen Markus Plois, Stefan Pelties, Dirk Hermann, Bernd Mühldorf und Babak Rezaei Rad für die diversen schönen Kaffeepausen, die Unterstützung während meiner Arbeit und das viele Korrekturlesen. Meiner Freundin Bianca Attenberger danke ich für ihre Freundschaft, Unterstützung und Gelduld.

Meiner Familie und meinen Freunden, insbesondere meinen Eltern samt neuen Lebensgefährten danke ich für ihre bedingungslose Unterstützung und den Glauben an mich. Nobbse danke ich für die wunderbare gemeinsame Zeit und die überaus ausdauernde Geduld mit mir.



## 10 Curriculum Vitae

### Jennifer Malberg

(Dipl. Chem. )

#### Personal Data

---

Birthday, -place                      29.07. 1984, Essen

Nationality                              German

#### Education

---

since 03/2010                      PhD Thesis in Inorganic Chemistry, in the group of Prof. Dr. Robert Wolf  
“ *Synthesis and Characterization of Oligonuclear Naphthalene and  
Diphosphacyclobutadiene Transition Metal Complexes* “

since 08/2011                      at the **University of Regensburg**

03/2010 - 08/2011                  at the **University of Münster**

01/2010                              Dipl.-Chem.

07/2009 - 01/2010                  Diploma Thesis in Inorganic Chemistry at the University of Münster under  
supervision of Dr. Robert Wolf and Prof. Dr. Hans Werner Uhl  
“*Synthese und Charakterisierung von niedervalenten Eisenverbindungen mit  
sterisch anspruchsvollen Cyclopentadienylliganden*“

11/2007                              Preliminary Diploma

10/2004                              Enrollment as student of Chemistry at the University of Münster

06/2004                              Abitur (A-level), Städtisches Mädchen-Gymnasium-Essen-Borbeck in Essen

Regensburg, Oktober 2013

## List of Publications

---

- (1) “*Synthesis and Electronic Structures of Dissymmetrical, Naphthalene-Bridged Sandwich Complexes  $[\text{Cp}'\text{Fe}(\mu\text{-C}_{10}\text{H}_8)\text{MCp}^*]^x$  ( $x = 0, +1$ ;  $M = \text{Fe, Ru}$ ;  $\text{Cp}' = \eta^5\text{-C}_5\text{H}_2\text{-1,2,4-tBu}_3$ ;  $\text{Cp}^* = \eta^5\text{-C}_5\text{Me}_5$ )*”, J. Malberg, E. Lupton, E. M. Schnöckelborg, B. de Bruin, J. Sutter, K. Meyer, F. Hartl, R. Wolf, *Organometallics* **2013**, published online at 10/09/2013. DOI: 10.1021/om4005862.
- (2) “*Gold(I) and Silver(I) Complexes of Diphosphacyclobutadiene Sandwich Anions*”, J. Malberg, T. Wiegand, H. Eckert, B. Bodensteiner, R. Wolf, *Chem. Eur. J.* **2013**, *19*, 2356.
- (3) “*Copper(I) and Silver(I) Complexes of 1,3-Diphosphacyclobutadiene Sandwich Anions: Synthesis, Crystal Structures, Solution and Solid-State NMR Characterization*”, J. Malberg, T. Wiegand, H. Eckert, M. Bodensteiner, R. Wolf, *Eur. J. Inorg. Chem.* **2013**, accepted for publication. DOI: 10.1002/ejic.201301173.
- (4) “*Preparation of an Organometallic Molecular Square by Self-Assembly of Phosphorus-Containing Building Blocks*”, J. Malberg, M. Bodensteiner, D. Paul, T. Wiegand, H. Eckert, R. Wolf, manuscript in preparation.
- (5) “*Solid-State NMR Studies and Chemical Shift Calculations of a Gold(I) Complex with a Diphosphacyclobutadiene Cobaltate Sandwich Anion*”, T. Wiegand, H. Eckert, S. Grimme, J. Malberg, R. Wolf, *Solid-State Nucl. Magn. Res.* **2013**, *53*, 13.
- (6) “*Highly Chemoselective Cobalt-Catalyzed Biaryl Coupling Reactions*”, S. Güllak, O. Stepanek, J. Malberg, B. Rezaei Rad, M. Kotorá, R. Wolf, A. Jacobi von Wangeling, *Chem. Sci.* **2012**, *4*, 776.